Geochemical fingerprinting of Icelandic silicic Holocene tephra layers

June 2011

By

Rhian Hedd Meara

A dissertation submitted to the College of Science and Engineering at the University of Edinburgh in fulfilment of the requirements for the degree of doctor of philosophy.

I, **Rhian Hedd Meara**, declare the following:

(a) that this thesis has been composed by myself, the candidate;

(b) that the incorporated work is entirely my own with any contribution from others clearly indicated; and

(c) that this work has not been submitted for any other degree or professional qualification.

……..

Dedication:

To my beautiful niece, who gave me a reason not to give up.

Ella Katherine Meara

12.10.2010

“I have never been wise.”

FitzChivalry Farseer and The Fool

Fool’s Fate, Book Three of the Tawny Man Trilogy

Robin Hobb

Acknowledgements

Many thanks go to the following for their contribution to the work involved in this thesis:

Financial assistance for this project was provided by RANNÍS - the Icelandic Science Foundation - and the School of GeoSciences at the University of Edinburgh. An additional grant was provided by NERC to fund Ion Probe analyses.

Thor Thordarson and Godfrey Fitton are thanked for their supervision and assistance during my 4 years at the University of Edinburgh. Staff within the School of GeoSciences have provided both assistance and friendship throughout my PhD, in particular Rosanna Macagnanno, Helena Sim, Nikki Reid, Rachel Palmer, Emma Latto, Sue Rigby, Barry Dawson, Anthony Newton and Pete Nienow.

Our colleagues Guðrun Larsen, Ármann Höskuldsson, Olgeir Sigmarsson and Guðrun Sverrisdóttir at the University of Iceland provided assistance in identifying proximal reference sections and helpful discussions. Thanks also go to Ben Schupack, Margaret Hartley, Tomos Davies, Katie Roberts and Jo Variava for their assistance during the field seasons of 2007 – 2009.

Thank you to Nic Odling, Mike Hall, Chris Hayward, John Craven, Richard Hinton and Cees Jan De Hoog at the University of Edinburgh for their support and supervision during sample preparation and use of the XRF, electron microprobe and ion probe facilities. Many thanks to Nick Pearce at the University of Aberystwyth for support and assistance when using the LA-ICP-MS facility, for being a friendly face during some hard times and for encouraging me to attend an amazing conference in Japan.

A huge thank you to my friends who have put up with me throughout this thesis. You've helped me laugh, shout and weep. You provided me with support, hugs and chocolate whenever it was needed and saw me through some incredible emotional roller-coasters. There are too many people to thank individually, but particular thanks go Team Edinburgh (Jenny Rapp, Louise Barron, Gillian McCay, Tanya Jude-Eton, Caroline Graham, Margaret

Hartley, Amber Annette, Sian Henley, Luke Ridley, Katie Noake, Matt Unterman, Dan Hobley and Tom Russon), Team Leicester (Richard Moakes, Jo Variava, Kirstie Wright, Ben Hedley, Pete Fitch, James Blight, Stephen Williams, James Beasant, Rebecca Blake, Jonathan Nimmo and Eleanor Chapman) and to Katie Roberts, Laura Roberts and Rachel Hawkins. I really couldn't have done it without you guys. Thanks to all the friends I made at the Edinburgh International Science Festival who helped me to realise that there was a life after this PhD. Thank you also to members of staff at Leicester University that encouraged me to believe in myself and my abilities – in particular Mike Norry, Sarah Davies, Gawen Jenkin, Mike Branney, Andy Saunders, Mike Lovell and Tim Brewer who will never be forgotten.

The biggest thanks go to my family. My Mam and Dad have provided continuous support and supervision, reading and correcting a seemingly endless stream of chapters and papers. They have listened to me ranting and raving and weeping uncontrollably and have comforted me every time I reached rock bottom. Never before has the Welsh saying "rhai weithiau, mae'n rhy gormod" meant so much. Thank you to my big brother Hefin and his fiancé Rosey for looking after me and giving me pep talks, and my Grandma, who has always encouraged me to believe that I could do anything. The biggest thanks of all however, go to Ella Katherine Meara, my beautiful niece to whom this thesis is dedicated. Ella was born during an incredibly difficult period of my life when I felt like I was completely falling apart and that I would never finish this thesis. Her birth gave me a reason to carry on and I hope I make her proud.

One final thank you goes to Jonas Rae who I met towards the end of this project. Thank you for helping me re-gain my confidence in myself.

Abstract

The overall aim of this research project has been to develop a reference dataset of 19 Holocene silicic Icelandic tephra layers sourced from the Torfajökull, Askja, Katla, Öræfajökull and Hekla volcanic systems. The dataset comprises geochemical data (including major, trace and rare earth element data for bulk and glass phases collected by XRF, electron microprobe, ion probe and laser ablation ICP-MS) and physical data (including sedimentary logs, field photographs, distribution maps and GPS localities of reference sections).

Results indicate that Icelandic volcanic systems show unique geochemical signatures which result from the systems proximity to the active rifting zone and the proposed upwelling mantle plume that underlies the island. Within individual volcanic systems, eruptions produce tephra with distinct geochemical characteristics, which allow for the independent confirmation of tephra identity. The identification and discrimination of tephra layers can in some cases be achieved using major element chemistry (e.g. Hekla, H1104 – H5) while other tephra layers can only be discriminated using trace element chemistry (e.g. Torfajökull, Landnám and Gràkolla). Certain tephra layers however show near-identical geochemistry and therefore discrimination is not possible (e.g. Hekla, HA, HB, HC, HM, HN, HX, HY, HZ) without the incorporation of other proxy data.

Icelandic micro-tephra horizons are identified in soil, lacustrine and marine sedimentary sequences and are used for dating and correlation in Quaternary studies. Data collected for this project will facilitate reliable data comparison and tephra identification between proximal and distal localities across the North Atlantic region. The data may also contribute to the debate regarding the formation of silicic rocks within Iceland, particularly with regard to the Hekla central volcano. The geochemical data collected for this thesis shows distinct age-dependant geochemical sub-groups suggesting temporal sub-surface relocation of the Hekla magma source.

Table of Contents

List of Figures

Chapter 2: Icelandic Geological Setting

Chapter 3: Tephra and Tephrochronology

Chapter 4: Methodology

Chapter 5: Establishing Icelandic tephra provenance using major element chemistry

Chapter 6: Major elements as a tool for identifying tephra layers sourced within the same volcanic system

Chapter 7: The application of major and minor element chemistry to the fingerprinting of Icelandic volcanic systems

Chapter 8: Discussion

List of Tables

Chapter 7: The application of major and minor element chemistry to the fingerprinting of Icelandic volcanic systems

List of Abbreviations

A - Askja volcano

BP - Before Present

BSE - Bulk Silicate Earth

DOM - Dosenmoor, Germany

DRE - Dense Rock Equivalent

EDS - Energy Dispersive Spectrometry

EMPA - Electron Microprobe Analysis

EVZ - Eastern Volcanic Zone

GRAM - Grambower Moor, Germany

H - Hekla volcano

IP - Ion Probe

JAM - Jardelunder Moor, Germany

K - Katla volcano

KR - Kolbinsey Ridge

LA-ICP-MS - Laser Ablation Inductively Coupled Mass Spectrometry

LOI - Loss on Ignition

Ma - Million years

MIB - Mid-Iceland Belt

MOR - An Loch Mór, Ireland

NAIP - North Atlantic Igneous Province

NIST - National Institute of Standards and Technology

NVZ - Northern Volcanic Zone

O or Ö - Öræfajökull volcano

ÖVB - Öræfi Volcanic Belt

PDCs - Pyroclastic Density Currents

RR - Reykjanas Ridge

SAR - Soil Accumulation Rate

SCD - Salisbury Cragg Dolerite

SG - Shapp Granite

SISZ - South Iceland Seismic Zone

SVB - Snæfelsness Volcanic Belt

T - Torfajökull volcano

TFZ - Tjörnes Fracture Zone

TAS - Total Alkali Silica

T-V - Torfajökull – Vatnaöldur volcanoes

VEI - Volcanic Explosivity Index

WDS - Wave Dispersive Spectrometry

WVZ - Western Volcanic Zone

XRF - X-Ray Fluorescence

Chapter 1:

Introduction

1.1 Background Information

The geologically instantaneous nature of volcanic eruptions combined with the ability of explosive Plinian eruptions to disperse ash across vast distances results in the presence of wide-spread time-parallel tephra marker horizons in sedimentary successions. The identification, characterisation and correlation of tephra layers for dating purposes forms the basis of tephrochronology (Thorarinsson, 1944, 1949, 1958, 1968; Larsen, 1981). Tephra markers can be used to date and correlate events such as climatic perturbations (e.g. Caseldine *et al*. 1998; Langdon and Barber, 2004), anthropological and archaeological episodes (e.g. Buckland *et al*. 1997) and variations in flora and fauna species concentrations (e.g. Blackford *et al*. 1992; Hall *et al*. 1994).

Tephra layers sourced from Icelandic volcanic systems account for a large number of the micro-tephra horizons identified across the North Atlantic region (e.g. A1875, Ö1362, H1104, Landnám, H3 and H4). The interaction of the spreading Mid-Atlantic ridge and the proposed mantle plume beneath Iceland results in individual volcanic systems showing specific geochemical signatures or provenance. The identification of micro-tephra horizons is typically achieved by analysing the major element compositions of individual glass shards by electron microprobe. This technique has proved effective for confirming the provenance of tephra layers and to some extent for identifying individual tephra layers sourced within the same system. The application of trace element chemistry is suggested as a possible mechanism for discriminating between tephra layers that show identical major element chemistry.

1.2 Study Objectives

The main aims of this thesis are as follows:

1. To Identify reference sections at proximal locations for important silicic tephra marker horizons in Iceland. To record the physical characteristics, and to collect samples that fully represent each eruption.
2. To develop a robust, reliable geochemical reference dataset for said marker tephra layers including major and trace element chemistry for bulk and glass phases.
3. To establish whether tephra provenance can be reliably confirmed using major element chemistry.
4. To determine whether tephra layers sourced within the same volcanic system can be distinguished using major elements.
5. To apply trace element chemistry to the discrimination and identification of tephra horizons.

These aims were developed in conjunction with a larger research project titled "**V**olcanism and the **A**rctic **S**yst**t**em" (VAST) which examines volcanic activity and climatic variations within the Arctic region during the Holocene. This component of the larger project focuses on developing an Icelandic tephrochronology framework for use in dating and correlating sedimentary successions by other workers within the group as well as the larger Quaternary research community.

Initially, only large silicic tephra layers sourced from explosive Plinian eruptions were selected for analysis as previous studies have indicated that these tephras are typically deposited over long-distances. In particular, tephras were selected from the Hekla, Askja, Torfajökull and Öræfajökull central volcanoes as these are linked with known episodes of environmental change and human activity e.g. H4 and the decline of the Scots Pine (Blackford *et al*. 1992) and Landnám with the human settlement of the Faroe Islands and Iceland (Wastegård *et al*. 2003). Subsequent field work focused on sampling smaller intermediate tephra layers. These tephras were sampled to provide information on local tephrochronology to correspond with tephra horizons identified in Icelandic lake cores as part of the extended VAST research. Sampling the smaller tephra layers also provided an opportunity to introduce a series of lesser known eruptions to the wider North Atlantic tephrochronology community. Ideally, this project would have analysed the entire Icelandic tephra succession, however this was outside the scope of the project. The basaltic tephra succession has been investigated by Jagan (2010), also a member of the VAST research group.

Physical and geochemical data have been collected in order to develop a robust, reliable data set of Icelandic Holocene silicic – intermediate tephra layers. No such data set exists at present. The development of methodologies for determining tephra provenance and identity were aimed at simplifying the task for workers both within the VAST group and the wider community. The analysis of trace and rare earth element chemistry in tephrochronology is relatively new and was incorporated into this project as its inclusion was in agreement with the overall aim of the project: to identify and discriminate between Icelandic tephra layers using geochemistry.

1.3 Thesis Structure

This research is presented in chapter format as follows:

Chapters 2 and 3 provide background information for this research project. Chapter 2 covers the geological and geographical context of Iceland, focusing on the islands formation, the development of active regional rifting zones and localised volcanic systems. The variability of volcano morphology and eruption styles are discussed and a brief overview of the origins of silicic magma is provided. The volcanic systems and associated tephra layers studied in this thesis are also introduced. Chapter 3 introduces the concept of tephrochronology and its application to interdisciplinary Quaternary studies. This chapter also presents the concepts of proximal and distal localities and details how tephra layers are identified at both localities. An explanation of the physical characteristics of tephra is provided along with an explanation of the interpretations gained from such information. A brief account of Icelandic tephrochronology is presented and some persistent problems are discussed.

Chapter 4 presents the methodology used during this study. The chapter provides detailed accounts of the methods used during field work, sample preparation and geochemical analyses including X-Ray Fluorescence, Electron Microprobe, Ion Probe and Laser Ablation Inductively Coupled Plasma Mass Spectrometry.

Chapter 5 is a geochemical study aimed at identifying tephra provenance using major element chemistry. The chapter presents field data including sedimentary logs and photographs, along with major element geochemical data for bulk and glass phases for tephra layers sourced from the Torfajökull, Askja, Katla and Öræfajökull volcanic systems.

Finally, a formal methodology for identifying tephra provenance using major element chemistry is presented.

Chapter 6 is a geochemical study aimed at identifying and discriminating between tephra layers sourced within the same volcanic system using major element chemistry. The Hekla volcanic system is used as a case study. The chapter presents field data including sedimentary logs and photographs, along with major element geochemical data for bulk and glass phases. A formal methodology for identifying discriminating between the Hekla tephra layers using major element chemistry is presented.

Chapter 7 is a geochemical study aimed at using major, trace and rare earth element chemistry to determine the geochemical fingerprints or signatures of volcanic systems and individual tephra layers. The first section of the chapter focuses on establishing the signatures of individual volcanic systems. The second section develops on the work conducted in Chapter 6 by investigating the possibility of discriminating between tephra layers sourced within the same system using trace and rare earth elements.

Chapter 8 discusses the implications of the work undertaken in Chapters 5 - 7, with particular focus on previous and future physical volcanology, igneous petrogenesis and tephrochronology studies. Magmatic signatures and generation processes are discussed. Suggestions for further work are also presented.

Chapter 9 provides the overall conclusions of the thesis.

Chapter 10 presents a bibliography of scientific papers and texts referenced within this thesis.

The attached Appendix CD comprises all geochemical data collected during this thesis.

Chapter 2:

Geology, volcanism and magmatism in Iceland

2.1 Introduction

The work presented in this thesis focuses on specific aspects of volcanism in Iceland. It is therefore appropriate to introduce the geological setting of Iceland, including the islands' formation, and the development of active regional rifting zones and localised volcanic systems. Volcano morphology and eruption styles recorded in Iceland are discussed and a brief overview of the origins of silicic magma is provided. The individual volcanic systems and tephra layers studied for this thesis are also introduced.

2.2 Geographical and Geological setting

Iceland is a volcanic island located in the North Atlantic Ocean at 63–67°N and 28–13°W. The island straddles the Mid-Atlantic rift system and resides over a stationary mantle hotspot (Sæmundsson, 1979; Wolfe, 1987; Wolfe *et al*. 1997; Larsen *et al*. 1998; Kristiansdóttir *et al*. 2007). The Icelandic plateau rises c. 3000 m above the surrounding abyssal plain and covers an area c. 350,000 km^2 with a crustal thickness of 10 – 40 km (Sæmundsson, 1979; Gudmundsson, 2000). The thickest crust is located in southern and central Iceland and the thinnest crust lies beneath the Reykjanes peninsula (Jónasson, 2006). The Icelandic plume is the principle source of the North Atlantic Igneous Province (NAIP) which currently extends from West Greenland to Scotland. Activity commenced c. 62 Ma and Iceland is the only active segment remaining (Talawani and Eldholm, 1977; Saunders *et al*. 1997). The formation of Iceland commenced c. 24 Ma during the Tertiary period; however the oldest outcropping rocks are typically 14 – 16 Ma (Fig. 2.1; McDougal, 1984). Iceland consists of three regional-scale geological formations relating to the construction of the island (Fig. 2.1; Thordarson and Höskuldsson, 2008). The oldest is the Tertiary Basalt Formation which extends to the east and western limits of the island and represents the period 16 – 3.3 Ma BP. The Plio-Pleistocene Formation represents 3.3 – 0.8 Ma BP and mirrors the axial rift. The Upper Pleistocene is the

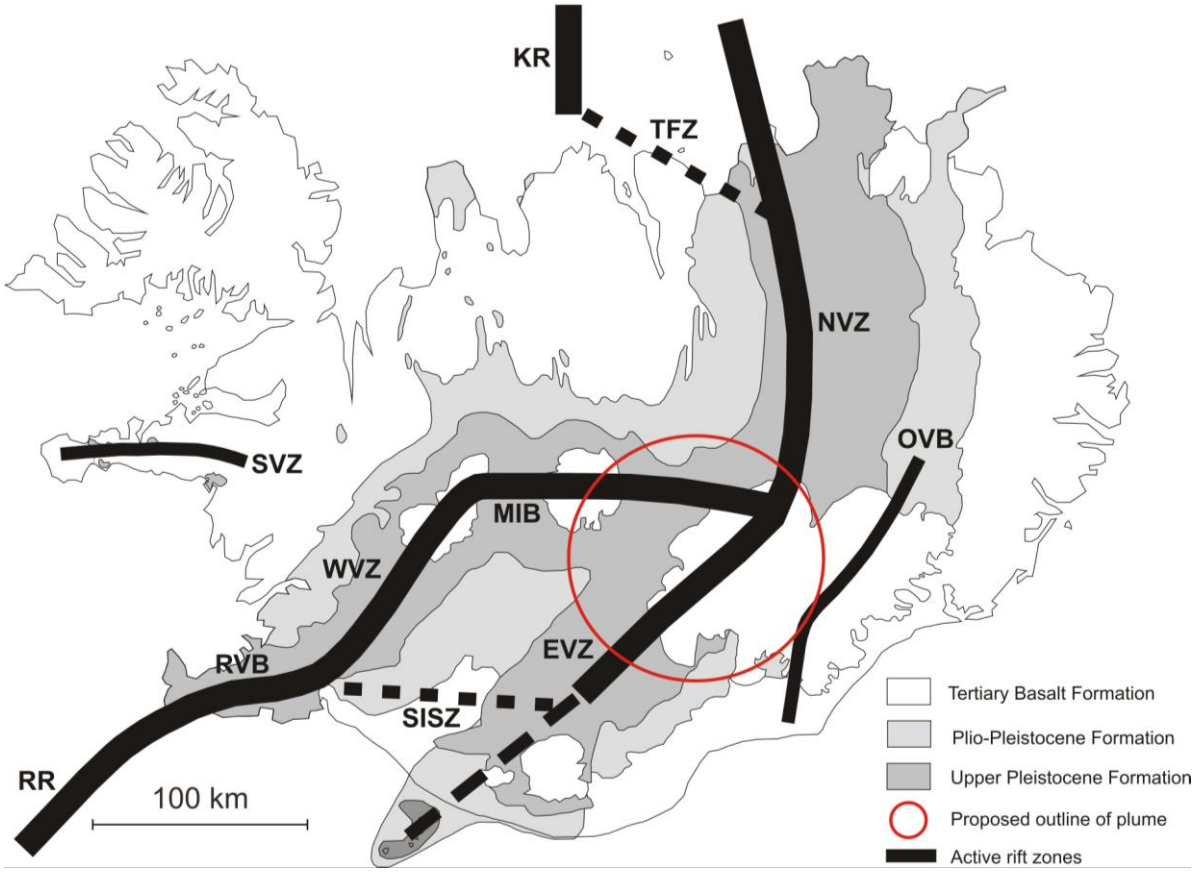

Figure 2.1: Map showing the active rifting structures within Iceland and the inferred location of the Icelandic mantle plume axis - as established by tomography studies (e.g. Bijwaard and Spakman 1999) superimposed onto the regional geological subdivisions. Kolbinsey Ridge (KR), Tjörnes Fracture Zone (TFZ), Northern Volcanic Zone (NVZ), Öræfi Volcanic Belt (OVB), Eastern Volcanic Zone (EVZ), Mid-Iceland Belt (MIB), South Iceland Seismic Zone (SISZ), Western Volcanic Zone (WVZ), Snæfellsnes Volcanic Belt (SVB) and Reykjanes Ridge (RR) (Adapted from Thordarson and Larsen, 2007).

is the youngest formation and represents 0.8 Ma BP to present and follows the axial rift as well as the propagating Eastern Volcanic Zone.

Iceland behaves as a continuation of the Mid-Atlantic rift system (Jónasson, 2006). Active rifting within Iceland is confined to the axial rift and the propagating Eastern Volcanic Zone. (Fig.2.1; Thordarson and Höskuldsson, 2008). The axial rift is the surface expression of the Mid-Atlantic rift and is represented by the Western Volcanic Zone (WVZ) which extends from the Reykjanes Peninsula in the south west to the Hofsjökull and Langjökull ice caps in the

north east, the Mid Iceland Belt (MIB) and the Northern Volcanic Zone (NVZ). These zones are dominated by tholeiitic magma compositions. The Eastern Volcanic Zone is a rift zone in the making via southwest propagation through older crust and exhibits systematic changes in magma compositions, from tholeiitic in the north to mildly alkalic at the southern tip (Jakobsson, 1979; Sæmundsson, 1979; Gudmundsson, 1995). The Öræfi volcanic belt (ÖVB) is a proto-rift in the east of the country postulated to represent avulsion of rifting to a new location at the surface (Thordarson and Höskuldsson, 2002). The Snæfellsnes Volcanic Belt (SVB) is a reactivated rift zone in the west of Iceland (Gudmundsson, 2000). For Iceland as a whole, the average spreading rate is 1.8 cm y^{-1} in N105°E direction; however there are variations along strike (Gudmundsson, 2000).

2.3 The volcanic system; concepts and definition

Volcanic systems are the principle structures within the volcano-tectonic zones and typically comprise a fissure swarm up to 100 km long, a central (composite) volcano or a combination of both. There are 30 active volcanic systems in Iceland; twenty of which feature fissure swarms and 19 systems have at least one central volcano (Fig. 2.2; Thordarson and Larsen, 2007). There are 40 – 55 extinct volcanic systems recognised in the eroded Tertiary and Pleistocene lava piles (Walker, 1966; Sæmundsson, 1979).

Fissure swarms are typically 5 – 20 km wide and 40 – 150 km long and mimic regional extensional trends. The structures are characterised by monogenetic basaltic fissure eruptions, sub-surface normal faults and dikes (Jakobsson, 1979; Sæmundsson, 1980; Gudmundsson, 2000). Sub-surface dikes are dominantly basaltic and show thickness variations $\leq$ 60 m Gudmundsson, 2000).

When present, central volcanoes are a locus of activity and typically produce a range of compositions from basalt through to rhyolite (Jakobsson, 1979; Sæmundsson, 1980). Central volcanoes typically erupt once every several hundred years and have lifetimes of 0.5 – 1 Ma. Typical dimensions are 5 – 20 km in diameter at the base and 1 – 2 km above sea level with volumes of many tens of cubic kilometres (Gudmundsson, 2000).

The formation of a volcanic system begins with the development of a fissure system which mimics regional extensional trends. Eruptive activity becomes focused on a series of vents,

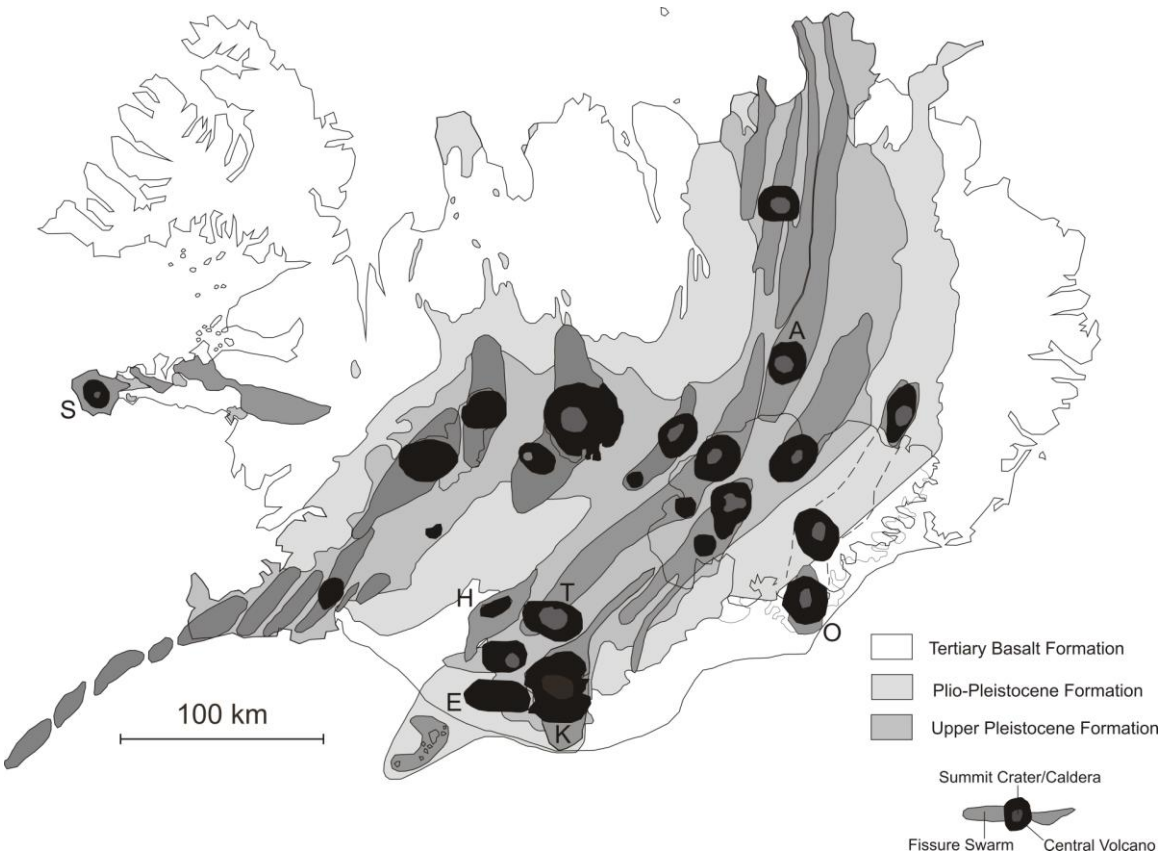

Figure 2.2: Map showing the location and the distribution of the 30 active volcanic systems identified within Iceland superimposed onto the regional geological subdivisions recorded in Iceland. Volcanoes known to have produced silicic magma are labelled: Hekla (H), Torfajökull (T), Katla (K), Öræfajökull (O) and Askja (A) Snæfellsnes (S) and Eyjafjallajökull (E) (adapted from Thordarson and Larsen, 2007).

producing small overlapping shield volcanoes. Finally, activity focuses onto a single vent, resulting in the development of an over-riding shield that buries other edifices. Gudmundsson (1987, 2000) suggests that the location of system development is explained by segregation and transportation of magma into areas of high permeability and crustal thinning. Central volcanoes are considered to be fed by two magma chambers – a primary reservoir in the base of the crust which feeds a magma chamber in the shallow crust. A central volcano and its associated magma chamber are considered to have reached maturity when the influx of magma is in equilibrium with the outflow, and when eruption and intrusion frequency and volumes are constant. Central volcanoes and their magma chambers are in their final stages when the influx of magma no longer maintains equilibrium. Volcanic extinction will occur following severance of a connection with the deep reservoir source.

2.4 Volcanic landforms

Iceland provides a perfect natural laboratory for studying volcanoes and their processes. The 30 volcanic systems in Iceland represent both polygenetic (i.e. showing multiple eruptions, compositions and styles) and monogenetic (i.e. represented by single, typically basaltic events) edifices. Icelandic volcanic systems showcase a complete range of volcanic structures and landforms (Francis and Oppenheimer, 2004; Thordarson and Höskuldsson, 2008):

Stratovolcanoes / Composite Cones: polygenetic volcanic structures with the main locus of activity focused on the summit craters and minor activity at parasitic monogenetic vents. Stratovolcanoes show a broad radial symmetry with gently sloping flanks which steepen near the summit producing an overall concave morphology. Stratovolcanoes have a layered or stratified appearance comprising alternating lava flows, airfall tephra, pyroclastic flows, volcanic mudflows and debris flows. Eruptive products show a range in compositions from basalt to rhyolite and reflect regional tectonic settings. Eruption styles vary from effusive Hawaiian lava flows to explosive Plinian ash clouds. Icelandic examples include: Snæfellsjökull (Fig. 2.3a), Hekla, Snæfell and Öræfajökull.

Shield volcanoes: polygenetic volcanic structures with the main focus of activity located within summit craters and minor activity from parasitic monogenetic vents and fissures. Shield volcanoes show a broad radial symmetry with very shallow slopes $\leq 10°$ producing an overall convex morphology reminiscent of warrior shields. Shield volcanoes are almost exclusively composed of stratified basaltic lava flows. Eruption styles are dominated by effusive Hawaiian lava flows. Icelandic examples include: Eyjafjallajökull (Fig. 2.3b), Skjaldabreður and Trölladyngja).

Table Mountains / Tuyas: Volcanic edifices formed in sub-glacial conditions. Tuyas are characterised by a distinctive stratigraphy: a sequence of polagonised tuffs, hyaloclastite breccias and pillow lavas and capped by horizontal sub-aerial lava flows. Icelandic examples include Herðubreið (Fig. 2.3c).

Caldera volcanoes: polygenetic volcanic structures capped with a cauldron-like depression. The depression structures are the result of rapid draining of a magma chamber. Evacuation of a sub-terraenean magma chamber results in structural failure and collapse of the overlying volcanic edifice. Caldera structures can measure up to 72 km in diameter and are often filled

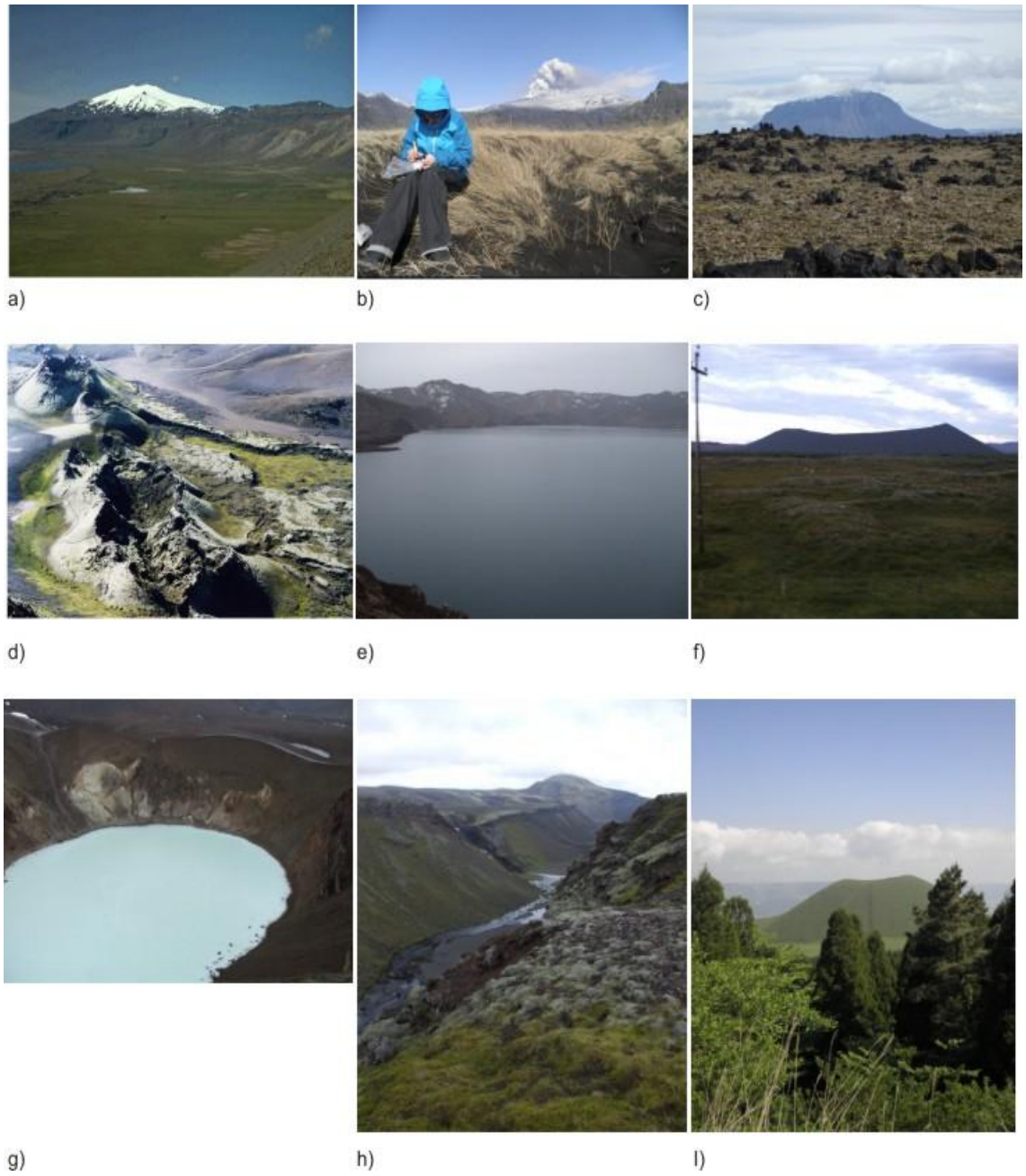

Figure 2.3: Photographs of the volcanic morphologies identified in Iceland. a) Stratovolcano – Snæfellsjökull. b) Shield volcano – Ejafjallajökull. c) Table mountain – Herðubreið. d) Cone row – Laki. e) Caldera volcano – Askja. f) Tuff cone - Hverfjall. g) Maar volcano – Viti. h) Chasm – Eldgjá. i) Scoria cone – Japan. Photographs b-c, e-i: Rh. Meara.

with water. Icelandic examples include: Torfajökull and Askja (Fig. 2.3e).

Scoria / Cinder cones: monogenetic volcanic edifice that forms during a single eruption. Post-

eruption, the sub-terranean plumbing system "freezes" restricting further activity. Scoria cones are dominated by loose basaltic scoria and rarely reach elevations higher than 300 m. Scoria cones are often asymmetrical, contain lava breaches and typically show slope angles of c. 35°. Icelandic examples include: Eldfell in Heimaey.

Spatter cones: monogenetic volcanic structures formed during a single eruption (Fig. 2.3i). Spatter cones differ to scoria cones in that spatter cones are formed when erupted molten lava agglomerates upon deposition. Icelandic examples include: Eldborg and Mýrum.

Tuff cones and Maars: monogenetic volcanic structures resulting from magma-water interaction. Tuff cones/rings represent positive structural features and are typically dominated by fresh juvenile material. Tuff structures can reach heights of 366 m and 800 m in diameter. Maars represent topographic depressions with low rims of ejected debris. Maar craters are often filled with lakes sourced from the ground water reservoirs responsible for initiating eruptions. Maar structures are typically 750 – 1750 m wide and 36 – 245 m deep. Icelandic examples include: Hverfjall near Mývatn (Fig. 2.3f).

Cone-row volcanoes: a series of volcanic cones representing eruption of an extensional fissure. Morphologically, cone-row structures show similar features to spatter and scoria cones, but are characterised by their linear relationships. Icelandic examples include: Laki (Fig. 2.3d).

Volcanic chasms: large fissures or deep volcanic canyons resulting from large fissure eruptions. Chasms show a range in sizes, the largest recorded is 270 m deep and 600 m wide. Icelandic examples include: Eldgjá (Fig. 2.3h).

Rootless cones: monogenetic small-scale scoria cones representing explosive interaction of mobile lava flows with surface water sources. Rootless cones represent explosion of lava sourced from a contemporaneous larger eruption and comprise no younger juvenile material. Icelandic examples include: Mývatn and Laki.

2.5 Holocene eruptive history, eruption styles and event frequencies

Icelandic volcanic systems show a variety of eruption styles and mechanisms including phreatic, phreato-magmatic and solely magmatic. Eruption style is dependent on a system's

proximity to and relationship with surface waters, ground waters and ice caps. Those volcanoes interacting with water sources produce the most explosive eruptions. Eruptions also vary between effusive and explosive. A volcanic eruption is deemed to be effusive if > 95 % of the eruptive products are lava, and deemed to be explosive if > 95 % of the eruptive deposits are pyroclastic in origin (Thorarinsson, 1981a). Icelandic volcanic systems showcase a complete range of volcanic eruption styles as detailed below (Newhall and Self, 1982; Francis and Oppenheimer, 2004; Mattson and Höskuldsson, 2003; Thordarson and Höskuldsson, 2008):

Hawaiian activity: characterised by eruption of non-viscous basaltic lava with minimal volatile contents, typically sprayed into the air to form fire fountains hundreds of metres high. Associated landforms are dependent on the cooling rate of lava within the fountain – quick cooling produces scoria cones while slow cooling produces spatter cones and clastogenic lavas. Generally, Hawaiian-style activity produces ≤ 10,000 m^3 of ejected material and represents a Volcanic Explosivity Index (VEI) of 0 (Fig. 2.4). Icelandic examples include eruptions at Krafla, and the Eldgjá and Laki eruptions of the Katla and Grimsvötn systems. The latter two are associated with small-scale continental flood basalt volumes.

Strombolian activity: characterised by a broad range of activity. Strombolian activity typically comprises intermittent, discrete explosive bursts which eject basaltic pyroclasts a few tens of hundreds of metres into the air. Eruption columns are not sustained. Eruptions produce low-viscosity magma with a moderate volatile content. Strombolian eruptions produce 10,000 – 1,000,000 m^3 of ejected material and represent a VEI of 1-2 (Fig. 2.4). Icelandic examples include: Eldfell on the island of Heimaey.

Surtseyan activity: characterised by a broad range of activity but dominated by phreato-magmatic processes. Powerful blasts allow ejected material to breach the constraints of a water/ice body. Such activity continues until the locus of activity is above the water/ice medium where Strombolian activity dominates with minor phreato-magmatic influences. A final effusive lava phase commences when all water influences are overcome. Icelandic examples include: Surtsey Island.

Vulcanian activity: characterised by typically brief explosive eruptions that last seconds to minutes. Eruption columns reach heights of 10 – 20 km and the resulting ejecta is deposited over a wide area. Vulcanian eruptions are dominated by volatile- and crystal-rich andesitic

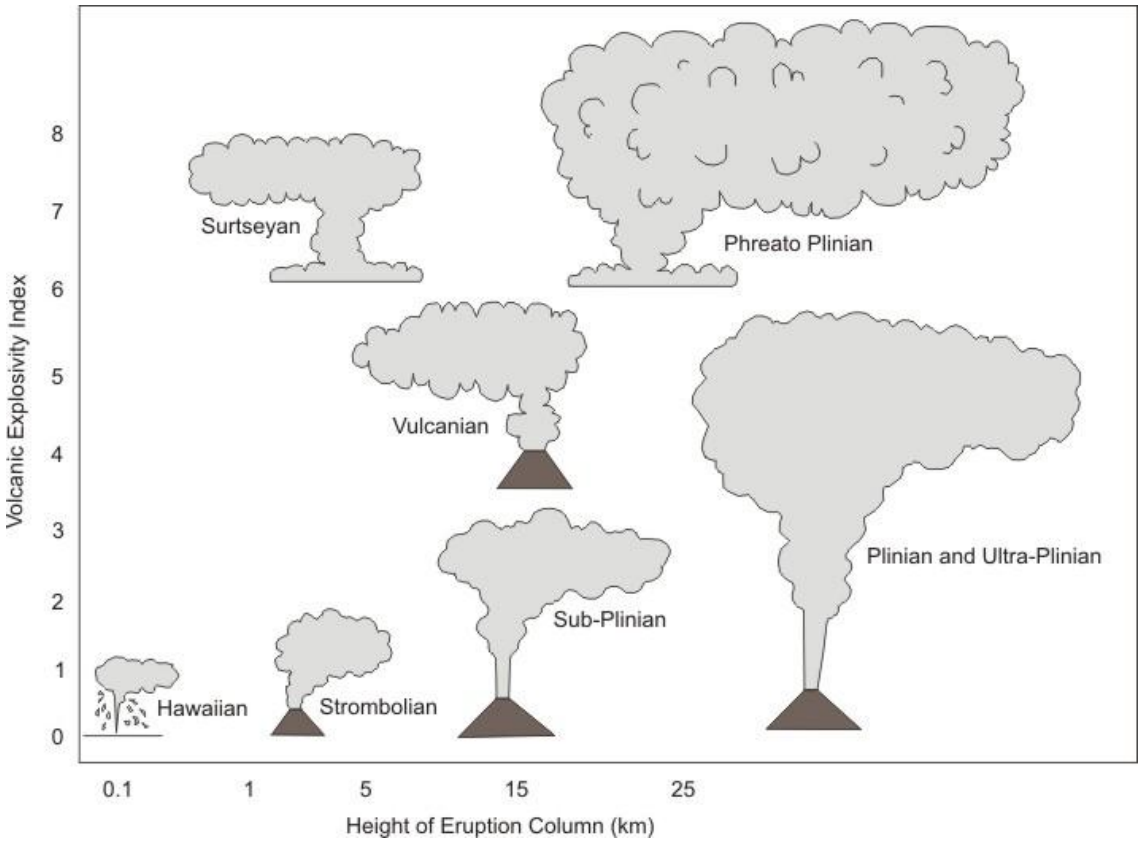

Figure 2.4: Characterisation of volcanic activity based on volcanic explosivity index and eruption column height. Adapted from Walker (1973).

magmas and are often associated with growing lava domes and pyroclastic density currents. Deposits often include non-juvenile material resulting from syn-eruptive vent clearing. Vulcanian eruptions produce 1,000,000 – 10,000,000 m^3 of ejected material and represent a VEI of 2 – 3 (Fig. 2.4). Icelandic examples include: Eyjafjallajökull (2010).

Sub-plinian activity: characterised by sustained explosive activity and eruption columns that reach 20 km. Sub-Plinian eruptions are dominated by volatile-rich dacitic and rhyolitic magmas although some eruptions comprise more mafic end members. Sub-Plinian eruptions produce 10,000,000 m^3 – 0.1 km^3 of ejected material and represent a VEI of 3 – 4 (Fig. 2.4). Icelandic examples include: Hekla.

Plinian/Ultra-Plinian/Phreato-Plinian activity: characterised by sustained extremely explosive activity and eruption columns that reach ≤ 40 km high, well into the stratosphere. The resultant ejected material is often transported and deposited over continents, and are felt across entire

hemispheres. Plinian/Ultra-Plinian eruptions are characterised by volatile-rich dacitic and rhyolitic magmas and are often associated with caldera formation and pyroclastic density currents. Phreato-Plinian eruptions represent incorporation of surface or ground waters with an ongoing Plinian/Ultra-Plinian eruption. Plinian/Ultra-Plinian/Phreato-Plinian eruptions produce 0.1 – 1,000 km^3 of ejected material and represent a VEI of 4 – 8 (Fig. 2.4). Icelandic examples include: Askja, Hekla, Torfajökull and Öræfajökull.

Current records indicate that there have been c. 500 effusive basaltic lava eruptions in Iceland during postglacial times, including 56 since the settlement of Iceland in 870 AD. When combined, these eruptions have produced around 390 +/- 50 km^3 of basaltic lava. During the same time period, there have been 29 intermediate and 15 silicic lava flows which have produced 23 km^3 and 1.2 km^3 respectively (Thordarson and Höskuldsson, 2008).

Establishing the number of explosive eruptions during postglacial times is difficult. During an explosive eruption, ash and pumice (see Chapter 3 for definitions) are ejected from the volcano and blanket the surrounding landscape, over time becoming incorporated and preserved within the underlying sedimentary sequence (Fig. 2.5). However, this process is only viable when certain conditions are met, i.e. the section must be ice-free and must have a high enough sediment accumulation rate (SAR) to ensure rapid burial of ash layers. Recent tephrochronology work conducted on sediment cores from a number of Icelandic lakes has highlighted this problem, indicating that many more layers may be preserved in proximal lacustrine sedimentary sequences than in proximal terrestrial sedimentary successions (Jagan, 2010).

Detailed logging and mapping has identified over 158 ash layers in terrestrial sequences dating from postglacial times, however this may be a serious under-estimation, with the total number of explosive eruptions closer to 2,400 (discussed further in Chapter 3). Of the confirmed 158 post-glacial eruptions, 87 % were sourced within the Eastern Volcanic Zone accounting for a dense rock equivalent (DRE) of 12.9 km^3 of magmatic material, while the remaining 13 % were sourced within the other volcanic zones and account for only 3.6 km^3 of magmatic material. Within the Eastern Volcanic Zones, Hekla and Katla are the most prolific producers of explosive eruptions accounting for 55 % of the 158 confirmed eruptions. This may be the result of the volcanoes' location: although both are ice-capped, neither lie within a large glacier as is the case for the Grímsvötn and Bardarbunga systems, and neither lie adjacent to

Figure 2.5: Terrestrial soil section showing a sequence of preserved basaltic (black), intermediate (green-grey) and silicic (white) tephra layers. Photograph is taken near Loðnugil on route F232, east of Mýrdalsjökull. The pale tephra horizon is thought to be the H3 tephra. (Photograph: Rh. Meara).

the sea shore as does Öræfajökull. Therefore, their eruptions deposit ash onto dry terrestrial sedimentary sequences and not into dynamic glacial and marine sequences (Thordarson and Larsen, 2007). Further information on Icelandic eruptions is provided in Chapter 3.

2.6 Volcanic systems and tephra layers studied for this thesis

Of the 30 active volcanic centres in Iceland, 7 have erupted silicic magmas during the Holocene period: Torfajökull, Askja, Katla, Öræfajökull, Hekla, Eyjafjallajökull and Snæfellsjökull (Fig. 2.2). These volcanic systems have erupted over 70 times since 10,300 BP and have a combined volume of > 40 km^3 DRE (Table 2.1). Tephra layers erupted from these volcanic systems were dominantly selected for research due to their widespread

Table 2.1: Volcanic systems and individual tephra layers discussed within this paper. The volume, area and age of each eruption is also recorded (Thorarinsson, 1958, 1963, 1967; Larsen and Thorarinsson, 1977; Sigurdsson and Sparks, 1981; Dugmore *et al*. 1995; Grönvold *et al*. 1995; Boygle, 1998; Larsen *et al*. 2001; Selbekk and Trønnes, 2007; Larsen and Eiríksson, 2008).

Source Volcano	**Eruptions**	**Age (BP)**	**Area (km^2) within the 0.1 cm Isopach**	**Volume ($km^{3)}$**
Askja	A 1875	125		2
Öræfajökull	Ö 1362	638	300,000	10
Hekla	H 1104, H3, HS, H4, H5	896, 2980, 3515, 4270, 7125	55,000; 80,000; > 10,000; 80,000; 62,000	2.5; 10-12; 2; 10-12; 3
Vatnaöldur / Torfajökull	Landnám, Grákolla	1126, unknown	0.4, unknown	
Katla	SILK-UN, SILK-LN	2660, 3440	< 15,000 > 15,000	0.16 0.12

identification across the North Atlantic region. Tephra layers from the Eyjafjallajökull and Snæfellsjökull volcanoes were not sampled and analysed due to constraints on the project. The following section introduces the seven volcanic systems investigated during this thesis and their associated tephra layers. Where available, information regarding main axes of distribution, isopach thicknesses and distal distribution are presented graphically. Major element chemistry collected by previous workers is presented in the Appendix CD.

2.6.1 Torfajökull

The Torfajökull volcanic system is located at the intersection between the EVZ and the SISZ (Fig. 2.2) and is the largest silicic centre in Iceland, covering over 400 km^2 (Walker, 1966; Blake, 1984; McGarvie, 1984). The volcano itself is a caldera ring complex measuring 18 x 13 km and elongated in a WNW-ESE direction (McGarvie, 1984; Sæmundsson, 1988). The complex is dominated by hyaloclastite acid breccias and silicic dome and ridge-shaped lava formations (Gunnarson *et al*. 1998). In post-glacial times, the volcano has interacted with the Barðarbunga-Veiðivötn fissure system causing simultaneous eruptions of both systems.

Injection of hot basaltic material from the Barðarbunga-Veiðivötn system into the Torfajökull complex causes the eruption of pre-existing silicic magma stored in its magma chamber. The result is mixing of tholeiitic basaltic magma from Veiðivötn and alkali rhyolite from Torfajökull (McGarvie, 1984; Gunnarsson *et al*. 1998). The Torfajökull system is the source for the silicic component of the Landnám and Grákolla tephra layers aged 1079 BP and 1840 +/- 100 years BP respectively. Both tephra layers are introduced in the following sections.

Landnám tephra layer: The Landnám or Settlement tephra is named after its period of eruption which coincided with the settlement of Iceland. The Landnám tephra is dated to 870 AD or 1079 BP (Grönvold *et al*. 1995). The associated tephra layer shows a bimodal composition due to the interaction of the two systems as noted above. For the purpose of this thesis, the focus will be on the rhyolitic component. The estimated volume of the tephra layer is 0.4 km^3 DRE (Larsen, 1984). Micro-tephra particles of the Landnám tephra layer are identified distally within sedimentary successions across Greenland, Norway, the Faroe Islands and in marine cores (Fig. 2.7; Grönvold *et al*. 1995; Wastegård *et al*. 2001, 2003; Pilcher *et al*. 2005).

Grákolla tephra layer: The Grákolla tephra is named after its type locality: Grákolla hill near Tjörvafell and Frostastadavatn, north of the Torfajökull volcanic complex (Larsen, *pers comm*. Fig. 2.8). The tephra, also known as the Domadalshraun tephra, is the culminating explosive phase of the eruption of the same name (Jakobsson, 1979). The advancing path of a tholeiitic fissure towards Torfajökull is denoted by a cone row NW of Domadalshraun (Blake, 1984). Field studies have concluded that the tephra was erupted following the rupture of an obsidian plug or carapace, resulting in the explosive release of degassing magma residing within the underlying conduit (Blake, 1984). The Grákolla tephra is dated at 1800 +/- 100 years BP or 150 +/- 100 years AD (Larsen, 1984) and has an estimated volume of 0.05 km^3 or 0.01 km^3 dense rock equivalent (DRE; Blake, 1982). The unit has a maximum thickness of approximately 3 m (Blake, 1984; Larsen, 1984). The main axis of deposition for the Grákolla tephra layer was north-east (Fig. 2.8). The tephra layer is relatively small-scale

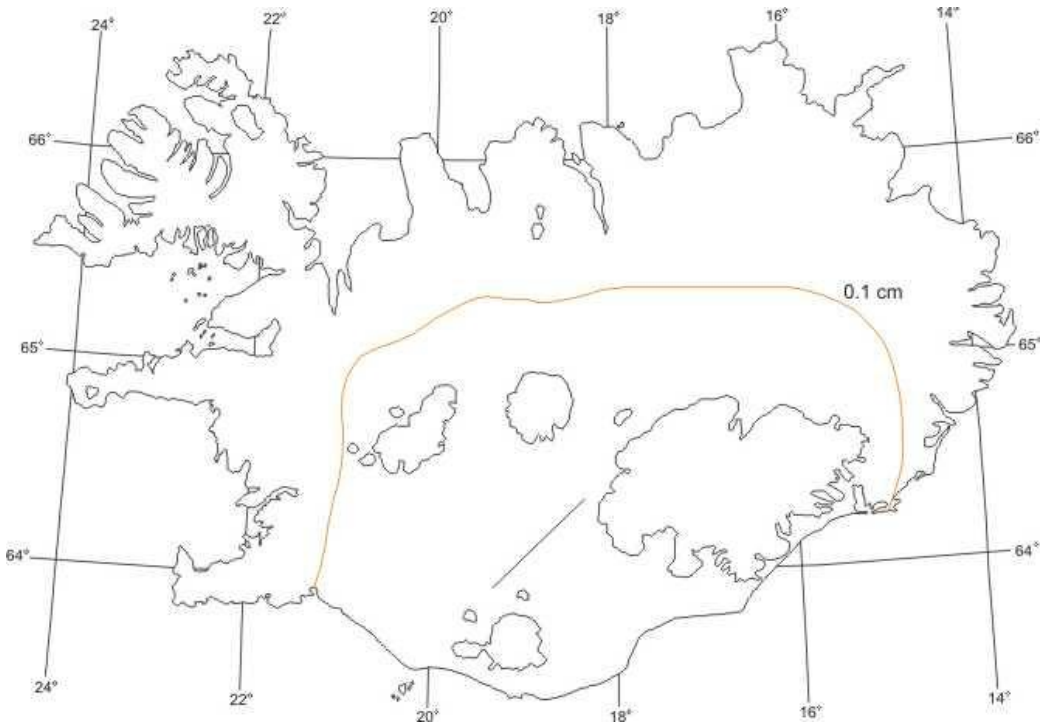

Figure 2.6: Isopach map representing the 0.1 cm thickness of the silicic component of the Landnám layer within Iceland. The map indicates a faintly north-east trend for maximum axis of deposition. Adapted from Larsen *et al*. 2002.

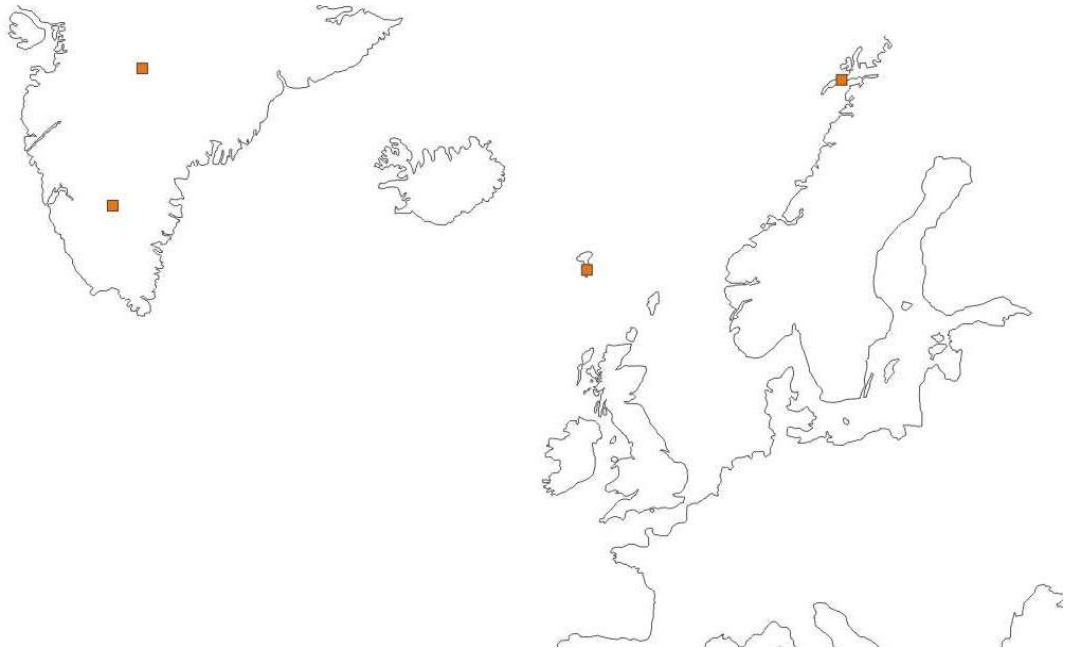

Figure 2.7: Known localities of the silicic component of the Landnám micro-tephra across the North Atlantic region sourced from terrestrial, marine, fluvial and glacial records (Grönvold *et al*. 1995; Wastegård *et al*. 2001, 2003; Pilcher *et al*. 2005).

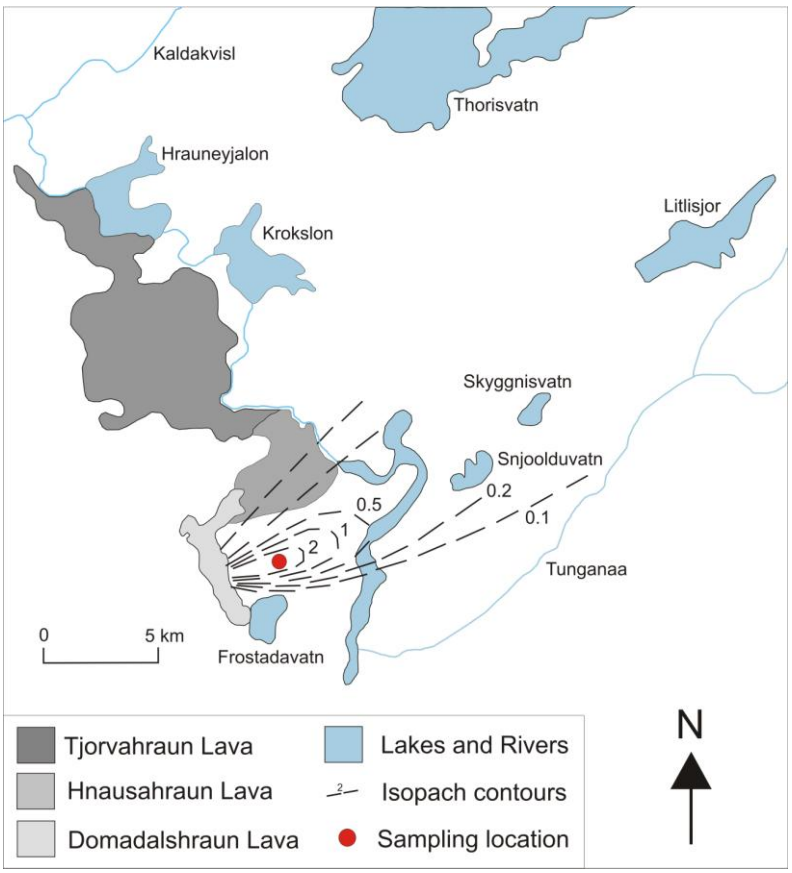

Figure 2.8: Local isopach map of the Grákolla tephra layer. The red circle in the south of the map represents the sampling location of the volcanic unit Grákolla on the hill bearing the same name. Numbers denote tephra thickness in metres. The main axis of deposition is recorded by the dominantly east-north-east orientation of the isopachs. Adapted from Larsen, 1984.

and is, as yet, not recorded outside of Iceland. However the layer shows potential for use in local tephrochronology studies in Iceland and has therefore been incorporated into this study.

2.6.2 Askja

Askja, also known as Dyngufjöll, is the central volcano to a 200 km long system within the NVZ (Fig. 2.2) and features three nestled calderas (Sigvaldason, 2002; Thordarson and Larsen, 2007). Country rock surrounding the Dyngufjöll complex is dominated by intercalated hyaloclastite and pillow lavas (Sigvaldasson, 1979). Among numerous basalt

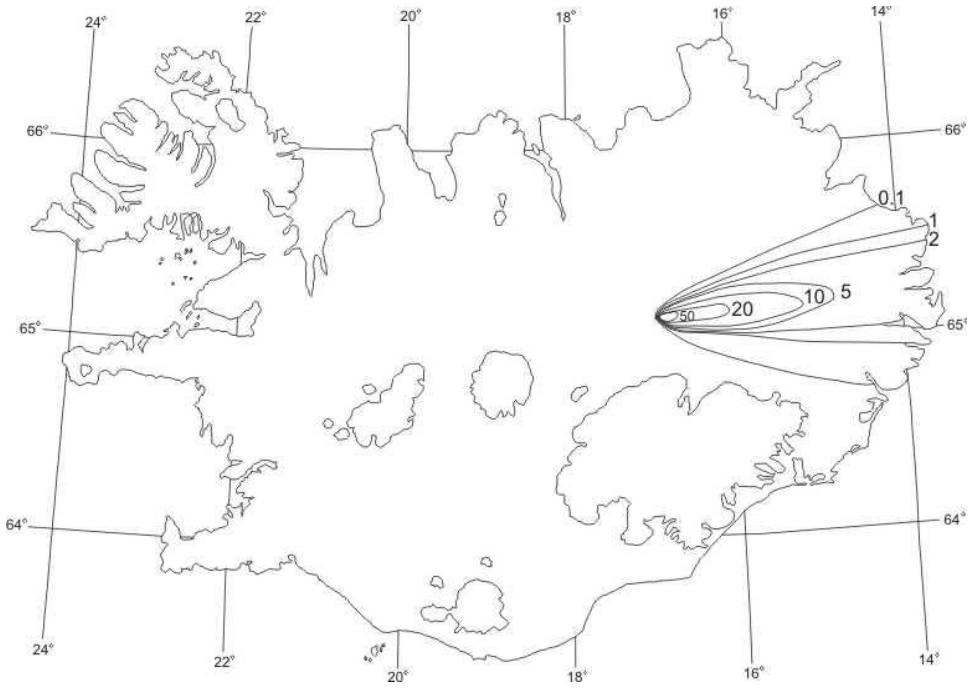

Figure 2.9: Isopach map representing the thickness of the A1875 layer within Iceland. The bold numbers represent tephra thickness in cm. Deposition of the tephra was dominantly eastwards as noted by the isopach pattern. Adapted from Carey *et al*. (2009).

Figure 2.10: Known localities of A1875 micro-tephra horizons across the North Atlantic region sourced from terrestrial, fluvial, marine and glacial records (Oldfield *et al*. 1997; Pilcher *et al*. 2005; Davies *et al*.2007).

eruptions, the Askja volcano is known to have produced three silicic explosive eruptions in postglacial times (Larsen and Eiríksson, 2008). The first event is thought to be a Plinian eruption that produced the Skolli tephra with an inferred age of 10 ka BP linked to the formation of the main Askja caldera, which covers an area of 45 km^2 with a diameter of 7 km (Sigvaldasson, 2002). Little is known about the second eruption; however it is inferred to have erupted c. 2 ka BP. The most recent event is the sub-Plinian/phreato-Plinian/Plinian eruption of the 28-29th March 1875 which resulted in the formation of the Öskjuvatn caldera which has a volume of 2.2 km^3 and a diameter of c. 5 km (Sigurdsson and Sparks, 1978; Sigvaldasson, 1979; Carey *et al*. 2009, 2010).

Askja 1875: The A1875 eruption is dated to 1875 AD or 125 BP by eye witness accounts. During its eruption, the main axis of deposition was east (Fig. 2.9). The associated tephra deposit is dominated by a rhyolitic composition. The volume of the tephra layer is estimated at 0.5 km^3 or 0.34 km^3 DRE (Carey *et al*. 2009). Micro-tephra particles of the A1875 tephra layer are identified distally within sedimentary successions across Norway, Sweden and Germany (Fig. 2.10; Oldfield *et al*. 1997; Pilcher *et al*. 2005; Davies *et al*. 2007). The A1875 tephra layer is also known as the GRAM-1 tephra layer in Germany (Van Den Bogaard and Schminke, 2002). The 2100 BP eruption of Askja is also known as the Stomyren tephra layer in Sweden (Borgmark, 2005), Glenn Garry in the UK (Dugmore *et al*. 1995) and as DOM-5, JAM-2 and GRAM-4 in Germany (Van Den Bogaard and Schminke, 2002).

2.6.3 Katla

The Katla volcanic system is located at the southern end of the EVZ (Fig. 2.2) and comprises a SW-NE trending 80 km-long fissure system and an ice-capped central volcano (Jakobsson, 1979; Thordarson and Larsen, 2007). The central volcano features a caldera with an area of 110 km^2 (Larsen, 2000). The volcano is superimposed onto Pleistocene lavas and hyaloclastite (Jóhannesson *et al*. 1990). Katla has erupted 21 times since the settlement of Iceland in 870 AD with dense rock equivalent (DRE) volumes for eruptions typically 0.02 – 1.5 km^3 (Larsen, 2000). The system is the source of the large scale rhyolitic Vedde eruption (10,300 years BP) identified in the North Atlantic Ash Zone 1 (Bond *et al*. 2001) and the large basaltic eruptions Eldgjá (934 AD) and Holmsá (680 ^{14}C years BP; Larsen *et al*. 2001). The Katla system is also the source for the sequence of intermediate Silk (**Sil**icic **K**atla) layers erupted between 1676 +/- 12 BP and 6800 BP.

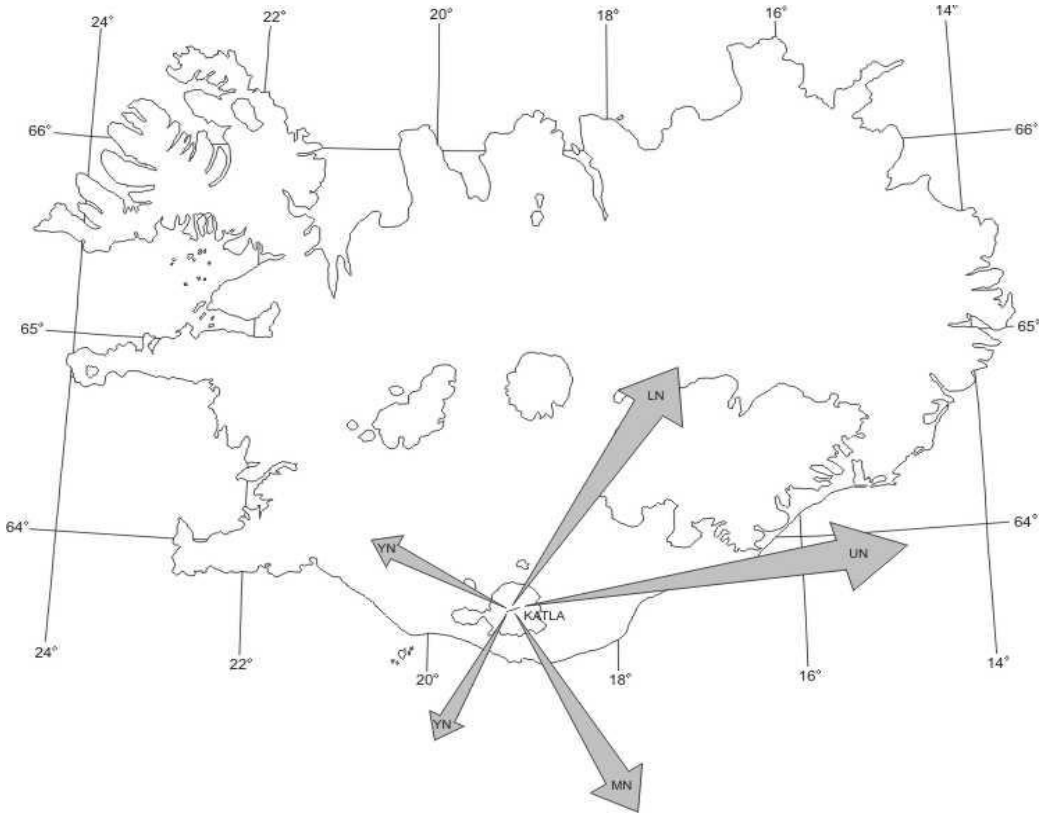

Figure 2.11: Main axis of thickness of the Silk needle tephra layers: upper needle layer, middle needle layer, younger needle layer and lower needle layer. The tephra layers show a range of depositional axes which may be manipulated during their identification. Adapted from Larsen and Eiriksson, 2008).

Silk UN and LN tephra layers: The Silk UN and LN tephra layers are dated to 2660 BP and 3440 BP respectively (Larsen *et al*. 2001). Neither tephra is identified outside Iceland and typically have only a local impact. The main axis of thickness for the UN tephra layer is east-north-east while the LN tephra layer is north-east (Fig. 2.11). The tephra layers show an intermediate composition and are characterised by a needle –like texture to their pumice clasts. The area of the Silk UN tephra layer within the 0.2 cm isopach is about 15,000 km^2 while the volume of the tephra layer is estimated at 0.27 km^3 or 0.16 km^3 DRE (Fig. 2.12; Larsen *et al*. 2001). The Silk LN tephra layer covers > 15,000 km^2 within the 0.1 cm isopach and has a volume of 0.2 km^3 or 0.12 km^3 DRE (Fig. 2.13; Larsen *et al*. 2001).

2.6.4 Öræfajökull

The Öræfajökull volcanic system is located at the southern margin of the Vatnajökull ice cap

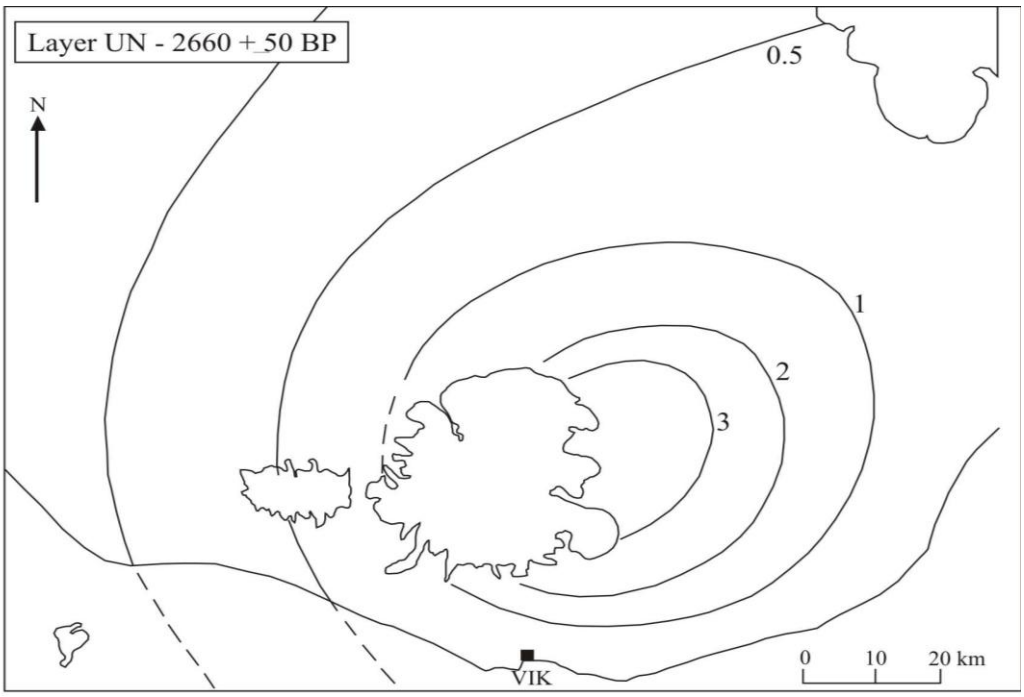

Figure 2.12: Isopach map of the thickness of the Silk UN layer at source, under the Mýrdalsjökull icecap in southern Iceland. Bold numbers represent tephra thickness in cm. Adapted from Larsen *et al*. (2001).

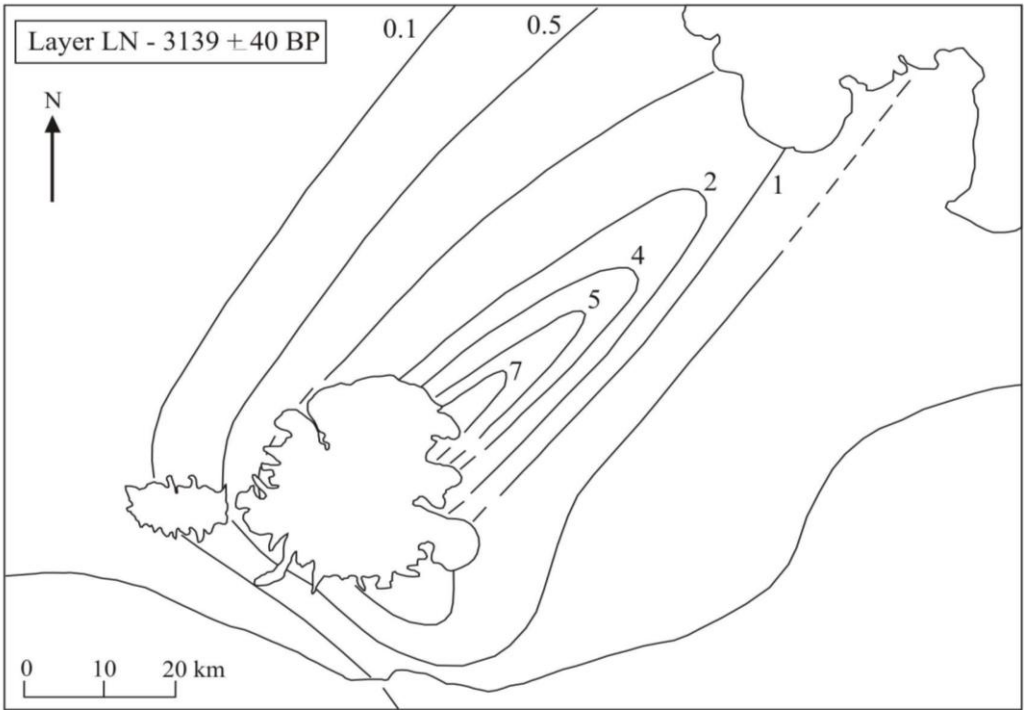

Figure 2.13: Isopach map of the thickness of the Silk LN at source, under the Mýrdalsjökull icecap in southern Iceland. Bold numbers represent tephra thickness in cm. Adapted from Larsen *et al*. (2001).

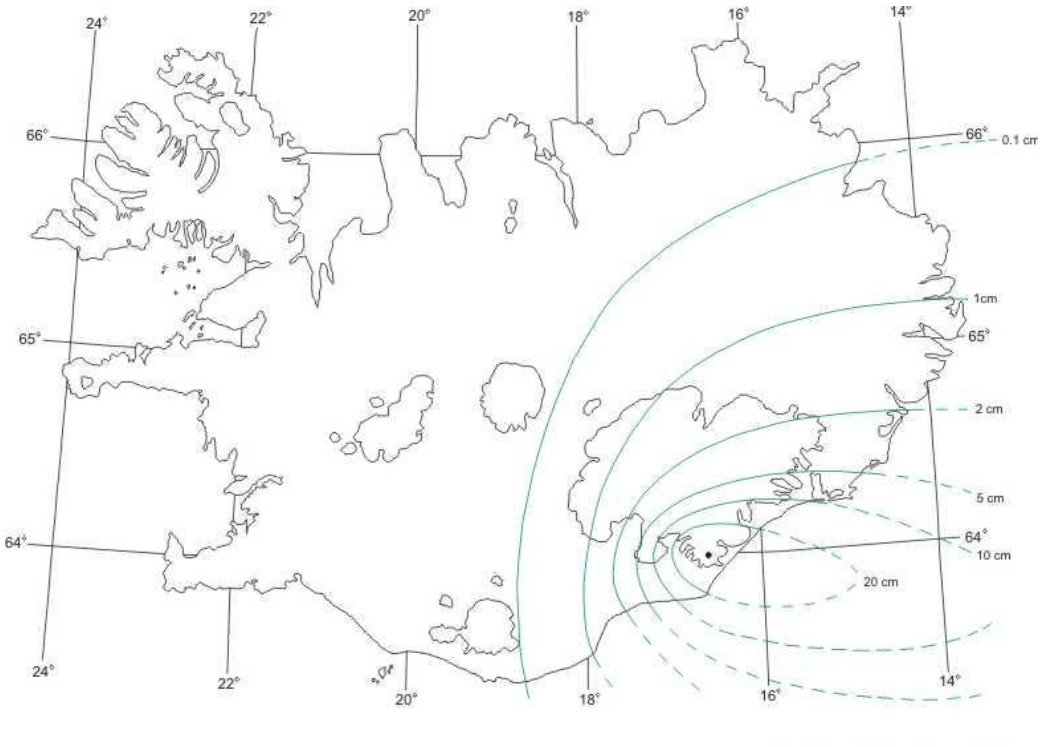

Figure 2.14: Isopach map of the thickness of the Ö1362 layer within Iceland. Bold numbers represent tephra thickness in cm. The main axis of deposition is highlighted as south-east by the pattern of the isopachs. Adapted from Selbekk and Trønnes (2007).

Figure 2.15: Known localities of Ö1362 micro-tephra horizons across the North Atlantic region, sourced by marine, fluvial, terrestrial and glacial records (Palais *et al*. 1991; Dugmore *et al*. 1995; Grönvold *et al*. 1995; Pilcher *et al*. 2005).

at the southern most point of the ÖVB in SE Iceland (Fig. 2.2; Prestvik, 1985; Stevenson *et al*. 2006; Sharma, 2008). Öræfajökull comprises a NE-SW trending 120 km-long fissure system and an ice-capped central volcano (Prestvik, 1985) including a summit caldera which covers 14 km^2 with a diameter of 5 km (Thorarinsson, 1958; Stevenson *et al*. 2006). The underlying basement comprises the glacially eroded roots of two Tertiary-aged extinct basaltic volcanoes located near Skaftafellsjökull and Breidarmerkurjökull (Prestvik, 1979, 1985). The Öræfi stratovolcano eruptive deposits are dominated by lavas and pyroclastic deposits ranging in composition from basalt through hawaiite, mugearite, benmorite, trachyte to rhyolite (Thorarinsson, 1958; Prestvik, 1985, 2001). There have been two notable eruptions during historical time: the 1362 Plinian rhyolitic eruption and the 1727 intermediate explosive eruption.

Öræfajökull 1362: Ö1362 eruption is dated to 1362 AD and 588 BP (Selbekk and Trønnes, 2007). During its eruption, the main axis of deposition was south-east (Fig. 2.15). The associated tephra deposit is dominated by a rhyolitic composition. The area within the 0.1 cm isopach (Fig. 2.14) is 30,000 km^2 and the volume of the tephra layer is 10 km^3. Micro-tephra particles of the Ö1362 deposit are identified distally within sedimentary sequences across Greenland, Norway and the UK (Fig. 2.15; Palais *et al*. 1991; Dugmore *et al*. 1995; Grönvold *et al*. 1995; Pilcher *et al*. 2005). The Ö1362 tephra layer is also known as the Loch Portain tephra in the UK (Dugmore *et al*. 1995).

2.6.5 Hekla

The Hekla volcanic system is located at the intersection between the propagating end of the Eastern Volcanic Zone and the South Iceland Seismic Zone (Fig. 2.2). Hekla is a ridge-shaped stratovolcano with a 5.5 km long active summit fissure, *Heklugjá* (Thorarinsson, 1967). The central volcano is built dominantly of basaltic andesite and rhyolite with a basement of sub-glacial Pleistocene basaltic hyaloclastite ridges (Sigvaldasson, 1974; Sigmarsson et al, 1992; Sverrisdóttir, 2007). The volcano has erupted at least 30 times since 7,000 years BP with erupted tephra of intermediate composition and volumes exceeding 12 km^3 (e.g. Larsen *et al*. 1999). Hekla eruptions begin with an explosive Plinian or sub-Plinian phase and most end with effusive eruption of lava (Thordarson and Larsen, 2007). Typically, the larger eruptions are rhyolitic while the smaller eruptions are of intermediate composition (e.g. Sigmarsson, 1992; Larsen et al. 1999; Sverrisdóttir, 2007). Hekla is the source of five large-scale rhyolitic eruptions H1104, H3, HSelsund, H4 and H5.

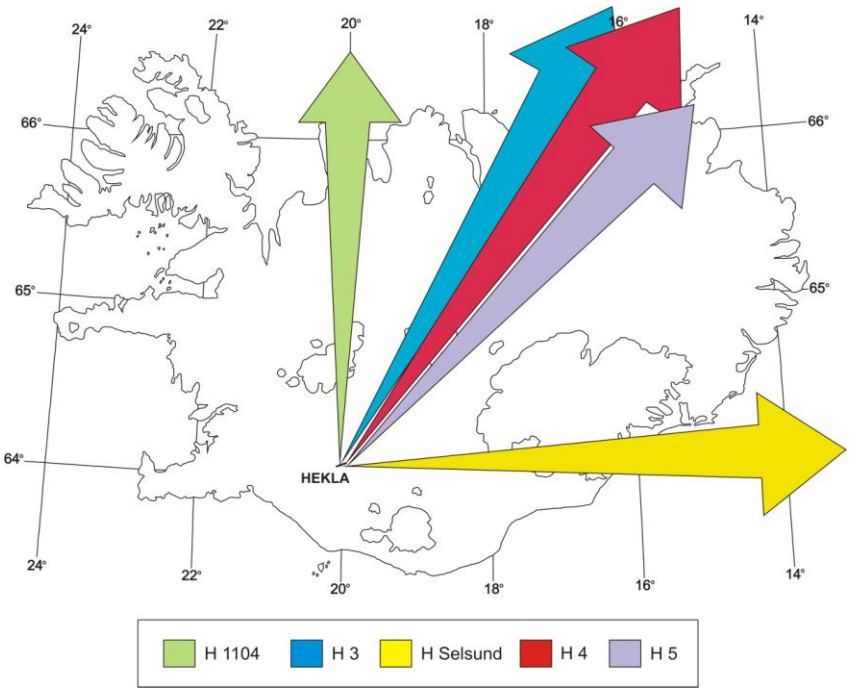

Figure 2.16: The assumed main axes of deposition of the five main Hekla eruptions: H1104, H3, HSelsund, H4 and H5. Adapted from Larsen and Thorarinsson (1977).

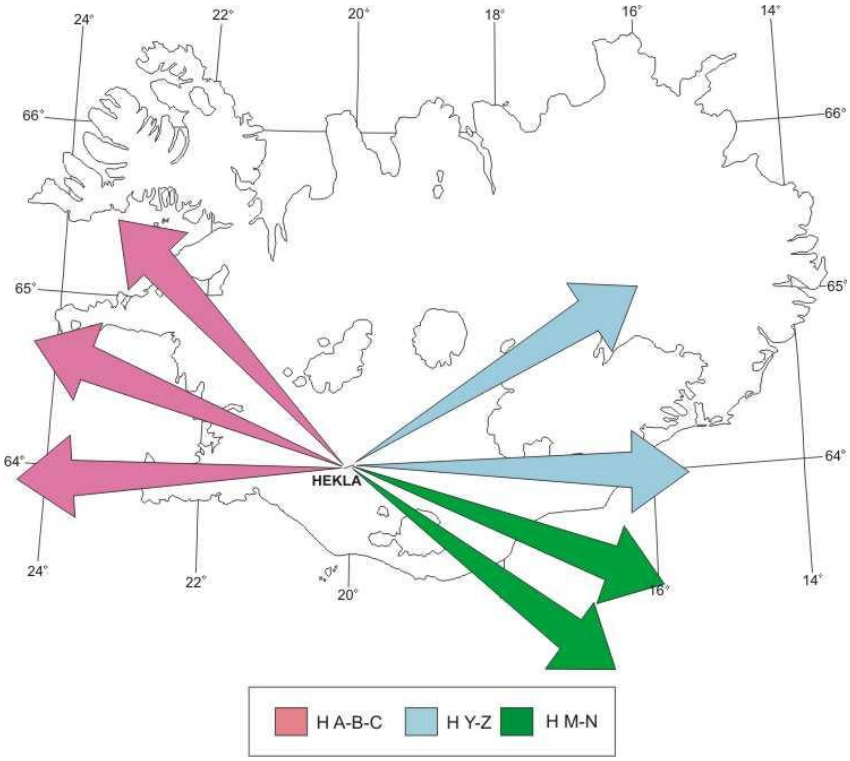

Figure 2.17: The assumed main axes of deposition for the seven intermediate Hekla eruptions: HA, HB, HC, HM, HN, HY and HZ. Larsen and Eiríksson (2008).

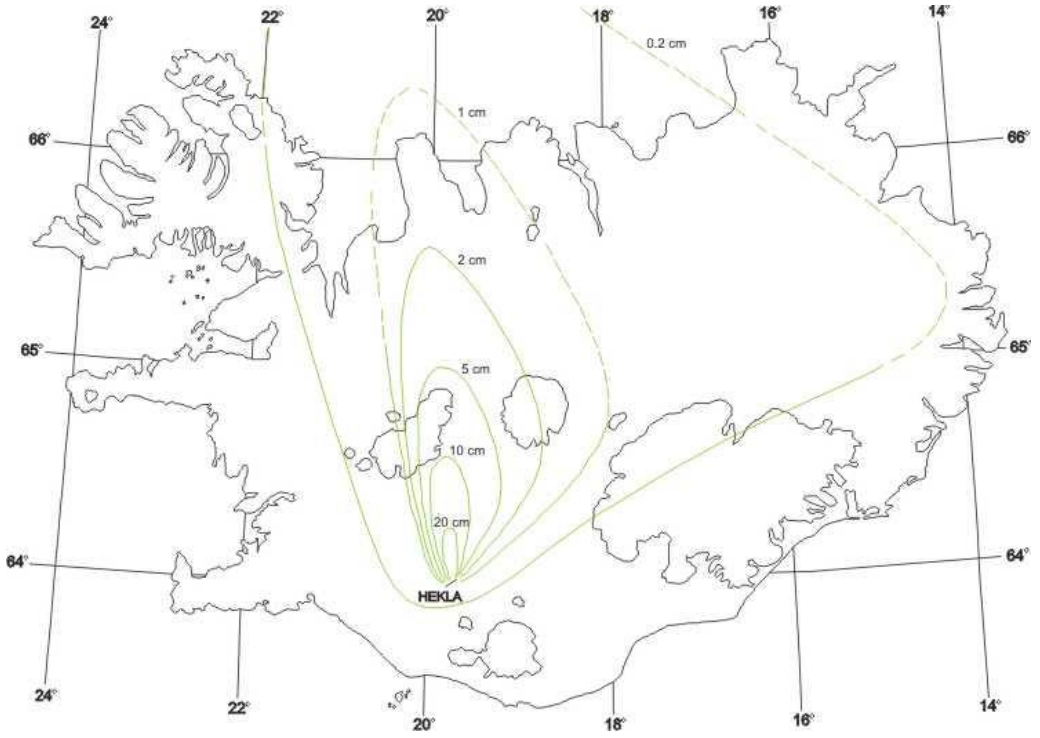

Figure 2.18: Isopach map of the thickness of the H1104 tephra layer in Iceland. Bold numbers represent tephra thickness in cm. Isopach patterns suggest that the main axis of deposition was to the north of the volcanic system. Adapted from Larsen and Thorarinsson (1977).

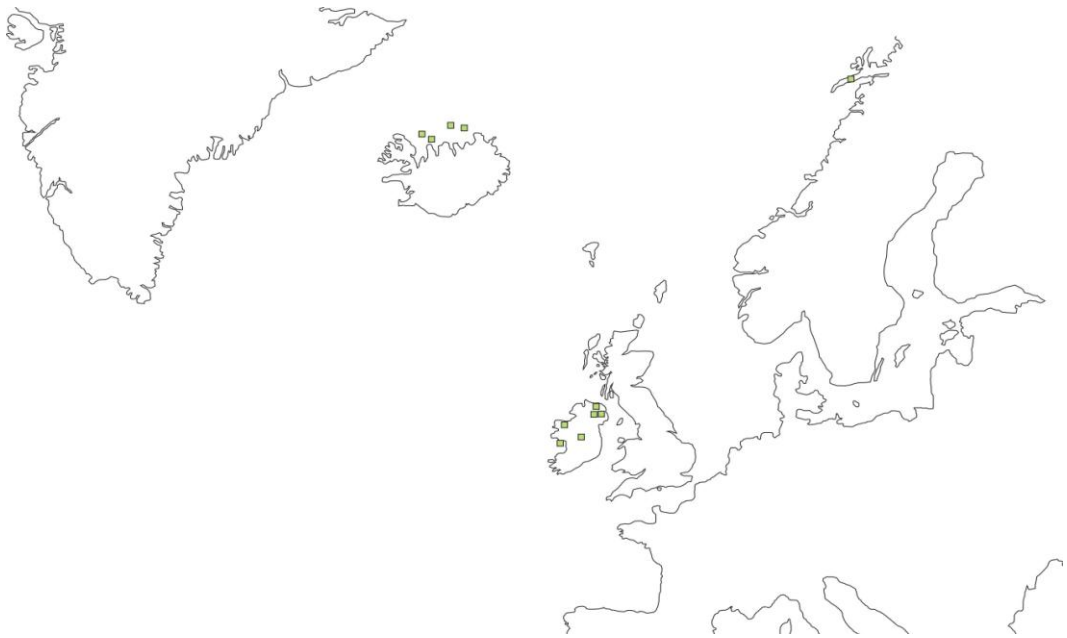

Figure 2.19: Known localities of H1104 micro-tephra horizons across the North Atlantic region, sourced from terrestrial, fluvial, marine and glacial records (Pilcher *et al*. 1995, 1996, 2005; Eiríksson *et al*. 2000, 2004; Larsen *et al*. 2002; Chambers *et al*. 2004; Kristiansdóttir *et al*. 2007).

Hekla 1104: The Hekla 1104 or H1 deposit is the tephra layer from the only rhyolitic eruption at the Hekla volcano during historic times occurring in 1104 A.D (896 BP). During its eruption, the main axis of deposition was due north (Fig. 2.16). The on land area of the deposit within the 0.1 cm isopach (Fig. 2.18) is c. 55 km^2 with volume estimates of c. 2.5 km^3 of tephra or 0.5 km^3 when calculated as dense rock equivalent or DRE. The H1104 tephra layer is also found in terrestrial sedimentary sequences in Ireland and Norway (Fig. 2.19; Pilcher *et al*. 1995, 1996, 2005; Chambers *et al*. 2004), in marine cores to the North of Iceland (Eiríksson *et al*. 2000, 2004; Larsen *et al*. 2002; Kristjánsdóttir *et al*. 2007) and in the Greenland ice cores (Vinther *et al*. 2006). The tephra layer is also known as the Mellstabromossen tephra in Sweden (Pilcher *et al*. 2005) and MOR-T3 tephra in Ireland (Chambers *et al*. 2004).

Hekla 3: the H3 eruption has been dated to 2980 years BP (Dugmore *et al*. 1995). During its eruption, the main axis of deposition was north-north-east (Fig. 2.16). The associated tephra deposit is the largest known tephra produced by the Hekla volcano and is dominantly rhyolitic in composition. The area within the 0.1 cm isopach (Fig. 2.20) is 80,000 km^2 and the volume of the tephra is estimated at 10-12 km^3 or 2.2 km^3 DRE (Larsen and Thorarinsson, 1977). Micro-tephra particles of the H3 deposit are identified distally within sedimentary sequences across Norway, Sweden and Germany (Fig. 2.21; Boygle *et al*. 1998, 2004; Van Den Bogaard *et al*. 2002; Zillén *et al*. 2002; Bergman *et al*. 2004 Wastegård, 2005) and within marine sediment cores north of Iceland (Eiríksson *et al*. 2000, 2004; Larsen *et al*. 2002; Kristjánsdóttir *et al*. 2007). The H3 tephra layer is also known as the DOM-7 tephra and JAM-4 tephra in Germany (Van Ven Bogaard and Schminke, 2002).

Hekla Selsund*:* Previously named H2, the Hekla Selsund eruption was originally considered to have occurred after the H3 eruption (Thorarinsson, 1951). Extensive field studies however have shown that the eruption took place prior to H3 and following the H4 eruption and is confirmed by radio carbon dating the deposit to 3515 BP +/- 55 years or 3515 years BP (Larsen and Thorarinsson, 1977; Dugmore *et al*. 1995; Boygle, 1998; Larsen *et al*. 2001). During its eruption, the main axis of deposition was due east (Fig. 2.16). The area on land within the 0.1 cm isopach is > 10,000 km^2 and the estimated volume is c. 2 km^3 or 0.1 – 1.5 km^3 DRE (Larsen and Thorarinsson, 1977; Sverrisdóttir, 2007; Larsen and Eiríksson, 2008), however there are no published isopach maps. During the Hekla Selsund eruption the majority of the tephra produced was supposedly transported via water saturated debris flow and not dominated by Plinian-style ash plumes as with the other major eruptions (Sverrisdóttir *et al*. 2006). Micro tephra horizons of the Hekla Selsund tephra layer have

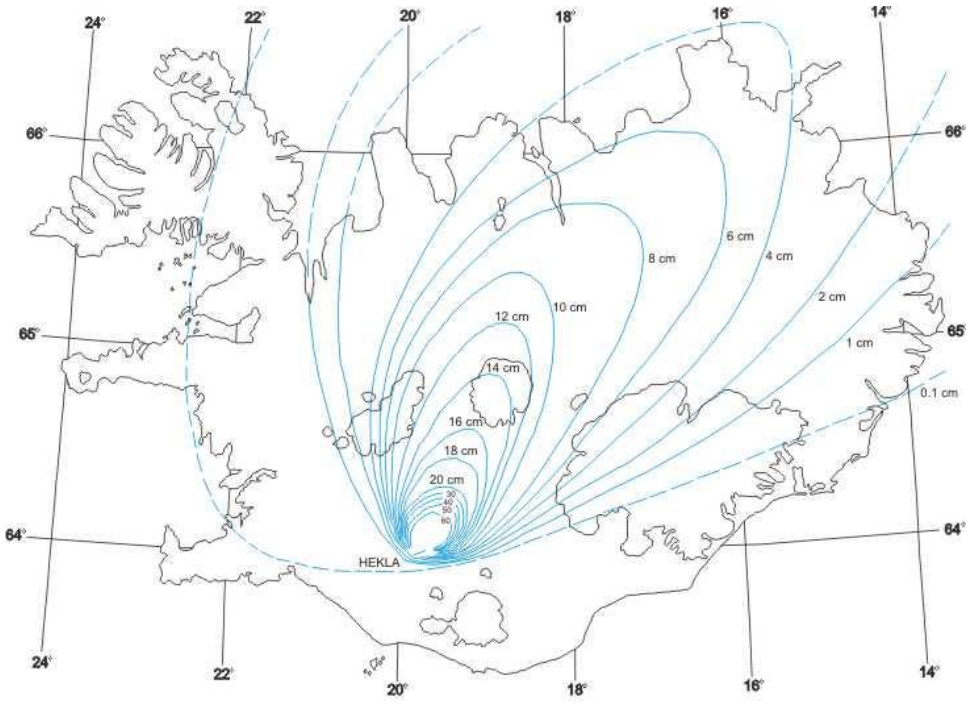

Figure 2.20: Isopach map of the thickness of the H3 tephra layer within Iceland. Bold numbers represent tephra thickness in cm. The main axis of deposition for the H3 tephra was north-north-east as indicated by the isopach pattern. Adapted from Larsen and Thorarinsson (1977).

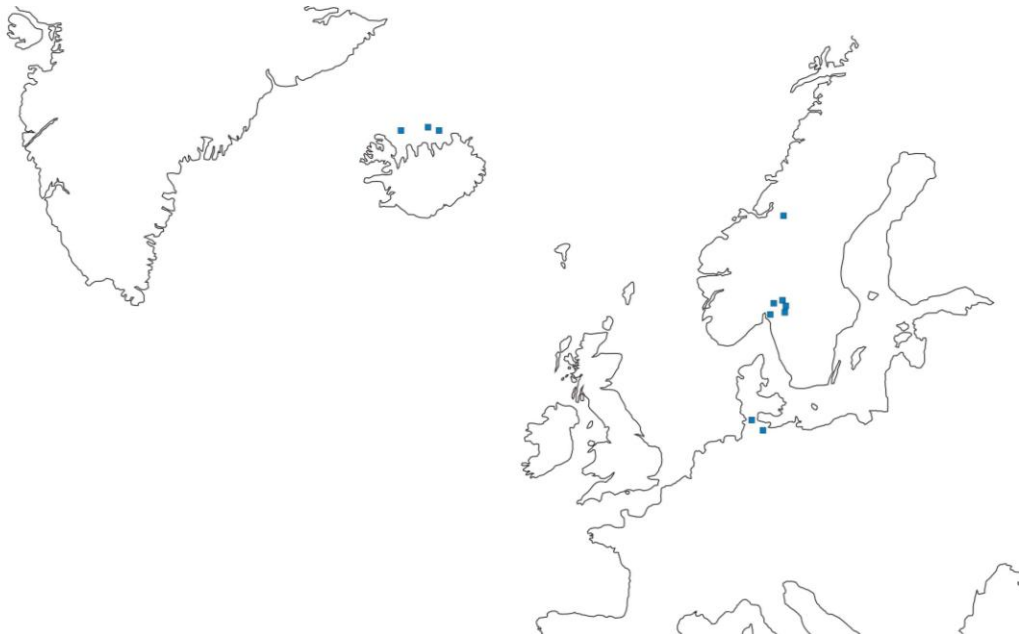

Figure 2.21: Known localities of H3 micro-tephra horizons across the North Atlantic region, sourced from glacial, marine, fluvial and terrestrial records (Boygle *et al*. 1998, 2004; Eiriksson *et al*. 2000, 2004; Larsen *et al*. 2002; Van Den Bogaard, 2002; Van Den Bogaard and Schminke, 2002; Zillén *et al*. 2002; Bergman *et al*. 2004; Wastegård, 2005; Kristjansdottir *et al*. 2007).

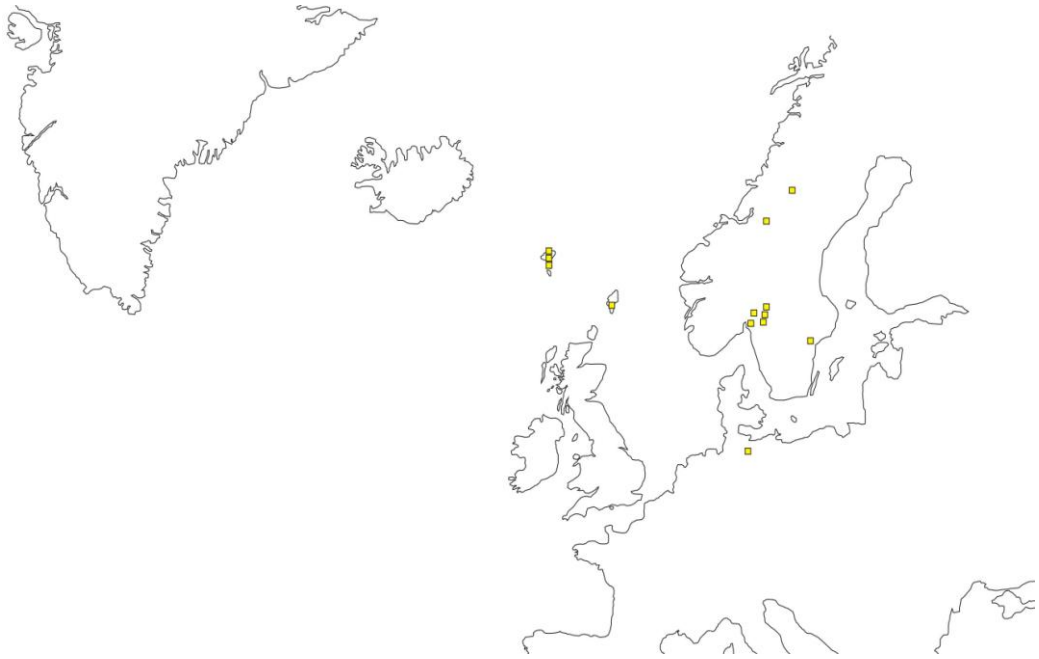

Figure 2.22: Known localities of HSelsund micro-tephra horizons of the HSelsund eruption across the North Atlantic region, sourced using marine, fluvial, glacial and terrestrial records (Boygle *et al*. 1998, 2004; Dugmore *et al*. 1995; Dugmore and Newton, 1998; Van Den Bogaard and Schminke, 2002; Zillén *et al*. 2002; Bergman *et al*. 2004; Wastegård, 2005; Wastegård *et al*. 2008).

been identified in terrestrial sedimentary sequences across Germany, Faeroe Islands, Shetland Islands, Norway and Sweden (Fig. 2.22; Dugmore *et al*. 1995; Boygle *et al*. 1998, 2004; Dugmore and Newton, 1998; Van Den Bogaard and Schminke, 2002; Zillén *et al*. 2002; Bergman, *et al*. 2004; Wastegård, 2005; Wastegård *et al*. 2008). The Hekla Selsund tephra layer is also known as the Kebister tephra in Shetland and Sweden and the Faroe Islands (Dugmore and Newton, 1998) and DOM-8 tephra in Germany (Van Den Bogaard and Schminke, 2002).

Hekla 4: The H4 eruption is dated to 4174 – 4202 years BP (Larsen and Thorarinsson, 1977; Larsen *et al*. 2001), confirmed by radio carbon dating providing an age of 3826 +/- 12 years (Dugmore *et al*. 1995). During its eruption, the main axis of deposition was north-east (Fig. 2.18). The area covered on land by the H4 deposit within the 0.1 cm isopach (Fig. 2.23 is estimated as c. 78,000 km^2 and volume estimates for the tephra indicate that c. 10 km^3 of pyroclastic material or 1.8 km^3 DRE were erupted (Larsen and Thorarinsson, 1977; Larsen and Eiríksson, 2008). The H4 tephra is the most widespread of the Hekla tephras, with micro tephra horizons identified within terrestrial sedimentary sequences across Ireland, UK,

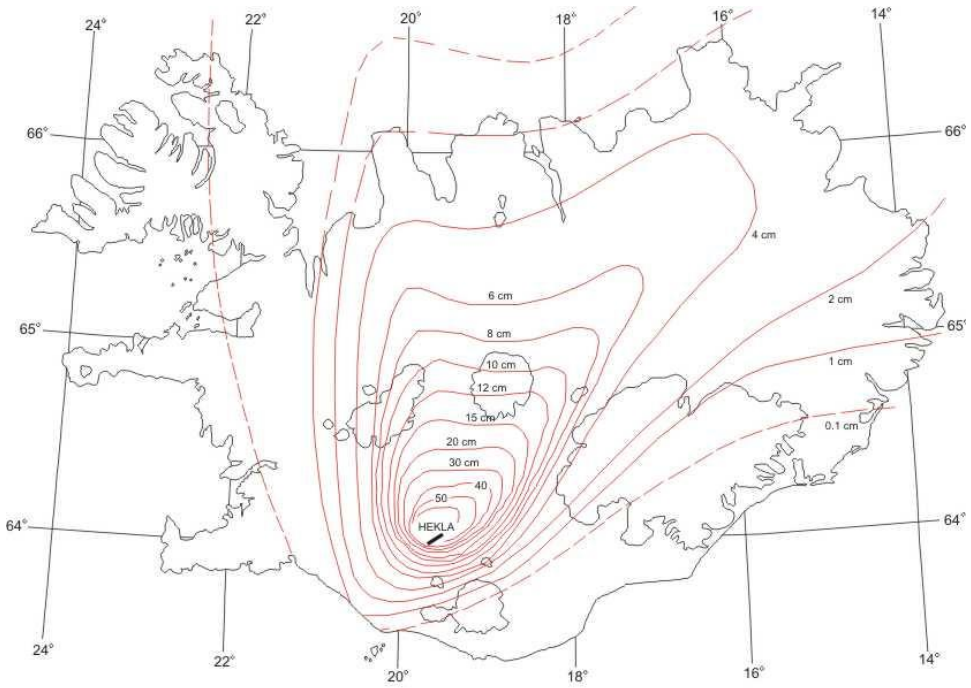

Figure 2.23: Isopach map of the thickness of the H4 tephra layer within Iceland. Bold numbers represent tephra thickness in cm. Isopach patterns suggest a dominant depositional axis towards the north-east, however a pattern also suggests deposition directly northwards. Adapted from Larsen and Thorarinsson (1977).

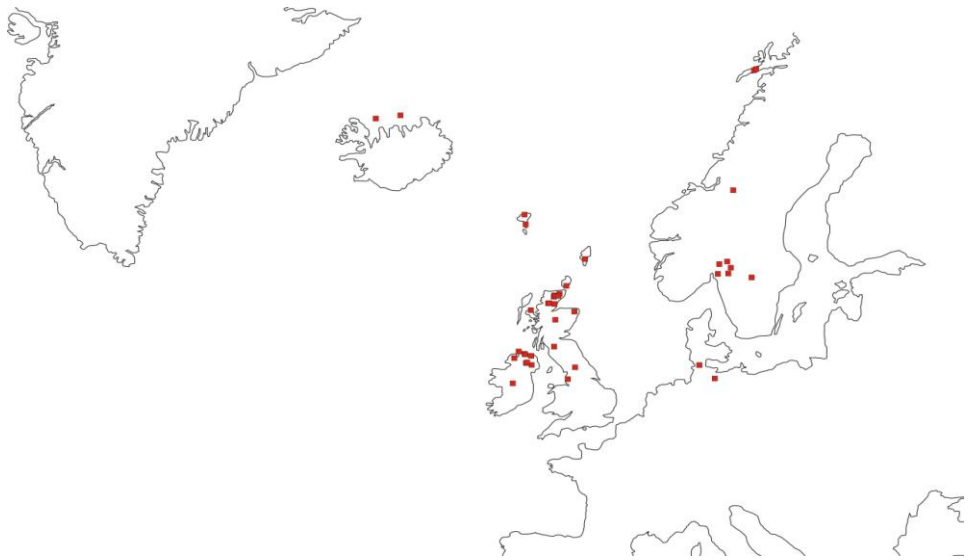

Figure 2.24: Known localities of H4 micro-tephra horizons across the North Atlantic region, sourced from marine, fluvial, terrestrial and glacial records (Blackford *et al*. 1992; Hall *et al*. 1994; Boygle *et al*. 1998, 2004; Charman *et al*. 1995; Dugmore *et al*. 1995, 1989; Pilcher *et al*. 1995, 1996, 2005; Pilcher and Hall, 1996; Caseldine *et al*. 1998; Dugmore and Newton, 1998; Eiríksson *et al*. 2000, 2004; Wastegård *et al*. 2001; Van Den Bogaard and Schminke, 2002; Bergman *et al*. 2004; Langdon and Barber, 2004; Wastegård, 2005; Kristiansdóttir *et al*. 2007).

Shetland, Germany, Sweden, Norway and the Faeroe Islands (Fig. 2.24; Blackfoot *et al*. 1992; Hall *et al*. 1994b; Charman *et al*. 1995; Dugmore *et al*. 1992, 1995, 1998; Pilcher *et al*. 1995, 1996, 2005; Pilcher and Hall, 1996; Boygle *et al*. 1998, 2004; Caseldine *et al*. 1998; Dugmore and Newton, 1998; Wastegård *et al*. 2001; Van Den Bogaard and Schminke, 2002; Zillén *et al*. 2002; Bergman *et al*. 2004; Langdon and Barber, 2004; Wastegård, 2005) as well as in marine sediment cores to the north of Iceland (Eiríksson *et al*. 2000, 2004; Larsen *et al*. 2002; Kristjánsdóttir *et al*. 2007). The H4 tephra is also known as the DOM-9 tephra and the JAM-5 tephra in Germany (Van Den Bogaard and Schminke, 2002).

Hekla 5: The Hekla 5 tephra layer is dated to 7125 years BP and is considered to be the first rhyolitic eruption at the Hekla central volcano during the Holocene (Larsen and Thorarinsson, 1977; Larsen and Eiríksson, 2008). During its eruption, the main axis of deposition was north-east (Fig. 2.18). On land the H5 tephra layer covers 62,000 km^2 within the 0.1 cm isopach (Fig. 2.25) and has an estimated volume of 3.0 km^3 or 0.3 km^3 DRE (Larsen and Thorarinsson, 1977). Micro tephra horizons of the H5 eruption are identified distally in terrestrial sedimentary sequences across Norway, Germany and Ireland (Fig. 2.26; Chambers *et al*. 2004; Pilcher *et al*. 2005; Van Den Bogaard and Schminke, 2002) and in marine sediment cores sourced north of Iceland (Eiríksson *et al*. 2004). The H5 tephra is also known as the MOR-T12 tephra in Ireland (Chambers *et al*. 2004), JAM-7 tephra and the GRAM-8 tephra in Germany (Van Den Bogaard and Schminke, 2002).

Hekla A-B-C-M-N-X-Y-Z: Following the H3 tephra layer is a sequence of tephra layers from the Hekla system erupted between 2900 – 1800 years BP. The tephra layers are identified in the field in three distinct groupings: The HA(youngest)-HB-HC tephra layers are found north-west of Hekla, the HM(youngest)-HN tephra layers are identified south-east of the volcano and the HX(youngest)-HY-HZ tephra layers are recognised to the west (Fig. 2.17). On-land area calculations are unpublished at present for all but the HA tephra layer which is estimated at 9,080 km^2 (Bryndisdóttir *et al*. 2002b). Conservative volume calculations are available for the HA, HX, HY and HZ tephra layers: 0.33 km^3, 0.27 km^3, 0.36 km^3 and 0.14 km^3 DRE respectively (Larsen *et al*. 1992; Bryndisdóttir *et al*. 2002b). Volumes for the HM and HN tephra layers are 0.28 km^3 and 0.4 km^3 DRE respectively; however these are based on estimations calculated within the 0.5 cm isopach and may therefore under-represent the actual volume (Larsen *et al*. 2002). At present, the smaller Hekla tephra layers are not identified in distal sedimentary successions, however their

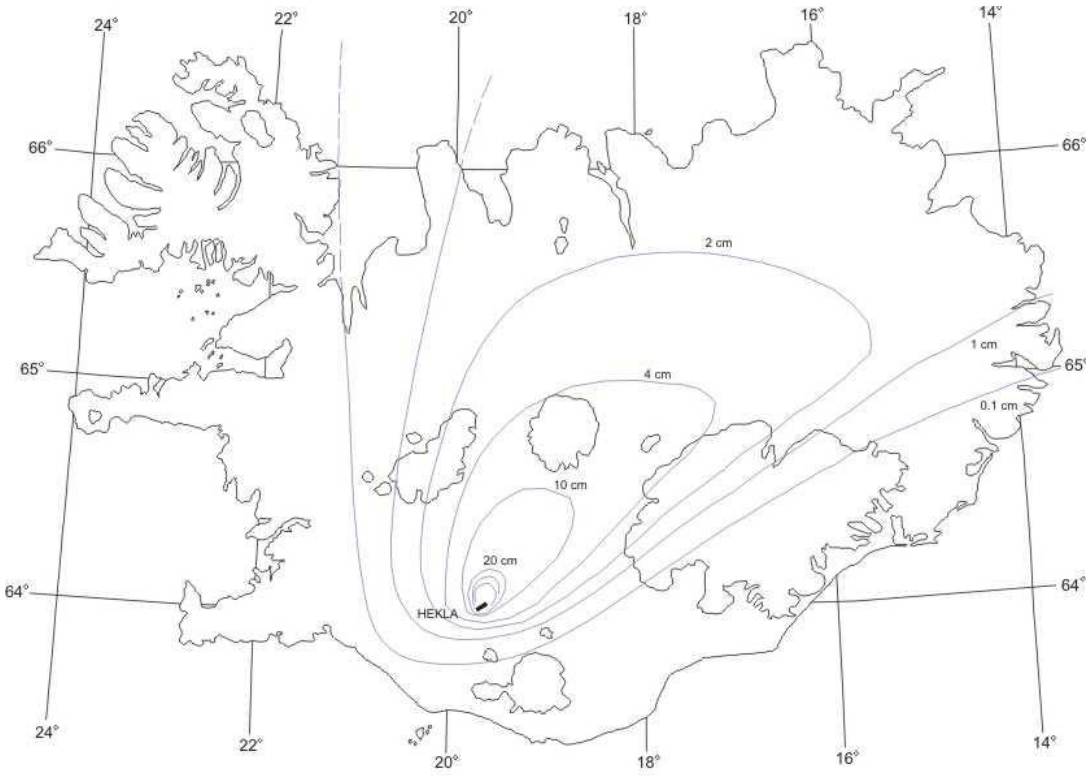

Figure 2.25: Isopach map of the thickness of the H5 tephra layer within Iceland. Bold numbers represent tephra thickness in cm. Isopach patterns suggest a main axis of deposition towards the north-east for the H5 eruption. Adapted from Larsen and Thorarinsson (1977).

Figure 2.26: Known localities of H5 micro-tephra horizons across the North Atlantic region, sourced from terrestrial, glacial, marine and fluvial records (Van Den Bogaard and Schminke, 2002; Chambers *et al*. 2004; Eiriksson *et al*. 2004; Pilcher *et al*. 2005).

usefulness as local Icelandic tephra marker horizons is increasing due to their preservation in lacustrine environments (Jagan, 2010).

2.7 Origin and formation of intermediate and silicic magmas in Iceland

The main focus of this thesis is silicic Icelandic Holocene tephra layers which are often identified in distal tephrochronological sites. Seven volcanic systems have produced silicic material during the Holocene period – Hekla, Askja, Katla, Eyjafjallajökull, Öræfajökull, Snæfellsjökull and Torfajökull (Fig. 2.2) – and have erupted at least 29 times. Icelandic silicic eruptions, both effusive and explosive, account for $\geq$ 70 km^3 which seem insignificant when compared to Icelandic mafic volumes ($\geq$ 500 km^3). The volumes are however unusually high considering the island's geological setting on an interacting hotspot and mid-ocean ridge setting with no external continental crustal rocks (Sæmundsson, 1979).

The formation of silicic rocks in Iceland is a highly debated topic. Understanding their formation may provide an insight into the formation of continental crust during Earth's early history (Gunnarson *et al*. 1998). Three main theories have been postulated to explain the origin of Iceland's silicic magma:

1. Origin by fractional crystallisation of primary basaltic magmas (e.g. Carmichael, 1964; Thy, 1990; Macdonald, 1991).
2. Formation through partial melting of hydrated crustal rocks (O'Nions and Grönvold, 1973; Sigvaldasson, 1974; Oskarsson, 1982; Thy *et al*. 1990; Sigmarsson *et al*. 1991; Gunnarson, 1998).
3. Generation as a result of injection of primary magma initiating partial melting of crustal material (Sigurdsson and Sparks, 1981; Macdonald, 1987; Nicholson, 1991, Sigmarsson *et al*. 1992);

Recent studies have concluded that each of the proposed mechanisms may play a part in the generation of silicic magma in Iceland. Martin and Sigmarsson (2007, 2010) have established that the most important factor is the location of a volcano with regard to the active rift zones and the Icelandic mantle plume (Fig. 2.1 and 2.2). Volcanic systems in the Eastern Volcanic Zone are influenced by the higher geothermal gradient associated with the mantle plume and

their silicic magmas are dominated by partial melting processes. Volcanic systems in the Western Volcanic Zone and the Northern Volcanic Zone are located further away from the plume and are not influenced by increased geothermal gradients. The silicic magmas in these systems develop in colder tectonic settings and are influenced more by fractional crystallisation processes than their eastern volcanic counterparts.

2.8 Summary

This chapter has provided information regarding the geographical and geological setting of Iceland and the volcanological processes occurring within the active rifting zones. The main volcanic systems have been presented with particular focus onto those known to have erupted silicic magma during the Holocene period. A brief overview of the generation of silicic magma has also been provided. The following chapter will introduce the terminology of explosive products erupted from Icelandic systems and the methods used to identify such material at proximal to distal localities. The chapter will also establish the concept of tephrochronology including a brief account of Icelandic tephrochronology with reference to some persistent problems associated with the methodology across the North Atlantic Region.

Chapter 3:

Tephra and Tephrochronology

3.1 Introduction

This chapter aims to introduce the concept of tephrochronology and its application to interdisciplinary Quaternary studies with particular reference to tephra stratigraphy in Iceland. Firstly, the chapter will introduce basic volcanology terminology before detailing how volcanic products are identified in proximal and distal sedimentary records. Secondly, the chapter will explain how volcanic products are used as a tool for dating sedimentary successions within the study of tephrochronology. Finally, the chapter will present an overview of North Atlantic tephrochronology with a brief discussion of some persistent problems arising from the technique.

3.2 What is tephra?

The term "tephra" is derived from the Greek word "ΤΕΦΡΑ" meaning "ash". The term was developed in 1944 by Thorarinsson, as a collective term for all solid fragmented material ejected from a volcano covering a range of chemical compositions. The term is now used to describe all forms of pyroclastic air fall deposits e.g. bombs, scoria, air-fall ash and pumice (Thorarinsson, 1974; Holmes *et al*. 1999). Tephras cover a wide range of sizes, including ash (< 2.0 mm), lapilli (2.0 – 64.0 mm) and blocks + bombs (> 64 mm) (Fig. 3.1; Francis and Oppenheimer, 2004).

The following section describes how tephra layers are identified in the field focusing on physical characteristics, sequence stratigraphy and geochemistry. Tephra layers are discussed under the umbrella terms of proximal and far-distal sampling locations. Definitions of distances from source are dependent on a number of features including location and eruption magnitude. For example, a Strombolian eruption will deposit tephra within a few km of the main vent, whereas a Plinian eruption will transport ash many hundreds of km from source. As this project is focusing mainly on the larger silicic

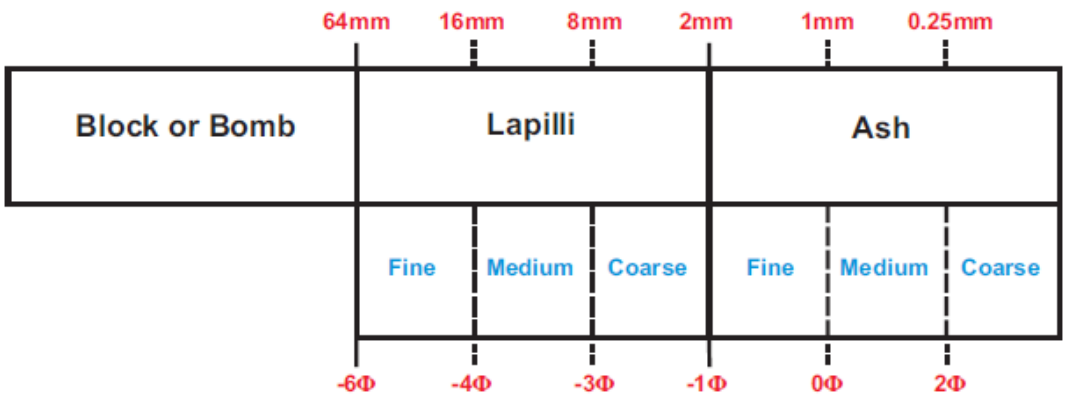

Figure 3.1: size terminology for volcanic ejecta. Note that the "fine" and "coarse" size fractions are frequently further sub-divided to denote "very coarse" and "very fine". Adapted from Wentworth (1922) and Fisher (1961).

eruptions, we will define proximal regions as those within 20 km of the source vent while far-distal locations are considered those representing locations outside of Iceland across the North Atlantic region. Medial and distal samples are not considered for simplicity. At far-distal localities, where tephra layers are typically preserved as micro-tephra horizons, grain sizes are so small as to prohibit identification with the naked eye. Micro-tephra recovery methods are described in section 3.2.2.

3.2.1 Proximal tephra

The identity of proximal tephra layers can be established by studying their physical, stratigraphical and chemical characteristics. The following section will provide a brief overview of these characteristics and how they are applied to ensure correct identification of individual tephra layers.

Physical characteristics: Tephra layers have distinct physical characteristics which vary depending on the mechanisms of magma generation, fragmenting processes, eruption intensity and depositional processes. These physical characteristics include tephra colour, unit thickness, grain size variation, componentry, clast morphology and phenocryst content (e.g. Fisher and Schminke, 1984; Cas and Wright, 1987; Óladóttir *et al*. 2005). Table 3.1 provides a summary of these characteristics. It is possible to use variations in these physical characteristics to determine the provenance of individual tephra layers. Individual

Table 3.1: Physical characteristics used to identify individual tephra horizons in the field at proximal sampling locations (adapted from Óladóttir *et al*. 2005).

Characteristics	**Description**
Colour	The colour of tephra is representative of its composition. Felsic layers are light coloured, with increasing SiO_2 content represented by a whiter appearance. Basaltic tephra are typically black – brown and intermediate compositions are brown – greyish brown.
Grain Size	Grain size range and sorting of each layer provides qualitative information on eruption style and intensity as well as depositional processes.
Unit Thickness	Thickness values of individual layers represent eruption intensities, original magma volumes and distance of the section from the source volcano.
Contacts	Tephra contacts should be sharp and non-erosional (with the exception of PDCs) and therefore a deviation from this may indicate post-depositional reworking.
Componentry	The relative abundance of juvenile material, phenocrysts and lithic wall fragments are used as an indicator of eruption type and style.
Depositional Structures	Transportation mechanisms can be deduced by studying the internal bedding, size grading, bed-forms and fabric, as well as identifying re-worked deposits.
Other	Material within tephra deposits can provide an insight into the environmental impact of the eruption i.e. The presence of archaeological findings and tree trunks.

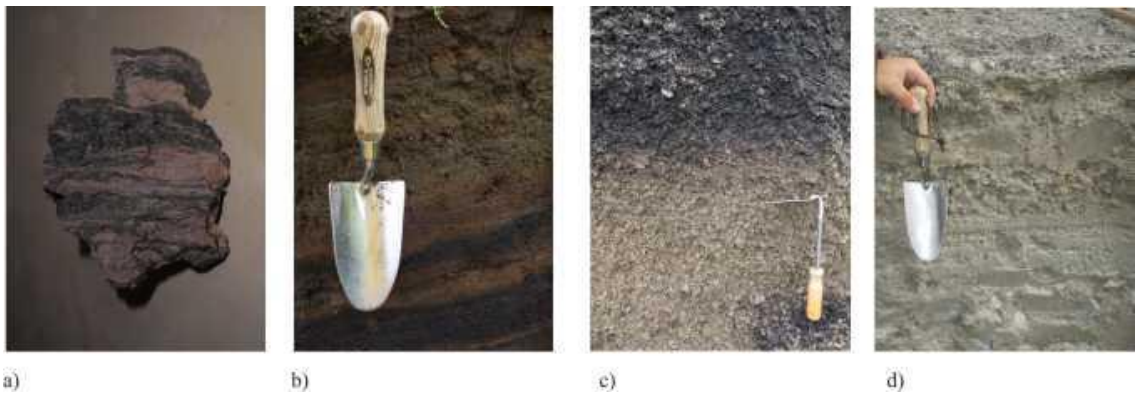

Figure 3.2: photographs of tephra layers showing the different physical characteristics of the volcanoes in Iceland. a) mingled pumice from Askja measuring c. 10 cm. b) needle-like clasts from the Katla SILK layers, trowel measures c. 25 cm. c) two-toned tephra from the Hekla volcano, scarping tool measures c. 35 cm. d) pale grey-white tephra from the Öræfajökull volcano, trowel measures c. 25 cm (photographs: Rh. Meara).

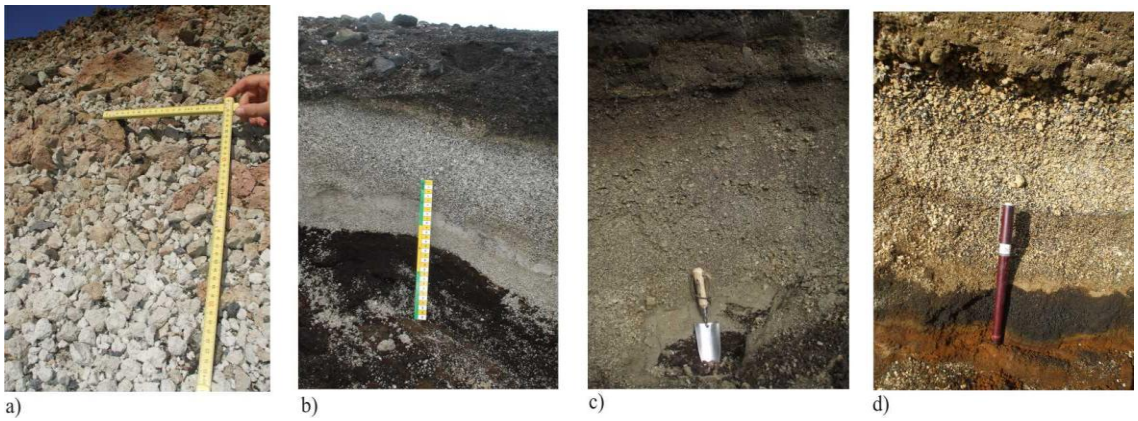

Figure 3.3: photographs of tephra layers from the Hekla volcanic system. a) H3 contains large tephra bombs and shows a colour change from white to orange pumices. Horizontal scale bar measures c. 23 cm. b) H4 has a pale white colour and a characteristic fine grained horizon low in the sequence. Scale bar measures c. 30 cm. c) HSelsund is a darker colour than the other tephra layers and has a fine grained base and a coarser upper. Trowel measures c. 25 cm. d) H5 overlays a dark tephra horizon and has a lithic-rich top. Pen used as scale measures c. 10 cm (photographs: Rh. Meara).

Icelandic volcanoes produce tephra with distinct physical appearances (Fig. 3.2 a-d). Askja pumice clasts are very sharp and angular, show a distinctive glossy appearance and demonstrate extensive mingling. Katla SILK tephras are green-grey in appearance and have a characteristic wood chip texture. Hekla tephras are often two toned, resulting from eruption

of a stratified magma chamber. Öræfajökull tephra is pale grey and highly vesicular. The deposits contain accretionary lapilli and armoured clasts.

The same physical properties can be applied to the identification of tephra layers that are sourced from within the same volcanic system. Such an example is provided by the Hekla volcanic system which has five large rhyolitic eruptions recorded since 7000 BP (Fig. 3.3 a – d; further information on Hekla and its associated tephra layers can be found in Chapters 2 and 6). The H3 tephra contains a horizon of large bomb-sized pumice clasts and a distinctive colour change from white to orange within the top 1 m of the proximal deposit. H4 has characteristic grain size variations within its stratigraphy and the upper horizons of the tephra layer are lithic-rich suggesting pulsations in eruption intensity and vent clearing. The HSelsund tephra also has a unique grain size variation and is darker in appearance than the other Hekla tephra layers. The H5 tephra layer is recognisable in proximal locations as it overlies a coarse black ash layer assumed to have erupted from Katla.

Sequence stratigraphy: The application of physical characteristics to the identification of tephra layers is generally very successful. However, when a sequence of tephra layers shares very similar characteristics they cannot be distinguished by this method alone. Examples of such situations include the Katla SILK needle layers – YN (youngest needle layer), UN (upper needle layer), MN (middle needle layer) and LN (lower needle layer) – and the sequence of small pre-historic Hekla eruptions HA, HB, HC, HM, HN, HX, HY and HZ. When such a situation arises, identification is reliant on sequence stratigraphy, which focuses on the age of eruptions and the stratigraphical order in which they appear in a sedimentary sequence. Within the sequence of Katla SILK tephra layers the YN layer is typically found to the west and south of the volcano; the UN layer consistently tops the sequence to the north-east of the volcano; the MN layer has a dominantly south-south east axis of thickness; the LN layer is the oldest tephra and has a dominantly north eastern axis of thickness (Fig. 2.13; Larsen *et al*. 2001). All three tephra layers have differing axes of thickness and isopach distribution patterns (Fig. 3.4). Basic discrimination is therefore possible by implementing sequence stratigraphy at proximal locations. Both sampling locations and stratigraphical height are important while studying the smaller Hekla eruptions. HA, HB and HC are found only to the north-west of the main volcanic edifice. HM and HN are found to the south-east of the volcano and HX, HY and HZ are found to the east of Hekla (Fig. 2.20; Larsen and Eiríksson, 2008). Within each sub-group, the youngest tephra layer is represented by the earliest alphabetical letter.

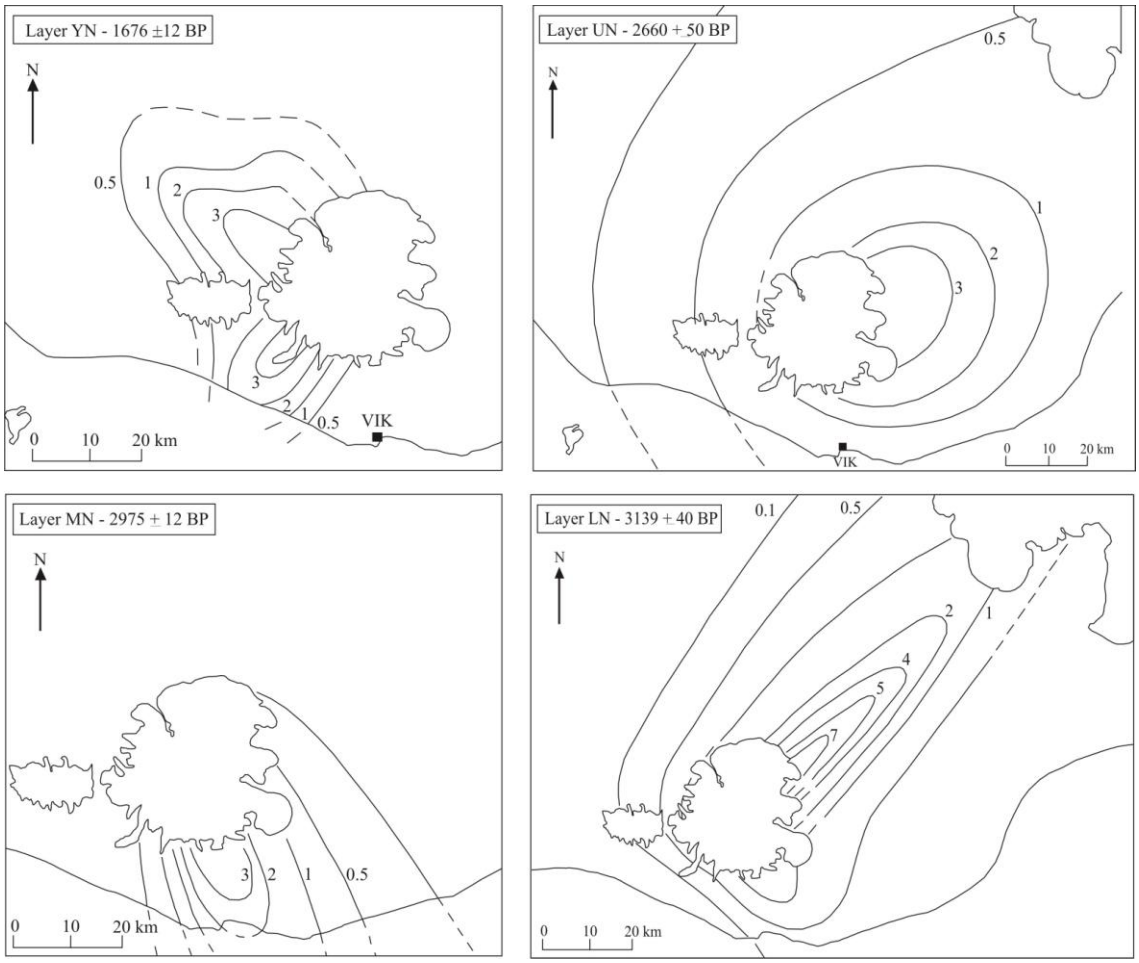

Figure 3.4: Isopach maps of the Katla SILK needle layers YN, UN, MN and LN at source, under the Mýrdalsjökull icecap in southern Iceland. Numbered lines represent tephra layer thickness in cm. Adapted from Larsen *et al* (2001).

Geochemical characteristics: The location of a volcanic system within the active rifting zones of Iceland strongly effects the geochemistry of products erupted from within that system. These differences are seen in the tholeiitic magmatic trend of the Western Volcanic Zone and Northern Volcanic Zone and alkaline to transitional alkaline magmatic trend for the Eastern Volcanic Zone (Fig. 2.1). As a result, individual volcanic systems have developed very distinct geochemical signatures and therefore their products can be identified. The process of identifying tephra provenance is typically conducted by analysing juvenile tephra shards on a WDS electron microprobe (EMPA) and collecting major element oxide data (e.g. Larsen, 1980, 1981). This technique is relatively cheap and fast and does not destroy or cause irreversible damage

to the samples. Micro-analysis of glass shards is preferred to bulk analyses as the latter often contains lithic fragments, non-juvenile material and a high phenocryst content and therefore do not represent true magmatic composition (Pearce *et al*. 2004). Bulk samples may also have undergone mineralogical and compositional fractionation during transportation (Dugmore *et al*. 1996). Application of major element chemistry to identify tephra provenance is discussed further in Chapter 5.

Major element chemistry can also be applied to the process of identifying and distinguishing between tephra layers sourced within the same volcanic system. Although tephra layers erupted within the same system will share an overall geochemical fingerprint, minor variations in major element concentrations resulting from minor changes in magma generation and storage between eruptions may provide an opportunity to distinguish between eruptions.

Discrimination of tephra layers sourced from the same system using major element compositions is only viable when there are noteworthy variations in magma generation and storage. If eruptions are closely spaced in time, and magma is generated from a similar source material the variation in major element concentrations are likely to be so minor as to prohibit reliable identification and discrimination of tephra layers. In such situations, geochemistry can still be used to determine the identity of a tephra layer. The focus must move onto the analysis of juvenile tephra shards for their trace element concentrations. Despite being present in minor concentrations, trace elements show a superior sensitivity to minor changes in magma generation and therefore allow for discrimination between tephra layers which would otherwise be identical. These ideas will be developed further in Chapters 6 and 7.

It should be noted that the majority of tephrochronology studies apply a selection of multi-proxy data to ensure the correct identification of tephra layers and do not rely solely on geochemical data.

3.2.2 Far-distal tephra

The term “far-distal” refers to tephra horizons deposited far from their original source volcano. In this instance, far-distal is taken to represent tephra deposited in glacial, marine, lacustrine and terrestrial sequences outside Iceland across the North Atlantic region. Distal tephra horizons are referred to as micro-tephra or crypto-tephra horizons (Lowe and Turney,

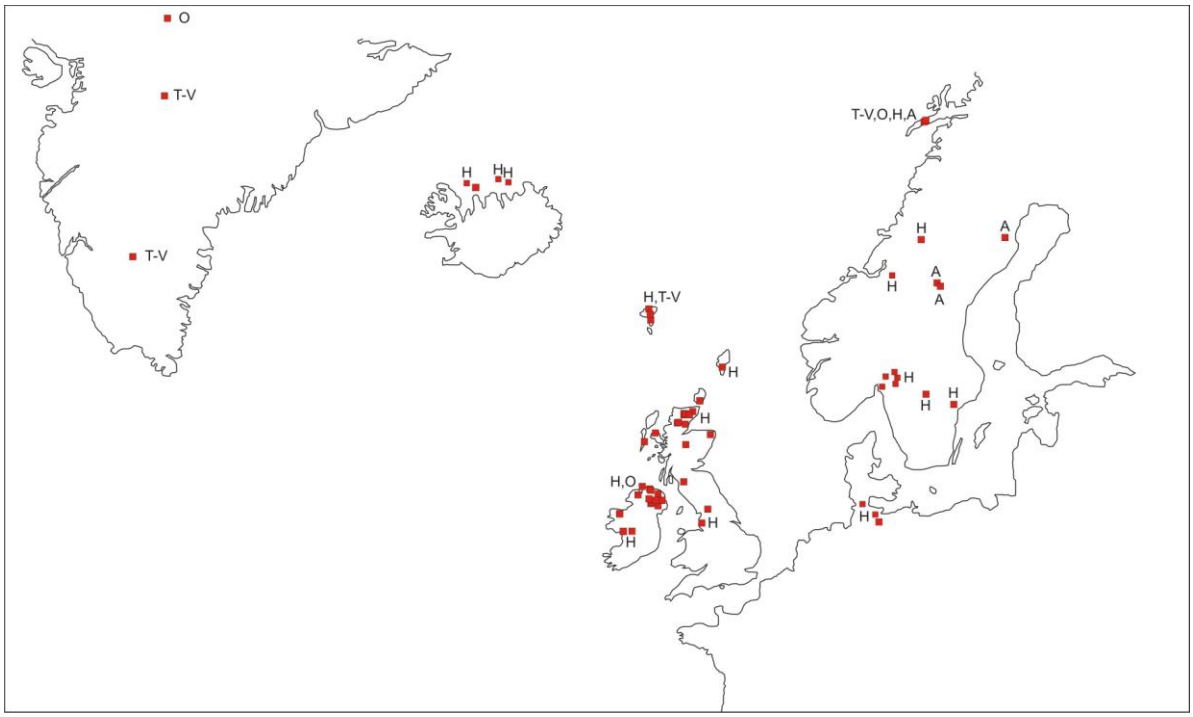

Figure 3.5: Known localities of Icelandic micro-tephra horizons across the North Atlantic region identified using marine, fluvial, glacial and terrestrial records. Letters denote which system produced the tephras identified at each location: O: Öræfajökull; T-V: Torfajökull – Vatnaöldur; H: Hekla; A: Askja (Dugmore, 1989; Palais *et al*. 1991; Blackford *et al*. 1992; Hall *et al*. 1994a; Van Den Bogaard *et al*. 1994, 2002; Charman *et al*. 1995; Dugmore *et al*. 1992, 1995, 1996; Pilcher *et al*. 1995, 1996, 2005; Pilcher and Hall, 1996; Oldfield *et al*. 1997; Boygle *et al*. 1998, 2004; Caseldine *et al*. 1998; Dugmore and Newton, 1998; Eiríksson *et al*. 2000, 2004; Wastegård *et al*. 2001, 2005, 2008; Larsen *et al*. 2002; Van Den Bogaard and Schminke, 2002; Zillén *et al*. 2002; Bergman *et al*. 2004; Chambers *et al*. 2004; Langdon and Barber, 2004; Davies *et al*. 2007; Kristijansdóttir *et al*. 2007)

1997) and typically describe ash particles of < 100 µm (Boygle, 2004; Pyne-O'Donnell, 2006). When volcanoes erupt explosively, an ash plume is carried up into the troposphere/stratosphere by density and buoyancy variations between the plume and surrounding air column. When the plume interacts with high speed winds, ash particles are transported across vast distances (see 3.3 Air-borne transportation of tephra during eruptions). The ash particles are deposited when they act as nuclei for water droplets or when wind speeds drop beneath that required for ash transportation (Wastegård and Davies, 2009). Since the 1960s, Icelandic micro-tephra horizons have been identified across the North Atlantic region, including Greenland, the Faeroe Islands, Norway, Sweden, Finland, Russia, Ireland, Scotland, England, Germany and the Netherlands (Fig. 3.5). One such example is

the recent eruption of the Eyjafjallajökull volcano which saw ash plumes reach heights of 8 - 12 km and ash deposited across Europe from Spain to Finland.

Micro-tephras are rarely preserved as distinct horizons in terrestrial soil sections due to bioturbation, repeated agricultural disturbances and due to the minor concentrations of tephra shards initially deposited at such locations. Marine, lacustrine and peat sedimentary sequences however are typically less disturbed and often contain a tephrastratigraphy extending thousands to tens of thousands of years before present (Holmes *et al*. 1999).

While some basaltic micro-tephra horizons have been identified, distal tephra deposits are dominated by silicic compositions (SiO_2 > 63 wt. %). This preservation bias is explained by the generally more explosive nature of silicic eruptions compared to their basaltic counterparts (Dugmore *et al*. 1995). Such a difference in explosive nature results in the transportation and deposition of more silicic tephra than basaltic tephra causing the apparent preservation bias. Pollard *et al*. (2003) and Wolff-Boenich *et al*. (2004) suggest that the bias towards silicic tephra in distal sedimentary sequences can be explained by post-depositional dissolution of basaltic glasses. Certain studies have suggested that when exposed to an environment with a pH of 4 and a temperature of 25 ºC, basaltic tephra shards have a life expectancy c. 10 times less than that of rhyolitic glass shards. Another valid suggestion is a bias resulting from the sampling technique used in certain environments at far distal localities. The density separation technique is designed to identify tephra shards based on their relative density, and is best applied to identifying low density rhyolitic tephra shards. The technique will be described in more detail in the following sub-section.

Identification of micro-tephras in sedimentary sequences: Due to their fine grained nature, distal tephra deposits cannot be as easily recognised and identified as those at proximal locations. The following section describes the five main techniques for confirming the presence of micro tephra in a far-distal sedimentary succession.

Density Separation: The density separation technique focuses on separating tephra grains from surrounding organic and minerogenic material by manipulating differences in density between the two mediums (Turney *et al*. 1997). Sodium polytungstate ($Na_6(H_2W_{12}O_{40}).H_2O$) is used as a floatation medium and is diluted to produce a liquid with a controllable specific gravity. Setting the specific gravity to 1.98 g cm^{-3} causes most detrital silicates (including diatoms and sponge spicules) and organic components to float and are removed. Adjusting

the specific gravity to 2.3 – 2.5 g cm^{-3} isolates any rhyolitic tephra shards within the sequence and these are removed for further investigation (Turney *et al*. 1997; Blockley *et al*. 2005). The density separation process is initially conducted on large samples of core i.e. 5 cm intervals to establish whether tephra is present within the section. Once tephra has been confirmed, the process is repeated on smaller sub-samples collected at 1 cm intervals within the appropriate horizons. Blockley *et al*. (2005) suggest minor improvements to the original methodology which provide a higher concentration of recovered tephra shards, successfully removes more detrital material and produces tephra with cleaner surfaces for analyses. Once individual tephra horizons have been identified within a sediment core, they are sampled and mounted onto thin sections ready for analysis. Density separation is the most commonly used technique in micro-tephra identification as it does not damage samples or cause any alteration to the geochemistry of the tephra shards.

Ashing: The process of ashing involves heating core sections to 550 ºC in order to remove any organic components. Remaining sample material is then dried over night at 105 ºC to remove any water moisture and are then returned to an oven at 650 ºC for 4 hours. Sedimentary material is then placed into a 10% HCl solution to disaggregate and dissolve any soluble inorganic material. Samples must then be thoroughly cleaned and dried to remove all impurities and moisture (Dugmore, 1989; Pilcher and Hall, 1992).

Chemical digestion: The chemical digestion technique focuses on identifying tephra shards by removing all other organic and non-organic detritus from the sample. This process is completed by submitting the sample to a sequence of acid solution baths to disaggregate the non-volcanic material (Dugmore, 1989. 1992).

Magnetic susceptibility: Magnetic susceptibility is a non-intrusive method for identifying tephra horizons within sedimentary sequences. The saturation isothermal remnant magnetization of a sediment core is analysed and the presence of tephra is inferred by peaks of > 0.2 $mAm2kn^{-1}$. Tephra-rich horizons can then be sampled with minimal damage to the remaining sediment core (Oldfield *et al*. 1989; Van Den Bogaard *et al*. 1994, Pawes *et al*. 1998). This technique however, is only applicable to the identification of basaltic tephra due to the poor magnetic susceptibility of silicic grains (Dugmore, *pers comm.*).

Ion chromatography: Micro-tephra horizons in ice cores are identified using ion chromatography, a process which analyses the concentration of water soluble catïons and

anïons deposited onto ice by a volcanic eruption. The process shows up peak concentrations of volcanic aerosols including H_2SO_4, HNO_3, HCl, and HF inferring the presence of tephra shards (Clausen *et al*. 1997). However, recent work on the NGRIP ice core by Davies et al (2010) has indicated that not all sulphate peaks correspond to tephra layers and not all tephra layers produce sulphate peaks. Therefore identification of micro-ash layers in ice cores is now completed by a combination of continuous flow analyses (CFA) and manual sub sampling and processing of ice cores.

3.3 Eruption and air-borne transportation of tephra

The removal of cap rock during explosive Plinian eruptions (see Chapter 2 for definition) causes rapid decompression of the underlying magma chambers which in turn releases volatile gases from within the stored magma. This release of gas triggers magma expansion, which is accommodated by upwards movement through the crust resulting in eruption at the surface. Upwelling of the ensuing volcanic plume is initially due to the driving force of further magmatic material exiting the conduit. Over time, this driving force diminishes and is replaced by the influence of density variations and buoyancy. The volcanic plume comprises hot gas-rich pumice and ash which have a lower density than the surrounding cool atmospheric air. This density variation allows the volcanic plume to rise buoyantly. At the troposphere – stratosphere boundary (the Tropopause, 8 – 15 km), the density of the surrounding air is equal to that of the plume and thus prohibits further ascent. At the boundary, the plume spreads out to form an umbrella cloud, named for its umbrella-like appearance. If no other forces act on the plume from this point forwards, then ash will gradually be deposited forming roughly circular isopach patters at proximal locations to the volcanic source (e.g. Fig. 2.12). If however, external forces i.e. jet stream winds influence the plume, ash will be transported in a downwind direction and may be cover large distances. Transportation by wind is indicated by non-circular isopach patterns (e.g. Fig. 2.9, 2.13 and 2.20) and the identification of micro-tephra horizons at far-distal localities (Fig. 3.5).

3.4 What is tephrochronology?

The identification, characterisation, dating and correlation of tephra horizons in glacial, marine, lacustrine and terrestrial sedimentary sequences forms the basis of tephrochronology

and tephrostratigraphy (Thorarinsson, 1949, 1958, 1967; Larsen, 1981). Volcanic eruptions are considered to be geologically instantaneous events which, when combined with the typically widespread nature of explosive eruptions results in detailed time-parallel marker horizons. Such marker horizons can be used to date and correlate events across contintental-scale distances.

Tephrochronology is used as a tool for dating events by various studies including archaeology and anthropology (e.g. Dugmore *et al*. 2000; Church *et al*. 2007), climate change and glacial fluctuations (e.g. Langdon and Barber, 2004; Kirkbride and Dugmore, 2003, 2008, 2011; Bradwell, Dugmore and Sugden, 2006), palynology (e.g. Hall *et al*. 1994) and geomorphology (Kirkbride and Dugmore, 2006). Three main assumptions are made when using tephrochronology for dating (Langdon and Barber, 2004; Lowe, 2011):

1. Tephra particles are deposited instantaneously in a geological context, with most eruptions lasting for just hours, days, weeks or even months.
2. Tephra grains are not mobile within sediment once deposited.
3. Each eruption produces geochemically distinct deposits.

The following sections will provide a brief overview of North Atlantic tephrochronology with respect to Icelandic volcanism. It is important to note that sedimentary successions within the North Atlantic region do not contain tephra horizons sourced solely from Iceland. Locations on mainland Europe also contain tephra horizons sourced within the Massif Central, the Eifel region and Italy (Davies *et al*. 2002). As these source regions are not the focus of this thesis, they are not discussed further. A summary of the problems associated with North Atlantic tephrochronology is also presented.

3.4.1 Icelandic Tephrochronology

The explosive nature of some of Iceland's volcanoes has resulted in the transportation and deposition of Icelandic Holocene aged micro-tephra layers across the North Atlantic region (Fig. 3.5). Icelandic tephra sourced from historic eruptions (post-870 AD) are of particular use to tephrochronology as eye witness accounts and written records often provide exact dates for the eruptions including the year, month, and day and in some circumstances the exact time of commencement (Watts, 1876; Larsen *et al*. 1999 and references therein).

More than 158 tephra layers have been identified in post-glacial sequences in Iceland; however the total number of eruptions that occurred in this time is believed to be closer to 2,400. Of the 158 tephra layers identified, over 80 represent important marker layers with at least 13 having been identified in sedimentary successions outside Iceland (e.g. Pilcher *et al*. 2005; Davies *et al*. 2007).

More than 50 intermediate to silicic explosive volcanic eruptions are known to have occurred in Iceland during the Holocene period. These eruptions are sourced from the Askja, Hekla, Katla, Eyjafjallajökull, Öræfajökull, Snæfellsjökull and Torfajökull volcanic systems and include the major marker horizons A1875, Ö1362, H1104, Landnám, H3 and H4 which are found at localities across the North Atlantic region.

The proximal Icelandic tephra stratigraphy has been studied in some detail (e.g. Larsen *et al*. 1999; Óladóttir *et al*. 2008). Late to mid Holocene tephra sequences are well characterised. However early Holocene tephra layers and those older than 10,000 years BP are often poorly studied due to poor preservation as a result of extensive ice coverage in Iceland during the last glacial maximum (Norddahl, 1991a). In such circumstances, the distal component of such tephra layers may be the only record of an eruption (Fig. 3.6) e.g. the Borrobol tephra (Turney *et al*. 1997; Davies *et al*. 2003).

Figure 3.6 is a graphical representation of the Icelandic tephra stratigraphy and its North Atlantic counterparts. The left column of the figure represents the on-land Icelandic sequence while the right column represents the sequence of micro-tephra horizons identified across the North Atlantic region (individual countries are not represented). The two columns are joined where a tephra layer has been identified at a far-distal locality and correlated to a known Icelandic source. Intermediate to silicic tephra layers are represented on the figure as these are the main focus of this thesis.

Figure 3.6 indicates abundant silicic volcanism in Iceland with over 50 intermediate to silicic eruptions since 10,300 BP. Of those recorded eruptions, 18 have been identified and correlated to sedimentary successions on the Scandinavian and European mainland ranging in age from 125 – 11,980 BP. Such correlations provide a framework for dating and correlating events across the region throughout the entire Holocene period. The remaining 32 tephra layers that have not been correlated to the far-distal record are still of great importance to Icelandic tephrochronology and can be used as marker horizons on a smaller

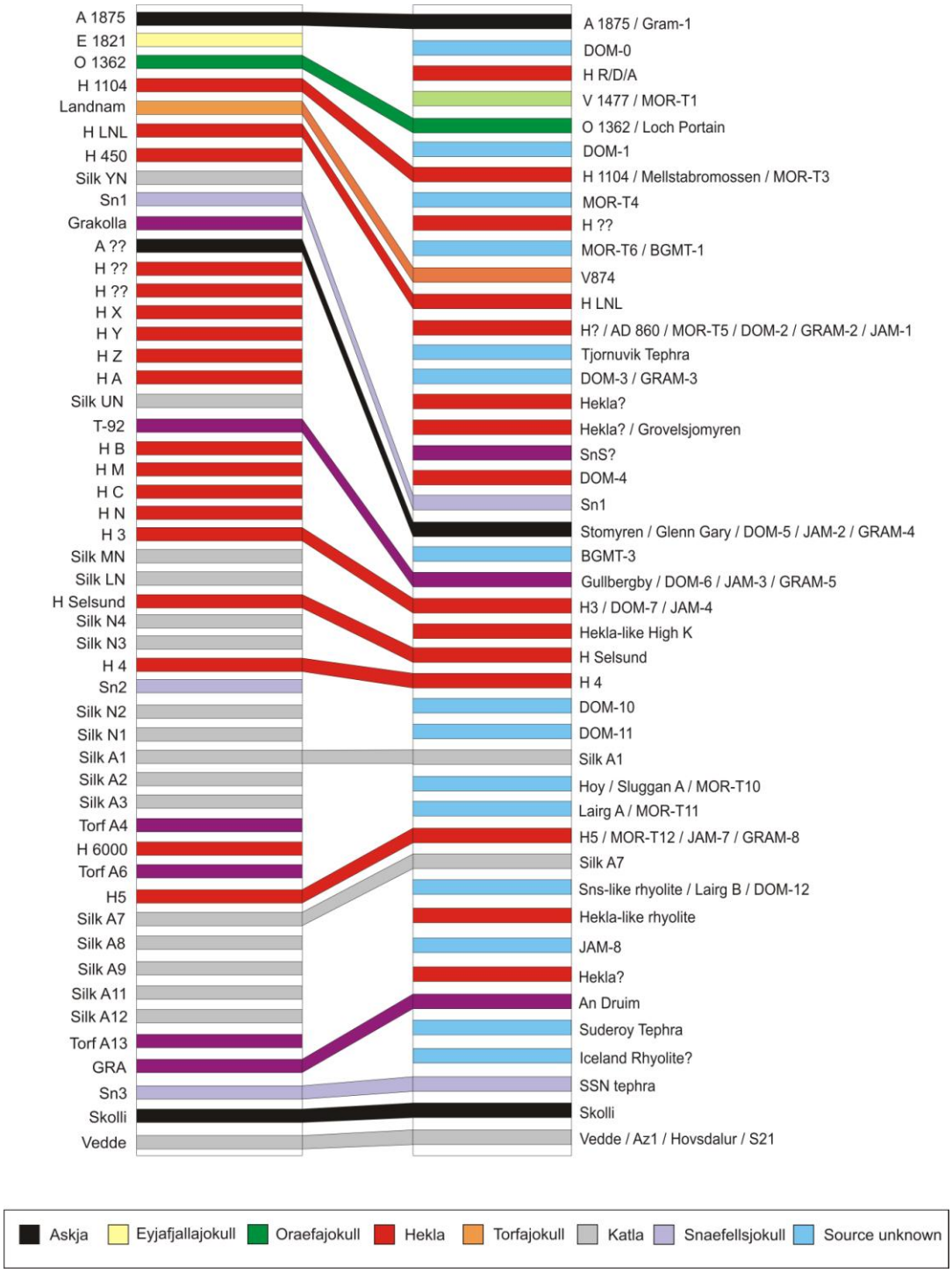

Figure 3.6: tephrostratigraphy of Iceland and the North Atlantic region. The column on the left depicts the main intermediate-silicic tephra layers known from the Holocene tephra record of Iceland. The column on the right depicts the main intermediate-silicic micro-tephra horizons identified in terrestrial, marine and lacustrine sedimentary sequences across the North Atlantic. Tephra layers correlated between proximal and distal locations are represented by a coloured band joining the two. Where the source of an eruption is unknown, the layer is coloured pale blue.

localised scale. The right hand column includes 26 tephra layers that do not correlate with a known proximal tephra. Volcanic systems have been suggested as sources for 11 of the unknown tephra layers based on their major element chemistry; however 15 tephra layers show no geochemical affinity to a known Icelandic source. Such an absence of affinity may be explained by poor preservation in the proximal succession, introduction of volcanic material from a non-Icelandic province or by mis-identification of a tephra layer by workers in the far-distal regions. It is also possible that the tephra layers are yet to be identified in the proximal succession.

3.4.2 Persistent problems associated with North Atlantic tephrochronology

The application of tephrochronology to Quaternary studies across the North Atlantic region has proved to be incredibly useful e.g. dating of the Scotts Pine decline across Scotland and Ireland using the H4 tephra layer (Blackford *et al*. 1992; Hall *et al*. 1994). However, there are a number of outstanding issues associated with the method which affect the quality of the data collected. Such issues may result in unreliable tephra identification and correlation with a knock on effect for any dates established using the technique. The four main issues are field work and sample collection, geochemical analyses and dating of tephra layers. A brief overview of these outstanding issues is provided below.

Field work and sample collection: When studying tephra deposits, it is essential to identify a reference section that comprises the full stratigraphy of an eruption in order to represent the complete magmatic characterisation of the deposit. This is particularly important for tephra layers which show geochemical stratification due to the zoned or stratified magma chamber that underlies the source volcano. A reference section located too far away from the volcano will not contain tephra from lower intensity phases of an eruption, while a section located too close to the volcano will have typically deposited tephra onto barren ground or onto a glacier and will be open to erosion and re-working (Óladóttir *et al*. 2005). Deposits erupted through ice capped volcanoes (e.g. Vatnajökull and Katla) do not typically show a full record of an eruption as the most proximal section will not be preserved within the seasonally melting ice caps. Similar problems are associated with volcanoes located in the Icelandic Highlands, where the absence of proximal deposits can be explained as a result of poor soil accumulation rates and a shortage of binding vegetation (Larsen and Eiríksson, 2008). The chosen section must show minimal post-depositional re-working to avoid contamination by other tephra layers. Topographic lows act as superior sediment traps therefore allowing for

rapid burials of tephra to avoid such re-working. The majority of these issues can be overcome with adequate investigation to identify a reliable reference section at proximal locations.

The identification of distal tephra layers is more problematic. In the majority of sections the tephra shards are microscopic and the horizons diffuse so as to be invisible to the naked eye therefore making it impossible to assess whether the section fully represents an eruption. The quality of samples is dependent on the sampling location, the processes which have affected the tephra shards since their deposition and the sampling techniques used. Post depositional physical processes occurring within sedimentary successions will impact the tephra stratigraphy (i.e. bio-turbation, agricultural processes such as ploughing, general gravitational slumping of sediments and chemical alteration of shards) causing contamination between horizons. Samples collected via coring systems have been associated with core stretching which disturbs sediments resulting in the draw down of younger sediment within the core providing tephra concentration peaks at incorrect stratigraphical horizons within the core (Davies *et al*. 2007).

A number of marine tephras linked to the Icelandic record are referred to as Ash Zones, which represent horizons of tephra within a sedimentary succession that do not form one continuous unit but are diffuse over a specified vertical height. These Ash Zones have in the past typically been considered as one unit and sampled in bulk rather than at specific intervals. In turn this has introduced artificial mixing to a deposit which in reality may contain several individual tephra layers (Kvamme *et al*. 1989; Sjøhlom *et al*. 1991; Lacasse *et al*. 1995; Austin *et al*. 2004). When analysing a core for micro-tephra horizons, their presence is typically confirmed by a marked peak in shard concentration with a gradual tail of decline within the overlying sediment. This peak is deemed to represent the commencement of the main eruptive event and not the first occurrence of tephra shards as these may represent downward migration of shards within the stratigraphic column (Enache and Cumming, 2006).

Geochemical analyses: The geochemical data for the tephra layers studied in this thesis collected by other workers is presented on the Appendix CD. Although the majority of previous data has been collected to the high standards, certain issues can influence the final product. Major elements are measured in relative wt. % during analysis; therefore errors encountered from analytical machines can drastically vary the overall chemical fingerprints

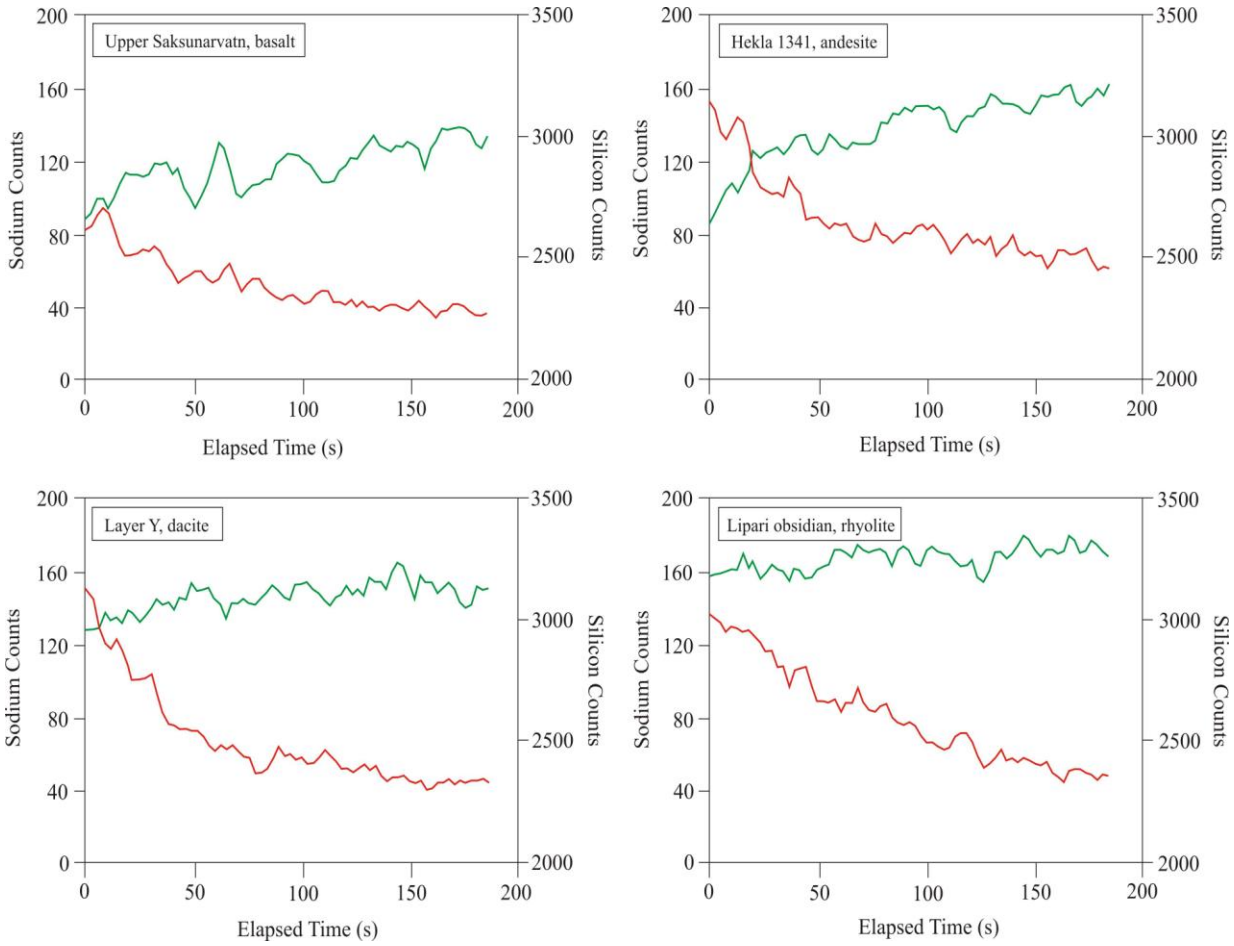

Figure 3.7: Electron microprobe data as absolute counts of X-rays at detector collected every two seconds for sodium (red) and silicon (green). The downward trend of the sodium profile is apparent in each example. The increasing trend of the silicon profile is less apparent but still clear. This steady increase is driven by the continual loss of sodium, thus silicon is readily over-represented in a sample, while sodium is systematically under-represented. The Saksunarvatn basalt, Hekla 1341 and Layer Y were sampled in Iceland and the Faroe Islands, while the Lipari obsidian was sourced from Italy. Adapted from Hunt and Hill (1993).

of individual glass shards. The typical reported error for microprobe analyses is c. 1%, which poses a problem for low concentration major elements (i.e. MnO and MgO in rhyolites). An important source of error during EMPA analysis is the time dependent loss of intensity of an element as a result of continuous bombardment from the electron gun (Nielsen and Sigurdsson, 1981). Mobile elements are the most affected by this, with up to 50 % underestimation of original Na contents within rhyolitic glasses (Mangerud *et al.* 1984; Hunt and Hill, 1993, 1996; Hayward, *in prep*). Figure 3.7 indicates the loss of Na and the resulting

relative increase of Si concentrations on four volcanic samples during electron microprobe analyses. Such a marked increase in Si concentrations will result in marked increase in SiO_2 wt. % thus potentially causing dramatic alteration to the overall composition of a tephra layer. Under such circumstances, analysis of a tephra layer with an intermediate silica composition would produce data suggesting a rhyolitic composition. Identification and correlation of the tephra would therefore focus onto known rhyolitic eruptions with the closest match assumed as correct. The potential for mis-identifying tephra layers is highlighted in figure 3.8. Samples collected by Kristjansdóttir *et al*. (2007) show significant Na-loss causing their data to plot some distance from the other data, potentially overlapping with that of another tephra layer.

It is common practice in some laboratories to normalise tephra data to an anhydrous basis. This involves re-scaling the analytical total to 100 wt. % to exclude any magmatic or meteoric water affecting the deposit. This practise is not universal and as a result the glass compositions published for a single deposit can differ significantly (Pearce *et al*. 2004).

The number of shards and size of samples analysed is thought to contribute towards reduced reliability of unit identification as the statistical significance of the results cannot be assessed. A number of microtephra horizons analysed across the North Atlantic Region are correlated to proximal deposits by the chemical finger printing of as little as six glass shards (Bond *et al*. 2001). This small number of shards does not provide any insight into the chemical variations encountered within eruptions, and does not guarantee definite identification of a primary tephra horizon as opposed to reworked secondary tephra deposits i.e. Vedde Ash layer identified in Loch Ashik, Isle of Skye (Davies *et al*. 2001).

The use of different machines during analysis is known to produce minor changes in chemical values of the elements recorded. Data collected via XRF and EMPA will differ as XRF analyses represent bulk samples including glass and phenocryst phases, while EMPA analyses are focused onto primary magmatic componentry by analysing singular points of glass material (Pearce *et al*. 2004). Bulk samples represent both the evolved final state of the magmatic glass material and the mineral assemblages which have crystallised from the melt before eruption. Variations in data collected are also noted between EDS and WDS microprobes (Birks *et al*. 1996). Newer machines are less accurate than their older counterparts, but do however use a cool finger technique which helps reduce problems with precision related to the migration of Na (Hunt and Hill, 1993). Rhyolitic glasses analysed on

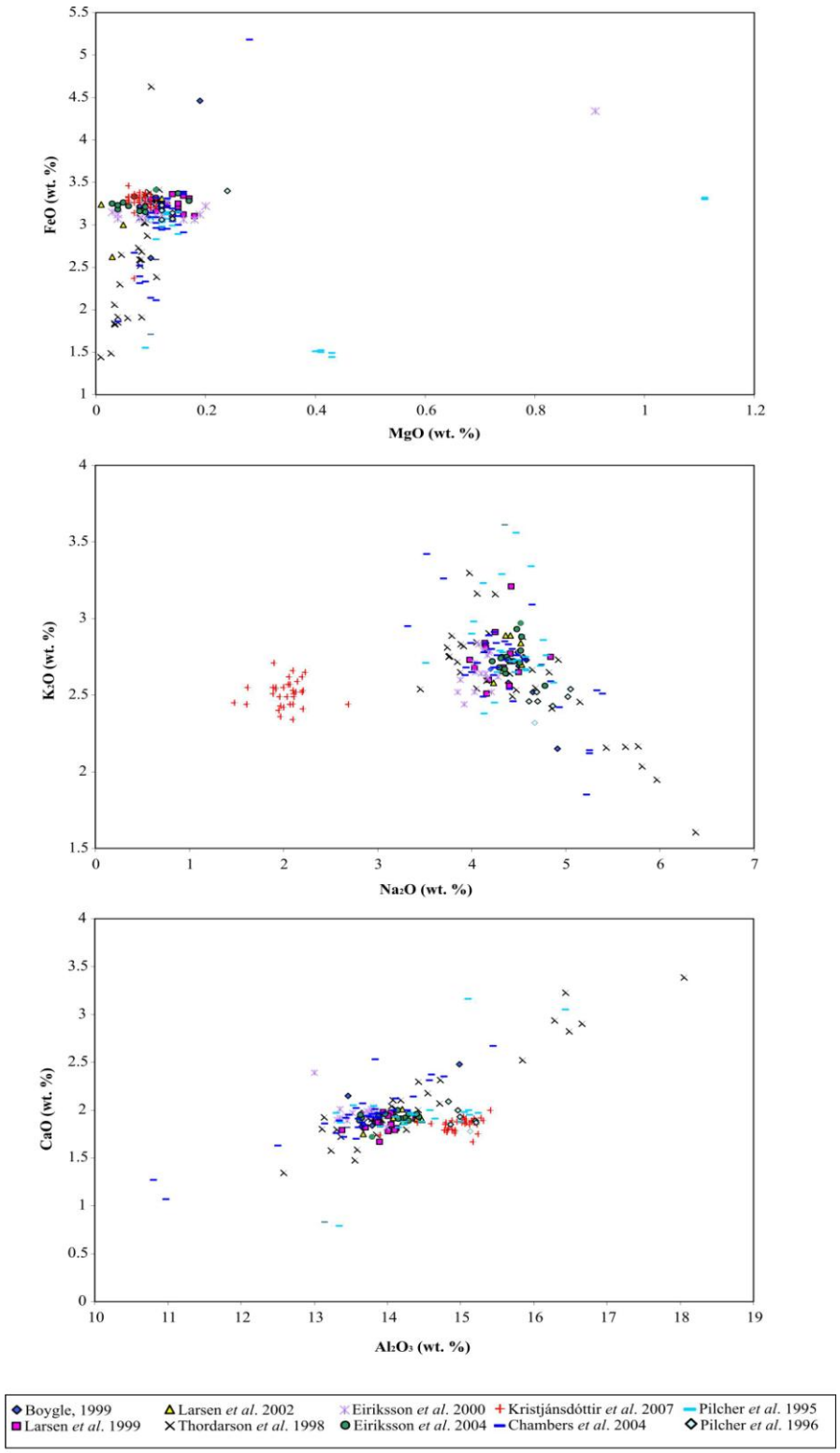

Figure 3.8: Bivariate plots of major element oxide values analysed for the H1104 samples. Plots show the variations in data collected for the same unit in a number of different institutions, caused by the issues discussed in the main text.

similar machines at different locations often show minor differences in precision and accuracy and the resultant major element values. Figure 3.9 shows a series of bi-variate plots showing major element data collected for the H1104 tephra layer. The data presented was collected at a number of different institutions and demonstrates the extent to which data can differ when subjected to inconsistent analytical set ups. Hunt and Hill (1993) and other workers have established criteria for the standardisation of analytical procedures to minimise the potential for inter-laboratory data variations which have resulted in a marked improvement in the quality of data collected.

Dating of tephra layers: Historic eruptions (post 870 AD) can often be dated to the exact year, month, day and in some cases to the hour of their eruption due to well preserved written records of volcanic occurrences since Icelandic settlement (Larsen *et al*. 1999 and references therein). Prehistoric tephra deposits identified in terrestrial glacial deposits can be dated by counting depositional layers in ice cores, which is accurate to +/- 10 years in the past 10,000 years (Grönvold *et al*. 1995; Pilcher *et al*. 2005).

Prehistoric tephra deposits found in non-glacial environments are typically dated using radiocarbon dating methods performed on organic material immediately above or below the tephra horizon. This method relies heavily on the soil age-depth model which assumes that the soil accumulation rate (SAR) is consistent and that tephra deposition was instantaneous with blanket-like coverage (not true in marine and fluvial environments due to ice rafting, sediment focusing and turbidity currents) and that no reworking has occurred (Boygle, 1999; Turney *et al*. 2006). However, the SAR is affected by a number of variables including topography, climate, drainage and vegetation (Thorarinsson, 1961; Bergman *et al.* 2004; Óladóttir *et al*. 2005). When dating of a tephra layer is calculated using the SAR values based on slow-deposition peat as found in Iceland precision can be worse than +/- 200 years (Pilcher *et al*. 2005). The age-depth method is also used to infer the identity of tephra horizons when the number of glass shards detected is too few for geochemical analyses to be undertaken (Bergman *et al*. 2004). Icelandic lake and marine sedimentary sequences are known to produce high ^{14}C ages when compared to terrestrial soils due the influx of mature terrestrial material into the fluvial environments through erosion (Jóhannsdóttir, 2006). The radiocarbon calibration curve suffers from a broad plateau between the ages of 4025 – 325 cal. yr. BP, and often has such a large error ($\leq$ 130 years at a 95% confidence level) that it makes the dating of prehistoric eruptions a futile task.

3.5 Summary

This chapter has introduced basic volcanology terminology and detailed how tephra horizons are identified and sampled at proximal and far-distal localities. The chapter has also defined the concept of tephrochronology and described its application to Quaternary studies across the North Atlantic region. A brief overview of Icelandic tephrochronology and a few associated problems with the technique in this region have also been presented.

Workers within the tephrochronology and analytical communities are developing methods and techniques to limit the influence of the issues raised in section 3.3.2 and some advancement as been achieved. In particular, laboratories across Europe and North America are analysing standardised reference materials to establish means for successfully comparing data collected at different institutions with different instrumentation (i.e. INTAV, 2010). To complement such work, this thesis presents a reference data set collected for a suite of Holocene Icelandic tephra layers collected at select reference localities near to source. By collecting and presenting this data set, we are providing the tephrochronology community with a reliable and robust reference for use when establishing tephra identities at far distal locations. Such a data set should minimise or indeed eliminate the potential for propagation of tephra mis-identification between studies. The data collected will be presented in Chapters 5, 6 and 7. The field and laboratory based methodologies used during data collection are described in Chapter 4.

Chapter 4:

Methodology

4.1 Introduction

The following chapter outlines and describes the methods used during sample collection, preparation and analyses for this research project. Field methods and sample collection are explained in section 4.2. Analytical methods applied to data collection and sample preparation are discussed in sections 4.3 (bulk analyses) and 4.4 (glass analyses). Geochemical data was collected for this thesis using X-Ray Fluorescence (XRF), Electron Microprobe Analysis (EMPA), Ion Probe (IP) and Laser Ablation Inductively Coupled Plasma Mass Spectrometry (LA-ICP-MS). XRF, EMPA and IP analyses were conducted at the University of Edinburgh while LA-ICP-MS analyses were conducted at the University of Aberystwyth.

4.2. Field sampling

During three consecutive field seasons to Iceland, key reference sites which represent tephra layers from key Holocene eruptions were identified. Following identification, each reference section was logged, photographed and described to record all physical characteristics. Sampling at multiple reference locations would have ensured the collection of all phases of the eruptions however this was outside the scope of the project. Instead, individual reference sections were selected following detailed discussions with local Icelandic experts to ensure the best localities. Reference sections were selected using the following criteria:

- Proximal location to source volcano – The location of a reference section greatly affects the level of detail recorded for an eruption. A reference section located too far away from the volcano will not contain tephra from the lower intensity phases of an eruption. A section selected too close to the volcano, will typically contain tephra deposited onto barren ground or onto a glacier and will be open to erosion and re-

working (e.g. Óladóttir *et al*. 2005). Topographic lows act as superior sediment traps therefore allowing for rapid burials of tephra to avoid such re-working. In this project, the term "proximal" refers to locations within 20 km of source.

- Inclusion of all known eruption phases – A large number of Icelandic tephra layers, in particular the Hekla volcano, are two-toned in appearance. Such tephra layers will have a white silicic base and a black mafic top indicating a bi-modal composition. In such circumstances, the bi-modal composition represents a zoned magma chamber beneath the volcano. It may also identify eruption of a dominantly silicic magma due to injection of hot basalt magma. Careful selection of a reference section allows for the identification of temporal changes in composition represented within the outcrop.

- Absence of re-working – A reference section must show minimal post-depositional re-working to avoid contamination by other tephra layers. Re-working of tephra layers is established during field studies based on the following criteria:

1. Re-worked tephra layers contain smooth rounded pumice clasts whereas fresh tephra layers contain rough often jagged and fragile tephra clasts. This variation in clast morphology results from abrasion during transportation via fluvial and gravity-based currents.
2. Tephra layers deposited via air fallout drape the landscape and typically show very good sorting as a result of gravitational segregation during deposition. A re-worked tephra layer should not drape the underlying topography, but will preferentially deposit in topographic lows, and will be moderately to poorly sorted.
3. A fresh tephra layer will contain juvenile pumice and lithic clasts ejected from the volcano during an eruption but little other material. When re-worked a tephra layer may contain a substantial amount of other sedimentary material incorporated during transportation (i.e. soil, non-juvenile lithic fragments, biogenic fragments) and small-scale sedimentary structures may be identified within the layer (i.e. mud-cracks, rivulets, ripples).

Fifteen reference sections were identified for the recording and sampling of tephra layers from the Torfajökull, Askja, Katla Öræfajökull and Hekla volcanic systems during three field seasons from 2007 – 2009 (Table 4.1; Fig. 4.1 – 4.6).

Table 4.1: sampling locations for the tephra layers studied in this chapter. GPS coordinates for sampling locations are provided along with unit thickness and average grain size of each tephra within the reference sections.

Eruption Name	GPS Location (N, E)	Unit Thickness	Average Grain Size
Landnám	63º 53.046', 19º 28.992'	2.73 m	Med – Coarse Lapilli
Grákolla	64º 02.123', 19º 03.828'	2.3 m	Med – Coarse Lapilli
A1875	64º 02.571', 19º 18.305'	5.5 m	Fine – Coarse Lapilli
Silk UN	63º 43.933', 18º 43.917'	0.16 m	Fine – Med Lapilli
Silk LN	63º 49.741', 18º 37.219'	0.055 m	Fine – Med Lapilli
Ö1362	63º 53.505', 16º 37.158'	2.9 m	Med Lapilli
H 1104	64º 03.478', 19º 46.398'	0.60 m	Med – Coarse Lapilli
H 3	64º 02.373', 19º 44.539'	2.70 m	V. Coarse Lapilli
H Selsund	64º 02.369', 19º 43.651'	0.75 m	Med – Coarse Lapilli
H 4	63º 53.046', 19º 28.992'	3.35 m	Coarse Lapilli
H 5	64º 05.876', 19º 34.903'	0.20 m	Fine – Med Lapilli
H A	64º 05.470', 19º 56.472'	0.08 m	Medium Lapilli
H B	64º 05.470', 19º 56.472'	0.15 m	Medium Lapilli
H C	64º 05.470', 19º 56.472'	0.40 m	Medium Lapilli
H M	63º 53.046', 19º 28.992'	0.40 m	Med – Coarse Lapilli
H N	64º 05.470', 19º 56.472'	0.80 m	Med – Coarse Lapilli
H X	64º 02.589', 19º 18.218'	0.30 m	Medium Lapilli
H Y	64º 02.589', 19º 18.218'	0.35 m	Medium Lapilli
H Z	64º 02.589', 19º 18.218'	0.75 m	Medium Lapilli

Once reference sections were identified using the above mentioned criteria, each tephra layer was thoroughly logged and photographed. The physical characteristics of each tephra layer were also recorded. The physical characteristics of individual tephra layers can provide important information for tephrochronology studies. Physical characteristics recorded at each locality include colour, grain size variation, pumice vesicularity, clast morphology and phenocryst content. Such details provide information regarding geochemistry, eruption intensity, explosivity and volatile content, depositional mechanisms and magma generation and storage.

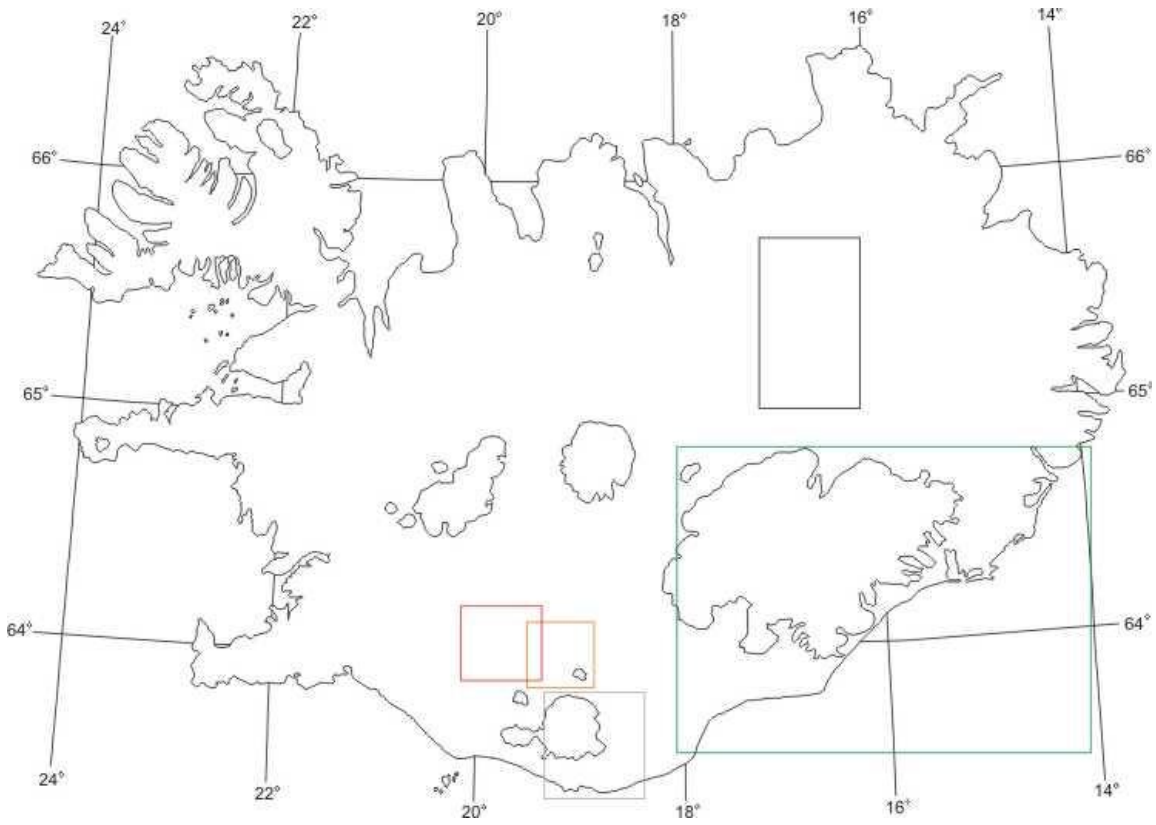

Figure 4.1: Map of Iceland indicating the sampling locations highlighted by Figures 4.2 – 4.6. Colours represent maps for each volcanic system: Hekla (red), Torfajökull (orange), Katla (grey), Askja (black) and Öræfajökull (Green).

These characteristics and the information they provide are of central importance to tephrochronology studies as they shed light on eruption intensity, transportation, deposition and preservation of distal and far-distal tephra horizons. By studying a tephra layer and developing stratigraphic logs at proximal locations we can collect samples that fully represent every phase of an eruption, thus providing more information for those working in distal locations. Providing chemical data for every phase of an eruption and not just the early rhyolitic phase may open up the possibility for identifying and correlating different phases of eruptions thus providing information on plume dispersal and ash transportation. Three main physical characteristics are explained below, while a brief explanation of all characteristics is provided in Chapter 3.

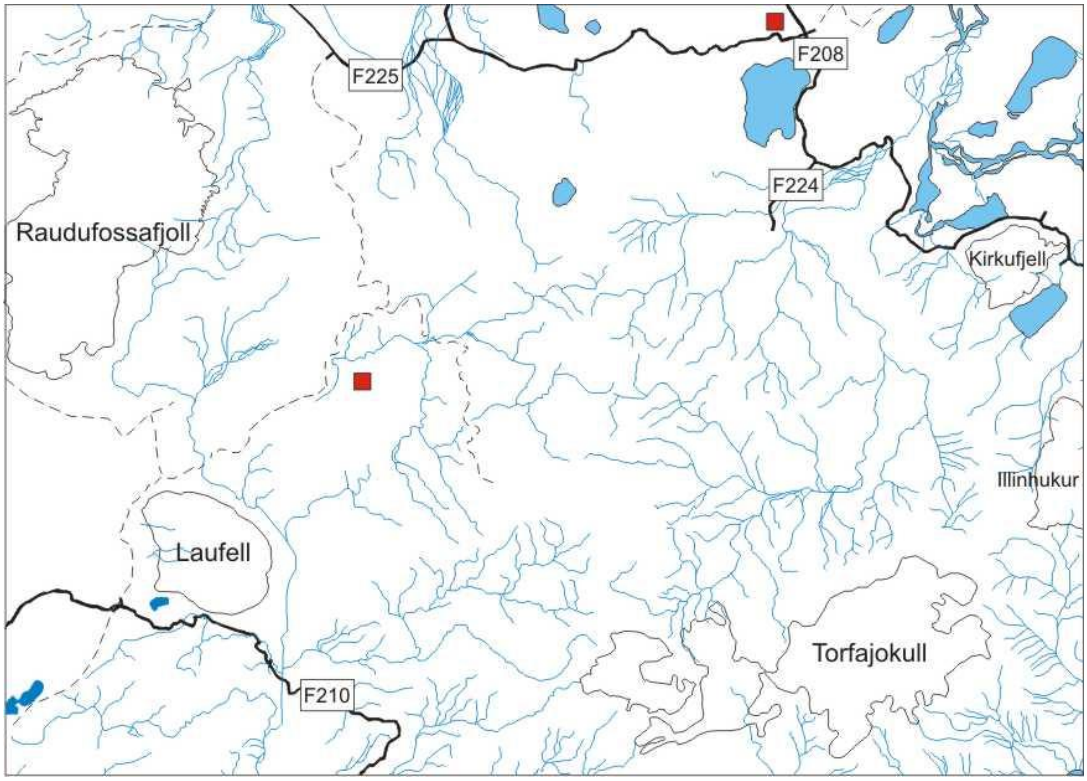

Figure 4.2: Map of the Torfajökull central volcano. The red square in the north of the map represents the sampling location of the volcanic unit Grákolla on the hill bearing the same name. The red square to the west of the map represents the sampling location of the silicic component of the Landnám tephra.

Colour provides information about the geochemistry of a tephra layer and any temporal variations associated with its eruption. Therefore, understanding geochemical variations within a tephra layer can aid identification and recovery of the distal component which often use techniques which utilise density variations between basaltic and rhyolitic shards.

Grain size variations within a tephra layer are of particular importance to tephrochronology. Recording the temporal variation in grain size at a specific location allows inferences to be made regarding the increasing and decreasing intensity of an eruption as well as inferring changes in wind direction during eruption. Ash-sized particles in a proximal sequence suggest a low intensity as the plume can only transport small clasts. Meanwhile, lapilli and bombs-sized fragments at the same locality suggest a much higher intensity for the eruption as the plume is able to transport larger sized fragments over a similar distance. The most explosive high intensity phases and the associated tephra are likely to be injected high into the atmosphere and are therefore most likely to represent the material identified in distal

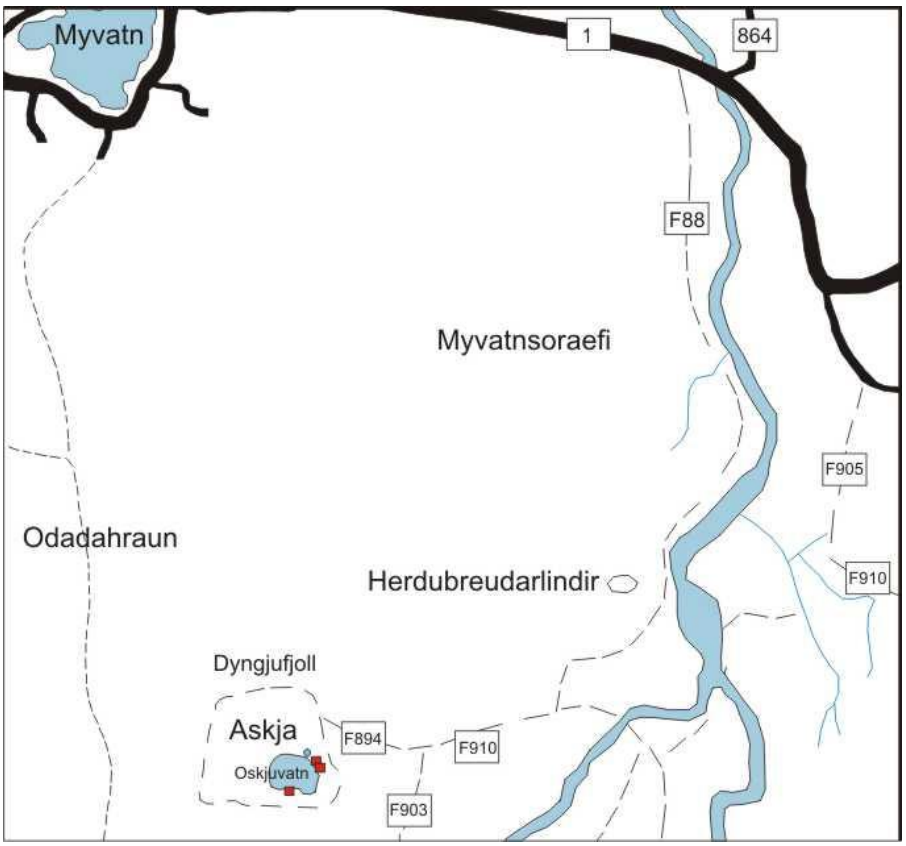

Figure 4.3: Map of the Askja central volcano. The red squares represent sampling locations for the A1875 eruption – the southern most location represents the B-unit, the eastern most location represents the C-unit and the northern most location represents the D-unit.

locations. It was previously believed that the first erupted material was representative of distal micro-tephra horizons as the earlier phases of an eruption should be the most explosive and therefore highest intensity. Our work suggests that this is not always the case, proving that a thorough understanding of volcanic eruptions and processes is essential before applying their products to other academic studies.

Clast morphology and sedimentary structures are used to infer depositional mechanisms and post-depositional re-working. Identifying the depositional mechanism of a tephra layer is important to tephrochronology as this will define the localities where a tephra layer may be preserved. If a tephra is deposited via ash fall out, the resulting layer will be uniform in thickness and will drape the landscape at proximal locations. Such a tephra is likely to be carried into the atmosphere by the volcanic plume, transported by winds and deposited across vast distances to produce a wide-spread marker horizon. Tephra deposited via

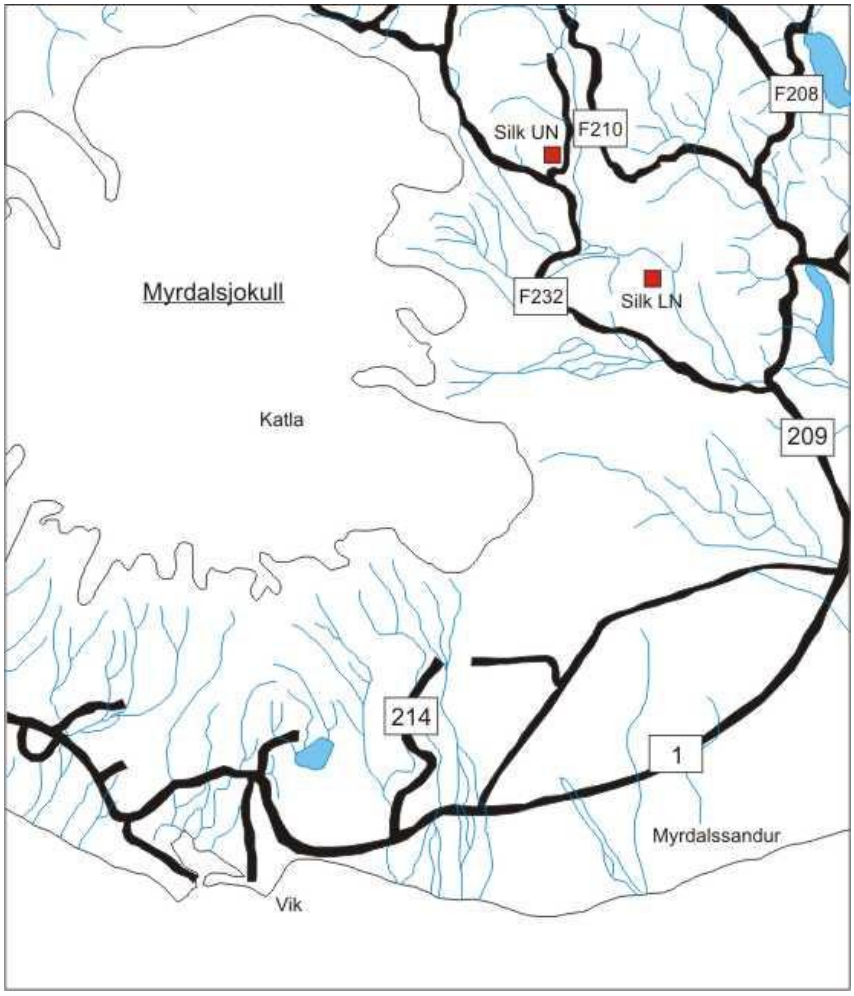

Figure 4.4: Map of the Katla volcanic system. The red squares represent sampling locations for the Katla Silk tephra layers. The northern square represents the Silk UN tephra while the southern square represents the Silk LN tephra.

pyroclastic density currents (PDCs) will produce deposits which do not drape the surrounding landscape and show variable thickness. Of the two PDC end-members, fully dilute currents will produce well sorted deposits with sedimentary structures such as cross bedding and anti-dunes, while granular-based currents will produce poorly sorted deposits without sedimentary structures. PDC-based tephra layers sourced in Iceland are typically not transported far and will not be identified at distal locations. Such tephra layers may however be of use as marker horizons in local terrestrial and marine tephrochronology studies. Ash Zones I and II, for example, are thought to source from large PDCs from the Katla and Tindfjöll volcanoes and their associated co-ignimbrite ash plumes (Lacasse *et al*. 1995).

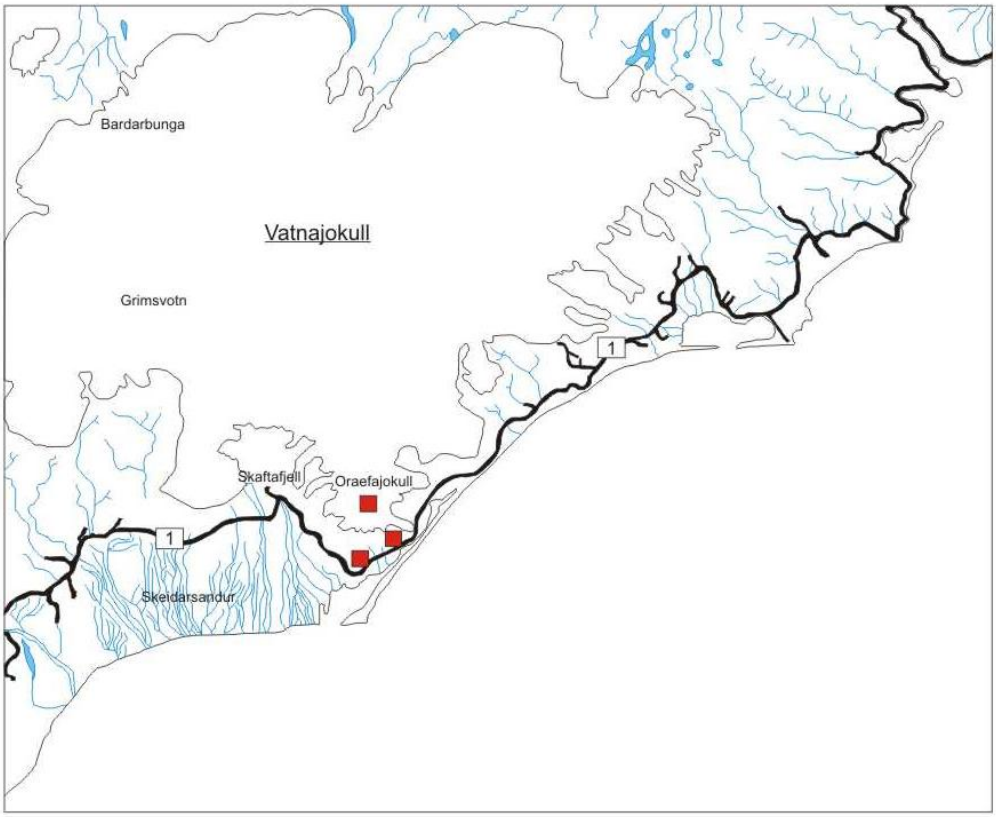

Figure 4.5: sample location map for the Öræfajökull samples collected for this thesis. Sampling locations are represented by red squares.

Following the logging, photographing and recording of each outcrop, the tephra layers were sampled so as to fully represent each eruption. Samples were collected at a selection of stratigraphic heights within each tephra layer to ensure representation of any variations. These inferred variations were based on visual observations during the logging process. Care was taken to ensure collection of the first erupted material at each site which is often inferred to correspond with material identified at distal locations across the North Atlantic.

4.3 Bulk Analyses

In this study, the term "bulk" refers to samples where whole pumice clasts have been analysed including glass, phenocryst and melt inclusion phases. Such data provides information regarding the final evolutionary state of a magma body.

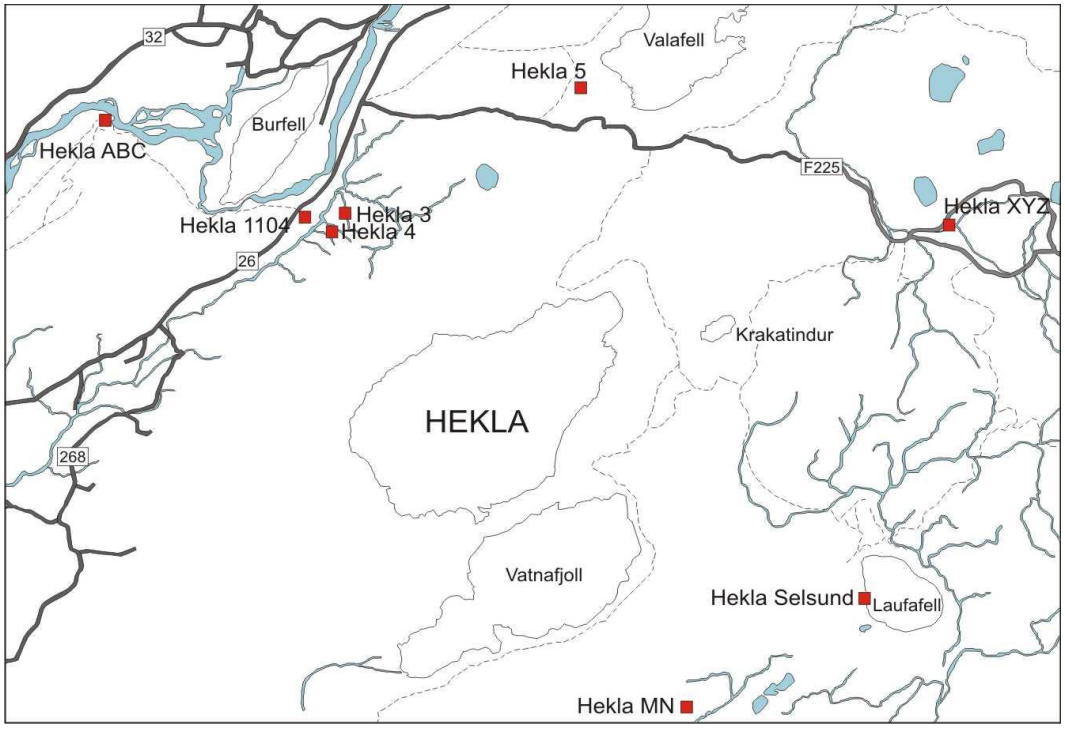

Figure 4.6: Map of the Hekla volcanic system. Red squares represent sampling locations for the Hekla tephra layers as noted on the image.

4.3.1 X-ray Fluorescence (XRF)

The XRF analytical method is used to investigate the bulk geochemistry of geological samples. The samples are irradiated with a beam of X-rays which excites electrons within the sample. This movement of electrons emits photons of energy which are detected by the analytical machines. Each element releases a distinct package of energy which can be identified by the analytical equipment and turned into information regarding element identity and concentration. The method is used to analyse major, trace and rare earth elements. The following sections describe overall sample preparation techniques and the methodology for fusing glass disks for major element data and pressing powder pellets for collection of trace and rare earth elements. Further information regarding XRF methodology can be found in Fitton *et al* (1998).

Sample Preparation: Samples were dried in a Gallenkamp hotbox oven at c. 70 ºC for a minimum of 24 hours before being sieved to remove the finer fractions. Smaller sub-samples were then individually hand-picked to select clean juvenile pumice samples for XRF preparation. All samples were ground into a fine powder to allow for the best analyses. The

samples were run through a crushing machine, to fragment the larger clasts. Samples were then placed into tungsten carbide grinding apparatus which in turn is placed into a milling machine for 4 minutes or until the samples had ground completely to a fine powder. A minimum of 10g of powder per sample was prepared in this way.

Fused Glass Disks: Prior to undertaking the glass disk lab work, samples were dried in an oven for a minimum of 2 hours at 120 ºC to ensure the loss of volatiles prior to disk fusion and Pt-5% Au crucibles were thoroughly cleaned in a HCL solution until all prior material has been dissolved. The following section details the exact methodology used for creating a fused disk.

Record the weight of the Pt-5% Au crucible to 4 decimal places. Add 0.95g of sample (S) to the crucible and record to 4 decimal places (UNIG). Ensure that samples are kept in a desecrator until required to ensure no interaction with external moisture sources. Add lithium borate (Li_2O_3) flux to the crucible on a 5:1 ratio (flux:sample). Stir the mixture thoroughly. Place the crucibles into a muffle furnace at 1000 ºC for 20 minutes to allow the mixture to melt. Extract the samples from the oven and allow to cool for 10 – 20 minutes. Typically, samples are fired in the oven for 20 minutes prior to the addition of flux to establish a value of loss on ignition (LOI), however this method resulted in re-crystallisation of unidentified solids when analysing rhyolitic samples and therefore was omitted in favour of a separate LOI analysis at the end of the session. When the samples are cooled, re-weigh and record the values to 4 decimal places. Add flux to the sample until pre-ignition weight is achieved. Place the crucible onto a Bunsen burner and melt the content. Swirl the mixture thoroughly to ensure homogenisation of the sample. When ready, pour the sample into a graphite mould and firmly compress using an aluminium plunger. Leave for 20 seconds before removing the aluminium plunger and allow the resultant fused glass disk to cool before labelling. The glass disk should measure c. 40 mm in diameter. To complete the missing LOI stage, weigh a crucible and record to 4 decimal places. Add 0.95g of sample to the crucible and record the combined weight to 4 decimal places. Place the crucible in the Lenton Thermal Design oven at 1000 ºC for 20 minutes then remove and allow to cool for a further 20 minutes. Weight the crucible and record the new weight to 4 decimal places (IG). The LOI value must be calculated in order to recover the final data from the sample set. To calculate the LOI use the equation:

$$\text{LOI (\%)} = 100 \times \frac{(\text{UNIG} - \text{IG})}{\text{S}}$$

Pressed Powder Pellets: Prior to sample preparation, samples were dried in an oven for a minimum of 2 hours at 120 ºC. All tools were washed in water and rinsed with Acetone to limit cross-contamination from previous studies. The following section details the exact methodology used for creating pressed powder pellets.

Record the weight of a glass beaker to 4 decimal places. Add 8 g of sample powder to the beaker and record to 4 decimal places. Add 8 drops of a 2 % aqueous solution of polyvinyl alcohol. Combine the mixture until a crumble-like texture has been attained and the polyvinyl has been spread throughout the sample. Place a 40 mm Al-cup into the tungsten carbide set and empty the beaker contents into the cup. Place the set-up into the SPEX 3630 X-PRESS hydraulic press and compress the sample at 0.6 tonnes/cm^2.

Both fused glass disks and pressed powder pellets were analysed using a Phillips PW2404 wavelength dispersive sequential X-ray spectrometer with an Rh-anode X-ray tube. The automated sample changer used was the Panalytical PW2540 VRC 168-position X-Y sample changer. Standards used during analyses are available in Govindaraju (1994). Corrections for matrix effects on intensity major element were applied using theoretical alpha coefficients calculated online using the Phillips software. Intensities of longer wave-length trace-element lines for matrix effects were corrected using alpha coefficients based on major element concentrations analysed with the pressed powder pellets. Matrix corrections were applied to the other trace element lines using the count rate from the RhKα Compton scatter line as an internal standard. Line-overlap corrections were applied using synthetic standards (Fitton *et al*. 1998).

4.4 Glass Analyses

In this study, the term “glass” refers to samples where analyses have focused onto clean amorphous quenched melt with no phenocryst or melt inclusion phases. Such data provides information regarding the final geochemical state of the liquid magma body. This section details the analytical techniques applied to data collection in this project including electron micro probe analyses, ion probe analyses and laser ablation inductively coupled plasma mass spectrometry analyses. The analytical set up for each technique is presented. Sample

preparation is described below as each technique uses the same sample set for comparable grain by grain analyses.

Sample Preparation: Samples were dried in a Gallenkamp hot box oven at c. 70 ºC for a minimum of 24 hours before being sieved to collect the 1Φ fraction. This fraction was selected as it would provide samples small enough to represent tephra grains found at medial to distal localities whilst also being large enough to allow grain by grain analyses using multiple techniques. Samples were individually hand-picked to select clean juvenile pumice and obsidian clasts for analyses. The grains were picked so as to represent the inferred range of chemistries for each deposit; however the main focus was on the rhyolitic clasts as these are the dominant focal point of the overall study. Lithic clasts and crystals were discarded as their analysis would not provide any data with tephrochronological applications. Samples were then placed into a 25.5 mm diameter disk and set with epoxy resin taking care to in-fill any vesicles or gaps with resin. Each disk was polished with 6 µm and 1 µm diamond pastes to ensure minimal topography to each sample and to present fresh surfaces for analyses. Each sample was photographed and digitally mapped using a Leica microscope, which were used to record the location of each individual grain analysis by electron microprobe and subsequent analyses using other techniques. Samples were coated prior to analyses with appropriate material: EMPA samples were coated with carbon using an Edwards Carbon Coater and ion probe samples were coated with gold using a BalTek SCD 050 gold coater.

4.4.1 Electron Micro Probe Analyses (EMPA)

The EMPA analytical method is used to investigate the glass geochemistry of geological samples. The samples are irradiated with a beam of electrons which excites electrons within the sample. This movement of electrons emits photons of energy which are detected by the analytical machines. Each element releases a distinct photon, and therefore the analytical equipment is able to identify the elements present and their concentrations. The method is used to analyse major elements. The following sections describe overall sample preparation techniques and the methodology for analysing pumice grains for major element data. Further information detailing the EMPA methodology used in this thesis can be found in Haywood (*submitted*).

Major element data used in this project was collected using a standardised EMPA technique. The set up was designed to minimise the loss of mobile elements during analyses, especially

Na (Hayward, *submitted*). Analyses were conducted on the Cameca SX100 electron microprobe at the University of Edinburgh. A standard wavelength dispersive setting was used at an accelerating voltage of 15 kV and a beam current of 2nA for major elements (Si, Al, Fe, Mg, Ca, Na, K) and 80 nA for trace elements (Mn, Ti). Beam diameter was 5 μm, counting times were 20 s for all elements with the exception of Mn and Ti which were 50 s and 40 s respectively. Total analysing time was 5 minutes. The Lipari1 (rhyolite) and BHVO2g (basalt) glass standards were measured at regular intervals for quality control and to monitor instrumental drift. ZAF corrections were applied to the data using XPhi Cameca PeakSight software.

The EMPA set up used for this research project implements analytical conditions which minimise the potential for remobilisation and loss of volatile elements such as Na (Haywood, *submitted*). In addition to this, the inclusion of all ten major elements during analysis, rejection of analyses with totals less than 97.5 wt. % and no normalisation of data to anhydrous has resulted in exceptionally high quality data. This data is presented in Chapters 5 and 6.

4.4.2 Ion Probe Analyses (IP)

Trace and rare earth element data were collected using the Cameca ims-4f ion microprobe at the University of Edinburgh. Sample preparation followed the methodology detailed at the beginning of section 4.4. Prepared samples were bombarded with a 15kV primary O- ion beam while positive secondary ions were accelerated to 4500 V, with an offset of 75±5 V to suppress molecular ion interference. Beam current was maintained at 5±1 nA and rastered over a 20±5 μm area. Peak positions were verified before each analysis. Isotopes recorded in each analysis include (counting times are noted in brackets following each isotope): The following isotopes were analysed in each cycle of a 10-cycle run, with counting time in seconds given in parentheses: ^{26}Mg (2), ^{30}Si (2), ^{39}K (2), ^{49}Ti (2), ^{85}Rb (3), ^{88}Sr (3), ^{89}Y (5), ^{90}Zr (3), ^{93}Nb (5), ^{138}Ba (5), ^{139}La (5), ^{140}Ce (3), ^{141}Pr (5), ^{143}Nd (5), ^{149}Sm (8), ^{151}Eu (5), ^{154}Gd (3), ^{156}Gd (3), ^{157}Gd (5), ^{159}Tb (5), ^{161}Dy (5), ^{165}Ho (5), ^{167}Er (5), ^{169}Tm (5), ^{171}Yb (5), ^{175}Lu (5). Mass 130.5 was measured as background for 5 s in each cycle and was always zero. Counts were normalised to pre-determined ^{30}Si concentrations collected via EMPA and used to calculate absolute elemental concentrations in the glass phases. Oxide interference was monitored by measurement of ^{154}BaO/Ba and ^{156}CeO/Ce. Systematic drift was

monitored by daily analyses of the standard material NIST SRM610. Further information can be found in Hinton *et al* (1995).

4.4.3 Laser Ablation Inductively Coupled Plasma Mass Spectrometry Analyses (LA-ICP-MS)

The LA-ICP-MS analytical method is used to investigate the trace and rare earth element glass geochemistry of geological samples. The samples are irradiated with a laser beam to produce a vaporised solid. The sample is aspirated into a high temperature (c. 6000 ºC) Ar-based ICP at atmospheric pressures. This ionises the samples to single positively charged ions. The samples is then sucked into a high vacuum chamber and focused into a beam by a series of ionised lenses before entering a mass spectrometer. Further information regarding the LA-ICP-MS methodology is given in Pearce *et al* (2004, 2007).

LA-ICP-MS analyses were conducted on the Coherent GeoLas ArF 193 nm Excimer laser ablation system coupled to the Thermo Finnegan Element 2 sector field ICP-MS at the University of Aberystwyth. Trace element data was collected for individual shards using 20 μm and 10 μm diameter ablation craters at a laser energy of 10 Jcm^{-2} and a repetition rate of 5 Hz over a 24 second acquisition. Crater size was dependant on the amount of material available for analyses. The minor ^{29}Si isotope was used as the chosen internal standard, with concentrations for individual shards determined by EMPA. SiO_2 concentrations were normalised to an anhydrous basis for calibration, which was achieved using NIST SRM 612 with concentrations given in Pearce *et al*. (1997). A different calibration was used for the 20 μm or 10 μm diameter craters to overcome any analytical variation resulting from different crater sizes (Pearce *et al*. this volume). Further details of the set up procedures and discussion of the precisions and accuracies is given in Pearce *et al*. (1996, 1999, 2004, 2007).

4.5 Summary

The field methods, sample preparation and analytical techniques used in this research project have been described in this chapter. The application of these methods and techniques has resulted in incredibly high quality data which will be presented in the following chapters.

The major element data collected using XRF and EMPA techniques will be presented in Chapters 5 and 6. Trace element data collected via XRF, IP and LA-ICP-MS will be presented in Chapter 7.

Chapter 5:

Establishing Icelandic Tephra Provenance Using Major Element Chemistry

5.1 Introduction

Icelandic tephrochronology was developed by Thorarinsson and later Larsen who identified and correlated tephra layers using their physical characteristics and stratigraphic relations (e.g. Larsen and Thorarinsson, 1977). Identification of the Askja 1875 tephra layer in Norway (e.g. Thorarinsson, 1981) opened up the possibility of using Icelandic tephra layers to date and correlate Quaternary sequences across the North Atlantic region. At such distal localities, physical characteristics and stratigraphic relations are unreliable tools for identification, as the tephra layers or micro-tephra horizons are often thin and discontinuous, comprising tephra shards < 100 micro metres in diameter. As discussed in Chapter 3, not all tephra layers are transported to far-distal localities and fewer still are preserved in the sedimentary record, thus making stratigraphic relations more challenging. Originally the identity of micro-tephra horizons was typically established by studying the refractive indices of individual shards.

The application of analytical geochemistry, in particular the electron microprobe, to the study of tephrochronology has opened up the possibility of identifying tephra layers by means of their geochemical composition, thus negating the issues associated with the previous techniques. The method focuses on collecting major element data for individual shards of glass, and is non-destructive, relatively fast and cheap. Evidence indicates that major element composition is sufficient to discriminate between volcanic systems within Iceland as many systems have an individual geochemical fingerprint or signature, resulting from the combined tectonic and magma generating processes occurring within each system (Dugmore, 1989; Larsen *et al*. 1999, 2001).

Identification of tephra provenance using geochemical analysis in conjunction with other multi proxy data is now an accepted technique in the Quaternary science community. However work can often be conducted without a robust reliable reference database. Most workers use their own "reference" data collected during previous studies. Using such data allows for the propagation of a tephra mis-identification at any stage through any subsequent studies, providing incorrect results.

The main aims of this chapter are as follows:

1. To locate appropriate proximal reference sections for a sequence of Holocene silicic Icelandic "marker" tephra layers and to present field data including sedimentary logs and field photographs of each tephra layer.
2. To present a robust reference dataset for key silicic marker layers from Iceland using a major element chemistry collected by electron microprobe (EMPA) and x-ray florescence (XRF) at the University of Edinburgh.
3. To use the data to establish a logical and systematic methodology for tephra provenance identification.

This chapter will focus on data collected from the Torfajökull, Askja, Katla and Öræfajökull volcanic systems. Hekla data is discussed; however data is presented separately in Chapter 6 where Hekla is used as a case study. Background information on each of the volcanic systems and individual tephra layers is presented in Chapter 2. Details of field sampling methods and analytical techniques are described in Chapter 4.

5.2 Results

This section presents the field and chemical data for the volcanic systems noted in Table 5.1 and their associated tephra layers with the exception of the Hekla volcanic system and its tephra layers. Hekla results are presented separately in Chapter 6 as an independent case study. Where more than one tephra layer is sourced within a volcanic system, each tephra layer is described separately under the initial system sub-heading (e.g. the Torfajökull sub heading will discuss both the Landnám and the Grákolla tephra). Field data includes field-based outcrop descriptions and interpretations, sedimentary logs of the reference sections and photographs of the outcrop. Chemical data includes tabulated EMPA and XRF data and

descriptions of the geochemistry aided with graphical figures. Note that geochemical data is presented as averages with 2σ values. Full data sets are available within the Appendix.

5.2.1 Torfajökull

The Torfajökull volcanic system is the source for both the silicic component of the Landnám and Grákolla tephra layers aged 1079 BP and 1800 BP respectively. Here, we present field and chemical data collected for these tephra layers.

5.2.1.1 Landnám Tephra Layer – Silicic Component

Field Data: The reference section for the Landnám tephra layer was selected at 63º 53.046'N 19º 28.992' E near Ljósárfjöll and Hrafntinnuhraun (Table 4.1, Fig. 4.2). Figure 5.1 is a stratigraphic log of the tephra layer compiled at this location while figure 5.2 is a set of field photographs of the tephra layer at the reference section. At the reference section, the tephra layer is 2.73 m thick (Fig. 5.1). The tephra layer is dominated by white rhyolitic pumice clasts, whilst at other locations in Iceland the layer has a mafic top, characterised by its prominent plagioclase crystals. The upper mafic component will not be discussed in this project as the focus of work is on the silicic to intermediate components. Despite its rhyolitic nature, the outcrop has an overall orange appearance caused by post-emplacement oxidation of the matrix ash. The oxidation of the pumice is superficial as fresh surfaces are un-affected. The tephra layer contains three distinct packages: Phase I, II and III which will be discussed individually below.

Phase III of the eruption is 0.73 m thick and dominated by dark grey rhyolitic pumice clasts. The tephra layer shows internal layering but no other depositional structures. Grain size is very coarse lapilli while average clast size is c. 4 cm. Maximum clast size is c. 20 cm due to the inclusion of pumiceous bombs. The lower 0.03 m of Phase III is a medium grade ash. The tephra layer is dominantly clast supported and poorly sorted. Pumice clasts are sub-angular and show no evidence of re-working. Phase III contains juvenile obsidian clasts and hydrothermally altered lithic clasts.

Phase II of the eruption is 1.1 m thick and dominated by pale grey rhyolitic pumice clasts.

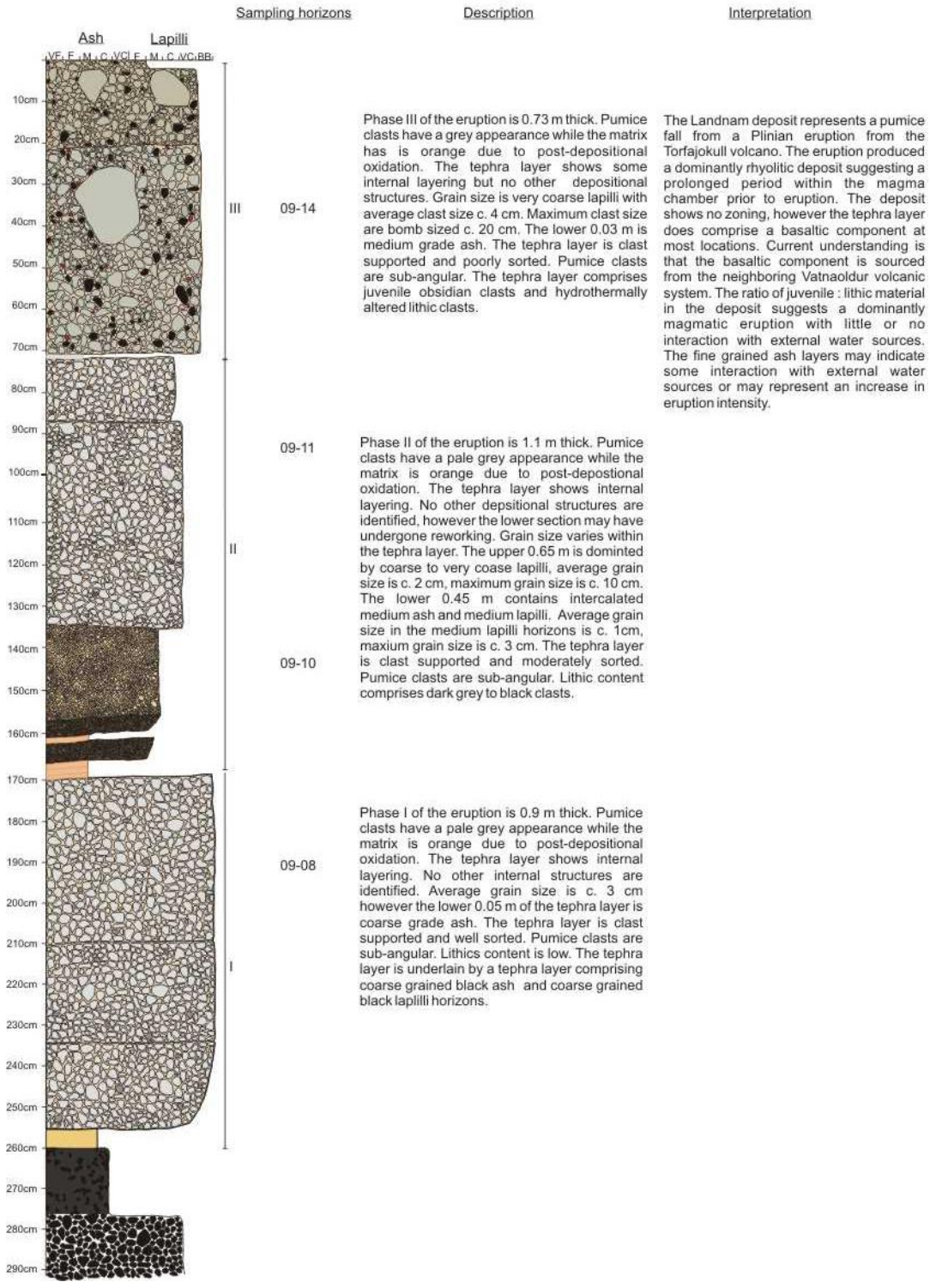

Figure 5.1: Stratigraphic log of the silicic component of the Landnám tephra showing physical characteristics e.g. colour, grain size and clast morphology. Drawn at the reference section near Hrafntinuhraun.

a)

b)

c)

Figure 5.2: Field photographs of the Landnám tephra layer. a) Base of the tephra layer overlying a coarse black tephra. Scraper measures c. 35 cm. b) Coarse rhyolitic pumice and obsidian clasts. Pen used as scale measures c. 10 cm. c) Outcrop at sampling location near Hrafntinuhraun. Shovel used as scale measures c. 75 cm. Photographs: Rh. Meara.

The tephra layer shows internal layering but no depositional structures, however the lower 0.35 m may have undergone some re-working. Grain size varies within the tephra layer. The upper 0.65 m of Phase II is dominated by coarse to very coarse lapilli. In this section, average grain size is c. 2 cm and maximum clast size is c. 10 cm. The lower 0.45 m contains intercalated medium ash and medium lapilli horizons. Average grain size in the lapilli phases is c. 1 cm and maximum clast size is c. 3 cm. The tephra layer is clast supported and moderately sorted. Pumice clasts are sub-angular. Lithic content includes dark grey to black clasts.

Phase I of the eruption is 0.9 m thick and is dominated by pale grey rhyolitic pumice clasts. The tephra layer shows internal layering but no other depositional structures. Grain size is very coarse lapilli. Average clast size is c. 3 cm; maximum clast size is c. 15 cm. The lowermost 0.05 m of the tephra layer is a coarse grade ash. The tephra layer is clast supported and well sorted. Pumice clasts are sub-angular. Lithics content is minimal, those identified are dark grey to black clasts. The tephra layer is underlain by a coarse grained black ash and a coarse grained black lapilli tephra layers.

The silicic component of the Landnám deposit represents a pumice fall from a Plinian eruption from the Torfajökull volcano. The eruption produced a dominantly rhyolitic deposit suggesting a prolonged period of repose prior to eruption. The deposit shows no zoning, however the tephra layer does comprise a mafic component at most locations. The basaltic component is sourced from the neighbouring Veiðivötn volcanic system. The ratio of juvenile:lithic material in the deposit suggests a dominantly magmatic eruption with little or no interaction with external water sources. This may vary in Phase III of the eruption which shows an increase in lithic material. The coarse grained ash layers may represent temporal increases in eruption intensity. The grain size distributions suggest that the early and final were the highest intensity. These grain size variations may also be the result of variations in wind direction and intensity and cannot be ruled out without investigation of multiple reference sections, which was outside the scope of this project.

Chemical Data: In total, six samples were analysed for the Landnám tephra layer collected from one sampling location. The new major element data collected via EMPA and XRF for the tephra layer is presented in Tables 5.1 and 5.2. The tephra layer shows two main geochemical sub-groups at the sampling location: a high silica and low silica phase. The chemical characteristics of the tephra layer are shown by figures 5.3 to 5.7. The tephra layer

Table 5.1: Glass chemistry of the silicic component of the Landnám tephra layer. Samples were collected near Ljósárfjöll and Hrafntinnuhraun c. 15 km north-west of the summit of Torfajökull. Ten electron probe analyses were collected for each sample and the data presented is the average of these analyses with two standard deviations. The complete data set is included in the Appendix.

Sample	SiO_2	TiO_2	Al_2O_3	FeO	MnO	MgO	CaO	Na_2O	K_2O	P_2O_5	Total
09-08w	70.79	0.25	14.21	2.36	0.08	0.22	0.90	5.19	4.60	0.03	98.62
2 σ	0.76	0.07	0.18	0.36	0.02	0.04	0.11	0.17	0.22	0.02	1.00
09-10w	70.75	0.26	14.26	2.34	0.08	0.23	0.88	5.08	4.66	0.03	98.58
2 σ	0.90	0.05	0.53	0.18	0.01	0.04	0.06	0.23	0.18	0.01	1.04
09-11w	70.81	0.25	14.11	2.33	0.07	0.24	0.87	5.21	4.64	0.03	98.58
2 σ	0.69	0.04	0.41	0.34	0.02	0.05	0.07	0.25	0.16	0.01	0.93
09-11b	45.53	2.55	15.41	12.72	0.20	7.28	10.69	2.59	0.40	0.22	97.60
2 σ	0.50	0.17	0.54	0.60	0.01	0.17	0.13	0.13	0.06	0.02	0.92
09-14w	70.87	0.25	14.29	2.23	0.08	0.24	0.85	5.18	4.6	0.03	98.63
2 σ	0.72	0.08	0.54	0.31	0.01	0.05	0.10	0.26	0.20	0.01	1.24
09-15w	70.83	0.26	14.17	2.23	0.08	0.23	0.87	5.12	4.66	0.03	98.47
2 σ	1.14	0.07	0.35	0.34	0.01	0.06	0.09	0.26	0.19	0.01	1.26

Table 5.2: Whole rock chemistry for the silicic component of the Landnám tephra layer. a) Samples were collected near Ljósárfjöll and Hrafntinnuhraun c. 15 km north-west of the summit of Torfajökull.

Sample	SiO_2	TiO_2	Al_2O_3	FeO	MnO	MgO	CaO	Na_2O	K_2O	P_2O_5	Total
09-08w	69.26	0.28	14.50	3.16	0.07	0.35	1.04	5.42	4.44	0.05	99.97
09-11w	69.52	0.29	14.44	3.19	0.08	0.31	0.96	5.02	4.47	0.04	99.74
09-14w	69.21	0.29	14.33	3.32	0.07	0.27	1.04	5.25	4.41	0.05	99.62
09-15w	69.47	0.31	14.35	3.17	0.07	0.33	0.95	5.18	4.54	0.05	99.63

has both a rhyolitic and a basaltic glass composition while the bulk composition is rhyolitic (Fig 5.3). The tephra layer is metaluminous (Fig. 5.4). The silicic phase of the tephra layer exhibits a restricted compositional range with minimal geochemical variation with stratigraphic height (Fig. 5.7) with the exception of a small sub-set of mafic grains taken at sampling height 09-11. The tephra layer shows a high alkaline nature as indicated by the compositional fields suggested in Rollinson (1993) and references therein. Deviation of the basaltic data set from the Torfajökull trend in Fig. 5.6 confirms the suggestion of interaction between two volcanic systems during the eruption.

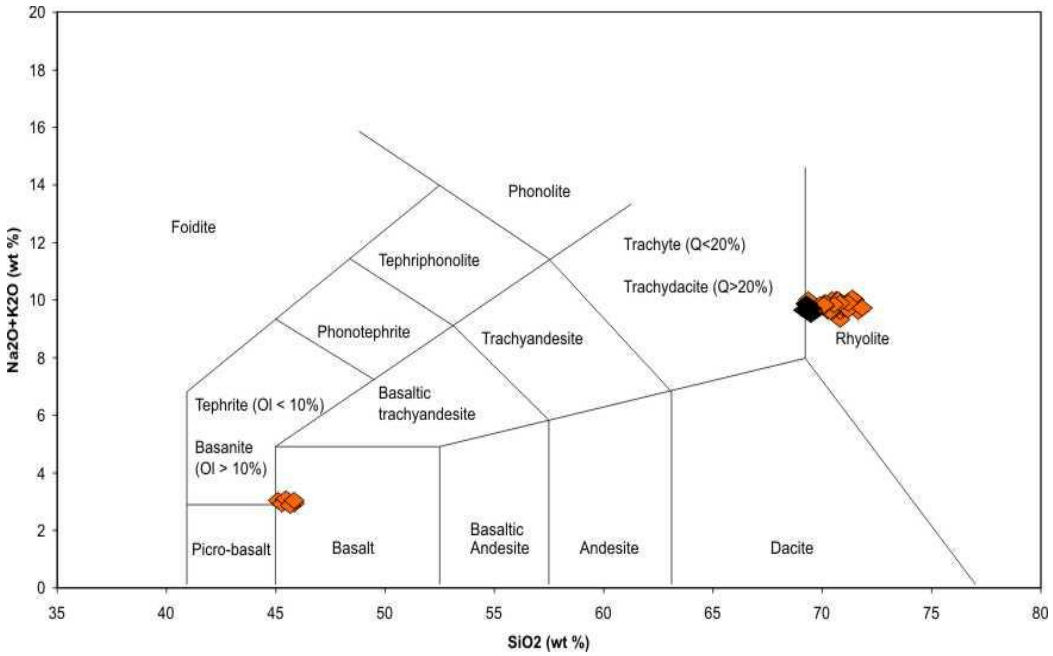

Figure 5.3: Total Alkali – Silica bivariate plot of the silicic component of the Landnám tephra layer. Orange diamonds represent EMPA data while black diamonds represent XRF data. Data indicate that the tephra layer shows a bimodal geochemistry of rhyolite and basalt. Grid lines adapted from La Maitre *et al*. (1989).

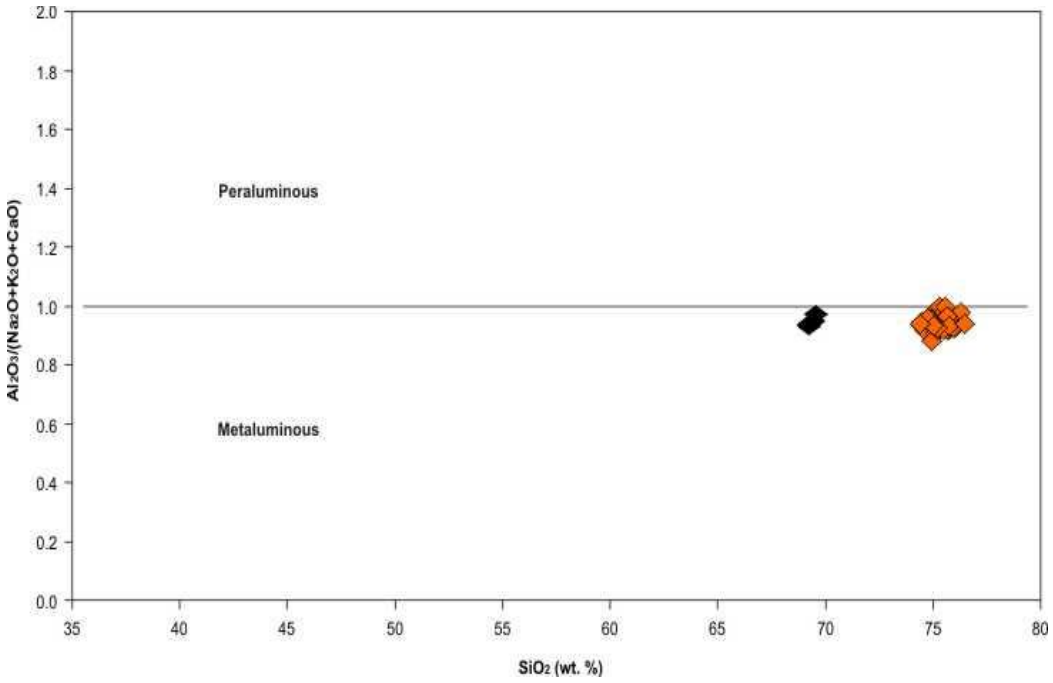

Figure 5.4: Silica – Aluminium and total alkali plot of the silicic component of the Landnám tephra layer. Orange diamonds represent EMPA data while black diamonds represent XRF data. Data indicate that the tephra layer shows a metaluminous geochemistry consistent with the geological setting.

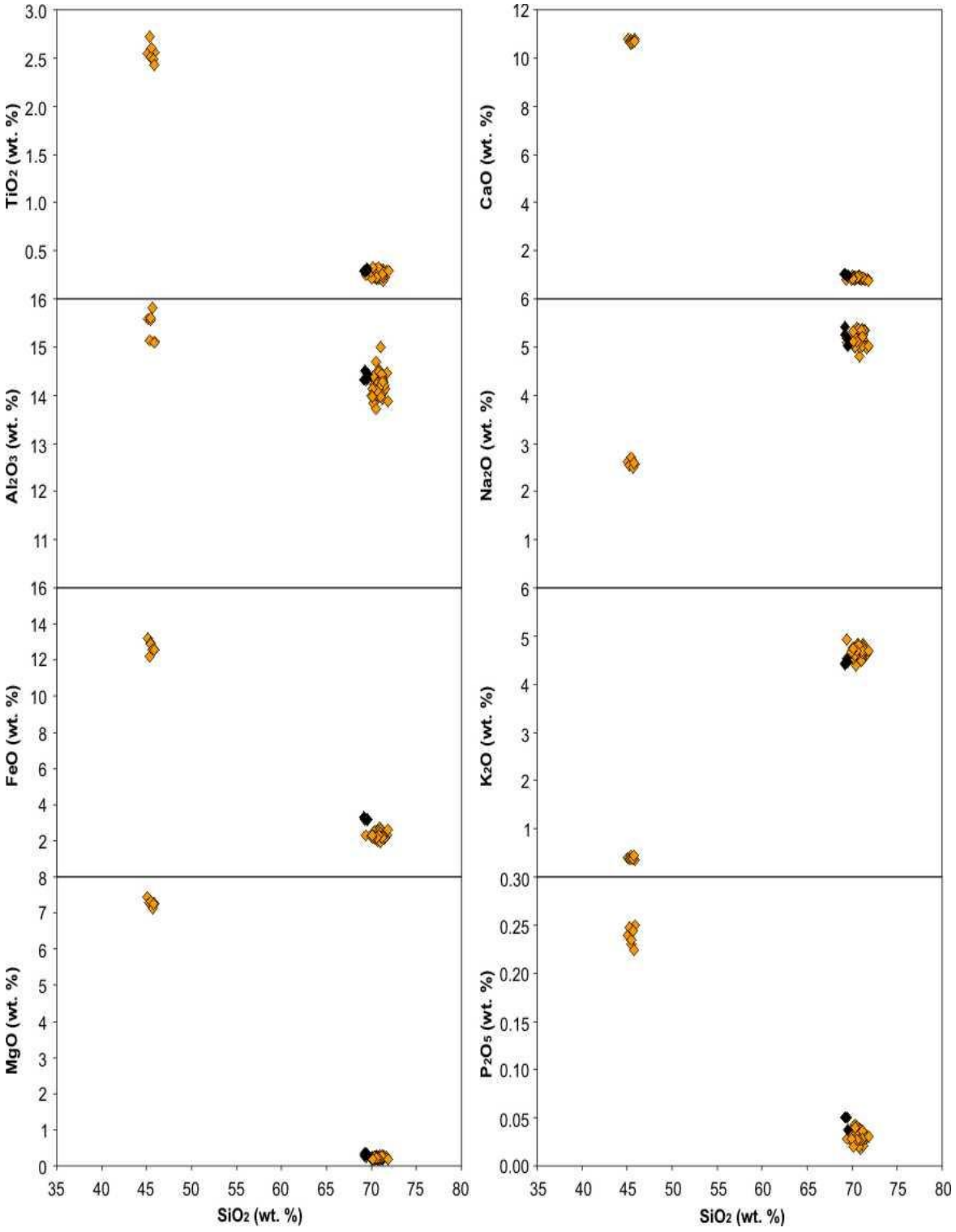

Figure 5.5: Bivariate plots of XRF and EMPA data for the silicic component of the Landnám tephra layer. Orange diamonds represent EMPA data whilst black diamonds represent XRF data. Very minor variations are recorded between XRF and EMPA data sets suggesting only minor amounts of fractional crystallisation prior to eruption.

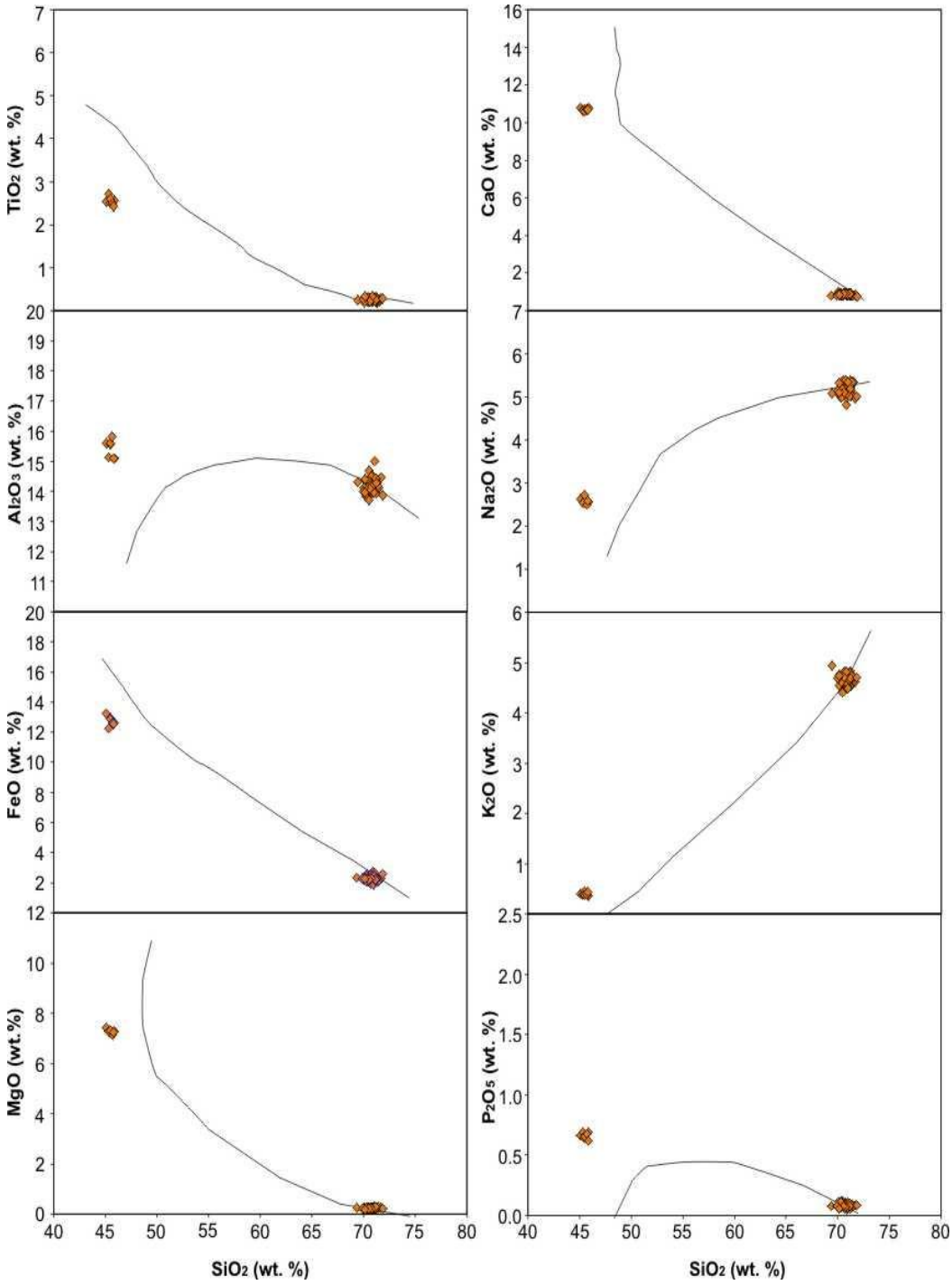

Figure 5.6: Harker plots of Landnám data plotted onto the crystallisation trends of major elements against SiO_2 (wt. %) for the volcanic system. Black lines represent data collected for the Torfajökull volcanic system by previous workers.

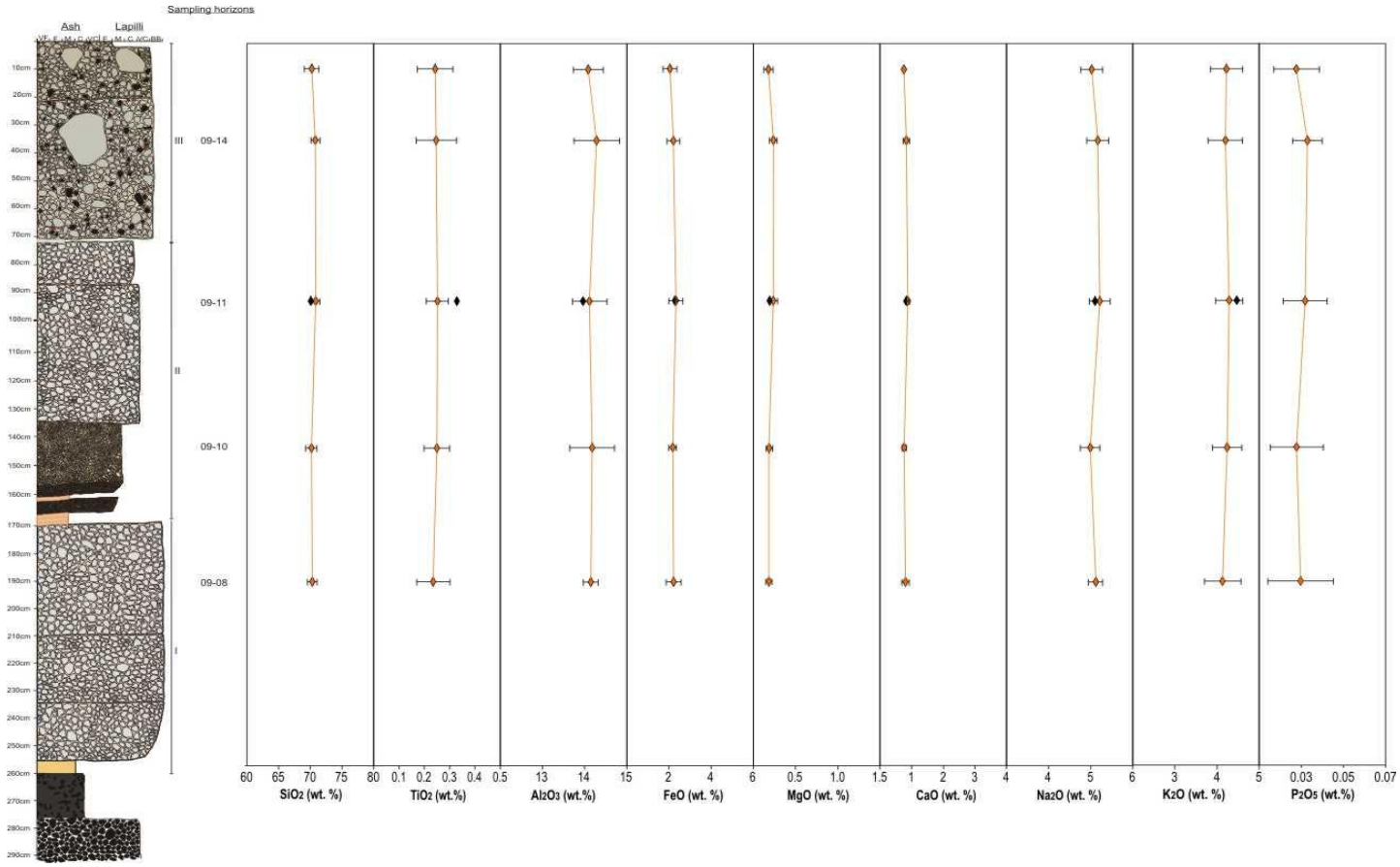

Figure 5.7: Chemical variation with stratigraphic height for the silicic component of the Landnám tephra. Elements depicted include the full range of elements analysed with the exception of MnO. Minor variation in elemental concentrations are seen in the tephra layer, mostly in phase III, however variations are within the error bars.

Comparing XRF and EMPA data highlights minor variation in SiO_2 concentrations between the data sets (Fig 5.5). Also highlighted are small increases in P_2O_5 concentrations in the XRF data compared with the glass data. These differences are the result of removal of these elements from the glass phase through fractional crystallization of apatite during melt generation.

5.2.2 Grákolla Tephra Layer

Field Data: The reference section for the Grákolla tephra layer was selected at 64º 02.123' N 19º 03.828'E on Grákolla Hill near Tjorvafell and Frostastadavatn, north of the Torfajökull volcanic complex (Table 4.1; Fig. 4.2). Figure 5.8 is a stratigraphic log of the tephra layer compiled at this location while figure 5.9 is a set of field photographs of the reference section. At this location, the tephra layer is 2.3 m thick. The tephra layer is dominated by alternating white and brown pumice layers. There are seven layers, however only three are studied in detail here due to constraints on fieldwork. The tephra layer contains three distinct packages: Phase I, II and III which will be discussed individually below.

Phase III of the eruption is 0.5 m thick and dominated by white to pale yellow pumice clasts. The tephra layer shows no obvious depositional structures. Grain size is medium to coarse lapilli while average clast size is c. 2.5 cm. Maximum clast size is c. 20 cm represented by pumiceous bombs. The bombs are shattered but retain their original shape, such as a jigsaw breccia. The tephra layer is moderately sorted and clast supported. The tephra layer comprises dark grey - black lithic clasts and juvenile obsidian fragments.

Phase II of the eruption is 0.8 m thick and dominated by dark brown pumice clasts. The tephra layer contains no obvious depositional structures. Grain size is medium lapilli. Average grain size is c. 2.5 cm and maximum clast size is c. 5 cm. The tephra layer is well sorted and clast supported. The tephra layer comprises mingled brown and white pumice clasts and white pumice clasts draped with a black tar-like substance at a height of 1 m (Figs. 5.11b and c). Pumice clasts are angular and comprise no obvious phenocryst phases.

Phase I of the eruption is 0.8 m thick and dominated by white to pale yellow pumice clasts. The tephra layer shows some internal layering but no other depositional structures. Grain size is medium lapilli in the lowermost 0.25 m of the tephra layer and coarse lapilli in the

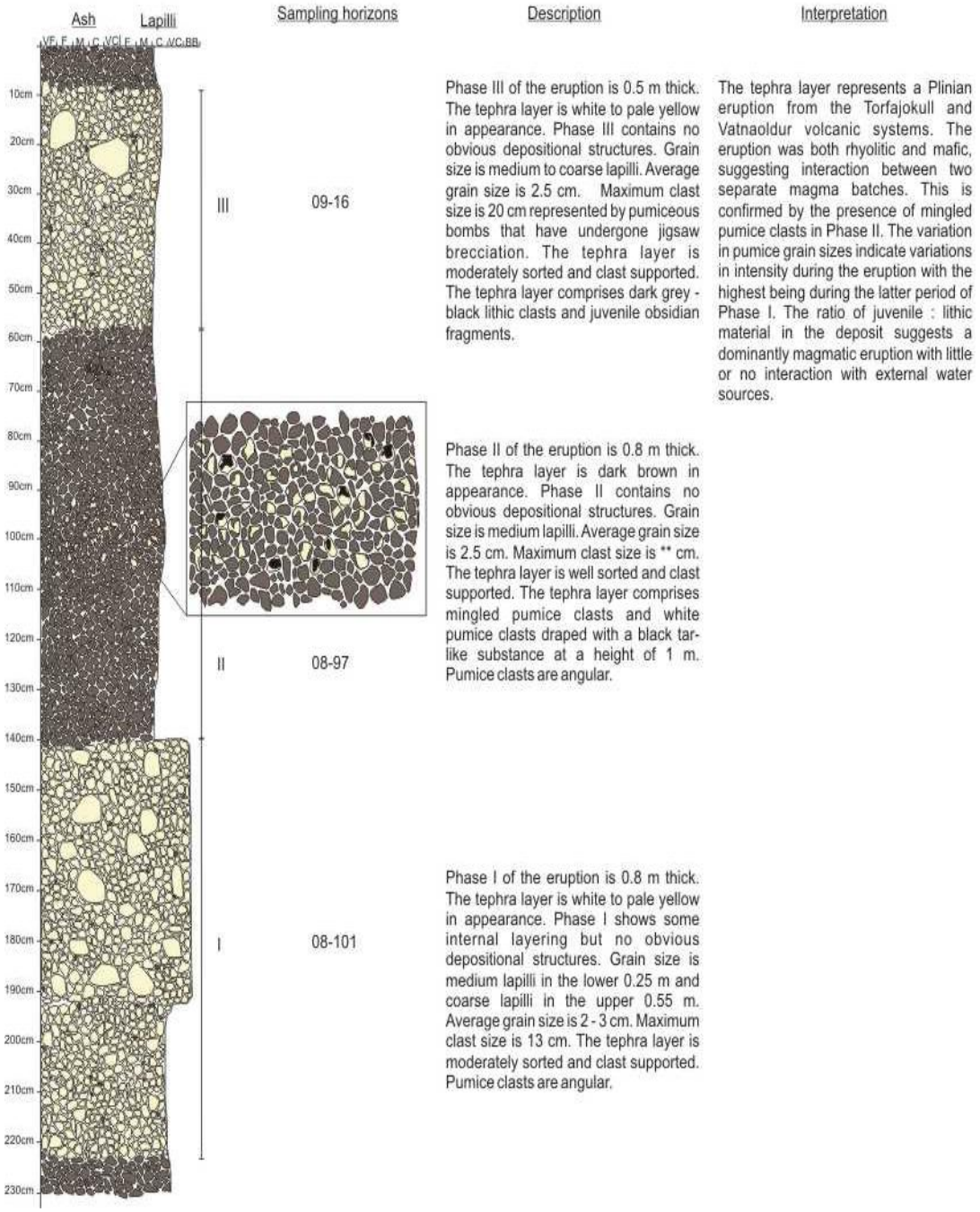

Figure 5.8: Stratigraphic log of the Grákolla tephra layer showing physical characteristics e.g. colour, grain size and clast morphology. Drawn at the reference section Grákolla hill near Tjörvafell and Frostastadavatn, north of the Torfajökull volcanic complex.

a)

b)

c)

Figure 5.9: Field photographs of the Grákolla tephra layer. a) Outcrop on the Grákolla Hill near Tjorvafell and Frostastadavatn, north of the Torfajökull volcanic complex. Person in the photograph measures c. 1.60 m. b) Rhyolitic pumice clast draped with black tar-like material. Pen used for scale measures c. 10 cm. c) Mingled pumice found within the deposit. Pen used for scale measures c. 10 cm. Photographs: Rh. Meara.

Table 5.3: Glass chemistry for the Grákolla tephra layers. Samples for the Grákolla tephra were collected from a section at Grákolla along route F225. Ten electron probe analyses were collected for each sample and the data presented is the average of these analyses with two standard deviations. The complete data set is available in the Appendix.

Sample	SiO_2	TiO_2	Al_2O_3	FeO	MnO	MgO	CaO	Na_2O	K_2O	P_2O_5	Total
09-16w	70.81	0.23	14.22	2.48	0.07	0.24	0.96	5.18	4.39	0.03	98.58
2 σ	2.44	0.10	1.18	0.38	0.01	0.05	0.27	0.51	1.11	0.02	1.00
09-16b	48.30	2.95	13.13	13.44	0.23	5.82	10.73	2.71	0.42	0.35	98.07
2 σ	2.51	2.66	0.97	1.97	0.03	1.62	1.63	0.74	0.53	0.48	1.24
08-97w	70.32	0.24	14.35	2.61	0.07	0.24	0.91	5.16	4.54	0.03	98.46
2 σ	0.83	0.07	0.62	0.49	0.02	0.08	0.16	0.13	0.18	0.01	1.17
08-97b	48.49	2.84	12.99	13.23	0.23	6.03	10.64	2.61	0.42	0.33	97.81
2 σ	2.24	2.61	0.92	1.78	0.02	1.73	1.84	0.78	0.54	0.46	1.21
08-101w	69.52	0.25	14.19	2.45	0.08	0.23	0.90	5.16	4.45	0.03	97.25
2 σ	5.50	0.11	1.05	0.36	0.01	0.04	0.12	0.50	0.36	0.01	7.46

Table 5.4: Whole rock chemistry for the Grákolla tephra layer. Samples for the Grákolla tephra were collected from a section at Grákolla along route F225.

Sample	SiO_2	TiO_2	Al_2O_3	FeO	MnO	MgO	CaO	Na_2O	K_2O	P_2O_5	Total
09-16b	55.51	1.19	14.62	10.48	0.16	4.83	8.23	2.97	1.63	0.12	99.92
08-97w	67.63	0.41	14.61	4.25	0.09	0.58	1.44	4.89	4.15	0.06	99.60

in the uppermost 0.55 m. Average grain size are 2 – 3 cm while maximum grain size is c. 13 cm. The tephra layer is moderately sorted and clast supported. Pumice clasts are angular.

The Grákolla deposit represents a pumice fall from a Plinian eruption from two interacting separate magma chambers, most likely within the Torfajökull and Vatnaöldur volcanic systems. The interaction of two separate magma bodies is confirmed by the presence of mingled pumice clasts (Fig. 5.9b) and the draping of white pumice clasts in Phase II of the eruption. The ratio of juvenile:lithic material in the deposit suggests a dominantly magmatic eruption with little or no interaction with external water sources. The coarse grained ash layers may represent temporal increases in eruption intensity. These grain size variations may also be the result of variations in wind direction and intensity and cannot be ruled out

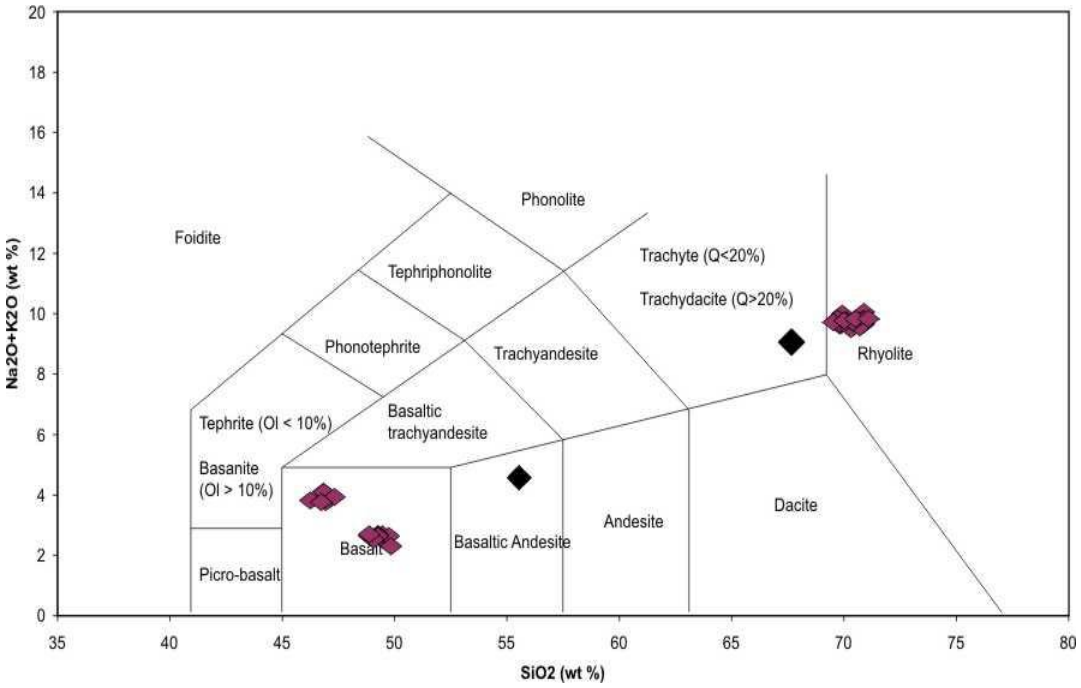

Figure 5.10: Total Alkali – Silica bivariate plot of the Grákolla tephra layer. Purple diamonds represent EMPA data while black triangles represent XRF data. Data indicate that the tephra layer shows a dominantly bimodal geochemistry with basaltic and rhyolitic components. One data point however suggests a basaltic andesite composition. Grid lines adapted from La Maitre *et al*. (1989).

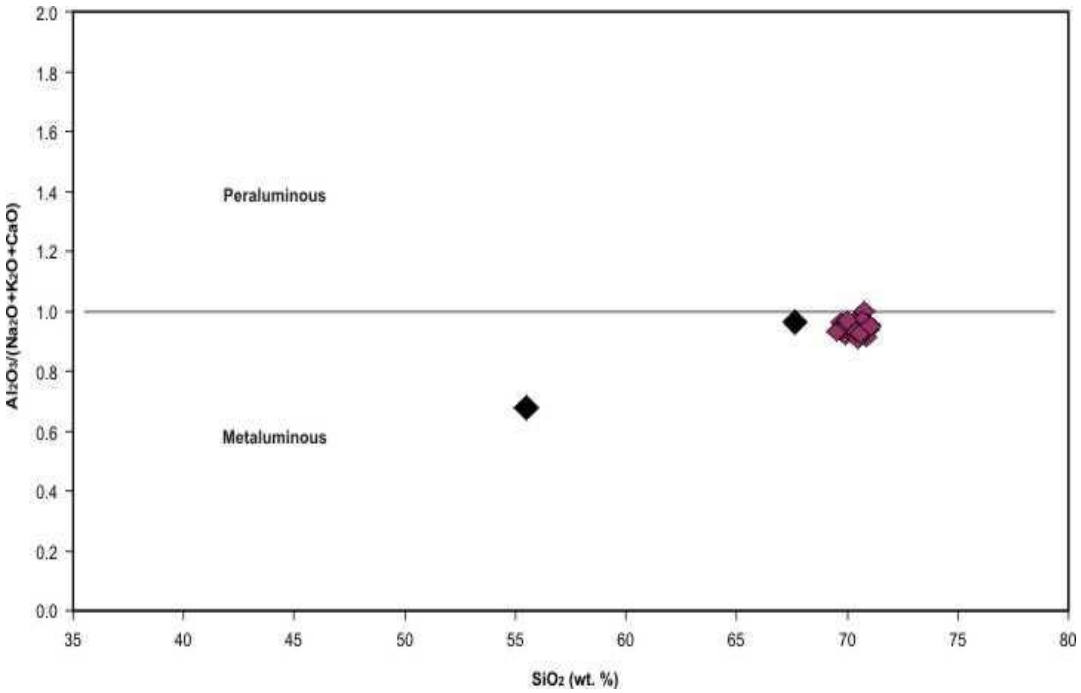

Figure 5.11: Silica – Aluminium and total alkali plot of the Grákolla tephra layer. Purple diamonds represent EMPA data while black triangles represent XRF data. Data indicate that the tephra layer shows a metaluminous geochemistry consistent with the geological setting.

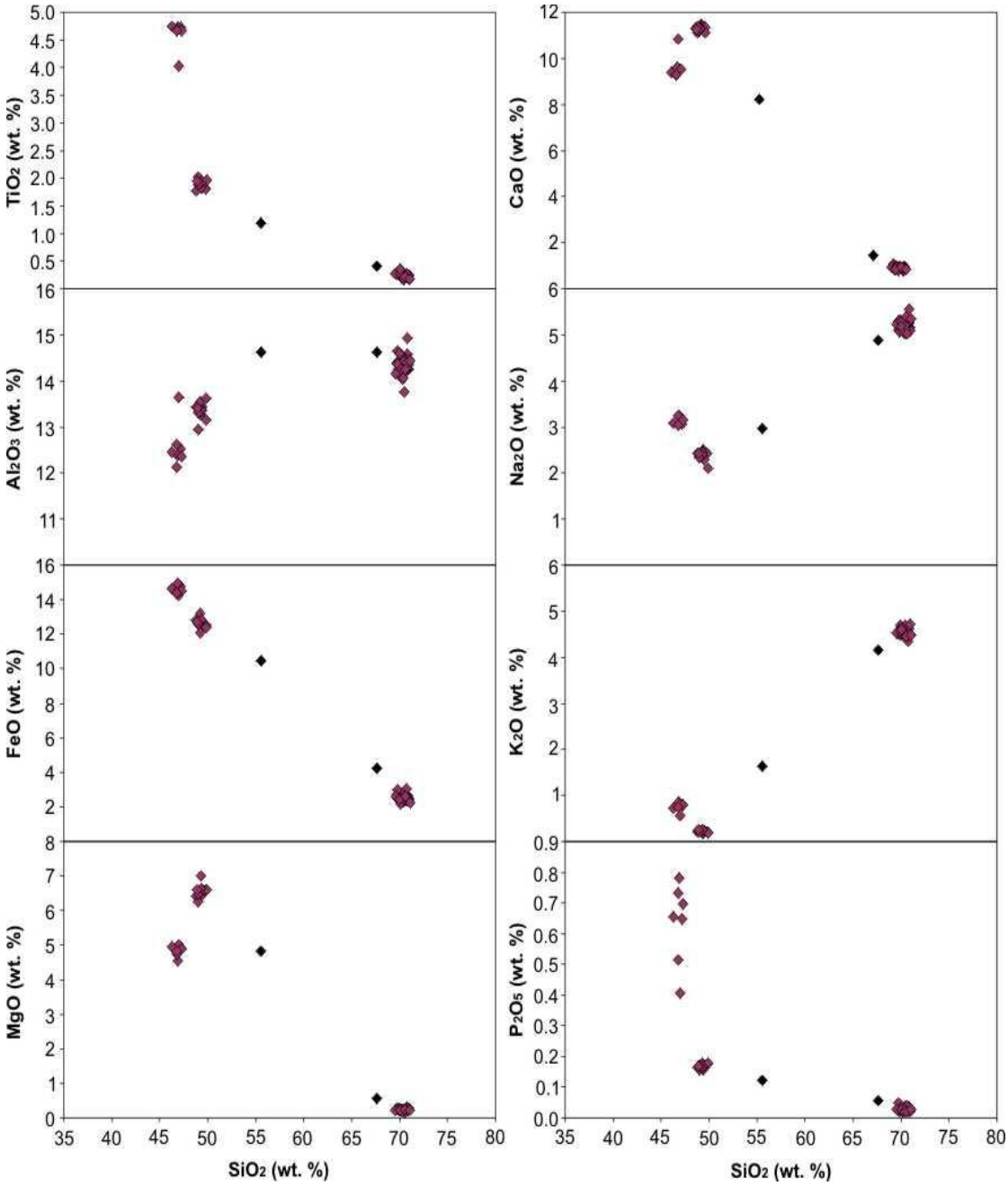

Figure 5.12: Bivariate plots of XRF and EMPA data for the Grákolla tephra layer. Purple diamonds represent EMPA data whilst black diamonds represent XRF data. Variations are recorded between XRF and EMPA data sets suggesting fractional crystallisation within the magma prior to eruption.

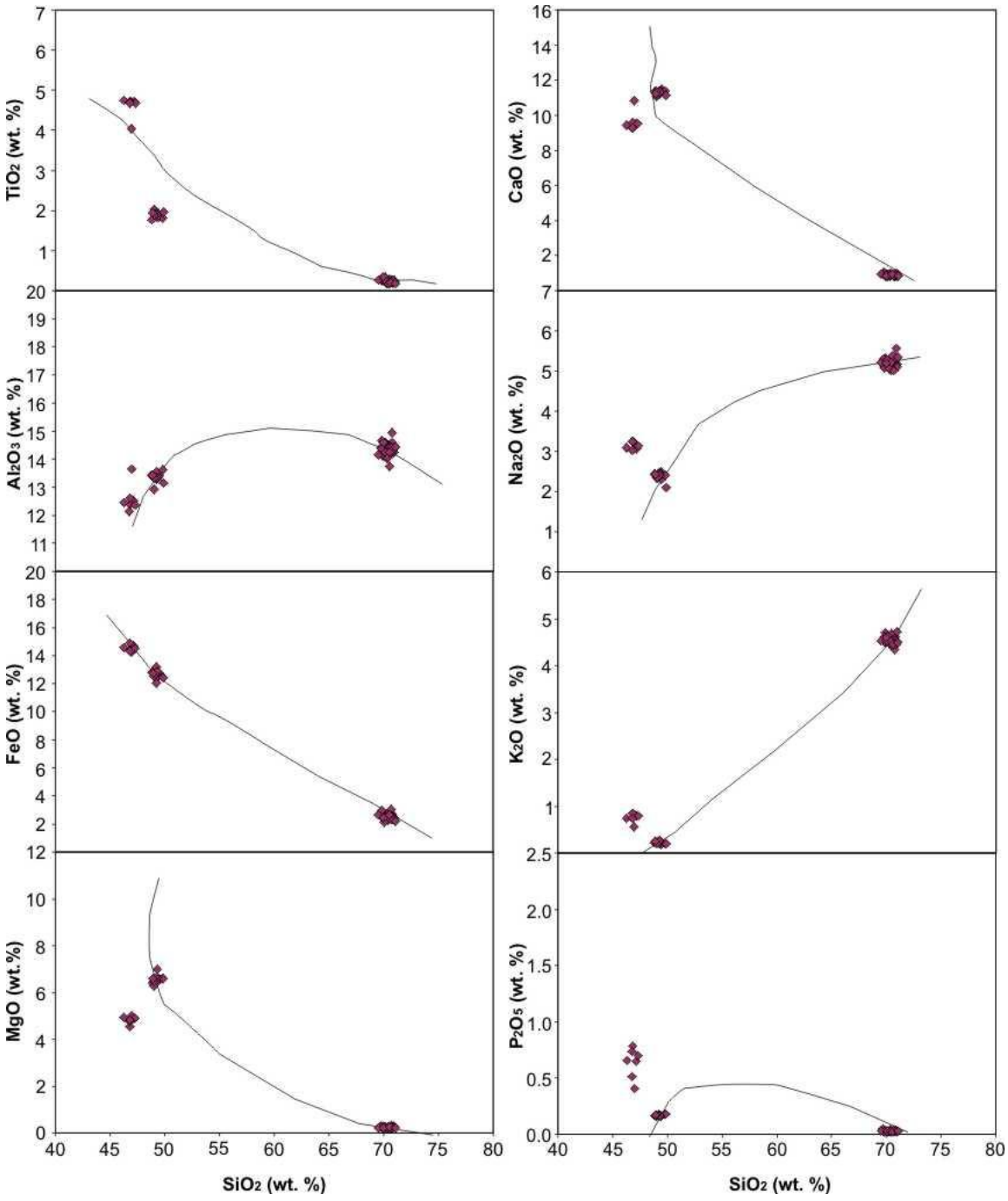

Figure 5.13: Harker plots for the Grákolla tephra layer plotted onto the crystallisation trends of major elements against SiO_2 (wt. %) for the volcanic system. Purple diamonds represent EMPA data while black triangles represent XRF data. Black lines represent data collected for the Torfajökull volcanic system by previous workers.

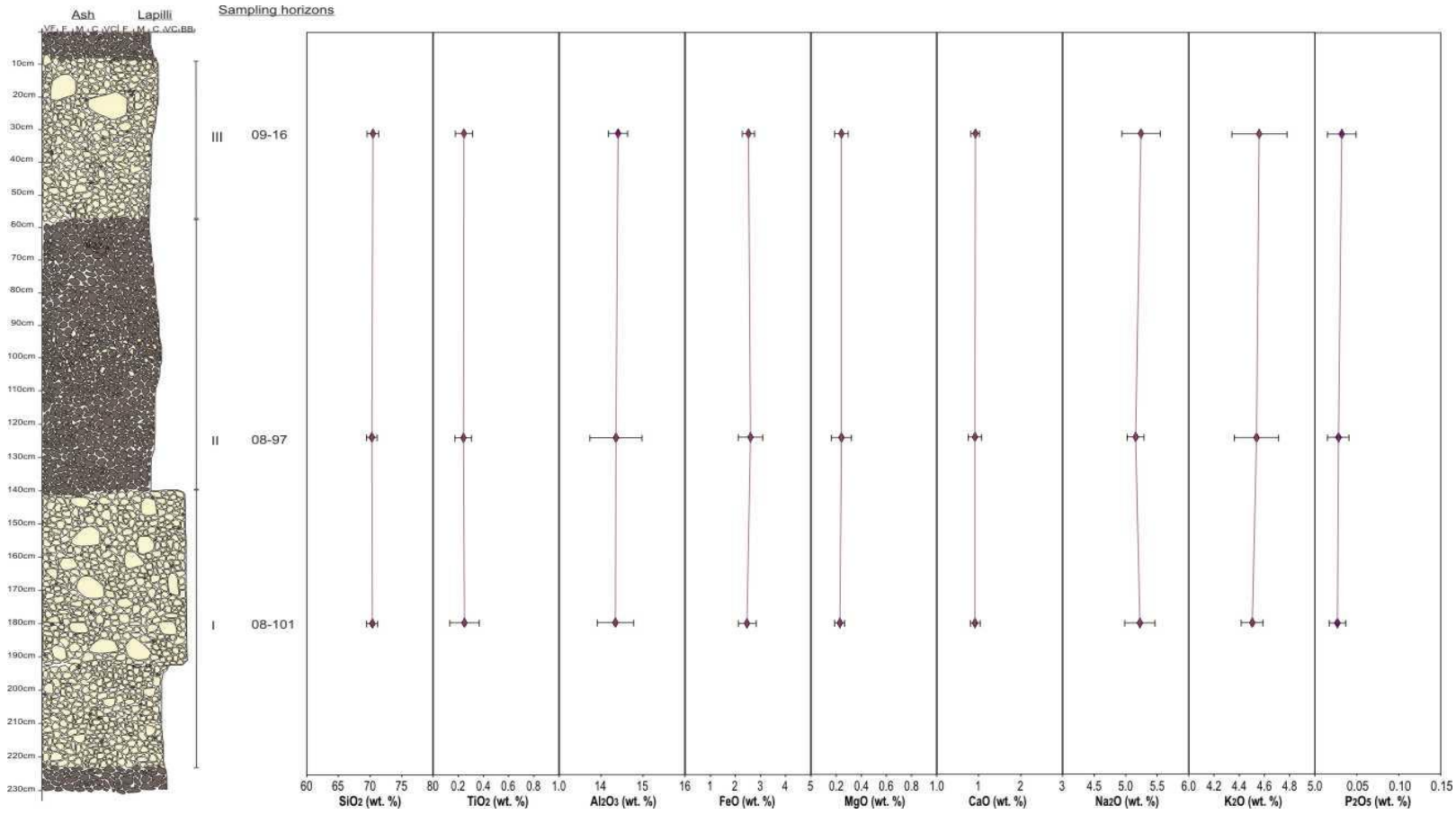

Figure 5.14: Chemical variation with stratigraphic height for the Grákolla tephra layer. Elements depicted include the full range of elements analysed with the exception of MnO. No major variations are recorded within the deposit despite the obvious changes in pumice colour

without investigation of multiple reference sections, which was outside the scope of this project.

Chemical Data: In total, five samples were analysed for the Grákolla tephra layer collected from the sampling location. The new major element data collected via EMPA and XRF for is presented in Tables 5.3 and 5.4. The tephra layer shows two main geochemical sub-groups at this location: a high silicic phase and a mafic phase. The chemical characteristics of the tephra layer are shown by figures 5.10 to 5.14. The tephra layer has both a rhyolitic and basaltic glass composition and a trachy dacite and basaltic andesite bulk composition (Fig 5.10). The tephra layer is metaluminous (Fig. 5.11). The tephra layer exhibits a restricted compositional range with no geochemical variation with stratigraphic height within the silicic phase (Fig. 5.14). The tephra layer shows a high alkaline nature as indicated by the compositional fields suggested in Rollinson (1993) and references therein.

Comparing XRF and EMPA data highlights variation in SiO_2 concentrations between the data sets (Fig 5.12). Also highlighted are minor increases in TiO_2, Al_2O_3, CaO and Na_2O as well as a more pronounced difference in FeO concentrations in bulk chemistry with respect to glass chemistry. These differences are the result of inclusion of phenocryst phases in the bulk phase, samples most likely pyroxenes, amphiboles, biotite mica, feldspars and quartz.

5.2.2 Askja

The Askja volcanic system is the source for the 1875 AD, 2100 BP and the 11000 BP Skolli tephra layers. The A1875 tephra layer is taken to represent the volcanic system. Field and chemical data collected for the tephra layer are presented in the following sections.

Field Data: The reference section for the Askja 1875 tephra layer was selected at 64º 02.571' N 19º 18.305' E to the north-north east of the Öskjuvatn caldera lake, next to the Víti geothermal crater (Table 4.1; Fig. 4.3). Figure 5.15 is a stratigraphic log of the tephra layer compiled at this location while figure 5.16 is a set of field photographs of the tephra layer at the reference section. At this location, the tephra layer is 5.5 m thick (excluding B-unit which is not found at this location). The tephra layer is comprised of three distinct packages: unit B, unit C_{1-2} and unit D_{1-5}. These packages will be discussed individually below.

The Units D_{1-5} are 2.9 m thick and comprise alternating layers of pale yellow-brown and dark

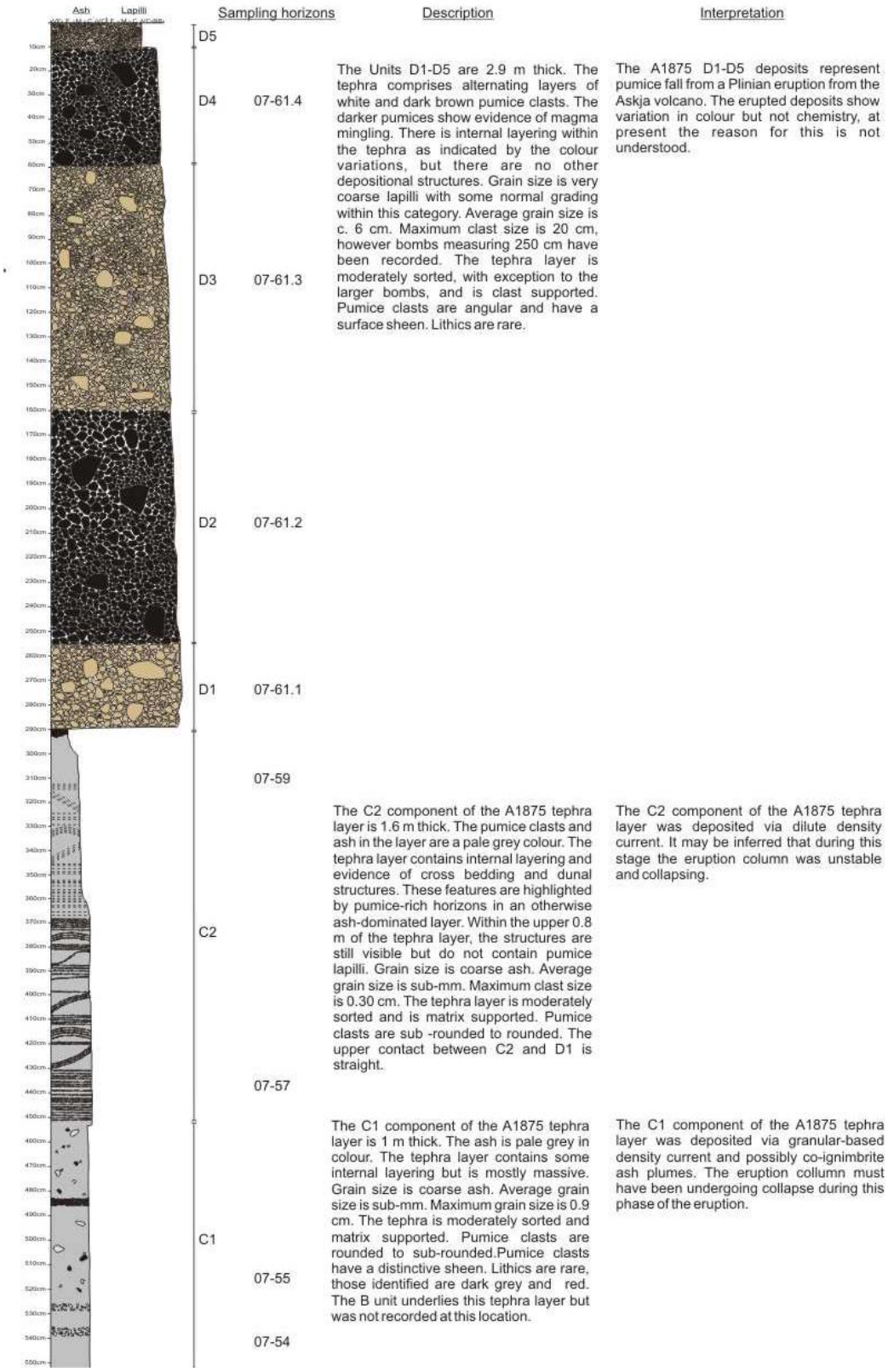

Figure 5.15: Stratigraphic log of the A1875 tephra layer showing physical characteristics e.g. colour, grain size and clast morphology. Drawn at the reference section in the Askja caldera near Öskjuvatn lake.

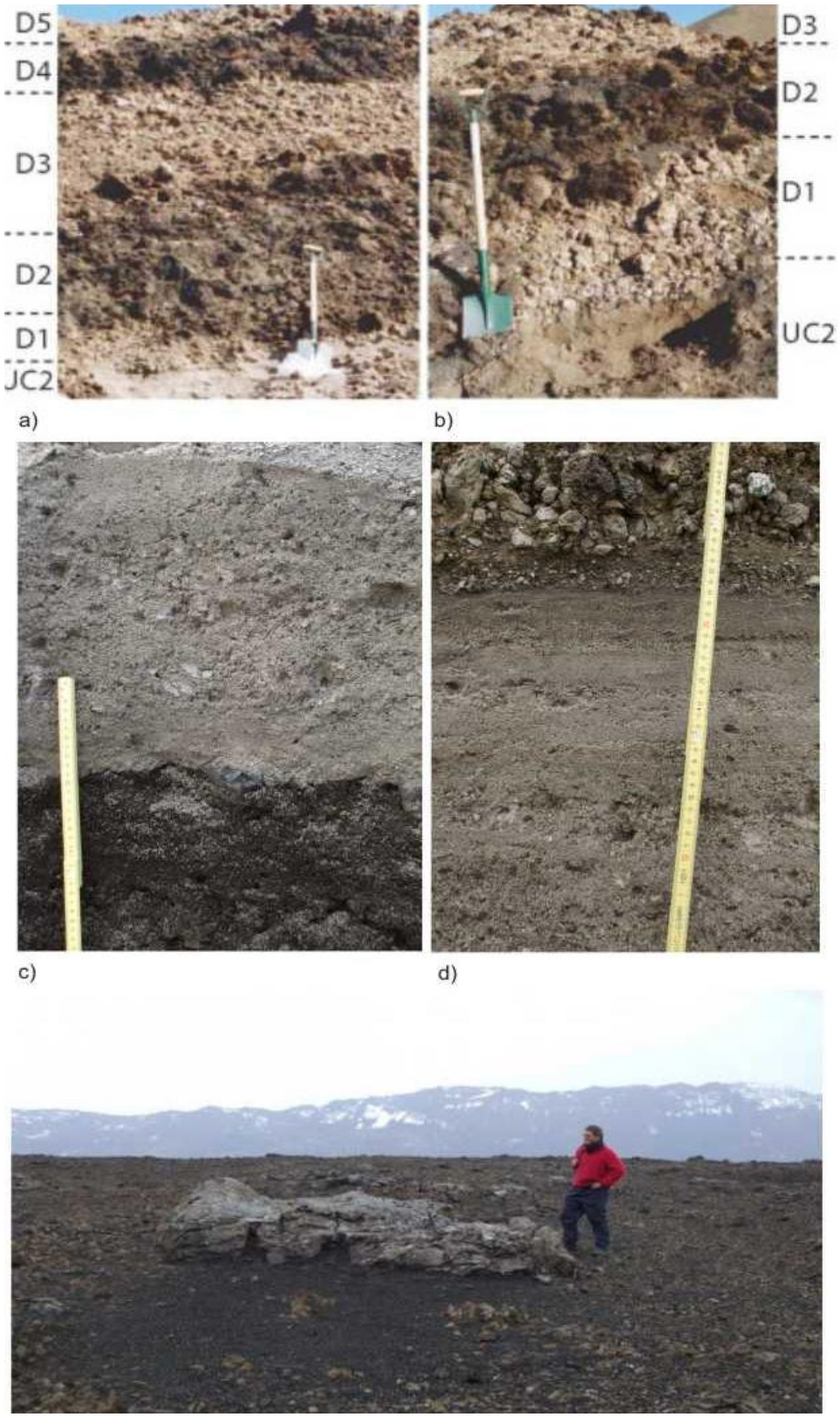

Figure 5.16: Field photographs of the A1875 tephra layer. a-b) A1875 $D_{1\text{-}5.}$ Shovel used for scale measures c. 75 cm. c) A1875 C_1. d) A1875 C_2. Scale bar shows 1 cm intervals. e) Pumice bomb above D_5 measuring c. 5 m. Photographs: a-b) R. Carey, c-e) Rh. Meara.

brown pumice clasts. The unit shows internal layering as defined by the changes in colour. The tephra layer shows some normal grading but no other depositional structures. Grain size is very coarse lapilli. Average grain size is c. 6 cm. Maximum clast size is c. 20 cm, however at other locations, pumice bombs are recorded measuring 500 cm (Fig. 5.16e). The tephra layer is moderately sorted and is clast supported. Pumice clasts are angular and have a recognisable surface sheen. The darker pumice clasts show evidence of magma mingling. Lithic clasts are rare.

The C unit is separated into C_1 and C_2. The C_2 component of the A1875 tephra layer is 1.6 m thick and dominated by pale grey ash. The unit shows internal layering and depositional structures such as cross-bedding and anti dunes. These features are visible throughout the tephra layer but are highlighted in the lower 0.8 m by concentrated horizons of fine grained pumice lapilli. Average grain size is in the coarse ash phase, maximum grain size is 0.30 cm. The tephra layer is moderately sorted and is matrix supported. Pumice clasts are sub – rounded to rounded. The upper contact between C_2 and the overlying D_1 is straight and shows no evidence of erosion. The C1 component of the A1875 tephra layer is 1 m thick and dominated by pale grey ash. The unit shows some internal layering but within packages is massive. Average grain size is coarse ash with a maximum grain size of 0.9 cm. The tephra is moderately sorted and matrix supported. Pumice clasts are rounded to sub-rounded. Pumice clasts have a distinctive sheen. Lithics are rare, those identified are dark grey and red.

The B unit underlies this tephra layer but was not recorded at this location.

The B, $C_{1\text{-}2}$ and $D_{1\text{-}5}$ units of the A1875 deposit represent the various phases of the eruption. The B unit represents the initial phase of the eruption and although not recorded here, is dominated by phreato-magmatic processes (Thordarson, pers com). The $C_{1\text{-}2}$ unit represent phases of plume collapse during the eruption. C_1 shows evidence of deposition via granular-based density currents while C_2 was deposited via dilute to fully dilute density currents. The $C_{1\text{-}2}$ tephra layers are only identified at very proximal locations within the Askja caldera and therefore do not present themselves to be long-distance marker horizons. The $D_{1\text{-}5}$ units represent pumice fall out from a Plinian eruption. The eruption produced dominantly rhyolitic tephra suggesting a prolonged repose period within the magma chamber before eruption. The prominent colour changes in the $D_{1\text{-}5}$ unit do not represent significant geochemical variation. The ratio of juvenile:lithic material in the deposit suggests a

Table 5.5: Glass chemistry of the Askja 1875 tephra units B, C and D. Samples were collected from proximal locations around Lake Öskjuvatn within the Askja caldera. Ten electron probe analyses were collected for each sample and the data presented are the average measurements and two standard deviations for these data points. Full data sets are available in the Appendix.

Sample	SiO_2	TiO_2	Al_2O_3	FeO	MnO	MgO	CaO	Na_2O	K_2O	P_2O_5	Total
07-61B	74.06	0.80	12.51	3.21	0.10	0.60	2.36	3.84	2.47	0.14	100.09
2 σ	1.18	0.08	1.12	0.50	0.01	0.10	0.70	0.38	0.24	0.02	0.70
07-54w	73.81	0.75	12.18	3.17	0.09	0.58	2.21	3.81	2.46	0.13	99.19
2 σ	1.77	0.10	0.70	0.49	0.02	0.12	0.36	0.14	0.18	0.03	1.78
07-54b	50.73	2.11	12.04	13.72	0.24	6.20	10.68	2.47	0.46	0.21	98.80
2 σ	1.73	0.25	5.65	2.48	0.02	5.09	6.05	1.42	0.23	0.03	1.24
07-55w	73.19	0.76	12.11	3.23	0.10	0.60	2.19	3.77	2.44	0.14	98.53
2 σ	1.60	0.08	0.36	0.32	0.02	0.07	0.23	0.13	0.16	0.02	1.43
07-55b	50.48	2.06	13.10	13.75	0.23	5.73	10.17	2.68	0.40	0.21	98.82
2 σ	0.95	0.26	0.62	1.59	0.02	0.96	1.11	0.26	0.16	0.04	1.05
07-57w	73.41	0.78	12.24	3.43	0.10	0.65	2.35	3.89	2.43	0.15	99.44
2 σ	1.34	0.10	0.63	0.48	0.02	0.17	0.49	0.18	0.12	0.05	1.21
07-57b	50.22	2.04	13.11	13.61	0.23	5.74	10.21	2.66	0.38	0.21	98.42
2 σ	1.31	0.30	0.64	1.06	0.02	0.94	1.28	0.17	0.20	0.03	0.75
07-59w	72.76	0.81	12.36	3.54	0.11	0.69	2.50	3.90	2.43	0.16	99.25
2 σ	0.94	0.07	0.45	0.23	0.02	0.08	0.22	0.16	0.12	0.01	0.84
07-59b	50.49	2.13	13.10	13.98	0.23	5.51	9.95	2.71	0.47	0.21	98.78
2 σ	1.98	0.27	0.67	1.14	0.02	1.15	1.46	0.27	0.28	0.05	0.95
07-D1w	72.71	0.88	12.67	3.67	0.11	0.73	2.63	3.82	2.42	0.16	99.81
2 σ	2.59	0.14	0.49	0.91	0.02	0.23	0.69	0.37	0.19	0.05	1.96
07-D2w	73.09	0.86	12.63	3.66	0.11	0.70	2.50	4.00	2.41	0.16	100.12
2 σ	1.32	0.10	0.52	0.77	0.01	0.17	0.46	0.15	0.16	0.04	0.82
07-D2b	52.21	2.28	13.04	14.30	0.22	4.64	8.83	2.81	0.67	0.23	99.24
2 σ	0.56	0.00	0.08	0.27	0.02	0.24	0.32	0.05	0.05	0.03	0.10
07-D3	73.11	0.89	12.53	3.59	0.11	0.73	2.71	3.86	2.46	0.16	100.15
2 σ	0.94	0.04	0.52	0.31	0.01	0.07	0.23	0.22	0.15	0.02	0.77
07-D4w	71.92	0.87	13.47	3.83	0.10	0.72	3.06	4.00	2.30	0.17	100.45
2 σ	2.61	0.39	2.91	1.54	0.06	0.41	1.52	0.62	0.43	0.11	1.33
07-D4b	49.97	1.90	13.73	12.66	0.22	6.38	10.78	2.59	0.34	0.19	98.77
2 σ	0.23	0.36	0.16	1.82	0.02	1.10	1.12	0.41	0.07	0.05	0.58

Table 5.6: Glass chemistry of the Askja 1875 tephra units B, C and D. Samples were collected from proximal locations around Lake Öskjuvatn within the Askja caldera.

Sample	SiO_2	TiO_2	Al_2O_3	FeO	MnO	MgO	CaO	Na_2O	K_2O	P_2O_5	Total
07-54w	71.18	0.85	12.35	4.80	0.11	0.83	2.56	3.76	2.35	0.17	99.82
07-55w	70.89	0.81	12.31	4.59	0.10	0.83	2.49	3.70	2.33	0.16	99.42
07-57w	71.23	0.84	12.34	4.68	0.10	0.86	2.54	3.78	2.36	0.17	99.64
07-59w	71.04	0.85	12.37	4.79	0.11	0.85	2.63	3.73	2.33	0.18	99.76
07-61.1	69.65	0.91	12.5	5.18	0.11	0.99	2.88	3.87	2.24	0.21	98.02
07-61.2	69.50	0.94	12.52	5.47	0.12	1.10	3.05	3.80	2.21	0.21	98.36
07-61.3	69.26	0.93	12.49	5.43	0.11	1.05	2.97	3.86	2.22	0.22	97.99
07-61.4	65.62	1.30	12.81	8.03	0.15	1.66	4.20	3.63	1.90	0.25	98.84
07-61.5	67.66	1.05	12.77	6.46	0.12	1.44	3.40	3.68	2.04	0.22	98.18

dominantly magmatic eruption with little or no interaction with external water sources. The increase in average grain size throughout the eruption may suggest an overall increase in intensity during the eruption or a change in the dominant wind direction during the eruptive period.

Chemical Data: In total, thirteen samples were analysed for the A1875 tephra layer collected from three discreet sampling locations. The new major element data collected via EMPA and XRF is presented in Tables 5.5 and 5.6. The chemical characteristics of the tephra layer are shown by figures 5.17 to 5.21. The tephra layer has both a rhyolitic and basaltic glass composition and a dacitic bulk composition (Fig 5.17). The tephra layer is metaluminous (Fig. 5.18). The tephra layer shows some chemical variation with stratigraphic height: SiO_2 values decrease slightly while there is a minor increases are seen in the concentrations of Al_2O_3, FeO, TiO_2, MgO, CaO and P_2O_5 (Fig. 5.21). The tephra layer shows a low alkaline nature as indicated by the compositional fields suggested in Rollinson (1993) and references therein.

Comparing XRF and EMPA data highlights variation in SiO_2 concentrations between the data sets (Fig 5.19). Also highlighted are increases in FeO, MgO, CaO and P_2O_5 as well as a subtle decrease in K_2O concentrations in the XRF data compared with the glass data. These differences are the result of removal of these elements from the glass phase through fractional crystallization of olivine, pyroxene and apatite during melt generation.

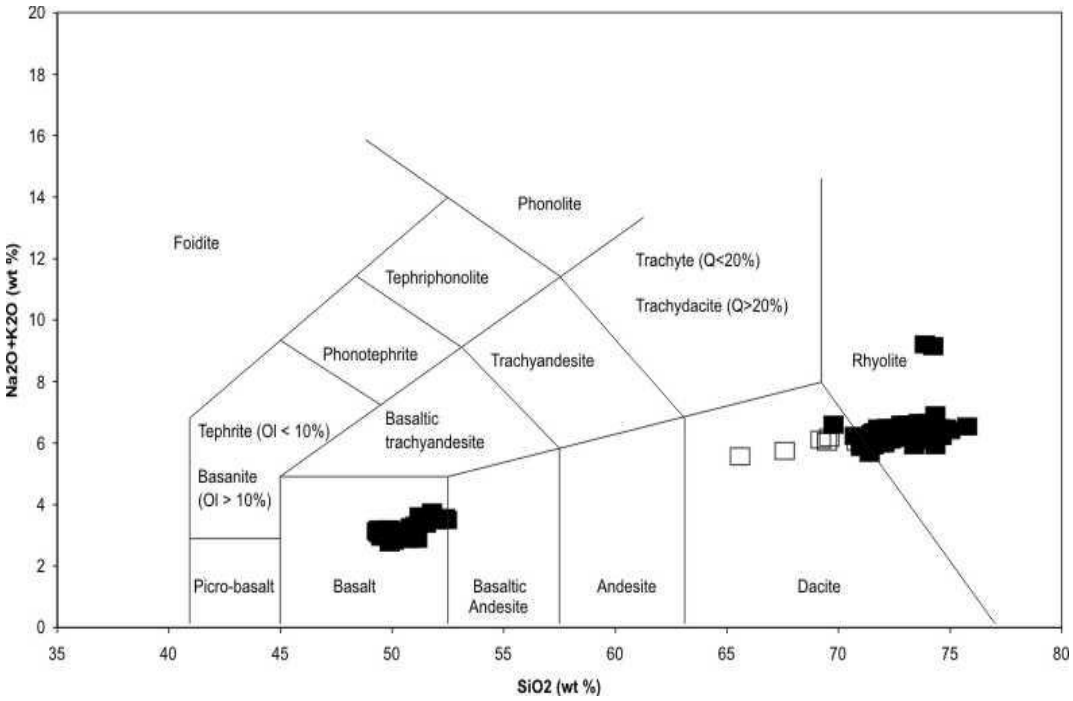

Figure 5.17: Total Alkali – Silica bivariate plot of the A1875 tephra layer. Black squared represent EMPA data while white squares represent XRF data. Data indicates that EMPA data is bimodal with basaltic and rhyolitic components, while XRF data is dacitic in composition. Grid lines adapted from La Maitre *et al*. (1989).

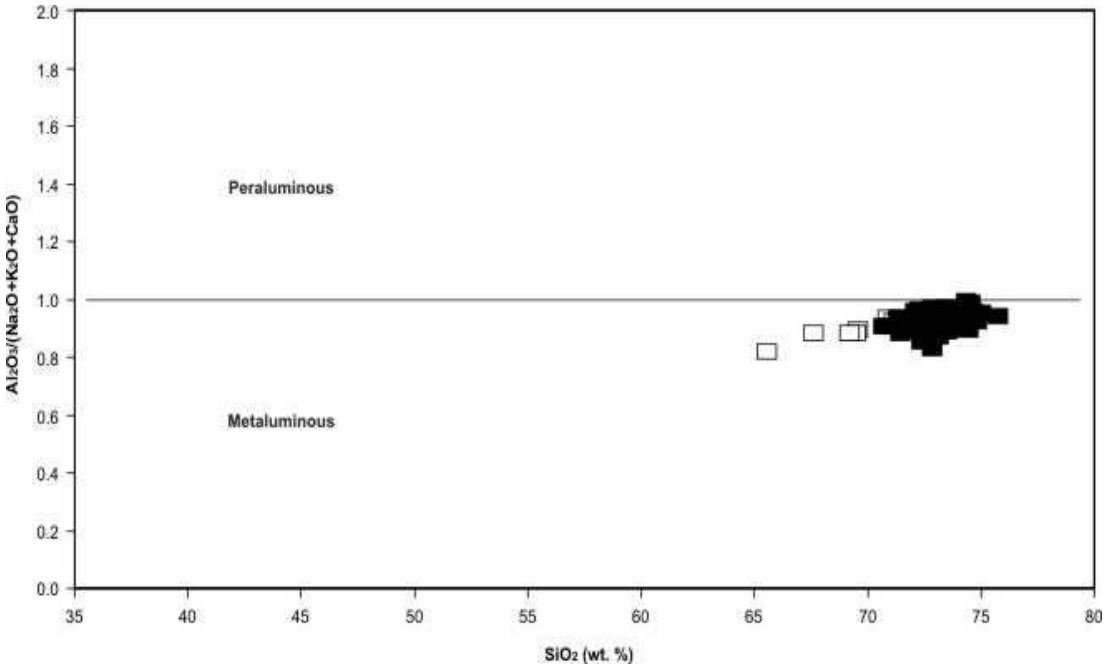

Figure 5.18: Silica – Aluminium and total alkali plot of the A1875 tephra layer. Black squares represent EMPA data while white squares represent XRF data. Data indicate that the tephra layer shows a metaluminous geochemistry consistent with the geological setting.

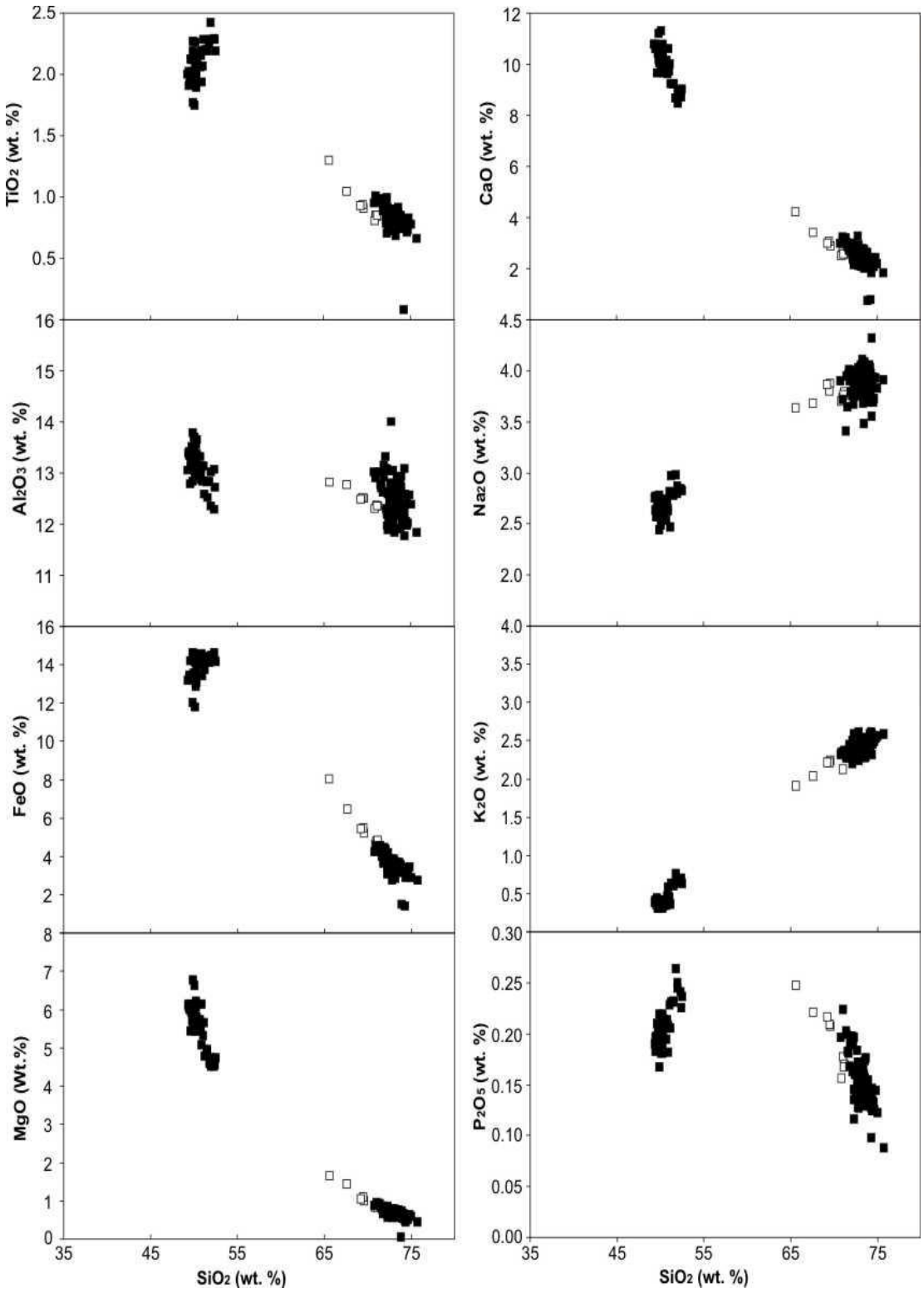

Figure 5.19: Bivariate plots of XRF and EMPA data for the A1875 tephra layer. Black squares represent EMPA data whilst white squares represent XRF data. Prominent variations between EMPA and XRF data suggest definite fractional crystallisation prior to eruption.

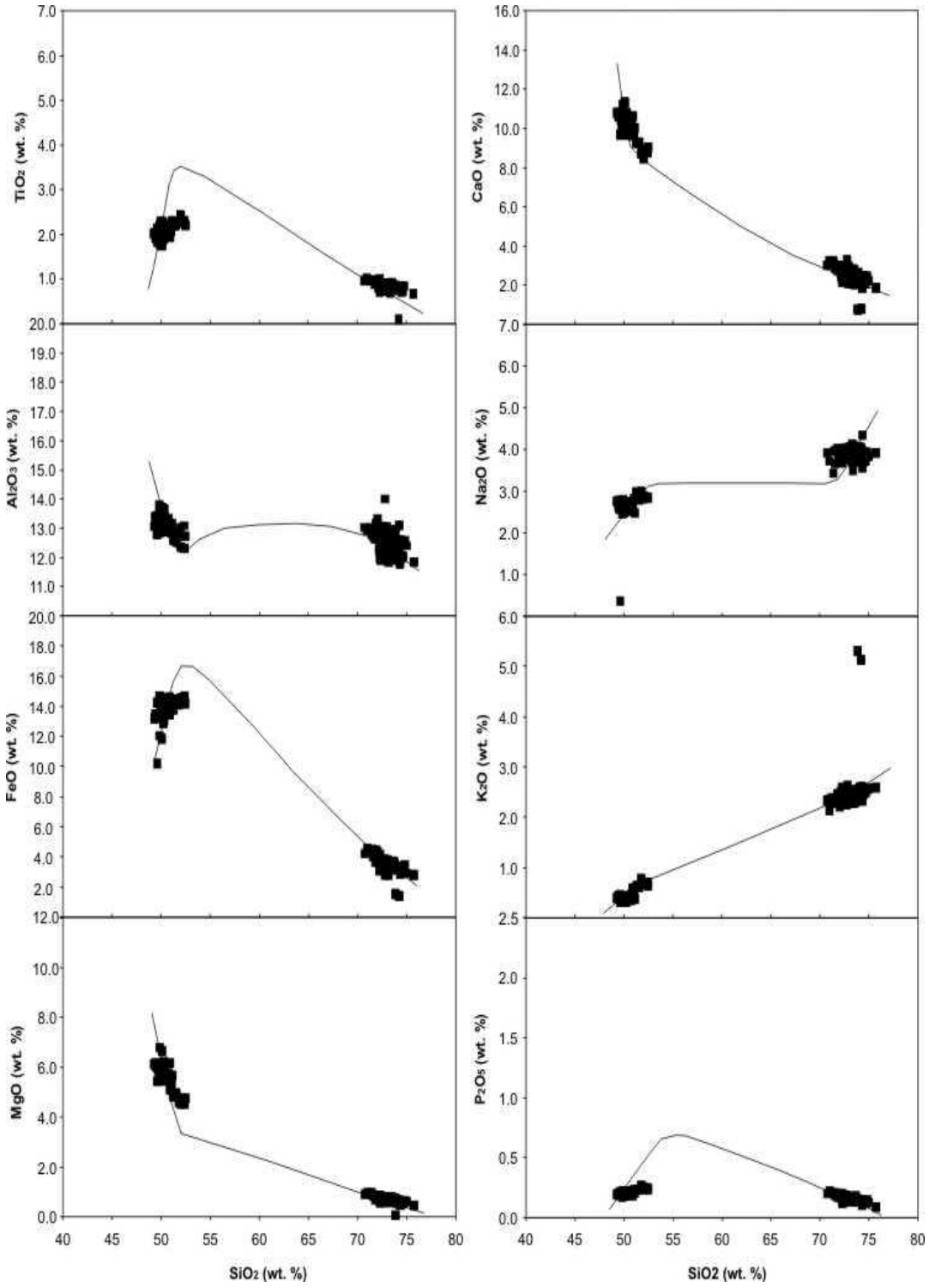

Figure 5.20: Harker plots of Askja 1875 data plotted onto the crystallisation trends of major elements against SiO_2 (wt. %) for the volcanic system. Black lines represent data collected for the Askja volcanic system by previous workers.

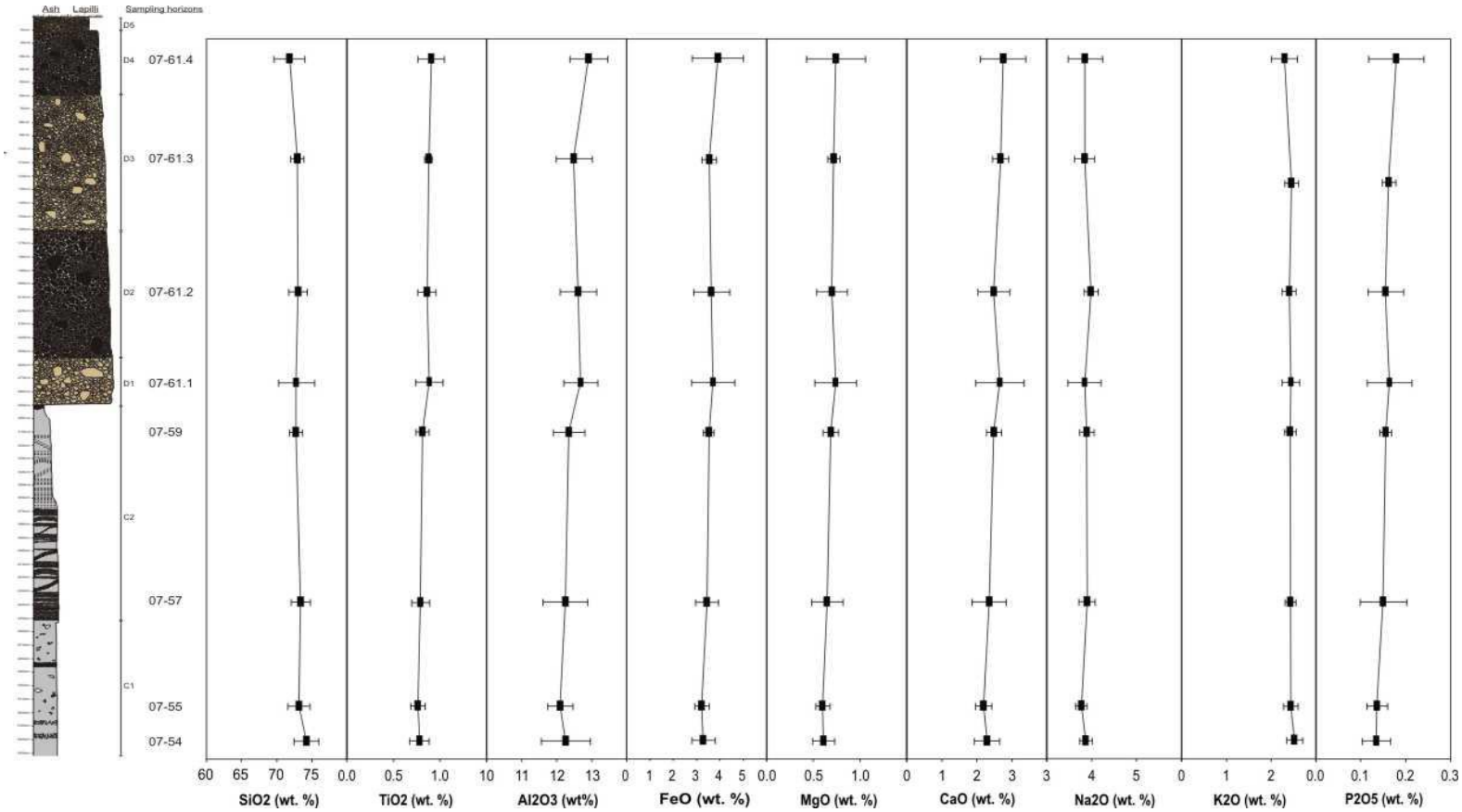

Figure 5.21: Chemical variation with stratigraphic height for the A1875 tephra. Elements depicted represent the full suite of major elements analysed with the exception of MnO. Geochemcial variations are noted at the C-D unit boundary and towards the top of the D unit.

5.2.3 Katla

The Katla volcanic system is the source of the sequence of andesitic Silk layers (**Sil**icic **K**atla) erupted between 1676 – 7200 BP and the widespread Vedde tephra layer aged 11980 BP. Here, we present field and chemical data collected for the Silk UN and LN tephra layers.

5.2.3.1 Katla Silk UN tephra layer

Field Data: The reference section for the Silk UN tephra layer was selected at 63º 43.933'N 18º 43.917'E near Loðnugil and Loðnugiljiahaus off the F232 route (Table 4.1; Fig. 4.4). Figure 5.22b,c are field photographs of the tephra layer at the reference section. At this location, the tephra layer is contained within a sequence of tephra layers dominated by black basaltic tephras presumably sourced from the Katla volcano. There is a white tephra layer within the sequence which underlies the Silk UN Layer which is presumably the H3 tephra from the Hekla volcanic system. Due to the small scale of the tephra layer it has not been logged at this location.

The Silk UN tephra is 0.16 m thick and dominated by green-grey pumice clasts. The tephra layer shows some faint internal layering and normal grading but no other depositional structures. Grain size is very fine to medium lapilli while average clast size is c. 1 cm. Maximum clast size is c. 2.6 cm. The largest clast sizes are recorded in the middle of the tephra layer, while the upper 0.02 m is dominated by coarse ash. The tephra layer is both clast and matrix supported and poorly sorted. The Silk needle layers are characterised by their pumice morphology: pumice clasts have a wood-chip texture and form fragile needles (Fig. 5.22c). The clasts are angular and show no evidence of re-working. Lithic clasts are minimal; those present are dominated by black basaltic clasts.

The Silk UN tephra layer represents a pumice and ash fall from an explosive sub-Plinian eruption from the Katla volcanic system. The eruption produced tephra with a dominantly andesitic composition. The tephra layer shows no obvious chemical zoning suggesting no mixing of separate magma batches. The ratio of juvenile:lithic material in the deposit suggests a dominantly magmatic eruption with little or no interaction with external water sources. The coarse grained ash horizon in the middle of the tephra layer represents an increase in eruption intensity during this phase. The fragile nature of the pumice clasts indicate that confirm that deposition must have occurred through fall out processes..

Figure 5.22: Field photographs of the Katla Silk UN and LN tephra layers. a) Outcrop near the banks of the Þorvaldsá river near Geldingasker off the F208 route. Notebook used for scale measures c. 15 cm. b) Outcrop near Loðnugil and Loðnugiljahaus off the F232 route. Trowel used for scale measures c. 25 cm. c) pumice clast showing the characteristic wood chip texture of the Silk needle layers. Scale on the ruler is in cm at top and inches at the bottom. Photographs: Rh. Meara.

Deposition via density currents would have caused irreversible damage to the clasts and would be visible in the resulting tephra layer.

5.2.3.2 Katla Silk LN tephra layer

Field Data: The reference section for the Silk LN tephra layer was selected at 63º 49.741'N 18º 37.219'E on the banks of the Þorvaldsá river near Geldingasker off the F208 route (Table 4.1; Fig. 4.4). Figure 5.22a is a field photograph of the tephra layer at the reference section (Silk LN is the lower grey-green tephra layer). At this location, the tephra layer is contained within a sequence of tephra layers dominated by black basaltic tephras presumably sourced from the Katla volcano. There is another Silk tephra within the sequence, presumed to be the Silk MN tephra. Due to the small scale of the tephra layer it has not been logged at this location.

The Silk LN tephra is 0.055 m thick and dominated by green-grey pumice clasts. The tephra layer shows some faint internal layering but no other depositional structures. Grain size is very fine lapilli while average clast size is c. 0.5 cm. The tephra layer is both clast and matrix supported and moderately sorted. The pumice clasts have a characteristic wood-chip texture and form delicate fragile needles. The clasts are angular and show no evidence of re-working. Lithics clasts are prominent, those present are black basaltic or obsidian clasts measuring < 0.05 cm. At the reference location the tephra layer shows some thickness variation and some discontinuity. These features are considered to represent post-depositional erosion of the tephra layer.

The Silk LN tephra layer represents a pumice and ash fall from an explosive sub-Plinian eruption from the Katla volcanic system. The eruption produced tephra with a dominantly andesitic composition suggesting some magma evolution prior to eruption. The tephra layer shows no obvious chemical zoning suggesting no mixing of separate magma batches. The ratio of juvenile:lithic material in the deposit suggests some interaction with an external water source during eruption. The constant grain size of the tephra layer implies no major changes in intensity during the eruption. The fragile nature of the pumice clasts confirm that deposition must have occurred through fall out processes. Deposition via density currents would have caused irreversible damage to the clasts and would be visible in the resulting tephra layer.

Katla Silk UN and LN Tephra Layers – Chemical Data: In total, two samples were analysed

Table 5.7: Glass chemistry of andesitic Silk UN and LN units of the Katla volcanic system. a) Samples of Silk-UN were collected from Loðnugil on route F232 to the east of Katla. b) Samples of Silk-LN were collected from the banks of the Þorvaldsá river near Geldingasker. Ten electron probe analyses were collected for each sample and the data presented is the average of these analyses and two standard deviations. Full data sets can be obtained as supplementary material.

a) SILK - UN

Sample	SiO_2	TiO_2	Al_2O_3	FeO	MnO	MgO	CaO	Na_2O	K_2O	P_2O_5	Total
07-64	65.24	1.33	13.85	6.08	0.20	1.32	3.48	4.61	2.59	0.36	99.06
2 σ	0.80	0.10	0.58	0.35	0.02	0.11	0.17	0.34	0.17	0.02	1.25

b) SILK – LN

Sample	SiO_2	TiO_2	Al_2O_3	FeO	MnO	MgO	CaO	Na_2O	K_2O	P_2O_5	Total
07-65	66.20	1.21	13.91	5.66	0.20	1.12	3.09	4.69	2.71	0.31	99.10
2 σ	1.25	0.11	0.54	0.41	0.02	0.11	0.23	0.19	0.14	0.02	1.68

Table 5.8: Whole rock chemistry of the Silk UN and LN units from the Katla volcanic system. a) Samples of Silk-UN were collected from Loðnugil on route F232 to the east of Katla. b) Samples of Silk-LN were collected from the banks of the Þorvaldsá river near Geldingasker. Ten electron probe analyses were collected for each sample and the data presented is the average of these analyses and two standard deviations. Full data sets can be obtained as supplementary material.

a) SILK - UN

Sample	SiO_2	TiO_2	Al_2O_3	FeO	MnO	MgO	CaO	Na_2O	K_2O	P_2O_5	Total
07-64	63.33	1.22	14.16	7.31	0.22	1.13	2.90	4.47	2.59	0.28	99.63

b) SILK – LN

Sample	SiO_2	TiO_2	Al_2O_3	FeO	MnO	MgO	CaO	Na_2O	K_2O	P_2O_5	Total
07-65	54.54	1.21	13.91	7.24	0.19	1.15	2.94	4.61	2.66	0.28	99.43

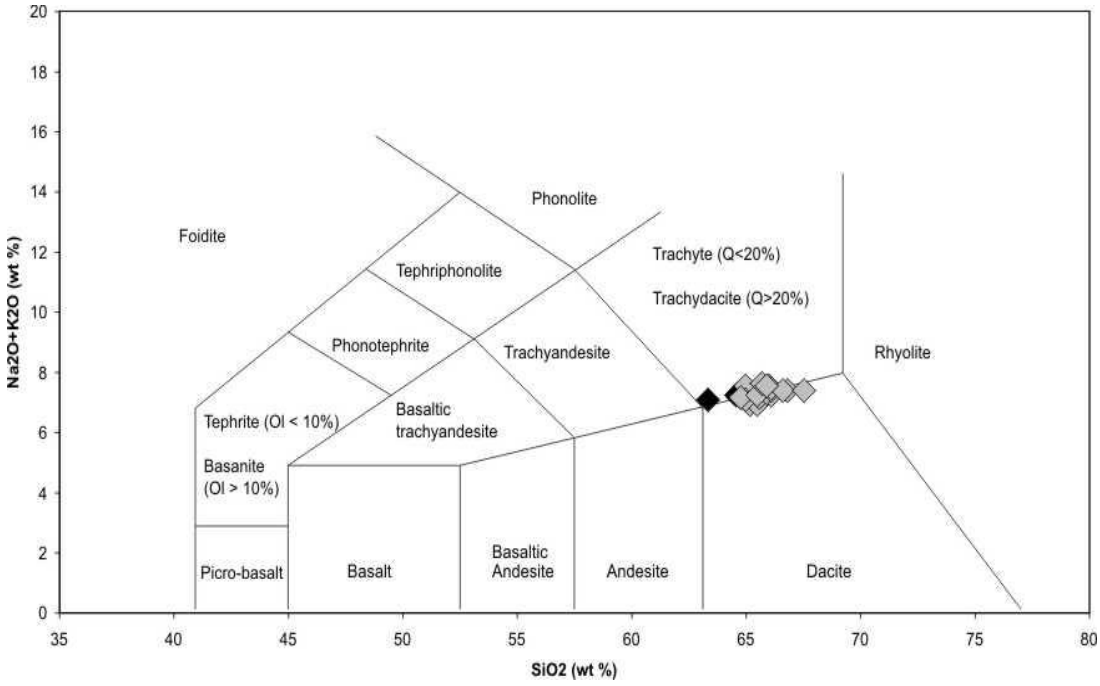

Figure 5.23: Total Alkali – Silica bivariate plot of the Katla Silk UN and LN tephra layers. Grey diamonds represent EMPA data while black diamonds represent XRF data. Data indicate that both XRF and EMPA data show a uni-modal chemistry which straddles the dacite-trachydacite boundary. Grid lines adapted from La Maitre *et al*. (1989).

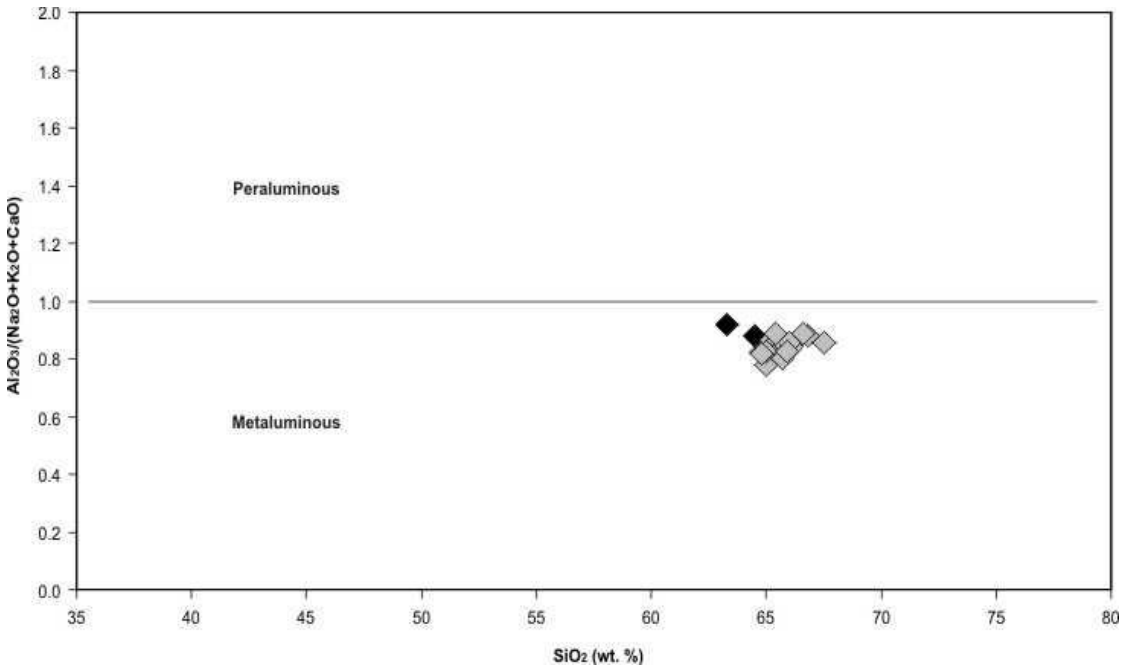

Figure 5.24: Silica – Aluminium and total alkali plot of the Katla Silk UN and LN tephra layers. Grey diamonds represent EMPA data while black diamonds represent XRF data. Data indicate that the tephra layer shows a metaluminous geochemistry consistent with the geological setting.

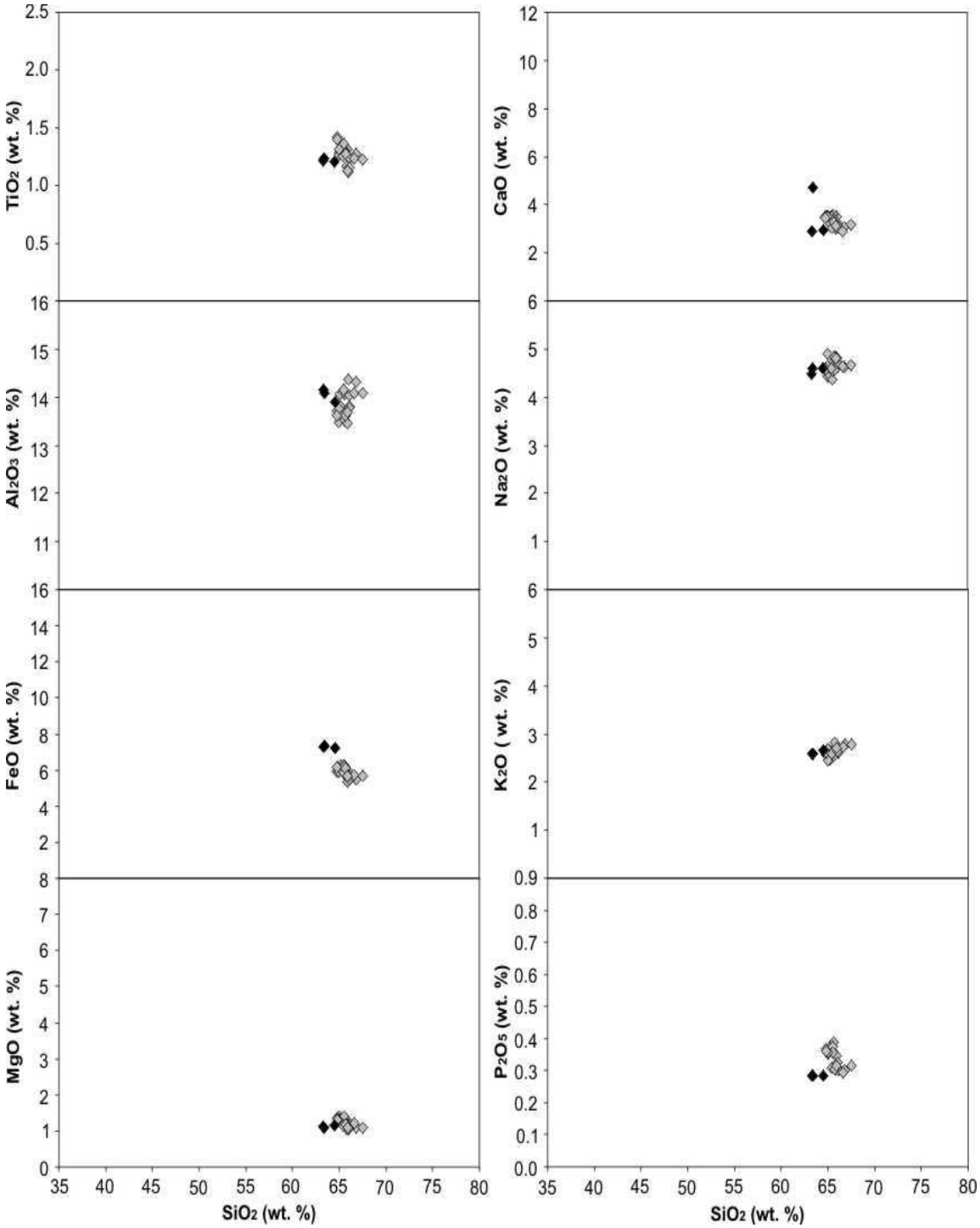

Figure 5.25: Bivariate plots of XRF and EMPA data for the Katla Silk UN and LN tephra layers. Grey diamonds represent EMPA data whilst black diamonds represent XRF data. Very minor variations are recorded between XRF and EMPA data sets suggesting only minor amounts of fractional crystallisation within the magma prior to eruption.

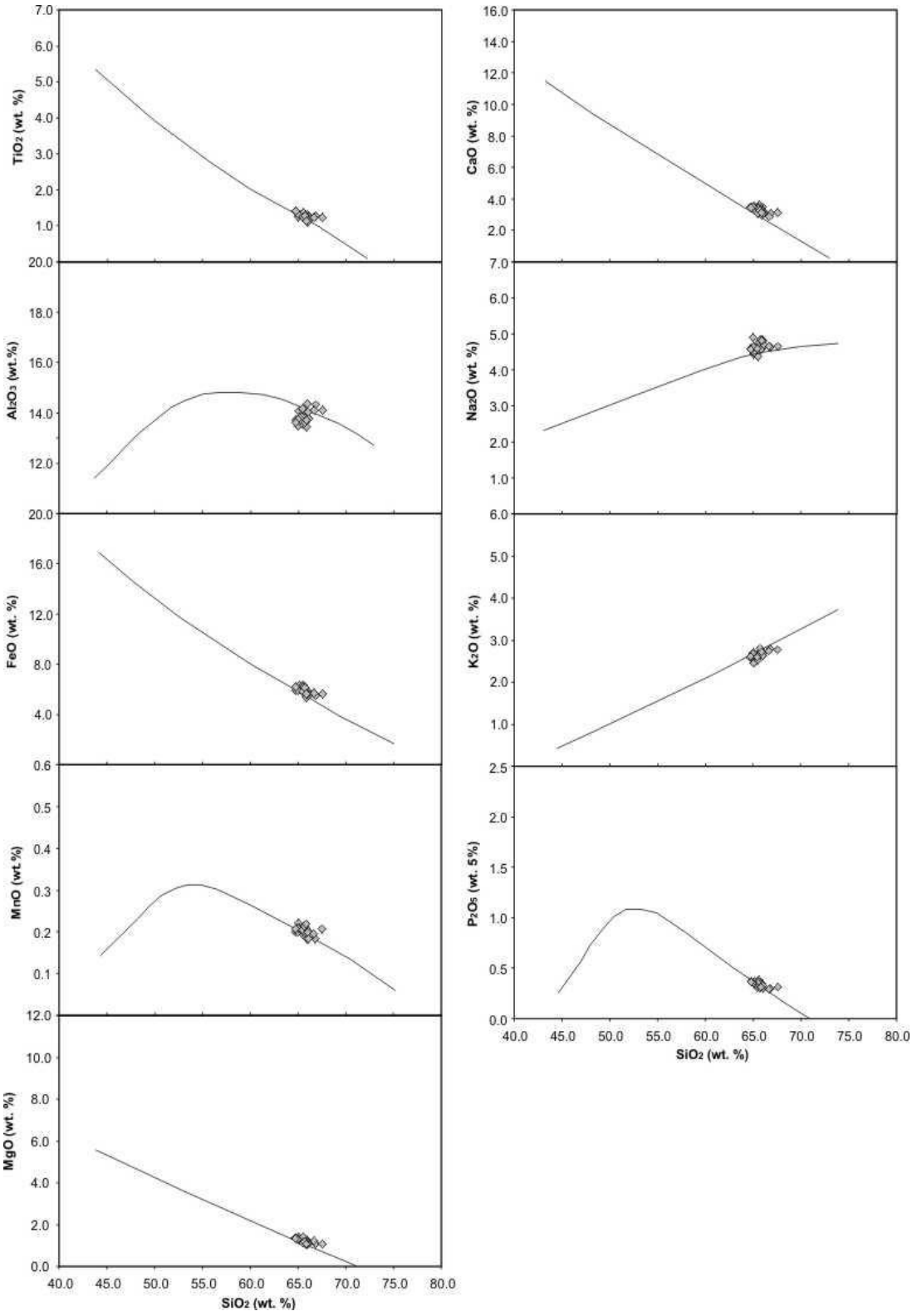

Figure 5.26: Harker plots of Katla Silk UN and LN data plotted onto the crystallisation trends of major elements against SiO_2 (wt. %) for the volcanic system. Black lines represent data collected for the Katla volcanic system by previous workers.

Katla Silk UN and LN Tephra Layers – Chemical Data: In total, two samples were analysed for the SILK UN and LN tephra layers collected from two separate sampling locations. The new major element data collected via EMPA and XRF for is presented in Tables 5.7 and 5.8.

The chemical characteristics of the tephra layer are shown by figures 5.23 to 5.26. The tephra layers have a dacitic to trachydacitic composition in both glass and bulk samples (Fig 5.23). The tephra layers are metaluminous (Fig. 5.24). The tephra layer shows a low alkaline nature as indicated by the compositional fields suggested in Rollinson (1993) and references therein.

Comparing XRF and EMPA data highlights variation in SiO_2 concentrations between the data sets (Fig 5.25). Also highlighted is an increase FeO in the XRF data compared with the glass data. This difference is the result of removal of these elements from the glass phase through fractional crystallization of olivine during melt generation.

5.2.4 Öræfajökull

The Öræfajökull volcanic system is the source for the 1362 AD and 1726 AD eruptions (Thorarinsson, 1958). Here, we present the field and chemical data collected for the 1362 tephra layer.

Field Data: The reference section for the Ö1362 tephra layer was selected at 63º 53.505'N 16º 37.158'E near Sigurðarholl and Sandsskarð (Table 4.1; Fig. 4.5). Figure 5.27 is a stratigraphic log of the tephra layer compiled at this location while figures 5.28 are a set of field photographs of the tephra layer at the reference section. At this location, the tephra layer is 2.9 m thick. The tephra layer is comprised of four distinct packages: Phase I, Phase II, Phase III and Phase IV. Phases I – III will be discussed below. Phase IV is not present at the reference location but will also be considered.

Phase III is 1.1 m thick and is dominated by pale grey ash. The tephra layer shows some internal layering but is otherwise massive. Grain size is medium to coarse ash, with two horizons dominated by fine lapilli. Within the coarser layers, average grain size is c. 0.5 cm and maximum clast size is 8 cm. The tephra layer is moderately sorted and dominantly matrix supported, excluding the lapilli-rich layers which are clast supported. Lithic fragments within the tephra layer are unaltered basalts or obsidian fragments. Phase III contains accretionary lapilli and armoured clasts. The outcrop is overlain by re-worked

material and a thin soil covering. Phase IV is identified in localities close to the Öræfajökull summit. The phase is dominated by pale grey ash-grade tephra layers that contain evidence of cross bedding and dunal structures. These depositional structures are highlighted by pumice-rich lobes (Fig. 5.28c).

Phase II is 1.3 m thick and dominated by pale grey – white pumice clasts. The tephra shows minimal internal layering and no other depositional structures. Grain size is medium lapilli. Average grain size is 2 – 4 cm while maximum clast size is 8.5 cm. The tephra layer is well sorted and clast supported. Pumice clasts are sub-angular. Lithic clasts are rare in Phase II. Phase I is 0.4 m thick and comprises a series of small tephra layers. Colour varies between pale grey – white to pale brown (Fig. 5.28d). The tephra layer shows prominent internal layering but no other obvious depositional structures. Grain size is medium to coarse ash with the exception of two horizons of fine lapilli. In the lapilli-rich layers, average grain size is 0.5 cm. Phase I is dominantly matrix supported and well sorted. Lithics are minimal in the outcrop.

The Ö1362 deposit represents an eruption from the Öræfajökull volcanic system. Phase I represents a series of PDC events. Phase II represents a fall out phase from a Plinian eruption column. Phase III represents continued deposition via Plinian fall out, with influences from external water sources as indicated by the armoured clasts and accretionary lapilli. Phase IV represents the final stages of the waning eruption with deposition of tephra occurring via dilute density currents as indicated by cross-bedding and pumice lobes. The limited extent of Phase IV suggests the phase will not be recorded as a prominent long distance marker horizon. The eruption produced only rhyolitic tephra suggesting a prolonged repose period within the magma chamber before eruption.

Chemical Data: In total, five samples were analysed for the Ö1362 tephra layer collected from three separate sampling locations. The new major element data collected via EMPA and XRF for is presented in Tables 5.9 and 5.10.

The chemical characteristics of the tephra layer are shown by figures 5.29 to 5.30. The tephra layer has a rhyolitic glass composition and a rhyolite – trachydacite bulk composition (Fig. 5.29). The tephra layer is metaluminous (Fig. 5.30). The tephra layer exhibits a restricted compositional range with no geochemical variation with stratigraphic height (Fig. 5.33). The tephra layer shows a high alkaline nature as indicated by the compositional fields suggested in Rollinson (1993) and references therein.

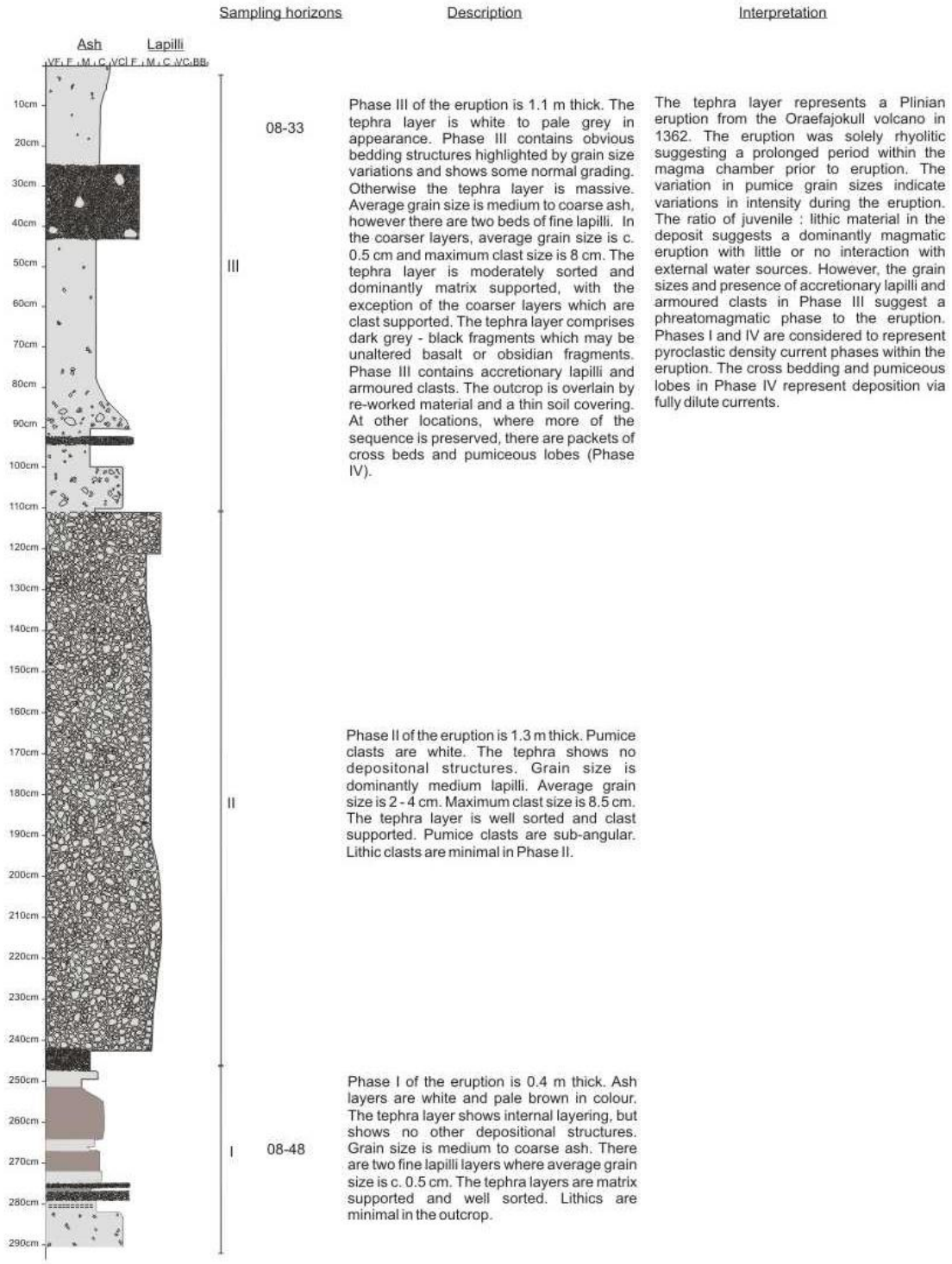

Figure 5.27: Stratigraphic log of the Ö1362 tephra layer showing physical characteristics e.g. grain size, clast morphology and overall outcrop colour. Drawn at the reference section near Sigurđarholl and Sandsskarđ.

Figure 5.28: Field photographs of the Ö1362 tephra layer. a) Top section in the outcrop showing phreato-magmatic ash. b) Coarse grained pumice fall deposit underlying a). c) Pumice lobes highlighting PDC flow lobes in the outcrop at a second exposure. d) thin layers of ash/PDCs at the base of the reference section. Trowel used for scale in photographs measures c. 25 cm. Photographs: Rh. Meara.

Table 5.9: Glass chemistry of the rhyolitic Ö1362 tephra. Samples were collected from proximal locations on the flanks of the volcano and on the sandur plain. Ten electron probe analyses were collected for each sample and the data presented is the average of these analyses and two standard deviations. Full data sets are available in the Appendix.

Sample	SiO_2	TiO_2	Al_2O_3	FeO	MnO	MgO	CaO	Na_2O	K_2O	P_2O_5	Total
08-20	71.94	0.24	13.97	2.98	0.10	nd	1.09	5.82	3.13	0.02	99.26
2 σ	4.61	0.07	4.86	1.94	0.01	nd	0.73	2.74	1.44	Nd	2.02
08-33	72.19	0.23	13.01	3.30	0.10	nd	0.99	5.30	3.49	0.02	98.62
2 σ	1.43	0.03	0.37	0.29	0.02	nd	0.09	0.22	0.24	nd	1.45
08-48	72.06	0.24	13.09	3.26	0.10	nd	0.99	5.15	3.41	nd	98.32
2 σ	0.64	0.03	0.45	0.30	0.01	nd	0.03	0.19	0.06	nd	1.21
08-59	72.27	0.23	13.06	3.22	0.11	0.05	1.01	5.44	3.40	nd	98.77
2 σ	1.30	0.06	0.47	0.16	0.02	nd	0.10	0.20	0.16	nd	1.54
08-65	72.27	0.23	13.07	3.23	0.10	nd	1.02	5.33	3.36	0.02	98.64
2 σ	1.14	0.07	0.26	0.30	0.01	nd	0.10	0.25	0.18	nd	1.28

Table 5.10: Whole rock chemistry of the rhyolitic Ö1362 tephra. Samples were collected from proximal locations on the flanks of the volcano and on the sandur plain. Full data set is available in the Appendix.

Sample	SiO_2	TiO_2	Al_2O_3	FeO	MnO	MgO	CaO	Na_2O	K_2O	P_2O_5	Total
08-20	68.94	0.31	13.10	3.96	0.10	0.14	1.05	5.28	3.30	0.03	96.21
08-33	69.36	0.26	12.87	3.72	0.10	0.05	0.98	5.45	3.35	0.02	96.15
08-48	69.21	0.29	13.17	3.83	0.10	0.09	1.06	5.48	3.30	0.02	96.54
08-59	69.58	0.26	13.09	3.79	0.10	0.10	1.02	5.43	3.33	0.02	96.73
08-65	69.29	0.26	13.05	3.82	0.10	0.11	1.01	5.34	3.34	0.02	96.34

Comparing XRF and EMPA data highlights variation in SiO_2 concentrations between the data sets (Fig. 5.31). Also highlighted are minor increases in TiO_2, CaO and Na_2O as well as a more pronounced difference in FeO concentrations in bulk chemistry with respect to glass chemistry. Also highlighted is a decrease in K_2O from the glass to the bulk samples. These differences are the result of removal of these elements from the glass phase through fractional crystallization of titanomagnetite, plagioclase, olivine and pyroxene during melt generation. These differences are the result of inclusion of phenocryst phases in the bulk phase, samples most likely pyroxenes, amphiboles, biotite mica, feldspars and quartz.

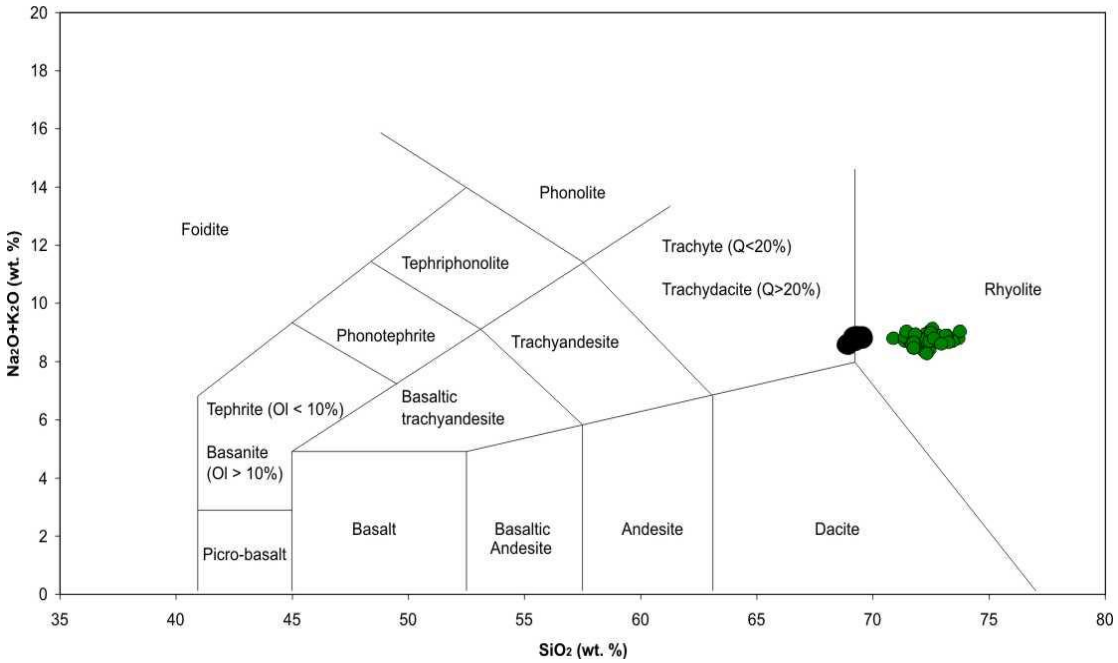

Figure 5.29: Total Alkali – Silica bivariate plot of the Ö1362 tephra layer. Dark green circles represent EMPA data while black circles represent XRF data. Data indicates that the tephra layer is dominated by rhyolitic compositions , however XRF data shows a more trachydacite composition. Grid lines adapted from La Maitre *et al*. (1989).

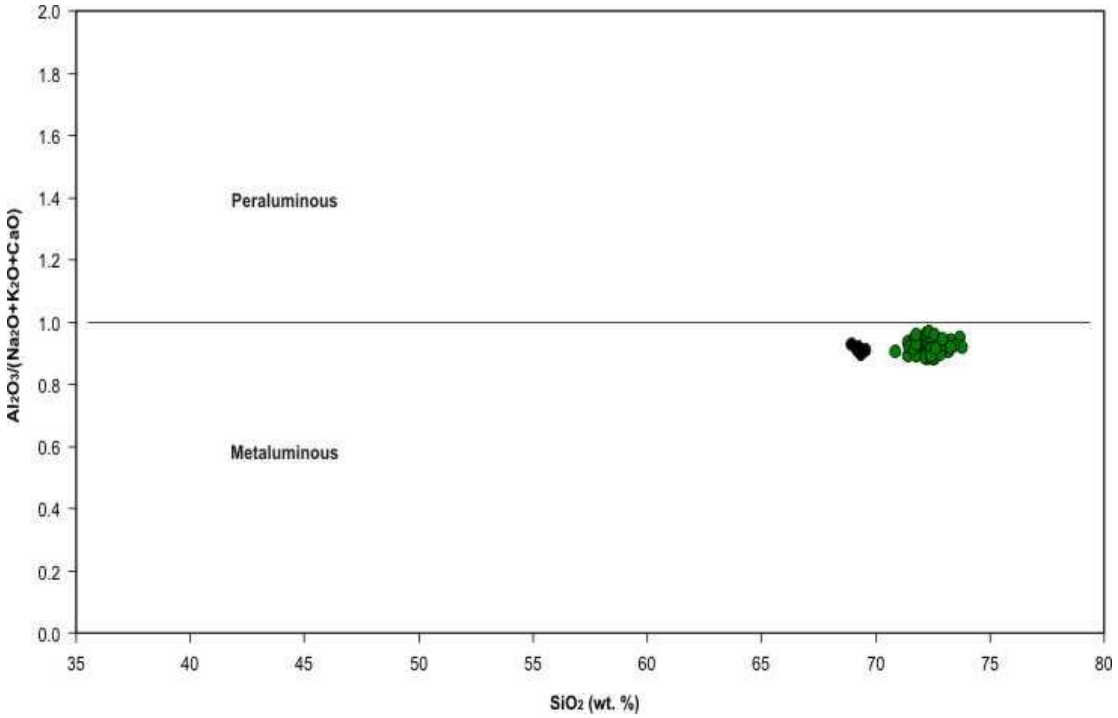

Figure 5.30: Silica – Aluminium and total alkali plot of the Ö1362 tephra. Dark green circles represent EMPA data while black circles represent XRF data. Data indicate that the tephra layer shows a metaluminous geochemistry consistent with the geological setting.

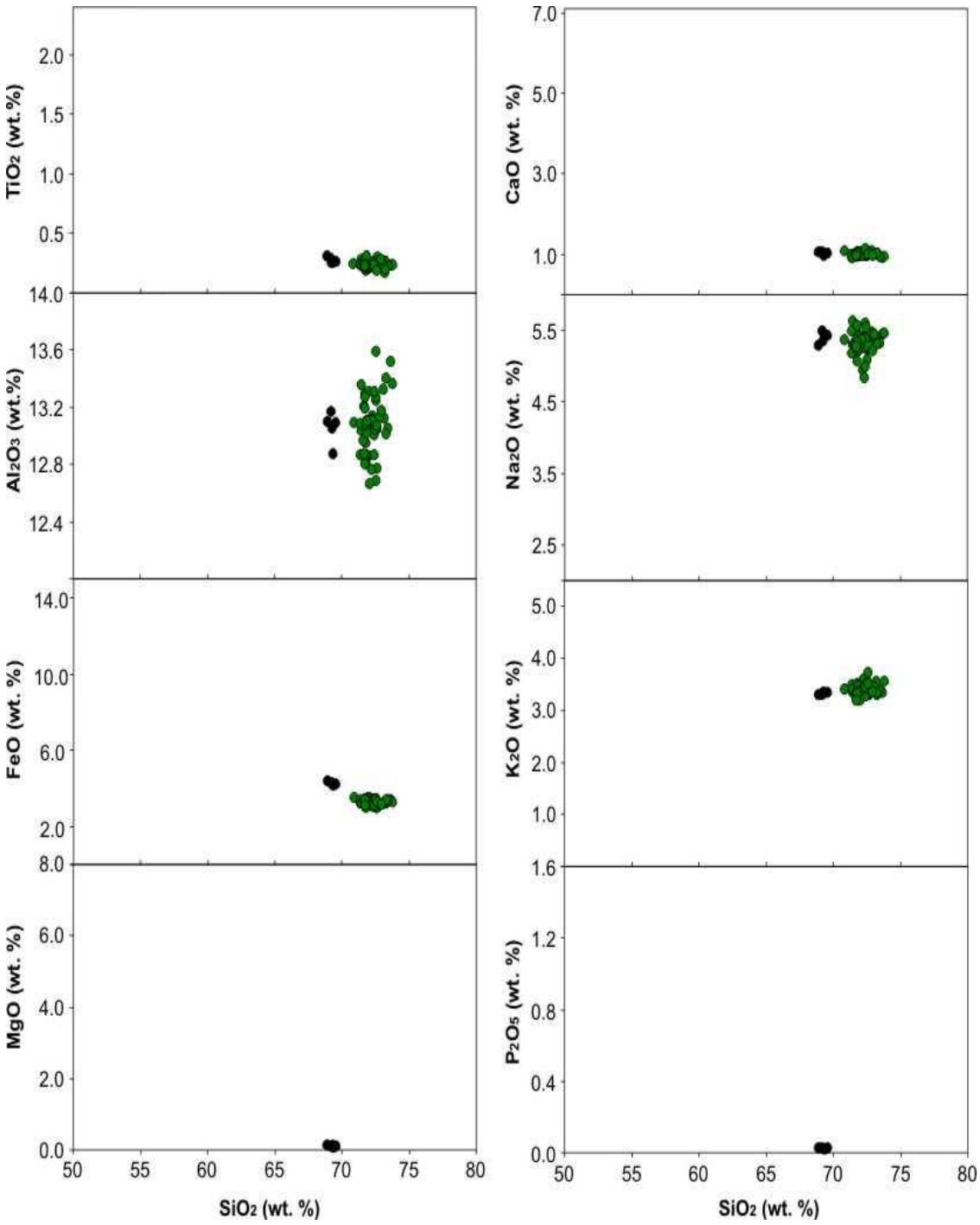

Figure 5.31: Bivariate plots of XRF and EMPA data for the Ö1362 tephra layer. Dark green circles represent EMPA data while black circles represent XRF data. Variations are recorded between XRF and EMPA data sets suggesting only minor amounts of fractional crystallisation within the magma prior to eruption, however these are dominated by SiO_2 and FeO.

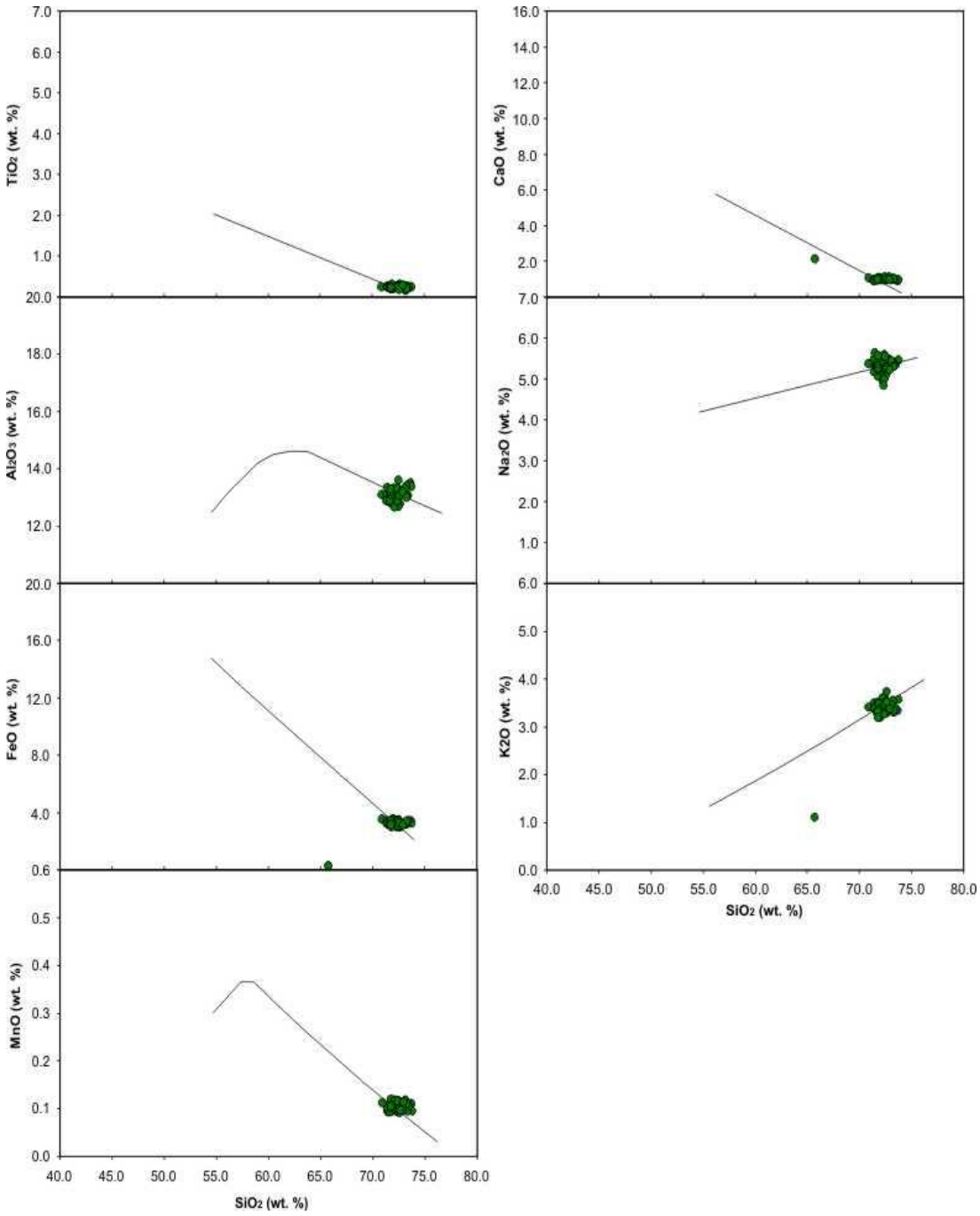

Figure 5.32: Harker plots of Ö1362 data plotted onto the crystallisation trends of major elements against SiO_2 (wt. %) for the volcanic system. Black lines represent data collected for the Öræfajökull volcanic system by previous workers.

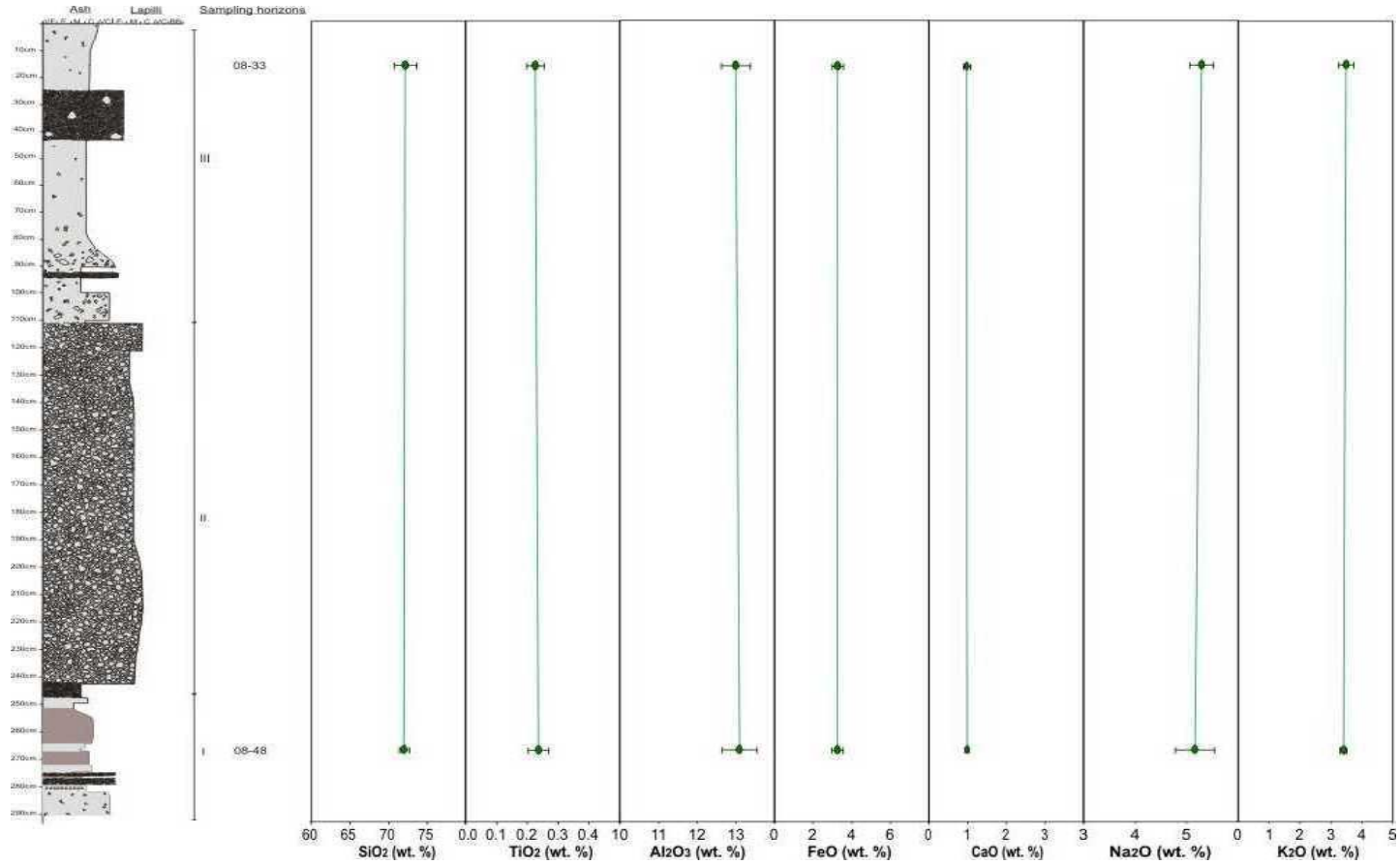

Figure 5.33: Chemical variation with stratigraphic height for the Ö1362 tephra. Elements depicted cover the full range of elements analysed with the exception of MnO. No elemental variations are recorded in the tephra layer, however to confirm this, more samples should be analysed.

This section has presented and described the field and geochemical data collected for the Torfajökull, Askja, Katla and Öræfajökull volcanic systems. The following section focuses on whether Icelandic tephra provenance can be established using the major element chemistry collected.

5.3 A formal system for the identification of tephra provenance

The following section focuses on whether Icelandic tephra provenance can be established using the major element data presented in the previous results section. The application of tephrochronology for dating and correlating sedimentary sequences is dependant on the reliable confirmation of tephra layer identity. Therefore, establishing a technique to reliably identify and correlate a tephra layer to its source origin is of great importance to the discipline.

The tephra layers selected for this study have been separated into high and low silica end members. This has been achieved by plotting all EMPA data onto a total-alkali-silica diagram (Fig. 5.34). An arbitrary point of 60 wt. % SiO_2 has been selected, with data points containing > 60 wt. % SiO_2 deemed "silicic" and those containing < 60 wt. % SiO_2 deemed "mafic". The silicic components of the eruptions are typically those correlated to far-distal localities, and are therefore the main focus of this work. The mafic components are also considered for completeness sake. For a more detailed account of basaltic geochemistry and tephrochronology in Iceland see Jagan (2010).

The separation of tephra layers into silicic and mafic sub-groups provides an opportunity to highlight patterns within the geochemical data which would go unnoticed if a wider dataset were used. Within the established silicic and mafic sub-groups, all data points are graphically plotted to cover each potential major element combination. Figures 5.35 to 5.37 represent the plots created for the silicic sub-group while figures 5.38 to 5.40 represent the plots created for the mafic sub-group. By plotting all major element combinations it is possible identify certain geochemical variations characteristic of individual volcanic systems. The manipulation of such variations allows a formal framework for discriminating between the volcanic systems to be established. The following sections will detail the frameworks established for identifying the silicic and mafic components of the eruptions discussed in this chapter.

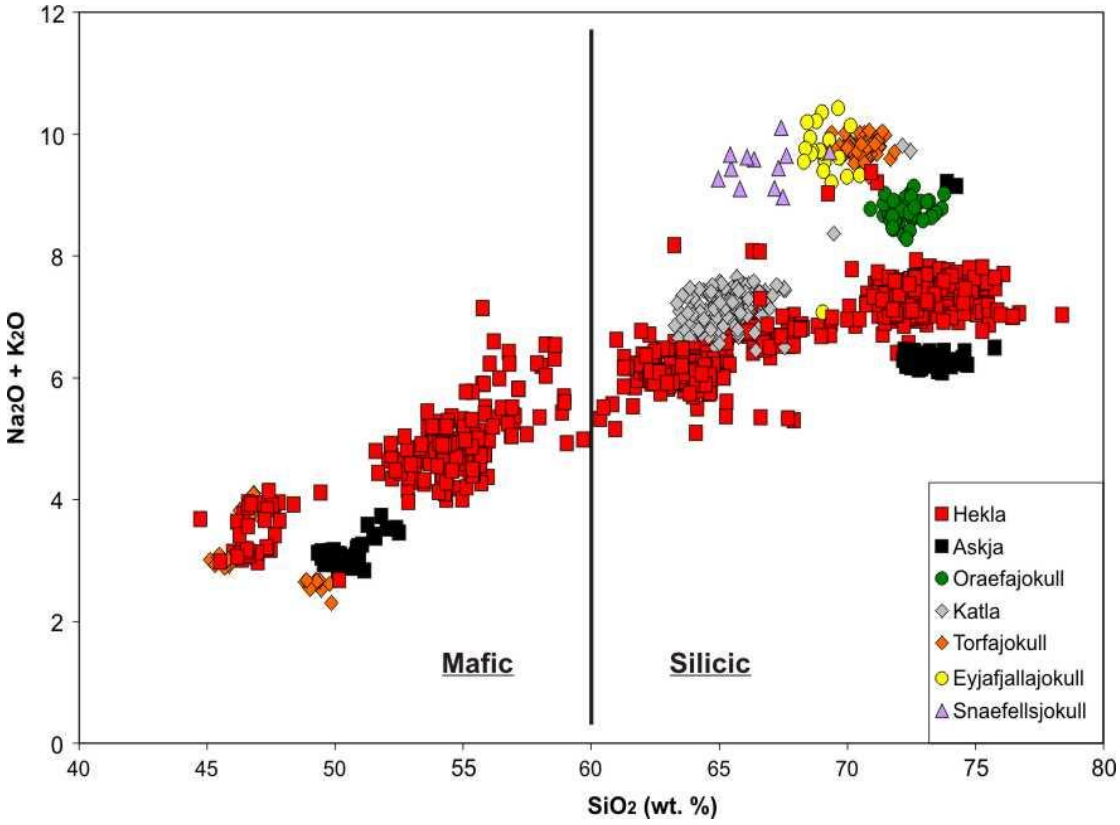

Figure 5.34: Total alkali silica plot of the seven volcanic systems discussed in this chapter. The graph is separated into silicic and mafic components which will be discussed in the next figure. The data presented is EMPA data collected during this project. Data for Eyjafjallajökull and Snæfellsjökull volcanic systems are sourced from Larsen *et al*. (1999).

Silicic Tephra Layers: the final methodology for identifying tephra provenance for silicic tephra layers is presented in Figure 5.41. To establish the provenance of a silicic tephra layer it is essential to produce a TAS diagram which separates the volcanoes into high and low alkali groups. The high alkali group comprises Eyjafjallajökull, Snæfellsjökull, Öræfajökull and Torfajökull. The low alkali group comprises Hekla, Askja and Katla. Once these sub-groups are established, it is possible to distinguish between the individual systems within each group. Plotting TiO_2 against FeO separates the low alkali group into three distinct clusters due to the higher TiO_2 and lower FeO contents of the Askja and Katla volcanoes compared to that of the Hekla volcano. Plotting FeO against K_2O allows for discrimination of the high alkali sub-group, however some overlap remains in data from the Eyjafjallajökull and Snæfellsjökull volcanic systems. This overlap can be overcome by plotting MgO against FeO.

Mafic Tephra Layers: the final methodology for identifying tephra provenance for the mafic components of silicic tephra layers is presented in Figure 5.42. Establishing the provenance of the mafic component of a silicic tephra layer is focused around the use of a TAS diagram. Such a plot will separate data into relatively high and low alkali groups. The high alkali group comprises the Hekla and Torfajökull (Landnám tephra layer) central volcanoes. The low alkali group comprises the Askja and Torfajökull (Grákolla tephra layer) central volcanoes. The Grákolla tephra layer of the Torfajökull volcanic system plots as two sub-groups and will thus be discussed as two separate data sets. The Grákolla and Askja data in the low alkali group show some data overlap in most elemental combinations with the exception of K_2O and SiO_2, therefore this plot is suggested for discrimination of the two tephra layers. Plotting MgO and SiO_2 for the high alkali group provides a distinct cluster for the Landnám tephra layer separate from the Hekla system and the Grákolla tephra layer. There is constant overlap between the Grákolla tephra layer and that of the Hekla volcanic system as indicated on the plot of FeO and CaO. No bivariate elemental combination allows for discrimination of these data sets. This may be due to geochemically identical parental magmas or due to inclusion and analysis of non-juvenile tephra grains within the Grákolla deposit at proximal localities.

Developing a standardised methodology for identifying the provenance of rhyolitic tephra will provide a serious contribution to tephrochronological studies, as will the reference database created for this study. The application of a TAS diagram at the first stage not only separates volcanic systems into silicic and mafic tephra, but also into high and low alkali sub-groups. Using Na_2O at such an early stage in identification in conjunction with a reliable reference data set highlights data which have undergone loss of volatiles during EMPA analysis or during preservation. This method is applicable to macro and micro-tephra horizons from proximal, medial, distal and far-distal sampling locations.

The methodology presented for identifying and discriminating between mafic tephra layers is focused solely on the mafic components of silicic tephra layers. The method does not incorporate all explosive mafic eruptions of Icelandic origin nor does it include data from every volcanic system in Iceland, only those known to produce silicic magmas. Such data would be required to reliably identify an unknown mafic tephra layer. Methodologies for identifying mafic tephra layers are presented in Oladóttir *et al*. (2008) and A. Jagan (2010).

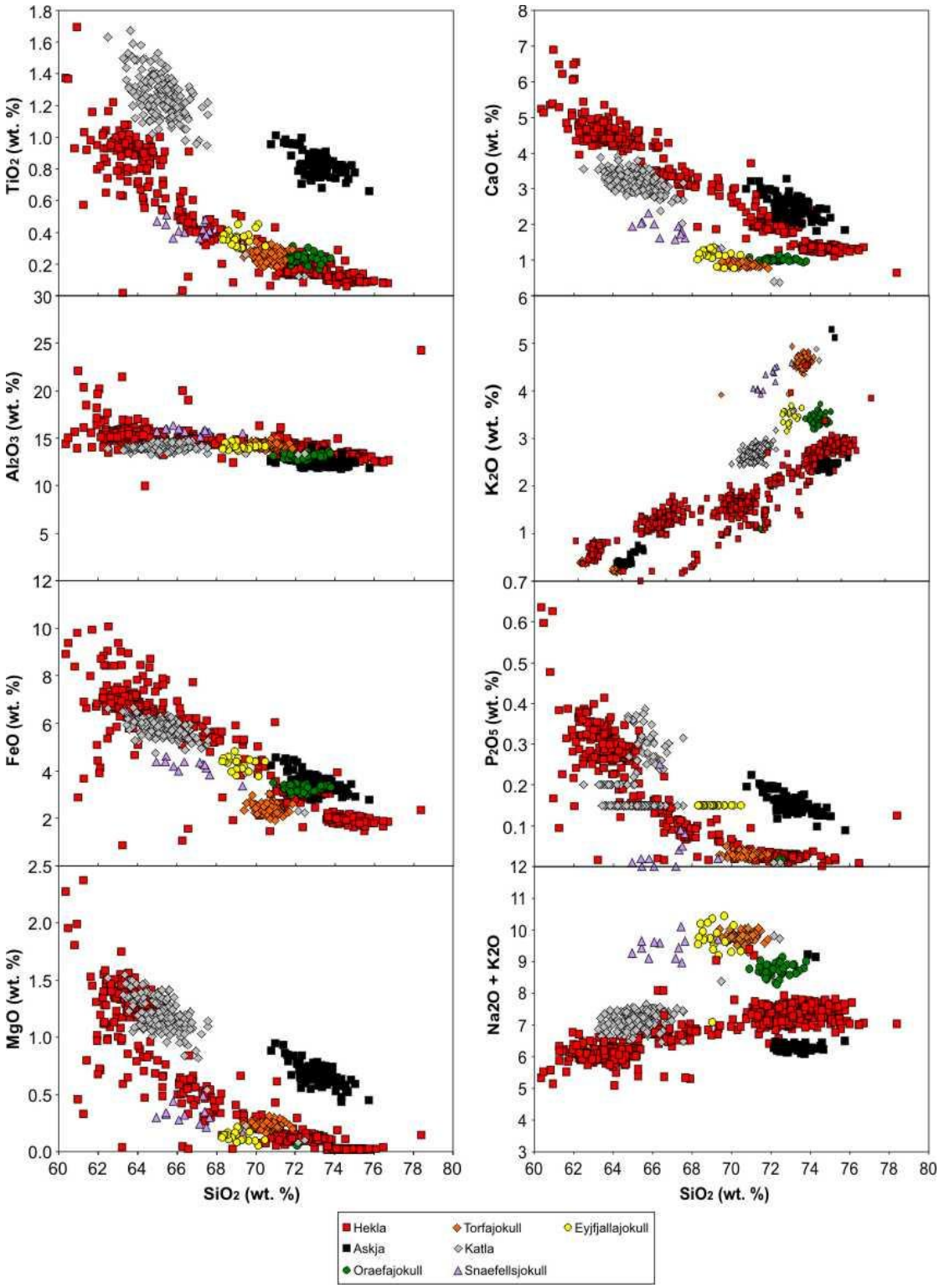

Figure 5.35: bivariate plots of the silicic components of each volcanic system plotting every element against SiO_2 wt. %. Plotting each element will establish which elemental combinations allow for identification and discrimination of tephra provenance. Red squares = Hekla, black squares = Askja, green circles = Öræfajökull, orange triangles = Torfajökull, grey diamonds = Katla, purple triangles = Snæfellsjökull and yellow diamonds = Eyjafjallajökull.

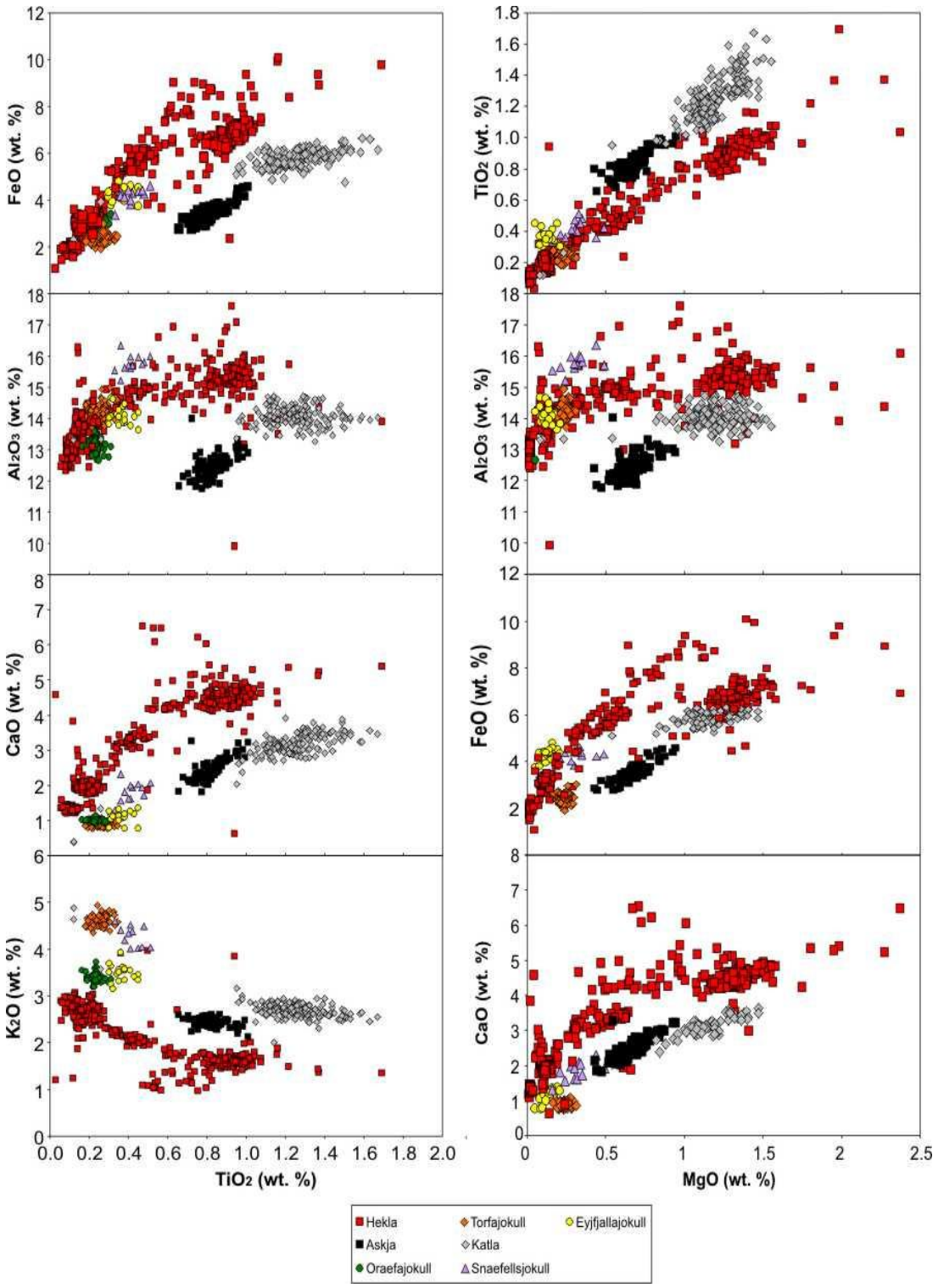

Figure 5.36: bivariate plots of the silicic components of each volcanic system plotting every element against TiO_2 and MgO wt. %. Plotting each element will establish which elemental combinations allow for identification and discrimination of tephra provenance. Red squares = Hekla, black squares = Askja, green circles = Öræfajökull, orange triangles = Torfajökull, grey diamonds = Katla, purple triangles = Snæfellsjökull and yellow diamonds = Eyjafjallajökull.

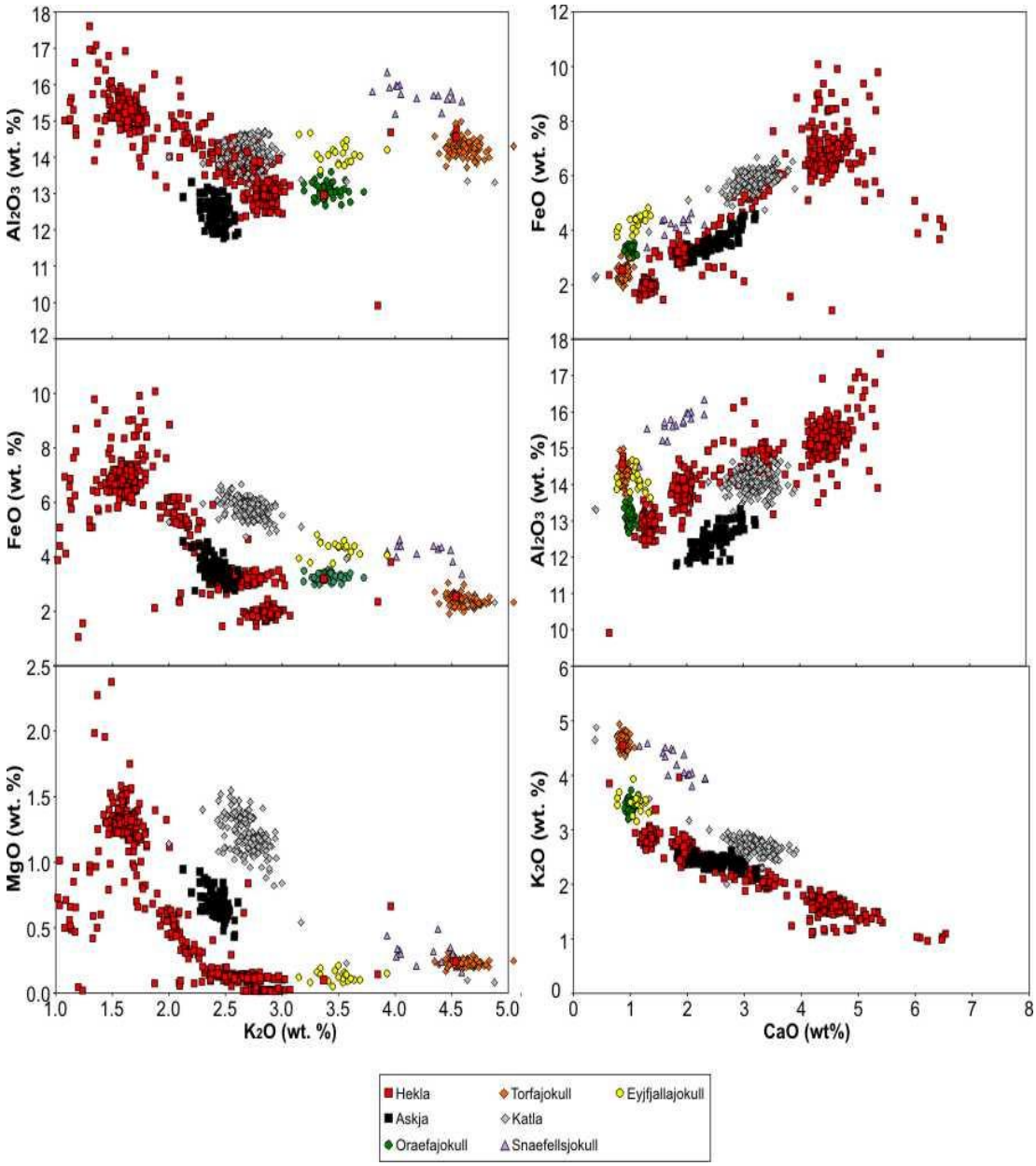

Figure 5.37: bivariate plots of the silicic components of each volcanic system plotting every element against K_2O and CaO. Plotting each element will establish which elemental combinations allow for identification and discrimination of tephra provenance. Red squares = Hekla, black squares = Askja, green circles = Öræfajökull, orange triangles = Torfajökull, grey diamonds = Katla, purple triangles = Snæfellsjökull and yellow diamonds = Eyjafjallajökull.

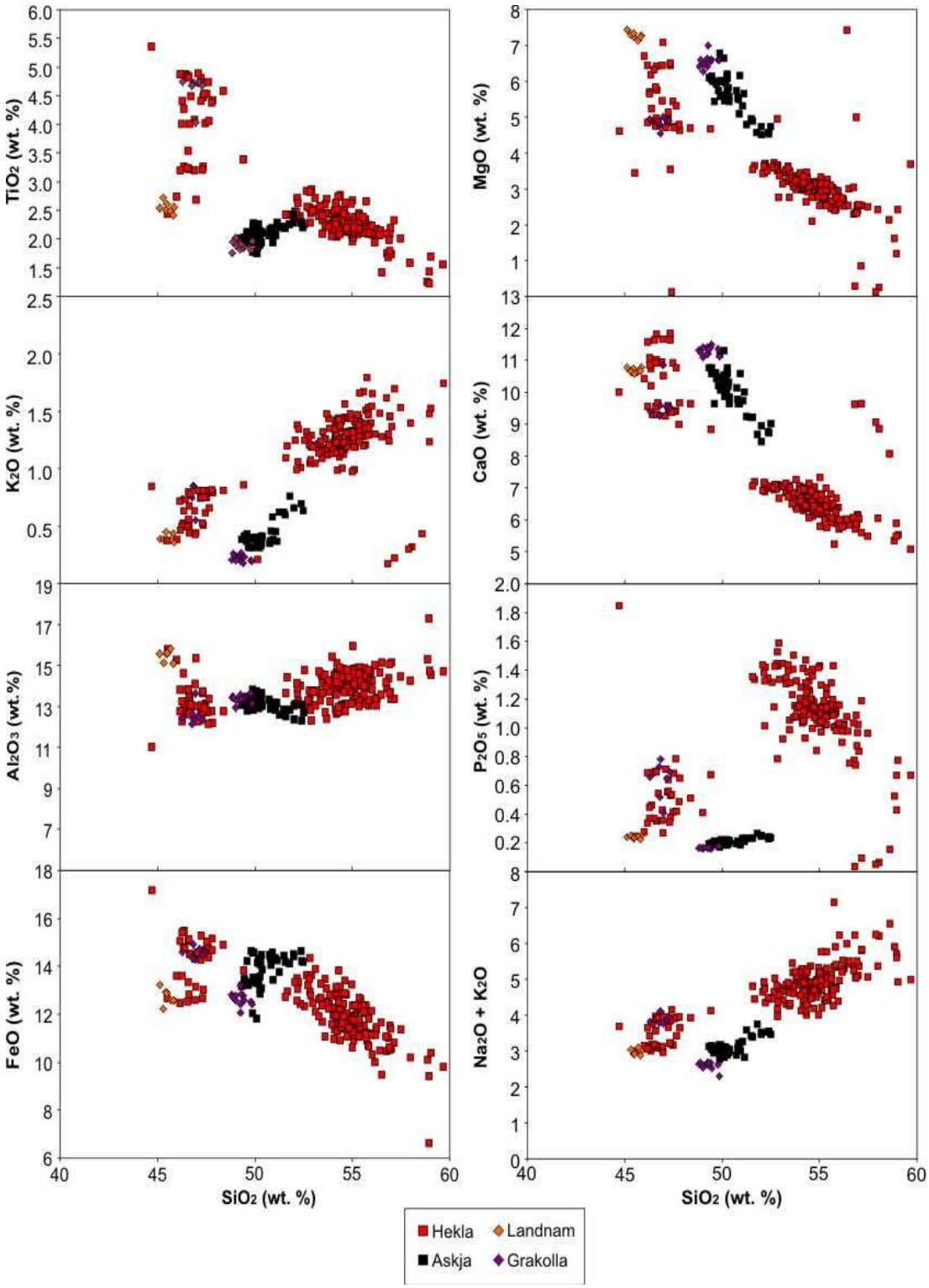

Figure 5.38: bivariate plots of the mafic components of each volcanic system plotting every element against SiO_2. Plotting each element will establish which elemental combinations allow for identification and discrimination of tephra provenance. Red squares = Hekla, black squares = Askja, orange and purples triangles = Torfajökull.

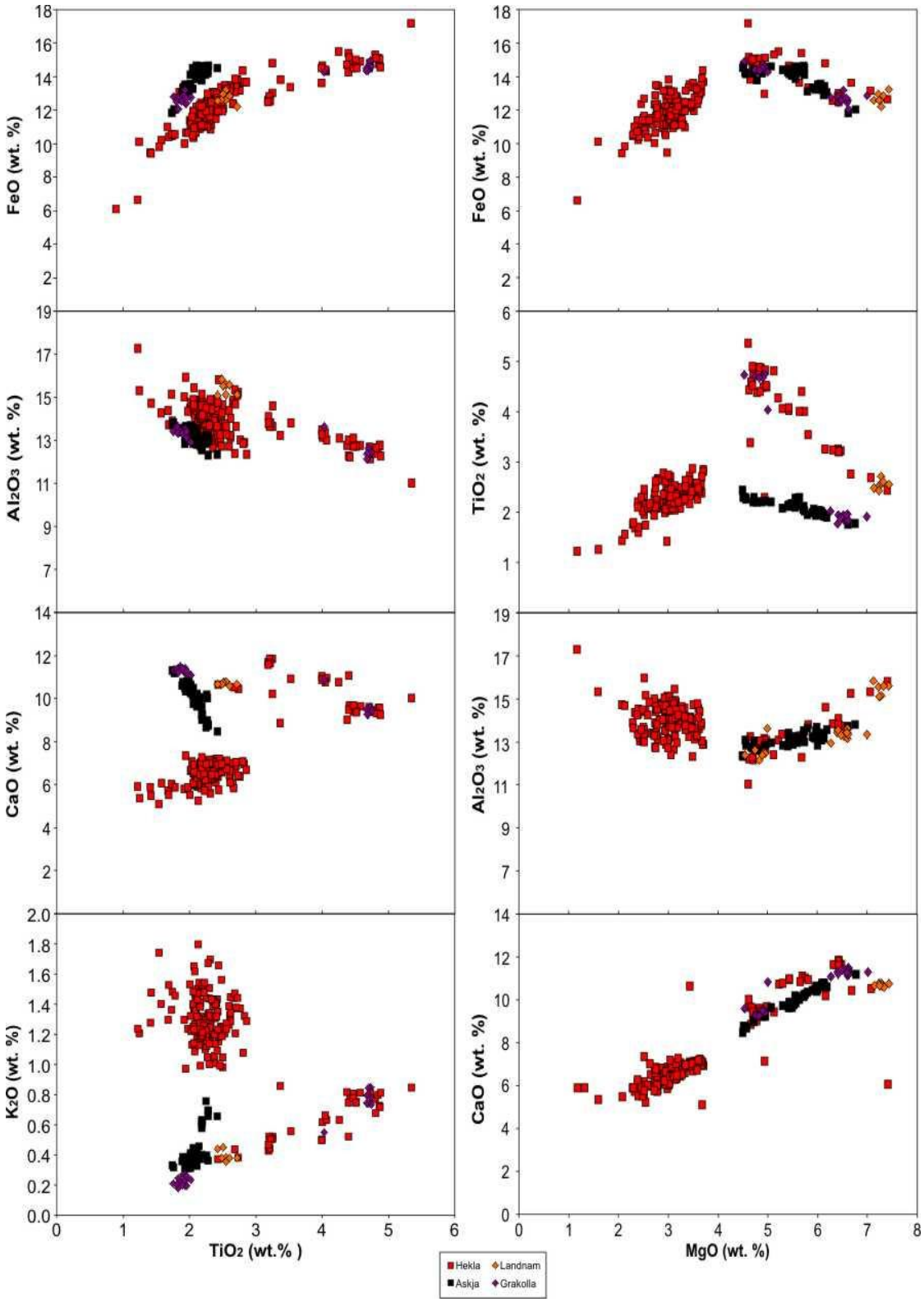

Figure 5.39: bivariate plots of the mafic components of each volcanic system plotting every element against TiO_2 and MgO. Plotting each element will establish which elemental combinations allow for identification and discrimination of tephra provenance. Red squares = Hekla, black squares = Askja, orange and purples triangles = Torfajökull.

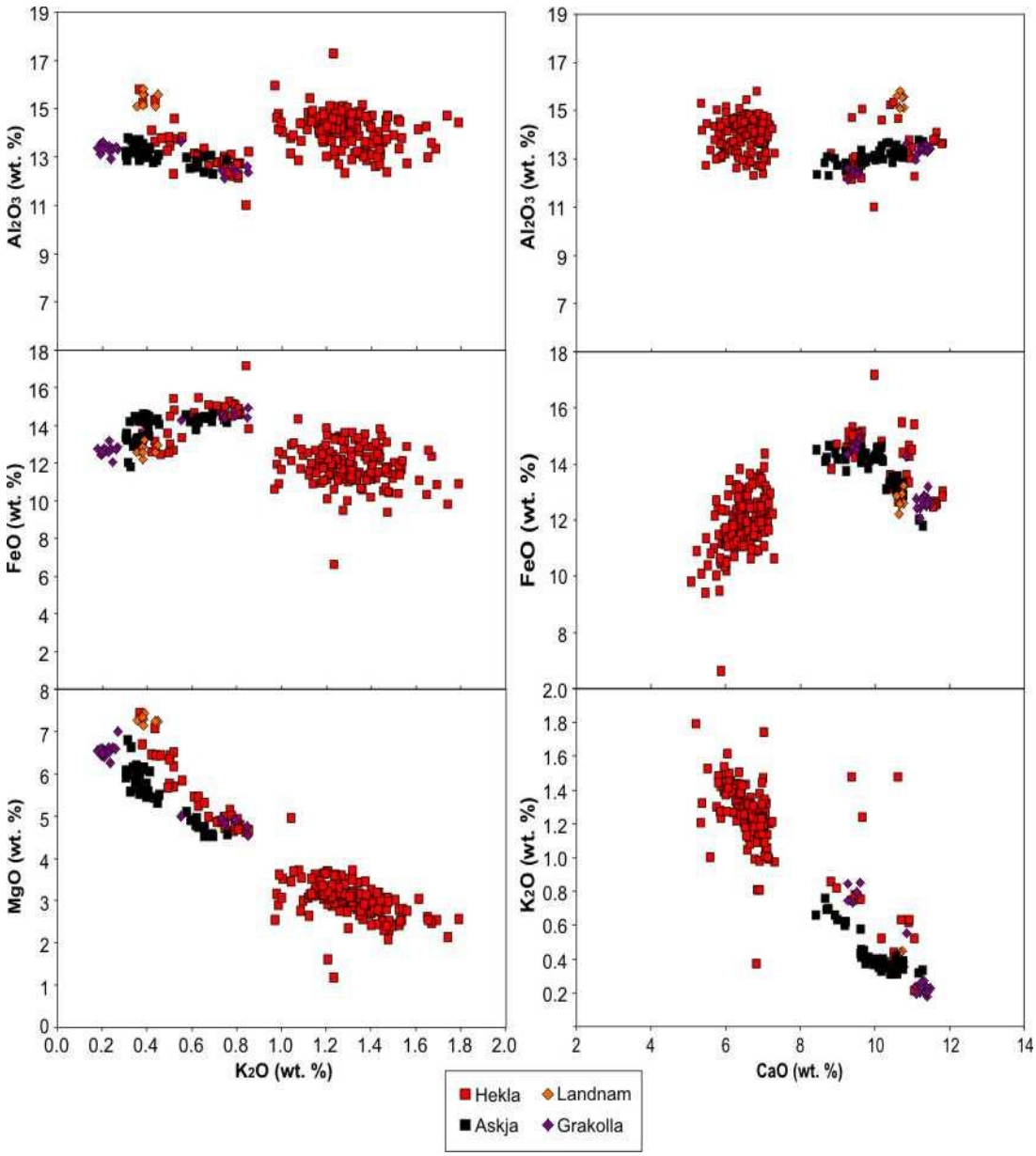

Figure 5.40: bivariate plots of the mafic components of each volcanic system plotting every element against K_2O and CaO. Plotting each element will establish which elemental combinations allow for identification and discrimination of tephra provenance. Red squares = Hekla, black squares = Askja, orange and purples triangles = Torfajökull.

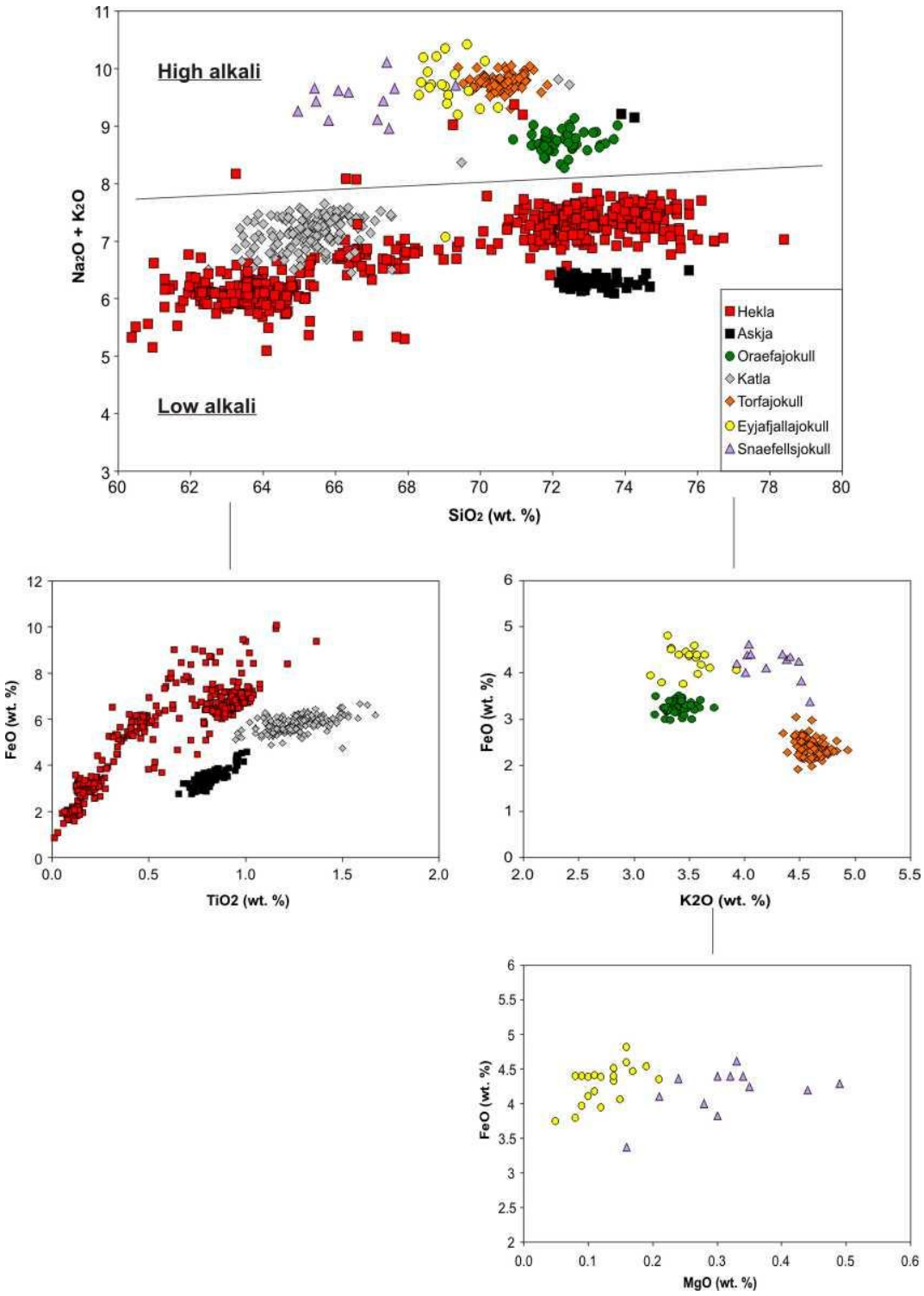

Figure 5.41: basic methodology for identifying tephra provenance of silicic tephra layers using major elements. The data used is new data, with the exception of data for Eyjafjallajökull and Snæfellsjökull volcanic systems which are sourced from Larsen *et al*. (1999).

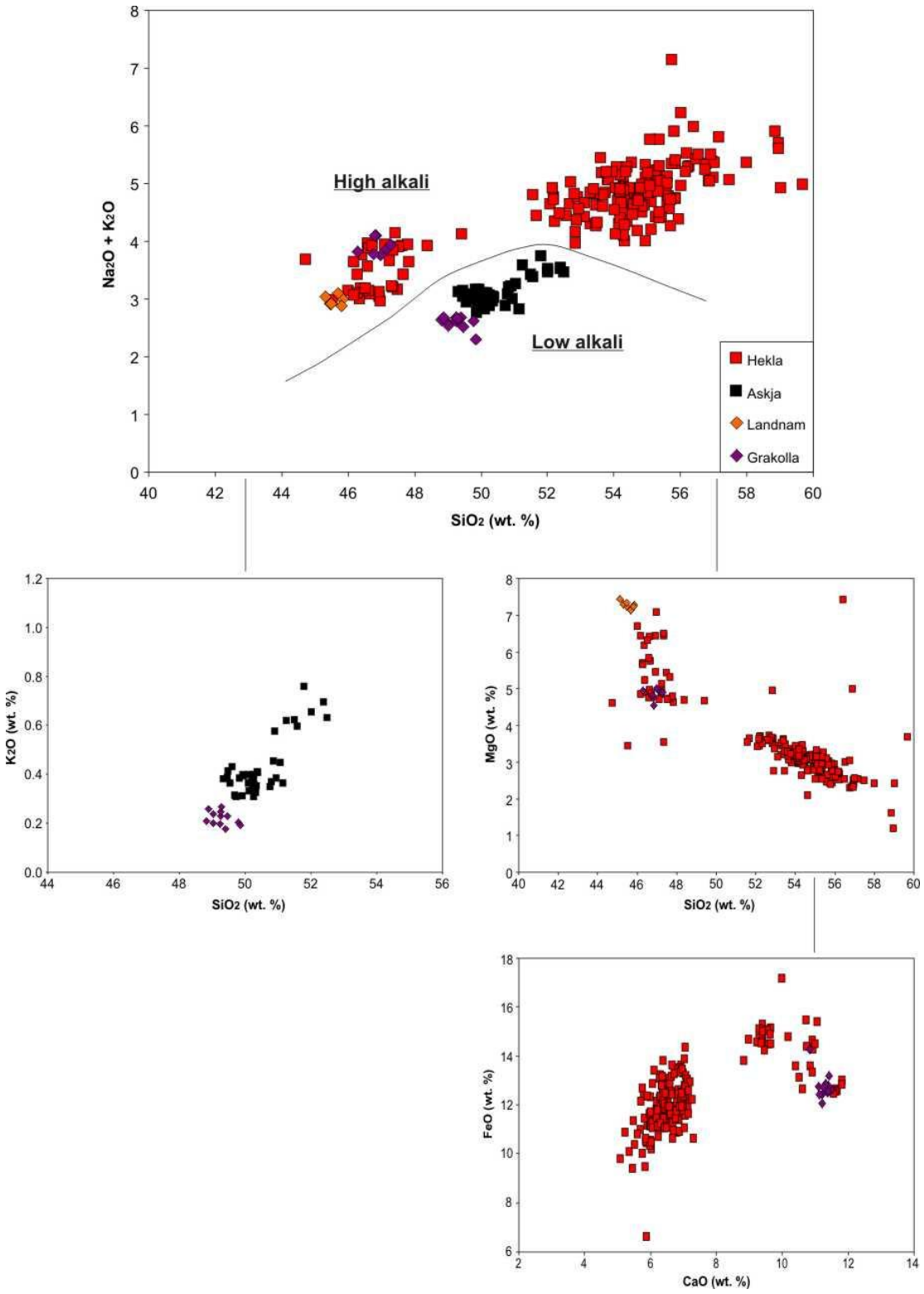

Figure 5.42: basic methodology for identifying tephra provenance of the mafic component of silicic tephra layers using major elements. The data used is new, however only covers the mafic component of the silicic tephra layers studied in this thesis and therefore does not represent the full suit of mafic tephra layers in Iceland.

reference data set highlights data which have undergone loss of volatiles during EMPA analysis or during preservation. This method is applicable to macro and micro-tephra horizons from proximal, medial, distal and far-distal sampling locations.

The methodology presented for identifying and discriminating between mafic tephra layers is focused solely on the mafic components of silicic tephra layers. The method does not incorporate all explosive mafic eruptions of Icelandic origin nor does it include data from every volcanic system in Iceland, only those known to produce silicic magmas. Such data would be required to reliably identify an unknown mafic tephra layer. Methodologies for identifying mafic tephra layers are presented in Oladóttir *et al*. (2008) and A. Jagan (2010).

5.6 Summary

This chapter has presented field and chemical data for tephra layers sourced from four Icelandic volcanoes. The physical and chemical characteristics of each tephra layer have been described. A formal framework for establishing the provenance of an unknown silicic tephra layer and in turn tephra identity has been proposed. When studying high silica tephra layers (> 60 wt. % SiO_2), plotting a TAS diagram groups volcanic systems into high and low alkali groups. Volcanic systems can then be identified and separated based on bivariate plots of major element combinations.

The work in this chapter has focuses on the identification of tephra provenance. However as established in Table 5.1, the volcanic systems studied here are often characterized by more than one explosive eruption. Successful identification and discrimination of individual tephra layers sourced within the same volcanic system is of equal if not greater importance to confirming tephra provenance. The Hekla central volcano is one such example with over 13 large intermediate to silicic eruptions occurring between 896 – 7125 BP. The following chapter will present field and chemical data for the Hekla system and will investigate the potential for discriminating between its tephra layers.

Chapter 6:

Major Elements as a tool for identifying tephra layers sourced within the same volcanic system. Hekla: a case study

6.1 Introduction

The previous chapter has enhanced the potential for identifying tephra provenance using major element chemistry. This chapter aims to develop on this work through the acquisition of new, high precision major element chemistry on key tephra layers sourced within the same volcanic system. In particular, this chapter focuses onto the Hekla central volcano.

The Hekla volcanic system is the most prolific producer of intermediate – silicic composition tephra in Iceland (Larsen *et al*. 1999). Tephra layers sourced from this system have been identified at widespread localities across the North Atlantic region (see Chapter 2) establishing these layers as valuable tools for dating in this area. The larger silicic eruptions are identified in distal localities across the North Atlantic region and provide reliable marker horizons for dating and correlating between marine, lacustrine and terrestrial sedimentary sequences (Fig. 6.5 a-e). The H4 tephra is used to date the decline in the Scots Pine in Scotland and Ireland (Blackford *et al*. 1992; Hall *et al*. 1994), the H1104, H3 and H4 tephra layers are used to date palaeo-oceanography events in the North Atlantic ocean (Eiríksson *et al*. 2000) and the H1104, H3, HSelsund and H4 tephra layers amongst others are used to date climatic changes occurring since the Younger Dryas period (Caseldine *et al*. 1998; Langdon and Barber, 2004; Vorren *et al*. 2007).

The Hekla tephra layers discussed in this chapter range in age from c. 7,000 BP to c.896 BP. Any mis-identification of a Hekla tephra layer could therefore introduce incorrect dates which propagate through interpretations based on such data. It is therefore imperative that when a tephra layer of Hekla provenance is identified in a sedimentary succession, its identity must be confirmed using robust methods, before any further work be conducted.

The main aims of this chapter are as follows:

1. To identify a list of key Holocene silicic tephra marker layers sourced from the Hekla volcanic system that complement previous studies and to identify new potential marker layers within the Hekla volcanic succession.
2. To locate an appropriate proximal reference section for each tephra layer. To log and sample each section for complete characterisation of chemical and physical properties.
3. To establish a robust reference dataset for key silicic marker layers from the Hekla volcanic system using major element chemistry collected by electron microprobe (EMPA) and x-ray florescence (XRF) at the University of Edinburgh.
4. To use the data to refine a logical and systematic methodology for identifying and discriminating between tephra layers sourced within the same volcanic system.

The work conducted in this chapter will focus on refined data collected from the Hekla volcanic system with particular reference to Holocene eruptions including the large-scale silicic eruptions (H1104, H3, HSelsund, H4 and H5) and the small-scale intermediate eruptions (HA, HB, HC, HM, HN, HX, HY, HX). Background information on each of the tephra layers is presented in Chapter 2. Details of field sampling methods and analytical techniques are described in Chapter 4.

6.2 Results

This section presents the field and chemical data for the tephra layers noted in section 6.1. Field data includes field-based outcrop descriptions and interpretations, sedimentary logs of the reference sections and photographs of the outcrop. Chemical data includes tabulated EMPA and XRF data and descriptions of geochemistry aided with graphical figures. Note that geochemical data is presented as averages with 2σ values. Full data sets are available within the Appendix.

6.2.1 Hekla 1104

The H1104 tephra layer is the only large rhyolitic eruption to have occurred at the Hekla

central volcano during historical time and erupted 846 BP. The following section presents field and chemical data collected for this tephra layers.

Field Data: The reference section for the H1104 tephra layer was selected at 64º 03'478N, 19º 46'398E near Búrfell on route 26 (Table 4.1; Fig. 4.6). Figure 6.1 is a stratigraphic log of the tephra layer compiled at this location while figure 6.2 is a field photograph of the tephra layer at the reference section. At this location, the tephra layer is 0.6 m thick. The tephra layer is dominated by white rhyolitic pumice clasts, with a thin, discontinuous mafic top. The tephra layer contains only one distinct package which will be discussed below.

The H1104 tephra layer is 60 cm thick and dominated by milky white rhyolitic pumice clasts. The tephra layer shows internal layering highlighted by the colour change in the pumice clasts, but no other depositional structures are recorded. Grain size is very medium to coarse lapilli while average clast size is c. 3 cm. The tephra layer is clast supported and well sorted. Pumice clasts are sub-angular to sub-rounded; however some clasts are flaky in appearance with sharp edges. The tephra layer contains minimal lithic components, those identified are hydrothermally altered. At the sampling location, the tephra layer is underlain by three white rhyolitic tephra layers. The lowermost is the H3 tephra layer, the second is the HC and the upper most is considered to be the HB tephra layer.

The H1104 tephra layer represents a pumice fall from a Plinian eruption from the Hekla volcano. The eruption produced a dominantly rhyolitic deposit suggesting a prolonged period of repose prior to eruption. The deposit shows some zoning, suggesting the presence of a zoned magma chamber beneath the volcano. The ratio of juvenile:lithic material in the deposit suggests a dominantly magmatic eruption with little or no interaction with external water sources. The fine- grained nature of the pumice clasts in the upper and lower 10 cm of the tephra layer represent temporal variation in eruption intensity. Grain size distributions suggest that the middle of the eruption was the highest intensity phase. These grain size variations may also be the result of variations in wind direction and intensity and cannot be ruled out without investigation of multiple reference sections, which was outside the scope of this project.

Chemical Data: In total, four samples were analysed for the H1104 tephra layer collected from one sampling location. The new major element data collected via EMPA and XRF for

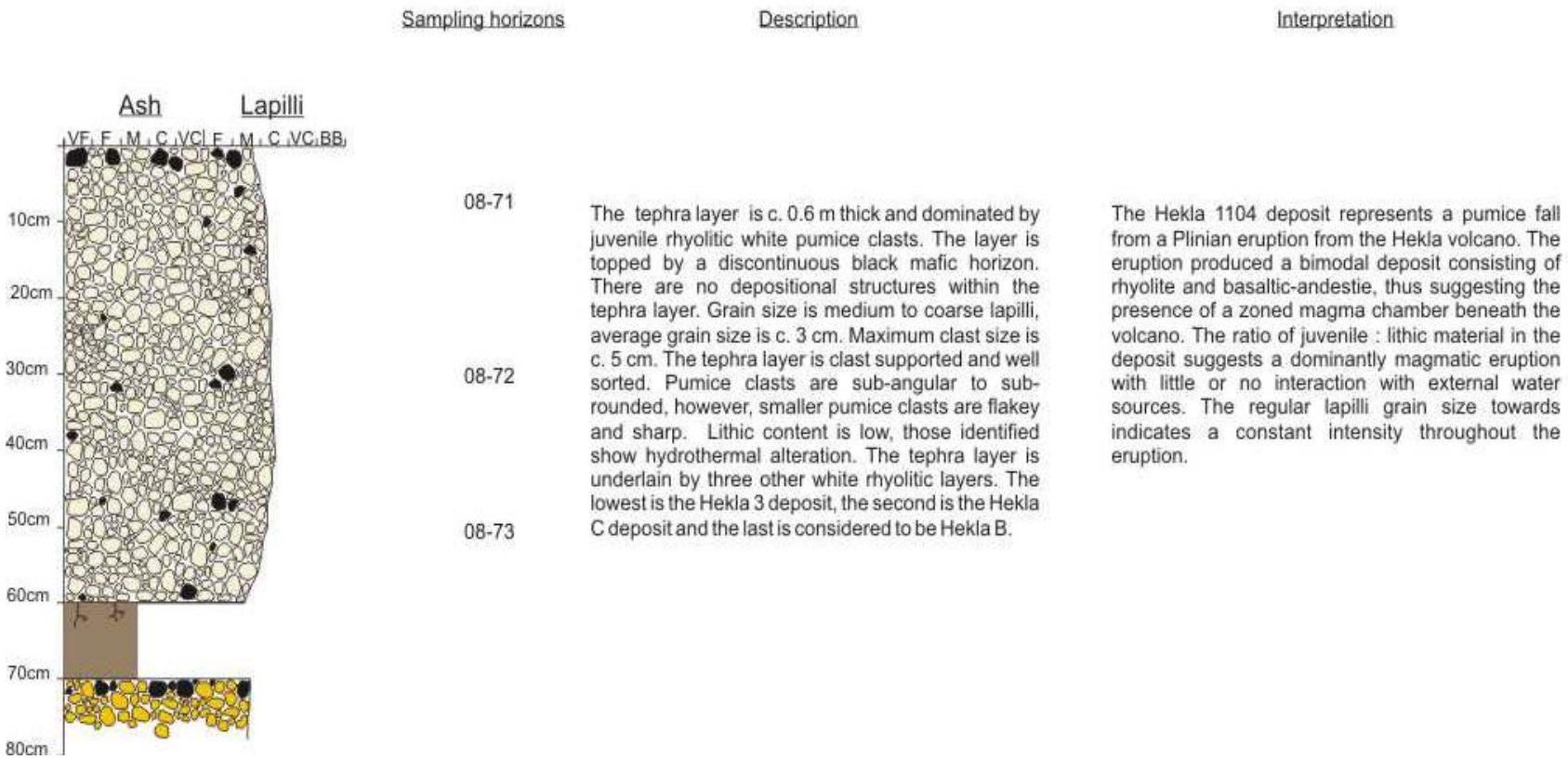

Figure 6.1: Stratigraphic log of the H1104 tephra layer showing physical characteristics e.g. colour, clast morphology and grain size. Drawn at the reference section near Burfell on route 26.

Figure 6.2: Field photograph of the H1104 tephra layer at the sampling location near Burfell on route 26. Trowel used as scale measures c. 25 cm. Photograph: Rh. Meara.

Table 6.1: Glass chemistry of the rhyolitic H1104 tephra layer. Samples were collected from proximal locations on the flanks of the volcano as indicated in Fig. 4.6. Ten electron probe analyses were collected for each sample (with the exception of sample 08-71 b) and the data presented is the average of these analyses and two standard deviations. Full data sets are available in the Appendix.

Sample	SiO_2	TiO_2	Al_2O_3	FeO	MnO	MgO	CaO	Na_2O	K_2O	P_2O_5	Total
08-71b	56.95	2.09	13.68	11.50	0.30	2.51	6.15	3.93	1.45	0.96	99.54
2 σ	na	na	na	na	na	na	na	na	na	na	na
08-71	72.50	0.20	13.78	3.20	0.12	0.11	1.96	4.76	2.72	0.02	99.38
2 σ	1.10	0.07	0.40	0.25	0.03	0.03	0.11	0.38	0.17	0.01	1.06
08-72	71.88	0.22	13.85	3.15	0.12	0.17	1.98	4.74	2.69	0.02	98.83
2 σ	1.62	0.04	0.72	0.29	0.02	0.32	0.10	0.30	0.12	0.01	1.83
08-73	72.55	0.17	13.84	3.17	0.12	0.11	1.99	4.73	2.70	0.02	99.40
2 σ	1.53	0.06	0.63	0.23	0.02	0.05	0.14	0.26	0.09	0.01	2.23

Table 6.2: Whole rock chemistry of the rhyolitic H1104 tephra layer. Samples were collected from proximal locations on the flanks of the volcano as described in Figure 4.6.

Sample	SiO_2	TiO_2	Al_2O_3	FeO	MnO	MgO	CaO	Na_2O	K_2O	P_2O_5	Total
08-70	66.07	0.39	14.59	6.61	0.17	0.37	3.04	4.65	2.13	0.08	104.05
08-71	67.48	0.37	14.27	5/04	0.14	0.27	2.59	4.75	2.40	0.07	102.98
08-72w	67.72	0.36	14.30	5.48	0.14	0.26	2.61	4.81	2.40	0.07	103.07
08-72g	67.92	0.38	14.28	5.54	0.14	0.28	2.63	4.79	2.44	0.07	103.47
08-73	67.64	0.37	14.28	5.56	0.14	0.28	2.60	4.81	2.41	0.07	103.16
08-74	67.42	0.38	14.32	5.60	0.14	0.31	2.65	4.71	2.38	0.07	103.03

the tephra layer is presented in Tables 6.1 and 6.2. The tephra layer shows two main geochemical sub-groups at the sampling location: a high silica and low silica phase.

The chemical characteristics of the tephra layer are shown by figures 6.3 to 6.7. The tephra layer has both a rhyolitic and a basaltic andesite glass composition while the bulk composition is dacitic (Fig. 6.3). The tephra layer is metaluminous (Fig. 6.4). The silicic phase of the tephra layer exhibits a restricted compositional range with minimal geochemical variation with stratigraphic height (Fig. 6.7) with the exception of a small sub-set of mafic grains taken at sampling height 08-71. The tephra layer shows a low alkaline nature as indicated by the compositional fields suggested in Rollinson (1993) and references therein.

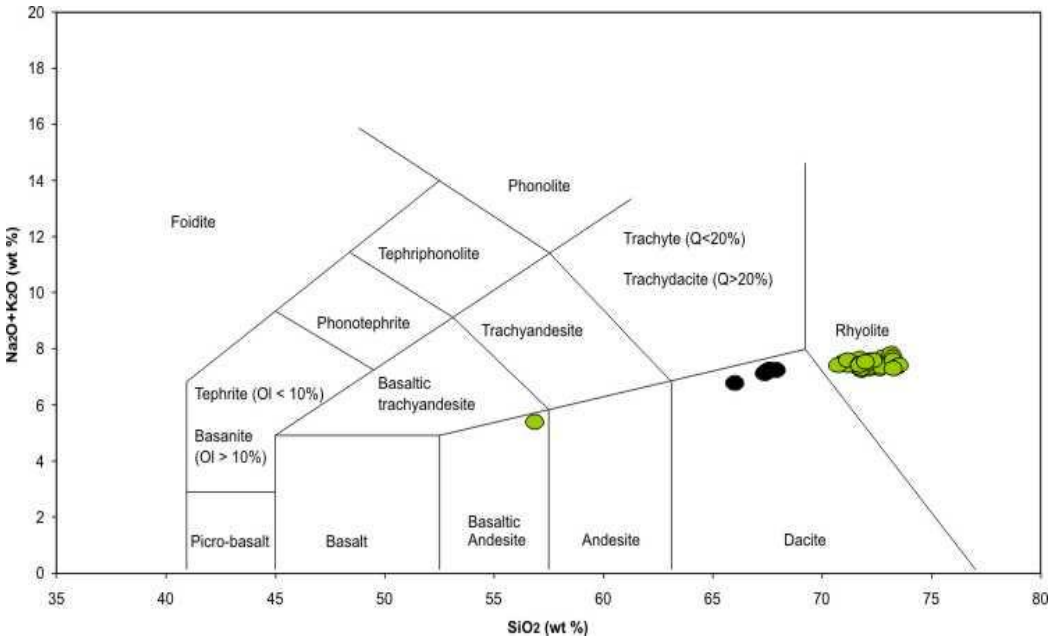

Figure 6.3: Total Alkali – Silica bivariate plot of the H1104 tephra layer. Green circles represent EMPA data, black circles represent XRF data. EMPA data indicate that the tephra layer shows a bimodal geochemistry with rhyolititc and basaltic andesite components. XRF data suggests that bulk chemistry is dacitic. Grid lines adapted from La Maitre *et al*. (1989).

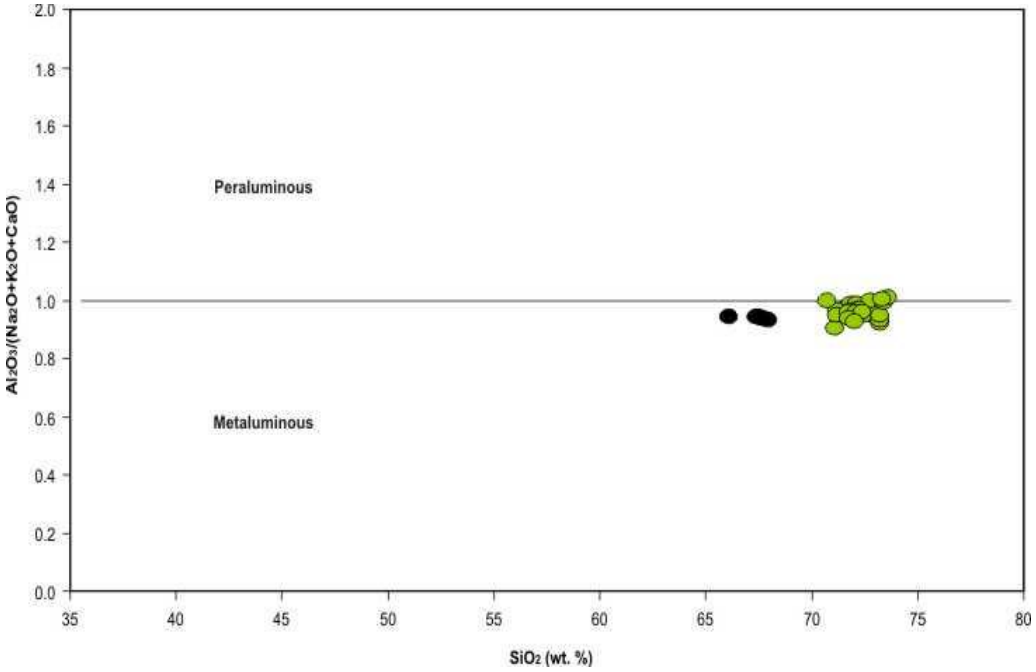

Figure 6.4: Silica – Aluminium and total alkali plot of the H1104 samples. Green circles represent EMPA data, black circles represent XRF data. Data indicate that the tephra layer shows a metaluminous geochemistry consistent with the geological setting.

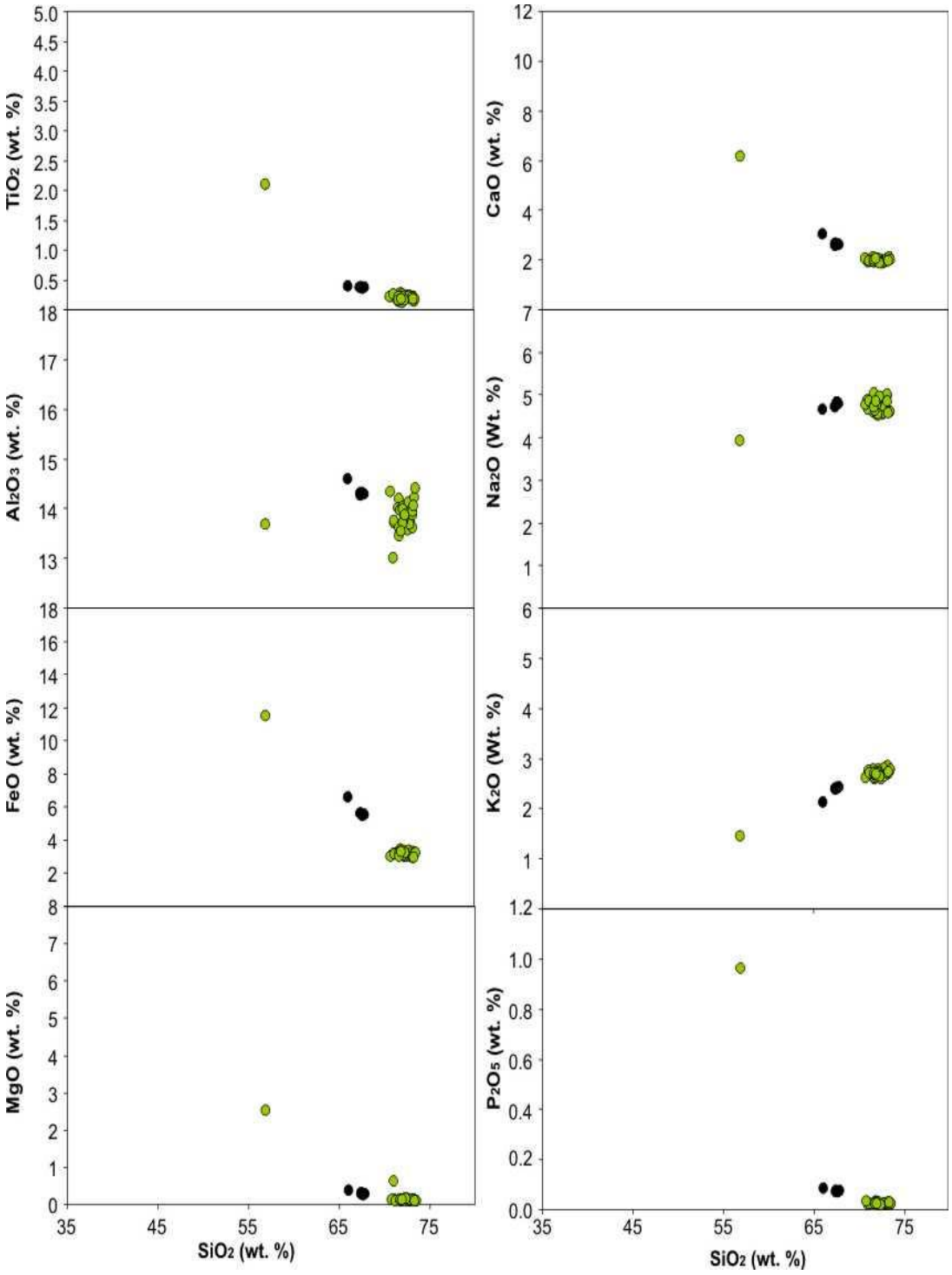

Figure 6.5: Bivariate plots of XRF and EMPA data for the H1104 tephra layer. Green circles represent EMPA data whilst black circles represent XRF data. Geochemical variations recorded between XRF and EMPA data sets confirm the occurrence of fractional crystallisation within the magma prior to eruption.

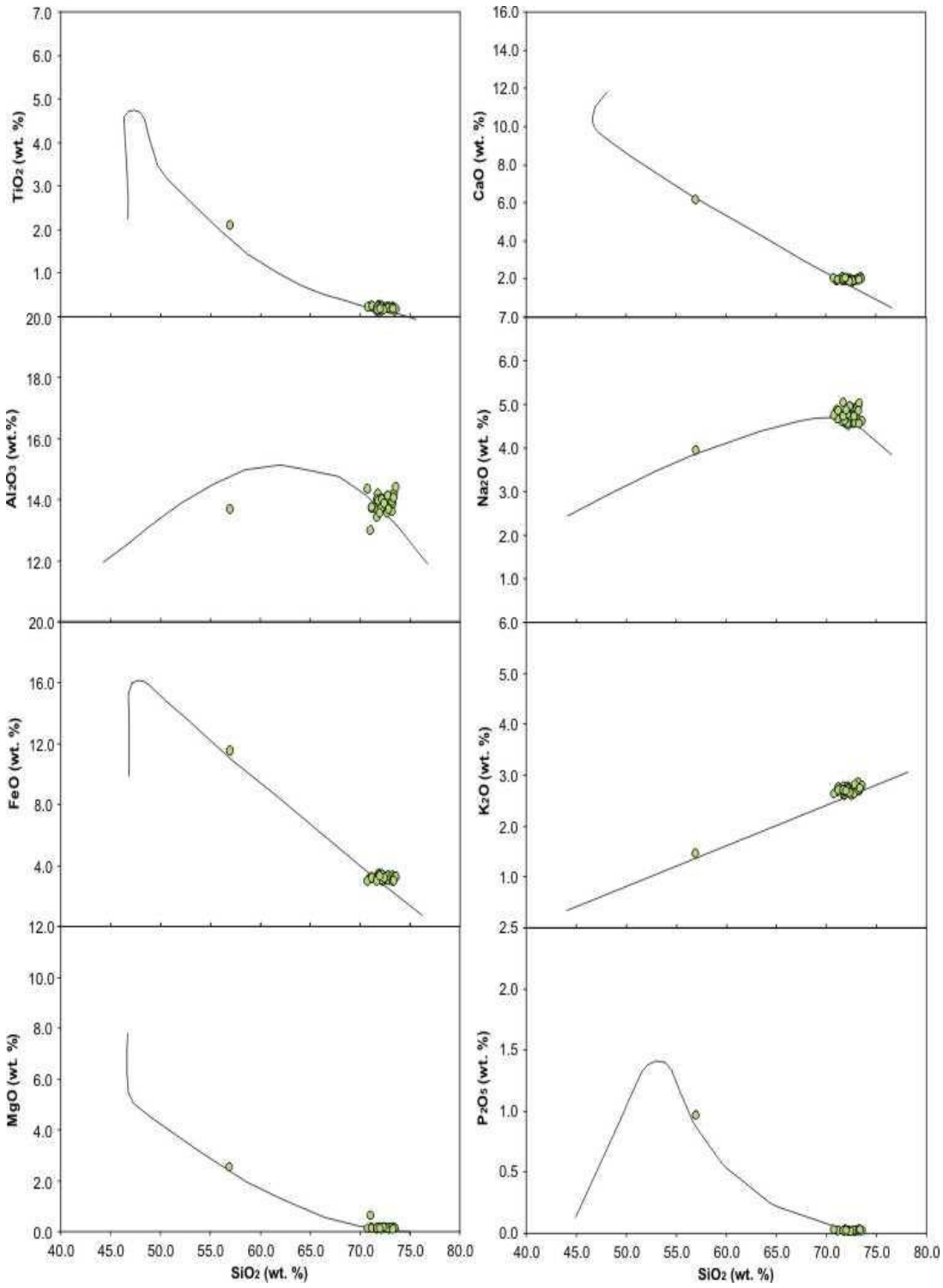

Figure 6.6: Harker plots of H1104 data plotted onto the crystallization trends of major elements against SiO_2 (wt. %) for the volcanic system. Black lines represent data collected for the Hekla volcanic system by previous workers.

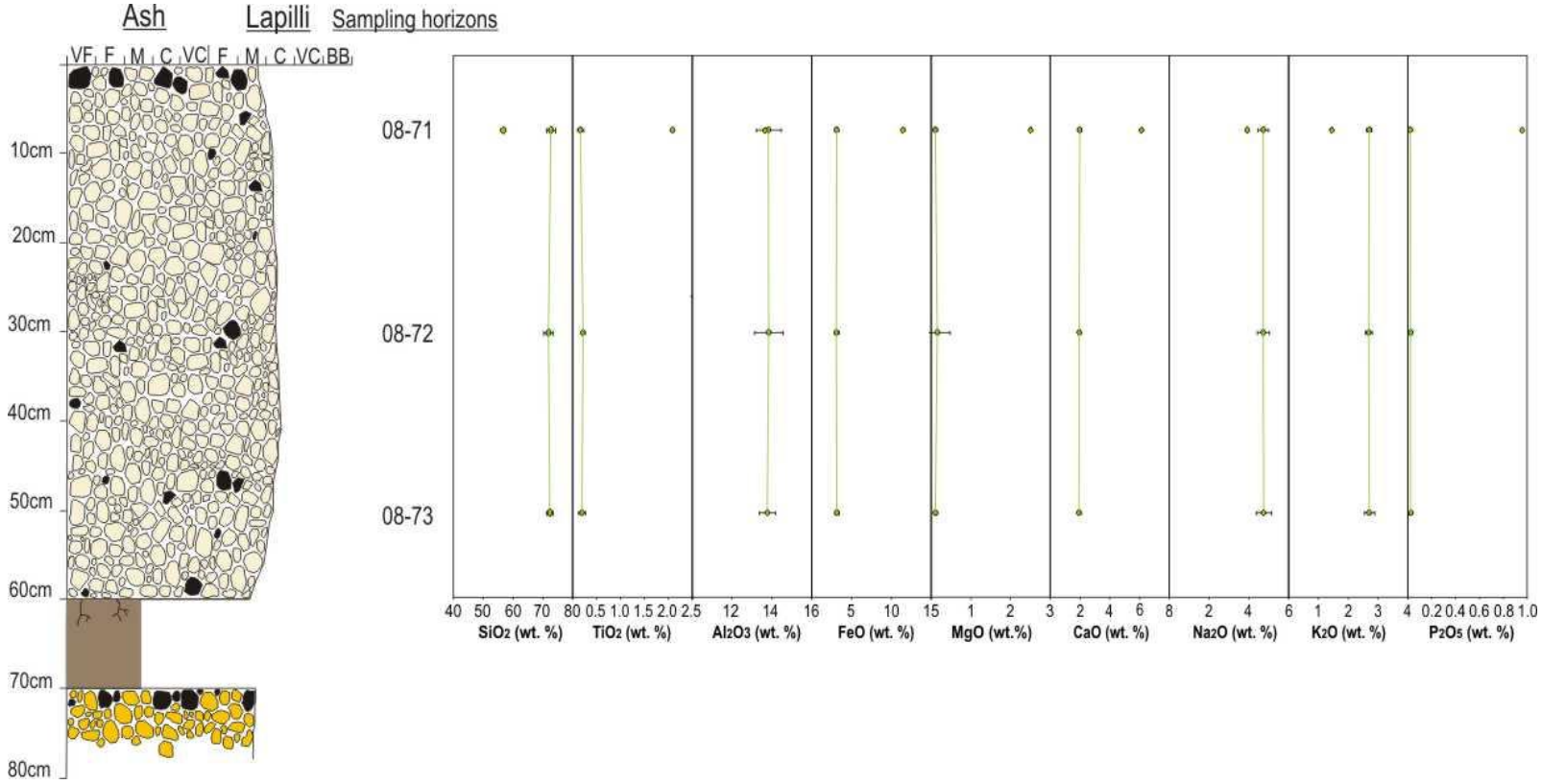

Figure 6.7: Chemical variation with stratigraphic height for the H1104 tephra. Elements depicted represent the full suite of major elements analysed with the exception of MnO. No major variations in elemental concentrations are recorded with the exception of sample 08-71 which comprises the upper mafic component of the tephra layer.

Comparing XRF and EMPA data highlights variation in SiO_2 concentrations between the data sets (Fig 6.5). Also highlighted are increases in Al_2O_3, FeO, MgO, CaO and P_2O_5 as well as a subtle decrease in K_2O concentrations in the XRF data compared with the glass data. These differences are the result of removal of these elements from the glass phase through fractional crystallization of titanomagnetite, plagioclase, olivine, pyroxene and apatite during melt generation.

6.6.2 Hekla 3

The H3 eruption occurred in 2879 BP. The field and chemical data collected for the H3 tephra layer is presented below.

Field Data: The reference section for the H3 tephra layer was selected at 64º 02.373'N 19º 44.539'E near Ófærugil (Table 4.1; Fig. 4.6). Figure 6.8 is a stratigraphic log of the tephra layer compiled at this location while figures 6.9 – 6.11 are field photographs of the tephra layer at the reference section. At this location, the tephra layer is 2.7 m thick. The tephra layer is comprised of three distinct packages: Phase I, Phase II and Phase III. These packages will be discussed individually below.

Phase III of the eruption is 1.0 m thick and is dominated by white pumice clasts with a thin top of dark brown-black clasts. The unit shows internal layering as defined by the changes in colour, but no other depositional structures are recorded. Grain size is very coarse lapilli. Average grain size is c. 4 cm. Maximum clast size is c. 27 cm, representing pyroclastic bombs within the stratigraphy (Fig. 6.9). The tephra layer is moderately sorted and clast supported. Lithic clasts are rare dark grey in appearance and show minimal alteration. Phase III shows a characteristic colour change in the pumice clasts from white to orange. This is presumed to be a localised artefact of post-depositional oxidation.

Phase II of the eruptions is 1.18 m thick and dominated by white pumice clasts with no post-depositional oxidation. The unit shows some internal layering highlighted by variations in grain size and normal grading. Average grain size is very coarse lapilli. Average grain size is6 cm. Maximum clast size is 15 cm, representing pyroclastic bombs within the sequence. The tephra layer is moderately sorted and clast supported. Pumice clasts are angular to sub-angular. Lithic clasts are dark grey to black and show no alteration.

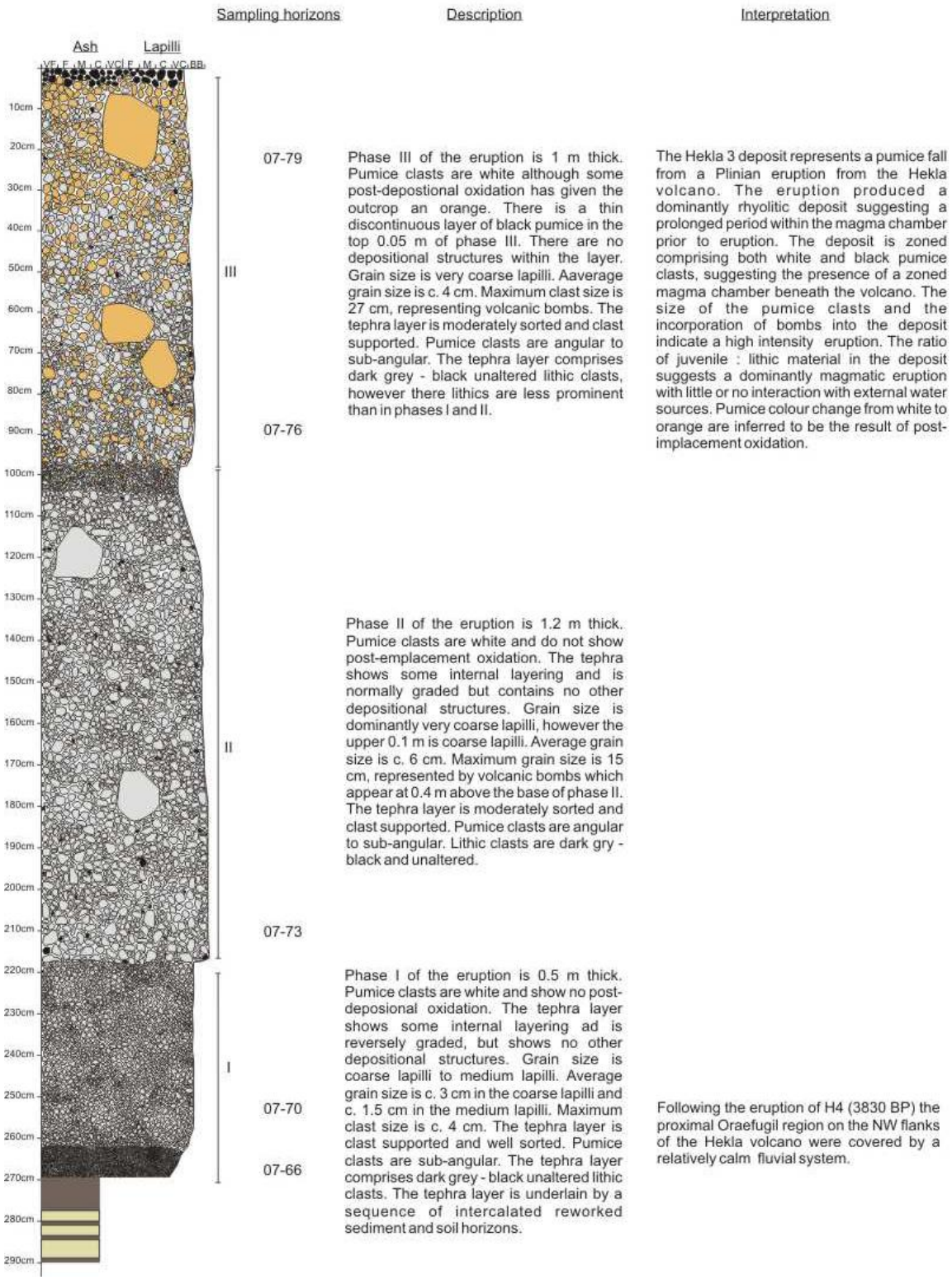

Figure 6.8: Stratigraphic log of the H3 tephra layer showing physical characteristics e.g. colour, clast morphology and grain size. Drawn at the reference section near Ófærugil.

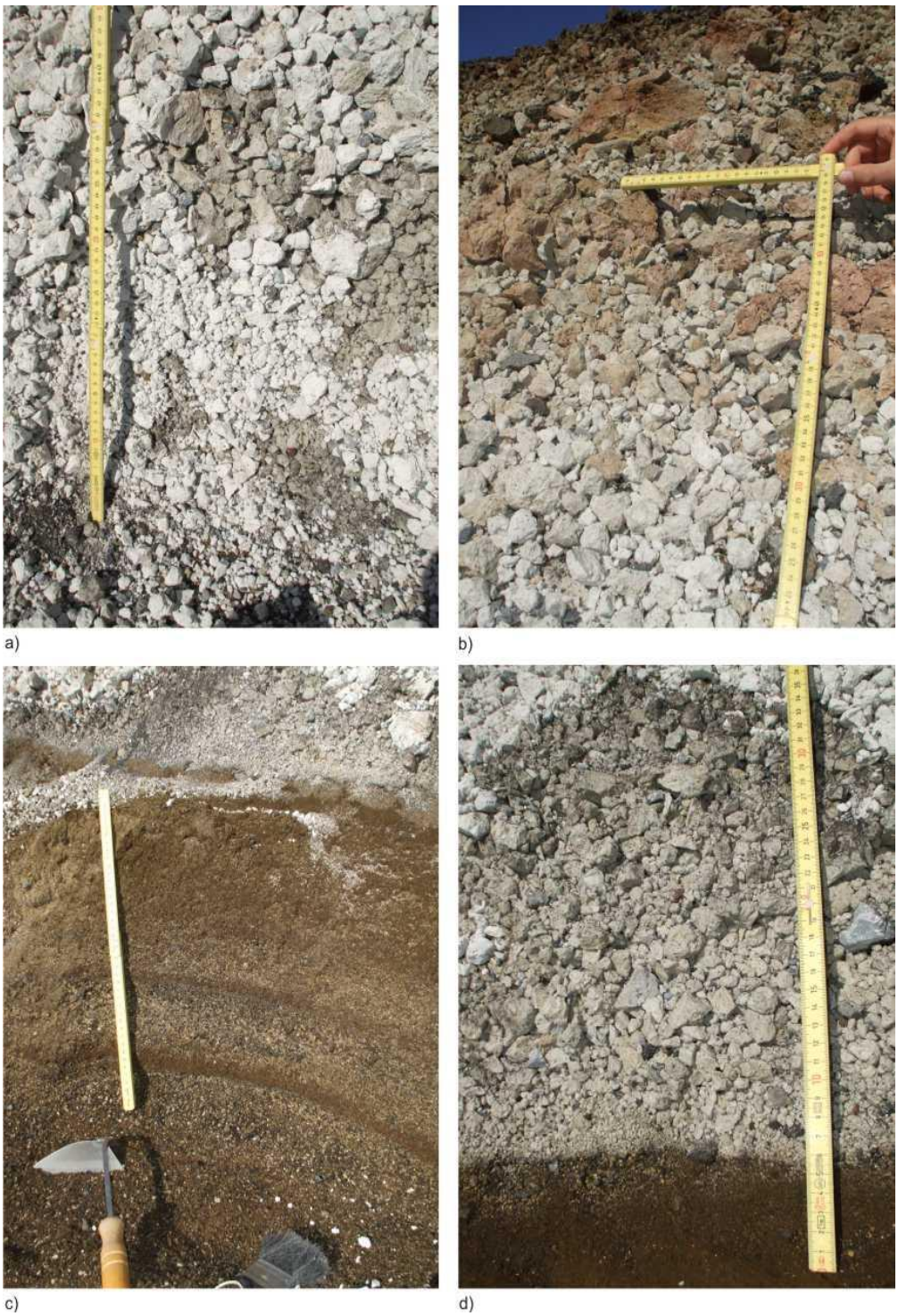

.

Figure 6.9: Field photographs of the H3 tephra layer at the reference section near Ófærugil. a) middle section of the H3 tephra showing coarse pumice clasts. Scale measures c. 50 cm. b) Upper section of the H3 tephra showing black mafic top, coarse orange pumices including bomb-sized clasts. Scale measures c. 40 cm vertically. c) Interacalated fluvial sediment underlying the H3 tephra layer. Scale measures c. 40 cm. d) Fine grained lapilli at the base of the H3 tephra layer. Scale measures c. 35 cm. Photographs: Rh. Meara.

Figure 6.10: Pyroclastic bomb measuring c. 25 cm within the H3 deposit at the pumice quarry near Ófærugil. The orange appearance is due to post eruptive oxidation and is indicative of this unit in proximal locations. Photograph: Rh. Meara.

Figure 6.11: H3 sampling location near Ófærugil. H3 is the highest white tephra layer, underlain by the H4 tephra layer. Note the thick packages of fluvial sediment preceding each tephra layer. Photograph: Rh. Meara.

6 cm. Maximum clast size is 15 cm, representing pyroclastic bombs within the sequence. The tephra layer is moderately sorted and clast supported. Pumice clasts are angular to sub-angular. Lithic clasts are dark grey to black and show no alteration.

Phase I of the eruption is 0.52 m thick and dominated by white pumice clasts with no post-depositional oxidation. The unit shows some internal layering highlighted by variations in grain size and reverse grading. Average grain size is coarse lapilli. Average grain size is c. 3 cm in the upper 0.44 m and c. 15 cm in the lower 0.08 m. Maximum clast size is c. 4 cm. The tephra layer is well sorted and clast supported. Pumice clasts are sub-angular. Lithic clasts are dark grey to black and show no alteration. The tephra layer is immediately underlain by a sequence of intercalated re-worked sediment (Fig. 6.9c), and by a succession of fluvial sediments (Fig. 6.11).

The H3 deposit represents a pumice fall from a Plinian eruption from the Hekla volcano. The eruption produced a dominantly rhyolitic deposit suggesting a prolonged period of repose prior to eruption. The deposit shows some zoning, suggesting the presence of a zoned magma chamber beneath the volcano. The ratio of juvenile:lithic material in the deposit suggests a dominantly magmatic eruption with phases of vent clearing but minimal interaction with external water sources. Variations in grain size throughout the tephra layer represent temporal variation in eruption intensity. The highest intensity phases are represented by the largest grain sizes, indicating that Phases II and III were the highest intensity due to the inclusion of decimetre sized pyroclastic bombs.

Chemical Data: In total, seven samples were analysed for the H3 tephra layer collected from one sampling location. The new major element data collected via EMPA and XRF for is presented in Tables 6.3 and 6.4.

The chemical characteristics of the tephra layer are shown by figures 6.12 to 6.16. The tephra layer shows a range in glass composition from andesite, dacite to rhyolite and an andesitic to dacitic bulk composition (Fig 6.12). The tephra layer is metaluminous (Fig. 6.13). With the exception of sampling horizon 07-70, the rhyolitic component of the tephra layer shows minimal chemical variation with stratigraphic height. The sampling horizon 07-70 shows decreased SiO_2 and K_2O, and increased TiO_2, Al_2O_3, FeO, MgO, CaO and P_2O_5 (Fig. 6.16). Andesitic components to the tephra layer are present at sampling horizons 07-70 and 07-76, their absence at other sampling horizons is presumed to be the result of the

Table 6.3: Glass chemistry of the rhyolitic H3 tephra layer. Samples were collected from proximal locations on the flanks of the volcano as described in Figure 6.6. Twenty electron probe analyses were collected for each sample (with the exception of 07-76 and 07-79) and the data presented is the average of these analyses and two standard deviations. Full data sets are available in the Appendix.

Sample	SiO_2	TiO_2	Al_2O_3	FeO	MnO	MgO	CaO	Na_2O	K_2O	P_2O_5	Total
07-79	69.59	0.28	14.33	4.24	0.31	0.23	2.60	4.62	2.31	0.05	98.54
2 σ	3.73	0.16	1.26	2.16	0.07	0.17	0.99	0.36	0.27	0.05	3.75
07-76b	64.55	0.67	15.18	7.70	0.23	0.77	4.44	4.88	1.50	0.20	100.12
2 σ	1.25	0.15	1.34	1.52	0.09	0.32	0.54	0.86	0.58	0.08	1.38
07-76w	72.33	0.18	14.05	2.96	0.10	0.12	2.98	4.81	2.49	0.02	99.13
2 σ	1.53	0.06	1.60	0.67	0.04	0.05	0.64	0.93	0.46	0.01	1.55
07-73	72.05	0.17	13.81	2.99	0.11	0.12	1.98	4.58	2.55	0.02	98.38
2 σ	0.94	0.08	0.54	0.21	0.02	0.04	0.11	0.55	0.15	0.01	0.93
07-70b	64.51	0.71	14.87	7.65	0.22	0.77	4.39	4.76	1.51	0.22	99.35
2 σ	2.86	0.38	1.31	3.03	0.07	0.56	0.40	1.20	0.56	0.18	0.94
07-70w	70.40	0.31	14.30	4.44	0.16	0.26	2.72	4.66	2.33	0.05	99.15
2 σ	5.03	0.17	1.38	2.31	0.07	0.23	1.35	0.50	0.51	0.05	1.76
07-66	72.20	0.17	13.75	3.04	0.11	0.14	1.98	4.72	2.51	0.02	98.65
2 σ	1.06	0.06	0.55	0.23	0.02	0.07	0.14	0.42	0.16	0.01	1.18

Table 6.4: Whole rock chemistry of the H3 tephra layer. Samples were collected from proximal locations on the flanks of the volcano as described in Figure 6.6.

Sample	SiO_2	TiO_2	Al_2O_3	FeO	MnO	MgO	CaO	Na_2O	K_2O	P_2O_5	Total
07-16w	66.36	0.34	14.01	5.46	0.14	0.32	2.58	4.64	2.24	0.07	101.06
07-16g	65.80	0.51	14.93	7.90	0.19	0.53	3.52	4.62	2.00	0.13	107.24
07-16b	61.82	0.75	14.82	9.99	0.23	0.98	4.26	4.38	1.71	0.25	108.17
07-79	68.14	0.51	14.81	8.11	0.19	0.57	3.54	4.58	1.94	0.14	105.88
07-76b	62.17	0.67	14.77	9.46	0.22	0.79	4.01	4.46	1.77	0.23	107.04
07-76w	64.19	0.51	14.81	8.11	0.19	0.57	3.54	4.58	1.94	0.14	105.88
07-73	67.01	0.31	14.02	4.93	0.13	0.27	2.37	4.67	2.29	0.06	100.50
07-70	62.16	0.72	14.95	9.82	0.23	0.88	4.12	4.41	1.74	0.25	108.12
07-66	68.46	0.31	14.32	5.16	0.13	0.24	2.51	4.81	2.33	0.06	102.97

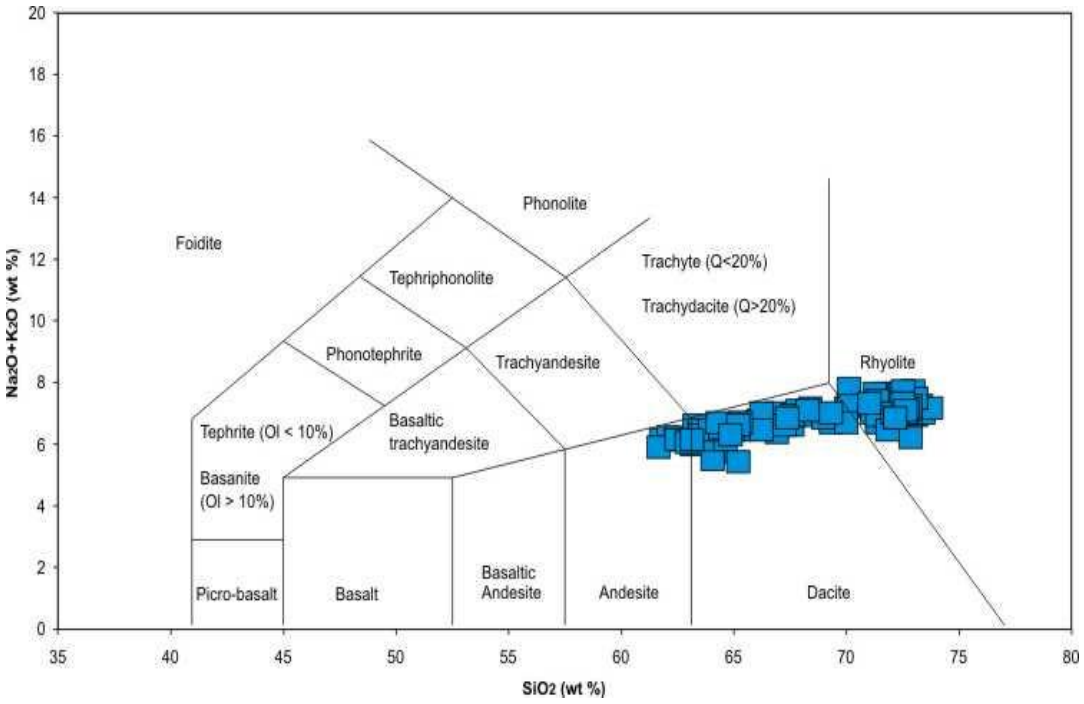

Figure 6.12: Total Alkali – Silica bivariate plot of the H3 tephra layer. Blue squares represent EMPA data, black squares represent XRF data. Data indicates that the H3 tephra shows a compositional range from andesite to dacite and rhyolite. Grid lines adapted from La Maitre *et al*. (1989).

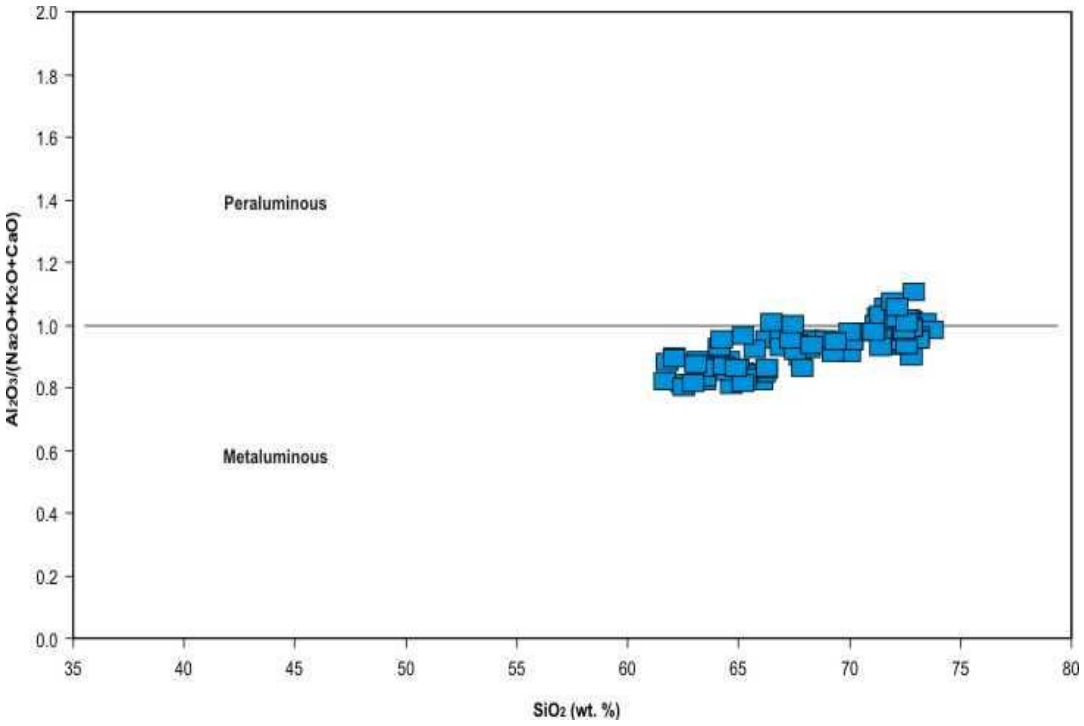

Figure 6.13: Silica – Aluminium and total alkali plot showing the H3 tephra layer. Blue squares represent EMPA data, black squares represent XRF data. . Data indicate that the tephra layer shows a metaluminous geochemistry consistent with the geological setting.

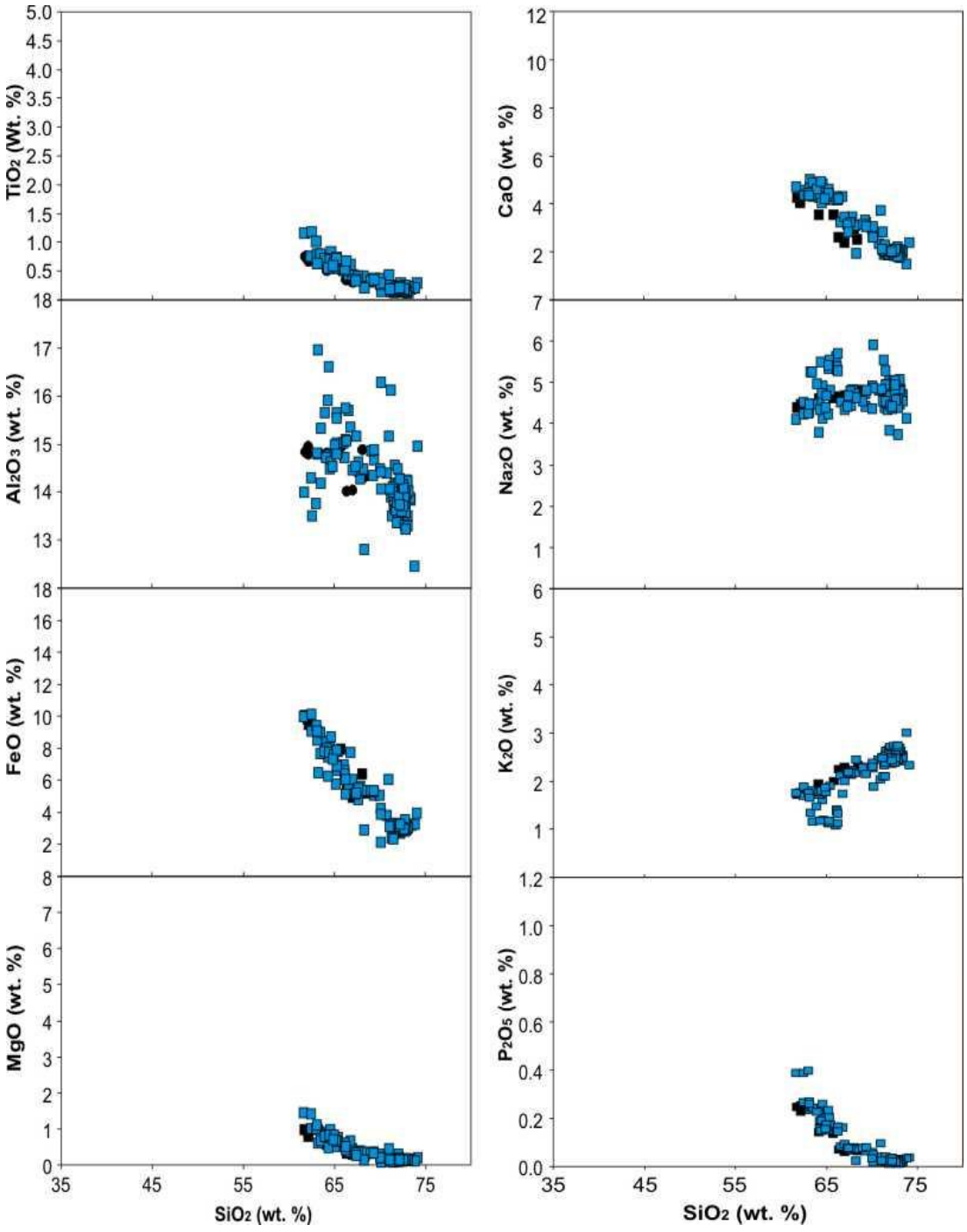

Figure 6.14: Bivariate plots of XRF and EMPA data for the H3 tephra layer. Blue squares represent EMPA data whilst black squares represent XRF data. EMPA and XRF data show persistent overlap which suggest minimal fractional crystallisation within the magma prior to eruption.

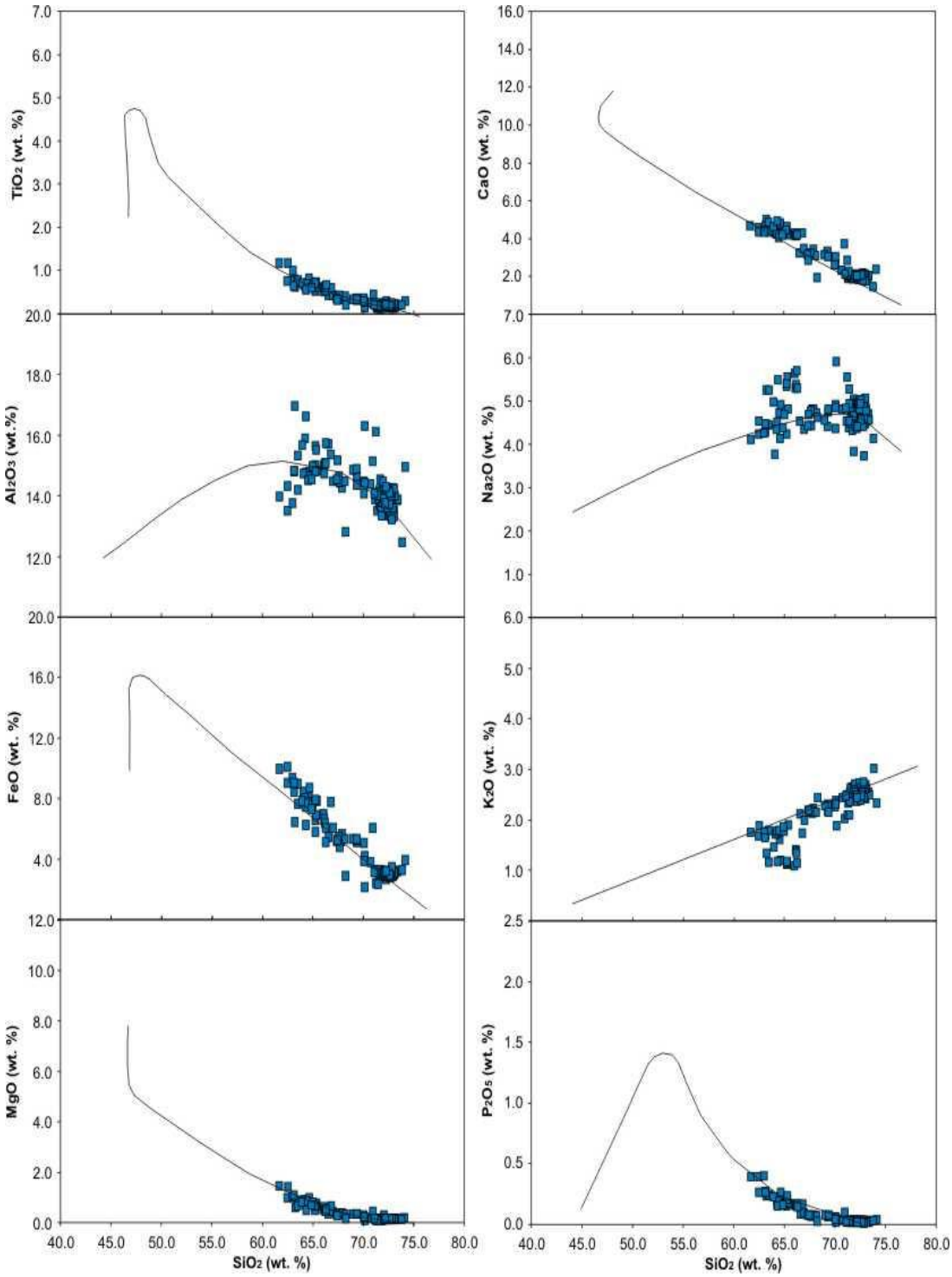

Figure 6.15: Harker plots of H3 data plotted onto the crystallization trends of major elements against SiO_2 (wt. %) for the volcanic system. Black lines represent data collected for the Torfajökull volcanic system by previous workers.

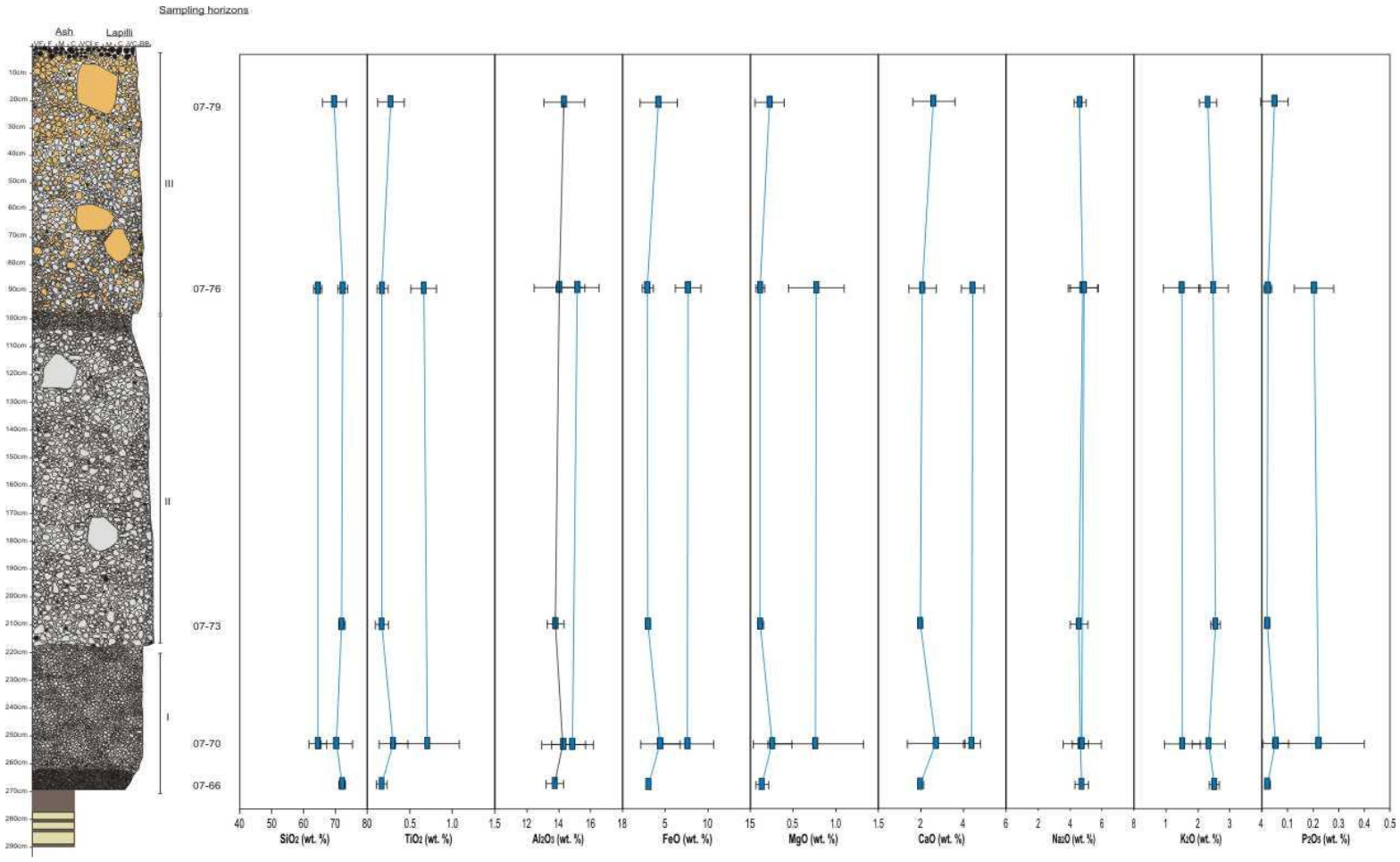

Figure 6.16: Chemical variation with stratigraphic height for the H3 tephra. Elements depicted represent the full suite of major elements analysed with the exception of MnO. Minor chemical variations are recorded in the lower most and upper most samples.

sampling technique. The tephra layer shows a low alkaline nature as indicated by the compositional fields suggested in Rollinson (1993) and references therein.

Comparing XRF and EMPA data highlights minimal variation between the data sets (Fig 6.20). Both glass and bulk data sets span the range of chemistries suggesting minimal influence of phenocryst phases on the samples.

6.2.3 Hekla Selsund

The HSelsund eruption occurred in 3515 BP. Field and chemical data collected for the HSelsund tephra layer is presented below.

Field Data: The reference section for the HSelsund tephra layer was selected at 63º 55'337 N, 19º 22'994 E near Laufafjell (Table 4.1; Fig. 4.6). Figure 6.17 is a stratigraphic log of the tephra layer compiled at this location while figures 6.18 a and b are field photographs of the tephra layer at the reference section. At this location, the tephra layer is 0.75 m thick. The tephra layer is comprised of four distinct packages: Phase I, Phase II, Phase III and Phase IV.

The HSelsund tephra layer is 0.75 m thick and is dominated by light brown to dark grey juvenile pumice clasts with a thin top of dark brown-black clasts. The unit shows internal layering as defined by the changes in colour and grain size, but no other depositional structures are recorded. Internal layering defines four phases of the eruption as noted in Figure 6.17. Grain size varies between fine lapilli in Phase I, coarse ash in Phase II, coarse lapilli in Phase III and medium lapilli in Phase IV. These grain size variations are a diagnostic characteristic of the HSelsund tephra layer. Average grain size is c. 2 cm. Maximum clast size is c. 3 cm. The tephra layer is moderately sorted and clast supported. Pumice clasts are sub-angular. Lithic clasts are rare dark grey to black in colour and show no alteration. The tephra layer is overlain by re-worked material and a coarse black pumice layer.

The HSelsund deposit represents a pumice fall from a Plinian eruption from the Hekla volcano. The eruption produced a dominantly dacitic deposit suggesting a shorter period of repose prior to eruption compared with that of the younger H3 eruption. The deposit shows some zoning, suggesting the presence of a zoned magma chamber beneath the volcano. The ratio of juvenile:lithic material in the deposit suggests a dominantly magmatic eruption with

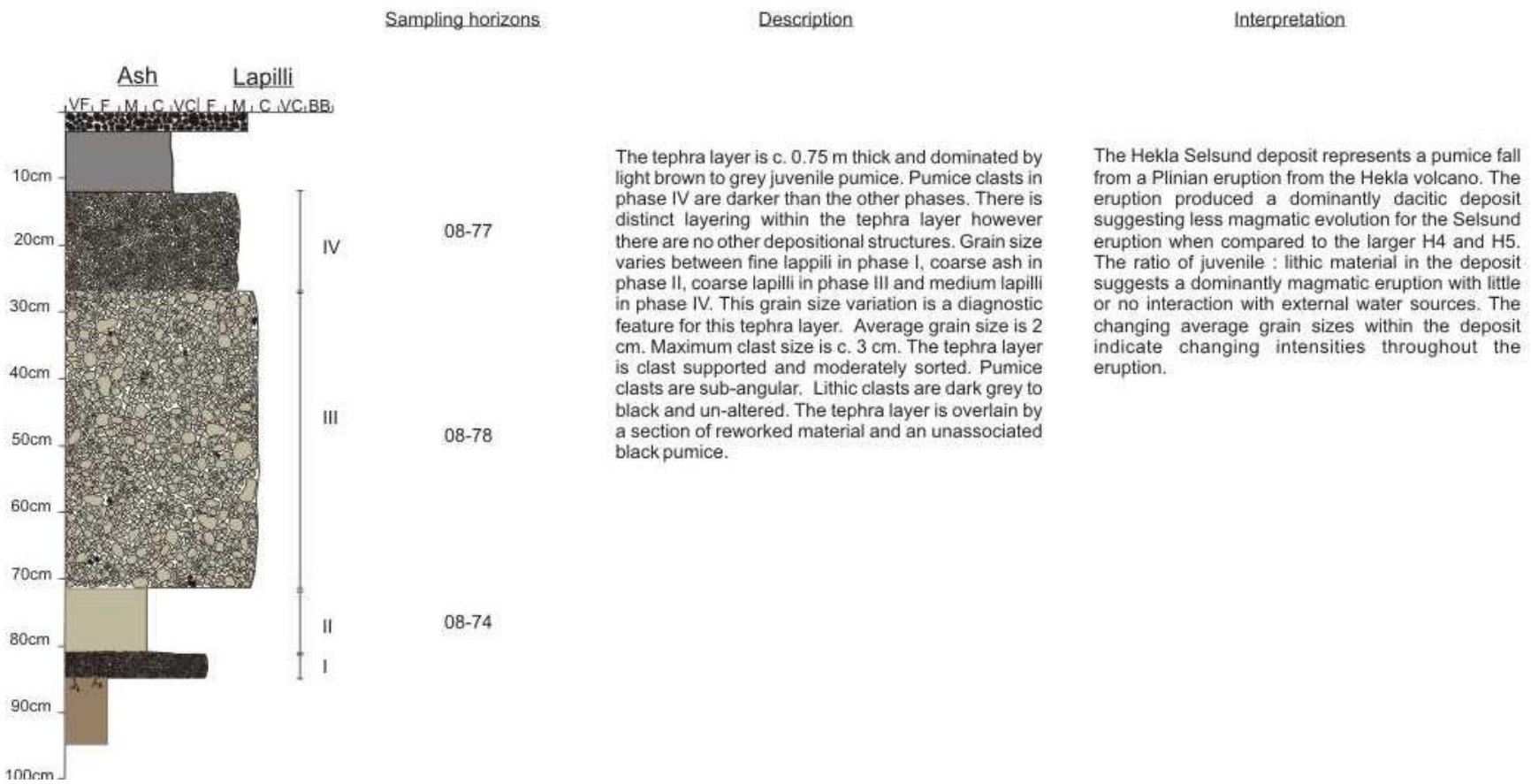

Figure 6.17: Stratigraphic log of the HSelsund tephra layer showing physical characteristics e.g. colour, grain size and clast morphology. Drawn at the reference location near Laufafjell.

Figure 6.18: Field photographs of the HSelsund tephra layer. a) H Selsund at the reference sampling location near Laufafjell. Trowel used for scale measures c. 25 cm. b) H Selsund on the banks of the Rauðufossakvísl near Sátubarn. Shovel used for scale measures c. 75 cm. Both photographs show a fine grained ash base to the tephra layer overlain by medium to coarse grained pumice clasts, topped with a dark brown mafic top. Photographs: Rh. Meara.

Table 6.5: Glass chemistry of the HSelsund tephra layer. Samples were collected from proximal locations on the flanks of the volcano as described in Figure 6.6. Ten electron probe analyses were collected for each sample and the data presented is the average of these analyses and two standard deviations. Full data sets are available in the Appendix.

Sample	SiO_2	TiO_2	Al_2O_3	FeO	MnO	MgO	CaO	Na_2O	K_2O	P_2O_5	Total
08-77b	56.60	1.99	13.56	11.09	0.29	2.40	5.88	3.96	1.43	0.92	98.14
2 σ	1.87	0.61	1.40	1.02	0.02	0.65	0.43	0.61	0.20	0.34	1.50
08-77w	68.05	0.41	14.70	5.13	0.16	0.46	3.12	4.64	2.11	0.09	98.86
2 σ	4.23	0.23	0.59	2.15	0.06	0.32	1.13	0.22	0.41	0.07	1.37
08-78	67.17	0.44	14.83	5.76	0.18	0.56	3.27	4.75	2.05	0.12	99.14
2 σ	3.00	0.16	0.62	1.35	0.03	0.25	0.60	0.15	0.20	0.07	0.62
08-79	68.48	0.39	14.65	5.22	0.17	0.45	3.02	4.72	2.14	0.09	99.32
2 σ	3.90	0.19	0.96	1.84	0.05	0.26	0.97	0.33	0.35	0.06	1.34

Table 6.6: Whole rock chemistry of the HSelsund tephra layer. Samples were collected from proximal locations on the flanks of the volcano as described in Figure 6.6. *Sample 07-75 was collected at a quarry further to the south to confirm unit correlation.

Sample	SiO_2	TiO_2	Al_2O_3	FeO	MnO	MgO	CaO	Na_2O	K_2O	P_2O_5	Total
08-77	64.56	0.50	14.82	7.48	0.17	0.62	3.37	4.63	1.97	0.14	105.00
08-78	64.41	0.52	14.86	7.74	0.18	0.63	3.42	4.57	1.96	0.20	105.42
08-79	65.19	0.49	14.82	7.29	0.17	0.57	3.30	4.65	2.02	0.13	105.18
08-75*	67.15	0.35	14.20	4.96	0.12	0.34	2.4	4.65	2.25	0.07	100.95

minimal interaction with external water sources. Variations in grain size throughout the tephra layer represent temporal variation in eruption intensity. The highest intensity phases are represented by the largest grain sizes, indicating that Phases II and IV were the highest intensity. Although not obvious at this locality, sampling locations to the south of the volcano showed evidence of fluidal transportation in the HSelsund tephra layer (Sverrisdottir, pers comm).

Chemical Data: In total, four samples were analysed for the HSelsund tephra layer collected from one sampling location. The new major element data collected via EMPA and XRF for is presented in Tables 6.5 and 6.6.

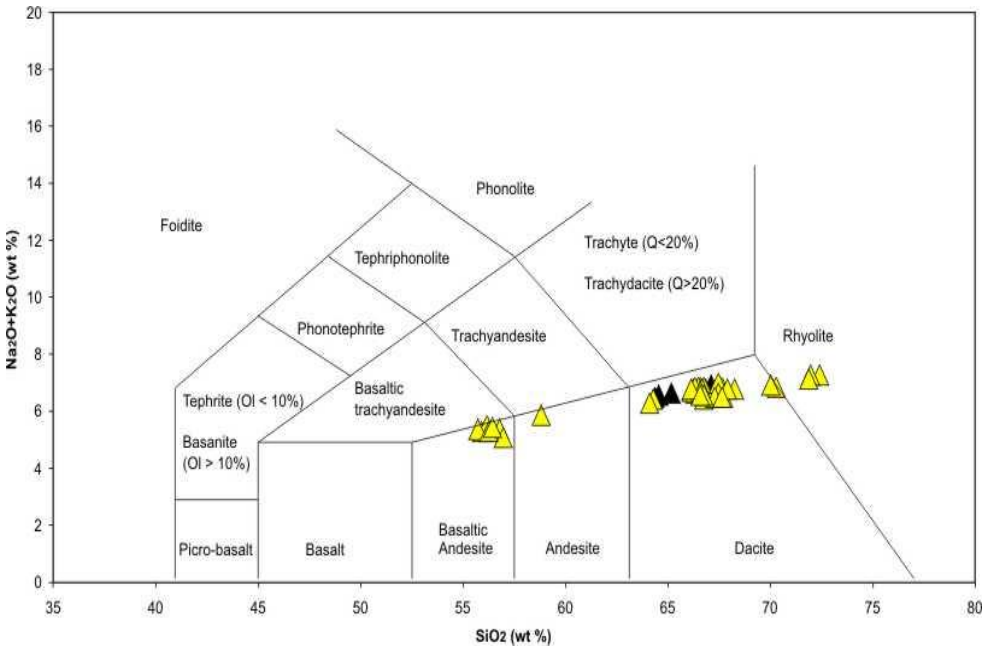

Figure 6.19: Total Alkali – Silica bivariate plot of the HSelsund tephra layer. Yellow triangles represent EMPA data, black triangles represent XRF data. Data indicates that the HSelsund tephra shows a compositional range of basaltic andesite to andesite, dacite and rhyolite. However there is a compositional gap in the andesitic phase which has not yet been explained. Grid lines adapted from La Maitre *et al*. (1989).

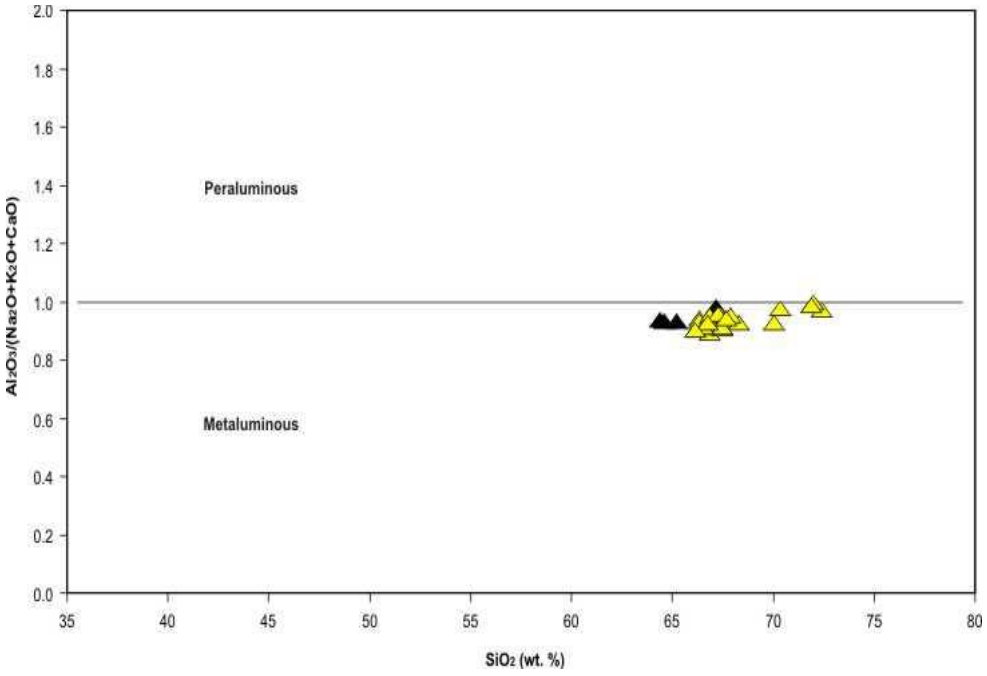

Figure 6.20: Silica – Aluminium and total alkali plot showing the luminosity of the HSelsund tephra. Yellow triangles represent EMPA data, black triangles represent XRF data. The data indicates that the tephra layer shows a metaluminous geochemistry consistent with the geological setting.

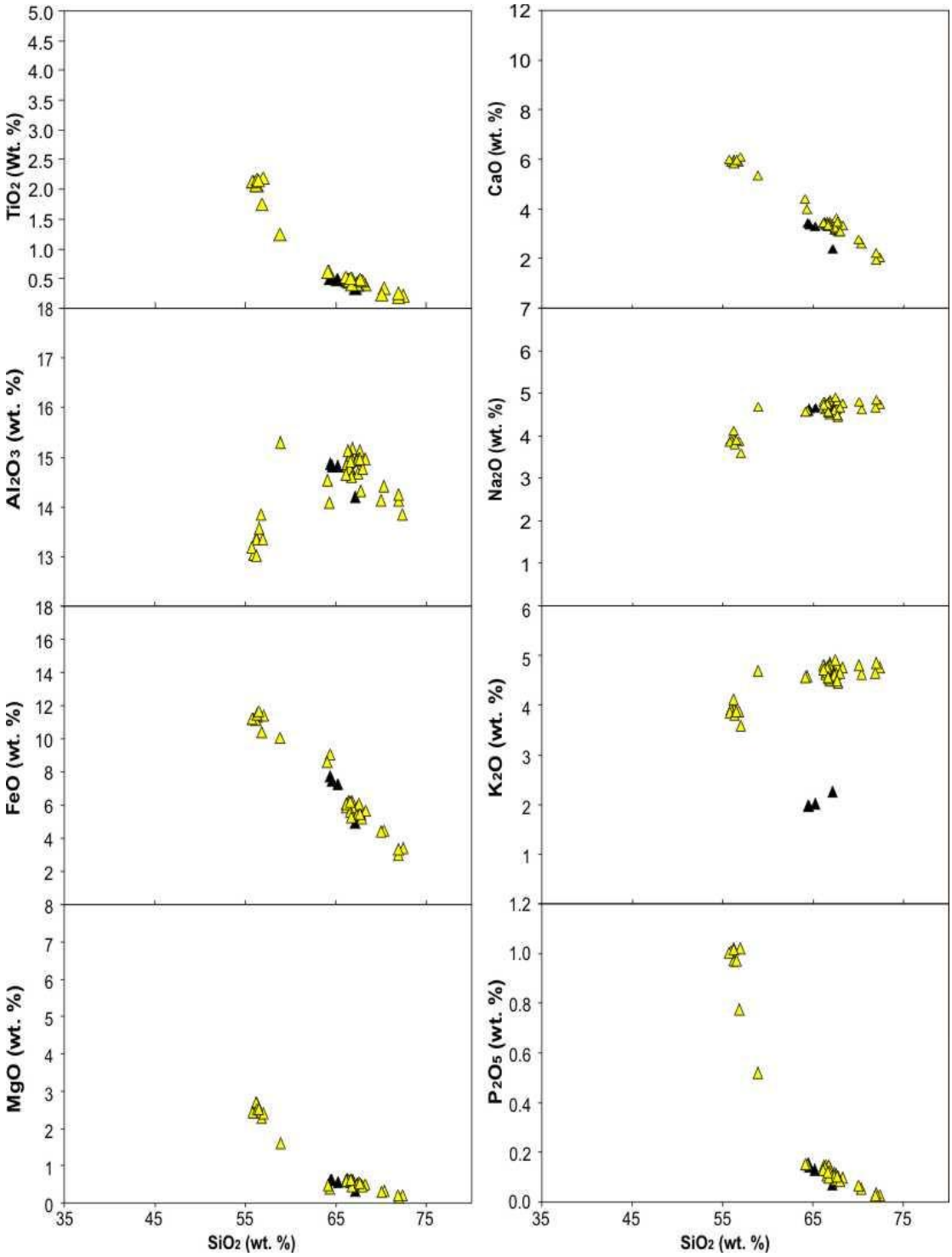

Figure 6.21: Bivariate plots of XRF and EMPA data for the HSelsund tephra layer. Yellow triangles represent EMPA data whilst black triangles represent XRF data. Geochemical variations are minimal between XRF and EMPA data sets suggesting only minor amounts of fractional crystallisation within the magma prior to eruption.

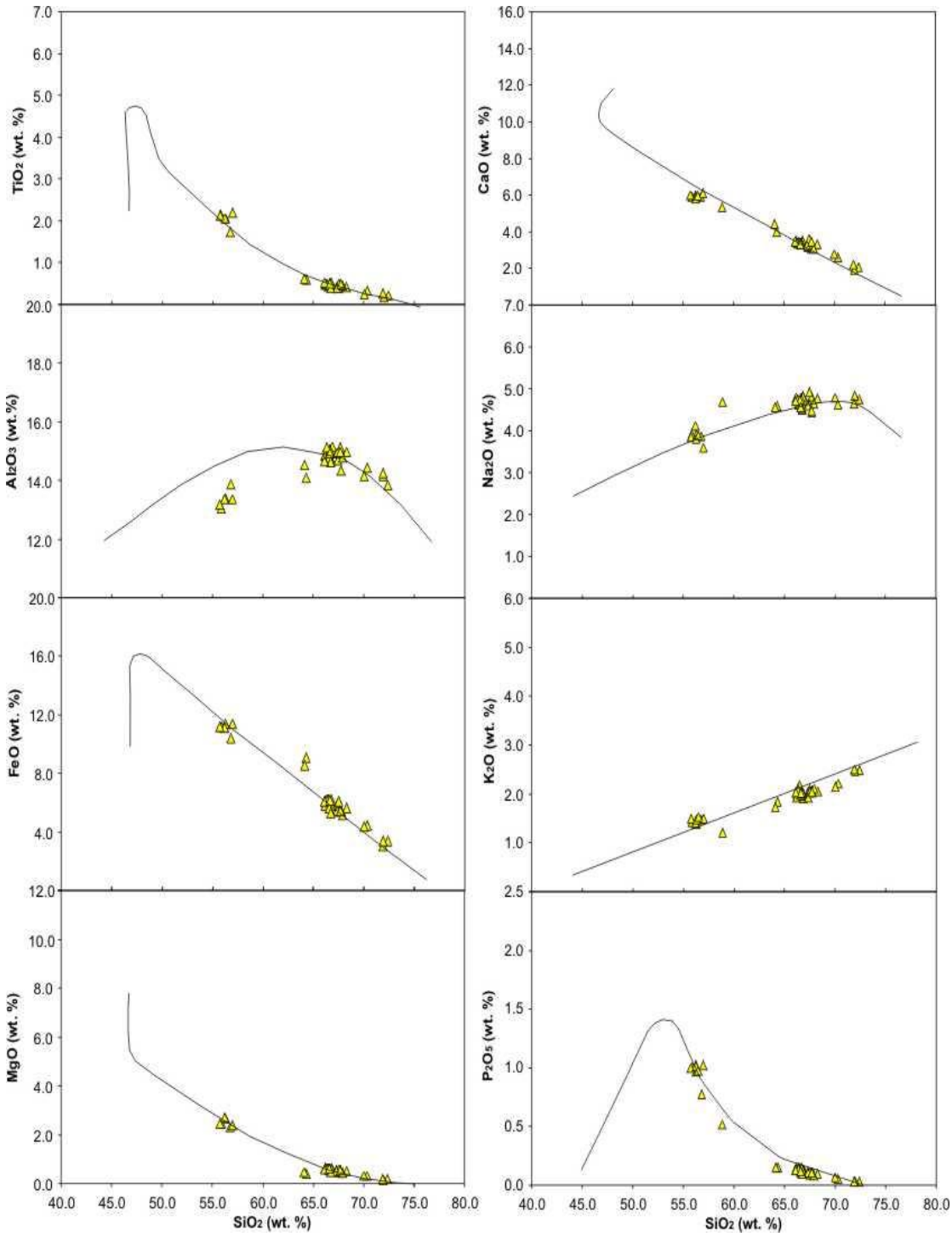

Figure 6.22: Harker plots of HSelsund data plotted onto the crystallization trends of major elements against SiO_2 (wt. %) for the volcanic system. Black lines represent data collected for the Torfajökull volcanic system by previous workers.

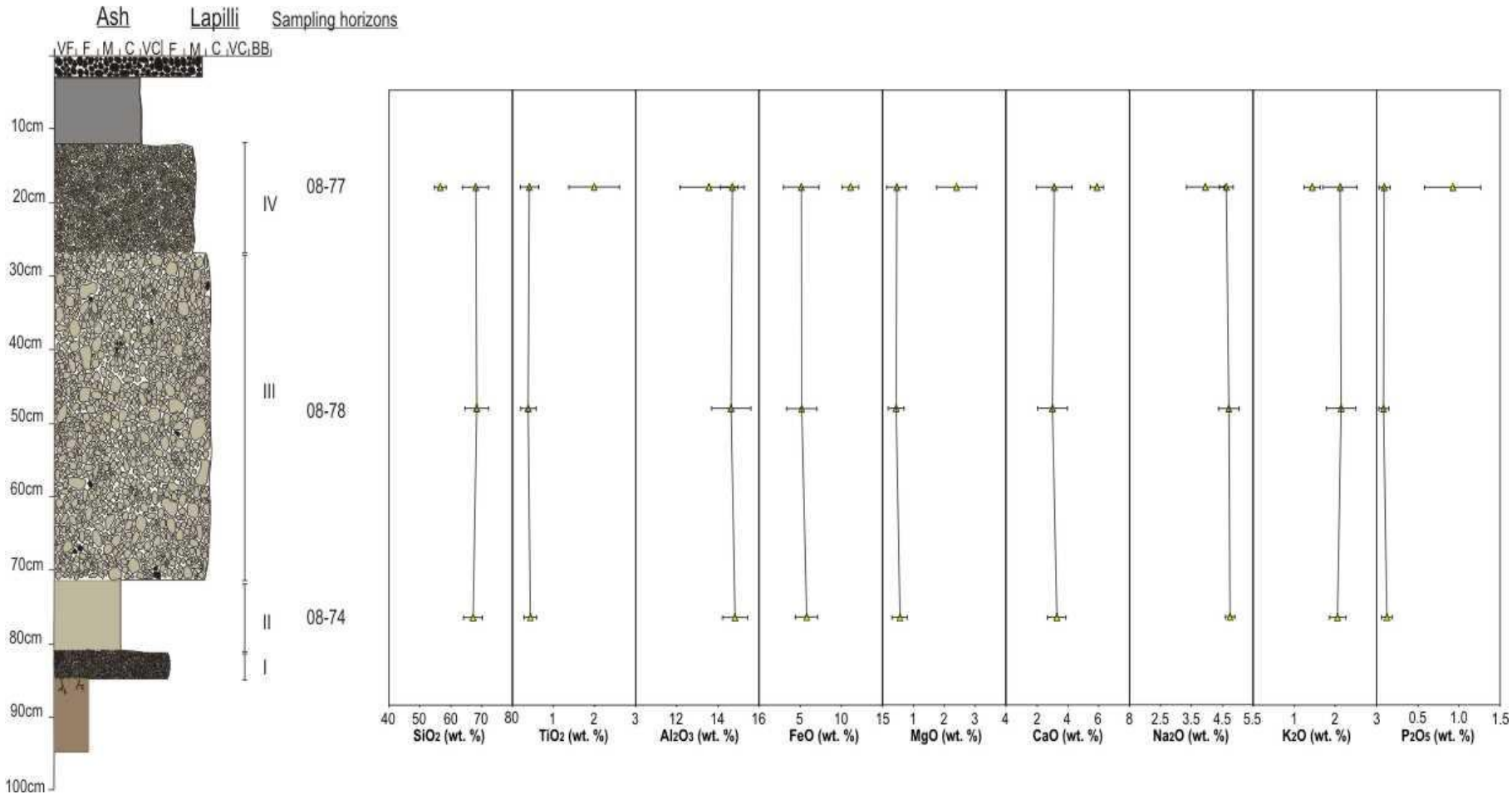

Figure 6.23: Chemical variation with stratigraphic height for the HSelsund tephra. Elements depicted represent the full suite of major elements analysed with the exception of MnO. Very minor variations in elemental concentrations are recorded, however all are within the error bars recorded.

The chemical characteristics of the tephra layer are shown by figures 6.19 to 6.23. The tephra layer shows a range in glass composition ranges from basaltic andesite, andesite, dacite to rhyolite and a dacite bulk composition (Fig 6.19). Figure 6.19 also highlights a gap in the compositional range of the HSelsund tephra and has now been recorded at both proximal and distal localities (Dugmore, *pers. com*.). It is not yet known whether this gap represents a true compositional jump or whether column collapse onto a poorly preserved sedimentary sequence has resulted in the loss of an eruptive face from the record. The former hypothesis would provide important information regarding the generation of silicic magma at the Hekla volcanic system, while the latter would explain the absence of the missing chemistries in the far-distal records. The tephra layer is metaluminous (Fig. 6.20). The tephra layer shows no chemical variation with stratigraphic height, with the exception of a sub-set of mafic grains analysed at sampling horizon 08-77 (Fig. 6.23). The tephra layer shows a low alkaline nature as indicated by the compositional fields suggested in Rollinson (1993) and references therein.

Comparing XRF and EMPA data highlights a minor variation in SiO_2 concentrations between the data sets (Fig 6.22). Also highlighted are increases in FeO and a decrease in K_2O concentrations in the XRF data compared with the glass data. These differences are the result of removal of these elements from the glass phase through fractional crystallization of plagioclase, olivine and pyroxene during melt generation.

6.2.4 Hekla 4

The H4 eruption occurred in 3830 BP. Here, we present field and chemical data collected for the H4 tephra layer.

Field Data: The reference section for the H4 tephra layer was selected at 63º 53.046'N 19º 28.992'E near Ófærugil (Table 4.1; Fig. 4.6). The section is missing the final stage of the eruption as indicated by its eroded top. The section however was sampled as it thoroughly represents the other phases of the eruption. Figure 6.24 is a stratigraphic log of the tephra layer compiled at this location while figures 6.25 – 6.26 are field photographs of the tephra layer at the reference section. At this location, the tephra layer is 3.3 m thick. The tephra layer is comprised of four distinct packages: Phase I, Phase II, Phase III and Phase IV. These packages will be discussed individually below.

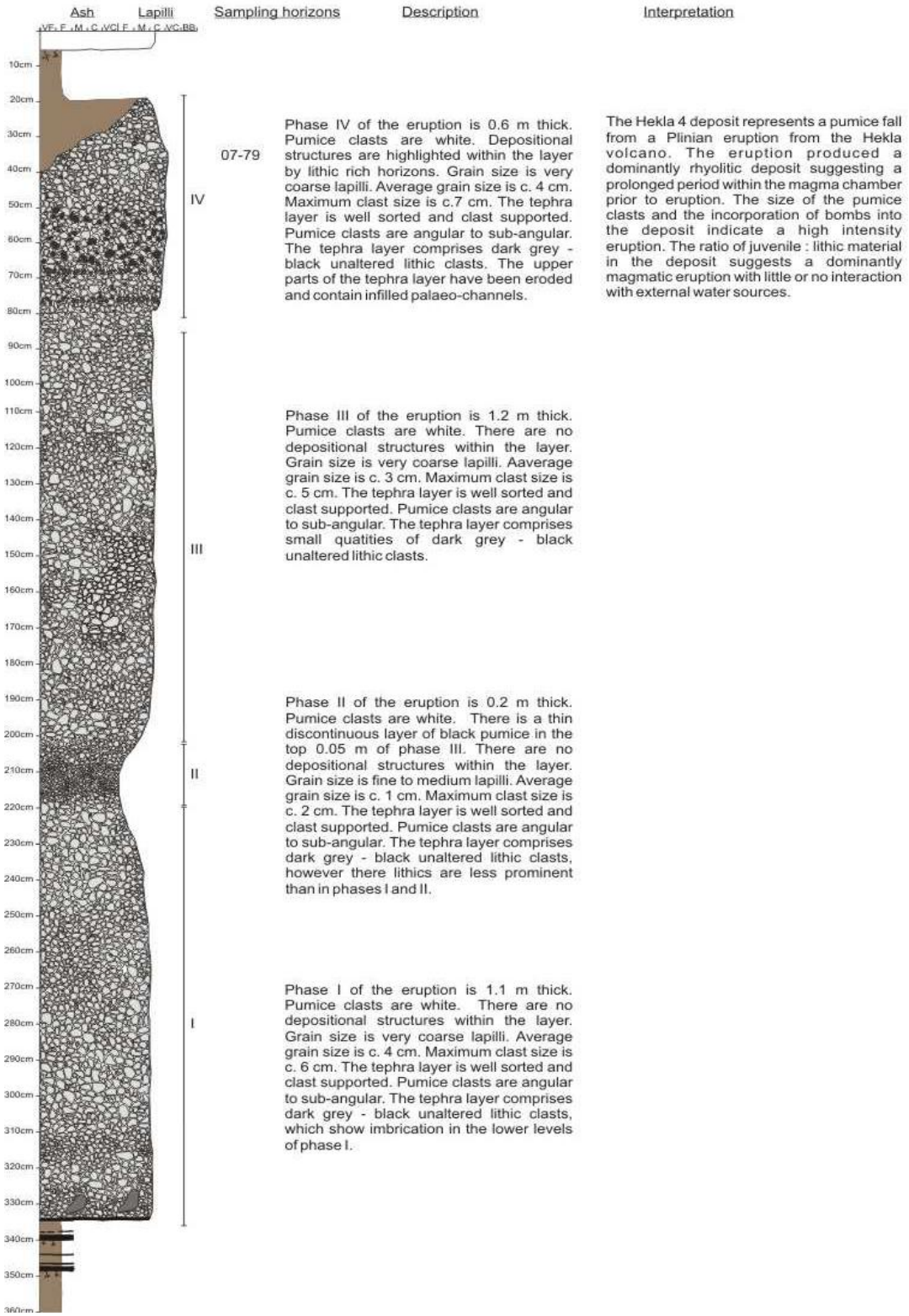

Figure 6.24: Field photographs of the H4 tephra layer showing physical characteristics e.g. colour, grain size and clast morphology. The upper section of the eruption has been eroded, however this section was selected as it represents in detail the majority of the eruption. Drawn at the reference section near Ófærugil.

Figure 6.25: Field photographs of the H4 tephra layer. a) lithic-rich bands in the upper 0.4 – 0.5 m of the tephra layer. Notebook measures c. 15 cm. b) Horizon of fine to medium lapilli pumice clasts, a feature which is diagnostic of the H4 tephra layer. Notebook measures c. 15 cm. c) Base of the tephra layer containing large lithic blocks angled away from source, indicating direction of transport. Pen used for scale measures c. 10 cm. d) H4 tephra layer taken at a second non-reference location. The outcrop is condensed and shows the diagnostic fine grained horizon and the mafic top. Scale measures c. 30 cm. Photographs: Rh. Meara.

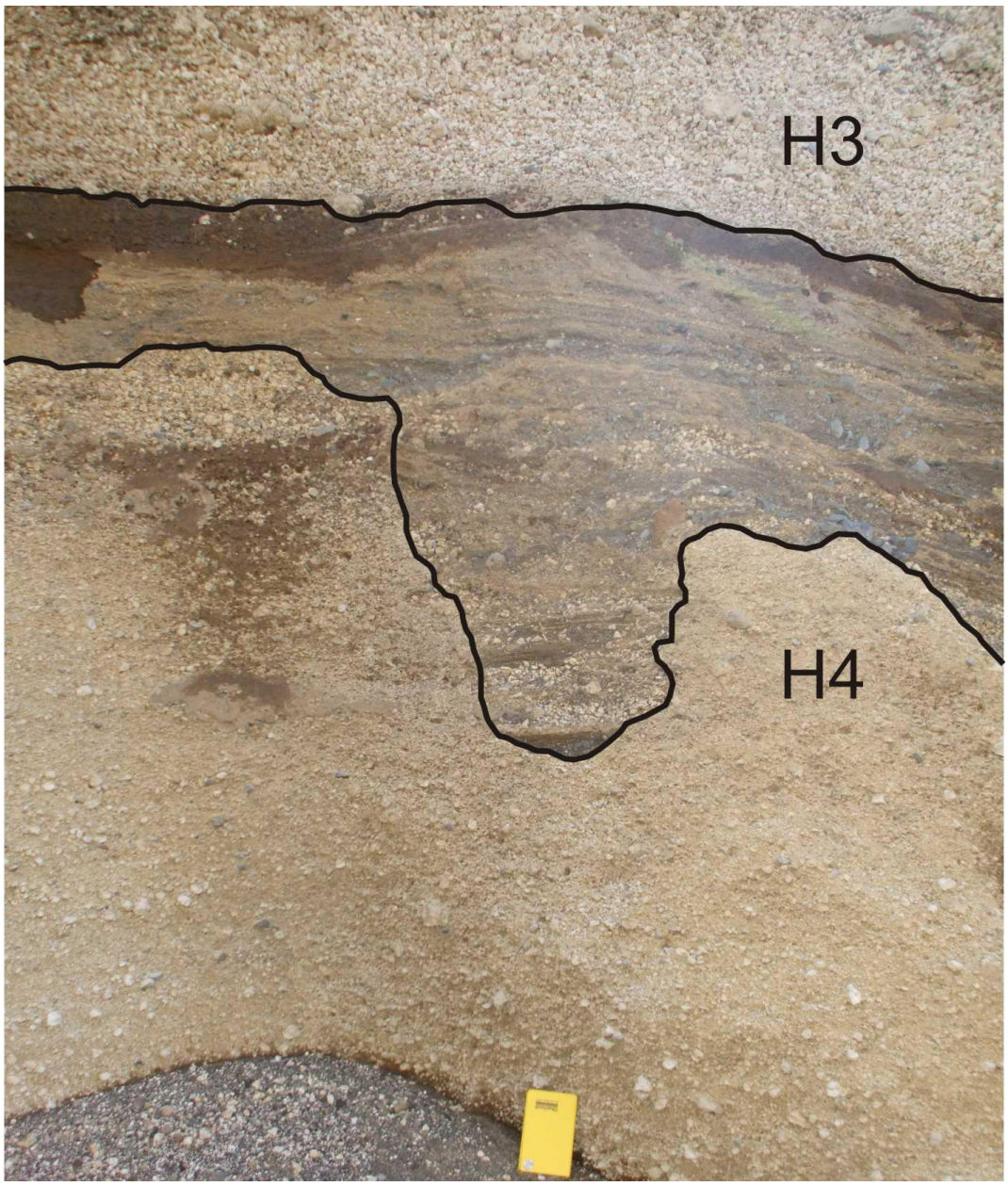

Figure 6.26: H4 tephra layer at the sampling location of Ófærugil. H4 is the lowermost pale brown tephra layer, overlain by the H3 tephra layer at the top of the photograph. Between the tephra layers is a package of fluvial sediments which erode into the underlying H4 tephra layer, evident by the small incised channel indicated on the photograph. This sedimentary sequence is observed throughout the Ófærugil region, is often < 5 m thick comprising large cross beds, ripples and massive flash flood-like deposits. Similar sequences are also found lower in the stratigraphy between the H4 and H5 deposits. Notebook measures c. 15 cm. (Photograph: Rh. Meara).

Phase IV of the eruption is 0.6 m thick and is dominated by white pumice clasts. There is a very thin, discontinuous top of dark brown-black pumice clasts on top of the deposit, however in most places this has been eroded by fluvial processes (Fig. 6.26). The unit shows internal layering as defined by lithic-rich horizons (Fig. 6.25a), but no other depositional structures are recorded. Grain size is coarse lapilli. Average grain size is c. 4 cm. Maximum clast size is c. 7 cm. The tephra layer is well sorted and clast supported. Lithic clasts are dark grey in appearance and show minimal alteration.

Phase III of the eruption is 1.15 m thick and is dominated by white pumice clasts. The unit shows no other depositional structures. Grain size is coarse lapilli. Average grain size is c. 3 cm. Maximum clast size is c. 5 cm. The tephra layer is well sorted and clast supported. Lithic clasts are rare, those recorded are dark grey in appearance and show minimal alteration.

Phase II of the eruptions is 0.10 m thick and dominated by white pumice clasts. The unit shows no depositional structures. Average grain size is fine lapilli. Average grain size is 1 cm. Maximum clast size is 2 cm. The tephra layer is well sorted and clast supported. Pumice clasts are angular to sub-angular. Lithic clasts are rare. The fine grained nature of Phase II is diagnostic of the H4 tephra layer, the change in grain size between Phases I-III can be used to recognise the deposit at more distal localities (Fig. 6.25d).

Phase I of the eruptions is 1.15 m thick and dominated by white pumice clasts. The unit shows some internal layering highlighted by variations in grain size and reverse grading. Average grain size is coarse lapilli. Average grain size is c. 4 cm. Maximum clast size is c. 6 cm. The tephra layer is well sorted and clast supported. Pumice clasts are sub-angular. Lithic clasts are dark grey to black and show no alteration. In the lowermost 0.05 m of the tephra layer there are blocky, angular lithic bombs measuring c. 5 cm and orientated west-north-west (Fig. 6.25c). The tephra layer is immediately underlain by a sequence of black ash layers and palaeosoils (Fig. 6.25c), and by a succession of fluvial sediments (Fig. 6.11).

The H4 deposit represents a pumice fall from a Plinian eruption from the Hekla volcano. The eruption produced a dominantly rhyolitic deposit suggesting a prolonged period of repose prior to eruption. The deposit shows some zoning, suggesting the presence of a zoned magma chamber beneath the volcano. The ratio of juvenile:lithic material in the deposit suggests a dominantly magmatic eruption with phases of vent clearing in the final stages of

Table 6.7: Glass chemistry of the H4 tephra layer. Samples were collected from proximal locations on the flanks of the volcano as described in Figure 6.6. Ten electron probe analyses were collected for each sample and the data presented is the average of these analyses and two standard deviations. Full data sets are available in the Appendix.

Sample	SiO_2	TiO_2	Al_2O_3	FeO	MnO	MgO	CaO	Na_2O	K_2O	P_2O_5	Total
07-101b	62.09	0.88	14.62	8.95	0.27	1.10	4.58	4.54	1.70	0.29	98.92
2 σ	1.49	0.10	0.37	0.98	0.02	0.15	0.25	0.27	0.23	0.07	1.15
07-101w	74.21	0.16	13.19	2.22	0.10	0.03	1.42	4.74	2.83	0.02	98.87
2 σ	2.85	0.16	0.76	1.37	0.07	0.03	0.75	0.24	0.44	0.02	1.48
07-96	74.55	0.13	13.07	1.98	0.09	0.02	1.31	4.67	2.87	0.01	98.67
2 σ	1.11	0.02	0.45	0.24	0.02	0.00	0.07	0.17	0.10	nd	1.14
07-94	73.56	0.10	12.82	1.89	0.17	0.02	1.31	4.55	2.81	0.02	97.22
2 σ	6.34	0.04	0.61	0.14	0.16	0.00	0.08	0.52	0.17	nd	7.51
07-92	74.07	0.11	12.95	2.05	0.24	0.02	1.32	4.53	2.87	0.02	98.16
2 σ	1.21	0.04	0.33	0.36	0.01	0.00	0.12	0.37	0.09	nd	1.20
07-89	74.34	0.13	12.96	2.02	0.12	0.03	1.38	4.69	2.84	0.02	98.48
2 σ	1.87	0.09	0.68	0.61	0.13	0.06	0.37	0.25	0.23	nd	1.42
07-87	74.56	0.11	12.98	1.89	0.24	0.02	1.28	4.49	2.80	nd	98.37
2 σ	1.01	0.03	0.45	0.26	0.01	0.00	0.13	0.22	0.15	nd	1.02
07-86	74.58	0.10	12.86	1.89	0.24	0.02	1.28	4.50	2.90	nd	98.36
2 σ	1.50	0.03	0.49	0.36	0.01	0.01	0.18	0.26	0.17	nd	1.77
07-85	74.39	0.10	13.07	1.95	0.24	0.02	1.32	4.44	2.84	nd	98.37
2 σ	0.89	0.04	0.41	0.17	0.01	0.01	0.13	0.26	0.21	nd	1.30
07-84	74.33	0.10	13.17	2.00	0.24	0.02	1.36	4.59	2.88	0.02	98.68
2 σ	1.01	0.03	0.30	0.24	0.01	0.00	0.09	0.33	0.10	nd	1.31

the eruption, but minimal interaction with external water sources. Variations in grain size throughout the tephra layer represent temporal variation in eruption intensity. The highest intensity phases are represented by the largest grain sizes, indicating that Phases I, III and IV were the highest intensity stages of the H4 eruption. Grain size variations may also be the result of variations in wind direction and intensity and cannot be ruled out without investigation of multiple reference sections, which was outside the scope of this project.

Chemical Data: In total, ten samples were analysed for the H4 tephra layer collected from one sampling location. The new major element data collected via EMPA and XRF for is presented in Tables 6.7 and 6.8.

Table 6.8: Whole rock chemistry of the H4 tephra layer. Samples were collected from proximal locations on the flanks of the volcano as described in Figure 6.6.

Sample	SiO_2	TiO_2	Al_2O_3	FeO	MnO	MgO	CaO	Na_2O	K_2O	P_2O_5	Total
07-101	72.89	0.14	13.18	2.66	0.08	0.07	1.39	4.76	2.87	0.02	100.44
07-98	71.90	0.14	12.98	2.67	0.08	0.07	1.39	4.68	2.83	0.02	99.16
07-94	72.09	0.15	13.04	2.69	0.08	0.08	1.40	4.72	2.83	0.02	99.52
07-92	71.03	0.15	12.94	2.70	0.08	0.11	1.36	4.56	2.79	0.02	98.17
07-89	72.02	0.14	12.98	2.58	0.08	0.08	1.35	4.67	2.86	0.02	99.09
07-87	71.75	0.15	12.97	2.68	0.08	0.09	1.39	4.57	2.82	0.02	98.92
07-87	72.70	0.14	13.14	2.64	0.08	0.05	1.38	4.69	2.85	0.02	100.07
07-86	71.05	0.15	12.86	2.66	0.08	0.10	1.37	4.62	2.79	0.02	98.09
07-86	72.14	0.15	13.01	2.67	0.08	0.10	1.38	4.59	2.83	0.02	99.37
07-85	71.82	0.14	12.95	2.63	0.08	0.10	1.38	4.64	2.84	0.02	98.97
07-84	71.79	0.15	12.92	2.64	0.09	0.09	1.36	24.59	2.83	0.02	98.85
07-82	71.89	0.18	13.09	2.86	0.09	0.11	1.49	4.57	2.80	0.03	99.66
07-82	72.33	0.18	13.15	2.91	0.09	0.15	1.48	4.58	2.80	0.02	100.31

The chemical characteristics of the tephra layer are shown by figures 6.27 to 6.31. The tephra layer shows a range in glass composition from basalt, basaltic andesite, andesite, dacite to rhyolite and a rhyolitic bulk composition (Fig 6.27). The tephra layer is metaluminous to peraluminous (Fig. 6.28). The tephra layer shows minimal chemical variation with stratigraphic height, with the exception of a sub-set of mafic grains analysed at sampling height 07-101 (Fig. 6.31). The tephra layer shows a low alkaline nature as indicated by the compositional fields suggested in Rollinson (1993) and references therein.

Comparing XRF and EMPA data highlights a minor variation in SiO_2 concentrations between the data sets (Fig 6.29). There are no other chemical variations between the XRF and EMPA data suggesting an aphyric nature to the bulk samples.

6.2.5 Hekla 5

The H5 eruption occurred in 6200 BP. Here, we present field and chemical data collected for the H5 tephra layer.

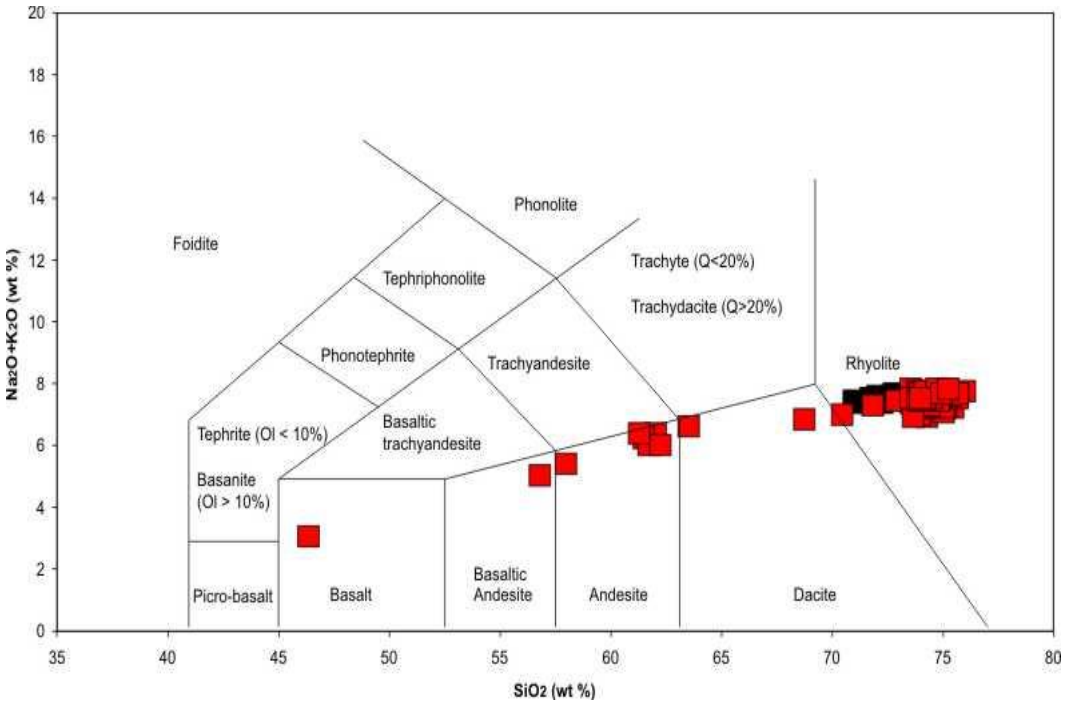

Figure 6.27: Total Alkali – Silica bivariate plot of the H4 tephra layer. Red squares represent EMPA data, black squares represent XRF data. Data indicates that the H4 tephra shows a compositional range from basalt, basaltic andesite, andesite, dacite and rhyolite. Grid lines adapted from La Maitre *et al.* (1989).

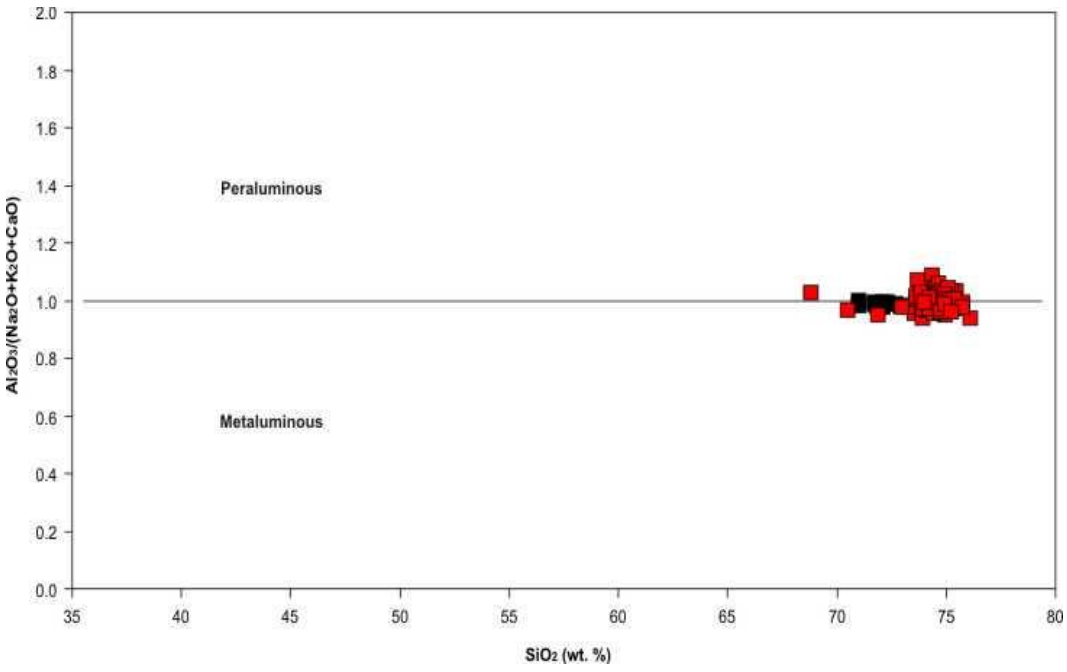

Figure 6.28: Silica – Aluminium and total alkali plot of the H4 samples. Red squares represent EMPA data, black squares represent XRF data. Data indicate that the tephra layer shows a mostly metaluminous geochemistry consistent with the geological setting.

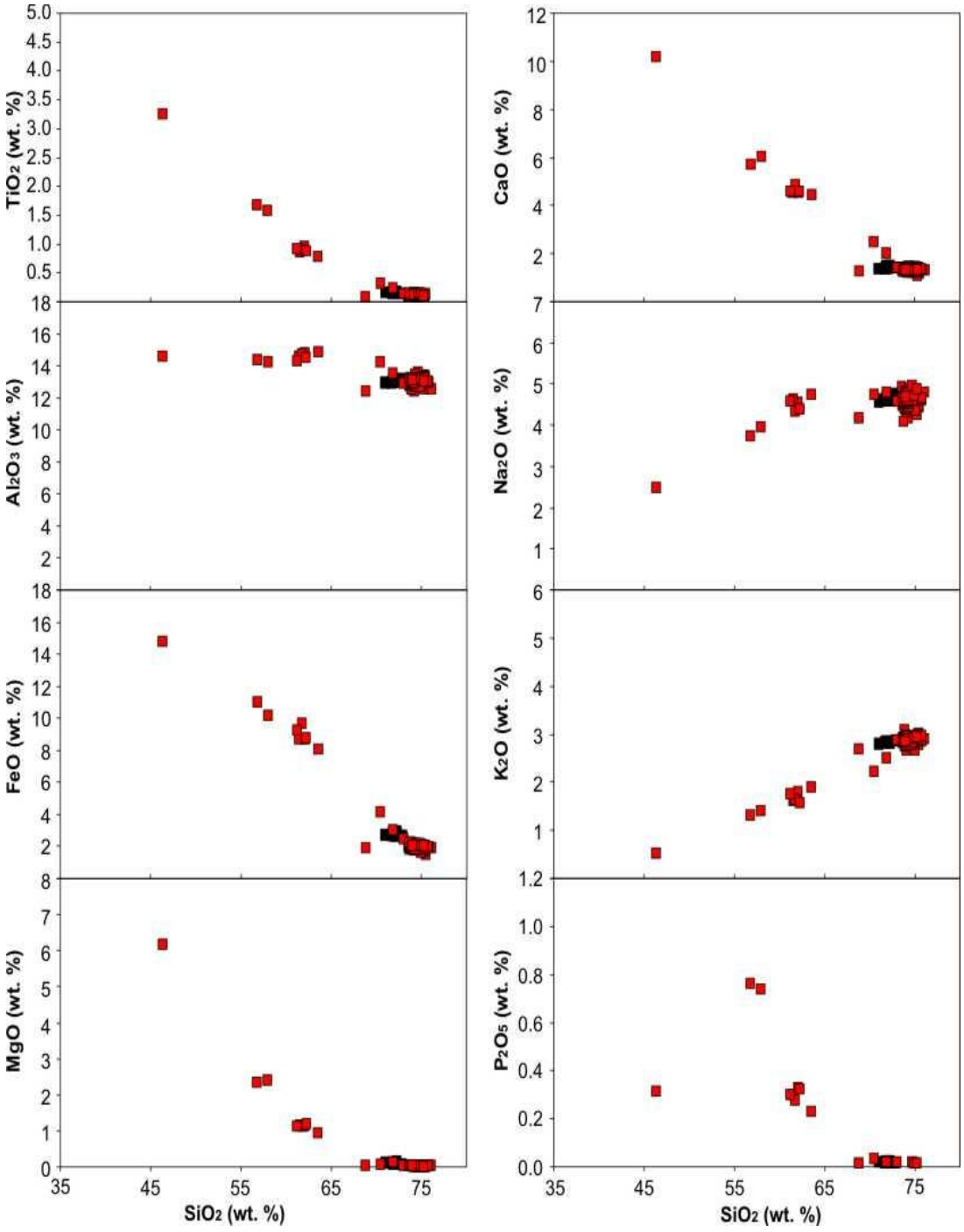

Figure 6.29: Bivariate plots of XRF and EMPA data for the H4 tephra layer. Red squares represent EMPA data whilst black squares represent XRF data. No geochemical variations are recorded between XRF and EMPA data sets suggesting very little or no fractional crystallisation within the magma prior to eruption.

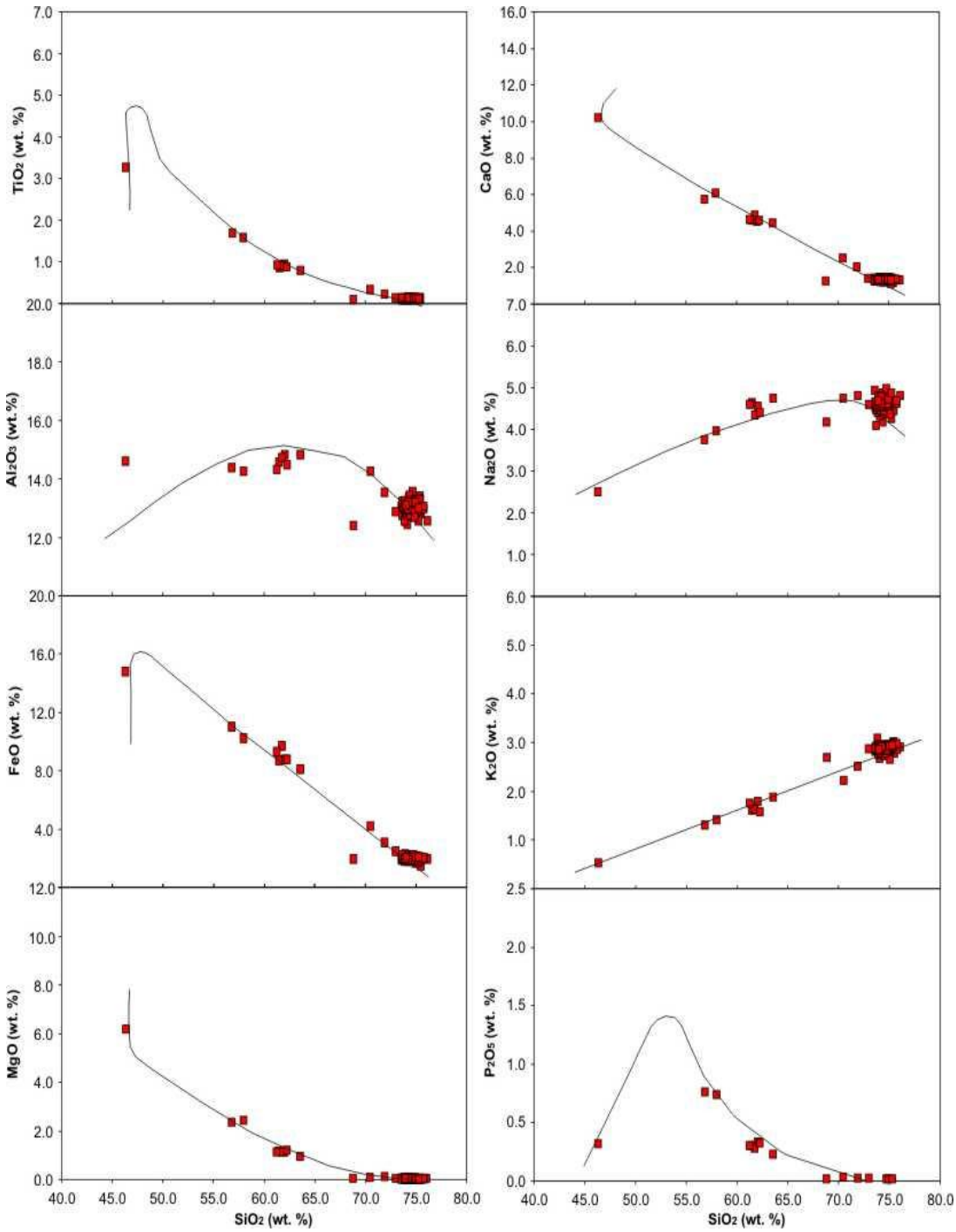

Figure 6.30: Harker plots of H4 data plotted onto the crystallization trends of major elements against SiO_2 (wt. %) for the volcanic system. Black lines represent data collected for the Torfajökull volcanic system by previous workers.

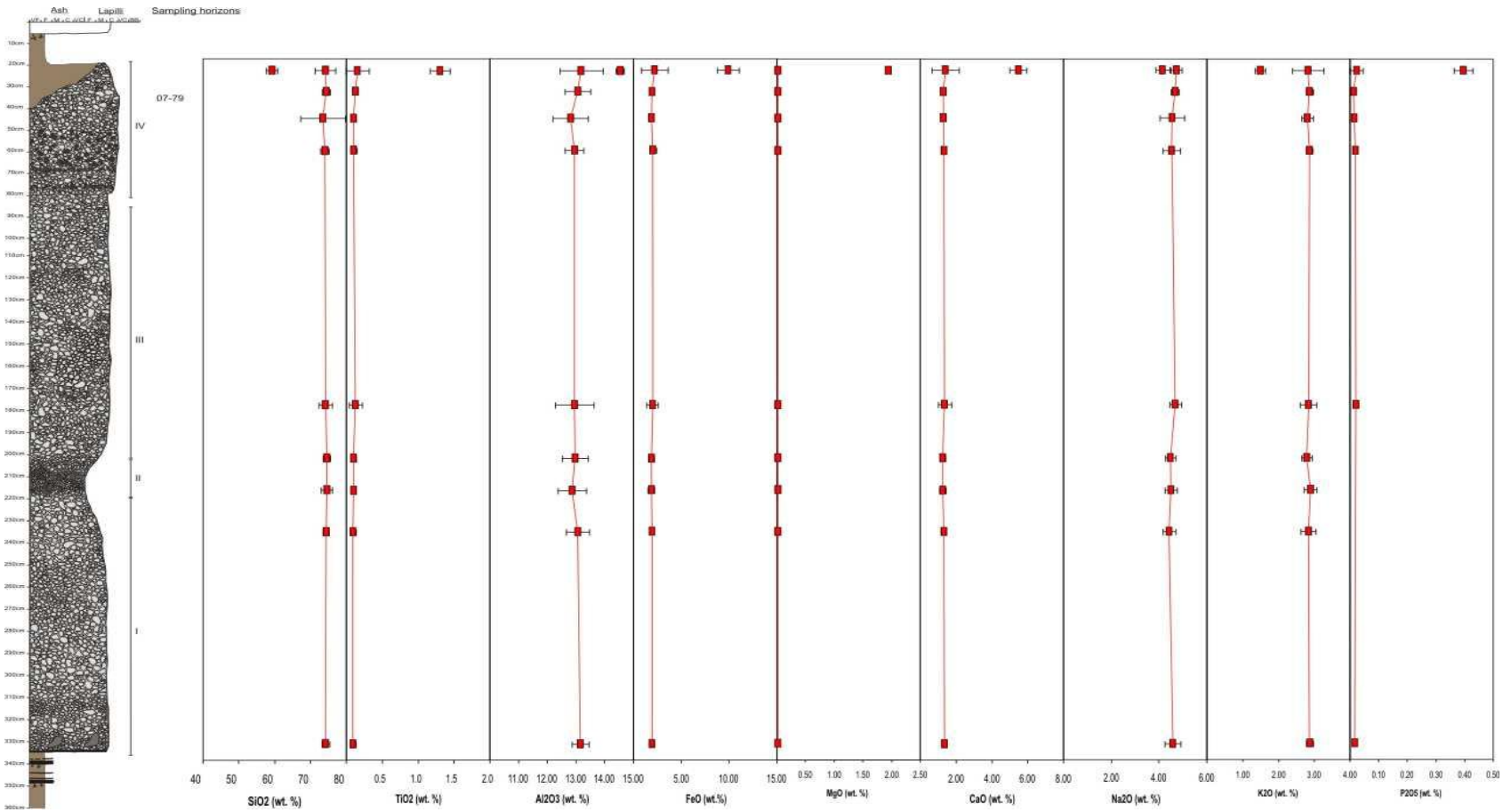

Figure 6.31: Chemical variation with stratigraphic height for the H4 tephra. Elements depicted represent the full suite of major elements analysed with the exception of MnO. Minot variations in elemental concentrations are recorded in the tephra, mostly in phases II and IV, however these are typically within error bars.

Field Data: The reference section for the H5 tephra layer was selected at 64º 05'876 N, 19º 34'903 E near Áfangagil (Table 4.1; Fig. 4.6). Figure 6.32 is a stratigraphic log of the tephra layer compiled at this location while figure 6.33a-b are field photographs of the tephra layer at the reference section. At this location, the tephra layer is 0.20 m thick. The tephra layer is comprised of two distinct packages: Phase I and Phase II. Both packages will be discussed individually below.

Phase II of the eruptions is 0.15 m thick and dominated by pale yellow to white pumice clasts. The unit is reversely graded but shows no depositional structures. Grain size is fine to medium lapilli. Average grain size is 0.5 - 1 cm. Maximum clast size is c. 2 cm. The tephra layer is well sorted and clast supported. Pumice clasts are sub-rounded. Lithic clasts are abundant; those recorded are dark grey in appearance and show no alteration. The tephra layer is overlain by re-worked pumice-rich sediment (Fig. 6.33a).

Phase I of the eruptions is 0.05 m thick and dominated by pale brown to pale yellow clasts. The unit shows some internal layering highlighted by variations in grain size. Grain size is fine lapilli. Average grain size is c. 0.5 cm. The tephra layer is well sorted and clast supported. Pumice clasts are sub-rounded. Lithic clasts are dark grey and are unaltered. Lithics are abundant but not as prominent as in Phase II. The tephra layer is immediately underlain by a coarse black ash layer and a green – grey fine ash (Fig. 6.33b).

The H5 deposit represents a pumice fall from a Plinian eruption from the Hekla volcano. The eruption produced a dominantly rhyolitic deposit suggesting a prolonged period of repose prior to eruption. The deposit shows very faint zoning, suggesting the presence of a zoned magma chamber beneath the volcano. The ratio of juvenile:lithic material in the deposit suggests a dominantly magmatic eruption with phases of vent clearing in the final stages of the eruption, but minimal interaction with external water sources. Variations in grain size throughout the tephra layer represent temporal variation in eruption intensity, suggesting that the final phases of Phase II were the highest intensity of the H5 eruption. These grain size variations may also be the result of variations in wind direction and intensity and cannot be ruled out without investigation of multiple reference sections, which was outside the scope of this project.

Chemical Data: In total, three samples were analysed for the H5 tephra layer collected from

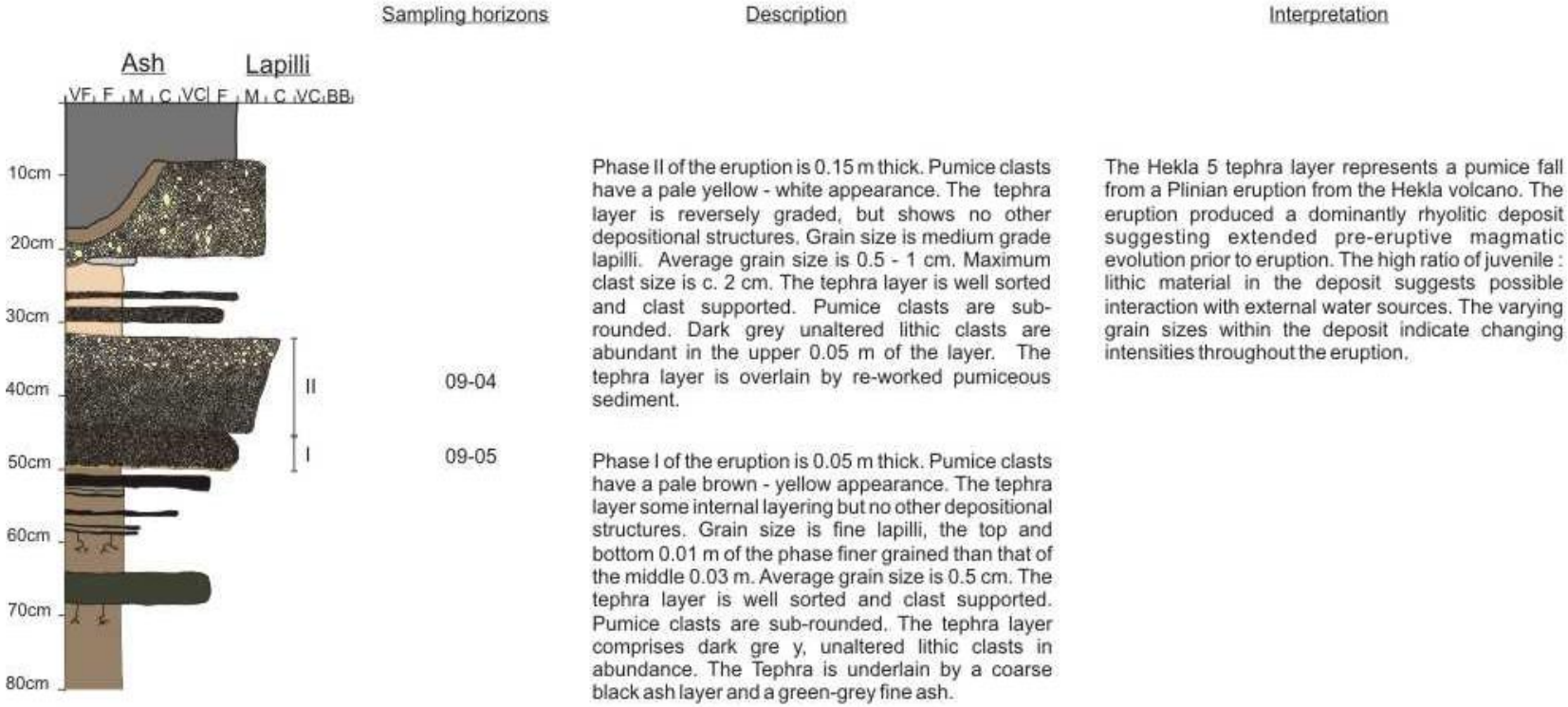

Figure 6.32: Sedimentary log of the H5 tephra layer showing physical characteristics e.g. colour, grain size and clast morphology. Drawn at the reference section near Áfangagil.

Figure 6.33: H5 tephra layer at the sampling location of Áfangagil. a) complete outcrop with overlying re-worked sediment (brown, grey and overlying pale brown layers). Pen used for scale measures c. 10 cm. b) The H5 tephra layer comprises a lower pale brown coarse ash – fine lapilli horizon and an upper pale yellow lithic-rich fine lapilli horizon which overlie a coarse black ash. Pen used for scale measures c. 10 cm. Photographs: Rh. Meara.

Table 6.9: Glass chemistry of the H5 tephra layer. Samples were collected from proximal locations on the flanks of the volcano as described by Figure 4.6. Ten electron probe analyses were collected for each sample and the data presented is the average of these analyses and two standard deviations. Full data sets are available in the Appendix.

Sample	SiO_2	TiO_2	Al_2O_3	FeO	MnO	MgO	CaO	Na_2O	K_2O	P_2O_5	Total
09-04w	75.68	0.08	12.72	1.76	0.07	nd	1.29	4.24	2.79	0.02	98.67
2 σ	1.20	0.01	0.39	0.17	0.02	nd	0.12	0.28	0.12	nd	1.23
09-04b	46.68	3.70	13.67	14.42	0.22	5.93	10.76	2.57	0.53	0.38	98.85
2 σ	1.00	1.41	2.35	1.73	0.04	1.40	0.47	0.20	0.20	0.16	0.82
09-05	72.57	0.07	12.53	1.65	0.06	nd	1.35	4.28	2.66	nd	95.22
2 σ	3.83	0.02	0.40	0.44	0.03	nd	0.41	0.81	0.41	nd	3.83

Table 6.10: Whole rock chemistry of the H5 tephra layer. Samples were collected from proximal locations on the flanks of the volcano as described by Fig. 4.6.

Sample	SiO_2	TiO_2	Al_2O_3	FeO	MnO	MgO	CaO	Na_2O	K_2O	P_2O_5	Total
09-04	73.06	0.17	13.03	2.74	0.08	0.14	1.50	4.32	2.65	0.02	99.82
09-05	72.00	0.24	13.22	3.11	0.09	0.24	1.61	4.22	2.59	0.04	99.33

one sampling location (Fig. 4.6). The new major element data collected via EMPA and XRF for is presented in Tables 6.9 and 6.10.

The tephra layer shows a bimodal glass composition from basalt to rhyolite and a rhyolite bulk composition (Fig 6.34). The tephra layer is faintly peraluminous (Fig. 6.35). The tephra layer shows some chemical variation with stratigraphic height, SiO_2, Al_2O_3 and K_2O values increase between the upper and lower phases of the eruption (Fig. 6.38). However, the MgO and P_2O_5 from the data set. The tephra layer shows a low alkaline nature as indicated by the compositional fields suggested in Rollinson (1993) and references therein.

Comparing XRF and EMPA data highlights increases in TiO_2, Al_2O_3 and FeO in the XRF data compared with the glass data (Fig. 6.36). These differences are the result of removal of these elements from the glass phase through fractional crystallization of titanomagnetite, plagioclase, olivine and pyroxene during melt generation.

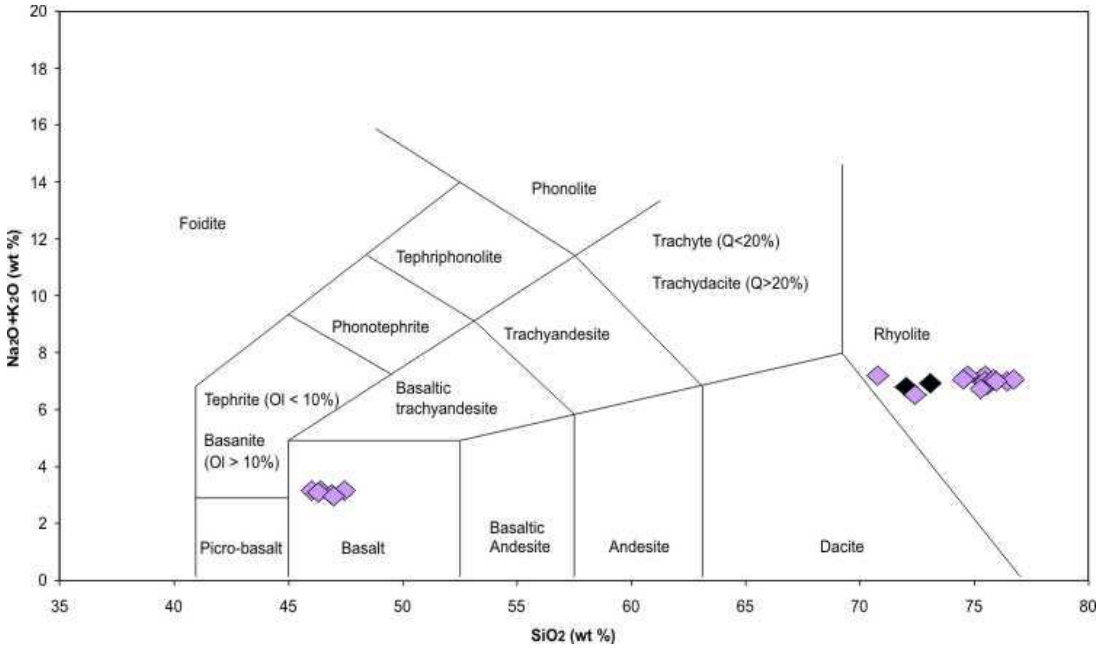

Figure 6.34: Total Alkali – Silica bivariate plot of the H5 tephra layer. Purple diamonds represent EMPA data, black diamonds represent XRF data. Data indicate that the H5 tephra layer shows a bimodal geochemistry of rhyolite and basalt. Grid lines adapted from La Maitre *et al*. (1989).

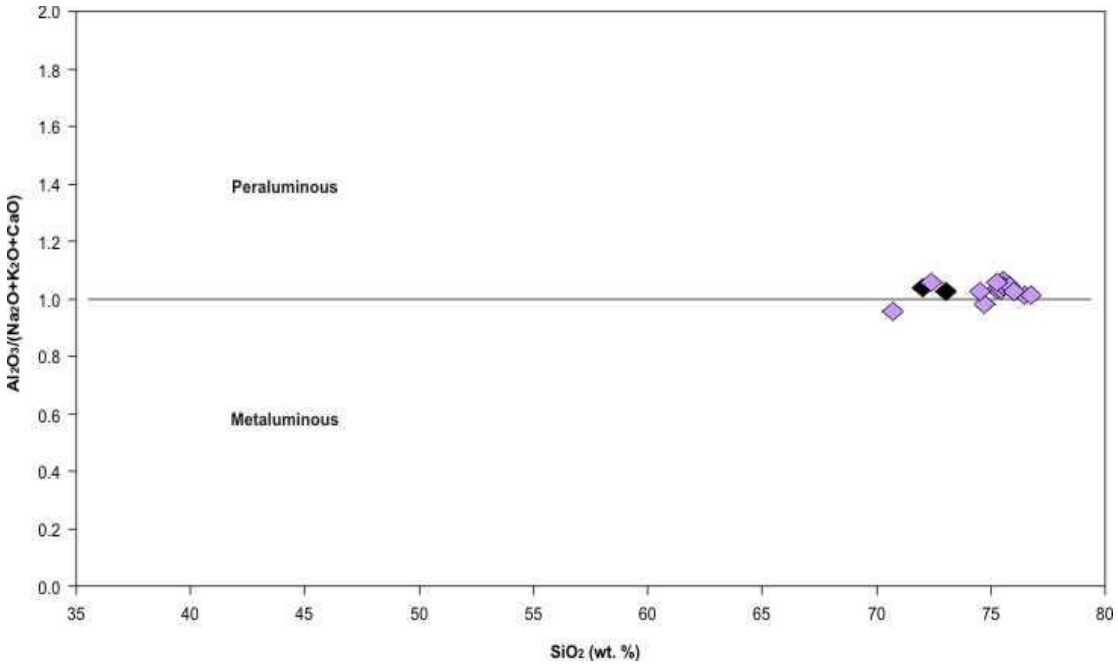

Figure 6.35: Silica – Aluminium and total alkali plot of the H5 samples. Purple diamonds represent EMPA data, black diamonds represent XRF data. Data indicate that the tephra layer shows a slightly peraluminous geochemistry which is inconsistent with the geological setting, perhaps suggesting data inadequacies.

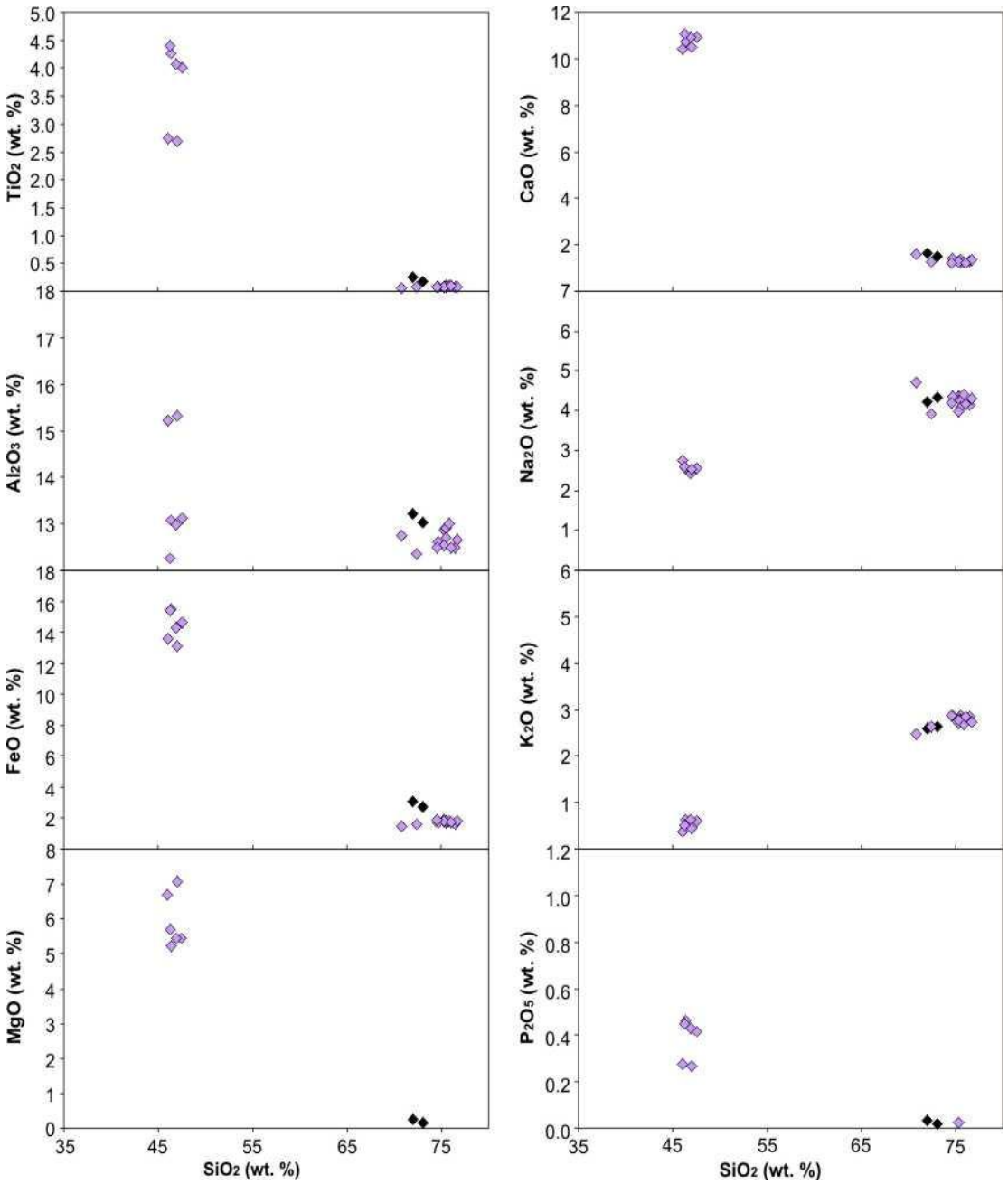

Figure 6.36: Bivariate plots of XRF and EMPA data for the H5 tephra layer. Purple diamonds represent EMPA data whilst black diamonds represent XRF data. Very minor variations are recorded for certain elements between XRF and EMPA data sets suggesting only some fractional crystallisation within the magma prior to eruption.

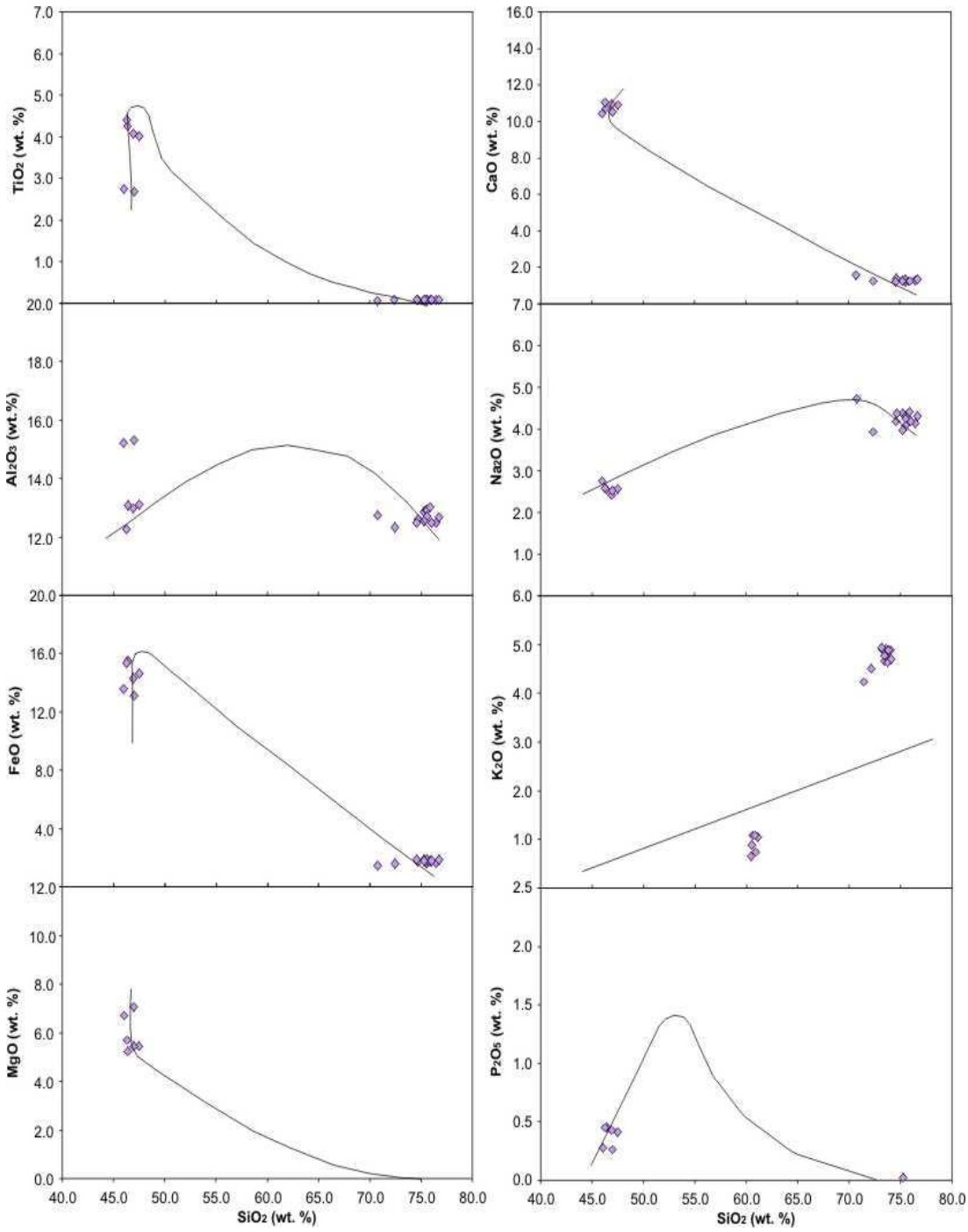

Figure 6.37: Harker plots of H5 data plotted onto the crystallization trends of major elements against SiO_2 (wt. %) for the volcanic system. Black lines represent data collected for the Torfajökull volcanic system by previous workers.

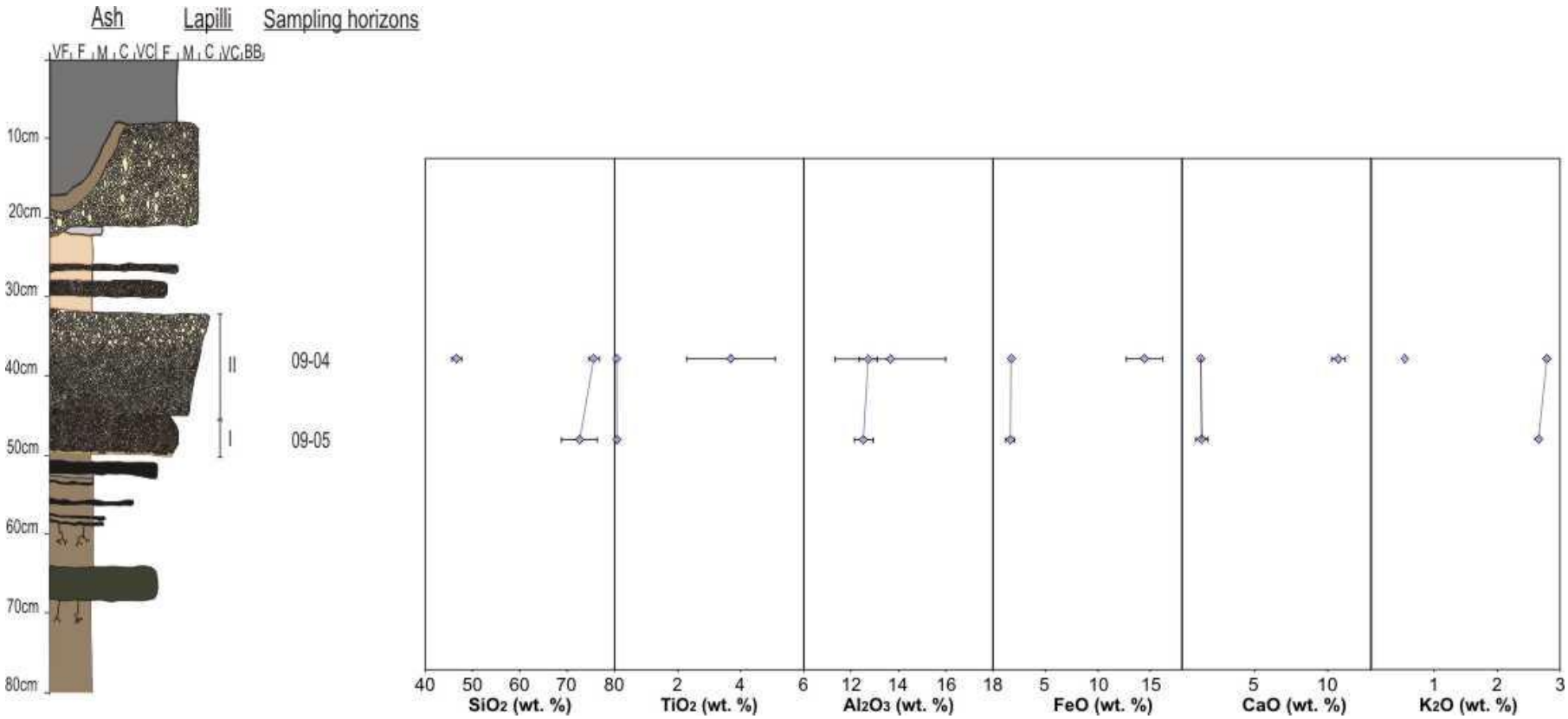

Figure 6.38: Chemical variation with stratigraphic height for the H5 tephra. Elements depicted represent the full suite of major elements analysed with the exception of MgO and P_2O_5 which were below the detection limit in the silicic samples and MnO. Some geochemical variation is recorded with stratigraphical height, however is unreliable due to the small number of samples analysed.

6.2.6 Hekla A, B and C

The HA, HB and HC tephra layers are three relatively small scale eruptions which occurred at the Hekla central volcano in the period 1850 – 2800 BP (Larsen, *pers comm*.). The three tephra layers are grouped together as they share common axes of deposition to the north-west (Fig. 2.19). HA is the youngest tephra layer in the sequence and HC is the oldest. The following section presents field and chemical data collected for the tephra layers.

Field Data: The reference section for the HA, HB and HC tephra layers was selected at 64º 05.470'N, 19º 56.472'E near Búrfell on the banks of the river Þorsjà off route 26 (Table 4.1; Fig. 4.6). Figure 6.39 is a stratigraphic log of the tephra layers compiled at this location while figure 6.40 a-d are field photographs of the tephra layer at the reference section. At this location, the tephra layers show thickness of 0.06 m (HA), 0.13m (HB) and 0.4 m (HC). The tephra layers are separated by thin palaeo-soil horizons. The tephra layers will be discussed individually below.

The HA tephra layer is 0.06 m thick and dominated by pale yellow pumice clasts with a thin discontinuous mafic top. The tephra layer shows internal layering highlighted by the colour change in the pumice clasts, but no other depositional structures are recorded. Grain size is fine lapilli while average clast size is c. 0.05 cm. Maximum clast size is c. 1 cm. The tephra layer is clast supported and well sorted. Pumice clasts are angular. The tephra layer comprises a minimal lithic content; those identified are hydrothermally altered and have an orange appearance. At the sampling location, the tephra layer is the uppermost tephra and overlies the older HB and HC tephra layers.

The HB tephra layer is 0.13 m thick and dominated by pale yellow pumice clasts with a thin top comprising black pumice clasts. The tephra layer shows internal layering highlighted by the colour change in the pumice clasts and some faint reverse grading. Grain size is fine to medium lapilli while average clast size is c. 1 cm. Maximum clast size is c. 2 cm. The tephra layer is clast supported and moderately sorted. Pumice clasts are angular; some clasts are flaky in appearance with sharp edges. The tephra layer contains minimal lithic components.

The HC tephra layer is 0.40 m thick and dominated by both pale yellow and black pumice clasts. The tephra layer shows internal layering highlighted by the colour change in the pumice clasts and some faint reverse grading. The HC tephra layer comprises a much thicker

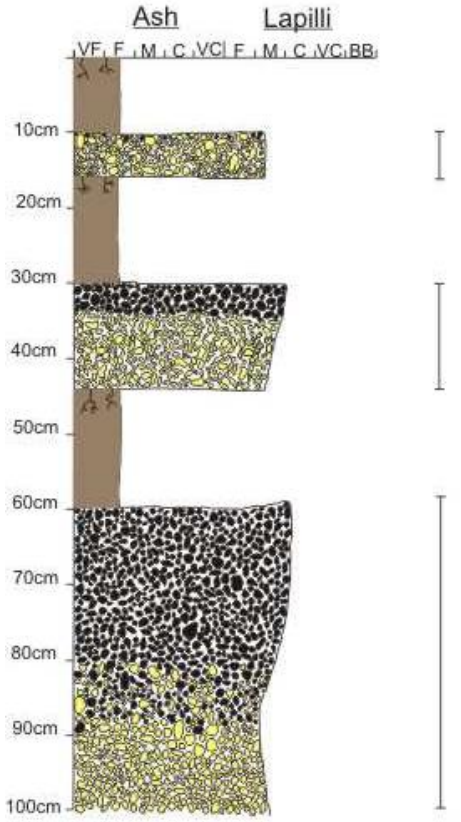

Hekla A

The HA tephra is 0.06 m thick. The deposit is dominated by pale yellow pumice clasts with a thin discontinuous mafic top. Bedding is highlighted by tephra colour change, however there are no other depositional structures. Grain size is fine lapilli. Average grain size is c. 0.5 cm. Maximum clast size is c. 1 cm. The tephra layer is well sorted and clast supported. Pumice clasts are angular. Lithic clasts are rare but when recorded are orange in colour and have an altered appearance.

The Hekla A deposit represents a pumice fall out from a Plinian eruption from the Hekla volcano. The constant grain size throughout the deposit suggests a constant intensity throughout the eruption.

Hekla B

The HB tephra is 0.13 m thick. The deposit is characterised by a two-tone appearance, the lower 0.1 m is dominated by pale yellow silicic pumice clasts and the upper 0.03 m is dominated by mafic pumice clasts. Bedding is highlighted by the colour change and the layer shows faint reverse grading. Grain size is fine to medium lapilli. Average grain size is c. 1 cm. Maximum clast size is c. 2 cm. The tephra layer is moderately sorted and clast supported. Pumice clasts are very angular with a sharp and flakey appearance.

The Hekla B deposit represents a pumice fall out from a Plinian eruption from the Hekla volcano. The deposit is bimodal indicating that the eruption was sourced from a stratified magma chamber. Low lithic components suggest a magma dominated eruption with little or no interaction with external water sources. The faint reverse grading suggests a slight increase in eruption intensity.

Hekla C

The HC tephra is 0.4 m thick. The deposit is characterised by a two-tone appearance, the lower 0.15 m is dominated by pale yellow silicic pumice clasts and the upper 0.25 m is dominated by mafic pumice clasts. Bedding is highlighted by the colour change but no other sedimentary structures are visible. The colour change between the upper mafic and lower silicic horizons is gradual over c. 0.06 m. Grain size is fine to medium lapilli. Average grain size is c. 1.2 cm. Maximum grain size is c. 2 cm. the tephra layer is moderately to well sorted and clast supported. Pumice clasts are angular.

The Hekla C deposits represents a pumice fall out from a Plinian eruption at the Hekla volcano. The bimodal chemistry of the deposit reflects zonation of the underlying magma chamber. The eruption was predominantly magmatic with little or no interaction with external water sources as suggested by the low lithic content within the deposit. The size of the deposit indicates a sustained eruption and the reverse grading suggests a an increasing intensity. The large vesicles suggest that the magma had undergone major de-gassing pre- and syn-eruption.

Figure 6.39: Sedimentary logs of the H A-B-C tephra layers at the reference section near Lambhagi on the banks of the Þjorsá river.

Figure 6.40: H A-B-C tephra layers at the sampling location near Lambhagi on the banks of the Þjorsá river. a) HA tephra layer showing a very thin and discontinuous mafic top layer. b) HB tephra layer showing angular shard like pumice clasts. c) HC tephra layer at the reference section showing gradual colour/chemical change. d) HC tephra layer at the south – east flanks of Búrfell. Photographs: Rh. Meara.

mafic component, in contrast to the HA and HB tephra layers. The increased mafic component may be the result of variations within the magma batches or due to different levels of erosion and preservation. Grain size is fine to medium lapilli while average clast size is c. 1.2 cm. Maximum clast size is c. 2 cm. The tephra layer is clast supported and moderately to well sorted. Pumice clasts are angular. Lithic components are rare.

The HA, HB and HC tephra layers represent three pumice falls from Plinian to sub-Plinian eruptions from the Hekla volcano. The eruptions produced strongly bi-modal deposits suggesting a stratified magma chamber or interaction between two magma batches. The ratio of juvenile:lithic material in the deposit suggests a dominantly magmatic eruption with little or no interaction with external water sources. The reverse grading within the HB and HC tephra layers suggest temporal variations in eruption intensity. Grain size distributions suggest that the mafic phases of these eruptions were the highest intensity. Another explanation for the differences in grain sizes is temporal variations in wind strength and direction at the specified locality.

Chemical Data: In total, one sample was analysed for HA, three samples for HB and five for HC, collected from one sampling location. The new major element data collected via EMPA and XRF for the tephra layers are presented in Tables 6.11 and 6.12. The tephra layers show two main geochemical sub-groups at the sampling location: a high silica and low silica phase.

The chemical characteristics of the tephra layer are shown by figures 6.41 to 6.45. The tephra layers show a range of glass chemistries including basaltic andesite, andesite, dacite and rhyolite. No rhyolitic phases have been recorded in the HA, HB and HC tephra layers previously. The rhyolitic grains show identical chemistry to the H4, H5, H3 and H1104 tephra layers. At present it is unclear whether the rhyolitic grains represent juvenile components of the tephra layers or entrainment of older pumiceous material during eruption. The data is recorded, but not included in the following sections. Bulk composition is basaltic andesite, andesite and dacite (Fig. 6.41). The tephra layer is metaluminous (Fig. 6.42). With the exception of the silicic to mafic transitions within each tephra layer, compositional variation is minimal with stratigraphic height (Fig. 6.45). The tephra layers shows a low alkaline nature as indicated by the compositional fields suggested in Rollinson (1993) and references therein.

Table 6.11: Glass chemistry of the HA, HB and HC tephra layers. Samples were collected from proximal locations on the flanks of the volcano as described in Figure 6.6. Ten electron probe analyses were collected for each sample and the data presented is the average of these analyses and two standard deviations. Full data sets are available in the Appendix.

Sample	SiO_2	TiO_2	Al_2O_3	FeO	MnO	MgO	CaO	Na_2O	K_2O	P_2O_5	Total
HA-08-19	64.39	0.83	15.20	6.47	0.17	1.19	4.26	4.42	1.70	0.26	98.89
2 σ	0.97	0.13	0.47	0.41	0.02	0.10	0.27	0.17	0.05	0.03	0.84
HB-08-17	54.98	2.09	14.39	11.66	0.24	2.76	6.84	3.53	1.09	1.05	97.12
2 σ	3.17	0.67	2.24	3.71	0.11	1.22	0.79	1.04	0.32	0.44	1.65
HB-08-17	65.93	0.72	14.35	6.02	0.18	1.22	3.62	4.39	2.04	0.36	98.62
2 σ	14.85	1.56	1.42	7.05	0.15	2.86	3.97	1.06	1.17	0.92	1.25
HB-08-18	65.45	0.94	15.25	7.05	0.19	1.34	4.53	4.49	1.65	0.33	99.21
2 σ	1.84	0.13	1.90	0.57	0.02	0.20	0.75	0.34	0.27	0.05	1.40
HC-08-13	54.79	2.46	13.66	12.29	0.30	2.98	6.33	3.30	1.36	1.31	98.78
2 σ	1.23	0.40	1.35	1.52	0.04	0.23	0.55	0.71	0.15	0.25	0.97
HC-08-14	55.65	2.19	14.16	11.89	0.29	2.90	6.16	3.68	1.40	1.11	99.43
2 σ	2.56	0.40	1.11	1.52	0.03	0.47	0.91	1.39	0.35	0.28	1.30
HC-08-14	63.33	0.88	15.31	6.84	0.19	1.24	4.48	4.61	1.63	0.30	98.81
2 σ	1.35	0.14	1.00	0.74	0.03	0.25	0.52	0.31	0.24	0.07	1.12
HC-08-15	63.66	0.88	15.26	6.77	0.18	1.31	4.42	4.44	1.62	0.29	98.84
2 σ	1.57	0.10	0.78	0.79	0.03	0.37	0.59	0.25	0.10	0.04	1.12
HC-08-16	65.80	0.85	14.70	5.78	0.16	1.08	3.94	4.37	1.94	0.25	98.85
2 σ	11.16	0.16	4.36	3.09	0.10	0.83	2.98	1.07	1.70	0.12	1.11

Table 6.12: Whole rock chemistry of the HA, HB and HC tephra layers. Samples were collected from proximal locations on the flanks of the volcano as described in Figure 6.6.

Sample	SiO_2	TiO_2	Al_2O_3	FeO	MnO	MgO	CaO	Na_2O	K_2O	P_2O_5	Total
HA-08-19	62.48	0.91	15.27	8.47	0.17	1.34	4.34	4.25	1.64	0.33	
HB-08-18	53.10	2.03	14.70	14.37	0.27	2.95	6.51	3.42	1.15	1.04	
HB-08-18	61.93	0.97	15.24	8.96	0.18	1.41	4.55	4.30	1.58	0.35	
HB-08-17	60.49	1.12	15.27	9.78	0.20	1.71	4.87	4.21	1.51	0.44	
HC-08-16	54.24	1.79	14.76	12.94	0.25	2.65	6.12	3.59	1.22	0.85	
HC-08-15	60.44	1.09	15.25	9.84	0.20	1.62	4.85	4.28	1.52	0.43	
HC-08-15	61.70	0..94	15.22	8.91	0.18	0.14	4.47	4.24	1.59	0.35	
HC-08-14	54.38	1.95	14.84	14.04	0.27	2.88	6.46	3.54	1.2	0.99	

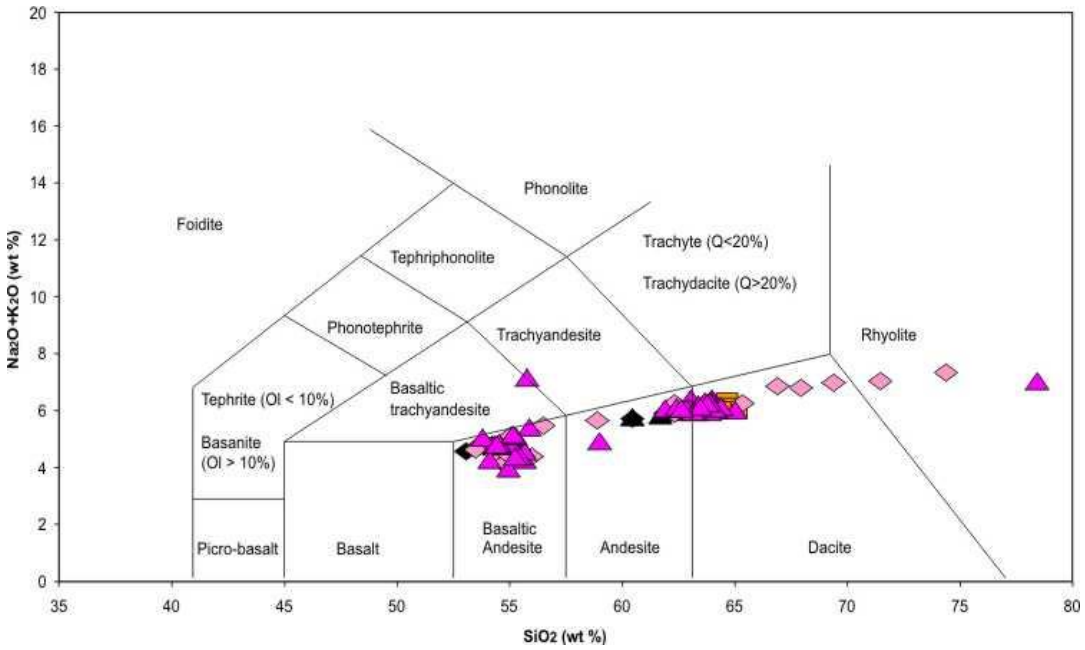

Figure 6.41: Total Alkali – Silica bivariate plot of the HA, HB and HC tephra layer. Coloured symbols represent EMPA data (Orange squares – HA, pale pink diamonds – HB, bright pink triangles – HC) while blackened symbols represent XRF data. Data indicate that the tephra layers show a geochemical range basaltic andestite, andesite, dacite and rhyolite. Grid lines adapted from La Maitre *et al*. (1989).

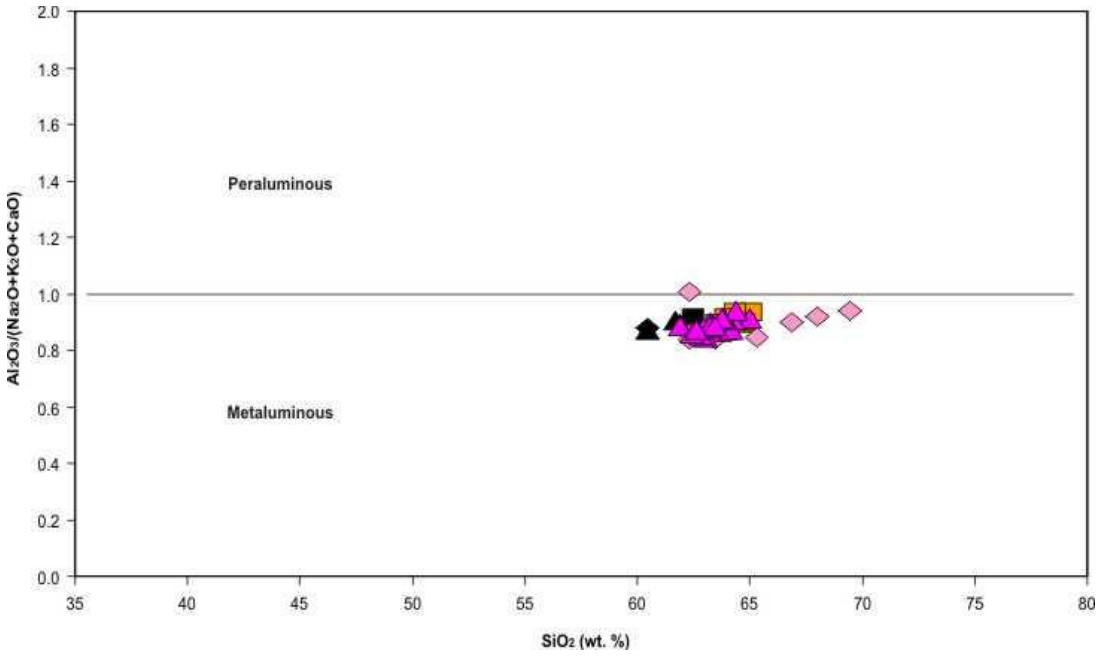

Figure 6.42: Silica – Aluminium and total alkali plot showing the luminosity of the HA, HB and HC samples. Coloured symbols represent EMPA data (Orange squares – HA, pale pink diamonds – HB, bright pink triangles – HC) while blackened symbols represent XRF data. Data indicate that the tephra layer shows a metaluminous geochemistry consistent with the geological setting.

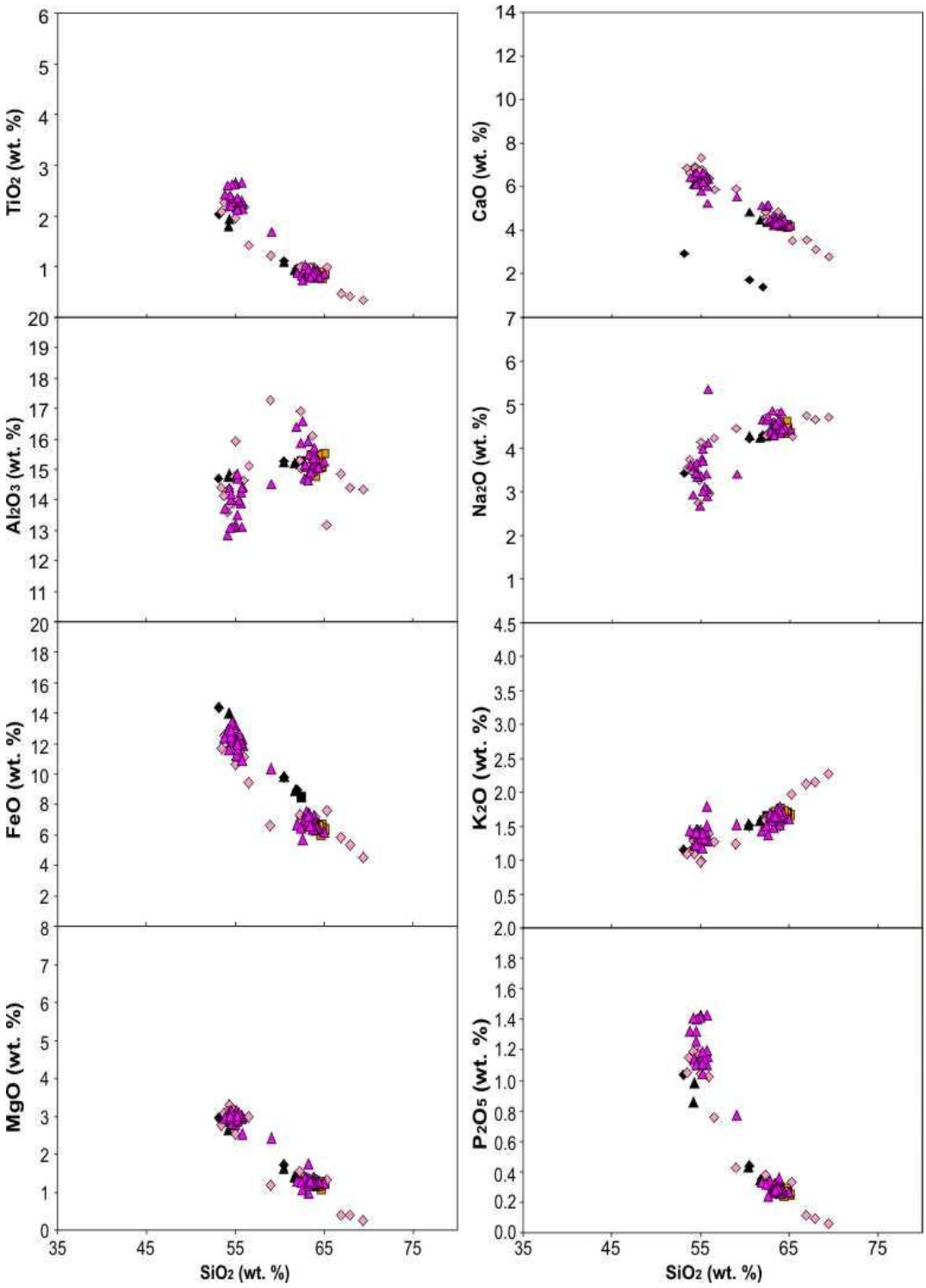

Figure 6.43: Bivariate plots of XRF and EMPA data for the HA, HB and HC tephra layers. Pink and orange colours represent EMPA data whilst black shapes represent XRF data Coloured symbols represent EMPA data (Orange squares – HA, pale pink diamonds – HB, bright pink triangles – HC) while blackened symbols represent XRF data. No major variations are recorded between XRF and EMPA data sets suggesting little if any fractional crystallisation within the magma prior to eruption.

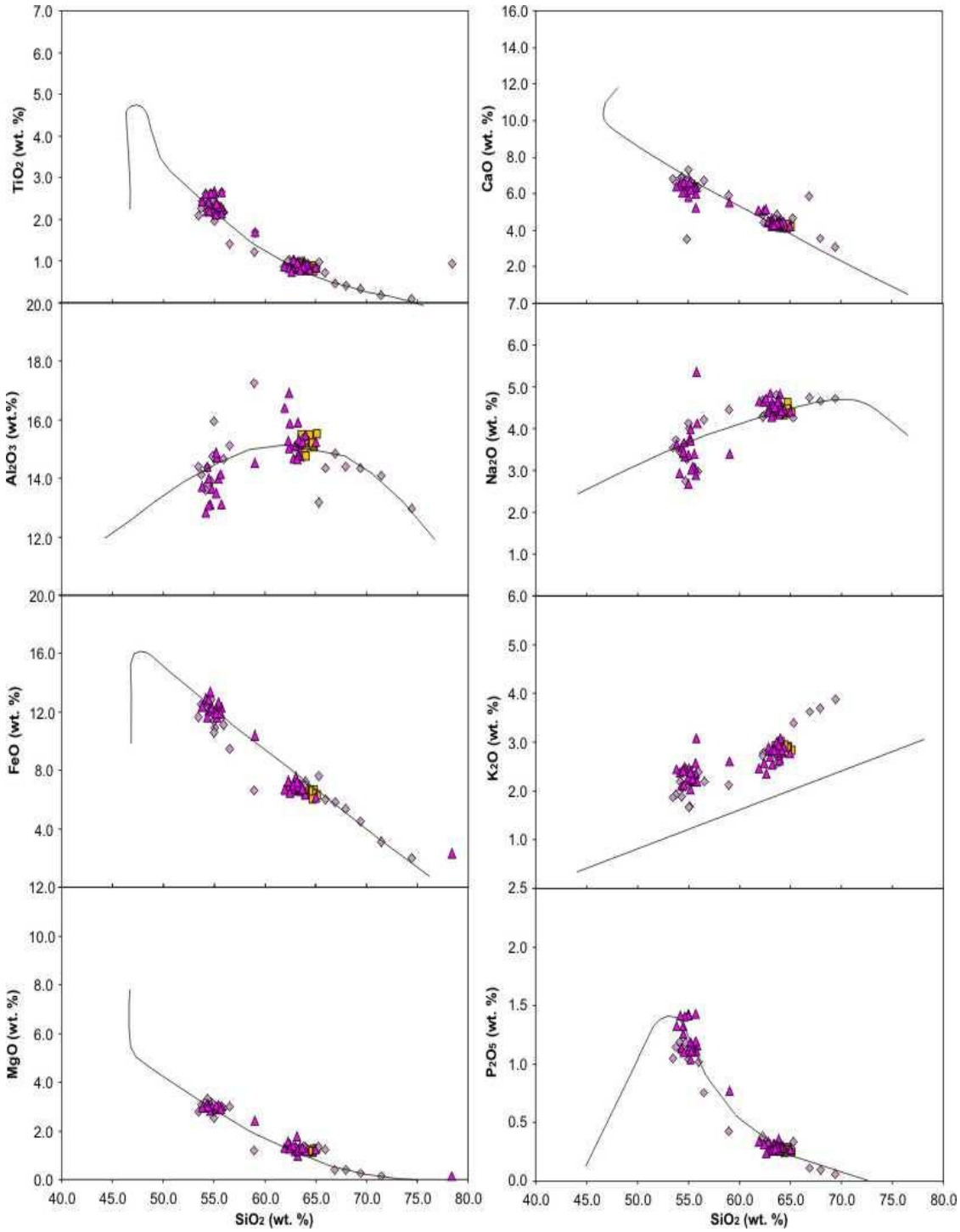

Figure 6.44: Harker plots of HA, HB and HC data plotted onto the crystallization trends of major elements against SiO_2 (wt. %) for the volcanic system. Coloured symbols represent EMPA data (Orange squares – HA, pale pink diamonds – HB, bright pink triangles – HC) while blackened symbols represent XRF data. Black lines represent data collected for the Torfajökull volcanic system by previous workers.

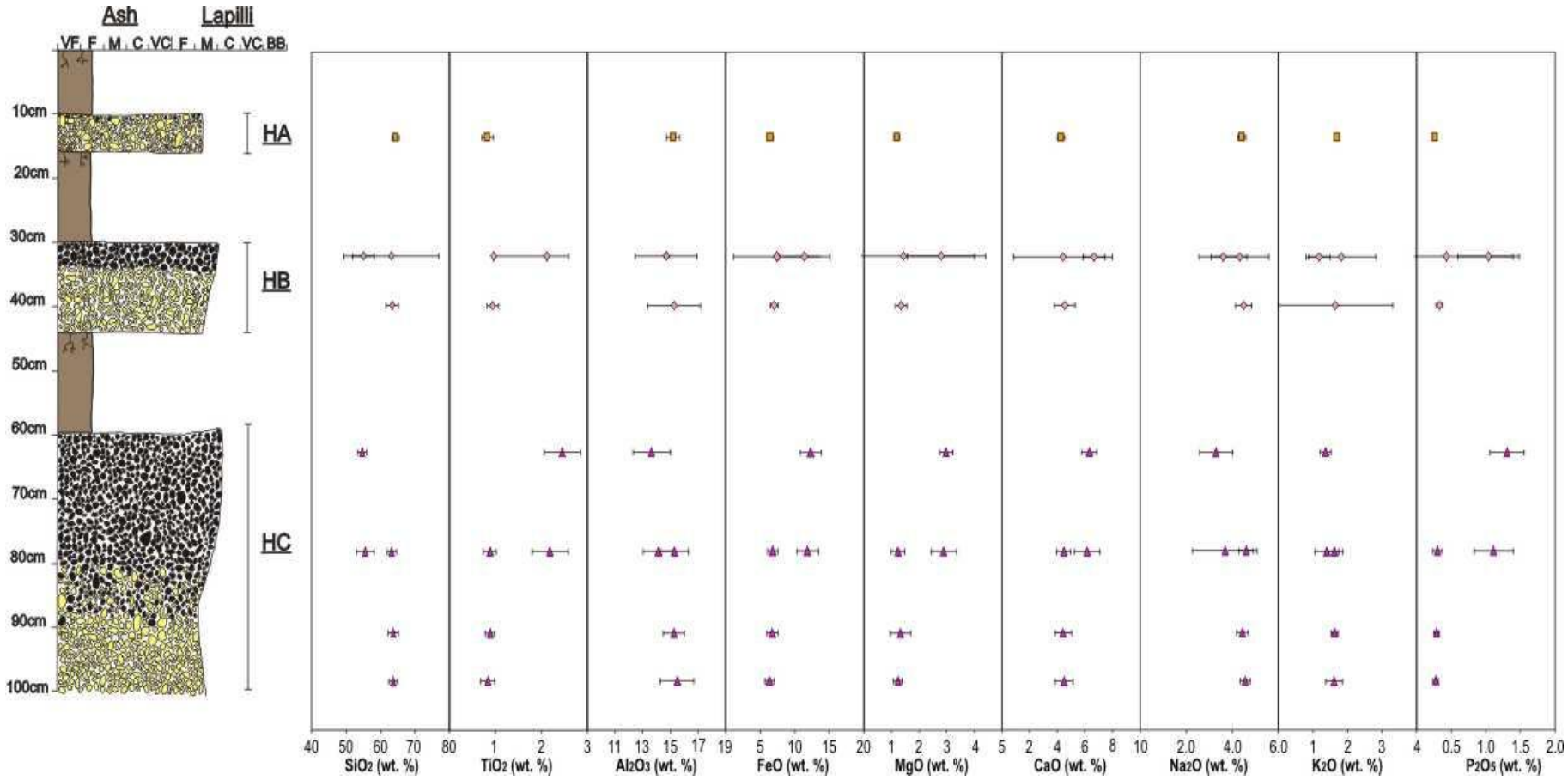

Figure 6.45: Chemical variation with stratigraphic height for the HA, HB and HC tephra layers. Elements depicted represent the full suite of major elements analysed with the exception of MnO. Geochemical variations are recorded with stratigraphical height where overall tephra chemistry becomes mafic.

Comparing XRF and EMPA data highlights variation in SiO_2 concentrations between the data sets (Fig 6.44). Also highlighted are increases in TiO_2, FeO, MgO and P_2O_5 in the XRF data compared with the glass data. These differences are the result of removal of these elements from the glass phase through fractional crystallization of titanomagnetite, olivine, pyroxene and apatite during melt generation. The mafic components of the tephra layers show distinct micro-crystalline textures in backscattered electron (BSE) images.

6.2.7 Hekla M and N

The HM and HN tephra layers are two relatively small scale eruptions which occurred at the Hekla central volcano in the period 2750 – 2800 BP (Larsen, *pers comm*.). The two tephra layers are grouped together as they share common axes of deposition to the south-east (Fig. 2.19). HM is the youngest tephra layer in the sequence and HN is the oldest. The following section presents field and chemical data collected for the tephra layers.

Field Data: The reference section for the HM and HN tephra layers was selected at 63º 53.046'N, 19º 28.992'E near Rangárhliðar on the mountain Grasleysufjöll on route F2010 near the Eystri-Rangá river (Table 4.1; Fig. 4.6). Figure 6.46 is a stratigraphic log of the tephra layers compiled at this location while figures 6.47 a) and b) are field photographs of the tephra layers at the reference section. At this location, the tephra layers show thickness of 0.4 m (HM) and 0.8 m (HN). The tephra layers are separated by a horizon of re-worked pumice clasts. The tephra layers will be discussed individually below.

The HM tephra layer is 0.4 m thick and comprises a dark yellow pumice basal phase and a dark brown to black pumice top. The tephra layer shows internal layering highlighted by the colour change in the pumice clasts and faint normal grading. No other depositional structures are recorded. Grain size is medium to coarse lapilli while average clast size is c. 2 cm. Maximum clast size is c. 3 cm. The tephra layer is clast supported and well sorted. Pumice clasts are sub-angular. The tephra layer comprises a minimal lithic content; those identified are hydrothermally altered and have an orange appearance. At the sampling location, the tephra layer is the uppermost tephra and overlies the older HN tephra layer.

The HN tephra layer is 0.8 m thick and comprises a dark yellow to pale brown basal pumice horizon with a dark brown to black pumice top. The tephra layer shows internal layering highlighted by the colour change in the pumice clasts and some faint normal grading. No

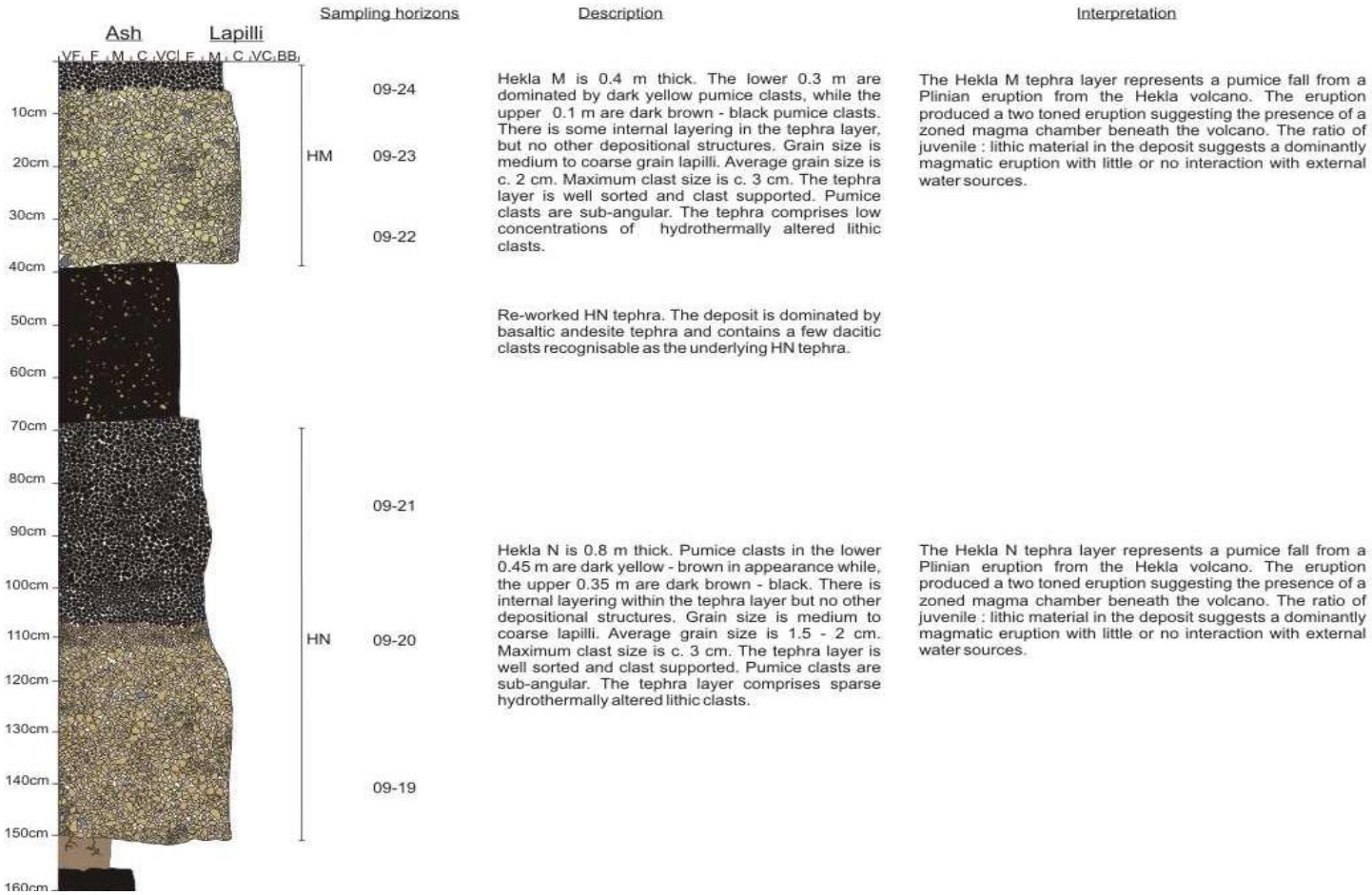

Figure 6.46: Sedimentary log of the H M-N tephra layers showing physical characteristics e.g. colour, clast morphology and grain size. Drawn at the reference section near Rangárhliðar on the banks of the Eystri-Rangá river and route F210.

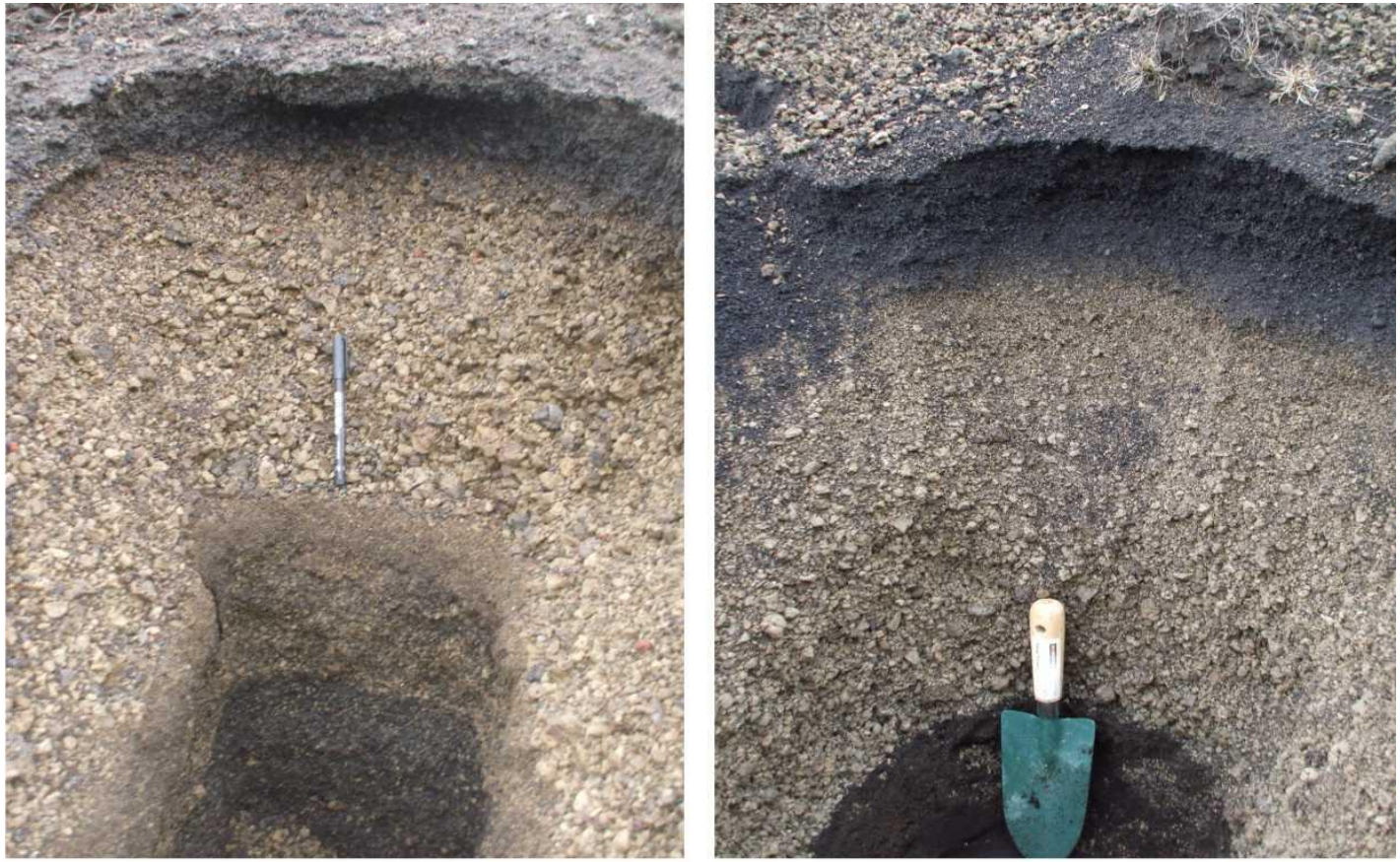

Figure 6.47: H M-N tephra layers at the sampling location near Rangárhliðar on the banks of the Eystri-Rangá river and route F210 a) HN tephra layer showing a pale yellow colour to the silicic pumice clasts. Pen used for scale measures c. 10 cm. b) HM tephra layer showing darker yellow – brown pumice clasts. Trowel used for scale measures c. 25 cm. Photographs: Rh. Meara.

Table 6.13: Glass chemistry of the HM and HN tephra layers. Samples were collected from proximal locations on the flanks of the volcano as described in Figure 6.6. Ten electron probe analyses were collected for each sample and the data presented is the average of these analyses and two standard deviations. Full data dets are available in the Appendix.

Sample	SiO_2	TiO_2	Al_2O_3	FeO	MnO	MgO	CaO	Na_2O	K_2O	P_2O_5	Total
HM-09-24	49.79	3.86	12.87	13.81	0.26	4.31	8.64	3.14	1.00	0.80	98.47
2 σ	8.95	2.40	1.12	3.31	0.07	2.60	4.07	0.76	0.89	0.53	1.03
HM-09-24	62.82	0.95	15.70	7.13	0.20	1.21	4.78	4.77	1.54	0.32	99.43
2 σ	1.51	0.18	2.35	2.36	0.09	0.32	1.08	0.61	0.53	0.06	1.21
HM-09-23	55.84	2.44	14.18	10.83	0.24	2.84	6.66	3.82	1.32	0.74	98.91
2 σ	5.01	0.52	0.88	2.47	0.05	0.81	1.06	0.32	0.21	0.34	1.65
HM-09-23	62.39	1.05	15.43	7.30	0.19	1.47	4.64	4.37	1.56	0.39	99.22
2 σ	5.01	0.52	0.88	2.47	0.05	0.81	1.06	0.32	0.21	0.34	1.65
HM-09-22	46.77	3.74	134.0	13.35	0.22	5.89	11.00	2.79	0.54	0.41	98.12
2 σ	0.82	1.38	1.18	1.86	nd	1.41	1.92	0.44	0.27	0.26	1.19
HM-09-22	63.58	0.93	15.63	6.52	0.18	1.30	4.66	4.48	1.55	0.29	99.11
2 σ	1.42	0.10	1.46	0.93	0.02	0.25	0.61	0.51	0.21	0.05	1.33
HN-09-21	55.22	2.17	13.99	11.63	0.30	2.80	6.29	3.61	1.39	1.08	98.48
2 σ	0.62	0.19	0.92	1.02	0.03	0.35	0.27	0.93	0.15	0.08	0.69
HN-09-21	63.14	0.95	15.88	6.56	0.18	1.31	4.77	4.53	1.51	0.30	99.14
2 σ	1.68	0.21	2.14	1.86	0.07	0.48	1.21	0.55	0.46	0.09	1.11
HN-09-20	63.77	0.93	15.44	6.82	0.18	1.34	4.48	4.47	1.60	0.29	99.32
2 σ	0.93	0.05	0.32	0.54	0.02	0.10	0.29	0.24	0.12	0.03	0.94
HN-09-19	53.87	2.42	13.86	12.42	0.30	3.22	6.75	3.34	1.31	1.09	98.66
2 σ	5.72	0.88	1.48	1.20	0.06	2.00	3.20	0.74	0.63	0.55	1.43
HN-09-19	64.39	0.88	15.20	6.27	0.17	1.24	4.23	4.47	1.71	0.29	98.75
2 σ	1.97	0.16	0.98	1.22	0.04	0.31	1.00	0.23	0.71	0.05	1.01

Table 6.14: Whole rock chemistry of the HM and HN tephra layers. Samples were collected from proximal locations on the flanks of the volcano as described in Figure 6.6.

Sample	SiO_2	TiO_2	Al_2O_3	FeO	MnO	MgO	CaO	Na_2O	K_2O	P_2O_5	Total
HM-09-24	58.26	1.58	15.36	11.29	0.21	2.75	5.75	3.67	1.29	0.38	99.56
HM-09-24	67.57	0.52	14.49	4.39	0.09	0.63	1.46	4.91	4.14	0.07	99.33
HM-09-23	62.91	0.95	15.39	8.84	0.18	1.42	4.50	4.21	1.57	0.33	99.89
HM-09-22	62.57	0.93	15.45	8.50	0.17	1.45	4.51	4.45	1.55	0.34	99.58
HN-09-19	63.39	0.903	15.32	8.45	0.17	1.36	4.40	4.29	1.60	0.31	99.96
HN-09-20	61.99	0.92	15.39	8.45	0.16	1.46	4.47	4.51	1.55	0.33	99.43

other depositional structures are recorded. Grain size is medium to coarse lapilli while average clast size is c. 1.5 – 2 cm. Maximum clast size is c. 3 cm. The tephra layer is clast supported and well sorted. Pumice clasts are sub-angular. The tephra layer contains minimal lithic components, those recorded are hydrothermally altered.

The HM and HN tephra layers represent two pumice falls from Plinian to sub-Plinian eruptions from the Hekla volcano. The eruptions produced strongly bi-modal deposits suggesting a stratified magma chamber or interaction between two magma batches. The ratio of juvenile:lithic material in the deposit suggests a dominantly magmatic eruption with little or no interaction with external water sources. The normal grading within the HM and HN tephra layers suggest temporal variations in eruption intensity. Grain size distributions suggest that the silicic basal components of these eruptions were the highest intensity. These grain size variations may also be the result of variations in wind direction and intensity and cannot be ruled out without investigation of multiple reference sections, which was outside the scope of this project.

Chemical Data: In total, six samples were analysed for HM and five for HN, collected from one sampling location (Fig. 4.6). The new major element data collected via EMPA and XRF for the tephra layers are presented in Tables 6.13 and 6.14. The tephra layers show two main geochemical sub-groups at the sampling location: a high silica and low silica phase.

The chemical characteristics of the tephra layera are shown by figures 6.48 to 6.52. The tephra layers show a range of glass chemistries including basanite, basalt, basaltic andesite, basaltic trachyandesite, andesite and dacite. Bulk composition is basaltic andesite, andesite, dacite and trachydacite (Fig. 6.48). The tephra layers are metaluminous (Fig. 6.49). With the exception of the silicic to mafic transitions within each tephra layer, compositional variation is minimal with stratigraphic height (Fig. 6.52). The tephra layers shows a low alkaline nature as indicated by the compositional fields suggested in Rollinson (1993) and references therein.

Comparing XRF and EMPA data highlights minor variation in SiO_2 concentrations between the data sets (Fig 6.50). No other distinct variations are highlighted between the XRF data compared with the glass data as both data sets show a range in composition. This absence of geochemical variation is surprising, as the mafic components of the HM and HN tephra layers show intense micro-crystalline textures in backscattered electron (BSE) images.

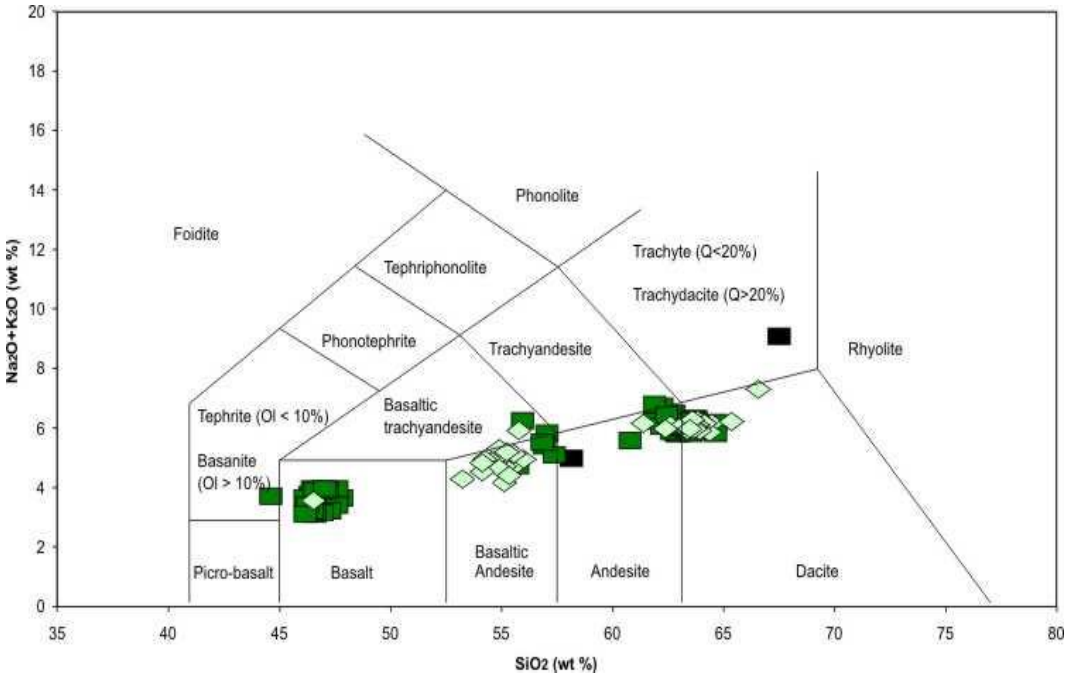

Figure 6.48: Total Alkali – Silica bivariate plot of the HM and HN tephra layers. Coloured symbols represent EMPA data (dark green squares – HM, pale green diamonds – HN) while blackened symbols represent XRF data. Data indicate that the tephra layers show a compositional range from basalt, basaltic andesite, andesite and dacite. Grid lines adapted from La Maitre *et al*. (1989).

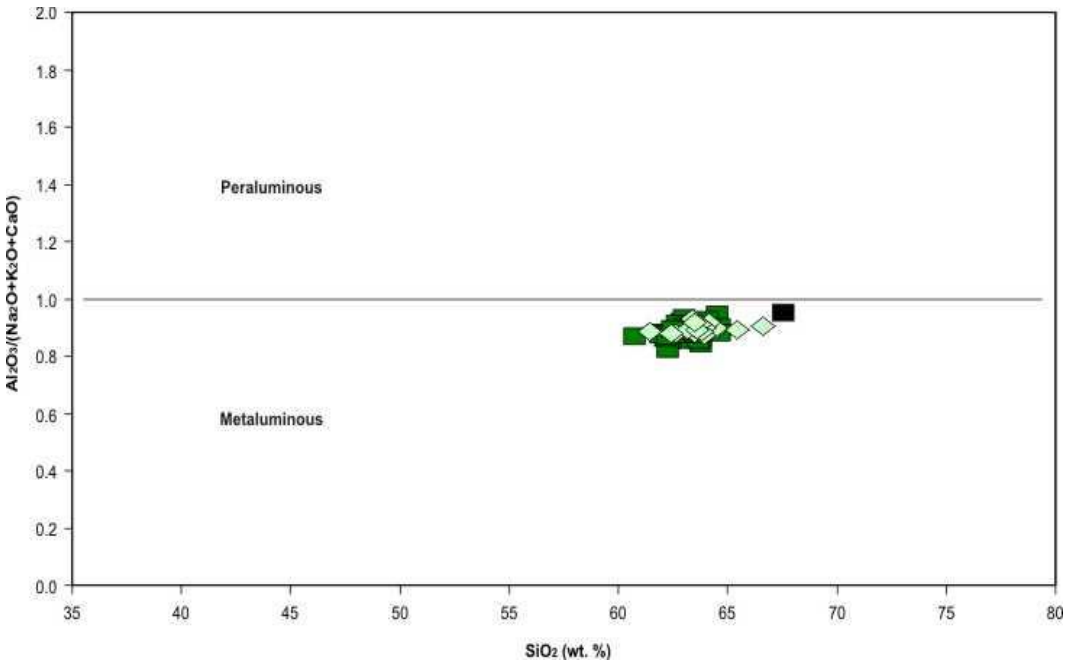

Figure 6.49: Silica – Aluminium and total alkali plot showing the luminosity of the HM and HN samples. Coloured symbols represent EMPA data (dark green squares – HM, pale green diamonds – HN) while blackened symbols represent XRF data. Data indicate that the tephra layer shows a metaluminous geochemistry consistent with the geological setting.

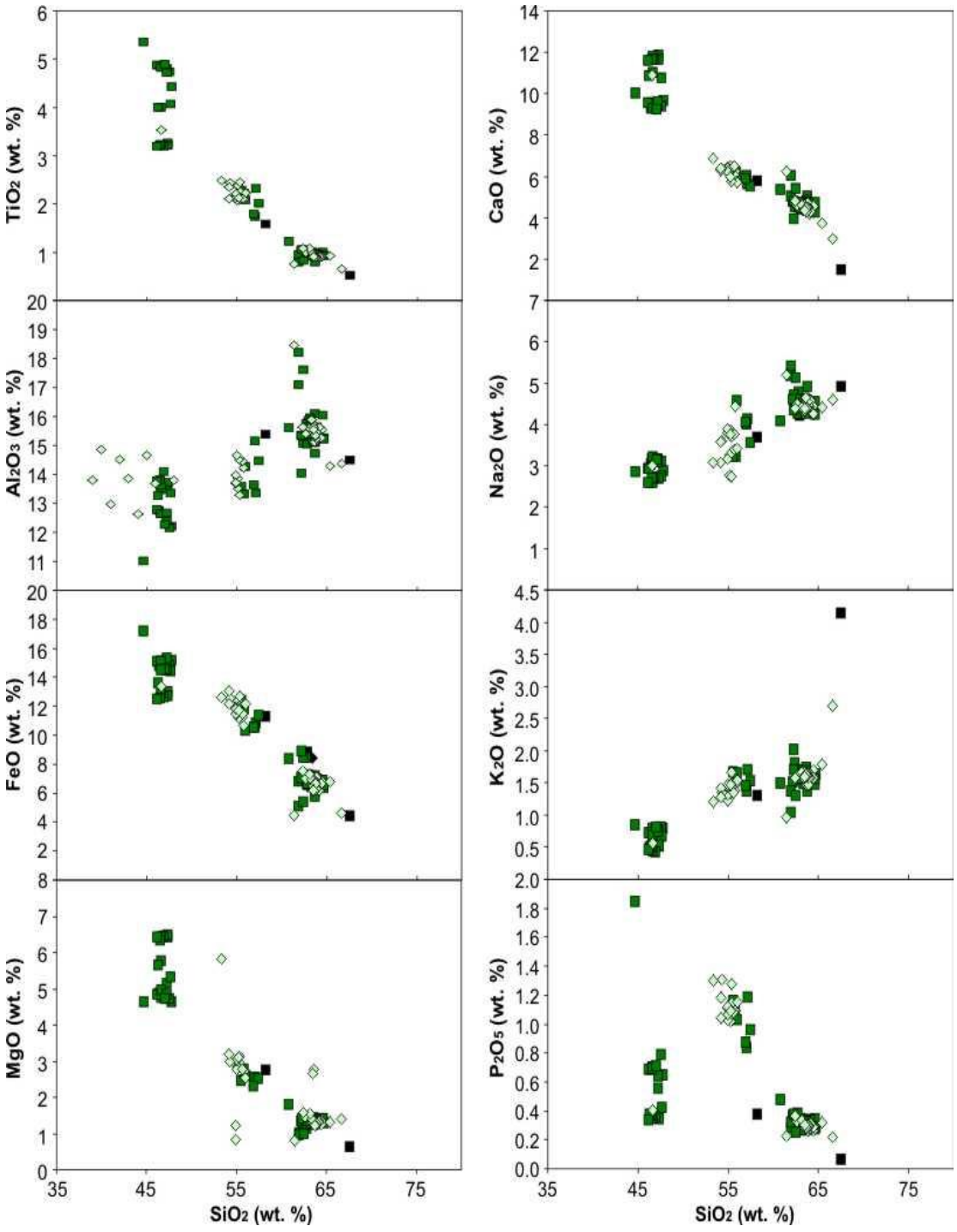

Figure 6.50: Bivariate plots of XRF and EMPA data for the HM and HN tephra layers. Coloured symbols represent EMPA data (dark green squares – HM, pale green diamonds – HN) while blackened symbols represent XRF data. No major variations are recorded between XRF and EMPA data sets suggesting little if any fractional crystallisation within the magma prior to eruption.

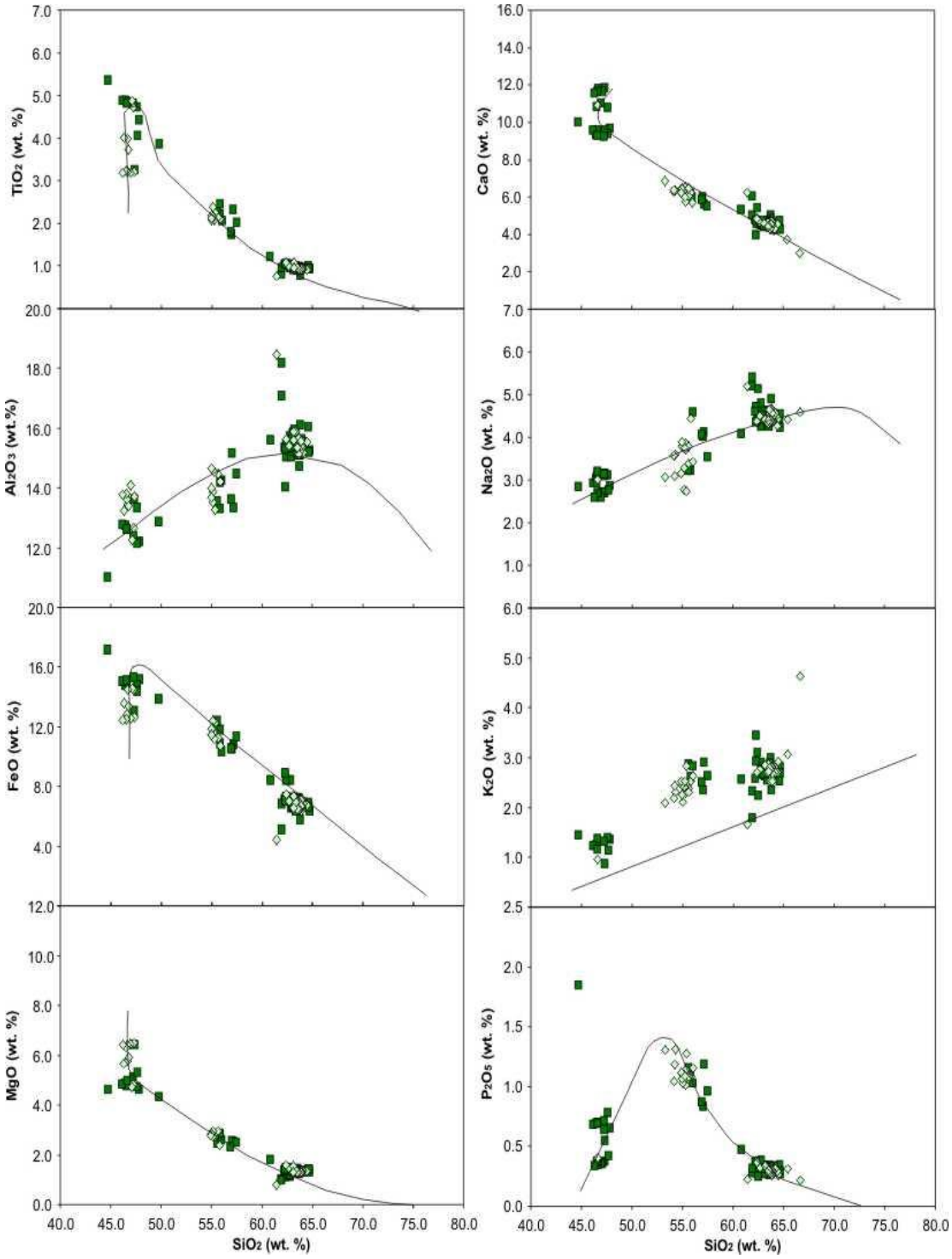

Figure 6.51: Harker plots of HM and HN data plotted onto the crystallization trends of major elements against SiO_2 (wt. %) for the volcanic system. Coloured symbols represent EMPA data (dark green squares – HM, pale green diamonds – HN). Black lines represent data collected for the Torfajökull volcanic system by previous workers.

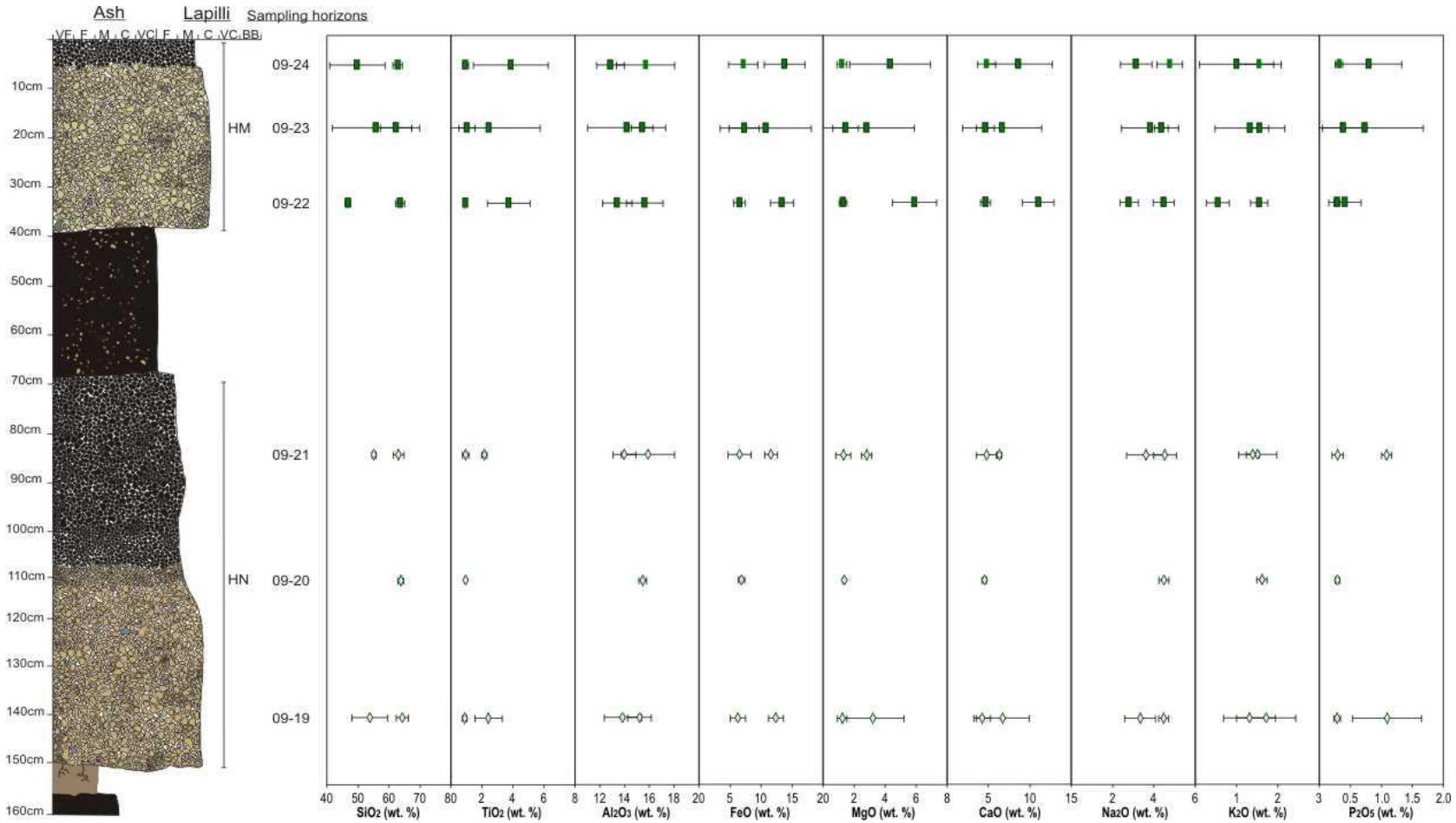

Figure 6.52: Chemical variation with stratigraphic height for the HM and HN tephra layers. Elements depicted represent the full suite of major elements analysed with the exception of MnO. No major geochemical variations with stratigraphical height are recorded within the HM – HN tephra layers.

6.2.8 Hekla X, Y and Z

The HX, HY and HZ tephra layers are three relatively small scale eruptions which occurred at the Hekla central volcano in the period 1850 – 2800 BP (Larsen, *pers comm*.). The three tephra layers are grouped together as they share common axes of deposition to the north-east (Fig. 2.19). HX is the youngest tephra layer in the sequence and HZ is the oldest. The following section presents field and chemical data collected for the tephra layers.

Field Data: The reference section for the HX, HY and HZ tephra layers was selected at 64º 02.589'N, 19º 18.218'E near Sauðleysur on route F225 near the banks of the river Helliskvísl (Table 4.1; Fig. 4.6). Figure 6.53 is a stratigraphic log of the tephra layers compiled at this location while figures 6.54 a – d are field photographs of the tephra layer at the reference section. At this location, the tephra layers show thickness of 0.32 m (HX), 0.33m (HY) and 0.75 m (HZ). There is no evidence for extensive palaeo-soil horizons separating the tephra layers. The tephra layers will be discussed individually below.

The HX tephra layer is 0.32 m thick and comprises a yellow pumice basal section with a black pumice top. The tephra layer shows internal layering highlighted by the colour change in the pumice clasts and some reverse grading. No other depositional structures are recorded. Grain size is fine to medium lapilli while average clast size is c. 1 cm. Maximum clast size is c. 3 cm. The tephra layer is clast supported and moderately sorted. Pumice clasts are angular. The tephra layer comprises a minimal lithic content; those identified are hydrothermally altered and have an orange and green appearance. At the sampling location, the tephra layer is the uppermost tephra and overlies the older HY and HZ tephra layers.

The HY tephra layer is 0.33 m thick and comprises a yellow pumice basal horizon with a black pumice top. The tephra layer shows internal layering highlighted by the colour change in the pumice clasts and some faint reverse grading. No other depositional structures are recorded. Grain size is fine to medium lapilli while average clast size is c. 1 cm. Maximum clast size is c. 3.8 cm. The tephra layer is clast supported and moderately sorted. Pumice clasts are angular. The tephra layer contains minimal lithic components.

The HZ tephra layer is 0.75 m thick and comprises a yellow pumice basal horizon and a black pumice top. The HZ tephra layer comprises a much thicker mafic component, in contrast to the HX and HY tephra layers. The increased mafic component may be the result

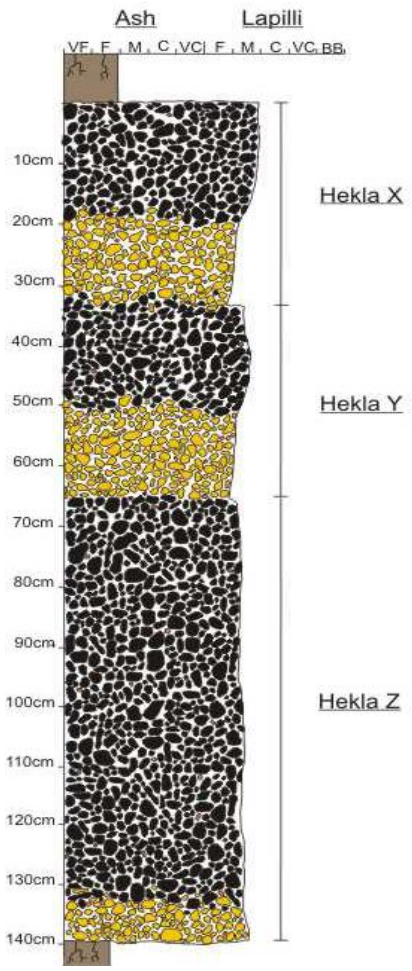

Description	Interpretation
The HX tephra layer is 0.32 m thick. The deposit is characterised by a two-tone appearance, the lower 0.12 m is dominated by yellow silicic pumice clasts and the upper 0.2 m comprising black mafic pumice clasts. Bedding is highlighted by the colour change and the layer shows faint reverse grading. Grain size is fine to medium lapilli. Average grain size is c. 1 cm. Maximum clast size is c. 3 cm. The tephra layer is moderately sorted and clast supported. Pumice clasts are angular. Lithics are rare within the deposit, but when visible are generally orange in colour and show minor alteration. Lithic clasts are c. 0.5 cm in size.	The Hekla X deposit represents a pumice fall out from a Plinian eruption from the Hekla volcano. The eruption produced a bimodal deposit consisting of rhyolite and basaltic-andestie, thus suggesting the presence of a zoned magma chamber beneath the volcano. The high ratio of juvenile : lithic material in the deposit suggests a dominantly magmatic eruption with little or no interaction with external water sources. The increase in lapilli grain size towards the top of the deposit indicates an increasing intensity towards the end of the eruption.
The HY tephra is 0.33 m thick. The deposit is characterised by a two-tone appearace, the lower 0.15 m is dominated by yellow silicic pumice clasts and the upper 0.18 m comprises black mafic pumice clasts. Bedding is highlighted by the colour change and faint reverse grading is seen in the mafic layer. Grain size is fine to medium lapilli. Average grain size is c. 1 cm. Maximum clast size is c. 3.6 cm. The tephra layer is moderately sorted and clast supported. Pumice clasts are angular. Altered orange lithics are found within the deposit but are rare.	The Hekla Y deposit represents a pumice fall out from a Plinian eruption at the Hekla volcano. The deposit is bimodal, with pumice chemistry ranging from rhyolite to basaltic andesite hinting at a certain extent of magmatic zoning within the chamber beneath the volcano. The poor lithic content suggests a magma dominated eruption with little or no interaction with external water sources. The reverse grading within the deposit is indicative of increasing intensity towards the end of the eruption. The small vesicles identified suggest that full de-gassing of the magma did not occur prior to cooling of individual pumice clasts.
The HZ tephra is 0.75 m thick. The deposit is characterised by a two-tone appearance, the lower 0.08 m is dominated by yellow silicic pumice clasts and the upper 0.68 m comprises black mafic pumice clasts. Bedding is highlighted by the colour change but no other depositional structures are recorded. Grain size is medium lapilli. Average grain size is c. 1.2 cm. Maximum clast size is c. 3 cm. The tephra layer is moderately sorted and clast supported. Pumice clasts are angular. Lithics are rare but predominantly orange in colour and hydrothermally altered.	The Hekla Z deposits represents a pumice fall out from a Plinian eruption at the Hekla volcano. Chemistry within the deposit is bimodal ranging from basaltic andesite to rhyolite indicating a certain degree of magmatic zonation within the underlying magma chamber. The eruption was predominantly magmatic with little or no interaction with external water sources as suggested by the low lithic content within the deposit. Full de-gassing of the magma was not compleated prior to eruption and cooling of the pumice clasts as indicated by the smaller vesicles within the clasts.

Figure 6.53: sedimentary log of the H X-Y-Z tephra layers at the reference section near Sauđleysur on the banks of the Helliskvísl river and route F225.

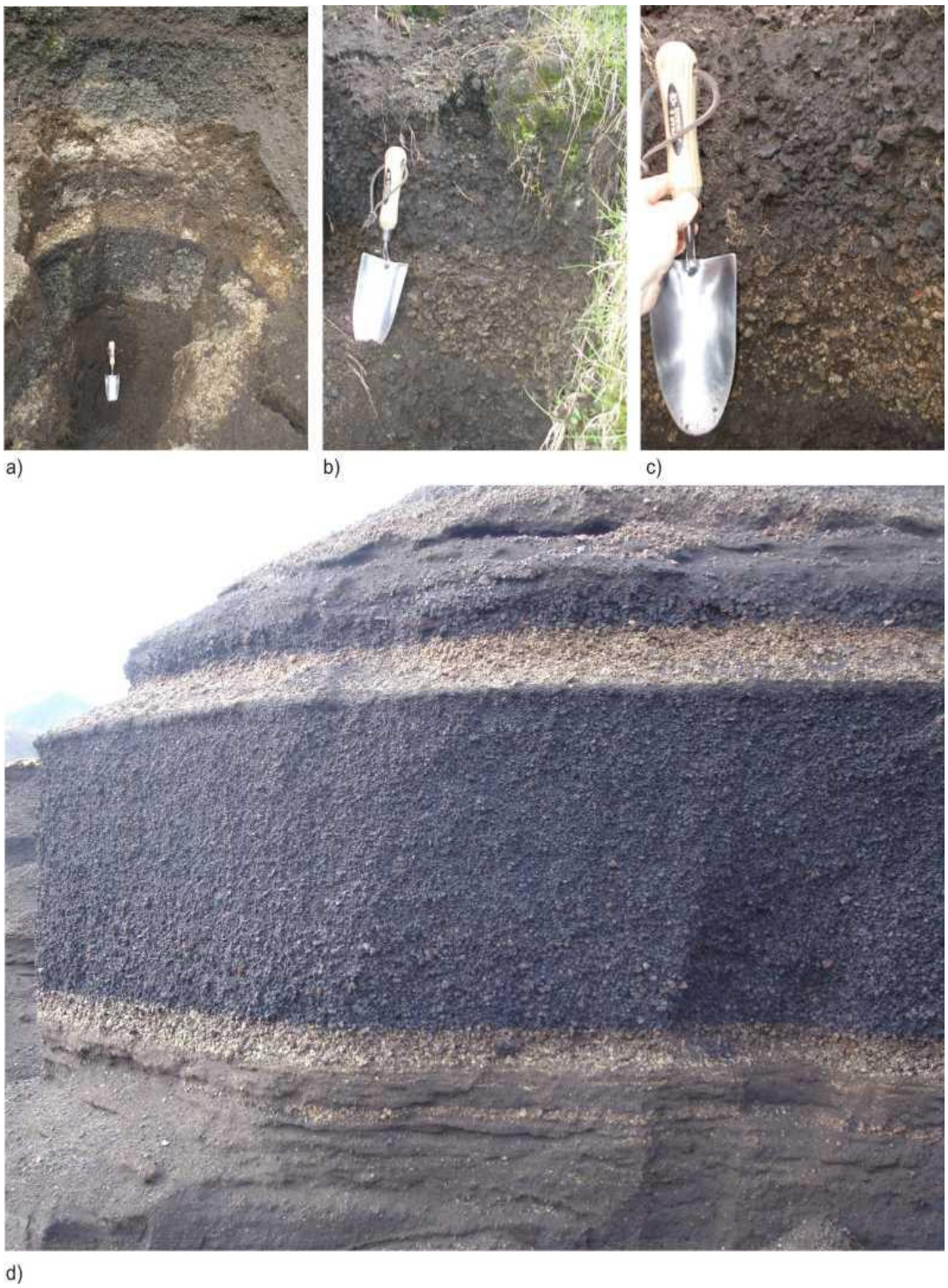

Figure 6.54: H X-Y-Z tephra layers at the sampling location near Sauðleysur on the banks of the Helliskvísl river and route F225. a) Reference section containing HX at the top, HY in the middle and HZ at the base of the deposit. b) HX tephra layer. c) HY tephra layer. d) HZ tephra layer taken on the banks of the Rauðufossakvísl near Sátubarn. Photographs: Rh. Meara (a-c) and K. Roberts (d).

of variations within the magma batches or due to different levels of erosion and preservation. The tephra layer shows internal layering highlighted by the colour change in the pumice clasts and some faint normal grading. No other depositional structures are recorded. Grain size is medium lapilli while average clast size is c. 1.2 cm. Maximum clast size is c. 3 cm. The tephra layer is clast supported and moderately sorted. Pumice clasts are angular. Lithic components are rare, those recorded are orange in appearance due to hydrothermal alteration.

The HX, HY and HZ tephra layers represent three pumice falls from Plinian to sub-Plinian eruptions from the Hekla volcano. The eruptions produced strongly bi-modal deposits suggesting a stratified magma chamber or interaction between two magma batches. The ratio of juvenile:lithic material in the deposit suggests a dominantly magmatic eruption with little or no interaction with external water sources. Grading within the layers suggest temporal variations in eruption intensity. Grain size distributions suggest that the mafic components of the HX and HY eruptions, and the silicic component of the HZ eruption, were the highest intensity phases.

Chemical Data: In total, one sample was analysed for HA, three samples for HB and five for HC, collected from one sampling location. The new major element data collected via EMPA and XRF for the tephra layers are presented in Tables 6.15 and 6.16. The tephra layers shows two main geochemical sub-groups at the sampling location: a high silica and low silica phase. These two phases will be discussed below for each tephra layer.

The chemical characteristics of the tephra layer are shown by figures 6.55 to 6.59. The tephra layers show a range of glass chemistries including basaltic andesite, basaltic trachyandesite, andestie, dacite and rhyolite. No rhyolitic phases have been recorded in the HX, HY and HZ tephra layers previously. The rhyolitic grains show identical chemistry to the H4, H5, H3 and H1104 tephra layers. At present it is unclear whether the rhyolitic grains represent juvenile components of the tephra layers or entrainment of older pumicous material during eruption. The data is recorded, but not included in the following sections. Bulk compositions are basaltic andesite and andesite (Fig. 6.55). The tephra layers are metaluminous (Fig. 6.56). With the exception of the silicic to mafic transitions within each tephra layer, compositional variations are minimal with stratigraphic height (Fig. 6.59). The tephra layers shows a low alkaline nature as indicated by the compositional fields suggested in Rollinson (1993) and references therein.

Comparing XRF and EMPA data highlights variation in SiO_2 concentrations between the data sets (Fig 6.57). No other distinct variations are highlighted between the XRF data

Table 6.15: Glass chemistry of the HX, HY and HZ tephra layers. Samples were collected from proximal locations on the flanks of the volcano as described in Figure 4.6. Ten electron probe analyses were collected for each sample and the data presented is the average of these analyses and two standard deviations. Full data sets are available in the Appendix.

Sample	SiO_2	TiO_2	Al_2O_3	FeO	MnO	MgO	CaO	Na_2O	K_2O	P_2O_5	Total
HX-08-1	54.60	2.26	14.14	11.57	0.27	3.08	6.59	3.55	1.28	1.06	98.41
2 σ	1.62	0.22	0.78	1.34	0.04	0.32	0.42	0.80	0.13	0.10	0.97
HX-08-1	69.89	0.41	14.37	4.40	0.13	0.44	2.53	4.45	2.56	0.10	99.29
2 σ	7.43	0.60	1.73	3.60	0.11	0.99	2.36	0.60	1.64	0.22	0.57
HX-08-2	53.34	2.55	13.90	12.22	0.27	3.69	7.31	3.44	1.12	0.89	98.72
2 σ	5.86	1.50	1.46	2.71	0.07	2.20	3.25	0.82	0.77	0.68	1.38
HX-08-2	71.55	0.27	13.86	3.68	0.13	0.25	2.21	4.40	2.63	0.06	99.03
2 σ	8.00	0.54	1.58	3.38	0.11	0.96	2.04	0.54	0.89	0.19	0.91
HX-08-3	53.20	2.84	13.45	12.82	0.29	3.60	7.26	3.38	1.16	0.90	98.90
2 σ	7.39	1.91	1.58	3.18	0.09	1.85	2.57	0.51	0.50	0.57	1.12
Hx-08-3	65.92	0.73	14.88	5.92	0.26	1.05	3.87	4.51	1.92	0.26	99.31
2 σ	9.15	0.81	1.82	4.41	0.26	1.41	2.78	0.67	1.10	0.36	1.87
HY-08-5	51.43	3.14	13.01	13.58	0.48	3.76	7.61	3.24	1.14	1.16	98.55
2 σ	6.22	1.86	1.13	1.83	0.10	1.72	2.66	0.63	0.56	0.87	1.08
HY-08-5	64.12	0.84	15.33	6.50	0.34	1.26	4.54	4.46	1.59	0.14	99.28
2 σ	4.20	0.49	1.23	2.25	0.07	0.78	1.12	0.40	0.39	0.28	1.16
HY-08-6	54.77	2.16	14.50	11.43	0.44	3.34	6.73	3.53	1.20	1.00	99.11
2 σ	8.70	0.97	1.76	4.03	0.10	2.94	3.01	1.40	0.60	0.77	1.21
Hy-08-6	68.12	0.55	14.65	4.63	0.30	0.77	3.14	4.69	2.24	0.19	99.26
2 σ	9.14	0.77	1.62	4.16	0.10	1.30	3.02	0.81	1.65	0.28	1.30
HY-08-7	54,58	2.20	14.35	11.71	0.46	3.19	6.60	3.68	1.26	1.17	99.20
2 σ	1.82	0.41	1.29	1.80	0.04	0.41	0.62	0.91	0.19	0.22	1.58
HY-08-7	64.20	0.88	15.15	6.38	0.34	1.33	4.53	4.42	1.65	0.30	99.18
2 σ	1.60	0.10	0.55	0.58	0.02	0.14	0.34	0.30	0.13	0.07	1.21
HZ-08-9	52.55	2.43	14.05	12.75	0.48	3.60	7.07	3.52	1.15	1.37	98.98
2 σ	1.22	0.17	1.03	0.90	0.02	0.12	0.13	0.47	0.17	0.10	1.75
HZ-08-9	68.58	0.48	14.65	4.59	0.30	0.65	2.93	4.43	2.37	0.14	99.12
2 σ	6.74	0.61	1.30	3.11	0.07	1.12	2.63	0.46	1.71	0.25	0.77
HZ-08-10	54.07	2.30	14.19	11.92	0.46	3.35	6.81	3.71	1.21	1.28	99.30
2 σ	1.99	0.30	0.99	1.54	0.03	0.39	0.45	0.87	0.21	0.16	1.43
HZ-08-10	70.16	0.33	13.93	4.12	0.29	0.36	2.33	4.43	2.36	0.08	99.23
2 σ	9.50	0.53	1.53	3.87	0.11	0.97	2.23	0.57	1.19	0.23	2.46
HZ-08-11	54.37	2.29	14.10	11.92	0.29	3.18	6.95	3.63	1.20	1.12	99.04
2 σ	1.34	0.22	1.06	0.83	0.04	0.20	0.44	0.47	0.21	0.18	1.33

Table 6.16: Whole rock chemistry of the HX, HY and HZ tephra layers. Samples were collected from proximal locations on the flanks of the volcano as described by Figure 4.6.

Sample	SiO_2	TiO_2	Al_2O_3	FeO	MnO	MgO	CaO	Na_2O	K_2O	P_2O_5	Total
HX-08-1	53.99	2.09	14.61	13.84	0.26	3.07	6.71	3.61	1.19	1.01	100.39
HX-08-2	56.30	1.81	15.05	12.79	0.24	2.74	6.28	3.75	1/27	0.82	101.06
HX-08-3	58.86	1.00	14.82	8.97	0.18	1.53	4.57	4.13	1.46	0.38	95.89
HX-08-3	61.34	1.05	15.24	9.24	0.18	1.55	4.77	4.35	1.53	0.38	99.63
HX-08-4	61.19	1.07	15.24	9.31	0.19	1.59	4.78	4.31	1.53	0.38	99.58
HY-08-5	52.83	2.11	14.65	14.49	0.28	3.14	6.70	3.46	1.14	1.02	99.81
HY-08-6	53.45	2.02	14.64	14.09	0.27	3.06	6.57	3.62	1.18	0.98	99.88
HY-08-7	62.78	0.97	15.05	8.40	0.17	1.46	4.52	4.30	1.58	0.33	99.56
HZ-08-9	51.89	2.33	14.57	15.26	0.29	3.39	7.04	3.40	1.08	1.25	100.50
HZ-08-10	52.86	2.20	14.71	14.62	0.28	3.24	6.88	3.48	1.13	1.14	100.54
HZ-08-11	54.63	1.95	14.90	13.61	0.27	2.88	6.44	3.66	1.21	0.96	100.50

compared with the glass data as both data sets show a range in composition. This absence of geochemical variation is surprising, as the mafic components of the HM and HN tephra layers show intense micro-crystalline textures in backscattered electron (BSE) images.

This section has presented and described the field and geochemical data collected for the H1104, H3, HSelsund, H4, H5, HA, HB, HC, HM, HN, HX, HY and HZ tephra layers sourced from the Hekla volcanic system. The following section focuses on establishing whether the afore mentioned tephra layers can be identified and distinguished using EMPA major element chemistry.

6.3 A formal system for the identification of tephra layers sourced within the Hekla volcanic system

Chapter 5 focused on establishing tephra identity by confirming tephra provenance using major element chemistry. In the following section, major element chemistry is applied solely to the Hekla volcanic system to investigate the potential for discriminating between tephra layers sourced within the same volcanic system. Both the mafic ($\leq$ 60 wt. % SiO_2) and silicic ($\geq$ 60 wt. % SiO_2) components of the tephra layers are considered, however the silicic

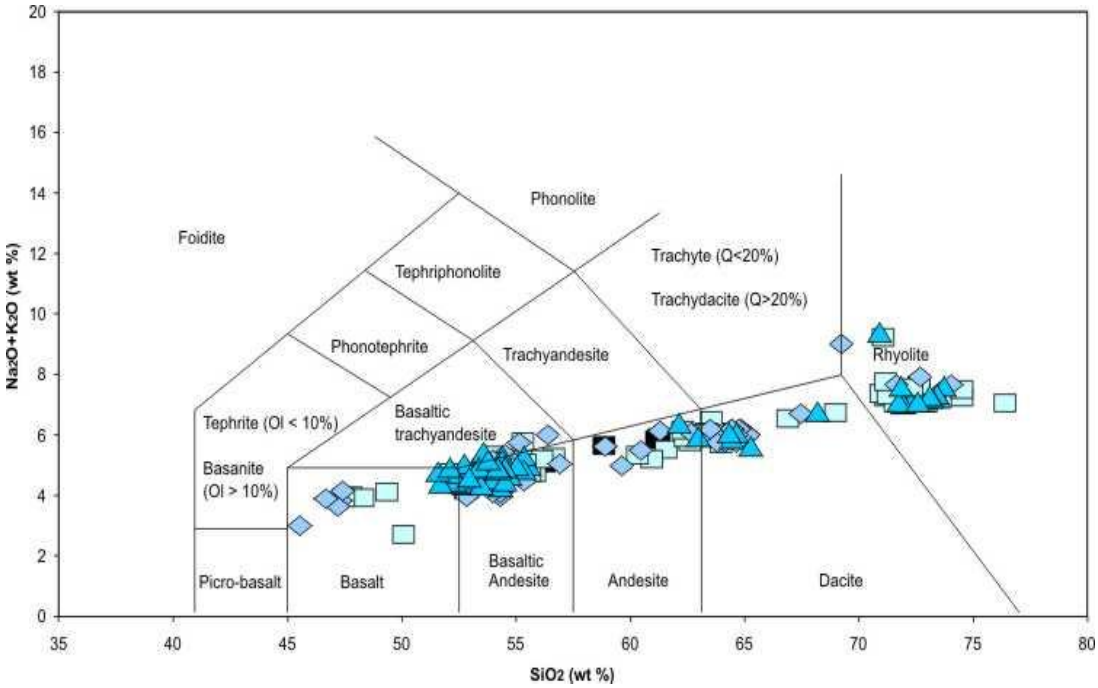

Figure 6.55: Total Alkali – Silica bivariate plot of the HX, HY and HZ tephra layers. Coloured symbols represent EMPA data (pale blue squares – HX, blue diamonds – HY, bright blue triangles – HZ) while blackened symbols represent XRF data. Data indicate that the tephra layers show a compositional range from basalt, basaltic andesite, andesite, dacite and rhyolite. Grid lines adapted from La Maitre *et al*. (1989).

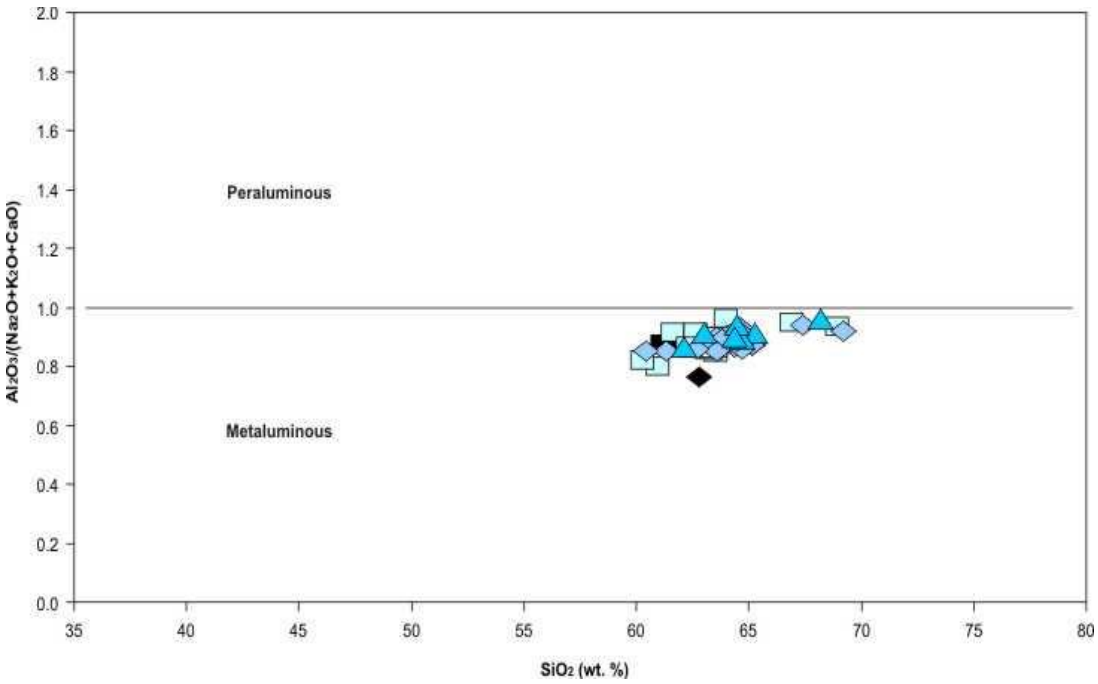

Figure 6.56: Silica – Aluminium and total alkali plot showing the luminosity of the HX, HY and HZ samples. Coloured symbols represent EMPA data (pale blue squares – HX, blue diamonds – HY, bright blue triangles – HZ) while blackened symbols represent XRF data. Data indicate that the tephra layer shows a metaluminous geochemistry consistent with the geological setting.

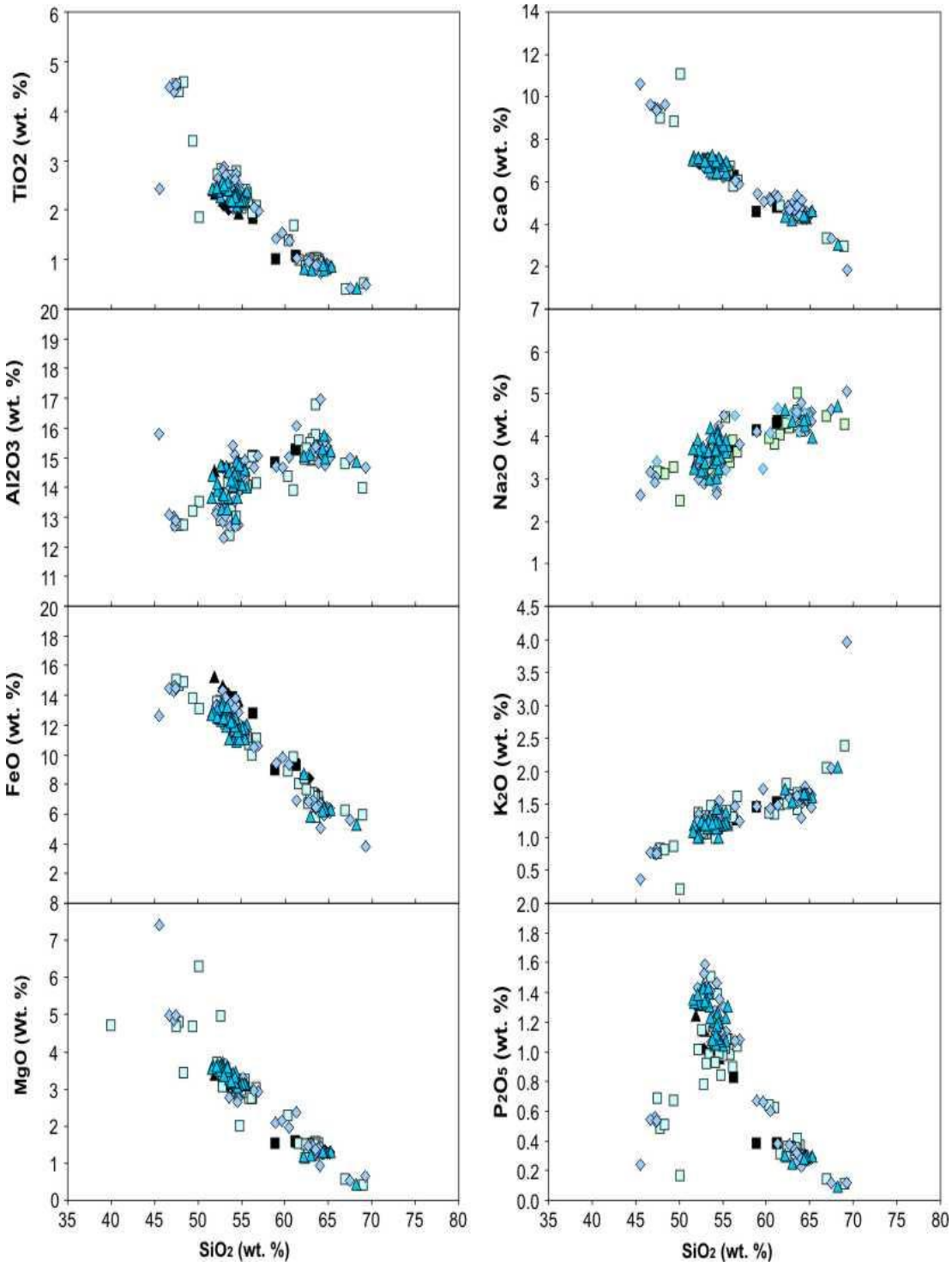

Figure 6.57: Bivariate plots of XRF and EMPA data for the HX. HY and HZ tephra layers. Coloured symbols represent EMPA data (pale blue squares – HX, blue diamonds – HY, bright blue triangles – HZ) while blackened symbols represent XRF data. No major variations are recorded between XRF and EMPA data sets suggesting little if any fractional crystallisation within the magma prior to eruption.

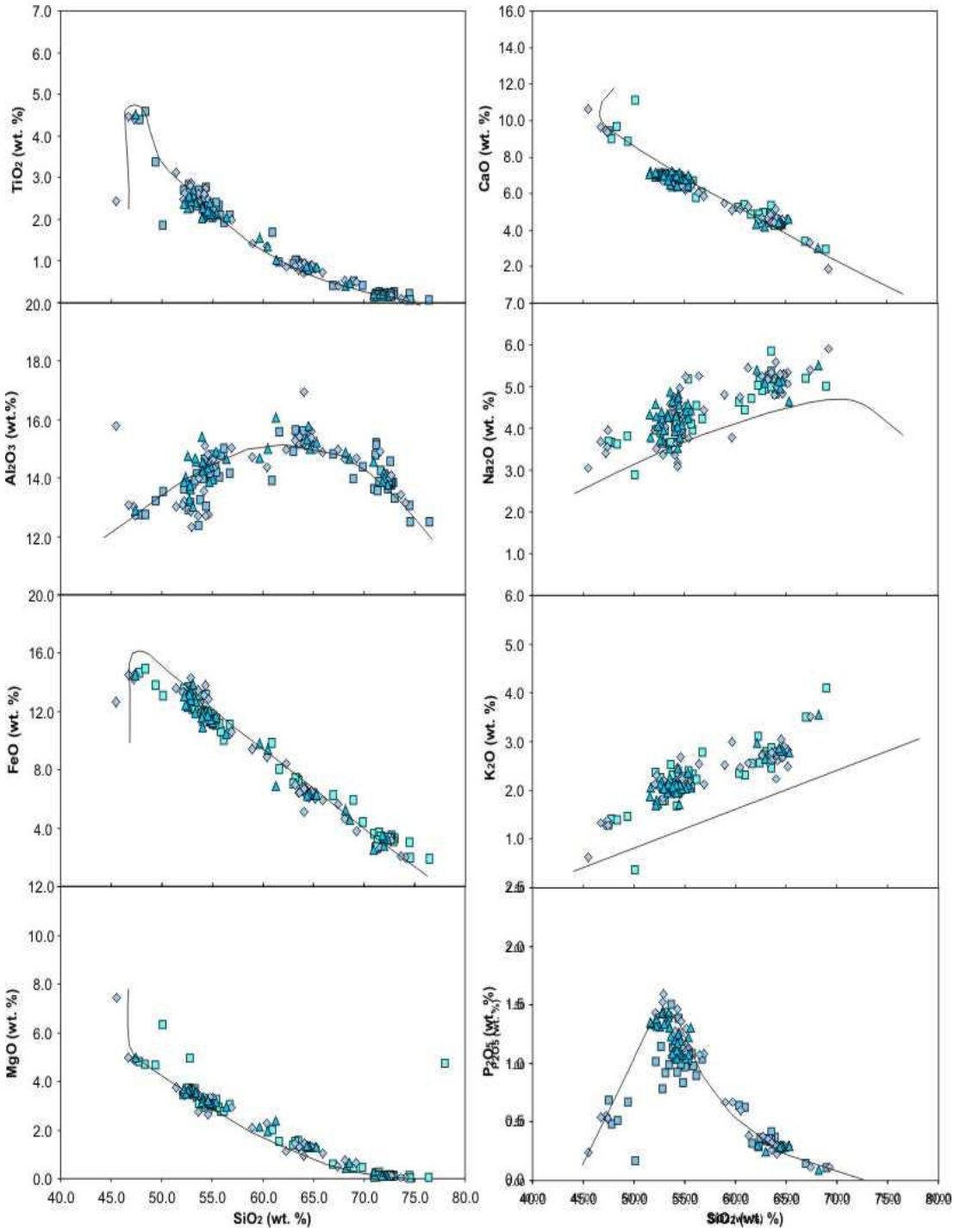

Figure 6.58: Harker plots of HX, HY and HZ data plotted onto the crystallization trends of major elements against SiO_2 (wt. %) for the volcanic system. Coloured symbols represent EMPA data (pale blue squares – HX, blue diamonds – HY, bright blue triangles – HZ). Black lines represent data collected for the Torfajökull volcanic system by previous workers.

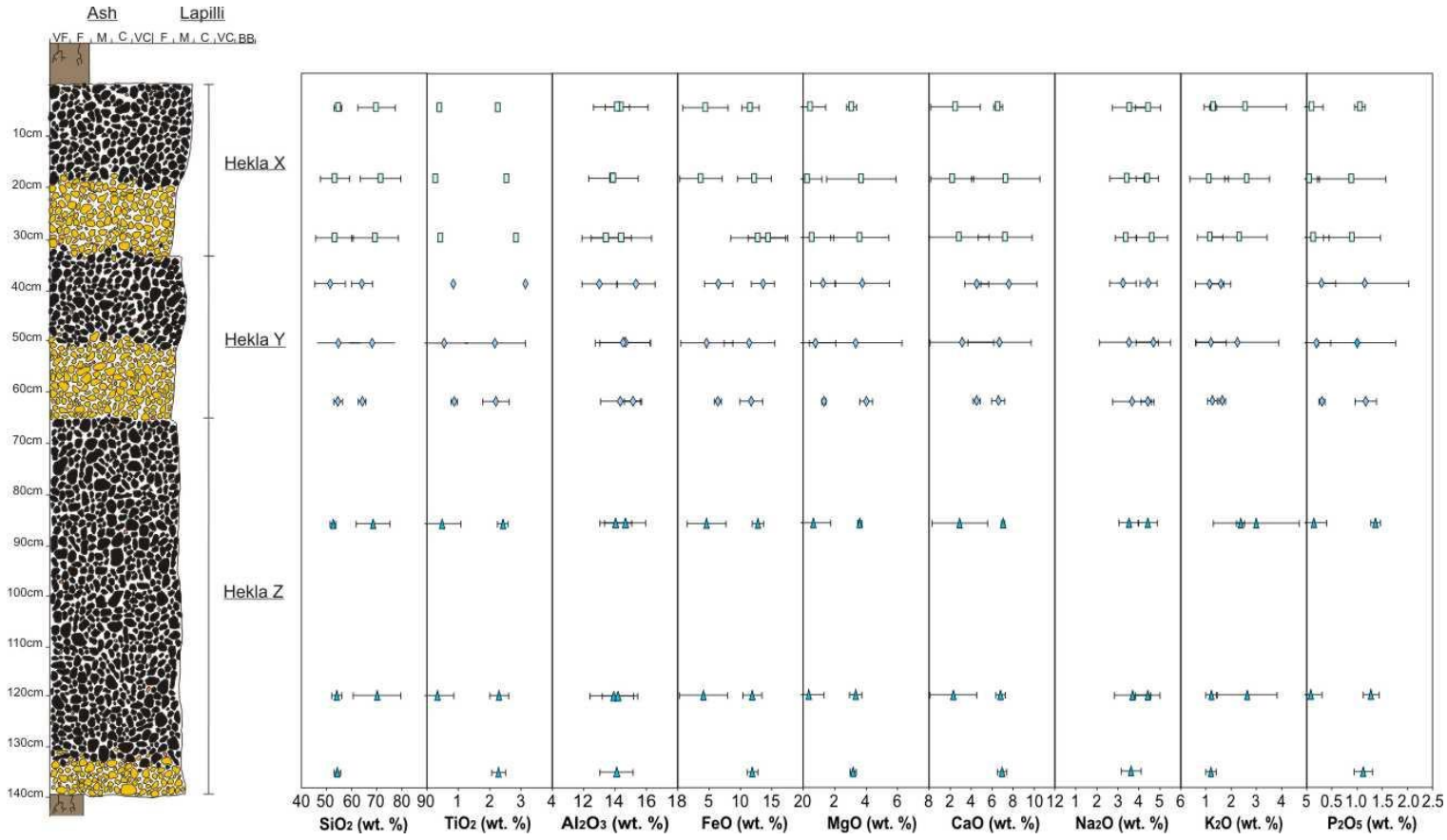

Figure 6.59: Chemical variation with stratigraphic height for the HX, HY and HZ tephra layers. Elements depicted represent the full suite of major elements analysed with the exception of MnO. Minimal geochemical variation is recorded with stratigraphical height.

components are the main focus of this project. For further analyses of basaltic tephra layers see Jagan (2010).

The tephra layers studied are plotted onto total alkali silica (TAS) diagrams (Fig. 6.60) which separates the data into mafic and silicic components. The separation occurs at an arbitrary point of 60 wt. % SiO_2. Data points containing > 60 wt. % SiO_2 are deemed "silicic" and those containing < 60 wt. % SiO_2 are deemed "mafic". The data may then be considered as two separate sub-groups and a formal method of identification can be determined for each group.

The separation of tephra layers into silicic and mafic sub-groups provides an opportunity to highlight patterns within the geochemical data which would go unnoticed if a wider dataset were used. Within the established silicic and mafic sub-groups, all data points are graphically plotted to cover each potential major element combination. Figures 6.61 to 6.63 represent the plots created for the silicic sub-group while figures 6.64 to 6.66 represent the plots created for the mafic group. By plotting all major element combinations it is possible identify certain geochemical variations characteristic of individual tephra layers. The manipulation of such variations allows a formal framework for discrimination between tephra layers sourced within the same volcanic system. The following sections will detail the frameworks established for identifying the silicic and mafic components of the eruptions discussed in this chapter.

Silicic Tephra Layers: The final methodology for establishing tephra identity for silicic Hekla tephra layers is presented in Figure 6.67. Plotting the tephra layers onto a bivariate plot of SiO_2 against FeO separates the layers into three distinct sub-groups – Group 1: H4-H5; Group 2: H1104-H3-HSelsund; Group 3: HA, HB, HC, HM, HN, HX, HY and HZ. The three sub-groups are recognisable in most elemental combinations (Figs. 6.61 – 6.63), however the data overlap between Group 3 and the low silica end of the H3 tephra layer is minimised when using the suggested plot.

Group 1 comprises the H4 and H5 tephra layers. Previous studies have found the tephra layers to show near-identical major element geochemical data. This study however, has revealed minor variations which can be manipulated to discriminate between the rhyolitic phases of the tephra layers. The H5 tephra layer comprises systematically lower TiO_2, FeO

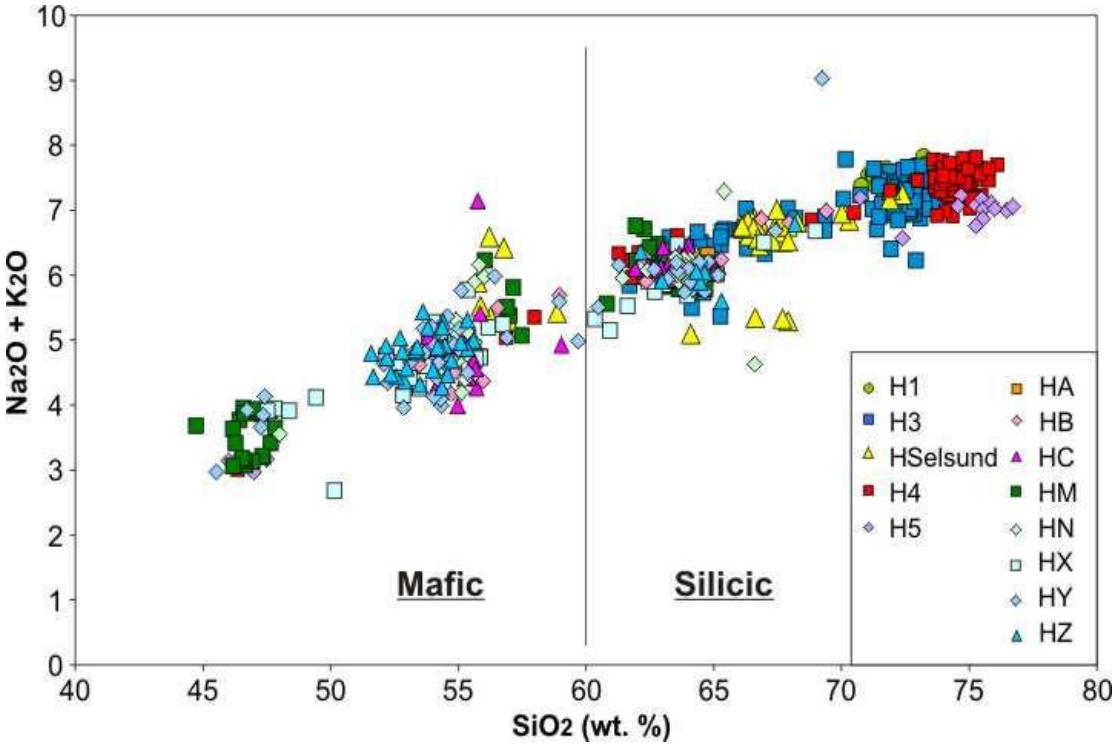

Figure 6.60: Total alkali silica plot of the thirteen Hekla tephra layers discussed in this chapter. The graph is separated into silicic and mafic components which will be discussed in the following sections. The data presented is EMPA data collected during this project.

and Al_2O_3 than the H4 tephra layer, thus allowing for these elements to be used as discriminators. Tephra layers in Group 1 are therefore best identified by plotting TiO_2 against FeO. This methodology is based on a minim of 10 electron probe analyses per sample, and a minimum of 2 samples per tephra layer depending on tephra thickness at the reference sections. The lower TiO_2 concentrations are due to the removal of the element from the melt by fractional crystallisation of titanomagnetite, while variations in Al_2O_3 can be explained by the removal of plagioclase and FeO by the removal of olivine phenocrysts from the melt.

Group 2 consists of the H1104, H3 and HSelsund tephra layers. Previous data has suggested that all three tephra layers show very similar chemical characteristics while our new data indicates minor differences in major element compositions between the tephra layers. The H3 and HSelsund tephra layers which are stratigraphically adjacent show minor variations in MgO and FeO values which are best recognised when plotted as Mg# (Mg# = $MgO_{wt.\%}$ / (($MgO_{wt.\%}$/MgO_{mol}) + ($FeO_{wt.\%}$/FeO_{mol})); Fig. 6.67). The HSelsund tephra shows a range of

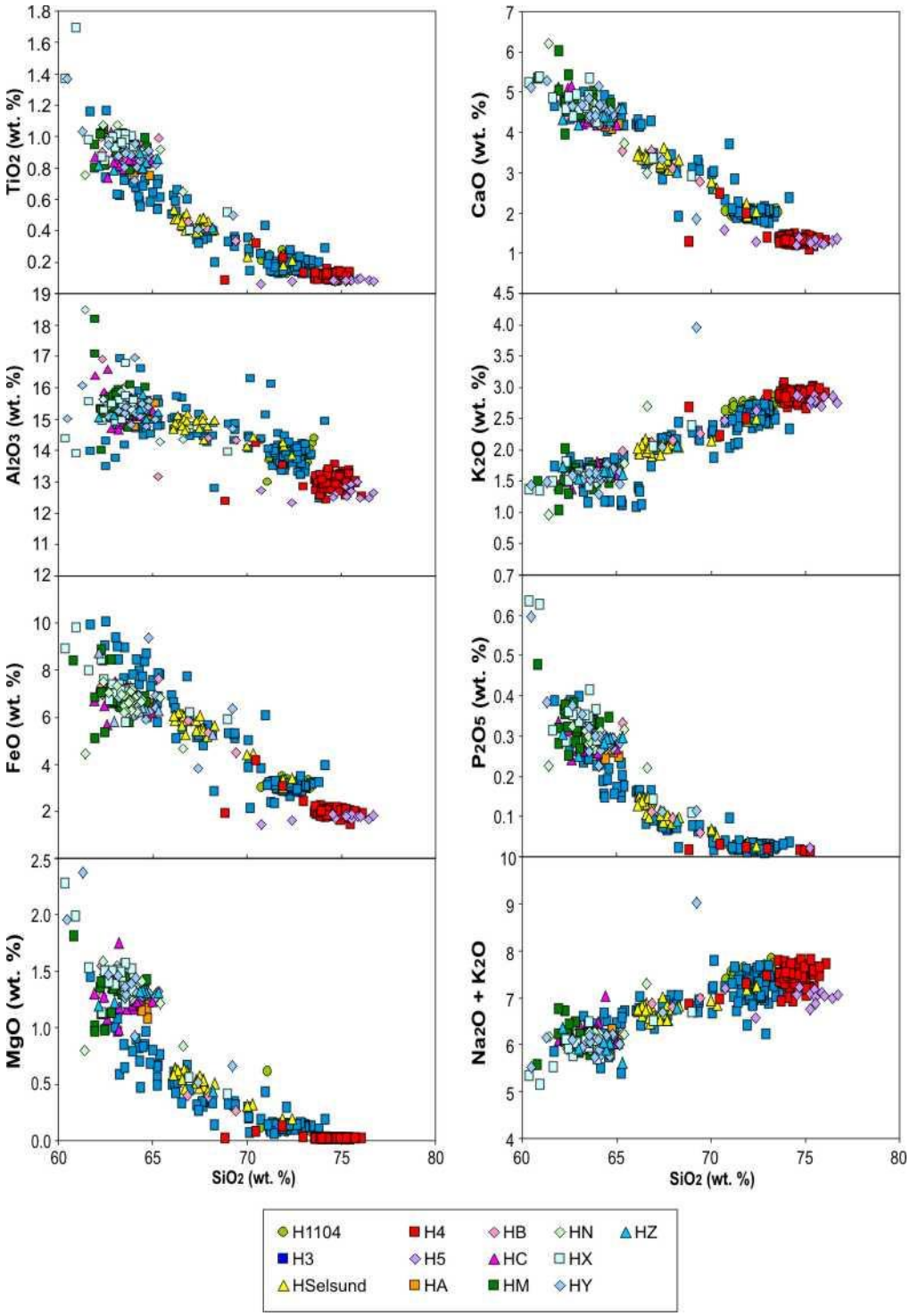

Figure 6.61: bivariate plots of the silicic components of each Hekla tephra plotting every element against SiO_2. Plotting each element will establish which elemental combinations allow for identification and discrimination of tephra provenance. Green circles = H1104, blue squares = H3, yellow triangles = HSelsund, red squares = H4, purple diamonds = H5, orange squares = HA, pink diamonds = HB, bright pink triangles = HC, dark green squares = HM, pale green diamonds = HN, pale blue squares = HX, blue diamonds = HY and bright blue triangles = HZ.

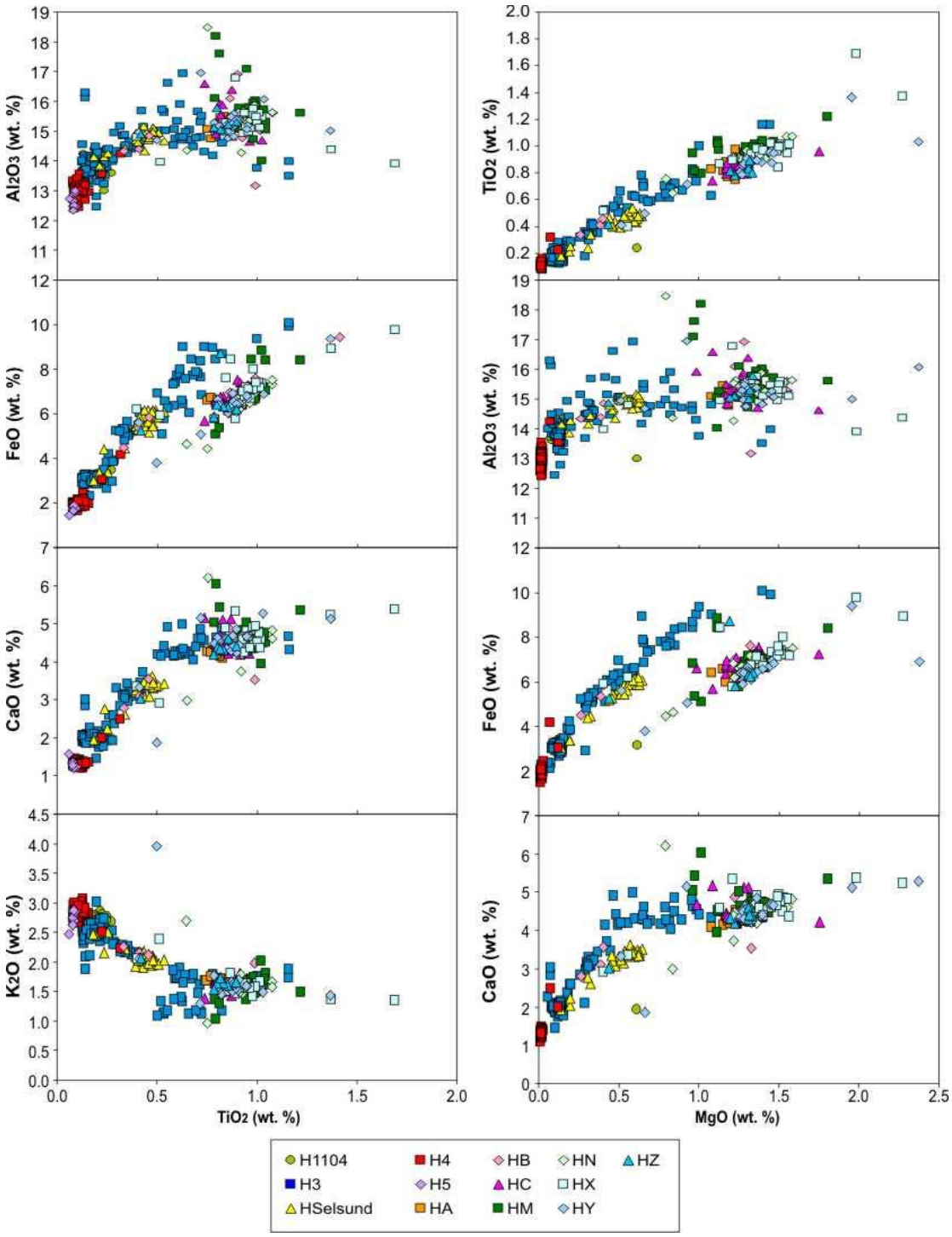

Figure 6.62: bivariate plots of the silicic components of each Hekla tephra plotting every element against TiO_2 and MgO. Plotting each element will establish which elemental combinations allow for identification and discrimination of tephra provenance. Green circles = H1104, blue squares = H3, yellow triangles = HSelsund, red squares = H4, purple diamonds = H5, orange squares = HA, pink diamonds = HB, bright pink triangles = HC, dark green squares = HM, pale green diamonds = HN, pale blue squares = HX, blue diamonds = HY and bright blue triangles = HZ.

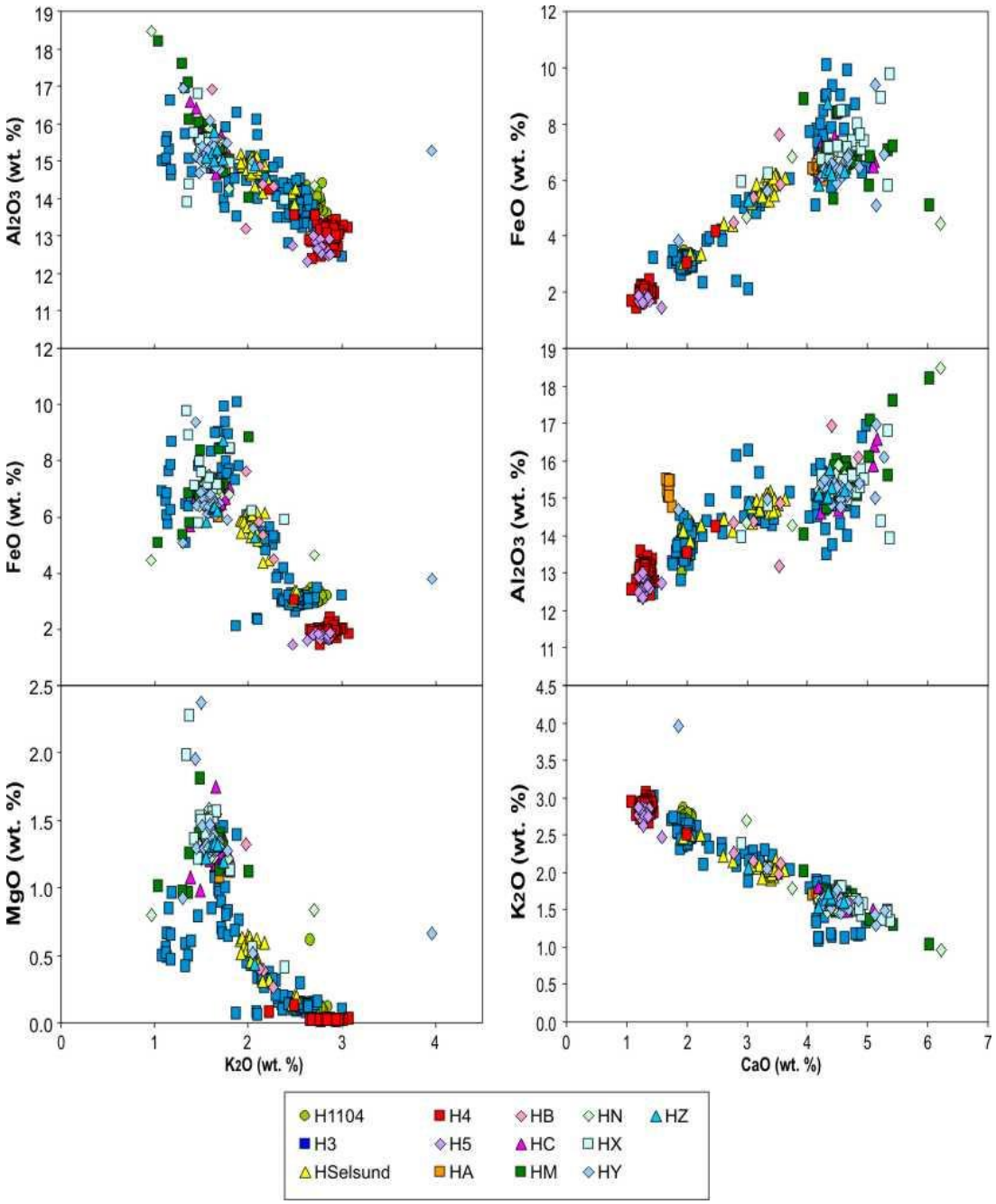

Figure 6.63: bivariate plots of the silicic components of each Hekla tephra system plotting every element against K_2O and CaO. Plotting each element will establish which elemental combinations allow for identification and discrimination of tephra provenance. Green circles = H1104, blue squares = H3, yellow triangles = HSelsund, red squares = H4, purple diamonds = H5, orange squares = HA, pink diamonds = HB, bright pink triangles = HC, dark green squares = HM, pale green diamonds = HN, pale blue squares = HX, blue diamonds = HY and bright blue triangles = HZ.

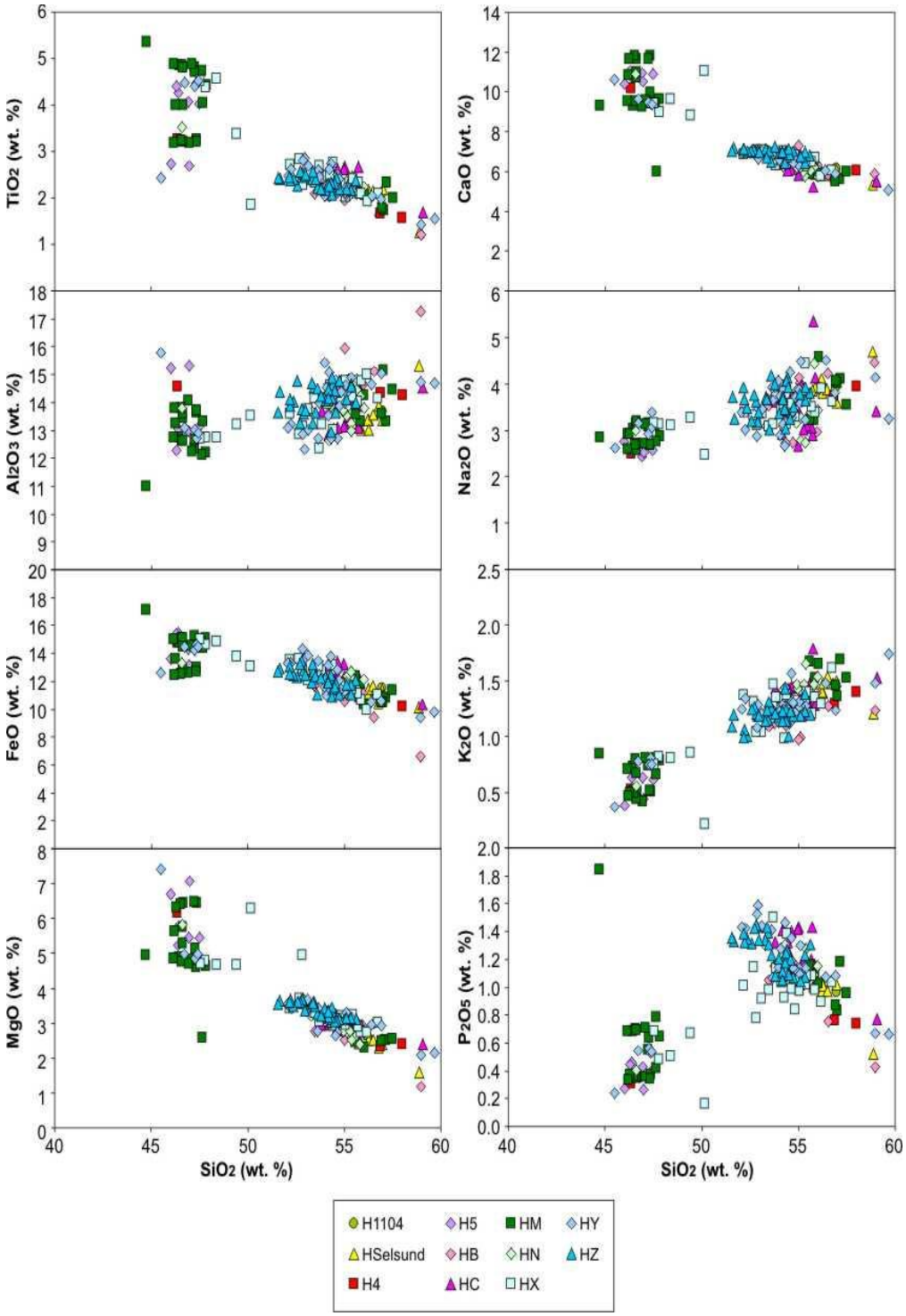

Figure 6.64: bivariate plots of the mafic components of each silicic Hekla eruption plotting every element against SiO_2. Plotting each element will establish which elemental combinations allow for identification and discrimination of tephra provenance. Green circles = H1104, yellow triangles = HSelsund, red squares = H4, purple diamonds = H5, orange squares = HA, pink diamonds = HB, bright pink triangles = HC, dark green squares = HM, pale green diamonds = HN, pale blue squares = HX, blue diamonds = HY and bright blue triangles = HZ.

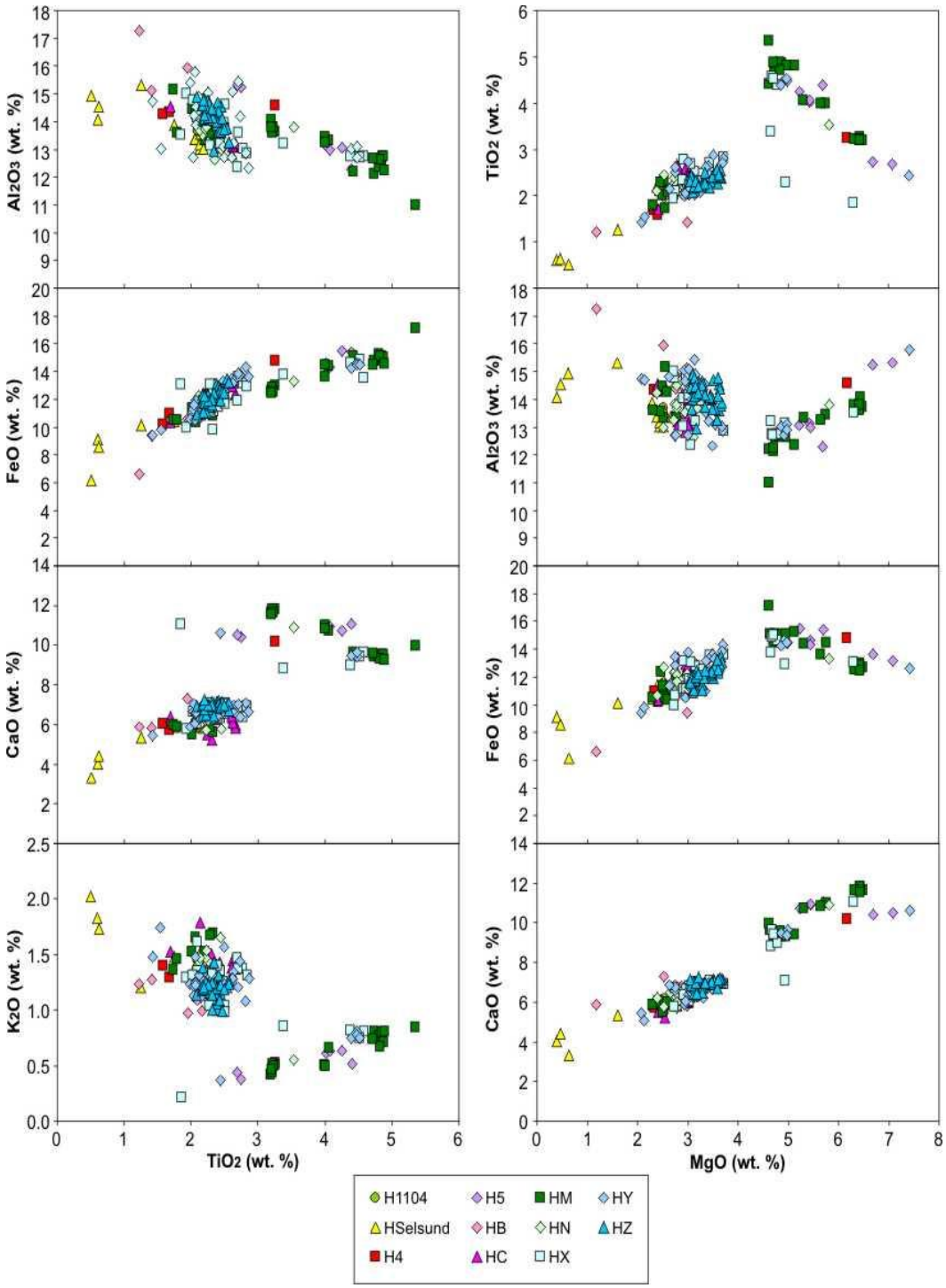

Figure 6.65: bivariate plots of the mafic components of each silicic Hekla eruption plotting every element against TiO_2 and MgO. Plotting each element will establish which elemental combinations allow for identification and discrimination of tephra provenance. Green circles = H1104, yellow triangles = HSelsund, red squares = H4, purple diamonds = H5, orange squares = HA, pink diamonds = HB, bright pink triangles = HC, dark green squares = HM, pale green diamonds = HN, pale blue squares = HX, blue diamonds = HY and bright blue triangles = HZ.

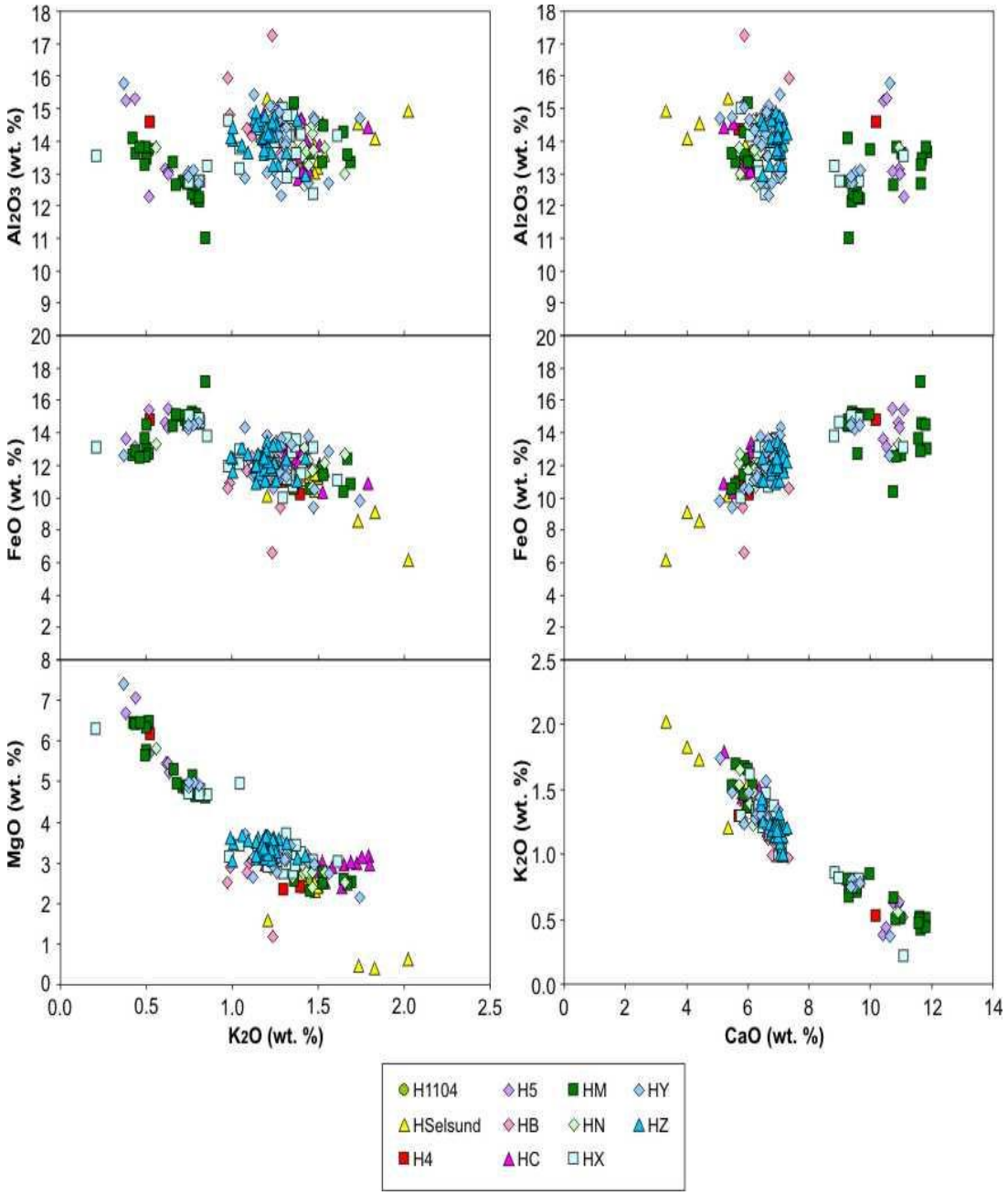

Figure 6.66: bivariate plots of the mafic components of each silicic Hekla eruption plotting every element against K_2O and CaO. Plotting each element will establish which elemental combinations allow for identification and discrimination of tephra provenance. Green circles = H1104, yellow triangles = HSelsund, red squares = H4, purple diamonds = H5, orange squares = HA, pink diamonds = HB, bright pink triangles = HC, dark green squares = HM, pale green diamonds = HN, pale blue squares = HX, blue diamonds = HY and bright blue triangles = HZ.

SiO_2 concentrations (55.74 – 73.19 wt. %) but is dominated by andesitic concentrations while the H3 and H1104 tephra layers are dominated by rhyolitic compositions. The H1104 and H3 tephra layers remain practically identical despite using the new EMPA methodology; however we have highlighted the very minor increase in K_2O concentrations in the H1104 tephra layer. Application of this element allows for differentiation of the two tephra layers although a marked data overlap remains (Fig. 6.74). The higher MgO and FeO contents of the HSelsund tephra layer can be explained by the less evolved nature of the parental magma and is confirmed by the lower SiO_2 concentrations recorded within the deposit. The minor variations in CaO and K_2O between the H3 and H1104 tephra layers are the result of differing fractional crystallisation rates of plagioclase phenocryst phases during melt storage during each eruption.

Group 3 consists of the sequence of smaller Hekla eruptions: HA, HB, HC, HM, HN, HX, HY and HZ. At present, minimal major element data has been presented or published for these tephra layers. The data collected for this project indicates that the tephra layers are geochemically identical and show consistent data overlap (Fig. 6.74). The tephra layers also show very similar physical characteristics at proximal locations, their only distinguishing features being their direction of deposition relative to the Hekla central volcano (Fig. 2.17) and their stratigraphical relationships within the sub-groups: HA-HB-HC; HM-HN; HX-HY-HZ.

Mafic Tephra Layers: Figures 6.64 – 6.66 represent all major elemental combinations plotted for the mafic components of the Hekla tephra layers discussed in this project. The figures indicate that it is not possible to discriminate between the tephra layers using major element chemistry. The work in this sub-section focuses solely on the mafic components of silicic tephra layers and does not incorporate all explosive mafic eruptions of Hekla origin. Such data would be required to develop a reliable method for identifying an unknown mafic Hekla tephra layer. Methodologies for identifying mafic Hekla tephra layers are presented in Jagan (2010).

Developing a standardised framework for identifying and discriminating between tephra layers sourced from within the same volcanic system will greatly benefit the tephrochronology community. Hekla is the largest contributor of silicic micro-tephra layers identified across the North Atlantic region. However due to the irregularities involved in deposition and preservation of micro-tephra layers, not all Hekla-derived tephra layers are

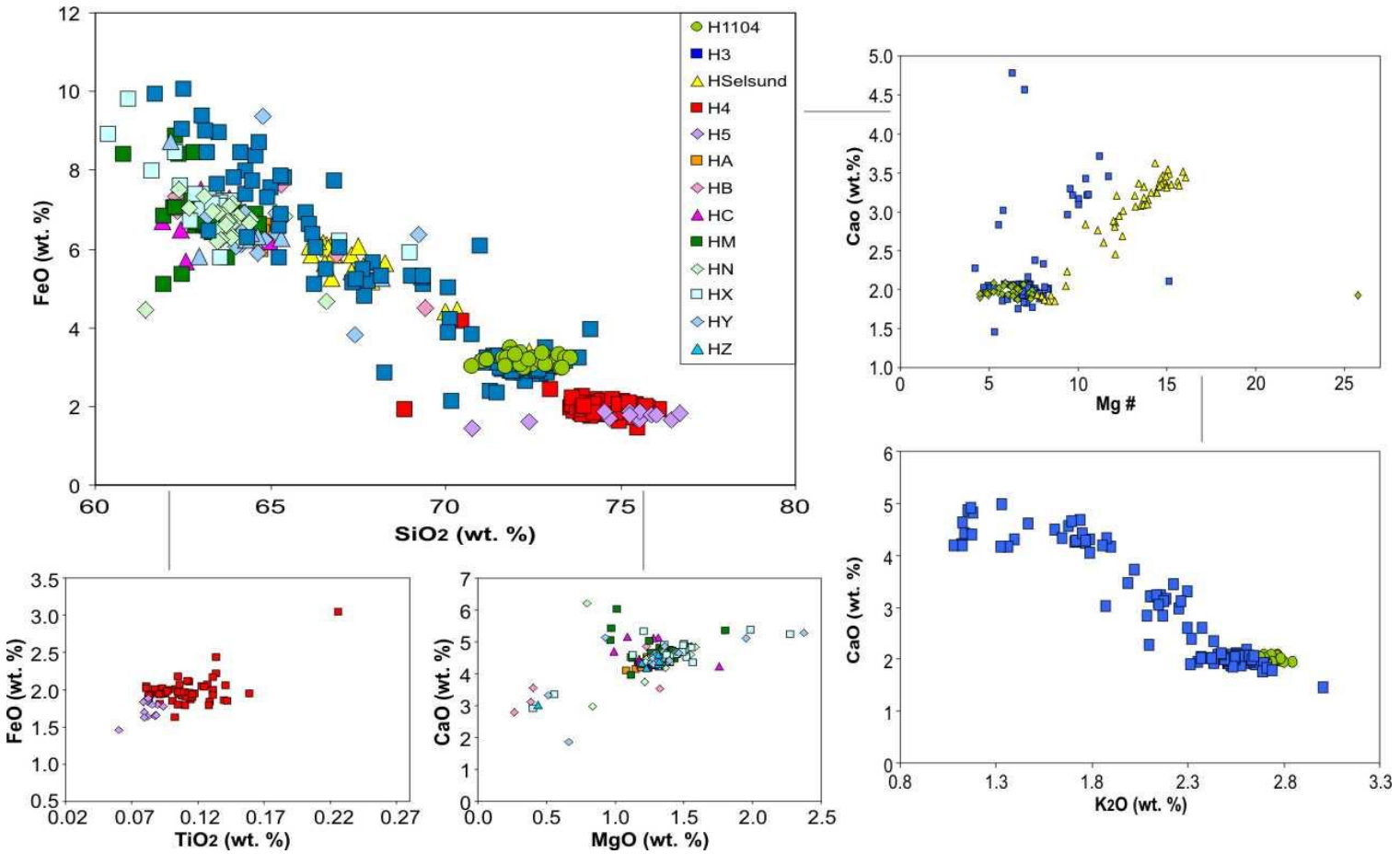

Figure 6.67: basic methodology for identifying tephra layers sourced within the Hekla volcanic system using major elements. The data shows that the Hekla tephra layers can be sub-divided into three groups 1. H4-H5, 2. H1104-H3-HSelsund, 3. HA-HB-HC-HM-HN-HX-HY-HZ. Within sub-groups 1 and 2, individual tephra layers are easily distinguished whilst group 3 remain identical. The data presented was collected via EMPA at the University of Edinburgh.

present in the far-distal sedimentary succession. It is therefore essential to ensure accurate identification and correlation when micro-tephra horizons are present. Application of the formal method of identification presented above should help to eradicate instances of tephra mis-identification and therefore improve dating techniques used in North Atlantic Quaternary studies.

It is also of great significance to have highlighted the geochemical similarity between the intermediate phases of the smaller eruptions and that of H3. This discovery has the potential to significantly alter dates and interpretations based on the identification of the H3 tephra at distal and far distal locations (see Chapter 8). Highlighting the minor variation in FeO content between the tephra layers will ensure that no such mis-identifications occur in the future.

6.4 Summary

This chapter has presented field and chemical data for thirteen tephra layers sourced from the Hekla volcanic system. The physical and chemical characteristics of each tephra layer have been described. A formal framework for establishing the identity of a silicic Hekla tephra layers has also been proposed based on the application of major element chemistry.

The work reported in this chapter has shown that silicic tephra layers sourced from the Hekla volcanic system fall into three geochemical groups when using a bivariate plot of SiO_2 and FeO. The work has also shown that within these three sub-groups, individual tephra layers can to some extent, be identified using major element chemistry. Previous workers have been unable to discriminate between tephra layers within the sub-groups, thus rendering the work presented here as great importance to the tephrochronology community. However, despite the successes of the work presented, is has confirmed that the smaller eruptions – HA, HB, HC, HM, HN, HX, HY and HZ – share such similar geochemical characteristics that it is impossible to discriminate between them using major element data alone.

Another important issue highlighted by the research conducted in this chapter is the geochemical similarity between the andesite and dacite components of the H3 tephra with those of the HA etc tephra layers. Due to the absence of any published data on the smaller eruptions, their geochemistry and to some extent even their existence has been unknown to

workers outside of Iceland. Therefore, identification of a tephra horizon within a sedimentary succession with a geochemistry similar to that of the H3 tephra layer and an age of approximately 2500 BP is presumed to represent correct identification of the H3 tephra layer. In actual fact, mis-identification of a tephra layer as H3 and not one of the smaller layers will introduce a 500 year discrepancy to any dating model based on tephrochronology. Further discussion of this work will be presented in Chapter 8.

The following chapter will present trace and rare earth element data for each of the tephra layers introduced in Chapters 5 and 6. The work will develop on the work conducted for these chapters by investigating whether individual volcanic systems show an individual geochemical fingerprint. The chapter will also investigate whether the application of minor elements can provide a means for discriminating between tephra layers that otherwise show identical major element chemistry.

Chapter 7:

The Application of Major and Minor Element Chemistry to the Fingerprinting of Icelandic Volcanic Systems

7.1 Introduction

Chapters 5 and 6 presented major element bulk and glass chemistry collected from a suite of Icelandic Holocene tephra layers. The chapters focused on developing new major element, firstly to refine tephra provenance and secondly, to evaluate the limitations of high precision major element data in the effective discrimination of tephra layers sourced within the same volcanic system – in this case Hekla, due to the far-travelled nature of its major silicic tephras.

This chapter will develop on the work presented in the previous chapters. New trace and rare earth element data is presented for the volcanic systems and eruptions previously described, collected via X-Ray fluorescence (XRF) and ion probe (IP) at the University of Edinburgh and laser ablation inductively coupled mass spectrometry (LA-ICP-MS) at the University of Aberystwyth.

The main aims of this chapter are as follows:

1. To establish a robust reference dataset for key silicic marker layers from the Torfajökull, Askja, Katla, Öræfajökull and Hekla volcanic systems (Fig. 2.2) using trace and rare earth element chemistry collected by X-Ray fluorescence (XRF) and ion probe (IP) at the University of Edinburgh and laser ablation inductively coupled mass spectrometry (LA-ICP-MS) at the University of Aberystwyth.
2. To use the data to establish whether individual volcanic systems show recognisable geochemical fingerprints.

3. To use the data to investigate whether trace and rare earth elements can be used to discriminate between tephra layers sourced within the same system, with particular reference to tephra layers that show identical major element chemistry.

The work conducted in this chapter will focus on data collected from the Torfajökull, Askja, Katla, Öræfajökull and Hekla volcanic systems and their associated tephra layers. Background information on each of the volcanic systems and tephra layers is presented in Chapter 2. Details of field sampling methods and analytical techniques are described in Chapter 4.

7.2 Geochemical Background

Trace or minor elements are conventionally defined by their concentrations in a particular sample, generally accepted as less than or equal to 0.1 wt. % or 1000 ppm. Such minor concentrations are sufficient for the stabilisation of accessory phase minerals but do not typically allow for inclusion into major rock forming minerals (Best, 2003).

Within the accepted definition, trace elements are sub-divided into sub-groups based on their geochemical behaviour. Each definition is based on different characteristics and there is therefore some overlap between groupings:

- Elements with the atomic numbers 57 to 71 are the *Rare Earth Elements* (REE). Elements with the atomic numbers 76 to 79 are the *Platinum Group Elements* (PGE). Elements with the atomic numbers 21 to 39 including Mn and Fe are the *Transition Metals* (Fig. 7.1). This grouping is used as elements within each group show similar geochemical behaviour and characteristics (Rollinson, 1993).
- Trace elements are also defined by their field strength, a value based on size ratio and overall charge or ionic potential (i.e. the electrostatic charge per unit surface area of the catïon). Small highly charged catïons are referred to as *High Field Strength Elements* (HFSE) and have an ionic potential of more than 2.0. Large poorly charged catïons are known as *Low Field Strength Elements* (LFSE) and have an ionic potential of less than 2.0. HFSE elements include La, Eu, Y, Sc, Lu, Th, U, Ce, Pb, Zr, Hf, Ti, Nb and Ta. LFSE elements include Cs, Rb, K, Ba, Pb, Sr, Eu.

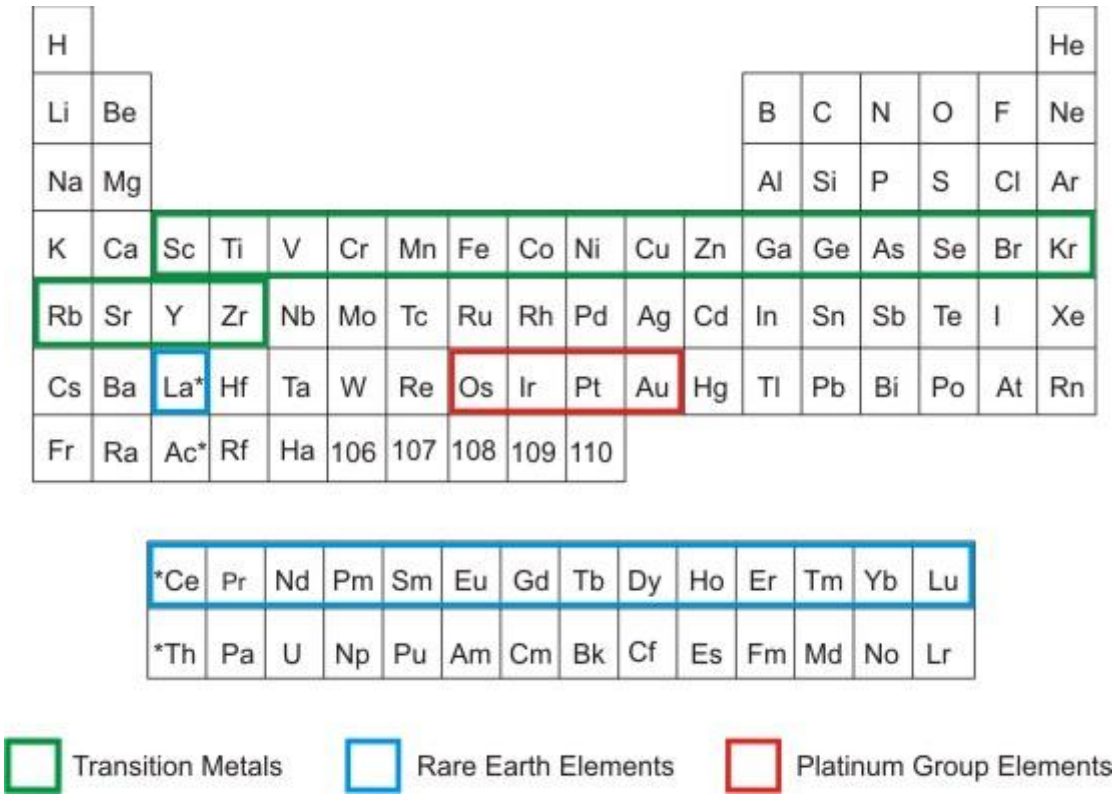

Figure 7.1: Periodic table with the main trace element groups annotated: transition metals (green), rare earth elements (blue) and platinum group elements (red).

- HFSE are typically immobile within crystals while LFSE elements are show much higher mobility and can be influenced by post-emplacement alteration (Rollinson, 1993).

Trace elements are also classed as compatible and incompatible elements. Compatible elements are preferentially incorporated into the crystalline structure of minerals during fractional crystallisation and typically remain in crystal form during partial melting. Incompatible elements remain in the melt during fractional crystallisation until accessory phases begin to crystallise and will preferentially return to the melt during early phases of partial melting. Compatible elements include Sc and Ni while incompatible elements include Zr and Y. The compatibility of an element in a mineral is defined by its partition coefficient (D) and is calculated using the Nernst equation:

$$K_d = \frac{\text{(Concentration in mineral)}}{\text{(Concentration in melt)}}$$

Where Kd is the Nernst distribution coefficient, and C is the concentration of a particular trace element in a specified mineral and the remaining melt. The calculated K_d value indicates the compatibility of an element. A K_d values of 1 represents equal distribution between melt and crystal, a value higher than 1 represents a compatible element while a value smaller than 1 represents an incompatible element. Pressure, temperature and magma evolution will influence trace element behaviour – increasing pressure and silica content encourage elemental compatibility as do decreasing temperatures (Best, 2003; Rollinson, 1993).

Tephrochronology studies have typically focused on the application of major element chemistry to the identification of tephra layers (e.g. Dugmore *et al*. 1995; Davies *et al*. 2005). The EMPA technique involved in the analysis of major element chemistry is relatively cheap, easily available and does not irreversibly damage samples. Analyses of trace elements has thus far been limited to its application in tephrochronology studies (e.g. Basile *et al*. 2001; Begét and Keskinen, 2003 and Pearce *et al*. 2004b), in particular to studies in the North Atlantic (e.g. Lacasse *et al*. 1995; Wallrabe-Adams and Lackschewitz, 2003) as the techniques are expensive, less readily available and irreversibly damage the samples analysed. However, continued development of the LA-ICP-MS technique and recent improvements in smaller beam size analyses, are increasing the potential for applying trace element data to tephrochronology studies (Pearce *et al*. 1996, 1999, 2004). Such developments are of great importance as trace elements show a much higher sensitivity to minor changes in melt generation than the major elements. Minor changes can be used to highlight small-scale variations between volcanic systems and tephra layers and potentially result in a more reliable method for identifying distal tephra layers.

7.3 Results

This section presents the trace and rare earth element data collected for the tephra layers noted in Table 4.1. Results include tabulated XRF, IP and LA-ICP-MS data and brief descriptions of the geochemical characteristics of each tephra layer. Note that geochemical data collected via LA-ICP-MS is presented as averages with 2σ values. Full data sets are

available in the Appendix. Where more than one tephra layer is sourced within a volcanic system, data for each tephra layer is tabulated separately under the initial volcano sub-heading (e.g. the Torfajökull sub-heading will discuss both the silicic component of the Landnám and the Grákolla tephra layers).

7.3.1 Torfajökull – Landnám and Grákolla tephra layers

In total, eleven samples were analysed for the Torfajökull volcanic system collected from two sampling locations (Fig. 4.1). The new trace and rare earth element data collected via XRF, IP and LA-ICP-MS for the Torfajökull tephra layers are presented in Tables 7.1 – 7.6. The Landnám and Grákolla tephra layers show two main geochemical sub-groups at the sampling location: a high silica and low silica phase. The characteristics of the tephra layers are discussed below.

Multi element plots of the Torfajökull data (Figs 7.2 and 7.3) indicate an overall negative trend from the incompatible to compatible elements. The incompatible elements (Ba – Ce) data represents a relatively flat trend with the exception of Ba which shows a negative anomaly. Pronounced negative anomalies are recorded for Sr, P and Ti. A small positive anomaly is recorded for Zr. The data shows tight clustering and therefore minimal deviation from the volcanic signature.

A rare earth element plot of the Torfajökull data (Fig 7.4) indicates a steeply dipping negative trend from the light rare earth elements (LREE) to the heavy rare earth elements (HREE) suggesting depletion of HREE relative to the LREE. The data presents a pronounced negative Eu anomaly and a small positive Ho anomaly. REE ratios of Gd/Yb for the tephra layers range from 1.16 – 4.70 but are typically less than 2.00, while La/Sm ratios range from 4.13 – 9.34. Data collected by LA-ICP-MS and IP techniques show overlap when plotted graphically. However, some variation is noted within the overlap, suggesting that data collected by the two techniques are not directly comparable.

Table 7.1: Bulk chemistry for the silicic component of the Landnám tephra layer collected via XRF. Samples for the Landnám tephra were collected near Ljósárfjöll and Hrafntinnuhraun c. 15 km north-west of the summit of Torfajökull.

Elements	09-08 Lndm	09-11w Lndm	09-14 Lndm	09-15 Lndm
Zr	641.20	638.80	663.00	729.60
Nb	122.60	122.00	126.30	134.30
Y	69.70	69.40	71.50	77.30
Sr	66.60	66.80	66.10	64.40
Rb	112.50	111.40	112.20	116.60
Th	17.50	17.20	17.60	17.60
Zn	92.10	92.70	97.90	94.50
Cu	6.80	6.30	13.40	6.20
Ni	2.80	3.60	3.30	3.30
Cr	5.10	6.00	4.90	5.20
Ba	402.20	402.90	406.40	434.70
La	101.30	100.20	101.90	108.40
Ce	190.50	188.60	192.30	204.10
Nd	75.40	74.00	77.40	83.20
Sc	0.40	0.60	0.70	0.90
U	5.50	5.60	5.50	5.80
Pb	9.10	9.20	9.60	9.40

Table 7.2: Glass chemistry for the silicic component of the Landnám tephra layer collected via IP. Samples for the Landnám tephra were collected near Ljósárfjöll and Hrafntinnuhraun c. 15 km north-west of the summit of Torfajökull.

Element	09-08 Lndm	09-11w Lndm	09-11b Lndm	09-14 Lndm	09-15 Lndm
Zr	581.67	573.94	147.87	575.77	568.08
Nb	104.79	104.67	17.04	101.68	101.02
Y	47.64	46.53	21.11	47.79	47.34
Sr	43.42	42.50	320.15	42.71	41.90
Rb	80.16	78.39	6.07	75.79	75.67
Ba	358.17	346.43	93.11	352.70	342.79
La	75.74	74.63	14.79	73.62	72.67
Ce	142.65	142.19	33.15	141.18	138.14
Pr	15.16	15.26	4.79	15.18	14.55
Nd	59.78	57.46	22.25	58.33	61.06
Sm	10.39	11.09	4.95	11.63	11.37
Eu	1.47	1.27	1.42	1.82	1.48
Gd	12.22	8.78	3.90	13.83	13.33
Ho	1.99	2.08	0.73	2.17	2.08
Yb	4.42	5.90	2.85	5.70	2.84
Sc	4.86	4.41	41.09	4.49	4.62

Table 7.3: Glass chemistry for the silicic component of the Landnám tephra layer collected via LA-ICP-MS. Samples for the Landnám tephra were collected near Ljósárfjöll and Hrafntinnuhraun c. 15 km north-west of the summit of Torfajökull. Ten points were analysed for each sample and the data presented is the average of these analyses with two standard deviations (numbers in brackets). The complete data set is available in the Appendix.

Element	09-08 Lndm	09-10 Lndm	09-11w Lndm	09-11b Lndm	09-14 Lndm	09-15 Lndm
Zr	690.24 *(136.81)*	664.84 *(94.32)*	635.76 *(165.56)*	105.04 *(15.01)*	832.29 *(357.86)*	658.43 *(77.96)*
Nb	127.33 *(20.04)*	125.33 *(12.61)*	126.65 *(12.80)*	15.94 *(1.50)*	142.15 *(37.42)*	126.83 *(8.81)*
Y	72.93 *(14.42)*	70.45 *(11.59)*	68.05 *(23.91)*	18.69 *(3.10)*	87.57 *(30.94)*	80.75 *(77.34)*
Sr	52.94 *(9.80)*	49.48 *(6.99)*	50.18 *(8.56)*	290.38 *(17.50)*	52.36 *(12.01)*	54.87 *(19.51)*
Rb	126.20 *(22.70)*	122.54 *(8.51)*	124.46 *(17.00)*	7.45 *(1.84)*	124.60 *(10.28)*	124.61 *(10.31)*
Th	21.30 *(6.43)*	19.67 *(2.23)*	19.06 *(4.05)*	0.99 *(0.37)*	22.10 *(5.26)*	20.19 *(3.54)*
Ba	423.85 *(61.23)*	397.14 *(49.75)*	414.48 *(55.95)*	80.22 *(7.04)*	430.68 *(89.96)*	418.39 *(35.69)*
La	101.37 *(17.98)*	98.00 *(16.68)*	93.74 *(20.39)*	11.38 *(1.86)*	110.59 *(25.32)*	117.79 *(109.22)*
Ce	179.84 *(28.14)*	173.26 *(29.13)*	175.25 *(20.57)*	24.67 *(1.79)*	198.47 *(73.18)*	223.68 *(252.89)*
Pr	19.84 *(3.62)*	19.14 *(3.75)*	18.43 *(3.16)*	3.52 *(0.58)*	21.06 *(4.58)*	25.58 *(32.26)*
Nd	74.48 *(13.51)*	71.03 *(16.31)*	69.55 *(15.70)*	16.67 *(2.23)*	82.48 *(25.86)*	96.67 *(135.68)*
Sm	14.58 *(2.40)*	13.85 *(4.06)*	13.22 *(3.25)*	4.51 *(1.12)*	16.46 *(5.67)*	18.61 *(27.30)*
Eu	1.91 *(0.78)*	1.53 *(0.42)*	1.66 *(0.78)*	1.11 *(0.40)*	2.27 *(2.10)*	2.06 *(2.31)*
Gd	13.48 *(2.92)*	12.78 *(1.99)*	12.60 *(6.29)*	4.42 *(0.79)*	16.07 *(6.80)*	17.07 *(23.82)*
Tb	2.96 *(0.65)*	1.96 *(0.37)*	1.96 *(0.56)*	0.61 *(0.16)*	2.42 *(0.94)*	2.68 *(3.15)*
Dy	13.98 *(3.68)*	12.44 *(3.38)*	12.93 *(4.32)*	3.85 *(0.44)*	15.93 *(6.19)*	15.73 *(16.99)*
Ho	2.55 *(0.58)*	2.44 *(0.45)*	2.59 *(0.82)*	0.80 *(0.24)*	4.01 *(4.91)*	3.09 *(2.65)*
Er	8.97 *(5.36)*	7.01 *(1.38)*	7.52 *(3.31)*	2.05 *(0.41)*	9.02 *(4.10)*	8.88 *(7.76)*
Tm	1.16 *(0.28)*	1.08 *(0.37)*	1.14 *(0.44)*	0.22 *(0.25)*	1.41 *(0.80)*	1.23 *(0.94)*
Yb	8.06 *(1.83)*	7.11 *(1.38)*	7.28 *(2.04)*	1.97 *(0.57)*	9.09 *(4.73)*	8.04 *(4.64)*
Lu	1.11 *(0.22)*	1.08 *(0.20)*	1.09 *(0.42)*	0.27 *(0.18)*	1.37 *(0.62)*	1.14 *(0.52)*
Hf	20.45 *(4.22)*	18.95 *(2.86)*	18.71 *(6.04)*	3.22 *(0.96)*	23.09 *(11.91)*	19.96 *(8.55)*
Ta	9.24 *(1.75)*	8.86 *(0.98)*	8.70 *(1.39)*	1.06 *(0.22)*	23.09 *(3.76)*	9.25 *(1.35)*
Sc	0.13 *(0.08)*	0.16 *(0.05)*	0.14 *(0.07)*	0.72 *(0.07)*	0.18 *(0.09)*	0.15 *(0.07)*
Cs	1.17 *(0.44)*	1.28 *(0.43)*	1.29 *(0.70)*	0.08 *(0.44)*	1.55 *(0.64)*	1.22 *(0.54)*
U	5.63 *(3.30)*	4.88 *(0.63)*	5.38 *(0.78)*	0.32 *(0.08)*	5.27 *(1.12)*	5.63 *(1.23)*
Pb	15.69 *(4.81)*	11.26 *(4.27)*	15.98 *(12.85)*	1.26 *(0.36)*	13.82 *(6.54)*	12.35 *(5.37)*

Table 7.4: Bulk chemistry for the Grákolla tephra layer collected via XRF. Samples for the Grákolla tephra were collected on Grákolla Hill near Torvafell and Frostastadavatn north of the Torfajökull volcanic complex.

Elements	09-16b Gka	08-97w Gka
Zr	297.9	646.0
Nb	48.2	48.2
Y	42.8	69.2
Sr	136.6	90.2
Rb	40.2	103.5
Th	6.8	16.0
Zn	101.6	103.0
Cu	96.1	16.1
Ni	52.8	4.9
V	222.5	25.0
Ba	196.2	416.8
La	38.6	94.6
Ce	80.1	180.3
Nd	34.2	73.4
Sc	34.5	4.3
U	1.5	4.8
Pb	3.6	8.4

Table 7.5: Glass chemistry for the Grákolla tephra layer collected via IP. Samples for the Grákolla tephra were collected on Grákolla Hill near Torvafell and Frostastadavatn north of the Torfajökull volcanic complex. Data presented represent average values and two standard deviations for two analyses.

Element	09-16w Gka	09-16b Gka	08-97w Gka	08-97b Gka	08-101w Gka
Zr	530.07 *(1.72)*	186.60 *(230.43)*	574.78 *(109.27)*	109.90 *(0.11)*	525.44 *(3.03)*
Nb	98.69 *(0.87)*	19.91 *(36.21)*	114.27 *(37.55)*	8.01 *(0.00)*	97.85 *(5.03)*
Y	46.68 *(1.21)*	28.98 *(14.63)*	46.40 *(1.69)*	24.90 *(0.33)*	46.58 *(0.06)*
Sr	46.50 *(1.32)*	255.90 *(373.48)*	44.69 *(2.12)*	125.43 *(3.32)*	42.69 *(0.04)*
Rb	73.17 *(0.13)*	5.94 *(9.52)*	84.02 *(27.02)*	2.08 *(0.94)*	72.84 *(3.36)*
Ba	359.33 *(4.61)*	94.24 *(172.86)*	363.63 *(3.31)*	34.87 *(1.78)*	354.31 *(4.98)*
La	74.10 *(0.22)*	17.00 *(28.33)*	75.20 *(4.10)*	7.03 *(0.50)*	72.72 *(0.16)*
Ce	138.29 *(2.07)*	39.05 *(62.97)*	139.77 *(6.16)*	18.08 *(1.06)*	136.91 *(1.59)*
Pr	15.13 *(0.37)*	5.55 *(8.68)*	15.24 *(0.38)*	2.56 *(0.55)*	15.05 *(0.25)*
Nd	60.26 *(0.02)*	27.39 *(41.11)*	60.79 *(4.73)*	15.12 *(2.68)*	61.80 *(0.35)*
Sm	11.35 *(0.71)*	6.68 *(10.01)*	10.09 *(0.99)*	3.98 *(0.45)*	10.00 *(1.85)*
Eu	1.44 *(0.57)*	2.00 *(2.42)*	1.14 *(0.81)*	1.10 *(0.49)*	1.40 *(0.28)*
Gd	13.52 *(3.40)*	6.59 *(7.80)*	10.54 *(6.47)*	3.81 *(1.57)*	12.62 *(1.62)*
Ho	2.03 *(0.08)*	1.28 *(0.97)*	2.13 *(0.31)*	1.07 *(0.26)*	2.01 *(0.05)*
Yb	4.30 *(0.43)*	2.92 *(0.30)*	5.09 *(1.56)*	3.23 *(0.75)*	5.27 *(0.80)*
Sc	4.56 *(0.92)*	43.52 *(9.52)*	5.34 *(1.07)*	50.52 *(0.22)*	4.75 *(0.54)*

Table 7.6: Glass chemistry for the Grákolla tephra layer collected via LA-ICP-MS. Samples for the Grákolla tephra were collected on Grákolla Hill near Torvafell and Frostastadavatn north of the Torfajökull volcanic complex. Ten points were analysed for each sample and the data presented is the average of these analyses with two standard deviations (numbers in brackets). The complete data set is available in the Appendix.

Element	09-16w Gka	09-16b Gka	08-97w Gka	08-97b Gka	08-101 Gka
Zr	481.92 *(250.33)*	0.85 *(0.80)*	474.45 *(142.78)*	0.76 *(0.69)*	476.18 *(155.62)*
Nb	105.64 *(32.41)*	0.21 *(0.30)*	103.73 *(12.43)*	0.20 *(0.30)*	107.74 *(18.03)*
Y	59.93 *(17.39)*	0.34 *(0.16)*	53.99 *(18.37)*	0.31 *(0.09)*	55.40 *(20.12)*
Sr	54.93 *(32.98)*	2.55 *(2.82)*	48.61 *(19.86)*	2.51 *(2.82)*	48.95 *(22.29)*
Rb	108.70 *(36.71)*	0.10 *(0.13)*	111.83 *(16.13)*	0.10 *(0.13)*	123.36 *(47.85)*
Th	13.71 *(7.27)*	0.03 *(0.04)*	14.20 *(4.36)*	0.03 *(0.04)*	14.59 *(5.10)*
Ba	406.58 *(163.00)*	1.13 *(1.61)*	343.74 *(90.69)*	1.14 *(1.75)*	375.87 *(67.49)*
La	76.76 *(26.41)*	0.23 *(0.32)*	74.87 *(18.43)*	0.21 *(0.31)*	76.52 *(18.92)*
Ce	143.04 *(43.50)*	0.54 *(0.73)*	140.76 *(32.11)*	0.53 *(0.73)*	149.51 *(35.07)*
Pr	15.78 *(3.67)*	0.09 *(0.11)*	15.49 *(3.19)*	0.08 *(0.11)*	15.91 *(3.79)*
Nd	57.84 *(16.68)*	0.05 *(0.06)*	56.27 *(16.44)*	0.05 *(0.05)*	60.32 *(20.24)*
Sm	11.57 *(2.85)*	0.01 *(0.01)*	10.84 *(3.06)*	0.01 *(0.01)*	10.65 *(4.98)*
Eu	1.23 *(1.31)*	0.01 *(0.01)*	1.34 *(0.48)*	0.01 *(0.01)*	1.30 *(0.45)*
Gd	11.41 *(4.52)*	0.02 *(0.02)*	10.18 *(3.10)*	0.02 *(0.02)*	10.47 *(1.88)*
Tb	1.67 *(0.72)*	0.01 *(0.01)*	1.47 *(0.47)*	0.01 *(0.01)*	1.65 *(0.35)*
Dy	11.70 *(2.12)*	0.02 *(0.01)*	9.80 *(3.30)*	0.02 *(0.01)*	11.00 *(2.84)*
Ho	2.25 *(0.76)*	0.01 *(0.01)*	1.89 *(0.65)*	0.01 *(0.00)*	2.12 *(0.38)*
Er	6.23 *(1.65)*	0.01 *(0.00)*	5.89 *(2.49)*	0.01 *(0.00)*	6.01 *(1.10)*
Tm	1.05 *(0.42)*	0.00 *(0.00)*	0.91 *(0.37)*	0.01 *(0.00)*	0.94 *(0.20)*
Yb	5.75 *(2.51)*	0.02 *(0.02)*	5.70 *(2.31)*	0.02 *(0.01)*	5.97 *(1.32)*
Lu	0.89 *(0.38)*	0.01 *(0.00)*	0.81 *(0.36)*	0.01 *(0.00)*	0.80 *(0.14)*
Hf	12.53 *(6.37)*	0.02 *(0.02)*	13.53 *(4.34)*	0.02 *(0.02)*	13.57 *(2.53)*
Ta	6.58 *(3.04)*	0.02 *(0.03)*	6.85 *(1.38)*	0.02 *(0.03)*	7.06 *(1.38)*
Sc	0.26 *(0.24)*	0.28 *(0.09)*	0.26 *(0.22)*	0.27 *(0.15)*	0.31 *(0.36)*
Cs	1.22 *(0.74)*	0.01 *(0.00)*	1.27 *(0.45)*	0.00 *(0.00)*	1.07 *(1.47)*
U	3.95 *(1.54)*	0.01 *(0.01)*	4.06 *(0.78)*	0.01 *(0.01)*	4.44 *(1.32)*
Pb	10.54 *(3.06)*	0.01 *(0.01)*	10.79 *(3.55)*	0.01 *(0.01)*	10.66 *(3.04)*

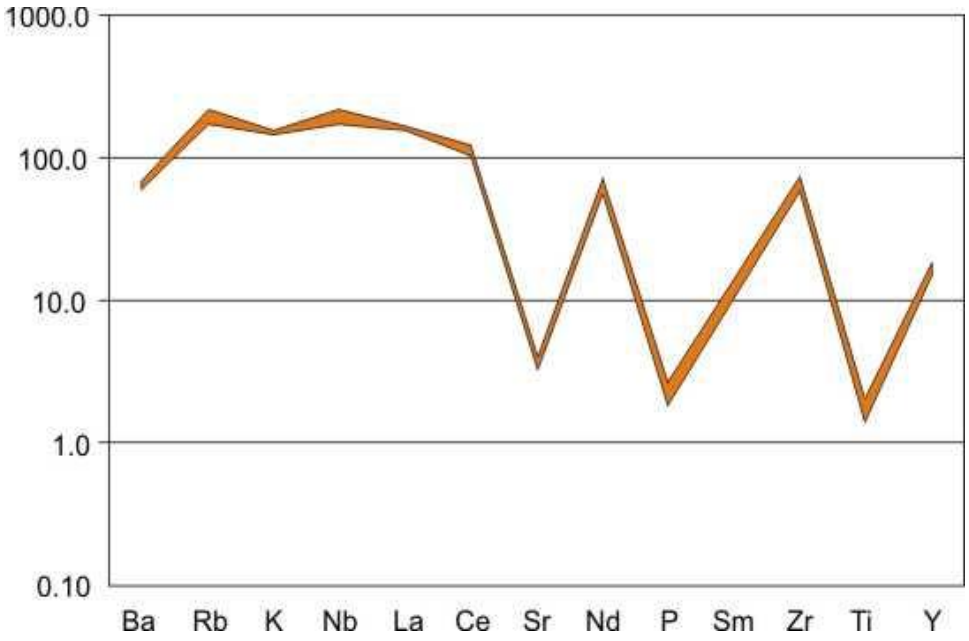

Figure 7.2: Multi element plot of the Torfajökull volcanic system using certain major, trace and rare earth element data collected via XRF. Data is normalised to bulk silicate earth (BSE) using the values in McDonough and Sun (1995). Negative data anomalies are recorded at Sr, P and Ti, while a positive anomaly is recorded at Zr.

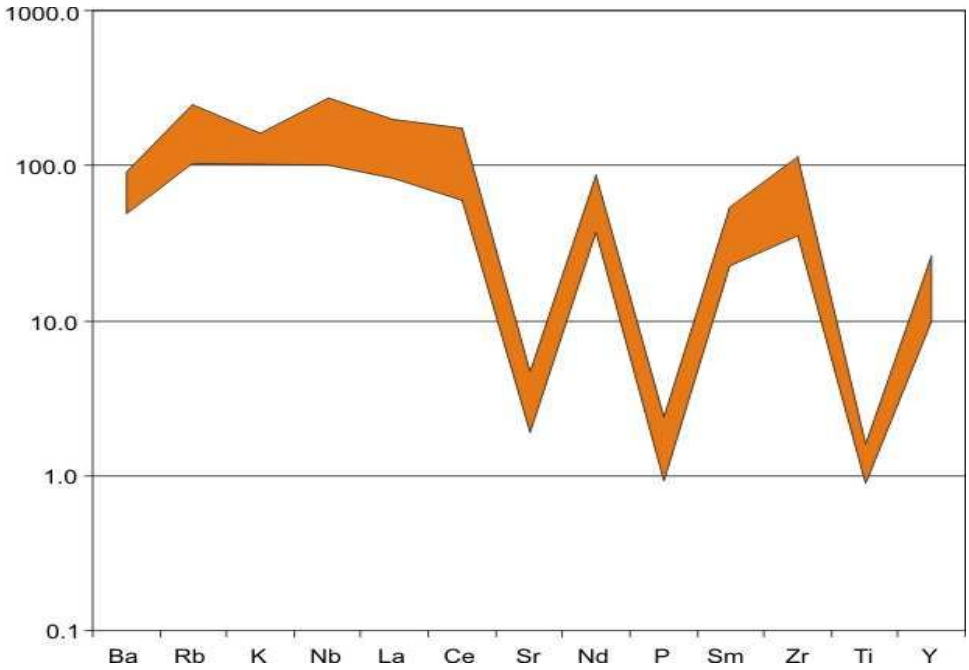

Figure 7.3: Multi element plot of the Torfajökull volcanic system using major, trace and rare earth data collected via electron microprobe and laser ablation ICP-MS. Data is normalised to bulk silicate earth (BSE) using the values in McDonough and Sun (1995). Negative data anomalies are recorded at Sr, P and Ti.

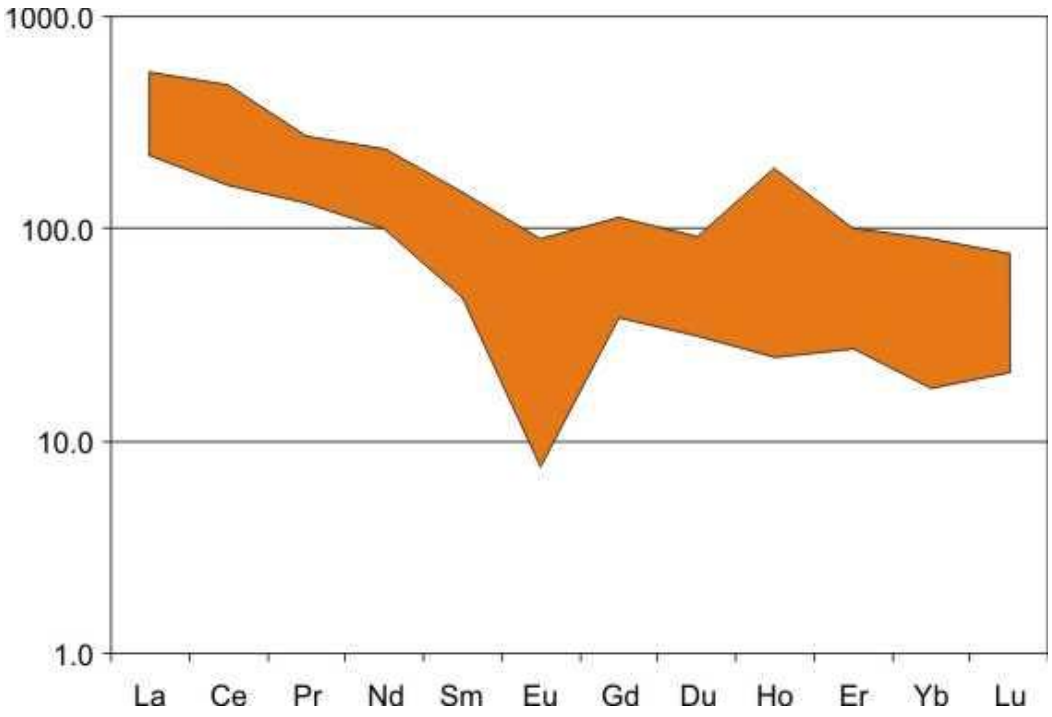

Figure 7.4: Rare earth element plot of the Torfajökull volcanic system using rare earth data collected via laser ablation ICP-MS and IP. Data is normalised to chondrite using the values in McDonough and Sun (1995). A negative data anomaly is recorded at Eu while a positive anomaly is recorded at Ho.

7.3.2 Askja – A1875 tephra layer

In total, eight samples were analysed for the Askja volcanic system layer collected from three sampling locations. The new trace and rare earth element data collected via XRF, IP and LA-ICP-MS for the tephra layer is presented in Tables 7.7 – 7.9. The A1875 tephra layer is separated into three main sub-groups (B, C_{1-2} and D_{1-5}) at the sampling locations.

Multi element plots of the Askja data (Figs 7.5 and 7.6) indicate a shallowly dipping overall negative trend from the incompatible to compatible elements. Small negative anomalies are recorded for Ba and Nb while larger negative anomalies are recorded for Sr, P and Ti. A small positive anomaly is recorded for Zr. The data shows tight clustering and therefore minimal deviation from the volcanic signature.

Rare earth element plots of the Askja data (Fig 7.7) indicates a shallowly dipping negative trend from the light rare earth elements (LREE) to the heave rare earth elements (HREE) suggesting some depletion of HREE relative to the LREE. The data presents a pronounced negative Eu anomaly and a small positive Sm anomaly. REE ratios of Gd/Yb for the tephra layers range from 1.21 – 2.00, while La/Sm ratios range from 2.30 – 16.78. Data collected by LA-ICP-MS and IP techniques show overlap when plotted graphically. However, some variation is noted within the overlap, suggesting that data collected by the two techniques are not directly comparable.

Table 7.7: Bulk chemistry for the A1875 tephra layer collected via XRF. Samples for the A1875 tephra layer were collected to the north-north east of the Öskjuvatn caldera lake, next to the Víti geothermal crater.

Elements	07-61 D_1	07-61 D_2	07-61 D_3	07-61 D_4	07-61 D_5
Zr	373.00	367.30	368.00	343.30	346.60
Nb	35.90	35.40	35.40	34.10	33.70
Y	64.60	63.80	64.00	63.70	61.40
Sr	112.30	114.60	114.70	130.80	118.20
Rb	55.10	53.90	53.40	48.60	49.70
Th	6.80	6.80	6.90	6.20	6.10
Zn	72.20	72.60	73.20	81.70	78.40
Cu	13.60	16.40	13.40	21.20	26.80
Ni	6.00	6.60	6.20	7.70	10.90
V	23.20	23.20	28.60	53.30	62.30
Ba	342.00	339.70	336.50	311.80	319.90
La	45.20	41.90	43.60	40.20	40.40
Ce	93.10	88.20	93.50	86.20	84.40
Nd	44.80	44.40	43.20	42.30	42.00
Sc	14.30	14.50	15.90	18.70	20.10
U	2.60	2.30	2.40	1.90	1.70
Pb	3.60	3.30	3.50	3.00	2.80

Elements	07-54 C_1	07-55 C_1	07-57 C_2	07-59 C_2
Zr	383.20	380.4	381.70	376.60
Nb	35.70	35.60	35.50	35.20
Y	65.10	64.80	64.80	64.30
Sr	105.60	105.10	105.00	107.40
Rb	57.10	56.80	56.80	56.20
Th	7.30	7.30	7.40	7.00
Zn	67.20	66.60	67.00	67.90
Cu	11.00	10.20	8.90	9.40
Ni	2.00	2.10	2.30	2.00
V	25.80	22.30	22.50	24.30
Ba	341.80	343.60	341.90	338.50
La	42.50	40.30	41.90	41.10
Ce	90.70	91.30	89.50	91.40
Nd	44.50	43.50	42.70	43.80
Sc	13.50	13.80	12.60	
U	2.00	2.10	2.10	1.90
Pb	4.40	4.20	4.00	4.00

Table 7.8: Glass chemistry for the A1875 tephra layer collected via IP. Samples for the A1875 tephra layer were collected to the north-north east of the Öskjuvatn caldera lake, next to the Víti geothermal crater.

Element	07-54 C_1	07-55w C_1	07-55b C_1	07-59w C_2	97-59b C_2
Zr	343.46	346.89	160.33	354.44	149.10
Nb	30.91	30.30	13.23	30.94	12.24
Y	40.05	40.84	31.41	41.31	31.10
Sr	76.62	77.91	158.40	80.94	165.68
Rb	40.06	40.04	5.66	39.69	4.35
Ba	284.26	284.39	76.47	290.07	71.23
La	30.94	30.67	12.01	31.57	10.83
Ce	62.13	64.78	27.38	64.95	27.54
Pr	7.05	7.33	3.80	7.48	3.50
Nd	34.55	31.38	21.12	32.47	18.32
Sm	6.62	1.83	4.78	6.31	4.14
Eu	0.94	1.29	1.25	1.41	1.35
Gd	7.81	7.60	4.31	6.68	4.16
Ho	1.20	1.80	1.25	1.83	1.39
Yb	5.73	6.20	3.64	5.26	3.78
Sc	11.70	11.49	55.14	11.69	58.25

Table 7.9: Glass chemistry for the A1875 tephra layer collected via IP. Samples for the A1875 tephra layer were collected to the north-north east of the Öskjuvatn caldera lake, next to the Víti geothermal crater. Ten points were analysed for each sample and the data presented is the average of these analyses with two standard deviations (numbers in brackets). The complete data set is available in the Appendix.

Element	07-61 D_1	07-61 D_2	07-61 D_3	07-61 D_4
Zr	378.77 *(49.91)*	342.61 *(142.26)*	369.46 *(61.49)*	265.82 *(175.57)*
Nb	33.54 *(3.07)*	29.91 *(10.36)*	33.18 *(3.53)*	26.25 *(14.94)*
Y	61.49 *(11.03)*	58.17 *(11.85)*	60.33 *(12.75)*	43.47 *(16.05)*
Sr	100.19 *(26.79)*	117.86 *(74.19)*	101.71 *(16.31)*	107.39 *(80.95)*
Rb	60.47 *(6.30)*	50.89 *(31.50)*	60.16 *(6.56)*	46.61 *(37.20)*
Th	7.55 *(1.05)*	6.40 *(4.82)*	7.54 *(2.23)*	5.43 *(4.64)*
Ba	314.73 *(35.08)*	281.33 *(159.22)*	319.78 *(51.27)*	240.30 *(171.20)*
La	38.41 *(5.84)*	35.22 *(18.49)*	38.50 *(6.62)*	27.31 *(18.03)*
Ce	70.98 *(8.52)*	64.55 *(28.32)*	71.77 *(13.38)*	56.41 *(34.22)*
Pr	8.76 *(0.83)*	8.18 *(3.16)*	8.93 *(1.58)*	6.94 *(3.66)*
Nd	39.37 *(9.14)*	36.62 *(11.70)*	37.93 *(8.18)*	30.44 *(13.46)*
Sm	8.76 *(2/09)*	8.74 *(3.21)*	9.15 *(3.76)*	7.57 *(2.88)*
Eu	1.56 *(0.95)*	1.57 *(1.34)*	1.83 *(0.70)*	1.61 *(1.31)*
Gd	9.79 *(2.59)*	9.53 *(3.55)*	10.49 *(1.75)*	7.67 *(3.06)*
Tb	1.63 *(0.41)*	1.48 *(0.60)*	1.66 *(0.53)*	1.19 *(0.46)*
Dy	10.66 *(3.18)*	10.24 *(2.64)*	10.85 *(4.05)*	8.59 *(3.66)*
Ho	2.33 *(0.48)*	2.16 *(0.80)*	2.21 *(0.86)*	1.59 *(0.71)*
Er	6.59 *(2.09)*	5.96 *(2.03)*	7.40 *(1.68)*	5.10 *(2.12)*
Tm	1.11 *(0.46)*	1.05 *(0.46)*	1.13 *(0.44)*	0.74 *(0.40)*
Yb	6.61 *(1.71)*	6.33 *(2.25)*	6.99 *(2.44)*	5.00 *(1.97)*
Lu	1.04 *(0.43)*	0.86 *(0.48)*	1.07 *(0.25)*	0.70 *(0.48)*
Hf	9.78 *(3.02)*	8.61 *(4.67)*	9.70 *(2.62)*	7.21 *(4.41)*
Ta	2.64 *(0.46)*	2.22 *(0.99)*	2.57 *(0.52)*	1.85 *(1.30)*
Sc	0.39 *(0.23)*	0.49 *(0.81)*	0.28 *(0.10)*	0.47 *(0.88)*
Cs	0.53 *(0.59)*	0.42 *(1.29)*	0.47 *(0.67)*	0.31 *(0.84)*
U	1.97 *(0.62)*	1.60 *(1.09)*	1.93 *(0.59)*	1.48 *(1.16)*
Pb	4.97 *(0.74)*	5.45 *(6.03)*	4.65 *(1.30)*	3.94 *(2.86)*

Table 7.9 continued

Element	07-61 B	07-54w C1	07-55w C1	07-55b C1
Zr	416.22 *(67.77)*	362.59 *(116.35)*	372.05 *(56.25)*	97.40 *(26.37)*
Nb	35.73 *(3.59)*	33.48 *(9.67)*	37.89 *(8.62)*	11.88 *(3.30)*
Y	67.16 *(11.88)*	59.05 *(19.88)*	61.32 *(12.14)*	25.68 *(5.60)*
Sr	98.56 *(13.12)*	102.55 *(55.81)*	98.88 *(24.01)*	144.67 *(9.38)*
Rb	63.41 *(5.80)*	58.83 *(9.02)*	65.28 *(9.76)*	7.72 *(2.73)*
Th	8.77 *(1.30)*	7.75 *(2.55)*	8.45 *(1.16)*	0.91 *(0.41)*
Ba	353.16 *(45.83)*	314.65 *(60.21)*	338.13 *(59.52)*	63.22 *(14.79)*
La	42.38 *(6.24)*	39.15 *(12.70)*	40.66 *(5.56)*	8.82 *(2.52)*
Ce	78.39 *(11.53)*	70.49 *(20.86)*	76.57 *(9.96)*	20.58 *(5.71)*
Pr	9.64 *(1.94)*	8.70 *(2.01)*	9.50 *(0.90)*	2.82 *(0.86)*
Nd	42.47 *(5.15)*	38.86 *(8.71)*	40.30 *(4.75)*	13.82 *(3.32)*
Sm	9.78 *(2.55)*	8.99 *(3.02)*	10.24 *(5.39)*	4.03 *(1.44)*
Eu	1.88 *(0.49)*	1.91 *(0.50)*	1.78 *(0.87)*	1.29 *(0.29)*
Gd	11.48 *(3.31)*	9.74 *(2.81)*	10.61 *(2.06)*	4.79 *(1.50)*
Tb	1.77 *(0.36)*	1.53 *(0.59)*	1.59 *(0.24)*	0.80 *(0.18)*
Dy	11.61 *(2.81)*	10.56 *(3.80)*	10.39 *(2.50)*	5.05 *(1.34)*
Ho	2.57 *(0.52)*	2.11 *(0.70)*	2.37 *(0.49)*	1.08 *(0.50)*
Er	7.62 *(2.07)*	6.51 *(2.09)*	6.96 *(3.10)*	3.40 *(0.81)*
Tm	1.19 *(0.42)*	0.95 *(0.47)*	1.06 *(0.37)*	0.51 *(0.12)*
Yb	7.66 *(1.56)*	6.59 *(2.21)*	6.86 *(2.04)*	3.00 *(0.97)*
Lu	1.26 *(0.36)*	1.04 *(0.47)*	1.09 *(0.43)*	0.42 *(0.16)*
Hf	11.96 *(2.13)*	10.85 *(4.27)*	11.10 *(2.96)*	2.84 *(0.97)*
Ta	2.84 *(0.58)*	2.62 *(1.07)*	3.07 *(0.49)*	0.80 *(0.27)*
Sc	0.30 *(0.11)*	0.33 *(0.10)*	0.32 *(0.12)*	1.01 *(0.06)*
Cs	0.55 *(0.58)*	0.44 *(0.97)*	0.57 *(0.68)*	0.13 *(0.23)*
U	2.11 *(0.42)*	1.93 *(0.44)*	2.22 *(0.71)*	0.27 *(0.09)*
Pb	5.18 *(1.25)*	5.10 *(3.57)*	5.85 *(2.92)*	1.20 *(0.51)*

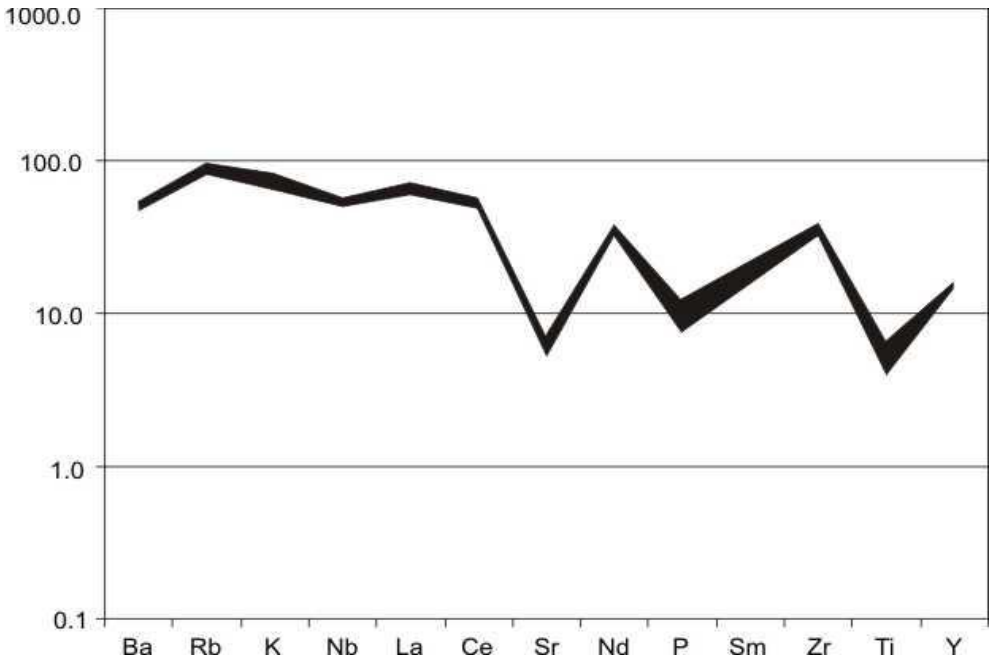

Figure 7.5: Multi element plot of the Askja 1875 tephra using certain major, trace and rare earth data collected via XRF. Data is normalised to bulk silicate earth (BSE) using the values in McDonough and Sun (1995). Negative data anomalies are recorded at Sr, P and Ti, while a positive anomaly is recorded at Zr.

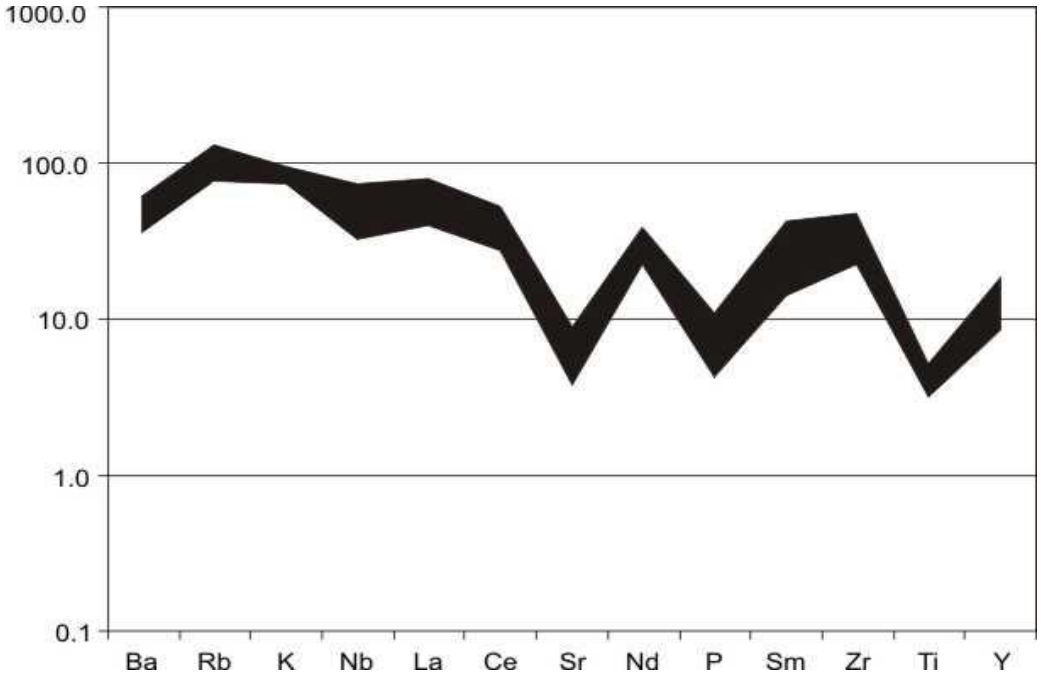

Figure 7.6: Multi element plot of the Askja 1875 tephra using major, trace and rare earth data collected via electron microprobe and laser ablation ICP-MS. Data is normalised to bulk silicate earth (BSE) using the values in McDonough and Sun (1995). Negative data anomalies are recorded at Sr, P and Ti, while a minor positive anomaly is recorded at Zr.

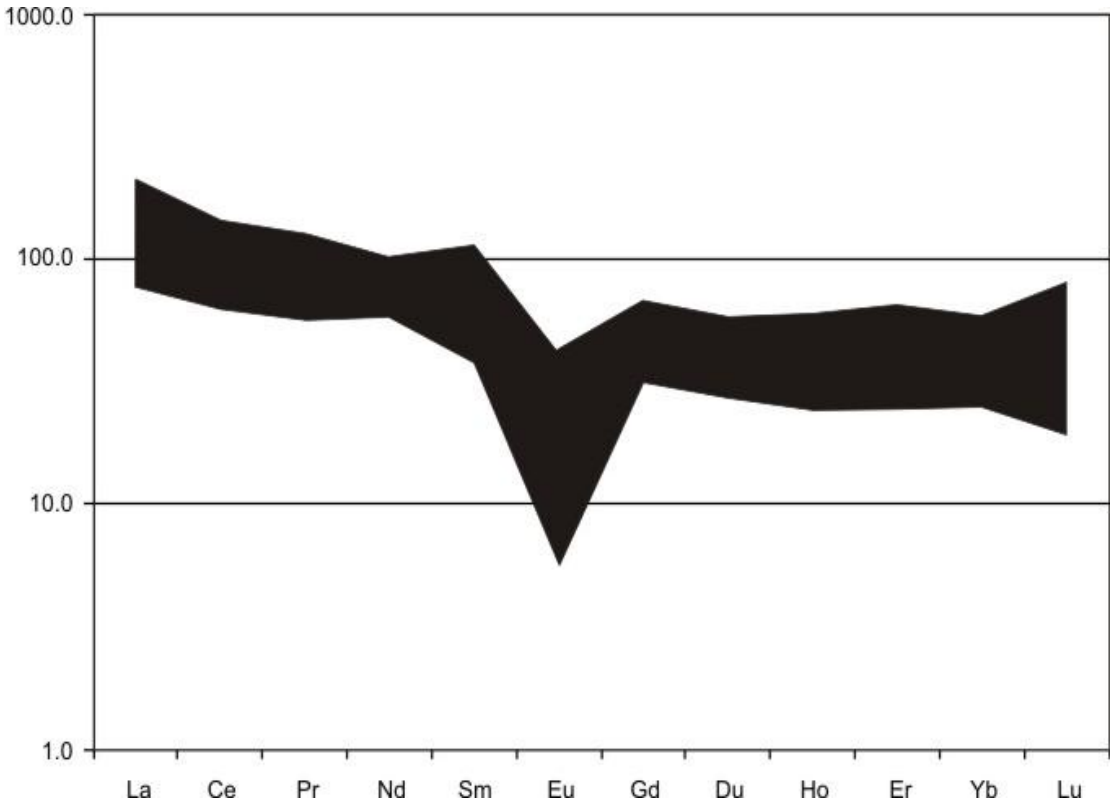

Figure 7.7: Rare earth element plot of the Askja 1875 tephra using rare earth data collected via laser ablation ICP-MS and IP. Data is normalised to chondrite using the values in McDonough and Sun (1995). A negative data anomaly is recorded at Eu, a positive anomaly is recorded at Sm and a broad range in data values is recoded at Lu.

7.3.3 Katla – Silk UN and LN tephra layers

In total, two samples were analysed for the Katla volcanic system layer collected from two sampling locations representing the Silk UN and Silk LN tephra layers. The new major element data collected via EMPA and XRF for the tephra layer is presented in Tables 7.10 – 7.12.

Multi element plots of the Katla data (Figs 7.8 and 7.9) indicate a shallowly dipping overall negative trend from the incompatible to compatible elements. The incompatible elements Ba, Rb and K show lower concentrations than Nb and La. Small negative anomalies are recorded for Sr, P and Ti. A small positive anomaly is recorded for Zr. The data shows tight clustering and therefore minimal deviation from the volcanic signature.

Rare earth element plots of the Katla data (Fig 7.10) indicates a shallowly dipping negative trend from the light rare earth elements (LREE) to the heavy rare earth elements (HREE) suggesting some depletion of HREE relative to the LREE. The data presents a subtle negative Eu anomaly and a small positive Nd and Er anomalies. REE ratios of Gd/Yb for the tephra layers range from 0.62 – 2.65 but are typically less than 2.00, while La/Sm ratios range from 4.01 – 11.17. Data collected by LA-ICP-MS and IP techniques show overlap when plotted graphically. However, some variation is noted within the overlap, suggesting that data collected by the two techniques are not directly comparable.

Table 7.10: Bulk chemistry for the Silk UN and LN tephra layer collected via XRF. Samples for the Katla tephra layers were collected near Loðnugil and Loðnugiljiahaus off the F232 route.

Elements	07-64 UN	07-65 LN
Zr	802.60	802.30
Nb	107.10	106.90
Y	80.10	82.00
Sr	291.80	299.00
Rb	55.80	57.10
Th	9.20	9.40
Zn	156.40	157.10
Cu	8.50	5.70
Ni	6.00	4.40
V	25.10	24.90
Ba	520.90	525.00
La	79.10	79.00
Ce	178.30	176.60
Nd	88.40	88.90
Sc	9.40	8.80
U	2.80	3.00
Pb	5.50	5.20

Table 7.11: Glass chemistry for the Katla Silk UN and LN tephra layers collected via IP. Samples for the Katla tephra were collected near Loðnugil and Loðnugiljiahaus off the F232 route.

Element	07-64 UN	07-65 LN
Zr	780.42 *(220.67)*	783.83 *(0.96)*
Nb	101.02 *(41.60)*	98.64 *(12.53)*
Y	57.55 *(9.47)*	55.25 *(7.23)*
Sr	269.71 *(38..69)*	246.78 *(1.28)*
Rb	49.84 *(33.49)*	44.43 *(14.31)*
Ba	508.43 *(219.54)*	486.24 *(56.13)*
La	69.85 *(30.35)*	66.50 *(0.65)*
Ce	155.41 *(65.23)*	143.74 *(3.52)*
Pr	19.36 *(8.40)*	17.51 *(0.46)*
Nd	82.95 *(35.47)*	75.50 *(4.68)*
Sm	12.13 *(19.34)*	16.33 *(0.90)*
Eu	2.65 *(1.70)*	2.73 *(1.04)*
Gd	9.26 *(9.67)*	8.81 *(13.12)*
Ho	2.43 *(0.26)*	2.38 *(0.10)*
Yb	7.12 *(2.62)*	6.65 *(0.21)*
Sc	10.83 *(0.81)*	10.70 *(0.82)*

Table 7.12: Glass chemistry for the Katla Silk UN and LN tephra layers collected via LA-ICP-MS. Samples for the Katla tephra layers were collected near Loðnugil and Loðnugiljiahaus off the F232 route. Ten points were analysed for each sample and the data presented is the average of these analyses with two standard deviations (numbers in brackets). The complete data set is available in the Appendix.

Element	07-64 UN	07-65 LN
Zr	721.47 *(180.65)*	726.04 *(100.62)*
Nb	97.83 *(9.22)*	103.67 *(9.08)*
Y	78.93 *(24.92)*	73.67 *(10.59)*
Sr	303.69 *(48.97)*	289.47 *(26.68)*
Rb	58.51 *(13.73)*	58.74 *(3.75)*
Th	9.15 *(2.61)*	
Ba	472.49 *(66.47)*	504.70 *(47.05)*
La	70.21 *(14.70)*	70.79 *(7.12)*
Ce	136.18 (18.78)	144.18 *(11.35)*
Pr	17.65 (3.17)	18.13 *(1.58)*
Nd	79.17 (16.99)	76.67 *(9.19)*
Sm	16.09 (4.55)	15.75 *(1.47)*
Eu	4.37 (1.11)	4.28 *(0.43)*
Gd	17.15 (6.94)	16.21 *(2.43)*
Tb	2.36 (1.04)	2.41 *(0.43)*
Dy	15.03 (4.72)	14.23 *(4.18)*
Ho	3.05 (1.11)	2.67 *(0.49)*
Er	8.52 (4.57)	7.81 *(1.62)*
Tm	1.01 (0.25)	1.11 *(0.31)*
Yb	7.57 (2.35)	7.25 *(1.59)*
Lu	1.11 (0.52)	1.00 *(0.49)*
Hf	18.30 (7.57)	18.44 *(3.09)*
Ta	6.49 (1.14)	6.55 *(0.74)*
Sc	0.34 (0.19)	0.30 *(0.08)*
Cs	0.31 (0.91)	0.48 *(0.26)*
U	2.38 (0.32)	2.63 *(0.27)*
Pb	6.46 (3.59)	6.40 *(0.93)*

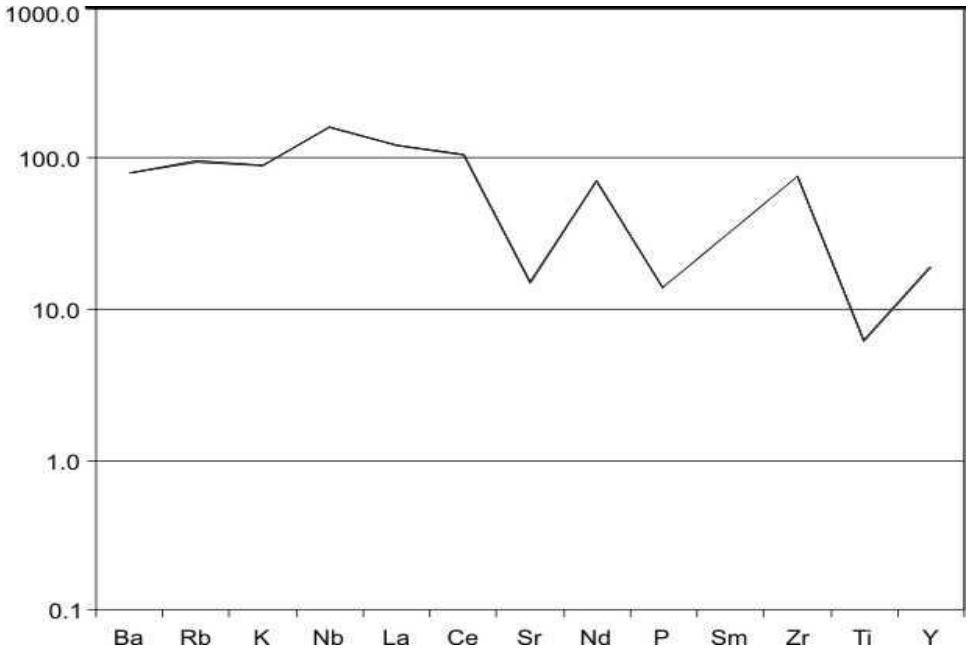

Figure 7.8: Multi element plot of the Katla Silk UN and LN tephra layers using certain major, trace and rare earth data collected via XRF. Data is normalised to bulk silicate earth (BSE) using the values in McDonough and Sun (1995). Negative data anomalies are recorded at Sr, P and Ti, while positive anomalies are recorded at Zr and Nb.

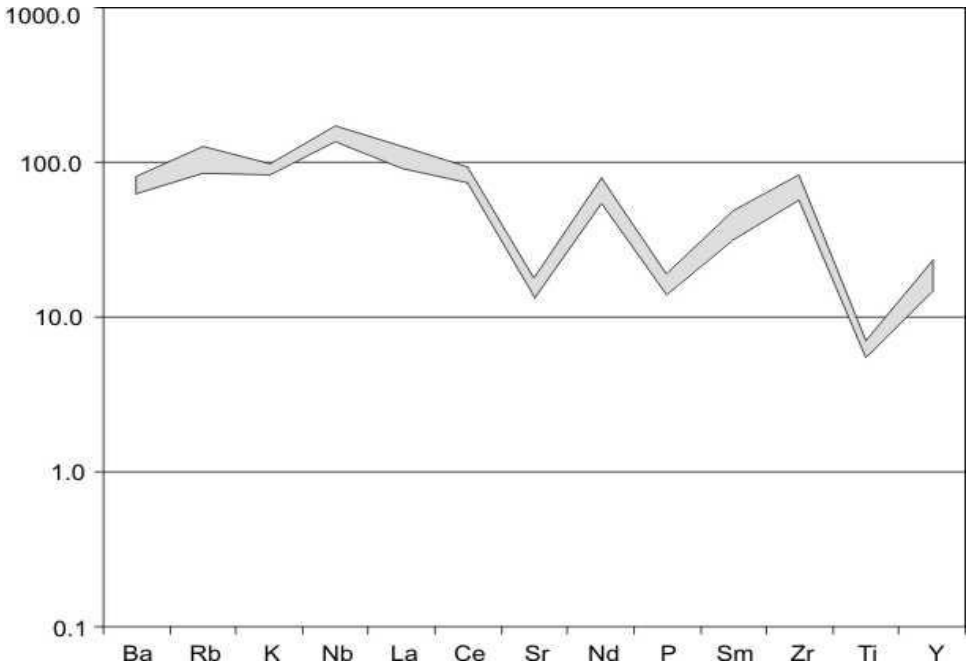

Figure 7.9: Multi element plot of the Katla Silk UN and LN tephra layers using major, trace and rare earth data collected via electron microprobe and laser ablation ICP-MS. Data is normalised to bulk silicate earth (BSE) using the values in McDonough and Sun (1995). Negative data anomalies are recorded at Sr, P and Ti, while positive anomalies are recorded at Zr and Nb.

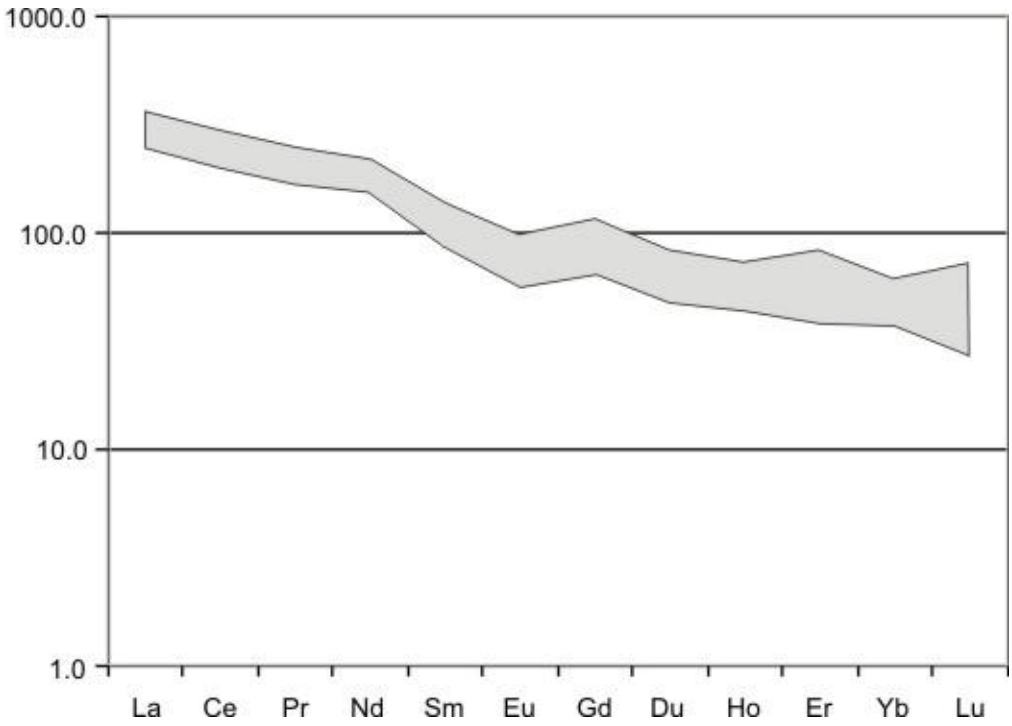

Figure 7.10: Rare Earth Element plot of the Katla Silk UN and LN tephra layers using rare earth data collected via laser ablation ICP-MS and IP. Data is normalised to chondrite using the values in McDonough and Sun (1995). A very minor negative data anomaly is recorded at Eu.

7.3.4 Öræfajökull – Ö1362 tephra layer

In total, five samples were analysed for the Öræfajökull volcanic system layer collected from two sampling locations. The new major element data collected via EMPA and XRF for the tephra layer is presented in Tables 7.13 – 7.15.

Multi element plots of the Öræfajökull data (Figs 7.11 and 7.12) indicate a shallowly dipping overall negative trend from the incompatible to compatible elements. The incompatible elements Ba - Ce show a flat lying trend. Pronounced negative anomalies are recorded for Sr, P and Ti. A small positive anomaly is recorded for Zr. The data shows tight clustering and therefore minimal deviation from the volcanic signature.

Rare earth element plots of the Öræfajökull data (Fig 7.13) indicates a shallowly dipping negative trend from the light rare earth elements (LREE) to the heavy rare earth elements (HREE) suggesting some depletion of HREE relative to the LREE. The data presents a subtle negative Eu anomaly and a small positive Sm anomaly. REE ratios of Gd/Yb for the tephra layers range from 0.03 – 2.10 but are typically less than 2.00, while La/Sm ratios range from 0.72 – 6.12. Data collected by LA-ICP-MS and IP techniques show overlap when plotted graphically. However, some variation is noted within the overlap, suggesting that data collected by the two techniques are not directly comparable

Table 7.13: Bulk chemistry for the Ö1362 tephra layer collected via XRF. Samples for the Ö1362 tephra were collected near Sigurðarholl and Sandsskarð.

Elements	08-20 O1362	08-33 O1362	08-48 O1362	08-59 O1362	08-65 O1362
Zr	788.10	764.50	776.80	796.20	779.00
Nb	82.50	80.70	82.20	82.80	82.30
Y	116.60	114.30	116.00	116.80	116.70
Sr	62.90	71.80	66.20	63.70	60.90
Rb	74.70	73.20	74.00	74.50	74.70
Th	9.70	9.60	10.00	9.90	9.90
Zn	150.10	149.60	153.30	151.20	149.60
Cu	7.30	6.70	8.00	6.60	6.90
Ni	1.20	2.80	2.30	0.90	0.80
V		1.60	6.00	0.80	0.20
Ba	598.50	601.00	600.20	603.40	594.60
La	79.10	77.00	77.20	77.60	78.60
Ce	167.10	163.50	165.40	166.30	167.60
Nd	82.40	80.40	81.40	81.70	80.60
Sc	0.20	0.90	1.50		
U	2.90	2.70	2.70	2.60	2.90
Pb	6.90	6.80	6.70	6.70	6.70

Table 7.14: Glass chemistry for the Ö1362 tephra layer collected via IP. Samples for the Ö1362 tephra were collected near Sigurđarholl and Sandsskarđ.

Element	08-33 O1362	08-48 O1362	08-59 O1362	08-65 O1362
Zr	700.64	685.18	698.75	729.41
Nb	73.91	74.39	75.63	79.13
Y	75.93	77.48	77.69	77.71
Sr	48.09	46.20	46.00	47.32
Rb	56.36	54.13	55.56	57.79
Ba	552.64	553.56	536.66	553.27
La	60.30	61.95	59.04	60.22
Ce	125.61	129.00	121.66	126.87
Pr	14.58	15.12	15.08	14.96
Nd	66.34	64.79	66.69	66.03
Sm	14.73	15.30	13.45	14.33
Eu	2.87	2.06	2.21	2.15
Gd	17.83	14.91	14.51	13.82
Ho	3.43	3.59	3.17	3.42
Yb	9.20	9.50	9.66	9.41
Sc	4.02	3.84	3.63	3.74

Table 7.15: Glass chemistry for the Ö1362 tephra layer collected via LA-ICP-MS. Samples for the Ö1362 tephra were collected near Sigurðarholl and Sandsskarð. Ten points were analysed for each sample and the data presented is the average of these analyses with two standard deviations (numbers in brackets). The complete data set is available in the Appendix.

Element	08-20 O1362	08-33 O1362	08-48 O1362	08-58 O1362	08-65 O1362
Zr	666.27 *(115.99)*	782.74 *(150.27)*	773.12 *(115.28)*	770.36 *(113.60)*	610.58 *(308.76)*
Nb	84.38 *(14.30)*	87.06 *(12.39)*	88.72 *(9.12)*	86.22 *(11.60)*	76.84 *(35.13)*
Y	110.17 *(21.35)*	128.04 *(33.43)*	125.88 *(23.68)*	129.28 *(21.65)*	103.86 *(53.85)*
Sr	47.15 *(21.87)*	61.00 *(8.12)*	59.56 *(8.47)*	63.54 *(34.04)*	86.87 *(167.58)*
Rb	79.09 *(11.16)*	83.77 *(6.86)*	81.27 *(7.36)*	75.33 *(10.68)*	72.93 *(34.98)*
Th	9.90 *(2.44)*	11.66 *(3.20)*	11.83 *(2.28)*	11.83 *(2.28)*	9.16 *(5.45)*
Ba	557.16 *(95.57)*	621.00 *(100.31)*	607.23 *(59.72)*	611.40 *(101.80)*	650.12 *(327.86)*
La	68.63 *(9.90)*	76.12 *(15.71)*	78.34 *(11.85)*	77.39 *(15.12)*	65.21 *(30.50)*
Ce	135.17 *(19.85)*	139.36 *(35.63)*	143.18 *(12.39)*	138.25 *(27.51)*	123.23 *(56.92)*
Pr	16.72 *(2.51)*	18.19 *(4.19)*	18.60 *(2.46)*	17.86 *(3.03)*	15.65 *(7.48)*
Nd	74.63 *(14.44)*	79.32 *(24.05)*	80.57 *(7.95)*	79.38 *(18.69)*	68.65 *(32.80)*
Sm	17.51 *(5.64)*	19.07 *(6.26)*	26.61 *(49.10)*	19.58 *(14.20)*	15.37 *(10.69)*
Eu	3.25 *(2.69)*	2.98 *(0.95)*	3.19 *(0.67)*	3.04 *(2.01)*	3.12 *(2.11)*
Gd	16.79 *(12.13)*	22.34 *(4.11)*	20.47 *(5.09)*	19..64 *(7.43)*	17.09 *(9.86)*
Tb	3.10 *(0.93)*	3.40 *(0.94)*	3.40 *(0.79)*	3.35 *(0.82)*	2.92 *(1.64)*
Dy	20.68 *(4.79)*	23.19 *(4.96)*	22.27 *(4.34)*	22.67 *(6.21)*	19.38 *(11.24)*
Ho	4.05 *(1.16)*	4.94 *(1.29)*	4.46 *(0.82)*	4.63 *(1.17)*	3.71 *(1.79)*
Er	10.69 *(7.82)*	13.62 *(2.62)*	13.72 *(2.79)*	13.07 *(3.93)*	11.57 *(6.49)*
Tm	1.60 *(1.17)*	1.94 *(0.50)*	2.09 *(0.43)*	1.94 *(0.64)*	1.60 *(1.24)*
Yb	11.35 *(2.19)*	12.92 *(3.45)*	13.26 *(2.94)*	12.74 *(4.16)*	10.49 *(5.64)*
Lu	1.80 *(0.63)*	1.84 *(0.65)*	1.97 *(0.50)*	1.91 *(0.70)*	1.42 *(0.84)*
Hf	18.75 *(3.01)*	21.42 *(5.51)*	22.20 *(5.03)*	21.04 *(5.64)*	18.04 *(9.50)*
Ta	5.47 *(1.41)*	6.13 *(1.39)*	6.38 *(0.62)*	5.94 *(1.85)*	5.03 *(2.84)*
Sc	0.12 *(0.09)*	0.14 *(0.06)*	0.14 *(0.10)*	0.11 *(0.11)*	0.10 *(0.07)*
Cs	0.75 *(0.82)*	0.73 *(0.67)*	1.01 *(0.50)*	1.00 *(0.65)*	0.71 *(0.41)*
U	2.54 *(0.73)*	2.97 *(0.93)*	2.75 *(0.54)*	2.47 *(0.69)*	2.37 *(1.23)*
Pb	8.17 *(4.48)*	8.99 *(2.05)*	16.07 *(54.78)*	8.59 *(11.07)*	7.38 *(3.46)*

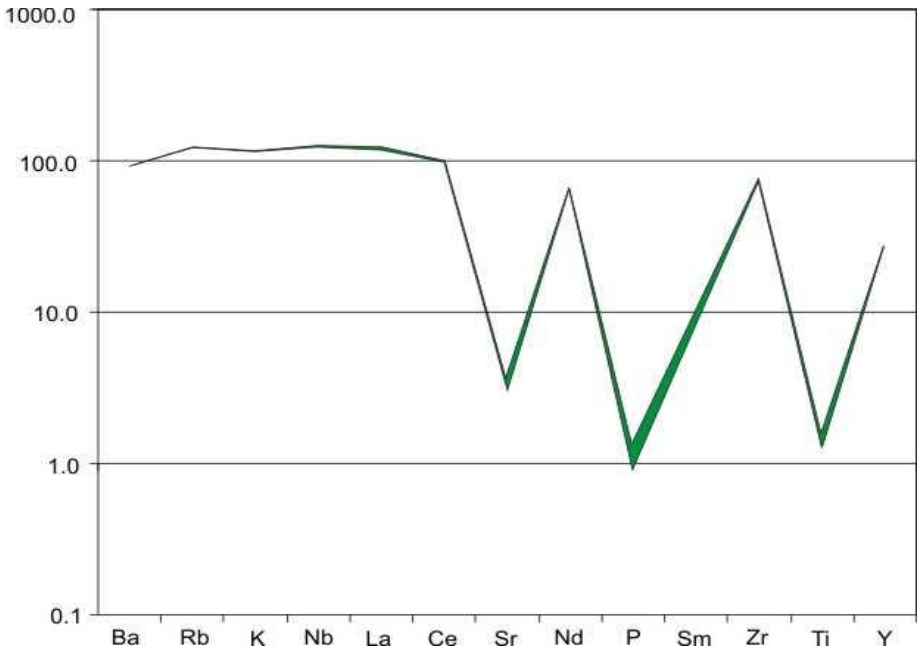

Figure 7.11: Multi element plot of the Öræfajökull 1362 tephra layer using certain major, trace and rare earth data collected via XRF. Data is normalised to bulk silicate earth (BSE) using the values in McDonough and Sun (1995). Negative data anomalies are recorded at Sr, P and Ti, while a positive anomaly is recorded at Zr.

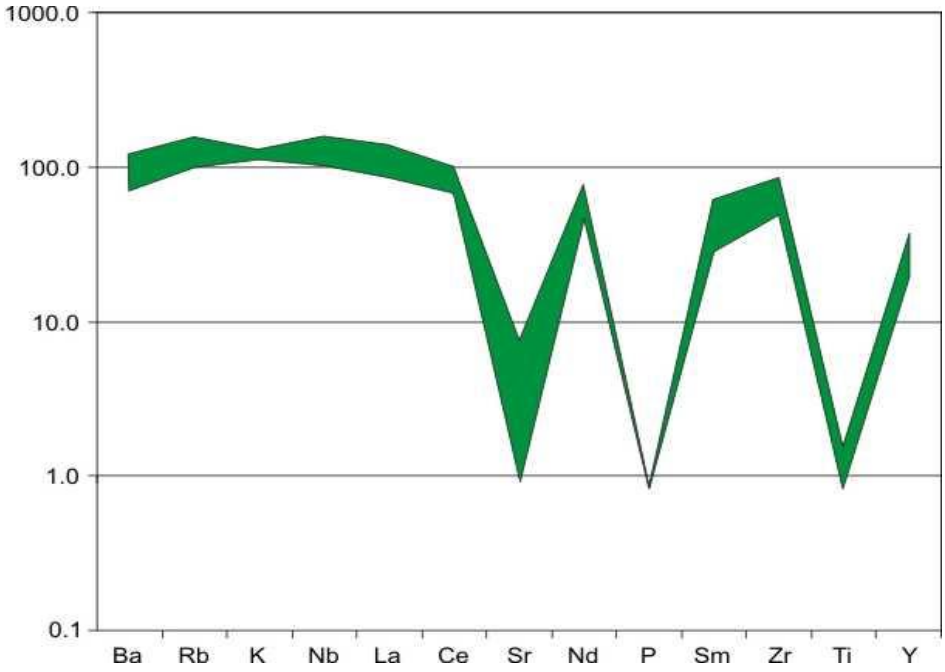

Figure 7.12: Multi element plot of the Öræfajökull 1362 tephra layer using major, trace and rare earth data collected via electron microprobe and laser ablation ICP-MS. Data is normalised to bulk silicate earth (BSE) using the values in McDonough and Sun (1995). Negative data anomalies are recorded at Sr, P and Ti, while a minor positive anomaly is recorded at Zr.

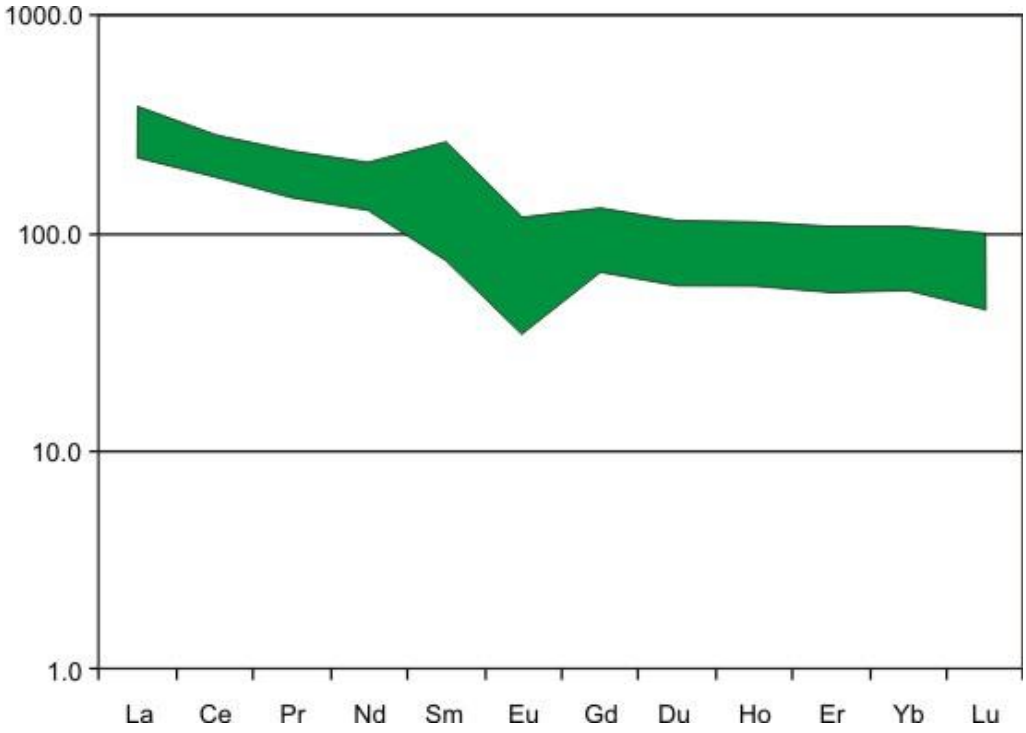

Figure 7.13: Rare Earth Element plot of the Öræfajökull 1362 tephra layer using rare earth data collected via laser ablation ICP-MS and IP. Data is normalised to chondrite using the values in McDonough and Sun (1995). A negative data anomaly is recorded at Eu, while a positive anomaly is recorded at Sm.

7.3.5 Hekla – H1104, H3, HSelsund, H4, H5, H-ABC-MN-XYZ tephra layers

In total, 27 samples were analysed for the Hekla volcanic system from thirteen tephra layers collected from eight sampling locations. The new trace and rare earth element data collected via XRF, IP and LA-ICP-MS for the tephra layers is presented in Tables 7.16 – 7.37. The Hekla tephra layers show stratigraphical zoning at each sampling location. As discussed in Chapter 6, the smaller Hekla tephra layers are recorded as showing a range in chemical compositions, including an unexpected rhyolitic component. At present it is unclear whether the rhyolitic grains represent juvenile components of the tephra layers or entrainment of older pumiceous material during eruption. The trace and rare earth element data collected on these grains is recorded in the data tables in the following sections but is not incorporated into the associated diagrams.

Multi element plots of the Hekla data (Figs 7.14 and 7.15) indicate a shallowly dipping overall negative trend from the incompatible to compatible elements. The incompatible elements Ba - Ce show a flat lying trend in the XRF data while the glass data shows a negative anomaly in K. Pronounced negative anomalies are recorded for Sr, P and Ti. A small positive anomaly is recorded for Zr in XRF data but is undetected in glass data. The data does not show tight clustering as with the other volcanic systems. However, this may be an artefact of the greater number of samples analysed for the Hekla system compared with the other volcanic systems.

Rare earth element plots of the Hekla data (Fig 7.16) indicates a shallowly dipping negative trend from the light rare earth elements (LREE) to the heavy rare earth elements (HREE) suggesting some depletion of HREE relative to the LREE. The data presents a pronounced negative Eu anomaly and a small positive Sm anomaly. REE ratios of Gd/Yb for the tephra layers range from 0.97 – 4.79, while La/Sm ratios range from 0.87 – 8.11. It is important to note that although LA-ICP-MS and IP data overlap they are consistently different to cast doubt on the comparability of the data sets.

Table 7.16: Bulk chemistry for the H1104 tephra layer collected via XRF. Samples for the H1104 tephra layer was selected near Burfell on route 26.

Elements	08-70 H1	08-71 H1	08-72 H1	08-73 H1
Zr	779.90	666.90 *(22.06)*	671.05 *(10.04)*	676.70
Nb	73.50	77.25 *(1.84)*	77.85 *(0.99)*	78.00
Y	84.70	85.85 *(1.27)*	86.00 *(0.00)*	86.30
Sr	233.60	224.10 *(21.89)*	216.60 *(6.76)*	214.20
Rb	46.20	52.43 *(1.31)*	52.43 *(0.53)*	52.60
Th	8.70	9.45	9.60	9.80
Zn	136.10	122.95 *(0.99)*	123.60 *(1.13)*	122.80
Cu	18.50	15.95 *(2.12)*	15.15 *(0.14)*	15.70
Ba	505.60	545.75 *(11.17)*	538.85 *(4.67)*	542.70
La	73.10	77.65 *(1.27)*	77.05 *(0.42)*	78.60
Ce	153.90	157.50 *(2.26)*	159.55 *(0.14)*	158.50
Nd	75.40	76.60 *(1.98)*	77.30 *(1.41)*	76.40
Sc	11.40	9.70 *(1.41)*	9.25 *(0.99)*	9.60
U	2.60	2.85 *(0.14)*	2.85 *(0.14)*	2.80
Pb	7.00	8.25 *(2.69)*	6.95 *(0.14)*	6.60

Table 7.17: Glass chemistry for the H1104 tephra layer collected via IP. Samples for the H1104 tephra layer was selected near Burfell on route 26.

Element	08-71 H1	08-72 H1	08-73 H1
Zr	394.32	399.64 *(15.04)*	417.81
Nb	64.70	65.22 *(1.48)*	70.52
Y	56.87	58.22 *(3.82)*	55.94
Sr	126.46	129.97 *(9.93)*	122.01
Rb	38.69	39.63 *(2.64)*	42.70
Ba	503.27	501.07 *(6.22)*	477.22
La	60.03	59.62 *(1.18)*	55.76
Ce	119.67	120.91 *(3.50)*	113.85
Pr	14.20	14.06 *(0.39)*	13.48
Nd	63.59	62.23 *(3.84)*	60.06
Sm	11.83	11.51 *(0.88)*	11.32
Eu	1.99	2.37 *(1.07)*	2.17
Gd	12.09	13.30 *(3.42)*	10.82
Ho	2.45	2.58 *(0.37)*	2.37
Yb	8.02	7.45 *(1.61)*	6.53
Sc	8.63	9.05 *(1.20)*	9.44

Table 7.18: Glass chemistry for the H1104 Landnám tephra layer collected via LA-ICP-MS. Samples for the H1104 tephra layer was selected near Burfell on route 26. Ten points were analysed for each sample and the data presented is the average of these analyses with two standard deviations (numbers in brackets). The complete data set is available in the Appendix.

Element	08-71 H1	08-72 H1	08-73 H1
Zr	447.83 *(177.20)*	418.82 *(59.34)*	409.50 *(71.30)*
Nb	78.00 *(27.56)*	78.91 *(13.91)*	75.22 *(8.00)*
Y	92.48 *(44.48)*	83.03 *(16.81)*	85.15 *(23.76)*
Sr	164.32 *(77.27)*	154.30 *(27.43)*	150.33 *(27.44)*
Rb	62.06 *(19.42)*	71.01 *(48.21)*	62.60 *(14.58)*
Th	11.27 *(5.07)*	10.56 *(3.05)*	9.99 *(2.55)*
Ba	554.42 *(182.67)*	546.53 *(86.46)*	543.84 *(52.04)*
La	77.81 *(31.72)*	72.98 *(11.12)*	77.67 *(24.87)*
Ce	132.72 *(46.14)*	129.59 *(19.19)*	134.40 *(30.59)*
Pr	16.37 *(5.13)*	17.22 *(4.24)*	16.70 *(3.10)*
Nd	70.51 *(28.09)*	67.46 *(14.19)*	72.43 *(13.29)*
Sm	18.63 *(16.32)*	15.88 *(4.66)*	17.46 *(7.27)*
Eu	2.88 *(1.31)*	2.99 *(1.99)*	3.49 *(2.94)*
Gd	16.99 *(6.92)*	16.52 *(5.17)*	16.64 *(8.97)*
Tb	2.58 *(1.10)*	2.53 *(0.82)*	2.49 *(0.96)*
Dy	17.54 *(8.27)*	17.69 *(6.76)*	18.13 *(7.74)*
Ho	3.53 *(2.30)*	3.62 *(1.24)*	3.16 *(1.48)*
Er	9.90 *(5.62)*	9.07 *(2.44)*	9.79 *(5.64)*
Tm	1.46 *(1.29)*	1.55 *(0.86)*	1.39 *(0.99)*
Yb	9.11 *(3.50)*	7.81 *(2.13)*	7.65 *(3.50)*
Lu	1.55 *(1.11)*	1.25 *(3.69)*	1.58 *(1.28)*
Hf	14.01 *(5.49)*	12..57 *(3.69)*	13.24 *(5.23)*
Ta	5.66 *(2.71)*	4.95 *(1.08)*	4.98 *(1.89)*
Sc	0.26 *(0.40)*	0.19 *(0.17)*	0.19 *(0.41)*
Cs	0.55 *(1.27)*	0.96 *(1.71)*	1.24 *(2.08)*
U	2.70 *(1.00)*	2.73 *(0.56)*	2.98 *(1.38)*
Pb	13.17 *(15.01)*	8.53 *(2.21)*	10.30 *(4.10)*

Table 7.19: Bulk chemistry for the H3 tephra layer collected via XRF. Samples for the H3 tephra layer was selected near Ófærugil.

Elements	07-66 H3	07-70 H3	07-73 H3	07-76 H3	07-79 H3
Zr	601.30	644.30	592.00	715.90	755.70
Nb	74.00	65.90	74.30	69.70	74.10
Y	86.20	76.20	86.00	79.70	85.30
Sr	203.50	286.60	197.20	262.00	229.00
Rb	49.90	37.50	50.10	42.30	47.00
Th	9.40	7.10	9.30	8.10	8.90
Zn	115.40	157.00	116.30	147.10	133.00
Cu	16.80	21.60	17.70	20.20	17.10
Ba	535.90	423.50	538.50	454.70	508.60
La	78.00	63.60	77.30	67.40	73.30
Ce	157.90	132.20	160.80	138.80	153.80
Nd	78.10	69.00	77.50	69.80	75.40
Sc	8.50	16.30	8.50	13.90	11.60
U	2.60	1.70	2.60	2.90	2.70
Pb	6.40	5.80	6.80	9.20	6.30

Table 7.20: Glass chemistry for the H3 tephra layer collected via IP. Samples for the H3 tephra layer was selected near Ófærugil.

Element	07-66 H3	07-70br H3	07-73 H3	07-76 H3
Zr	394.27	665.21 *(55.43)*	380.54 *(45.25)*	413.95 *(119.11)*
Nb	75.89	69.28 *(1.86)*	74.72 *(16.38)*	78.73 *(19.56)*
Y	60.74	58.03 (*4.83)*	58.55 *(1.04)*	62.37 *(24.07)*
Sr	132.96	239.00 *(9.27)*	127.75 *(7.12)*	136.24 *(16.79)*
Rb	41.97	28.79 *(0.75)*	44.86 *(14.10)*	50.81 *(19.18)*
Ba	532.80	385.49 *(45.98)*	520.35 *(24.59)*	583.70 *(228.34)*
La	65.37	54.76 (*1.08)*	61.64 *(0.16)*	71.30 *(38.55)*
Ce	134.56	116.79 *(8.99)*	128.60 *(5.33)*	147.99 *(89.23)*
Pr	15.45	14.39 *(1.56)*	14.83 *(0.90)*	17.15 *(11.32)*
Nd	70.42	67.14 *(8.87)*	63.45 *(6.90)*	72.11 *(40.91)*
Sm	13.34	12.84 *(1.64)*	12.39 *(0.90)*	13.30 *(6.13)*
Eu	2.58	3.17 *(1.12)*	2.20 *(0.61)*	1.67 *(1.35)*
Gd	17.55	20.43 *(5.82)*	17.20 *(1.50)*	12.47 *(5.79)*
Ho	2.68	2.79 *(5.82)*	2.71 *(0.13)*	2.92 *(1.33)*
Yb	7.49	6.27 *(1.40)*	7.03 *(0.13)*	8.17 *(4.47)*
Sc	9.31	18.52 *(2.12)*	8.91 *(0.70)*	9.51 *(2.78)*

Table 7.21: Glass chemistry for the H3 tephra layer collected via LA-ICP-MS. Samples for the H3 tephra layer was selected near Ófærugil. Ten points were analysed for each sample and the data presented is the average of these analyses with two standard deviations (numbers in brackets). The complete data set is available in the Appendix.

Element	07-66 H3	07-73 H3	07-76 H3
Zr	382.51 *(81.76)*	380.74 *(48.19)*	385.40 *(217.18)*
Nb	74.45 *(6.39)*	75.32 *(6.02)*	66.99 *(20.81)*
Y	82.85 *(16.23)*	86.21 *(14.24)*	79.04 *(35.38)*
Sr	157.62 *(25.89)*	155.27 *(20.20)*	236.*73 (231.86)*
Rb	61.21 *(15.58)*	72.39 *(37.22)*	58.51 *(21.10)*
Th	10.13 *(2.63)*	10.77 *(2.13)*	9.85 *(4.59)*
Ba	640.95 *(270.50)*	567.69 *(37.86)*	559.68 *(109.21)*
La	73.03 *(15.44)*	75.41 *(9.31)*	69.24 *(28.03)*
Ce	138.89 *(18.42)*	138.81 *(16.35)*	128.44 *(48.20)*
Pr	16.90 *(5.12)*	17.14 *(2.07)*	16.01 *(6.02)*
Nd	64.39 *(27.37)*	67.11 *(10.25)*	63.89 *(27.05)*
Sm	13.71 *(10.01)*	25.65 *(52.58)*	15.20 *(5.52)*
Eu	2.75 *(0.69)*	2.50 *(1.73)*	3.20 *(1.69)*
Gd	16.23 *(4.89)*	16.13 *(5.45)*	14.68 *(7.00)*
Tb	2.21 *(1.13)*	2.21 *(0.72)*	2.33 *(1.11)*
Dy	15.84 *(4.79)*	16.37 *(6.21)*	14.95 *(5.97)*
Ho	3.21 *(0.99)*	3.08 *(1.25)*	3.11 *(1.44)*
Er	9.11 *(5.48)*	9.50 *(3.09)*	9.27 *(4.44)*
Tm	1.14 *(0.68)*	1.*53 (0.93)*	1.32 *(0.41)*
Yb	9.12 *(2.77)*	8.77 *(2.99)*	8.47 *(4.37)*
Lu	1.36 *(0.64)*	1.34 *(0.39)*	1.33 *(0.80)*
Hf	10.18 *(5.45)*	11.95 *(4.16)*	12.11 *(6.11)*
Ta	4.19 *(3.17)*	5.16 *(0.52)*	4.77 *(1.82)*
Sc	0.26 *(0..09)*	0.23 *(0.13)*	0.25 *(0.29)*
Cs	1.04 *(2.04)*	0.86 *(0.48)*	0.50 *(0.68)*
U	2.61 *(0.83)*	2.90 *(1.59)*	2.37 *(0.98)*
Pb	10.13 *(2.63)*	19.78 *(30.36)*	9.50 *(4.59)*

Table 7.22: Bulk chemistry for the HSelsund tephra layer collected via XRF. Samples for the HSelsund tephra were collected near Laufafjell.

Elements	08-77 HS	08-78 HS	08-79 HS
Zr	706.90	689.40	719.50
Nb	70.90	70.40	71.10
Y	80.60	80.10	80.80
Sr	255.60	257.70	250.70
Rb	42.60	42.10	43.00
Th	7.80	8.00	8.40
Zn	137.60	140.50	135.20
Cu	20.40	20.20	19.60
Ba	470.20	463.30	477.30
La	70.30	69.40	74.60
Ce	145.30	145.90	148.40
Nd	71.70	72.60	72.40
Sc	12.40	11.40	12.10
U	2.40	2.50	2.10
Pb	6.60	6.20	6.00

Table 7.23: Glass chemistry for the HSelsund tephra layer collected via IP. Samples for the HSelsund tephra were collected near Laufafjell.

Element	08-77 HS	08-78 HS	08-79 HS
Zr	489.71 *(505.10)*	686.35 *(29.59)*	648.35 *(576.98)*
Nb	57./84 *(2.52)*	70.64 *(2.91)*	82.14 *(5.51)*
Y	52.92 *(1.73)*	56.28 *(0.35)*	63.03 *(0.05)*
Sr	155.81 *(104.69)*	196.26 *(59.97)*	180.35 *(118.07)*
Rb	31.45 *(6.12)*	35.15 *(2.65)*	45.65 *(6.12)*
Ba	427.12 *(25.99)*	473.98 *(39.13)*	558.03 *(50.94)*
La	52.75 *(2.59)*	57.91 *(3.51)*	68.45 *(2.48)*
Ce	106.79 *(3.41)*	123.49 *(6.16)*	143.35 *(3.68)*
Pr	13.45 *(0.48)*	14.58 *(0.16)*	17.05 *(1.14)*
Nd	55.83 *(4.13)*	64.59 *(1.06)*	72.61 *(5.40)*
Sm	10.98 *(1.17)*	13.00 *(0.44)*	14.78 *(1.40)*
Eu	2.21 *(0.26)*	2.59 *(0.62)*	2.71 *(1.09)*
Gd	11.37 *(1.06)*	17.59 *(3.80)*	16.90 *(0.19)*
Ho	2.42 *(0.26)*	2.68 *(0.25)*	2.97 *(0.16)*
Yb	7.17 *(0.90)*	7.55 *(1.75)*	7.62 *(0.96)*
Sc	10.74 *(5.95)*	12.13 *(2.40)*	11.39 *(6.88)*

Table 7.24: Glass chemistry for the HSelsund tephra layer collected via LA-ICP-MS. Samples for the HSelsund tephra were collected near Laufafjell. Ten points were analysed for each sample and the data presented is the average of these analyses with two standard deviations (numbers in brackets). The complete data set is available in the Appendix.

Element	08-77 HS	08-78 HS	08-78 HS
Zr	661.36 *(200.45)*	518.50 *(91.44)*	437.87 *(267.98)*
Nb	69.93 *(7.01)*	61.64 *(5.64)*	59.59 *(6.95)*
Y	79.43 *(23.67)*	66.07 *(14.93)*	60.81 *(20.66)*
Sr	226.97 *(52.05)*	202.91 *(45.89)*	168.40 *(83.34)*
Rb	49.53 *(7.68)*	44.41 *(10.08)*	48.46 *(6.80)*
Th	9.01 *(2.70)*	6.24 *(1.39)*	6.28 *(2.37)*
Ba	468.35 *(91.27)*	332.05 *(63.36)*	338.34 *(78.90)*
La	64.88 *(16.06)*	52.41 *(10.19)*	51.97 *(15.28)*
Ce	113.73 *(16.81)*	99.48 *(12.93)*	101.42 *(24.52)*
Pr	15.09 *(3.66)*	12.46 *(2.16)*	12.50 *(2.58)*
Nd	66.96 *(20.47)*	56.24 *(13.19)*	52.87 *(12.49)*
Sm	15.07 *(3.35)*	12.09 *(3.51)*	12.79 *(5.19)*
Eu	3.51 *(1.53)*	3.33 *(1.08)*	2.19 *(0.67)*
Gd	17.09 *(3.90)*	11.68 *(4.09)*	12.04 *(3.43)*
Tb	2.23 *(1.08)*	1.87 *(0.28)*	1.64 *(0.59)*
Dy	16.78 *(6.66)*	13.86 *(3.20)*	11.23 *(3.17)*
Ho	3.35 *(1.03)*	2.44 *(0.47)*	2.20 *(0.92)*
Er	10.35 *(3.79)*	7.99 *(3.12)*	7.59 *(2.31)*
Tm	1.65 *(0.86)*	1.10 *(0.40)*	1.22 *(0.81)*
Yb	8.18 *(2.81)*	6.56 *(2.33)*	6.27 *(2.49)*
Lu	1.29 *(0.65)*	1.03 *(0.50)*	1.05 *(0.49)*
Hf	17.79 *(4.05)*	13.12 *(2.83)*	10.68 *(4.97)*
Ta	4.74 *(1.38)*	3.83 *(0.69)*	3.72 *(1.17)*
Sc	0.31 *(0.29)*	0.33 *(0.14)*	0.26 *(0.18)*
Cs	0.46 *(0.69)*	0.54 *(0.69)*	0.74 *(0.70)*
U	2.24 *(0.56)*	2.24 *(2.54)*	2.01 (*0.30)*
Pb	7.74 *(3.05)*	6.38 *(2.26)*	8.26 *(4.06)*

Table 7.25: Bulk chemistry for the H4 tephra layer collected via XRF. Samples for the H4 tephra were collected near Ófærugil.

Elements					
Zr	321.90	313.20	315.90	320.30	319.80
Nb	90.10	89.80	90.20	90.70	90.90
Y	97.30	96.70	96.60	97.60	97.60
Sr	114.10	112.10	112.20	111.30	111.60
Rb	60.10	60.00	60.20	60.00	59.40
Th	10.90	11.00	10.70	10.70	10.90
Zn	120.80	119.50	119.40	120.30	119.80
Cu	16.40	16.10	15.60	16.50	14.90
Ni	5.00	5.50	4.60	4.90	4.10
Ba	631.40	621.20	631.10	628.60	628.50
La	90.50	95.40	85.90	87.50	89.10
Ce	178.80	184.80	170.50	172.80	176.30
Nd	85.90	88.70	83.60	83.80	85.50
Sc	4.20	3.20	3.80	4.10	3.30
U	3.30	3.20	3.10	3.30	3.20
Pb	6.70	7.00	6.90	6.90	6.90

Elements					
Zr	317.30	334.00	329.70	331.00	324.40
Nb	91.10	91.20	91.30	91.70	91.30
Y	97.60	98.00	97.50	98.60	98.00
Sr	108.40	111.70	112.70	113.10	112.30
Rb	59.50	59.50	59.20	59.10	59.70
Th	10.60	10.90	10.90	10.90	10.70
Zn	121.70	120.90	121.40	121.00	119.50
Cu	14.90	16.50	16.20	15.60	16.00
Ni	5.00	4.10	4.90	4.90	4.90
Ba	630.50	626.80	625.80	623.70	623.60
La	89.90	92.80	90.60	89.90	88.90
Ce	178.50	182.00	175.90	179.60	175.30
Nd	86.50	87.20	86.10	85.00	83.20
Sc	3.50	4.00	4.40	4.20	4.40
U	3.10	3.20	3.10	3.30	3.20
Pb	7.00	6.70	6.70	6.80	6.70

Table 7.26: Glass chemistry for the H4 tephra layer collected via IP. Samples for the H4 tephra were collected near Ófærugil.

Element	07-84 H4	07-87 H4	07-101w H4	07-101b H4
Zr	226.16 *(17.11)*	352.45 *(62.66)*	229.75 *(15.71)*	522.00 *(145.62)*
Nb	83.16 *(3.96)*	138.56 *(2.76)*	87.85 *(5.81)*	51.78 *(28.33)*
Y	63.10 *(4.25)*	92.65 *(14.79)*	62.98 *(5.26)*	48.87 *(23.42)*
Sr	81.93 *(2.40)*	106.24 *(17.25)*	79.65 *(6.61)*	265.35 *(16.42)*
Rb	46.86 *(3.13)*	73.08 *(13.99)*	46.46 *(5.06)*	20.46 *(2.79)*
Ba	569.96 *(38.00)*	876.66 *(37.59)*	556.51 *(48.25)*	326.50 *(44.40)*
La	52.70 *(4.02)*	78.32 *(35.59)*	51.21 *(4.99)*	42.72 *(19.86)*
Ce	115.90 *(11.48)*	172.50 *(70.32)*	110.25 *(10.85)*	93.45 *(46.32)*
Pr	13.44 *(1.46)*	20.91 *(10.09)*	13.28 *(2.21)*	11.76 *(6.48)*
Nd	60.66 *(4.68)*	91.01 *(36.30)*	57.54 *(7.99)*	56.14 *(281.6)*
Sm	12.44 *(0.76)*	19.75 *(6.79)*	12.18 *(1.67)*	10.92 *(5.75)*
Eu	1.43 *(1.50)*	0.98 *(1.58)*	2.04 *(0.71)*	3.16 *(2.31)*
Gd	14.19 *(2.25)*	19.69 *(2.01)*	16.73 *(3.86)*	15.95 *(2.86)*
Ho	2.78 *(0.25)*	4.63 *(1.79)*	2.82 *(0.60)*	2.43 *(1.19)*
Yb	6.52 *(0.68)*	11.83 *(4.57)*	8.03 *(1.77)*	6.12 *(2.83)*
Sc	5.57 *(0.42)*	6.93 *(0.78)*	5.43 *(0.71)*	20.16 *(6.18)*

Table 7.27: Glass chemistry for the H4 tephra layer collected via LA-ICP-MS. Samples for the H4 tephra were collected near Ófærugil. Ten points were analysed for each sample and the data presented is the average of these analyses with two standard deviations (numbers in brackets). The complete data set is available in the Appendix.

Element	07-84 H4	07-87 H4	07-101 H4
Zr	225.01 *(57.98)*	241.56 *(36.52)*	272.78 *(82.60)*
Nb	91.25 *(23.19)*	94.54 *(23.23)*	95.79 *(30.43)*
Y	92.55 *(25.08)*	100.70 *(12.11)*	106.48 *(31.92)*
Sr	102.21 *(38.84)*	103.77 *(18.73)*	111.42 *(27.27)*
Rb	84.35 *(44.64)*	75.20 *(11.30)*	65.59 *(12.28)*
Th	10.19 *(2.63)*	11.79 *(1.88)*	12.72 *(2.68)*
Ba	619.00 *(98.41)*	668.01 *(40.07)*	629.39 *(115.94)*
La	60.40 *(13.28)*	65.27 *(7.37)*	68.63 *(15.88)*
Ce	118.32 *(25.64)*	135.35 *(25.09)*	125.58 *(22.31)*
Pr	15.08 *(2.67)*	16.77 *(2.76)*	16.99 *(3.56)*
Nd	61.75 *(14.60)*	69.86 *(14.79)*	72.22 *(19.32)*
Sm	16.09 *(5.42)*	17.27 *(4.07)*	18.63 *(9.40)*
Eu	2.97 *(1.49)*	3.23 *(1.52)*	3.08 *(2.27)*
Gd	16.62 *(3.94)*	18.44 *(5.64)*	18.62 *(9.13)*
Tb	2.48 *(1.30)*	2.51 *(0.87)*	2.90 *(1.36)*
Dy	16.86 *(6.52)*	20.97 *(3.03)*	20.74 *(7.75)*
Ho	3.58 *(1.07)*	3.99 *(1.55)*	3.98 *(1.34)*
Er	10.46 *(3.10)*	11.36 *(2.79)*	11.87 *(3.98)*
Tm	1.74 *(0.79)*	1.72 *(1.03)*	1.87 *(0.78)*
Yb	8.45 *(3.20)*	9.98 *(3.05)*	11.19 *(3.49)*
Lu	1.26 *(0.72)*	1.43 *(0.71)*	1.68 *(0.68)*
Hf	8.81 *(4.10)*	9.98 *(3.68)*	10.74 *(5.06)*
Ta	5.52 *(1.68)*	6.52 *(2.92)*	7.37 *(3.28)*
Sc	0.13 *(0.17)*	0.16 *(0.23)*	0.10 *(0.14)*
Cs	0.95 *(1.15)*	0.60 *(0.87)*	1.50 *(1.96)*
U	3.04 *(1.84)*	3.03 *(0.81)*	3.02 *(0.80)*
Pb	19.03 *(18.75)*	19.01 *(14.62)*	10.83 *(3.18)*

Table 7.28: Bulk chemistry for the H5 tephra layer collected via XRF. Samples for the H5 tephra were collected near Áfangagil.

Elements	09-04 H5	09-05 H5
Zr	256.30	253.60
Nb	75.00	73.70
Y	84.90	83.00
Sr	117.10	124.10
Rb	58.00	56.40
Th	10.40	10.00
Zn	95.50	97.10
Cu	14.00	20.10
Ni	2.30	5.00
V	2.50	13.70
Ba	588.10	590.10
La	66.40	61.90
Ce	137.90	132.30
Nd	65.90	63.80
Sc	5.80	6.40
U	3.20	2.80
Pb	6.80	7.10

Table 7.29: Glass chemistry for the H5 tephra layer collected via IP. Samples for the H5 tephra were collected near Áfangagil.

Element	09-04w H5	09-04b H5	09-05 H5
Zr	166.49 *(14.64)*	191.14 *(76.64)*	177.05 *(43.00)*
Nb	72.23 *(4.34)*	24.58 *(12.07)*	77.72 *(20.35)*
Y	55.50 *(1.13)*	24.75 *(5.94)*	57.43 *(7.64)*
Sr	75.16 *(0.06)*	328.16 *(36.21)*	72.43 *(2.52)*
Rb	44.50 *(1.42)*	7.00 *(5.74)*	48.63 *(5.69)*
Ba	516.27 *(9.95)*	119.11 *(46.72)*	552.20 *(108.34)*
La	39.37 *(2.27)*	18.98 *(8.33)*	42.12 *(10.46)*
Ce	82.85 *(6.04)*	44.61 *(20.92)*	90.31 *(18.26)*
Pr	10.30 *(0.80)*	5.99 *(3.11)*	11.03 *(2.10)*
Nd	46.33 *(0.59)*	29.32 *(17.76)*	48.38 *(6.64)*
Sm	10.57 *(2.01)*	6.10 *(1.22)*	10.33 *(2.28)*
Eu	1.43 (*1.02)*	2.01 *(0.32)*	0.79 *(0.27)*
Gd	14.39 *(4.16)*	7.04 *(1.23)*	12.33 *(2.45)*
Ho	2.44 *(0.48)*	1.16 *(0.13)*	2.60 *(0.19)*
Yb	7.11 *(2.00)*	2.57 *(0.75)*	7.67 *(3.51)*
Sc	6.31 *(0.34)*	40.26 *(1.20)*	6.94 *(1.17)*

Table 7.30: Glass chemistry for the H5 tephra layer collected via LA-ICP-MS. Samples for the H5 tephra were collected near Áfangagil. Ten points were analysed for each sample and the data presented is the average of these analyses with two standard deviations (numbers in brackets). The complete data set is available in the Appendix.

Element	09-04 H5	09-05 H5
Zr	177.51 *(32.15)*	182.50 *(36.90)*
Nb	78.42 *(5.40)*	79.76 *(10.20)*
Y	84.30 *(17.59)*	85.98 *(12.09)*
Sr	97.75 *(21.44)*	123.88 *(39.66)*
Rb	64.32 *(3.95)*	64.53 *(7.77)*
Th	10.15 *(2.29)*	11.48 *(2.18)*
Ba	573.99 *(75.66)*	627.32 *(28.49)*
La	47.36 *(7.96)*	50.38 *(6.95)*
Ce	94.85 *(11.92)*	101.84 *(15.17)*
Pr	12.34 *(2.03)*	13.01 *(1.84)*
Nd	53.85 *(9.61)*	56.27 *(9.14)*
Sm	13.72 *(3.45)*	14.24 *(4.78)*
Eu	2.24 *(0.71)*	2.45 *(0.61)*
Gd	15.13 *(2.74)*	14.85 *(0.97)*
Tb	2.41 *(0.84)*	2.69 *(0.51)*
Dy	16.05 *(3.95)*	16.89 *(3.31)*
Ho	3.32 *(0.60)*	3.44 *(0.69)*
Er	9.12 *(2.48)*	10.01 *(2.50)*
Tm	1.42 *(0.34)*	1.60 *(0.37)*
Yb	8.12 *(2.00)*	8.64 *(1.44)*
Lu	1.22 *(0.33)*	1.37 *(0.25)*
Hf	7.07 *(1.53)*	8.33 *(1.30)*
Ta	5.49 *(0.97)*	5.98 *(0.91)*
Sc	0.19 *(0.06)*	0.24 *(0.08)*
Cs	0.85 *(0.35)*	0.97 *(0.26)*
U	2.83 *(0.62)*	2.98 *(0.88)*
Pb	10.56 *(9.16)*	10.08 *(3.08)*

Table 7.31: Bulk chemistry for the HA, HB and HC tephra layers collected via XRF. Samples for the HA, HB and HC tephras were collected near Búrfell on the banks of the river Þorsjà off route 26.

Elements	08-19 HA	08-18 HB	08-17b HB	08-17w HB	08-15w HC	08-15b HC	08-14 HC
Zr	476.00	489.20	453.20	478.30	488.40	488.20	465.70
Nb	51.90	54.80	61.20	56.00	57.80	54.60	65.70
Y	63.20	66.10	72.50	66.70	68.20	65.60	77.10
Sr	287.70	312.30	354.10	312.30	319.30	300.50	371.10
Rb	35.30	304.00	25.00	31.70	32.10	34.40	24.20
Th	6.60	33.70	5.70	5.70	5.60	6.40	5.50
Zn	117.10	124.90	162.40	133.30	137.20	126.10	175.20
Cu	25.90	24.20	25.70	26.10	22.90	24.10	17.70
Ni	5.50	5.50	7.60	7.10	3.90	7.30	6.20
V	28.90	29.50	76.90	37.70	29.40	25.20	72.40
Ba	382.80	374.50	309.00	358.40	368.00	377.20	309.20
La	51.60	52.40	49.90	52.40	52.90	55.10	52.20
Ce	116.40	115.10	116.90	115.10	117.50	116.60	124.50
Nd	59.50	59.50	66.20	59.50	61.20	60.80	72.00
Sc	14.90	14.70	22.60	17.00	16.50	15.70	24.80
U	1.90	1.90	1.40	1.70	1.80	1.40	1.10
Pb	4.60	4.10	3.80	4.50	5.60	4.80	3.60

Table 7.32: Bulk chemistry for the HM and HN tephra layer collected via XRF. Samples for the HM and HN tephras were collected near Rangárhliðar on the mountain Grasleysufjöll on route F210 near the Eystri-Rangá river.

Elements	09-24 H4w	09-24 HMb	09-23 HM	09-22 HM	09-20 HN
Zr	412.40	473.00	475.20	468.80	486.50
Nb	50.00	66.30	53.50	51.70	53.80
Y	57.10	74.50	62.60	61.50	63.20
Sr	316.30	358.70	291.50	286.60	288.90
Rb	27.00	25.40	33.00	33.20	33.10
Th	5.30	5.70	6.30	6.50	6.40
Zn	137.80	174.70	123.20	119.30	120.70
Cu	56.00	23.20	27.80	31.00	31.00
Ni	24.20	8.30	7.40	7.00	7.00
V	106.90	52.40	21.00	21.80	21.80
Ba	310.90	309.90	357.90	360.60	376.40
La	45.40	52.40	53.60	51.50	52.40
Ce	99.50	119.20	111.80	110.20	113.90
Nd	53.80	71.60	55.10	56.40	57.70
Sc	22.20	22.90	14.40	13.10	14.60
U	1.60	1.40	1.80	1.80	1.80
Pb	4.20	5.70	4.60	4.30	4.60

Table 7.33: Bulk chemistry for the HX, HY and HZ tephra layers collected via XRF. Samples for the HX, HY and HZ tephras were collected near Sauðleysur on route F225 near the banks of the river Helliskvísl.

Elements	08-01 HX	08-02 HX	08-03 HX	08-05 HY	08-06 HY	08-7 HY	08-09 HZ	08-10 HZ	08-11 HZ
Zr	435.90	437.50	470.90	440.10	447.00	440.80	437.60	438.10	446.80
Nb	61.00	58.20	53.50	62.80	63.00	47.10	64.10	62.80	61.10
Y	73.30	69.60	64.30	74.50	74.70	58.90	78.30	76.40	73.20
Sr	363.60	346.70	302.6	368.70	368.10	289.20	376.10	371.70	359.80
Rb	23.70	25.80	33.00	22.50	23.50	34.70	21.40	22.30	24.20
Th	5.50	5.30	5.90	5.10	5.10	6.70	4.00	5.20	5.50
Zn	167.50	157.10	124.90	177.90	175.80	113.40	180.60	178.10	169.10
Cu	26.40	29.30	27.20	22.70	21.30	29.10	16.10	19.00	23.10
Ni	5.40	4.30	2.40	7.60	5.00	2.10	4.10	3.80	7.40
V	87.50	73.60	28.00	79.10	70.50	29.50	83.80	78.80	68.10
Ba	296.60	309.90	366.60	294.60	299.70	373.60	281.30	291.90	306.30
Sc	22.90	20.70	16.10	23.80	23.50	13.40	24.30	23.70	22.70
U	1.10	1.70	1.90	1.30	1.10	2.00	1.20	1.30	1.30
Pb	6.10	5.40	5.00	4.30	5.00	5.60	6.00	4.20	4.20

Table 7.34: Glass chemistry for the HZ tephra layer collected via IP. Samples for the HZ tephra layer were collected near Sauðleysur on route F225 near the banks of the river Helliskvísl.

Element	08-11w HZ	08-11b HZ
Zr	406.25 *(90.83)*	460.78 *(17.92)*
Nb	66.78 *(17.49)*	53.70 *(0.57)*
Y	55.35 *(0.86)*	60.02 *(4.48)*
Sr	106.82 *(43.35)*	260.97 *(110.38)*
Rb	43.75 *(18.46)*	15.40 *(4.50)*
Ba	482.05 *(41.03)*	249.02 *(10.10)*
La	57.41 *(3.24)*	45.83 *(3.34)*
Ce	116.56 *(7.41)*	105.04 *(5.95)*
Pr	13.73 *(0.28)*	13.86 *(1.46)*
Nd	60.56 *(0.70)*	68.44 *(4.44)*
Sm	11.42 *(1.03)*	14.15 *(1.74)*
Eu	2.10 *(1.18)*	3.77 *(0.20)*
Gd	12.86 *(2.91)*	14.38 *(1.76)*
Ho	2.46 *(0.26)*	2.47 *(0.03)*
Yb	6.46 *(2.78)*	6.85 *(0.88)*
Sc	7.70 *(2.01)*	26.91 *(0.15)*

Table 7.35: Glass chemistry for the HA, HB and HC tephra layers collected via LA-ICP-MS. Samples for the HA, HB and HC tephras were collected near Búrfell on the banks of the river Þorsjà off route 26. Ten points were analysed for each sample and the data presented is the average of these analyses with two standard deviations (numbers in brackets). The complete data set is available in the Appendix.

Element	08-19 HA	08-18 HB	08-14 HC
Zr	325.68 *(216.64)*	317.78 *(175.90)*	356.62 *(96.85)*
Nb	38.70 *(19.96)*	38.42 *(13.70)*	44.78 *(12.55)*
Y	42.74 *(27.09)*	38.97 *(17.84)*	49.84 *(19.66)*
Sr	223.27 *(133.11)*	228.39 *(97.93)*	268.93 *(61.82)*
Rb	40.09 *(22.51)*	41.43 *(16.55)*	42.03 *(6.33)*
Th	5.16 *(3.60)*	4.30 *(3.25)*	5.15 *(1.33)*
Ba	319.13 *(193.23)*	290.76 *(98.79)*	353.62 *(80.19)*
La	36.99 *(21.87)*	36.23 *(16.13)*	41.40 *(11.14)*
Ce	76.02 *(38.24)*	72.38 *(30.38)*	90.61 *(39.49)*
Pr	9.28 *(4.57)*	10.46 *(9.71)*	11.21 *(6.14)*
Nd	39.62 *(21.50)*	34.43 *(17.57)*	47.12 *(24.86)*
Sm	8.53 *(5.99)*	8.56 *(4.27)*	10.50 *(5.80)*
Eu	2.74 *(1.57)*	2.28 *(1.06)*	3.50 *(0.80)*
Gd	8.26 *(5.42)*	8.07 *(3.97)*	10.78 *(6.31)*
Tb	1.47 *(0.91)*	1.09 *(0.69)*	1.53 *(1.10)*
Dy	8.14 *(3.03)*	7.10 *(5.02)*	10.71 *(4.66)*
Ho	1.89 *(0.86)*	1.71 *(0.87)*	2.18 *(0.73)*
Er	4.54 *(3.83)*	5.08 *(3.89)*	6.03 *(3.59)*
Tm	0.81 *(0.75)*	0.91 *(0.95)*	1.00 *(0.91)*
Yb	4.86 *(2.89)*	4.77 *(3.44)*	5.01 *(2.72)*
Lu	0.64 *(0.58)*	0.59 *(0.24)*	0.79 *(0.42)*
Hf	8.00 *(6.40)*	7.76 *(5.16)*	8.74 *(3.00)*
Ta	2.48 *(1.82)*	2.20 *(1.34)*	2.62 *(0.88)*
Sc	0.50 *(0.44)*	0.34 *(0.34)*	0.41 *(0.28)*
Cs	0.81 *(1.09)*	0.93 *(1.03)*	0.59 *(1.30)*
U	1.57 *(1.07)*	1.37 *(0.72)*	1.70 *(0.44)*
Pb	6.55 *(4.67)*	5.50 *(4.24)*	7.25 *(4.49)*

Table 7.36: Glass chemistry for the HM and HN tephra layers collected via LA-ICP-MS. Samples for the HM and HN tephras were collected near Rangárhliðar on the mountain Grasleysufjöll on route F210 near the Eystri-Rangá river. Ten points were analysed for each sample and the data presented is the average of these analyses with two standard deviations (numbers in brackets). The complete data set is available in the Appendix.

Element	08-24 HM	08-20 HN
Zr	402.69 *(155.35)*	386.42 *(100.11)*
Nb	50.50 *(27.99)*	42.83 *(7.21)*
Y	58.50 *(25.61)*	49.71 *(15.60)*
Sr	262.20 *(56.88)*	250.33 *(51.90)*
Rb	38.88 *(7.93)*	41.09 *(7.46)*
Th	5.10 *(1.90)*	5.42 *(1.78)*
Ba	345.74 *(0.53)*	339.52 *(52.58)*
La	43.06 *(16.12)*	42.56 *(9.07)*
Ce	93.42 *(42.02)*	85.33 *(14.16)*
Pr	11.64 *(4.37)*	10.43 *(2.50)*
Nd	51.68 *(28.13)*	45.00 *(12.60)*
Sm	14.91 *(9.61)*	11.54 *(2.09)*
Eu	3.74 *(2.09)*	2.95 *(1.97)*
Gd	13.31 *(6.98)*	10.08 *(4.37)*
Tb	1.82 *(0.90)*	1.51 *(0.68)*
Dy	11.26 *(4.90)*	9.86 *(2.76)*
Ho	2.22 *(0.89)*	2.25 *(0.78)*
Er	6.68 *(4.49)*	5.83 *(2.68)*
Tm	0.88 *(0.83)*	0.79 *(0.56)*
Yb	5.95 *(2.33)*	5.31 *(2.64)*
Lu	0.94 *(0.44)*	0.85 *(0.38)*
Hf	10.66 *(4.69)*	10.45 *(2.57)*
Ta	3.19 *(2.01)*	3.02 *(0.97)*
Sc	0.48 *(0.26)*	0.29 *(0.27)*
Cs	0.60 *(0.53)*	0.71 *(0.70)*
U	1.82 *(0.83)*	1.68 *(0.36)*
Pb	8.17 *(7.87)*	6.24 *(2.26)*

Table 7.37: Glass chemistry for the HX, HY and HZ tephra layers collected via LA-ICP-MS. Samples for the HX, HY and HZ tephras were collected near Sauðleysur on route F225 near the banks of the river Helliskvísl. Ten points were analysed for each sample and the data presented is the average of these analyses with two standard deviations (numbers in brackets). The complete data set is available in the Appendix.

Element	08-1 HX	08-2 HX	08-3 HX	08-7 HY	08-9 HZ	08-14 HC
Zr	502.15 *(279.27)*	112.21	342.23 *(204.93)*	390.69 *(77.28)*	385.58 *(376.37)*	351.93 *(185.05)*
Nb	62.63 *(27.62)*	24.86	44.80 *(10.92)*	38.46 *(7.98)*	43.18 *(26.13)*	53.32 *(28.17)*
Y	61.04 *(22.32)*	29.22	48.10 *(19.06)*	53.57 *(15.21)*	54.47 *(46.23)*	64.43 *(42.03)*
Sr	221.09 *(82.73)*	582.17	270.68 *(23.97)*	268.06 *(45.28)*	243.54 *(45.18)*	220.33 *(104.42)*
Rb	53.58 *(42.93)*	19.97	42.89 *(12.03)*	41.25 *(8.65)*	43.01 *(13.80)*	46.38 *(11.88)*
Th	7.17 *(2.74)*	2.69	5.20 *(2.22)*	6.56 *(1.95)*	6.87 *(4.36)*	6.64 *(2.15)*
Ba	380.57 *(203.84)*	566.54	341.79 *(144.44)*	350.34 *(47.57)*	362.89 *(162.23)*	367.01 *(146.05)*
La	53.03 *(17.43)*	24.84	40.94 *(13.52)*	43.60 *(8.90)*	45.18 *(25.40)*	50.33 *(24.13)*
Ce	108.99 *(40.98)*	45.37	86.32 *(15.17)*	87.17 *(32.02)*	89.70 *(43.16)*	94.82 *(37.11)*
Pr	14.30 *(5.43)*	5.20	10.68 *(5.32)*	11.08 *(3.99)*	11.23 *(6.89)*	12.27 *(6.92)*
Nd	56.32 *(7.03)*	21.46	41.75 *(15.20)*	46.51 *(11.04)*	48.93 *(28.45)*	54.88 *(29.03)*
Sm	11.41 *(2.41)*	4.49	10.83 *(3.23)*	11.07 *(5.63)*	9.53 *(7.64)*	12.19 *(6.07)*
Eu	2.88 *(3.46)*	6.61	3.11 *(1.43)*	2.61 *(1.77)*	2.91 *(1.13)*	3.49 *(2.09)*
Gd	12.87 *(3.23)*	4.12	10.92 *(5.92)*	9.24 *(3.13)*	12.00 *(6.81)*	10.64 *(5.80)*
Tb	1.91 *(1.51)*	0.66	1.68 *(1.16)*	1.78 *(1.36)*	1.77 *(1.61)*	2.11 *(2.14)*
Dy	23.38 *(7.30)*	3.88	9.70 *(3.20)*	10.39 *(3.44)*	11.41 *(7.69)*	10.37 *(5.06)*
Ho	2.53 *(0.87)*	0.87	2.22 *(0.82)*	2.18 *(1.08)*	2.51 *(2.92)*	2.41 *(2.14)*
Er	7.22 *(1.12)*	2.78	4.90 *(3.06)*	6.01 *(2.15)*	7.08 *(4.61)*	7.40 *(2.01)*
Tm	1.32 *(1.63)*	0.04	0.66 *(0.65)*	0.96 *(0.63)*	0.99 *(1.73)*	1.19 *(1.44)*
Yb	6.00 *(1.67)*	1.45	4.58 *(1.94)*	5.06 *(2.55)*	6.01 *(4.50)*	6.33 *(2.71)*
Lu	0.88 *(0.61)*	0.48	0.89 *(0.70)*	0.82 *(0.65)*	1.27 *(0.67)*	0.84 *(0.45)*
Hf	13.35 *(7.74)*	2.75	8.76 *(5.84)*	10.59 *(2.59)*	10.50 *(10.25)*	9.99 *(4.73)*
Ta	4.34 *(2.29)*	1.52	2.99 *(1.18)*	3.00 *(1.16)*	3.86 *(5.01)*	3.83 *(1.78)*
Sc	0.67 *(0.84)*	0.19	0.49 *(0.54)*	0.41 *(0.49)*	0.40 *(0.43)*	0.43 *(0.68)*
Cs	1.40 *(2.84)*	0.05	1.28 *(1.08)*	1.00 *(2.57)*	0.69 *(1.68)*	0.47 *(0.20)*
U	2.16 *(1.18)*	1.02	1.62 *(0.47)*	1.72 *(0.46)*	1.99 *(0.91)*	2.01 *(0.90)*
Pb	8.26 *(4.87)*	3.80	13.26 *(11.67)*	14.36 *(37.04)*	8.30 *(2.55)*	5.56 *(1.21)*

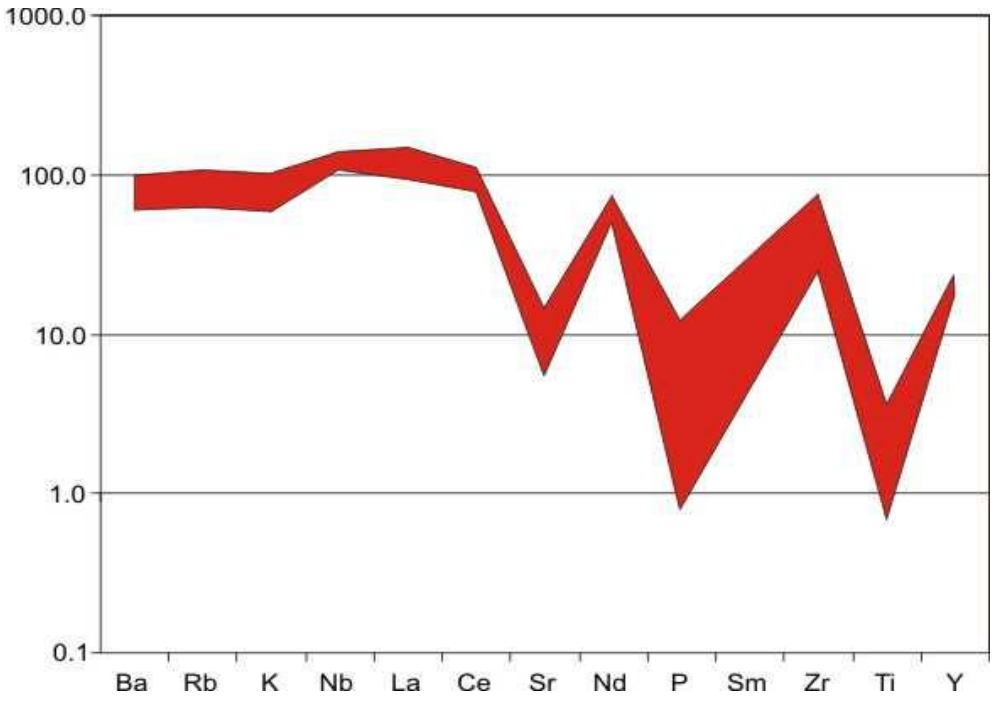

Figure 7.14: Multi element plot of the tephra layers from the Hekla volcanic system using certain major, trace and rare earth data collected via XRF. Data is normalised to bulk silicate earth (BSE) using the values in McDonough and Sun (1995). Negative data anomalies are recorded at Sr, P and Ti, while a positive anomaly is recorded at Zr and Nb.

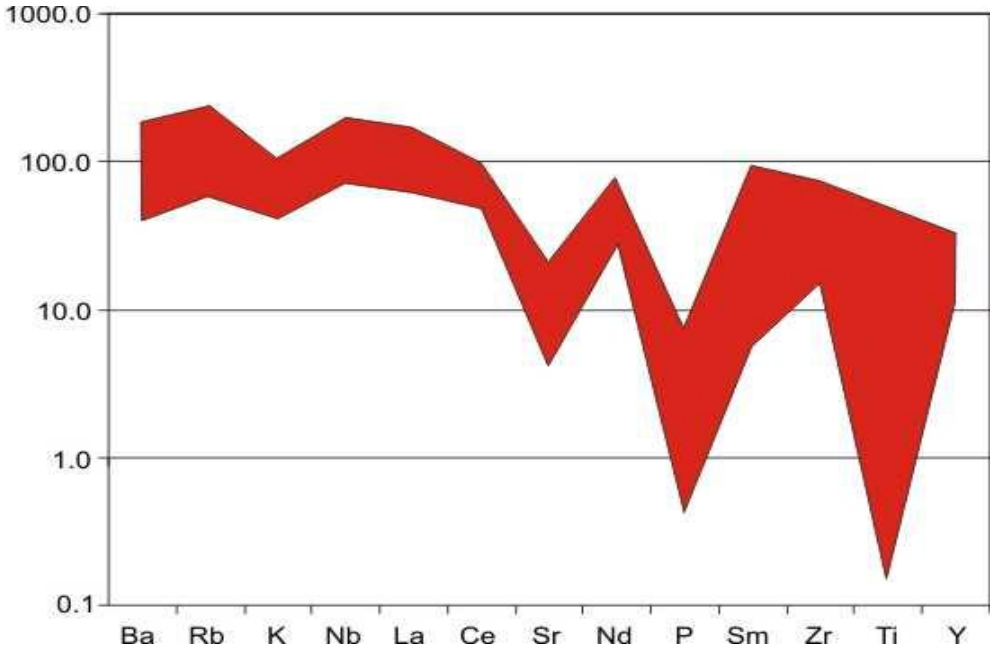

Figure 7.15: Multi element plot of the tephra layers from the Hekla volcanic system using major, trace and rare earth data collected via electron microprobe and laser ablation ICP-MS. Data is normalised to bulk silicate earth (BSE) using the values in McDonough and Sun (1995). Negative data anomalies are recorded at K, Sr, P and Ti, while a positive anomaly is recorded at Zr.

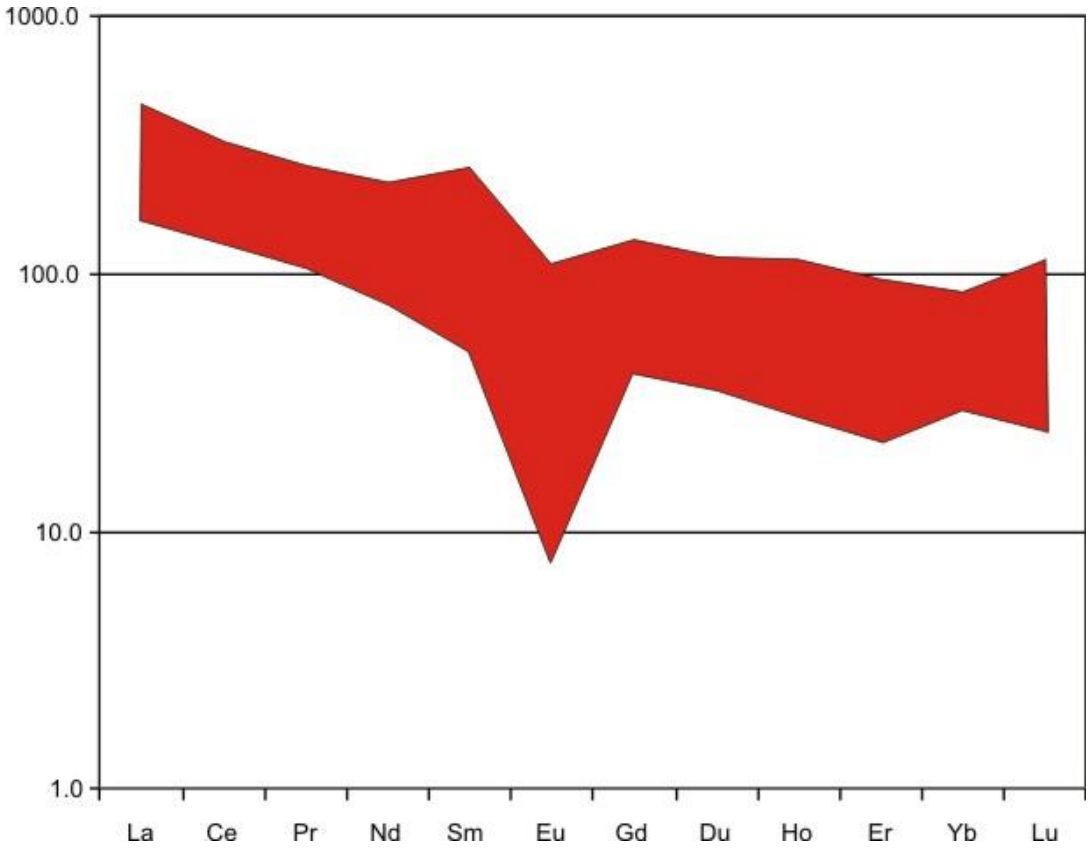

Figure 7.16: Rare Earth Element plot of the tephra layers from the Hekla volcanic system using rare earth data collected via laser ablation ICP-MS and IP. Data is normalised to chondrite using the values in McDonough and Sun (1995). Negative data anomalies are recorded at Eu and Er, while a positive anomaly is recorded at Sm.

7.4 Establishing volcanic signatures using multi element diagrams

The previous section presented the new trace and rare earth data collected via XRF, IP and LA-ICP-MS for the volcanic systems Torfajökull, Askja, Katla, Öræfajökull and Hekla. The following section will investigate whether the new data can be used to establish definitive geochemical signatures or fingerprints for each of the five volcanic systems studied.

Figures 7.2 – 7.16 are multi element and rare earth element diagrams for the five named volcanic systems showing averaged data collected by LA-ICP-MS and IP. Data on the multi element diagrams are normalised to Bulk Silicate Earth (BSE) while the rare earth element plots of normalised to Chondrite as defined by Sun and McDonough (1995). The coloured fields represent the spread of data collected for each volcanic system. Figures 7.17 and 7.18 are averaged representations of the data sets collected by LA-ICP-MS for each volcanic system.

The multi element diagram (Fig. 7.17) is a plot of the averaged overall LA-ICP-MS data values for each system. The plot indicates that all five volcanic systems show the same overall trend: shallow negatively dipping pattern highlighting a higher concentration of incompatible elements than compatible elements. Each volcano also shows pronounced negative Ba, Sr, P and Ti anomalies. The rare earth element diagram (Fig. 7.18) is a plot of the averaged overall LA-ICP-MS data values for each system. The data plotted mirrors the trace element trend with each volcanic system demonstrating a shallowly dipping negative trend indicating a higher concentration of light rare earth elements (LREE) than heavy rare earth elements (HREE). Each data set indicates a negative Eu anomaly. The common characteristics highlighted by the plots are the result of a shared tectonic setting for magma generation (i.e interaction of an oceanic spreading centre with an active mantle plume) and similar fractional crystallisation and assimilation processes.

Despite the common trends shared by each volcanic system, there are subtle geochemical variations between the data sets in Figures 7.17 and 7.18:

- The Torfajökull volcanic system has the highest concentrations of the incompatible elements Rb – Ce as well as the highest concentrations in the lightest rare earth elements La and Ce.

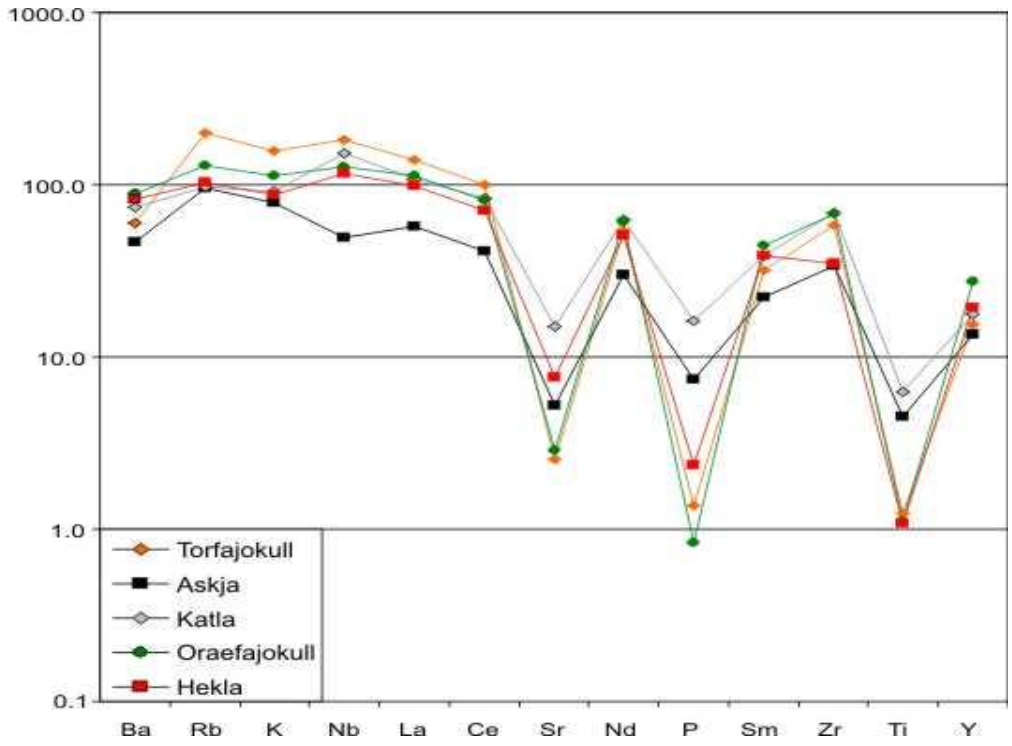

Figure 7.17: Multi element diagram of the averaged major element data for each system collected via IP and LA-ICP-MS. Data is normalised to bulk silicate earth (BSE) using the values in McDonough and Sun (1995). Each volcanic system shows individual characteristics e.g. Askja shows lower concentrations of Nb, La and Ce; Torfajökull shows higher concentrations of Rb – Ce; Katla shows the highest concentrations of Sr, P and Ti, while Öræfajökull shows the lowest. Hekla is notable in that it shows no obvious individual geochemical characteristics.

- The Askja volcanic system consistently shows the lowest concentration of incompatible and rare earth elements in particular Nb, La, Ce, Pr, Nd and Sm. Askja data contains the negative Sr, P and Ti anomalies recorded for all systems, however the Askja values show much smaller negative values that the Torfajökull, Öræfajökull and Hekla volcanic systems.
- The Katla volcanic system has the smallest negative Sr, P, Ti and Eu anomalies of the five systems.
- The Öræfajökull volcanic system shows high concentrations of incompatible elements and has both the highest and lowest extremes of the compatible elements, in particular P, Zr and Y. The system contains the highest concentrations of HREE of all the systems.
- The Hekla volcanic system is identifiable as it does not show distinctive

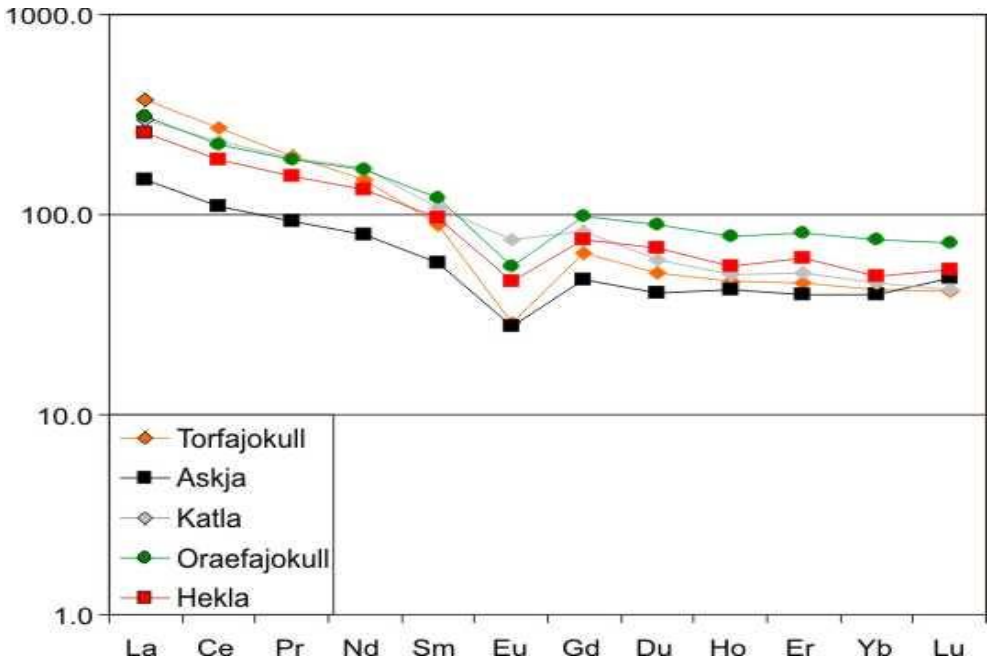

Figure 7.18: Rare earth multi element diagram of the averaged major element data for each system collected via IP and LA-ICP-MS. Data is normalised to chondrite using the values in McDonough and Sun (1995). Each volcanic system shows individual characteristics e.g. Askja shows the lowest concentrations of all elements with the exclusion of Lu; Torfajökull shows the highest concentrations of La – Ce; Katla shows the highest concentration of Eu; while Öræfajökull shows the highest concentrations of Gd – Lu. Hekla is notable in that it shows no obvious individual geochemical characteristics.

geochemistry. The other volcanic systems in this study are recognised by their notable geochemical characteristics. Therefore the absence of such features for the Hekla volcanic system allows for its identification following the initial eliminating of other volcanic systems.

Although only minor, such geochemical variations can be manipulated to allow for identification and discrimination of the individual volcanic systems discussed in this chapter. Figure 7.19 is a series of bivariate plots using the trace and rare earth element data collected by LA-ICP-MS to identify the afore mentioned systems. LA-ICP-MS data has been preferentially used as the analytical technique as it provides more analyses per sample than the IP technique. Once a volcanic system is identified, it is not incorporated into the following plots. This allows for a straightforward scheme for discriminating between data sets to establish the provenance of tephra layers for this study.

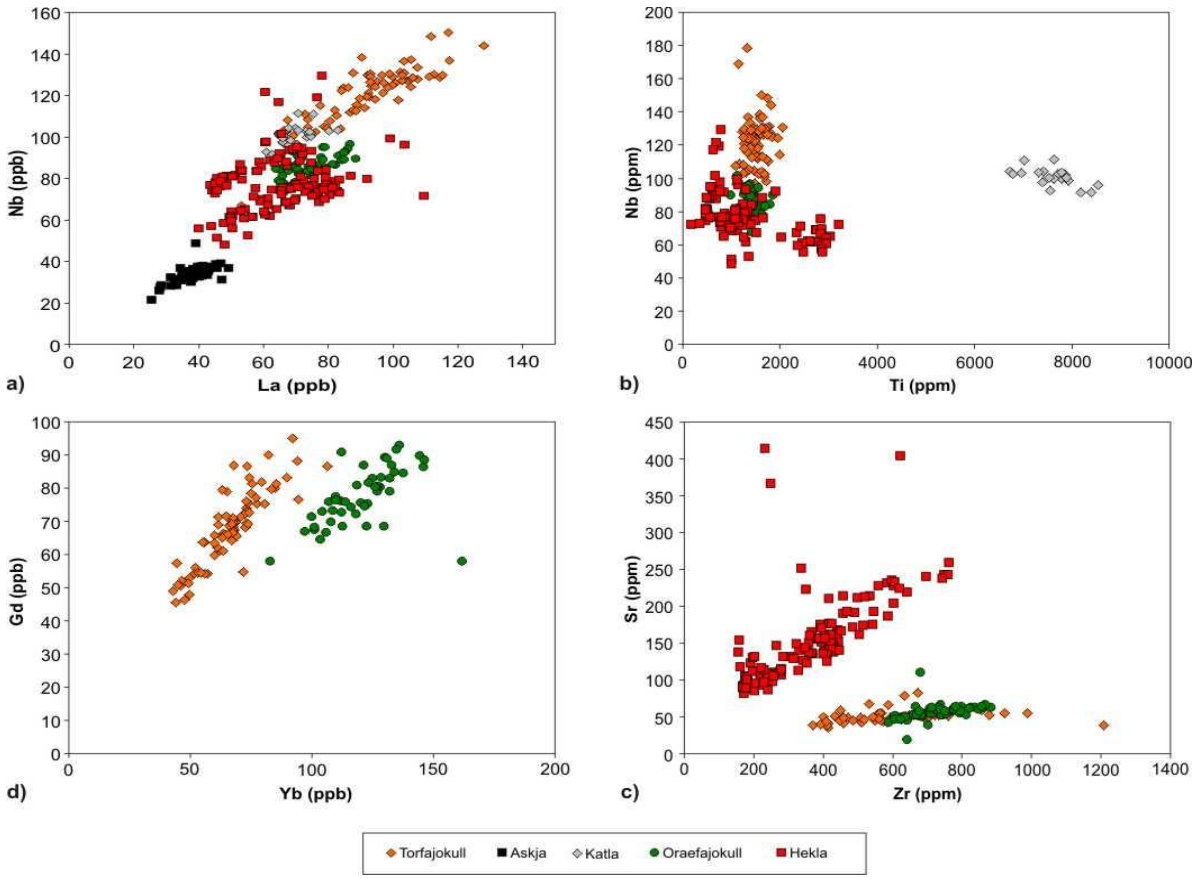

Fig. 7.19: Bivariate plots of trace and rare earth element combinations for the five volcanic systems. a) Plotting La against Nb separates the Askja data set from the other systems. b) Plotting Ti and Nb concentrations segregates the Katla data set from the other systems. c) Plotting Sr and Zr values allows for segregation of the Hekla data set from the other volcanic systems. d) The Torfajökull and Öræfajökull data sets can be distinguished by their different heave rare earth element patterns, in this case Gd and Yb.

Fig. 7.19a highlights the lower concentrations of both La and Nb in the Askja data set compared with that of the other volcanic systems. Fig 7.19b reveals significantly higher concentrations of Ti in the Katla volcanic than the remaining systems. Figure 7.19c highlights high concentrations of Sr in the tephra layers of the Hekla volcanic system. Figure 7.19d allows for separation of the final two volcanic systems Torfajökull and Öræfajökull on the basis of their differing heavy rare earth element concentrations, in particular Yb and Gd.

Discriminating between the volcanic systems is simple once geochemical variations have been highlighted. By initially plotting multi element diagrams, the individual fingerprint of a system can be identified and minor elemental variations allows for a rapid identification and discrimination of tephra provenance. Incorporation of multi element plots also eliminates the need to draw all possible elemental bivariate combinations in order to establish a systematic methodology as in Chapters 5 and 6. The multi element and rare earth element plots can also be used to infer a great deal about each volcanic system e.g. tectonic setting, depth of magma generation and identification of phenocryst phases (see Chapter 8: Discussion). However, the collection of trace and rare earth element data from the glass phase of tephra shards via IP or LA-ICP-MS is an expensive and destructive process. With particular reference to LA-ICP-MS, data must be processed and normalised to an internal standard, typically grain by grain concentrations of SiO_2 which must be collected by electron microprobe prior to analyses.

As in chapter 5, the work discussed in this section focuses solely onto five of Iceland's active volcanic systems. The Torfajökull, Askja, Katla, Öræfajökull and Hekla volcanic systems are studied as they are the most prolific producers of silicic magma in Iceland. Tephra layers from these volcanic systems have been selected for trace element analyses as they have typically formed the basis for tephrochronology studies across the North Atlantic region. Of the remaining volcanic systems, Snæfellsjökull and Eyjafjallajökull are noteworthy. These systems are known to have erupted evolved material during the Holocene period with chemistries ranging from andesite – dacite – rhyolite (Larsen *et al*. 1999, 2002). Both systems were included into the work in Chapter 5 as major element data was available from reliable sources. However, the systems have been excluded from this study as at present, no trace or rare earth element data has been published for either system, and undertaking such analyses was outside the scope of this project. Inclusion of data from the Snæfellsjökull and Eyjafjallajökull volcanic systems may alter the final detail of the method for identification and discrimination presented in Figure 7.19. The underlying theory however remains the same and can be adapted as more extensive data sets become available.

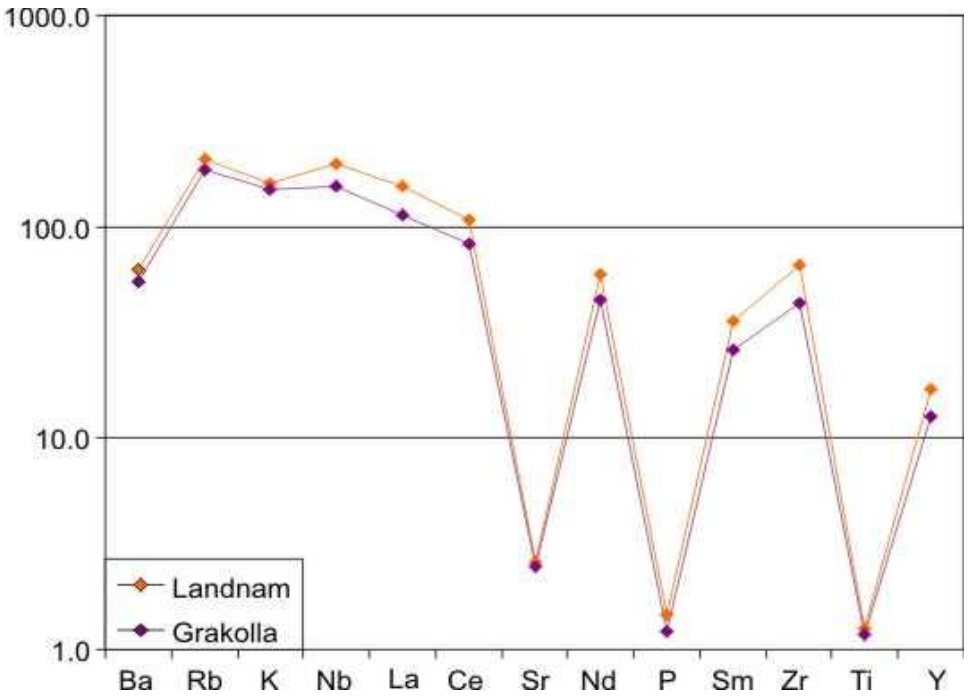

Figure 7.20: Multi element diagram of the averaged major element data for the silicic component of the Landnám and Grákolla tephra layers collected via LA-ICP-MS. Data is normalised to bulk silicate earth (BSE) using the values in McDonough and Sun (1995). Each tephra layer shows specific individual characteristics e.g. Landnám shows the highest concentrations of all elements while the Grákolla tephra layer shows consistently lower concentrations of all elements.

It should also be noted that figures 7.17 – 7.19 have focused onto the most evolved components of each system. This is particularly important for the Hekla volcanic system, which is defined by its five largest eruptions H1104, H3, HSelsund, H4 and H5. The smaller less evolved eruptions H-ABC-MN-XYZ are not included. The larger eruptions are taken as representative of the highest silica phase of this system and is in agreement with the other systems. The only exception is the Katla system which is included despite its typically andesitic eruptions and absence of large-scale rhyolitic eruptions during the Holocene. Further work should focus on fingerprinting the andesitic to dacitic components of every Icelandic volcanic system.

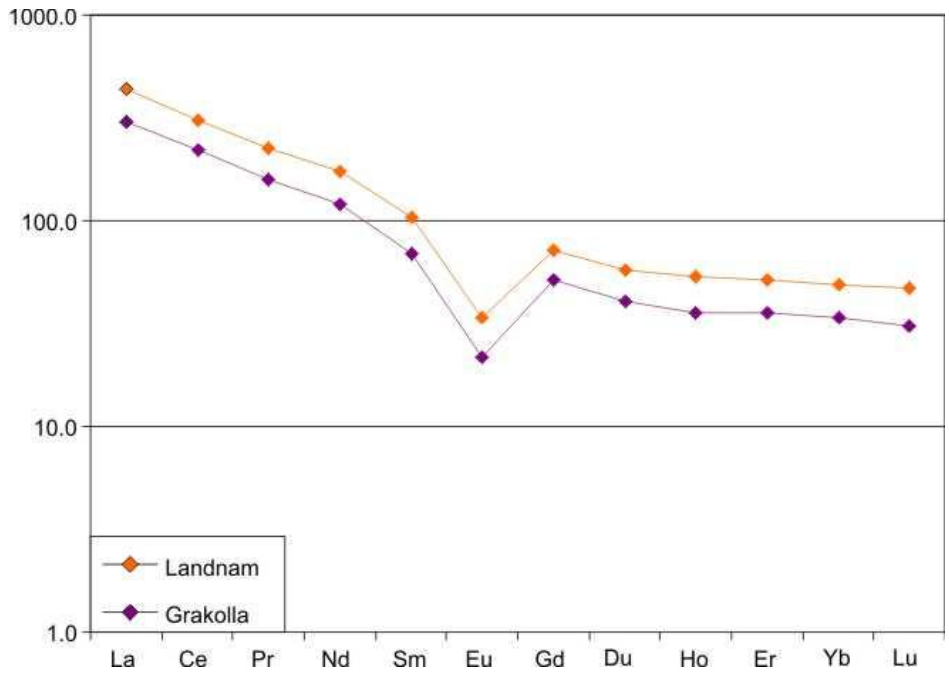

Figure 7.21: Rare earth multi element diagram of the averaged major element data for the silicic component of the Landnám and Grákolla tephra layers collected via LA-ICP-MS. Data is normalised chondrite using the values in McDonough and Sun (1995). Each tephra layer shows specific individual characteristics e.g. Landnám shows the highest concentrations of all elements while the Grákolla tephra layer shows consistently lower concentrations of all elements.

7.5 Discrimination of tephra layers sourced from within the same system using trace and rare earth element data.

Section 7.5 presented a method for discriminating between volcanic sources using trace and rare earth elements. The following section develops on this work by investigating whether tephra layers sourced within the same volcanic system can be discriminated by the application of trace and rare earth element data. The focus is tephra layers sourced from the Torfajökull (*silicic component of the Landnám and Grákolla*), Katla (*Silk UN and Silk LN*) and Hekla (*H1104, H3, HSelsund, H4, H5, HA, HB, HC, HM, HN, HX, HY and HZ*) volcanic systems. The Askja and Öræfajökull volcanic systems are not discussed as both are represented solely by one tephra layer. The data used are the LA-ICP-MS and IP presented in section 7.3. Each of the three systems will be dealt with separately in the following sections.

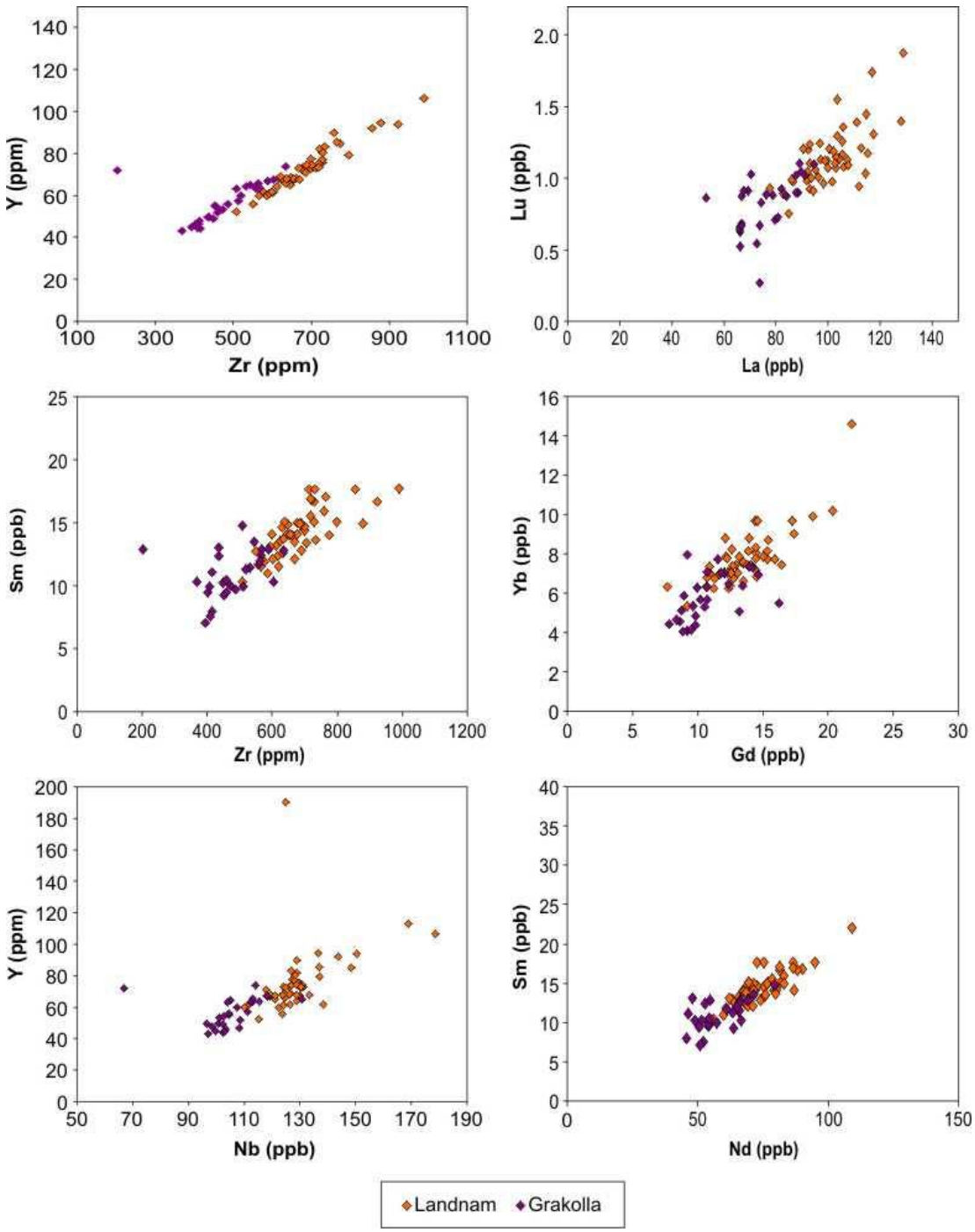

Fig. 7.22: Bivariate plots of trace and rare earth element combinations for the silicic component of the Landnám and Grákolla tephra layers collected via ICP-MS.

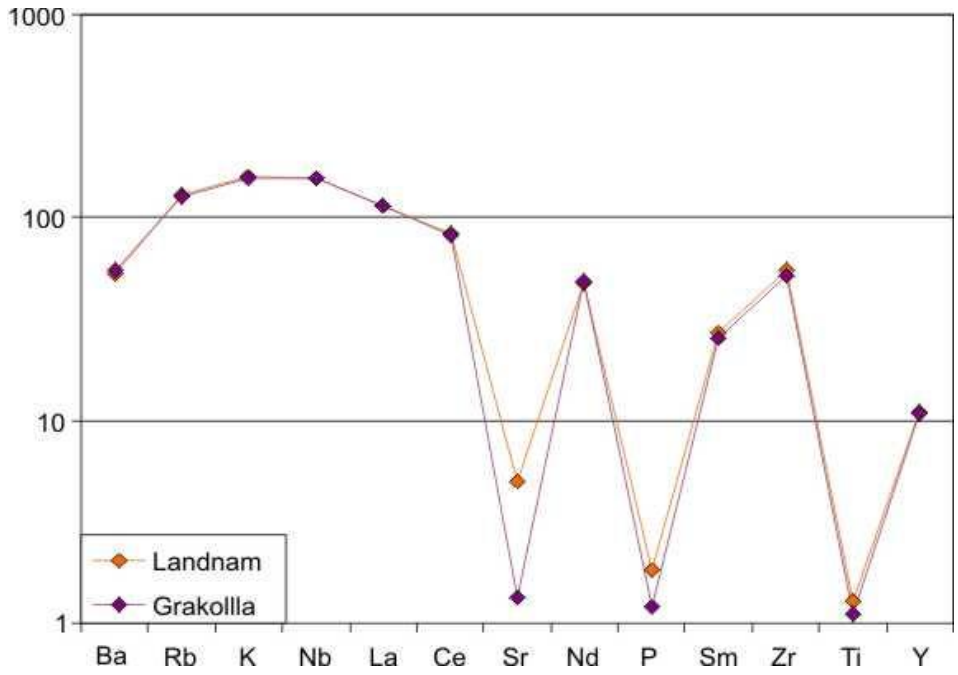

Figure 7.23: Multi element diagram of the averaged major element data for the silicic component of the Landnám and Grákolla tephra layers collected via IP. Data is normalised to bulk silicate earth (BSE) using the values in McDonough and Sun (1995). Each tephra layer shows specific individual characteristics e.g. Landnám shows the highest concentrations of Sr, P, Sm, Zr and Ti, while the Grákolla tephra layer shows consistently lower concentrations in the same elements.

- Torfajökull: The Torfajökull volcanic system is represented by two major Holocene tephra layers, the silicic component of the Landnám (871 +/- 2 AD) and Grákolla (150 AD) tephra layers. The major element chemistry shown by the tephra layers is identical. Figures 7.20 and 7.21 are averaged multi element and rare earth element diagrams of the LA-ICP-MS data for the tephra layers, while figures 7.23 and 7.24 are the averaged IP data. Data on the multi element diagrams are normalised to Bulk Silicate Earth (BSE) while the rare earth element plots of normalised to Chondrite as defined by Sun and McDonough (1995).

The multi element diagrams (Figs. 7.20 and 7.21) indicate that both tephra layers show the same overall trends: shallow negatively dipping from Ba to Y with a positive Zr anomaly and negative anomalies at Ba, Sr, P and Ti. The LA-ICP-MS data shows a small negative K anomaly that is not highlighted in the IP data set. The REE patterns also confirm a negative trend from light rare earth elements (LREE) to heavy rare earth elements (HREE) with a

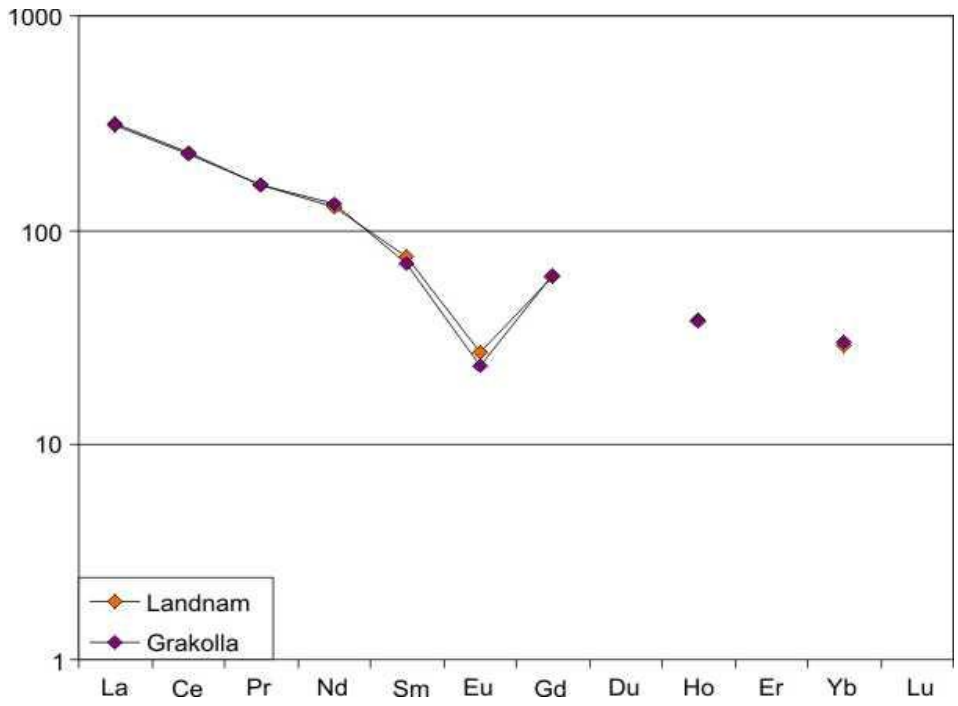

Figure 7.24: Rare earth multi element diagram of the averaged major element data for the silicic component of the Landnám and Grákolla tephra layers collected via IP. Data is normalised to chondrite using the values in McDonough and Sun (1995). Overall rare earth geochemistry of both tephra layers is very similar; however Landnám shows the highest concentrations of all Sm and Eu.

consistent negative Eu anomaly. The shared trends are expected as they represent the large-scale tectonic and magmatic settings affecting the Torfajökull volcanic system.

Despite the common trends shared by both tephra layers, there are subtle geochemical variations between the data sets in Figures 7.20 – 7.21 and 7.23 – 7.24:

- The silicic component of the Landnám tephra layer is consistently higher in all REE and the majority of the trace elements in the LA-ICP-MS data set with the exception of Sr.
- The IP data indicates that both tephra layers are much closer in composition with clear differences only notable at Sr, P and Ti and minor variations at Sm, Eu and Zr.

Although only minor, such geochemical variations can be manipulated to allow for identification and discrimination between the tephra layers. Figures 7.22 and 7.25 are a series of bivariate plots using the trace and rare earth element data collected by LA-ICP-MS

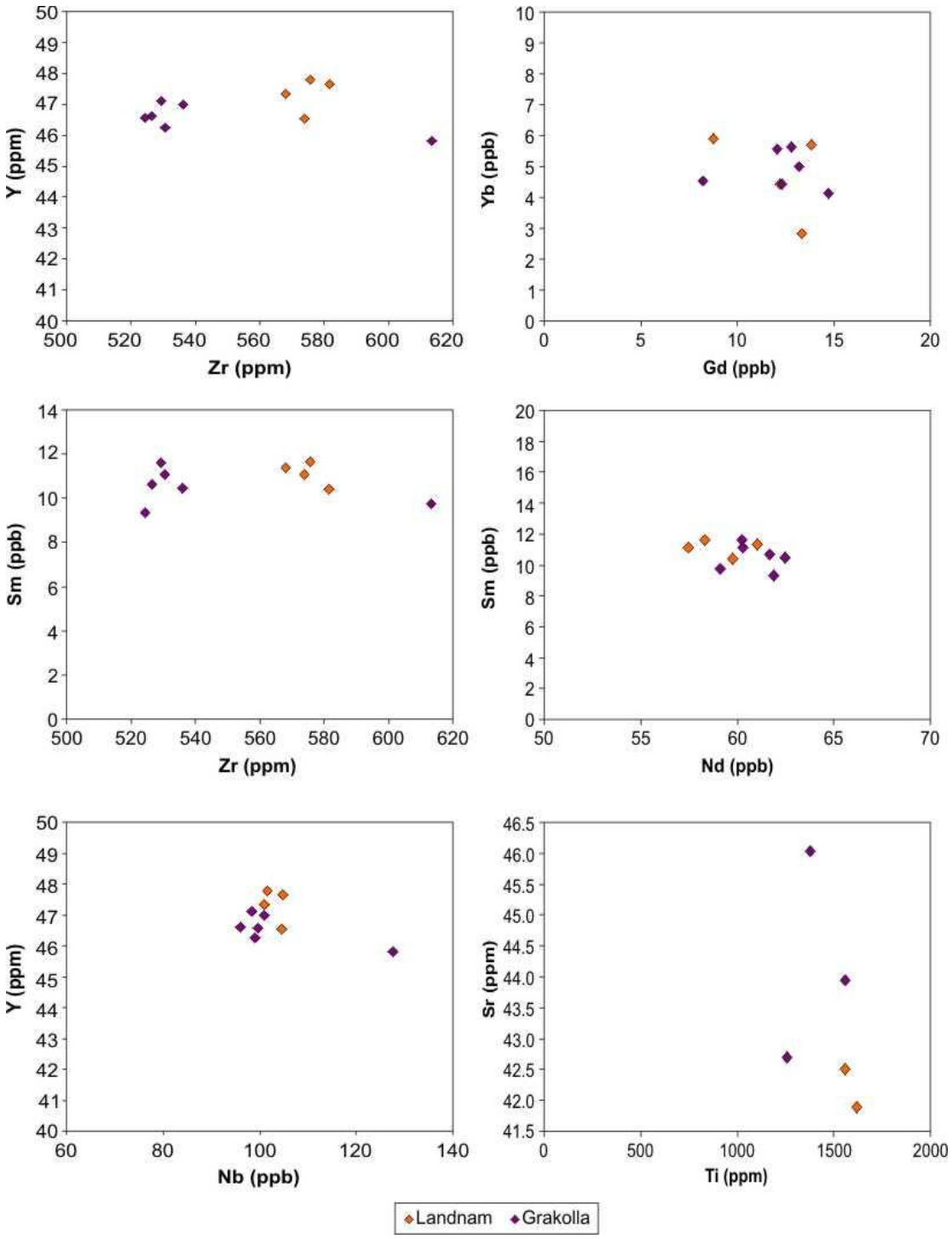

Fig. 7.25: Bivariate plots of trace and rare earth element combinations for silicic component of the Landnám and Grákolla tephra layers collected via IP. The tephra layers show substantially different geochemistry to allow for tephra discrimination, however some data overlap remains.

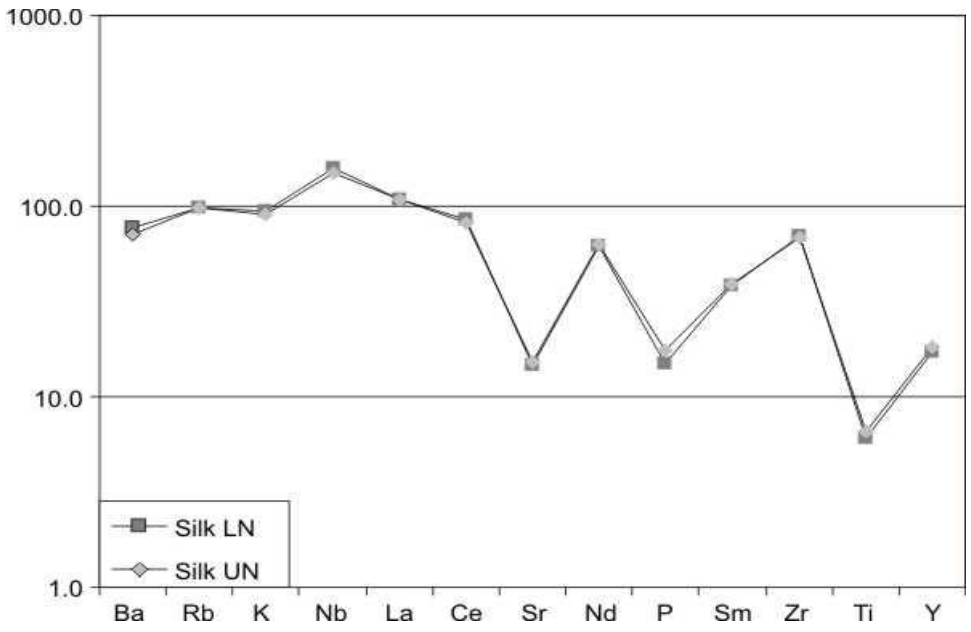

Figure 7.26: Multi element diagram of the averaged major element data for the Silk UN and Silk LN tephra layers collected via LA-ICP-MS. Data is normalised to bulk silicate earth (BSE) using the values in McDonough and Sun (1995). Both tephra layer near-identical geochemical signatures.

and IP to identify the tephra layers. Elements were assigned to the plots based on the minor variations highlighted in the multi element diagrams. Those deemed most useful for the discrimination process in this situation were Zr, Y, Lu, La, Sm, Gd, Yb Nb, Nd, Sr and Ti. Plotting these elements allows for reasonable discrimination between the tephra layers, however there still remains a minor data overlap.

The work discussed in this section focuses solely on the silicic component of the Landnám and Grákolla tephra layers; however these are not the only products to have been erupted from the Torfajökull volcanic system during the Holocene. The system has also produced a number of basaltic eruptions of varying explosivity. The silicic component of the Landnám and Grákolla eruptions have been selected for this study as they are sourced from large-scale evolved explosive eruptions and have potential for transportation and deposition across large areas of the North Atlantic. The Landnám tephra has been identified at many sites (see Chapter 2) and is used as an important time parallel marker horizon in tephrochronology studies (e.g. Wastegård *et al*. 2003). At present, the Grákolla tephra layer has not been identified outside of Iceland, however its identical major element chemistry may have resulted in its mis-identification as the younger Landnám tephra (see Chapter 8).

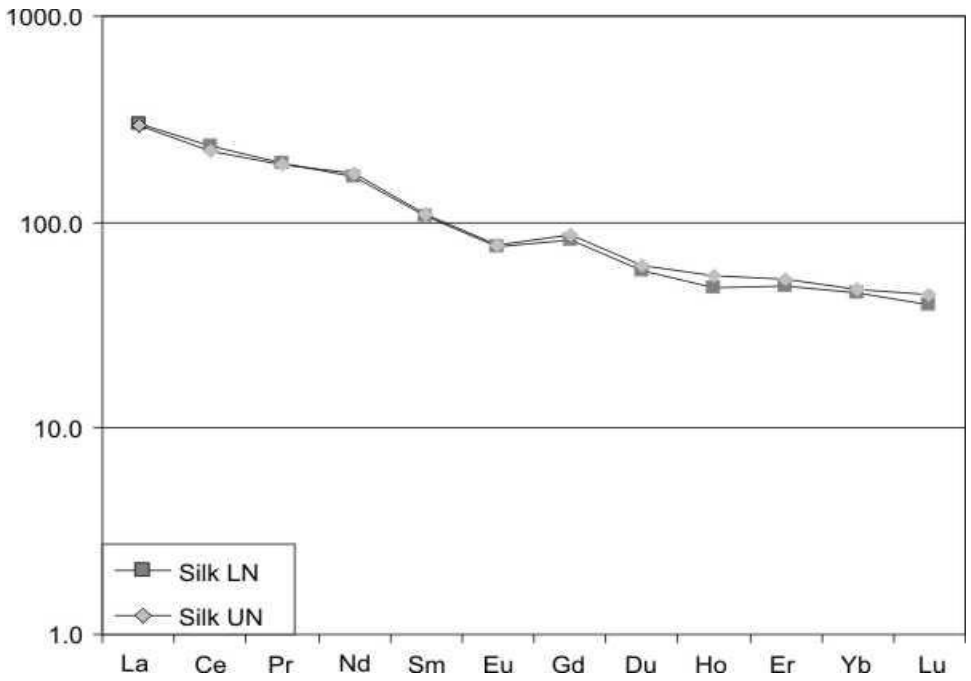

Figure 7.27: Rare earth multi element diagram of the averaged major element data for the Silk UN and Silk LN tephra layers collected via LA-ICP-MS. Data is normalised to chondrite using the values in McDonough and Sun (1995). Both Katla tephra layers show near-identical rare earth element geochemical signatures.

Katla: The Katla volcanic system is represented here by two tephra layers, the Silk UN (2660 BP) and LN (3440 BP). Figures 7.26 and 7.27 are averaged multi element and rare earth element diagrams of the LA-ICP-MS data for the tephra layers, while figures 7.29 and 7.30

are the averaged IP data. Data on the multi element diagrams are normalised to Bulk Silicate Earth (BSE) while the rare earth element plots of normalised to Chondrite as defined by Sun and McDonough (1995).

The multi element diagrams (Figs. 7.26 and 7.27) indicate that both tephra layers show the same overall trends: shallow negatively dipping from Nb to Y. Ba, Rb and K are lower than expected however this may be due to weathering and alteration of the samples. The tephra layers show a positive Zr anomaly and negative anomalies at Sr, P and Ti. The REE patterns also confirm a negative trend from light rare earth elements (LREE) to heavy rare earth elements (HREE) with a minor negative Eu anomaly. The shared trends are expected as they represent the large-scale tectonic and magmatic settings affecting the Katla volcanic system.

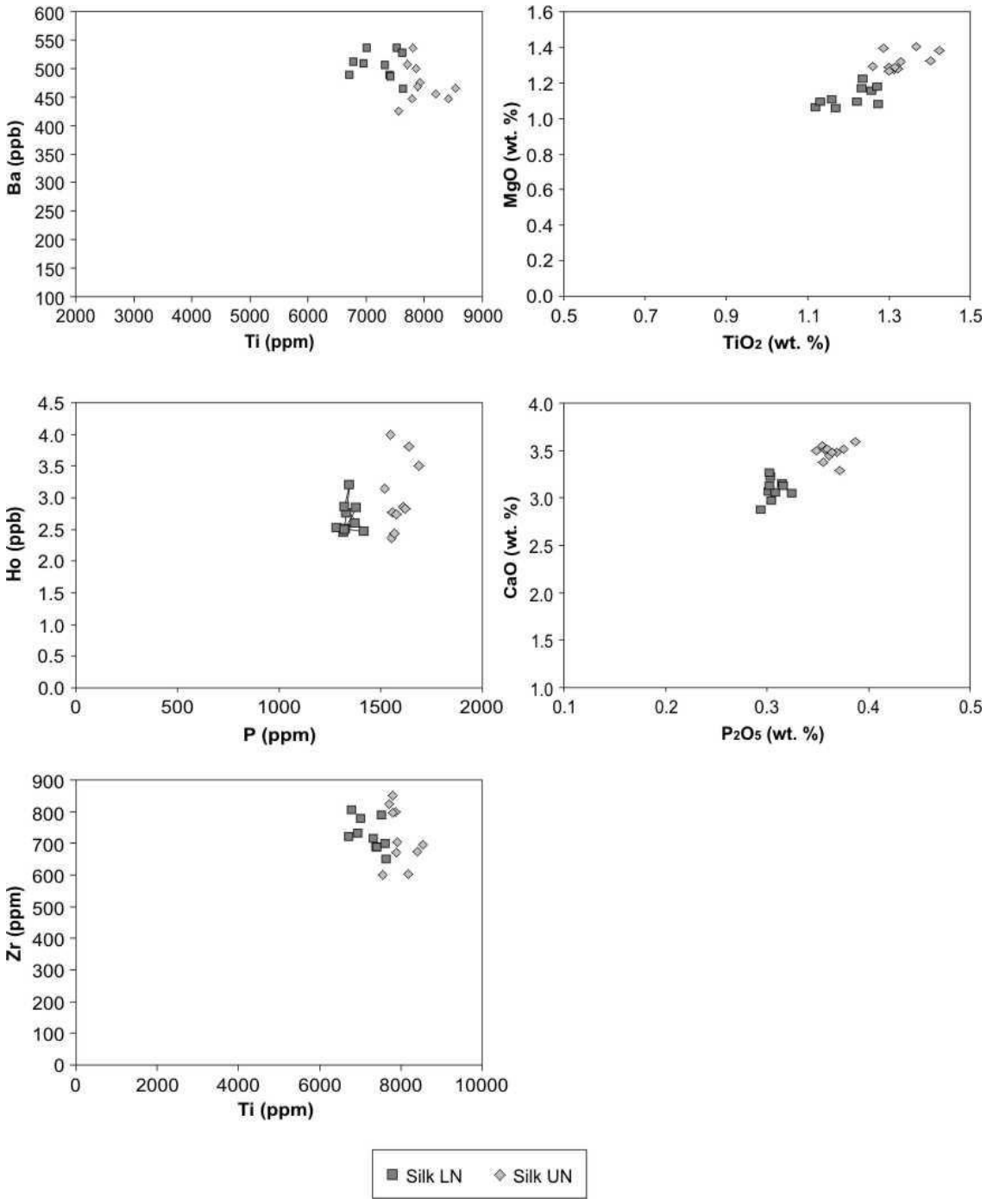

Fig. 7.28: Bivariate plots of trace and rare earth element combinations for the Silk UN and Silk LN tephra layers collected via ICP-MS. Bivariate plots of the Katla tephras indicate that trace and rare earth element chemistry cannot be utilised to discriminate between the tephra layers. The plots do however highlight the use of major elements such as P Ti in the discrimination of the tephra layers.

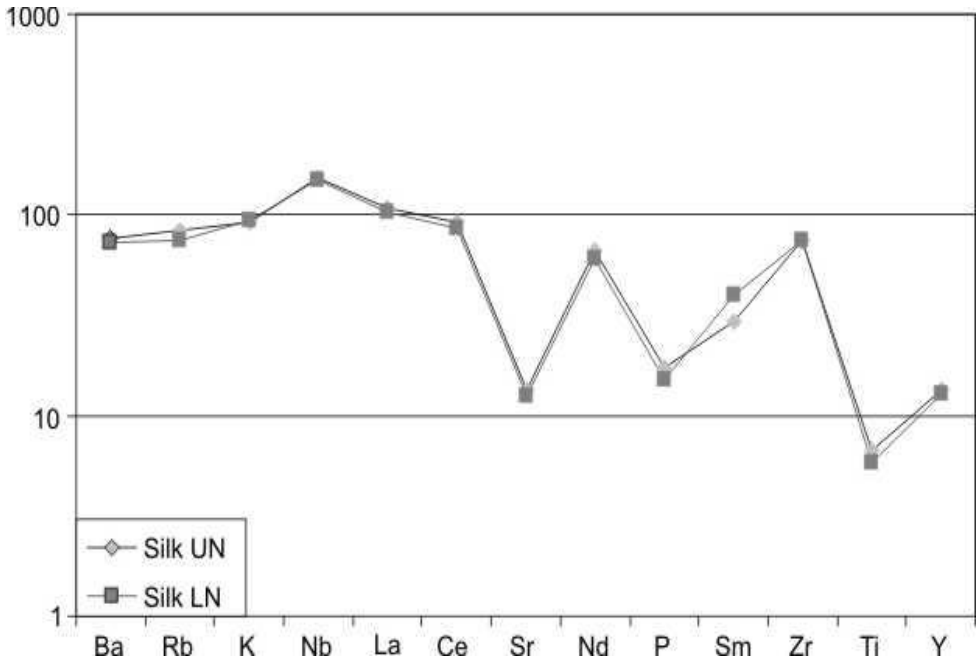

Figure 7.29 Multi element diagram of the averaged major element data for the Silk UN and Silk LN tephra layers collected via IP. Data is normalised to bulk silicate earth (BSE) using the values in McDonough and Sun (1995). Both Katla tephra layers show near-identical rare earth element geochemical signatures.

The data sets for both tephra layers are tightly clustered showing minimal geochemical variations between the layers. The few minor differences are highlighted in Figures 7.26 – 7.27 and 7.29 – 7.30:

- The Silk LN tephra layer shows slightly higher concentrations of Ba and Nb and slightly lower concentrations in P, Ho and Lu when considering the LA-ICP-MS data set.
- The Silk LN tephra layer shows a slightly higher concentration of Sm and lower concentrations of Rb, P and Ti when considering the IP data.

The geochemical variations for the Katla tephra layers are very subtle; however such geochemical variations can still be used to discriminate between the tephra layers. Figures 7.28 and 7.31 are a series of bivariate plots using the trace and rare earth element data collected by LA-ICP-MS and IP to identify the tephra layers. Elements were assigned to the plots based on the minor variations highlighted in the multi element diagrams. Those deemed most useful for the discrimination process in this situation were Zr, Ti, Ba and P. Figure 7.28

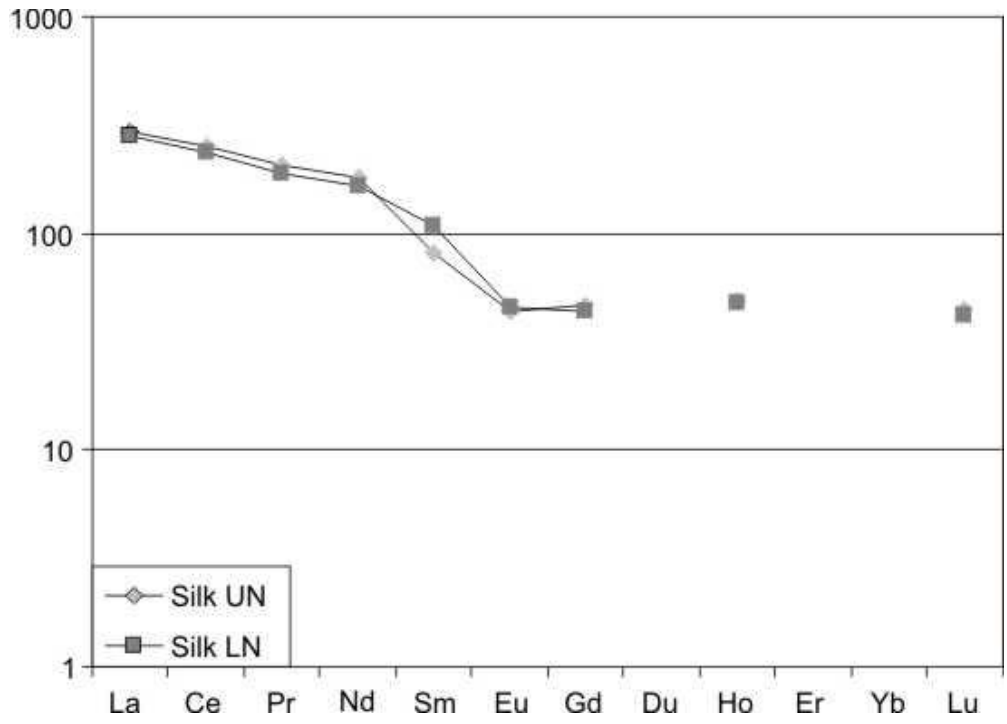

Figure 7.30: Rare earth multi element diagram of the averaged major element data for the Silk UN and Silk LN tephra layers collected via IP. Data is normalised to chondrite using the values in McDonough and Sun (1995). Both Katla tephra layers show near-identical rare earth element geochemical signatures.

also contains two plots based on major element chemistry. These plots indicate that discrimination of the Silk LN and UN tephra layers is possible using major element compositions indicating that discrimination by trace elements is redundant.

The work discussed in this section focuses solely on the Silk LN and UN tephra layers; however these are not the only products to have been erupted from the Katla volcanic system during the Holocene. The system has produced two other Silk Needle tephra layers and sequence of intermediate Silk tephra layers. The system has also erupted a number of basaltic eruptions. The Silk LN and UN eruptions have been selected for this study as they are sourced from medium-sized explosive eruptions and have potential to be important marker horizons in the Icelandic tephra stratigraphy with regards to environmental change and glacier fluctuations. At present, none of the Silk tephra layers have been identified outside of Iceland, however as micro-tephra retrieval techniques improve they may become more important.

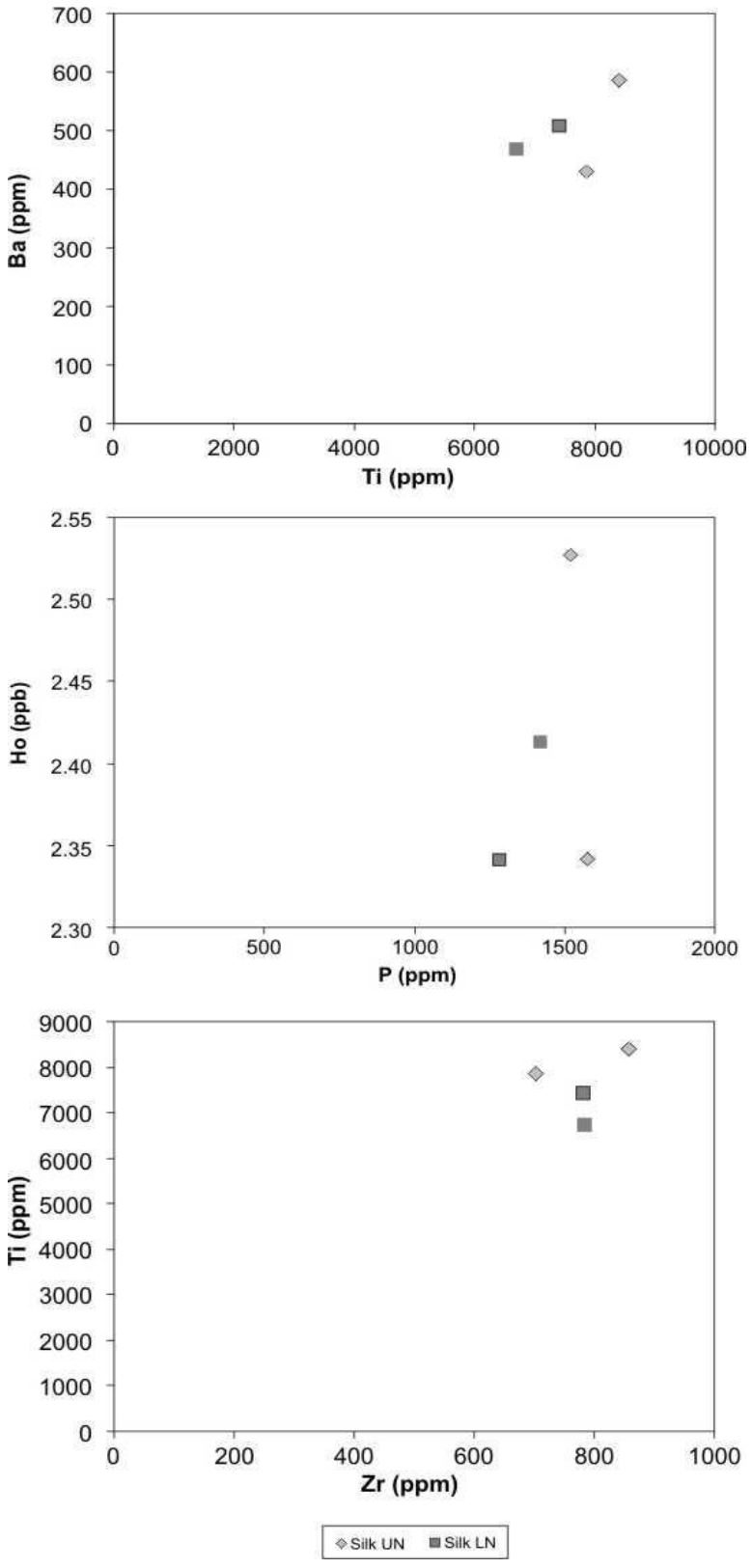

Fig. 7.31: Bivariate plots of trace and rare earth element combinations for Silk UN and Silk LN tephra layers collected via IP. Bivariate plots of the Katla tephras indicate that trace and rare earth element chemistry cannot be utilised to discriminate between the tephra layers. The plots do however highlight the use of major elements such as P Ti in the discrimination of the tephra layers.

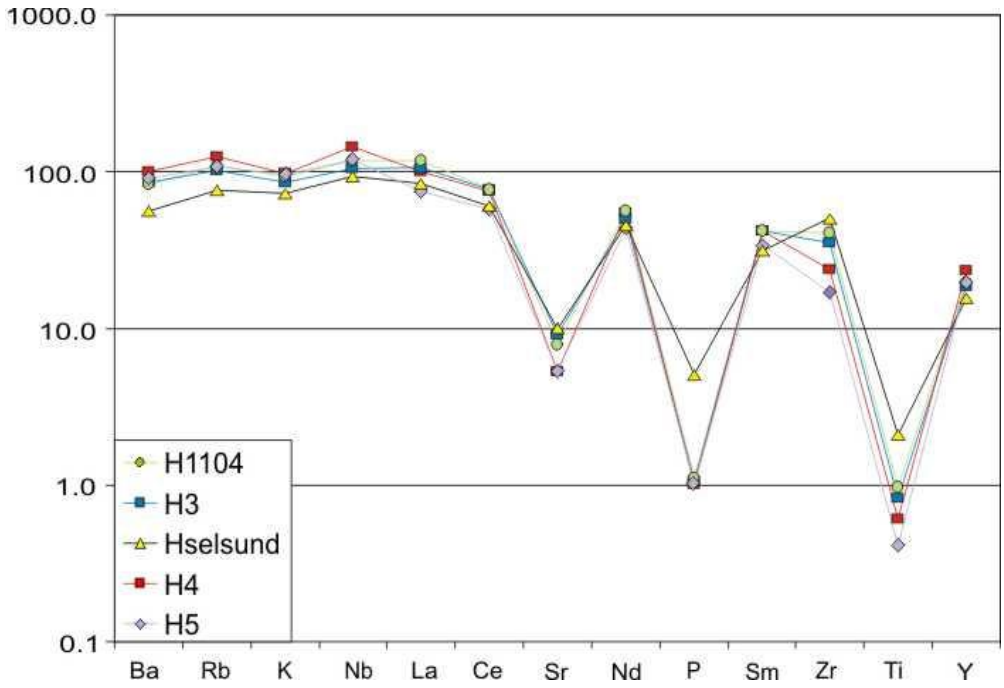

Figure 7.32: Multi element diagram of the averaged major element data for the Hekla silicic tephra layers collected via LA-ICP-MS. Data is normalised to bulk silicate earth (BSE) using the values in McDonough and Sun (1995). Each tephra layer shows specific individual characteristics e.g. H5 shows the lowest concentration of Ti; H4 shows the highest concentrations of Ba, Rb and Nb; HSelsund shows both the lowest concentrations of Ba – Nb, Y and the highest concentrations of P, Zr and Y; H3 and H1104 do now show individual characteristics which in itself can be manipulated for their identification.

Hekla: The Hekla volcanic system is represented by five major silicic and eight intermediate tephra layers: H1104 (846 BP), H3 (2980 BP), HSelsund, (3515 BP), H4 (4270 BP) and H5 (7125 BP); HA-HB-HC-HM-HN-HX-HY-HZ (1850 – 2800 BP). Figures 7.32 – 7.33 and 7.38 – 7.39 are averaged multi element and rare earth element diagrams of the LA-ICP-MS data for the tephra layers, while figures 7.35 – 7.36 are the averaged IP data. Data on the multi element diagrams are normalised to Bulk Silicate Earth (BSE) while the rare earth element plots of normalised to Chondrite as defined by Sun and McDonough (1995). The tephra layers have been separated into silicic (H1104, H3, HSelsund, H4 and H5) and intermediate (HA, HB, HC, HM, HN, HX, HY and HZ) compositional groups based on the work conducted in Chapter 6. There is limited IP data for the intermediate group due to limited equipment availability. The data is presented in Table 7.34 but is not incorporated into the following figures.

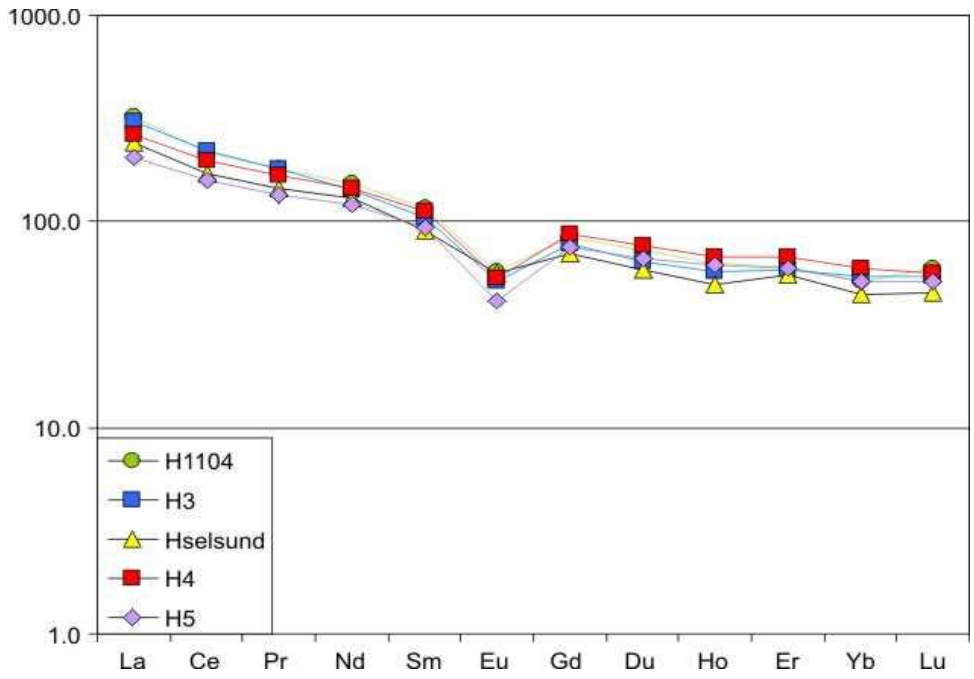

Figure 7.33: Rare earth multi element diagram of the averaged major element data for the Hekla silicic tephra layers collected via LA-ICP-MS. Data is normalised to chondrite using the values in McDonough and Sun (1995). Each tephra layer shows specific individual characteristics e.g. H5 shows the lowest concentration of La - Eu; H4 shows the highest concentrations of Gd - Yb; HSelsund shows both the lowest concentrations of Gd – Lu; H3 and H1104 show the highest concentrations of La and Ce.

The multi element diagrams (Figs. 7.32, 7.35 and 7.38.) indicate that each tephra layer shows the same overall trend: shallow negatively dipping from Ba to Y with a positive Zr anomaly and negative anomalies at Ba, Sr, P and Ti. The REE patterns confirm a negative trend from light rare earth elements (LREE) to heavy rare earth elements (HREE) with a consistent negative Eu anomaly. The shared trends are expected as they represent the large-scale tectonic and magmatic settings affecting the Hekla volcanic system.

Despite the common trends shared by tephra layers in both sub-groups, there are subtle geochemical variations between the data sets highlighted in Figures 3.32 – 7.33, 7.35 – 7.36 and 7.38 – 7.39:

- The LA-ICP-MS multi element data for the silicic group show that HSelsund has the lowest concentrations of Ba, Rb, K, Nb and Y and the highest concentrations of P, Zr and Ti. The H4 tephra layer has the highest Ba, Rb, Nb and Y concentrations. H4

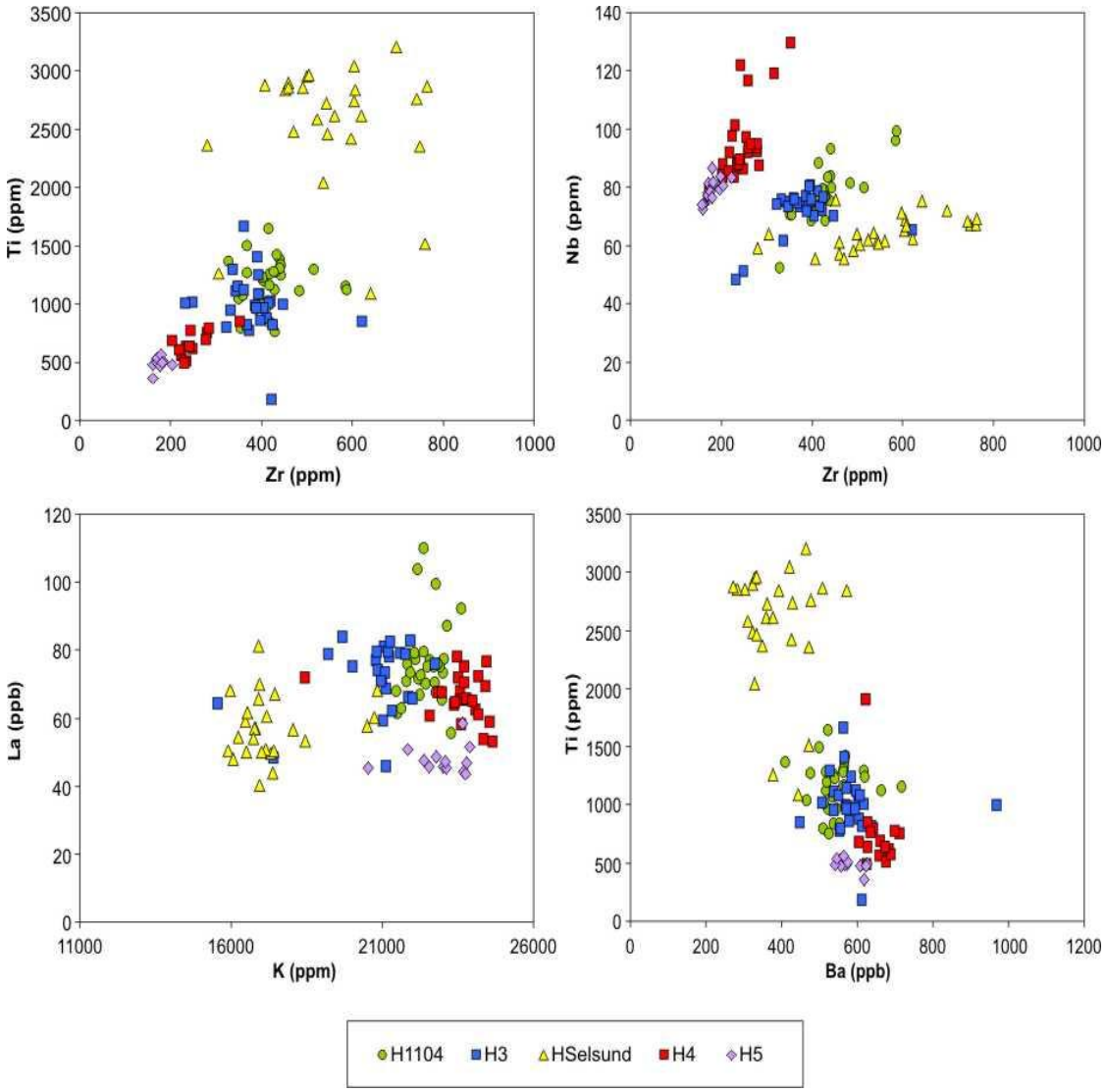

Fig. 7.34: Bivariate plots of trace and rare earth element combinations for the Hekla silicic tephra layers collected via ICP-MS. The tephra layers show substantially different geochemistry to allow for tephra discrimination, however some data overlap remains.

and H5 have the lowest values of Sr, P, Ti and Zr. The H3 and H1104 tephra layers are notable by the absence of any outstanding high or low elemental concentrations.

- The LA-ICP-MS rare earth element data for the silicic group shows that HSelsund has the lowest concentrations of the heavy rare earth elements (Gd – Lu) while H4 has the highest concentration of the same elements. H5 has the deepest Eu anomaly.
- The IP multi element data for the silicic group indicates that HSelsund has the lowest Ba and Rb concentrations as well as the highest Sr, P, Zr and Ti. He has the highest concentrations of the incompatible elements Ba – Nb. H4 and H5 have the

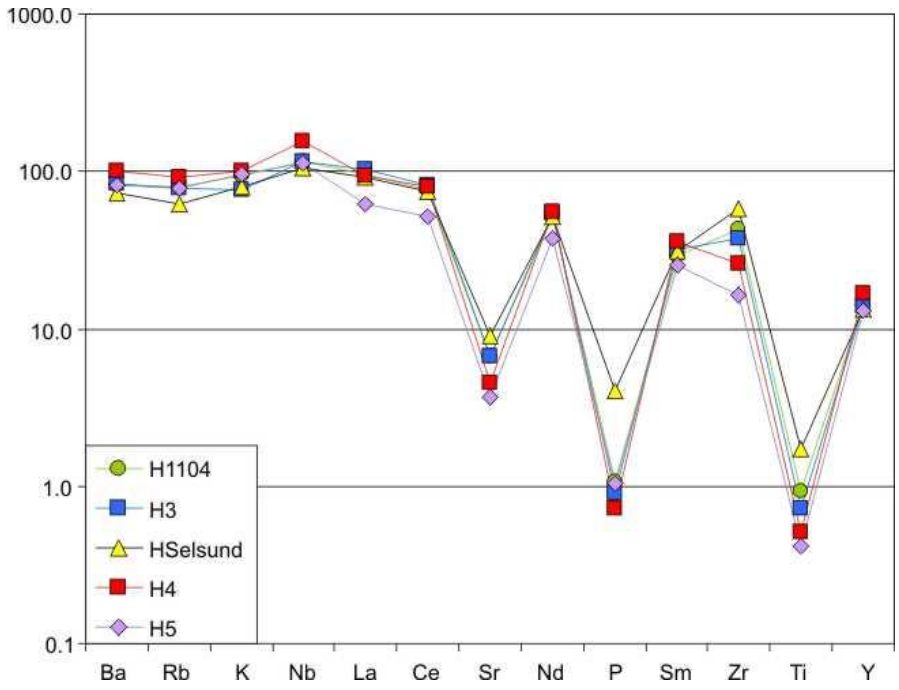

Figure 7.35 Multi element diagram of the averaged major element data for the Hekla silicic tephra layers collected via IP. Data is normalised to bulk silicate earth (BSE) using the values in McDonough and Sun (1995). Each tephra layer shows specific individual characteristics e.g. H5 shows the lowest concentration of La – Nd, Sm – Ti; H4 shows the highest concentrations of Ba – Nb, Nd, Sm, Y; HSelsund shows both the lowest concentrations of Ba and Rb, but the highest concentrations of P, Zr and Ti; H3 and H1104 show no major geochemical individualities.

lowest concentrations of Sr and Ti. H5 shows the lowest values for La, Ce and Zr.

- The IP rare earth element data for the silicic group shows that H5 has the lowest concentrations of light rare earth elements (La – Eu) and HSelsund has the shallowest Eu anomaly.
- The LA-IC-MS multi element data for the intermediate group suggests that HX contains the lowest concentrations of P and Ti, HM the highest Sm values and that HA and HB typically show the lowest concentrations for Ba, La, Ce, Nd, Sm, Y.
- The LA-ICP-MS rare earth element data for the intermediate group confirms that HM has the highest concentrations of Sm and that HA and HB generally show the lowest concentrations for most of the REE.

Figures 7.34 and 7.37 are a series of bivariate plots created for the Hekla tephra layers plotting the trace and rare earth element data collected by LA-ICP-MS and IP to identify and

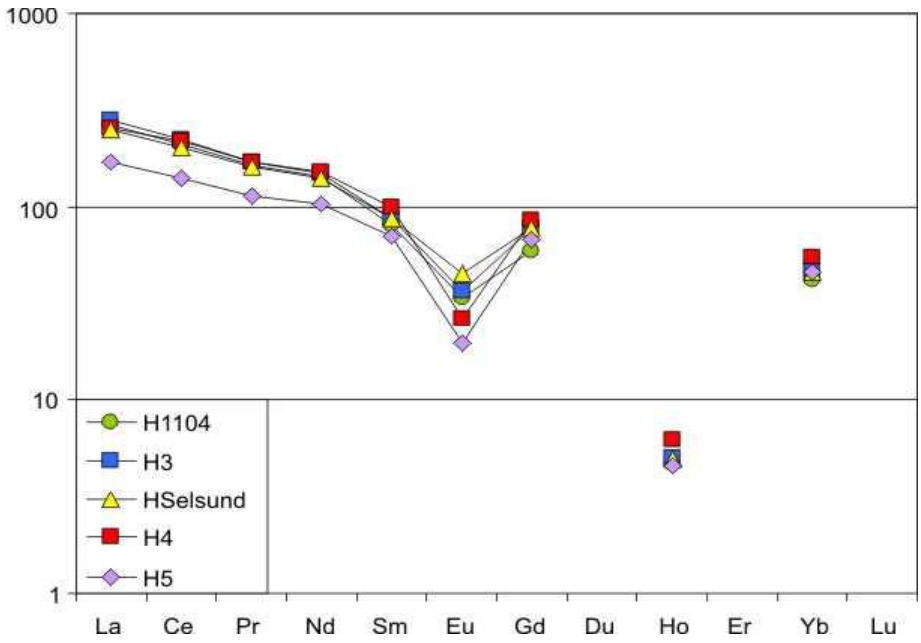

Figure 7.36: Rare earth multi element diagram of the averaged major element data for the Hekla silicic tephra layers collected via IP. Data is normalised to bulk silicate earth (BSE) using the values in McDonough and Sun (1995). Each tephra layer shows specific individual characteristics e.g. H5 shows the lowest concentration of La – Eu, Ho and Yb; H4 shows the highest concentrations of Pr – Sm, Gd, Ho and Yb, Y; HSelsund and H3 show no major geochemical individualities. H1104 shows the lowest concentrations of Gd and Yb.

discriminate between the tephra layers. Elements were assigned to the plots based on the minor variations highlighted in the multi element diagrams. Those deemed most useful for the discrimination process in this situation were Zr, Ti, Nb, K and Ba. When using major element chemistry, the silicic layers produce two distinct sub-groups: H4 – H5 and H1104 – H3 – HSelsund. The same groupings are also clear when plotting trace element data. H4 and H5 are easily separated by plotting La, Zr, Ti, Ba and Nb. HSelsund is identified easily by plotting K, Zr and Ti. H3 and H1104 remain geochemically similar and as established in Chapter 6, are only separated using K and to some extend Ti. There still however remains some data overlap between the two tephra layers.

Figure 7.40 is a series of bivariate plots created for the intermediate tephra layers created using trace and rare earth element data collected using LA-ICP-MS. Despite highlighting potential possible elemental variations that might lead to discrimination, the intermediate tephra layers show a consistent data overlap. Plotting P against Ti allowed for a very basic

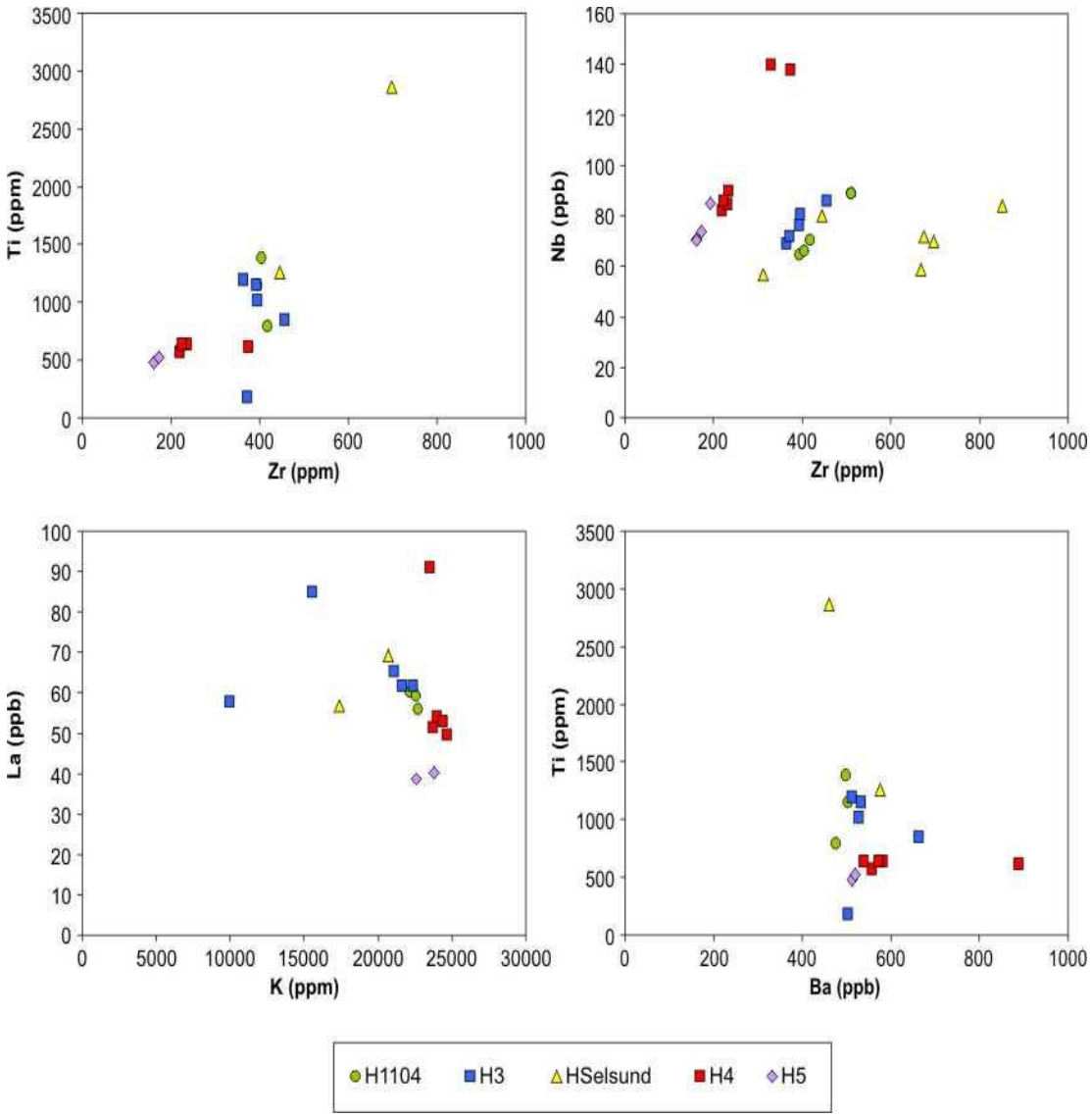

Fig. 7.37: Bivariate plots of trace and rare earth element combinations for Hekla silicic tephra layers collected via IP. The tephra layers show substantially different geochemistry to allow for tephra discrimination, however these calculations are based on very small data sets. Some data overlap also remains.

discrimination between the HA, HB and HC tephra layers however once the remaining tephra layers were included, they overlay the original discrimination.

The work discussed in this section focuses on thirteen Hekla eruptions; however these are not the only products to have been erupted from the system during the Holocene period. The

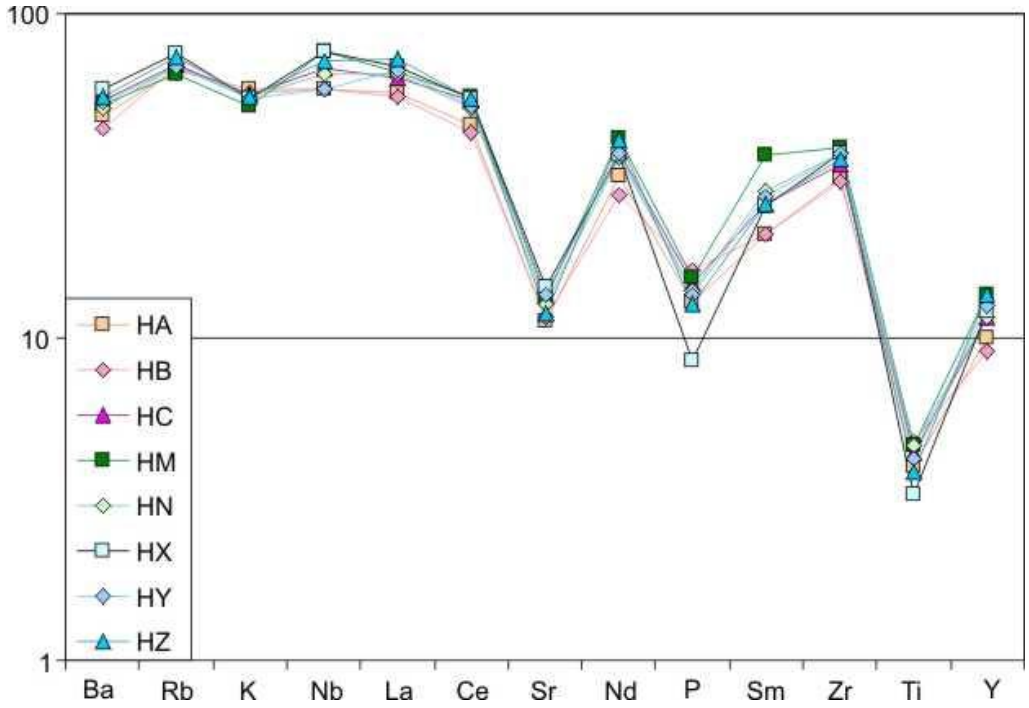

Figure 7.38: Multi element diagram of the averaged major element data for the Hekla intermediate tephra layers collected via LA-ICP-MS. Data is normalised to bulk silicate earth (BSE) using the values in McDonough and Sun (1995). The sequence of intermediate Hekla tephra layers do not show any substantial geochemical variation which might allow for their discrimination.

system has also produced a number of basaltic eruptions of varying explosivity. The silicic eruptions are studied as they are known to be useful marker horizons indentified across the North Atlantic region. The intermediate eruptions have been included as they are useful local marker horizons and may become more important as climate and oceanography-based tephrochronology studies focus research onto marine sedimentary cores sampled on the Icelandic shelf (see Chapter 8). Further work could focus onto geochemically characterising the post-H1104 tephra layers erupted from the Hekla volcano which are dominated by intermediate compositions.

It should also be noted that the figures in Section 7.5 have focused onto the most evolved components of each eruption. The high silica phases of each tephra layer are typically associated with the most explosive phases of an eruption and are therefore taken as representative of the material transported and deposited across North Atlantic region.

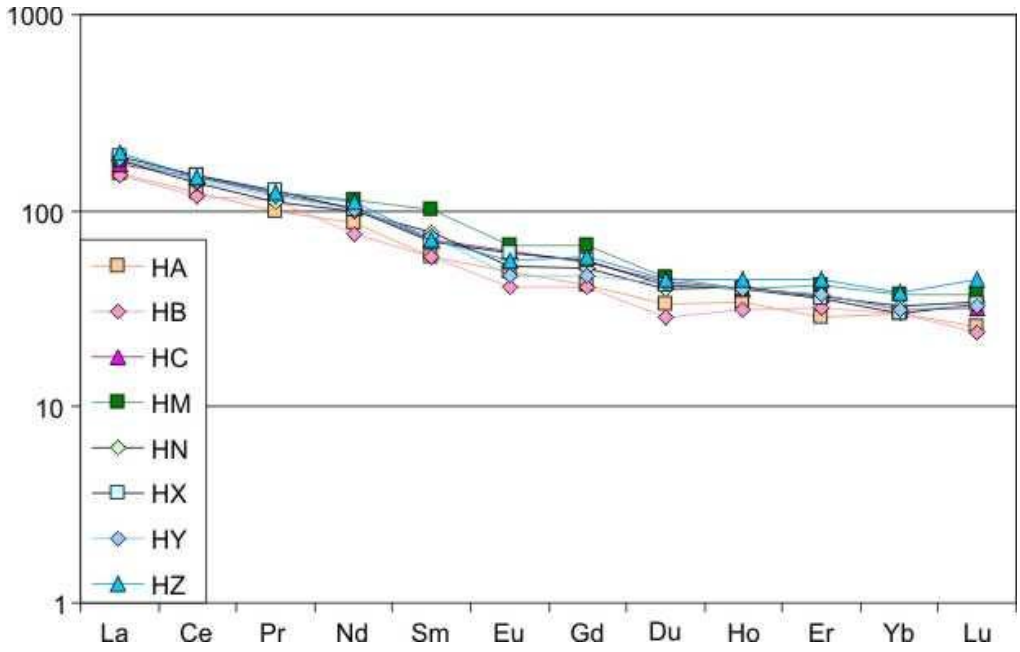

Figure 7.39: Rare earth multi element diagram of the averaged major element data for the Hekla intermediate tephra layers collected via LA-ICP-MS. Data is normalised to bulk silicate earth (BSE) using the values in McDonough and Sun (1995). The sequence of intermediate Hekla tephra layers do not show any substantial geochemical variation which might allow for their discrimination.

7.6 Summary

This chapter has presented the trace and rare earth element data for a suite of Icelandic Holocene tephra layers sourced from the Torfajökull, Askja, Katla, Öræfajökull and Hekla volcanic systems.

A formal framework for establishing tephra provenance using trace and rare earth element chemistry has been proposed. By initially plotting multi element diagrams for each volcanic system it is possible to identify individual geochemical signatures or fingerprints and to highlight any minor geochemical variations between sources. Any such minor geochemical variations can then be plotted onto a series of bivariate plots to discriminate between tephra sources. Tephra from the Askja volcano is identified by plotting La and Nb; Katla is identified by plotting Ti and Nb; Hekla is noted by plotting Zr and Sr; Torfajökull and Öræfajökull are discriminated by their Yb and Gd concentrations.

A formal framework has also been established to determine whether tephra layers sourced

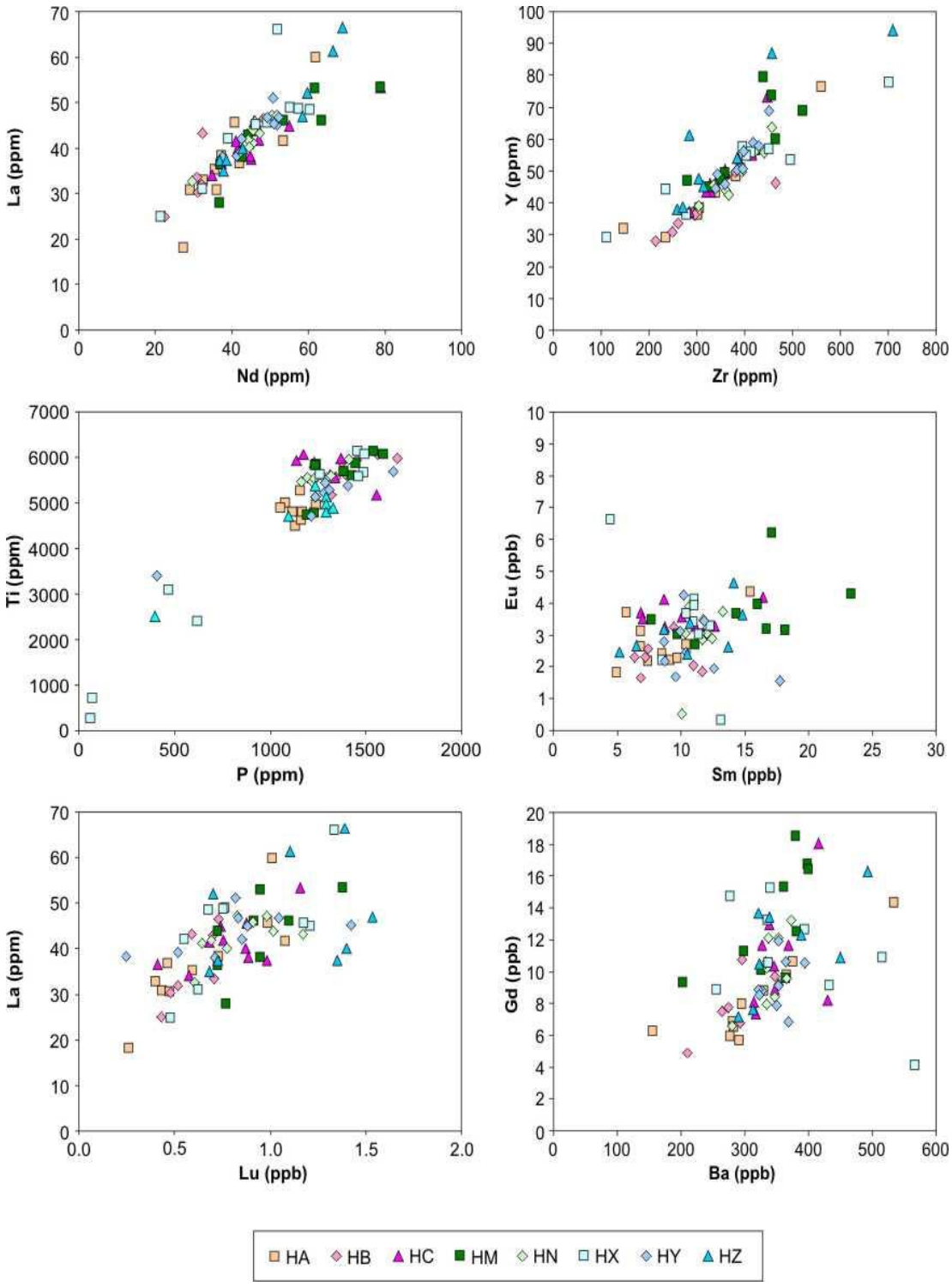

Fig. 7.40: Bivariate plots of trace and rare earth element combinations for the Hekla intermediate tephra layers collected via ICP-MS. The sequence of intermediate Hekla tephra layers do not show any substantial geochemical variation which might allow for their discrimination.

within the same system can be discriminated using trace element chemistry. The work has focused onto the Torfajökull, Katla, and Hekla volcanic systems as these systems are represented by more than one tephra layer. Plotting multi element diagrams for each tephra layer within the three volcanic systems highlight any minor geochemical variations between sources. Plotting the minor geochemical variations onto a series of bivariate plots allows for their discrimination. The Grákolla and Landnám tephra layers of the Torfajökull share identical major element chemistry but are easily distinguished with minimal data overlap. The Silk UN and Silk LN layers are distinguishable by plotting trace elements however their major element chemistry suffices for this purpose. The Hekla tephra layers are separated into silicic and intermediate sub-groups as defined in Chapter 6. Within the silicic sub-group the H1104, H3, HSelsund, H4 and H5 tephra layers are easily discriminated by plotting Zr, Ti, Nb, La and Ba. There remains some data overlap between H3 and H1104 with minimal data overlap achieved by plotting the element K. The intermediate Hekla tephra layers show some potential for discrimination when plotted on multi element and rare earth element plots. However when plotted onto bivariate plots there remains such a data overlap between the tephra layers that no discrimination can be established.

The following chapter will be a discussion of the data presented in Chapters 5, 6 and 7. The discussion will focus onto the applications and implications of the data set for North Atlantic Quaternary studies. The chapter will also discuss interesting questions that have arisen during this research and will present options for further work.

Chapter 8:

Discussion

8.1 Introduction

Chapters 5, 6 and 7 presented major, trace and rare earth element chemistry for a suite of Holocene Icelandic tephra layers sourced from the Torfajökull, Askja, Katla, Öræfajökull and Hekla volcanic systems. The chapters investigated whether application of the new data in conjunction with the old data (e.g. Larsen *et al*. 1999), could be used to refine identification of tephra provenance and in turn discriminate between tephra layers sourced within the same volcanic system.

The main aims of this chapter are as follows:

1. To discuss the influence, applications and implications of the new data set for future North Atlantic Quaternary studies.
2. To discuss any questions arising from the new data set, including implications for previous tephrochronology studies and existing models for silicic magma generation, with particular reference to the Hekla volcanic system.
3. To discuss suggestions for further work highlighted during this thesis.

8.2 Development of the reference data set

Chapter 3 introduced the idea that the comparability of geochemical data sets is influenced by analytical set up, sample preparation techniques and the precision, accuracy, age and makeup of the equipment used. Some work has been conducted to improve the comparability of data collected at different institutions (e.g. Hunt and Hill, 1993; INTAV 2010 session) and as a result standardised analytical set ups are being developed (e.g. Hayward, *in review*). Such work is of great importance to the tephrochronology community as it increases the reliability and quality of the geochemical data collected and increases the credibility of

interpretations based on the resulting tephra identification and correlation. Despite the successful enforcing of standardised sample preparation and analytical techniques, there remains an absence of standardised geochemical reference data sets. At present, workers in the North Atlantic tephrochronology community designate a data set to be "reference data" without properly investigating the accuracy of such assertions. Typically, such a data set is one collected in an earlier study and used to infer the identity of an unknown tephra layer. Any mis-identification and subsequent dating based on such a data set at this early stage would permeate discrepancies through ensuing studies based on the original work.

Undertaking the development of a robust geochemical reference dataset of Icelandic Holocene tephra layers was the main objective of this research project. Development of the geochemical dataset, should improve the robustness and reliability of the already established technique of identifying and correlating tephra layers using their major element chemistry. The importance of using recognised reference data when using trace and rare earth elements to identify tephra layers will be instilled. Geochemical analyses included in the dataset were analysed at the Tephra Analytical Unit at the University of Edinburgh to the highest standards to ensure the best quality data. Standardised set up procedures were implemented, recognised international reference materials were used for calibration and tephra shards with totals less than 97.5 wt. % were discarded. Samples were collected from proximal reference locations in Iceland as defined in Chapters 3 and 4 to ensure the best reflection of the stratigraphy of each eruption. The analysis of such a large number of tephra layers using identical analytical conditions also allows for regulation of any variations within the equipment at Edinburgh.

It should be noted that the dataset does not solely comprise geochemical data, but also includes field data and photographs for each tephra layer (see Chapters 5 and 6) and maps and sampling information to allow the identification of reference localities for future studies (see Chapter 4). Additional information includes general background data on the individual tephra layers including, where available, information regarding main axes of thickness, isopach maps, thickness and volume estimates (see Chapter 2). Major element data from previous studies has been compiled (Appendix), with appropriate reference sources acknowledged, as well as maps of distal limits within the North Atlantic region and a list of alternative names for each tephra layer at each sampling location. Tephrochronology studies typically rely on the identification, dating and correlation of tephra layers as a stepping stone in a greater interdisciplinary research project. However, access to such an array of

information as catalogued within the dataset provides an easily accessible forum for sharing such information and will be of critical importance to early stage researchers and PhD students working across the North Atlantic region from a range of disciplines. The dataset will also greatly reduce the difficulty of researching, obtaining and disseminating information from multiple sources that might otherwise be unavailable to individual users by identifying information and directing users to its location. The geochemical data collected for this thesis will also be incorporated into the tephra database Tephrabase which is available online for use by other workers.

The information collected for the dataset could contribute to the fields of physical volcanology and natural hazards including field photographs and sedimentary logs for 15 intermediate to silicic Icelandic tephra layers. The sedimentary logs visually present information regarding each tephra layer including grain size and morphology, colour, vesiculation, sedimentary structures and componentry. Such information can be used to infer information about each tephra layer including eruption explosivity, transportation mechanisms, chemistry, volatile content, depositional mechanisms and magma generation (see Chapter 3 for more information). Such information can be used by the scientific community in a number of ways. Grain size, morphology and vesiculation can be used to understand eruption processes occurring at individual volcanic systems e.g. at ice- and non-ice covered edifices. The sedimentary logs are also used to establish a chronology of events within a volcanic eruption. Depositional processes (i.e. ash fall or PDC) can be established via sedimentary structures and clast morphology within the logs. Volatile content can be studied by analysing the size, shape and distribution of vesicles in the samples collected. The recorded grain size can be a direct proxy for eruption intensity with smaller grain sizes typically representing low intensities and larger grain sizes indicated increasing eruption intensities (Fig. 8.1a-c).

Previous studies have suggested that the first erupted material (i.e. at the base of the deposit) represents an initial high intensity eruptive phase that correlates with the farthest dispersed distal micro-tephra horizons (Fig. 8.1c). Our work however, indicates that eruption intensity varies during each event with some eruptions peaking early and others much later. This suggests that correlation of eruptive phases is only possible once the proximal stratigraphy of an eruptive event has been thoroughly recorded. This work could be developed by studying each deposit at a number of reference sites to ensure that changes in grain size do in fact represent changes in eruption intensity rather than changes in wind direction.

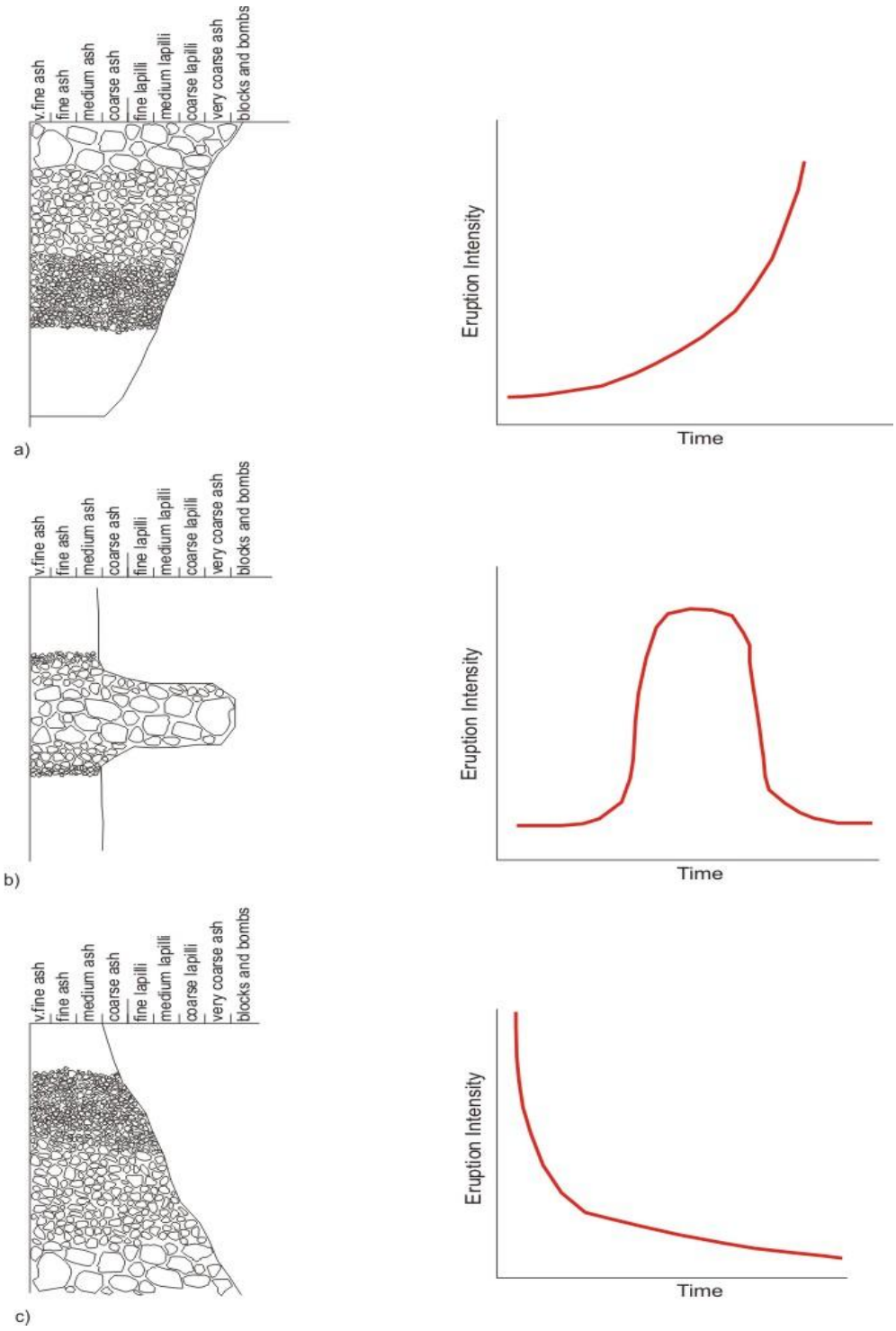

Figure 8.1: Sedimentary logs of three eruptive scenarios with matching graphical profiles. a) increasing grain size indicating increasing eruption intensity or explosivity. b) a grain size peak during the eruption indicates a short-lived peak in eruption intensity. c) decreasing grain size indicates decreasing eruption intensity or explosivity. Grain size variations in stratigraphic profiles may also be the result of variations in wind direction and intensity and cannot be ruled out without investigation of multiple reference sections, which was outside the scope of this project.

Isopach maps and distribution maps can be used while studying the transportation and deposition of tephra. For example, the intermediate Hekla tephra layers HA-HZ are grouped and defined by their main axes of dispersal (Fig. 2.19). Combining this information with currently unpublished isopach maps by Brandsdóttir provides a more thorough data set for these tephra layers and allows for inferences of potential sampling locations.

8.3 Questions arising from this thesis

The following sections present and discuss a number of interesting questions which have arisen from the research conducted for this thesis.

8.3.1 Incorporation of small-scale Icelandic tephra layers

Tephrochronology studies across the North Atlantic typically focus on large-scale silicic Icelandic eruptions (e.g. A1875, Ö1362, H1104, H3 and H4). These silicic tephra layers are preferentially studied as they are widespread, easily identified and recovered in sedimentary successions and are generally geochemically distinct.

Figure 8.2 (Fig. 3.5 in Chapter 3) indicates a large discrepancy between the established Icelandic and North Atlantic tephra stratigraphies. There are at least 31 silicic to intermediate composition eruptions represented in the proximal stratigraphy that do not yet appear in the distal stratigraphy. Conversely, 26 tephra layers have been identified in distal sedimentary successions that do not correlate with any known eruptions in the proximal Icelandic stratigraphy. Of the distal tephra layers, 15 show no recognised Icelandic geochemical affinity. The tephra layers may be sourced outside of Iceland, from the Jan Mayen, Eifel or Italian volcanic fields. Tephra provenance can be established by plotting multi element diagrams (see Chapter 7) which highlight modes of magma generation based on overall trends (i.e. mid-ocean ridge, ocean island or subduction settings). This highlights the need for a full suite of geochemical data when conducting tephrochronology studies to ensure a full understanding of each tephra layer. The large number of uncorrelated tephra layers may also be explained by the apparent dismissal of intermediate compositions from tephrochronology studies. Such tephra layers are typically ignored and assumed not to be useful long distance markers due to their association with smaller-scale eruptions.

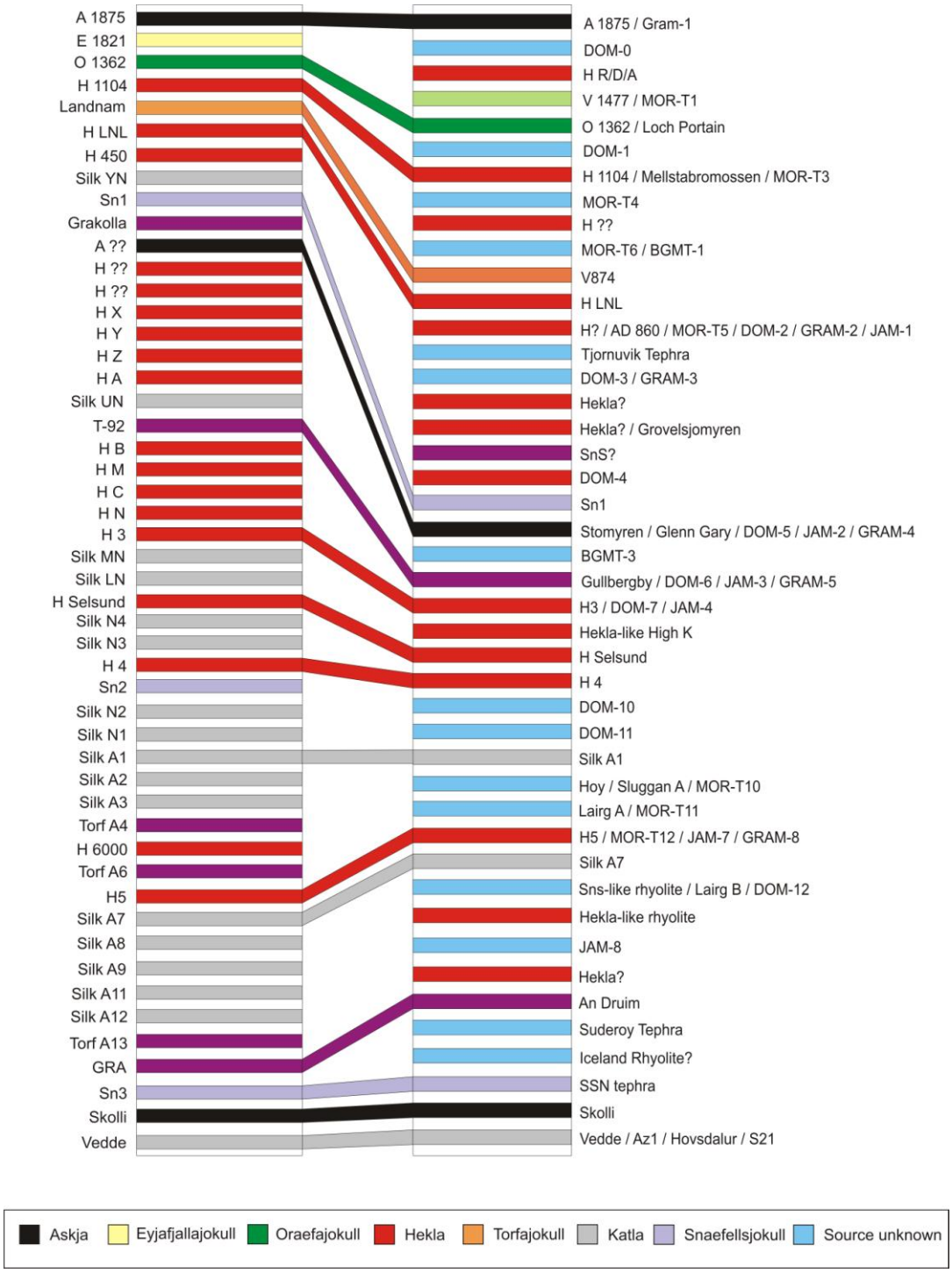

Figure 8.2: tephrostratigraphy of Iceland and the North Atlantic region. The column on the left depicts the main intermediate-silicic tephra layers known from the Holocene tephra record of Iceland. The column on the right depicts the main intermediate-silicic micro-tephra horizons identified in terrestrial, marine and lacustrine sedimentary sequences across the North Atlantic. Tephra layers correlated between proximal and distal locations are represented by a coloured band joining the two. Where the source of an eruption is unknown, the layer is coloured pale blue.

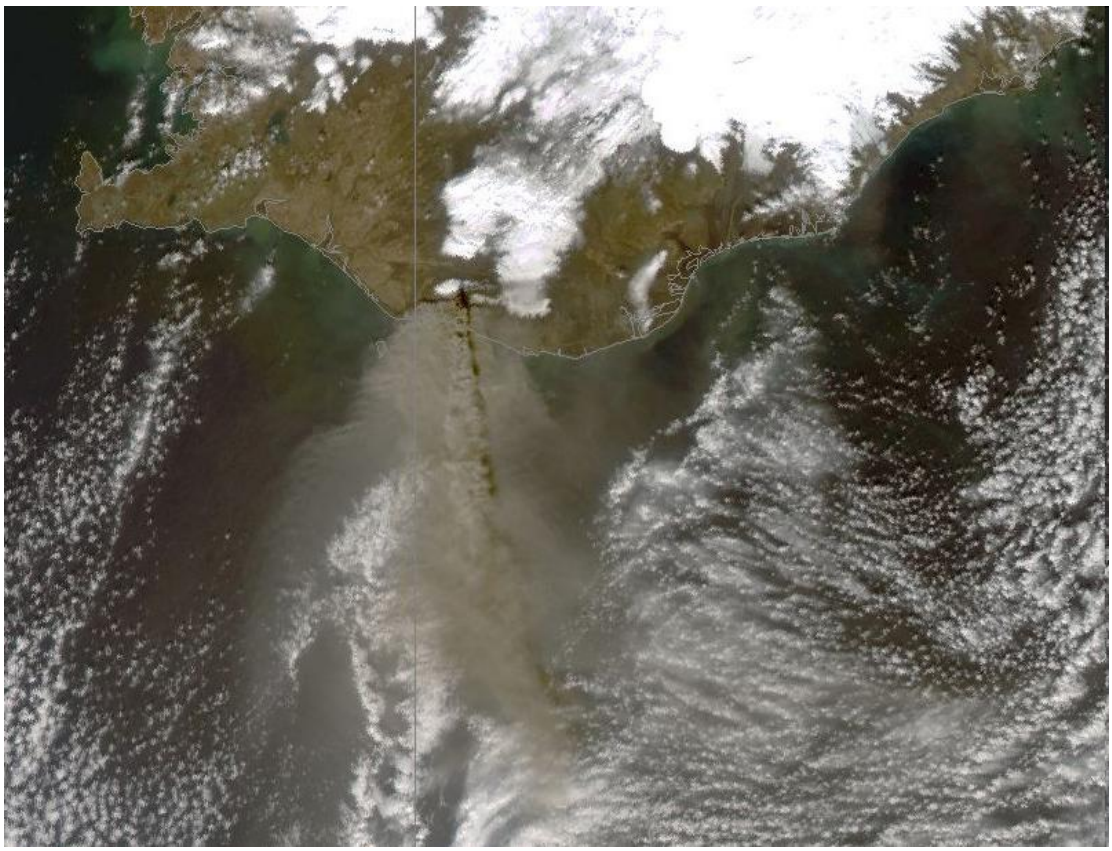

Figure 8.3: Satellite image of the Eyjafjallajökull 2010 eruption plume dispersing in a due south direction from the active edifice towards Europe (Met Office UK).

Intermediate tephra layers may be present in the successions, but are missed due to the current micro-tephra recovery techniques which are best suited for low density silicic tephra shards (see Chapter 3). Tephra layers may also be missing from the known distal record to due to localised changes in wind direction at the source.

The importance of smaller-scale intermediate tephra layers is underestimated and that the layers may become a vital component of North Atlantic tephrochronology. The 2010 eruption of the Eyjafjallajökull volcano in Iceland provided an opportunity to study the impact of a small-scale intermediate tephra layer. The eruption was relatively small (VEI c. 3), was volumetrically insignificant (0.14 km^3, Larsen *et al*. 2010), had minimal impact on the Icelandic mainland as indicated by its isopach pattern (Fig. 8.4) and a year on is recorded only in local stratigraphic profiles. Despite the small size of the eruption, the resulting tephra was transported due south (Fig. 8.3) across Western Europe causing chaos to the international aviation industry. Very fine ash fall was recorded in Scotland, England, Wales,

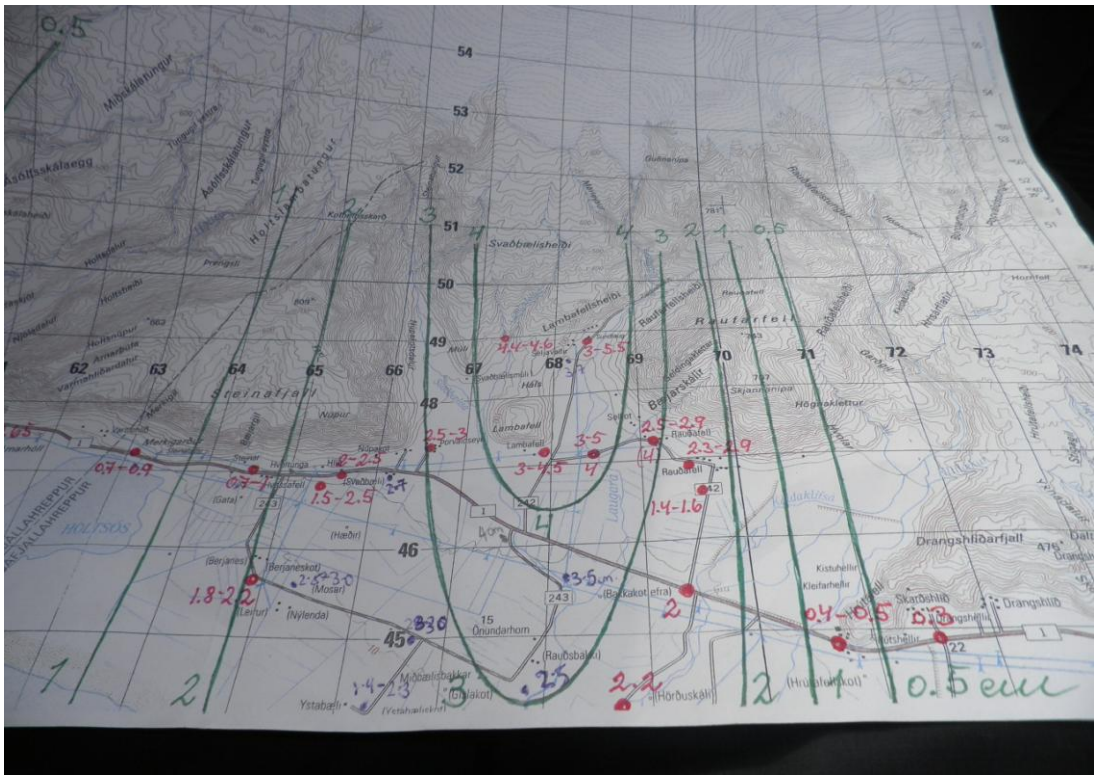

Figure 8.4: Isopach map (in progress) of the Eyjafjallajökull 2010 eruption. Blue and red circles represent sampling locations and corresponding numbers represent tephra thickness in cm at the noted location. Green lines and numbers represent tephra isopach thicknesses in cm. The isopach pattern indicates dominant transportation and deposition of tephra in due south from the volcanic edifice which is located to the north of the image, beneath the white glacier. Photograph: Rh. Meara.

Northern Ireland, the Republic of Ireland, Norway, and the Faroe Islands (J. Stevenson, *pers. comm*.). Icelandic tephra is typically transported east to east–south east across Scandinavia and the northern UK in line with North Atlantic weather patterns. Transportation and deposition due south is also recorded in the 1947 Hekla eruption (Larsen *et al*. 1999). The behaviour of the Eyjafjallajökull 2010 eruption can be used as a proxy for older intermediate eruptions, suggesting a real potential for identifying similar eruptions in far-distal successions.

Small-scale tephra layers have been included into this research project and the resulting dataset with the aim of introducing such layers to the wider tephrochronology community. The tephra layers include the Grákolla tephra layer from the Torfajökull volcanic system, Silk UN and Silk LN from the Katla system and HA, HB, HC, HM, HN, HX, HY and HZ

from the Hekla volcanic system. The tephra layers are found in terrestrial and lacustrine sedimentary successions across Iceland (Jagan, 2010) and are used as regional time markers. At present, the tephra layers are not identified in sedimentary successions at distal to far-distal localities.

Of particular interest are the smaller Hekla layers which occur stratigraphically between the H3 and H1104 tephra layers (2900 – 1800 years BP). The short repose periods between these eruptions allow for accurate correlation of sedimentary successions over tightly constrained time-scales for the study of pre-settlement baselines for environmental change (Dugmore, *pers comm.*). Major and trace element concentrations for the tephra layers are identical (Chapters 6 and 7), making their dispersal patterns relative to the Hekla volcano the only reliable method for their identification: HA, HB and HC are identified solely to the north-west, HM and HN are found to the south-east and HX, HY and HZ are dispersed to the east (Fig. 2.17). The tephra dispersal patterns may also be used to infer potential locations where the tephra layers might be identified. HA, HB and HC follow a north-west trajectory and should appear in lake sediments and marine cores north of Iceland, and potentially within the Greenland ice cores. The HM and HN tephra layers should be identified in marine cores to the south of Iceland and potentially across the Faroe Islands, the UK and Ireland. HX, HY and HZ should be identified in lake sediments and marine cores to the east of Iceland and potentially as far afield as Norway and Sweden.

8.3.2 Impact of the new data for previous studies

The following section focuses on two previous North Atlantic tephrochronology studies and the impact of the new reference data on the original interpretations concluded from the studies.

The first study is that presented by Wastegård *et al*. (2003). The authors identify a micro-tephra horizon within a sedimentary succession in the Faroe Islands that shares the major element geochemical signature of the Landnám tephra, sourced from the Torfajökull volcanic system. They assign the accepted age of 870 AD to this tephra layer and infer similar ages for other micro-tephra horizons within the succession. This inferred age is then applied to the dating and correlation of first human colonisation of the Faroe Islands, a topic currently under debate (e.g Jóhanssen, 1985; Arge *et al*. 1991; Dugmore *et al*. 2005).

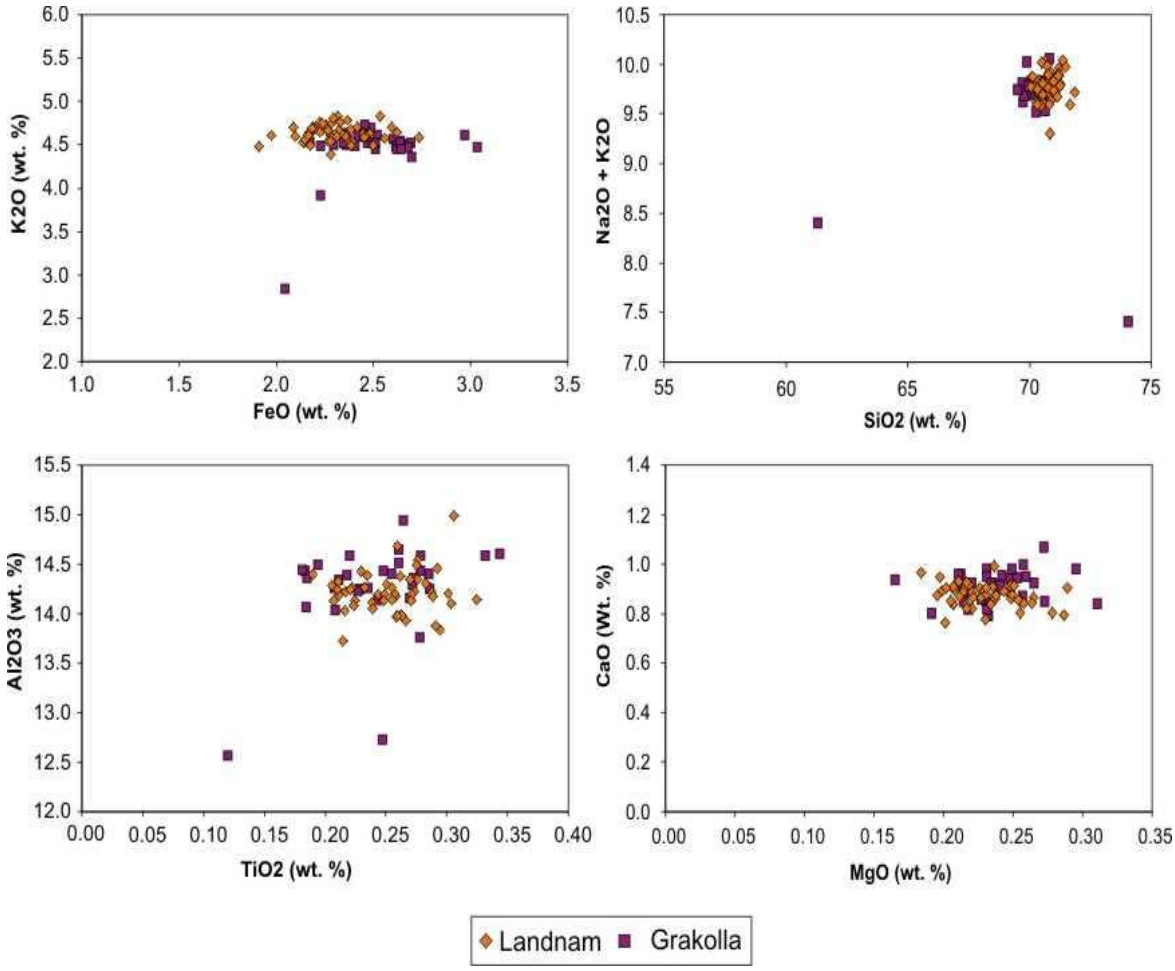

Figure 8.5: Bivariate plots of major element chemistry of the Landnám and Grákolla tephra layers. Both tephras show a near identical major element chemistry thus restricting the application of such data for identification and discrimination of the layers.

Identification of the tephra layer based solely on major element chemistry allows potential for mis-identification of the tephra layer which may in fact be an older Torfajökull tephra layer known as Grákolla. The tephra is related to the Domadalshraun eruption (1840 +/- 100 BP), but is not commonly discussed outside Icelandic literature (e.g. Jakobsson, 1979; Blake, 1984; Larsen, 1984). Both the Grákolla and Landnám tephra layers show identical major element chemistry (Fig. 8.5). Wastegård *et al* (2003) acknowledge that the succession cannot be independently carbon dated due to a radio carbon plateau at this stratigraphic level which prohibits exact dating of the over- and underlying organic sediments. The ages inferred for settlement are therefore based solely on the correct identification of the Landnám

tephra layer. Were the tephra layer mis-identified an age discrepancy of 600 years would be introduced to any subsequent interpretations.

Trace and rare earth element data collected for this research project and presented in Chapter 7 indicates that the Landnám and Grákolla tephra layers can be reasonably discriminated with minimal data overlap (Figs. 7.24 and 7.27). Availability of trace element data for the succession presented in Wastegård *et al*. (2003) would allow for comparison of the data sets with reliable confirmation of tephra identify and a robust reliable dating tool for dating the first human settlement in the Faroe Islands.

It must be stressed that we are not questioning the findings of Wastegård *et al*. (2003). The aim of this work is to highlight that assigning an identity to a major tephra horizon based solely on major element chemistry with no external dating methods can result in incorrect dating and correlation of events.

The second study is presented by Eiríksson *et al*. (2000, 2004). The authors use tephra layers identified in a sedimentary succession on the Icelandic shelf to date regional palaeo-oceanographic and climatic events and ^{14}C reservoir age variations. The tephra layers used in the study are H1104 (896 BP), H3 (2980 BP) and H4 (4270 BP) with particular interest in the H3 sampling horizon.

Major element chemistry collected via EMPA and terrestrial tephra layers are used to infer tephra identity. Identities are confirmed by the northerly pattern of transportation and deposition of the tephra layers indicated by isopach maps (Larsen and Thorarinsson, 1977). Data presented by Eiríksson *et al*. (2000, 2004) for the H3 tephra layers indicate a tephra dominated by intermediate compositions with SiO_2 values ranging from 60.94 – 69.76 wt. % with one rhyolitic analysis. Major element data collected for the H3 tephra layer for this thesis indicates a more rhyolitic composition with SiO_2 values ranging from 61.71 – 74.15 wt. %. Meanwhile, major element data collected for the smaller Hekla tephra layers – HA, HB, HC, HM, HN, HX, HY, HZ – show dominantly intermediate compositions similar to those presented by Eiríksson *et al*. (2000, 2004).

Figure 8.6 is a series of bivariate plots of major element data collected for the H3 and HA-HZ tephra layers collected for this thesis and by Eiríksson *et al*. (2000, 2004). The high-silica analyses for the HA-HZ tephra layers have been included in the figure despite the

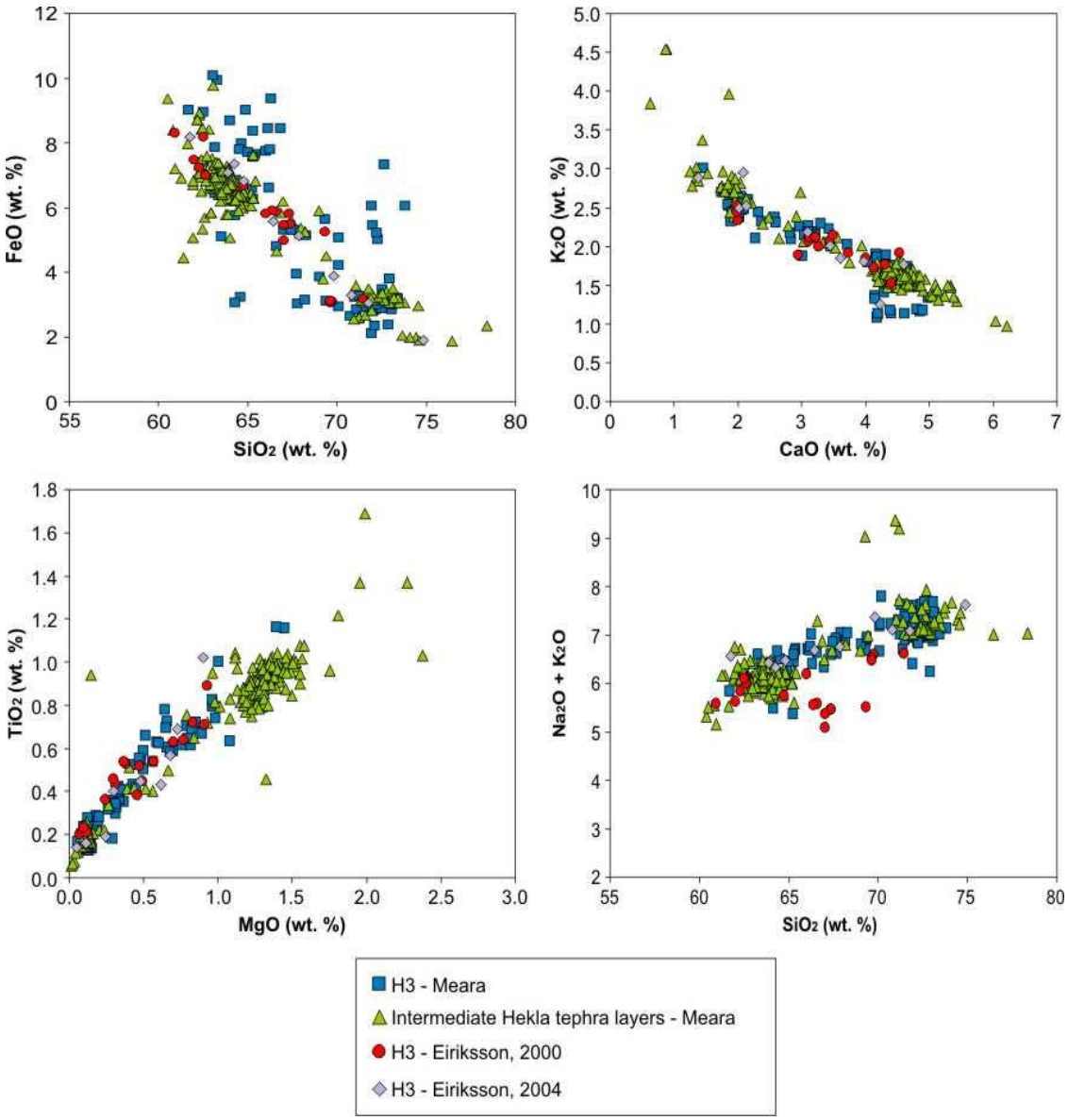

Figure 8.6: Comparison of major element chemistry collected for this study for the H3 and intermediate tephra layers with data collected by Eiríksson *et al*. (2000, 2004).

uncertainty regarding their origin. Data collected for this thesis shows consistent overlap between the H3 tephra and the HA-HZ tephra layers – the intermediate compositions representing the later stages of the H3 eruption but representing the earlier phases of the HA-HZ eruptions. Data collected by Eiríksson *et al*. (2000, 2004) plots directly onto the data overlap between the H3 and intermediate data collected for this thesis. Plotting SiO_2 against FeO highlights subtle trends between the H3 and intermediate data sets, and suggests that the

data collected by Eiríksson *et al*. (2000, 2004) follows the trend set by the intermediate HA-HZ tephra layers.

Eiríksson *et al*. (2000, 2004) state that the tephra layers represent fresh ash fall and are not influenced by ice-rafted debris or secondary deposition. However, the authors provide no photographic evidence or field descriptions of the cores to support such a statement. The authors do note that the tephra layers are associated with an increased influx of terrestrial sediment suggesting potential contamination.

We hope to highlight the potential for mis-identification of the H3 tephra layer and application of incorrect dates to subsequent research. The H3 and HA-HZ tephra layers are similar in age (2980 BP and 2800 – 1800 BP respectively) and are identified in a sequence where the radio carbon reservoir is unreliable and shows substantial temporal variation. Eiríksson *et al*. (2000, 2004) focus on dating two climatic events: the Little Ice Age (AD 1350 – 1900) and the Medieval Warm Period (800 – 1350 AD). Climatic studies such as those presented in Eiríksson *et al*. (2000, 2004) typically focus on decadal to centennial dating schemes and therefore the introduction of a dating error of 180 – 1180 years would be of great significance.

The case studies discussed in this section confirm the importance of introducing the full Icelandic tephra succession to the wider tephrochronology community. Doing so would ensure correct identification and correlation of micro-tephra horizons and would improve the overall quality and reliability of the resulting research.

8.3.3 Geochemical fingerprinting of volcanic systems and tephra layers

The main aims of this thesis were to establish:

i) Whether individual Icelandic volcanic systems showed distinct geochemical signatures or fingerprints by analysing the bulk and glass major and trace element geochemistry of a suite of silicic tephra layers.
ii) Whether individual eruptions sourced within the same system showed distinct deviations from the over-riding fingerprints by analysing the bulk and glass major and trace element geochemistry of a suite of silicic tephra layers sourced from the Hekla central volcano.

The existence of volcanic fingerprints has long been assumed for Icelandic volcanoes, and has to some extent been investigate for the North Atlantic Region (e.g. Larsen *et al*. 1999).

Confirming the existence of geochemical fingerprints for both volcanic systems and individual tephra layers has enhanced the potential for successful identification of unknown proximal to far-distal tephra layers in sedimentary successions across the North Atlantic. This includes enhancing our understanding of the proximal Icelandic stratigraphy which in turn provides an insight into the history and evolution of volcanic activity in Iceland.

Presentation and collation of such detailed geochemical data sets will be of use to the fields of Icelandic geochemistry and igneous petrogenesis. The five silicic volcanic systems studied are now represented by a suite of major, trace and rare earth element chemistry as well as detailed sedimentary logs. By combining data and logs it is possible to track stratigraphic geochemical variations within each tephra layer, which provides information regarding evolution and development of an eruption. Geochemical variations may be indicative of changes in magma source regions, injection of new material or magma chamber storage processes. This will be discussed further in the next section while section 8.4.3 will focus in particular on the Hekla volcanic system.

The multi element plots presented in Chapter 7 (see also Figs. 8.7 and 8.8) indicated that the geochemical fingerprints of each volcanic system are dominated by over-riding patterns. Each system is characterised by a negative trend indicating relative enrichment between incompatible and compatible elements. A relatively flat trend is observed within the incompatible element group. Pronounced negative anomalies are recorded for Sr, P and Ti. Small positive anomalies are recorded for Zr (Fig. 8.7). The rare earth element plots show shallowly negative trends indicating relative enrichment from light rare earth elements (LREE) to heavy rare earth elements (HREE). Pronounced negative Eu anomalies are recorded. Rare earth element ratios indicate relatively low La/Sm and Gd/Yb values (Fig. 8.8).

The trends identified in the multi element and rare earth element plots can be used to infer information regarding the generation of magma at each volcanic system. The negative trends indicate melts enriched in incompatible elements compared to bulk silicate earth or primordial mantle (McDonough and Sun, 1995). The negative trends also indicate melts

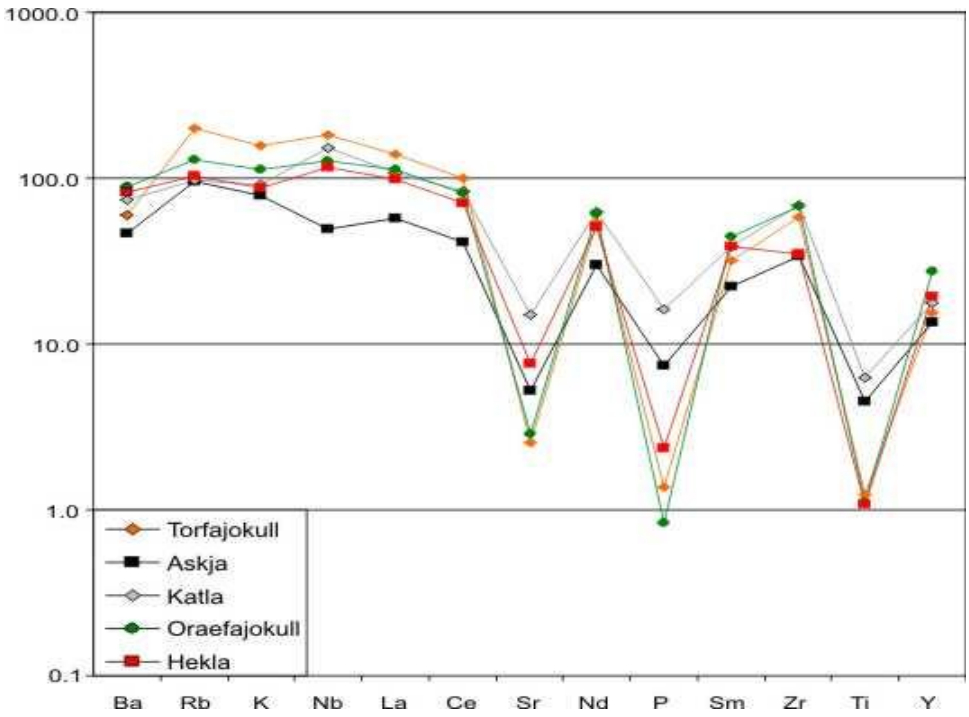

Figure 8.7: Multi element diagram of the averaged major element data for each system collected via IP and LA-ICP-MS. Data is normalised to bulk silicate earth (BSE) using the values in McDonough and Sun (1995). Each volcanic system shows individual characteristics e.g. Askja shows lower concentrations of Nb, La and Ce; Torfajökull shows higher concentrations of Rb – Ce; Katla shows the highest concentrations of Sr, P and Ti, while Öræfajökull shows the lowest. Hekla is notable in that it shows no obvious individual geochemical characteristics.

sourced from small amounts of partial melting within the mantle. The negative anomalies indicate removal of plagioclase, apatite and titanomagnetite as phenocryst phases from the melt prior to eruption. The positive Zr anomalies indicate relative enrichment of the element during melt evolution. The generally low (< 2.00) La/Sm values confirm minimal interaction with continental crust as expected from the Icelandic geological setting. Gd/Yb ratios show a range in values (0.03 – 4.79) suggesting some variation in depth of melt generation between the spinel and garnet zones. Such variations are consistent with the Icelandic regional tectonic model proposed in Chapter 2 – interaction of a spreading ridge with an upwelling mantle plume (e.g. Sæmundsson, 1979). Confirming this model would require an extensive primary basaltic data set, as the processes involved in the evolution of intermediate to silicic melts as studied in this thesis typically overprint any evidence of the original tectonic regime.

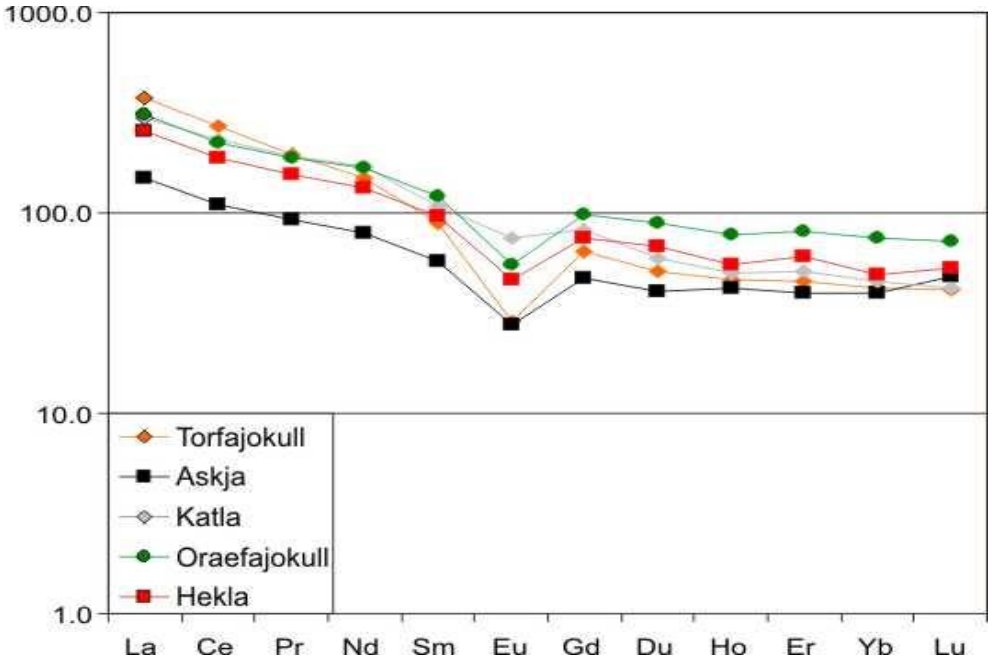

Figure 8.8: Rare earth multi element diagram of the averaged major element data for each system collected via IP and LA-ICP-MS. Data is normalised to chondrite using the values in McDonough and Sun (1995). Each volcanic system shows individual characteristics e.g. Askja shows the lowest concentrations of all elements with the exclusion of Lu; Torfajökull shows the highest concentrations of La – Ce; Katla shows the highest concentration of Eu; while Öræfajökull shows the highest concentrations of Gd – Lu. Hekla is notable in that it shows no obvious individual geochemical characteristics.

The work conducted in Chapter 7 also indicated that eruptions sourced within the same volcanic system show distinct geochemical variations. As shown in section 8.3.2, tephra layers sourced from the Torfajökull volcanic system show identical major element compositions but very distinct trace and rare earth element compositions. A similar pattern is observed within the Hekla system where the tephra layers produce three distinct geochemical sub-groups. This suggests the influence of four imprints recorded in a tephra layer's individual fingerprint:

1. The potential for regional tectonic settings influencing magma generation in all Icelandic volcanic systems due to the interaction of a spreading ridge with an upwelling mantle plume.

2. The proposition that the location of a volcanic system relative to active rifting (i.e. the older western volcanic zone or the younger propagating eastern volcanic zone) and the mantle plume may influence overall magmatic geochemistry.
3. That localised magma generating conditions vary at each volcano during individual eruptions (i.e. depth, temperature, pressure and alteration of source rock during melting) thus influencing the resulting magma compositions.
4. That magma storage at each volcano prior to and during individual eruptions (i.e. duration of storage, assimilation of wall rock, injection of fresh material during storage and fractional crystallisation) influence the final magmatic composition as a result of fractional crystallisation processes.

8.3.4 Magma generation and storage at the Hekla volcanic system

Section 8.3.3 highlighted the potential for minor variations in geochemical signatures between tephra layers sourced within the same volcanic systems. Such geochemical variations are particularly noted for tephra layers from the Hekla volcanic system. In chapters 6 and 7, Hekla tephra layers fall into three distinct geochemical sub-groups (Figs. 6.74 and 7.35): group 1 – H4 and H5; group 2 – H1104, HSelsund, H3; group 3 – HA-HZ. The three geochemical sub-groups correspond to stratigraphical assemblages and categorize tephra layers of similar ages. H4 and H5 are successive eruptions which occur between 5000 and 7000 BP. The H3 and HSelsund events occur between 3600 and 2900 BP. The HA-HZ tephra layers are a cluster of small-scale intermediate eruptions which occur post-H3 c. 2800 – 1850 BP. The only exception to the pattern is the H1104 tephra layer which, shares an almost identical geochemistry with the group 2 tephra layers despite occurring c. 2000 years after the eruption of H3.

Another pattern highlighted in the Hekla data is a minor variation in the spread of major element data collected for the H3 and HA-HZ tephra layers. The subtle differences seen in the data indicate unexpected independent magma mixing lines for both groups (Fig. 8.9). Such a pattern suggests generation of magma from separate locations and source materials for both groups.

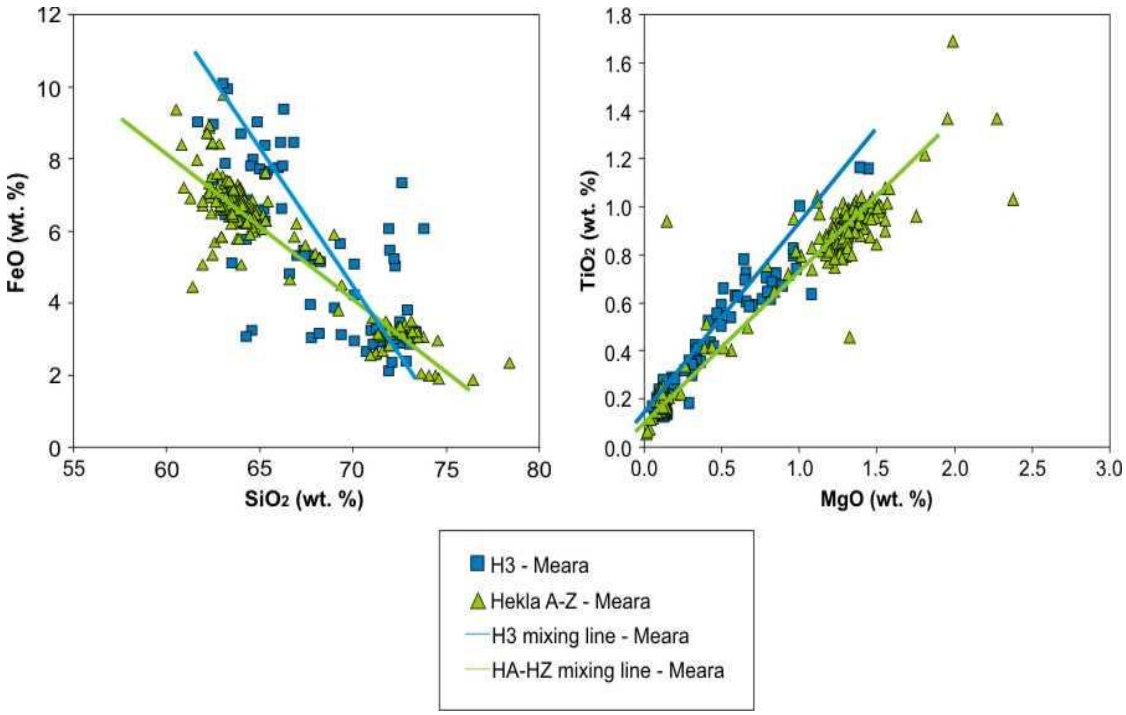

Figure 8.9: Bivariate plots of major element data for the H3 and HA-HZ tephra layers. Estimated lines of best fit have been added which represent theoretical magma mixing lines. The magma mixing lines show distinct trends for both groups suggesting separate sources and / or processes influencing the formation and evolution of magma for both groups.

Several models have been proposed to explain magma generation at the Hekla volcanic system. The accepted model is that proposed by Sigmarsson *et al*. (1992) which successfully explains the presence of a full magmatic suite from basalt to rhyolite. The model uses Th and U isotopes to establish magmatic sources. The study concludes that primary basaltic material is injected from the crust-mantle boundary and undergoes crystal fractionation to form basaltic andesite magma. The presence of hot basaltic magma initiates in-situ melting of meta-basic country rock to produce a dacitic melt fraction. The dacitic fraction undergoes fractional crystallisation to produce a rhyolitic melt. Any remaining non-fractionated dacite melt mixes with the basaltic andesite component to form an andesitic melt. The model is dependent on prolonged repose periods and substantial partial melting of country rock.

Sigmarsson *et al*. (1992) also briefly suggest that the melting source may be mobile within the crust and not restricted to a fixed magma chamber setting. They suggest that mobility within the crust explains the presence of rhyolitic magma due to the availability of un-tapped un-depleted country rock. The data collected for this thesis supports and develops this

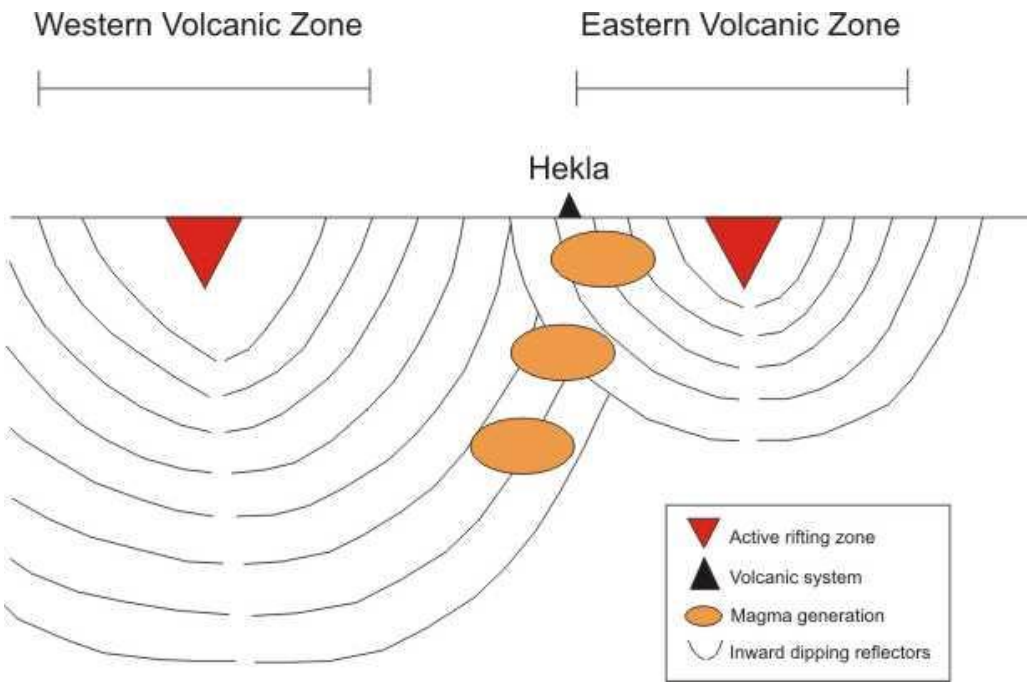

Figure 8.10: Proposed model for magma generation model at Hekla volcano. Temporal movement of the magma generation location or magma chamber causes interaction with young crust from the Eastern Volcanic Zone and old hydrated crust from the Western Volcanic Zone.

hypothesis. We believe the site of magma generation beneath the Hekla volcanic system is free to migrate within the crust and that such movement is recorded by the distinct geochemical sub-groups highlighted for the tephra layers analysed for this thesis. Each silicic eruption represents a phase of migration to an untapped source to account for the large volumes of rhyolitic melt produced. Migration may be represented by the geochemical sub-grouping seen in the Hekla tephra layers, e.g. vertical migration could be characterised by the geochemical signatures attributed to the tephra sub-groups 1-3, while horizontal migration would be characterised by variations in geochemical signature within each sub-group, i.e. geochemical variation between the H4 and H5 tephra. This work is however merely speculative and extensive further work would be require to develop a definitive answer.

Figure 8.10 illustrates the adapted model for melt generation at the Hekla volcanic system. Melt production occurring in the lower crust would be sourcing silicic melt from old typically hydrothermally altered tholeiitic rocks sourced from the Western Volcanic Zone.

Magma production occurring at shallower depths in the crust will be sourcing material from young un-altered transitional alkali rocks produced in the Eastern Volcanic Zone. Magma production occurring in between these regions would produce magma with a hybrid signature. Confirming the accuracy of the model would require further analyses to determine the conditions of magma generation i.e. pressure, temperature and volatile contents. Many questions are raised by the model with regards to sub-surface processes, e.g.:

1. Is magma generation and storage confined to a singular magma chamber or spread across a series of lenses as suggested by Checkol *et al*. (2011)?
2. To what extent has the lower crust been altered and how does this influence the residual melt it sources?
3. What influence does sub-terranean plumbing have on magma en route to the surface?

Such questions must be investigated and answered before a full petrogenetic model can be presented and confirmed for the Hekla volcanic system. Such an investigation is however outside the scope of this project.

8.4 Further Work

The research conducted for this thesis has focused on the geochemical fingerprinting of a series of major Icelandic silicic tephra marker horizons along with some lesser known intermediate tephra layers. The aim of this work has been to develop a reliable robust geochemical reference data set that can be used to aid identification and correlation of micro-tephra horizons across the North Atlantic. Due to various funding and time constraints on the project, only nineteen proximal tephra layers have been studied. Any further work conducted on this research project should initially focus on adding to the dataset by studying other silicic and intermediate tephra layers within the Icelandic succession e.g. Öræfajökull 1727, Snæfellsjökull 1-3, Katla Silk MN and YN, Askja 2000 and Skolli, Hekla Ö. Identifying smaller-scale intermediate to silicic tephra layers in the proximal record will increase the potential for correlating micro-tephra layers from currently un-known sources.

The tephra layers studied for this thesis were analysed using a variety of analytical techniques – XRF, EMPA, IP and LA-ICP-MS – to monitor any instrumental variations.

This method proved successful in highlighting differences both between bulk and glass chemistry but also within the glass analyses for IP and LA-ICP-MS. Limited availability of the ion probe facility at Edinburgh University restricted analyses to only a few grains in selected samples, compared to multiple grain and sample analyses using LA-ICP-MS. We were also unable to analyse bulk samples for rare earth element values using ICP-MS or to collect any isotopic or volatile data for the tephra layers. Further geochemical work should certainly focus on characterising the isotopic and volatile compositions of the tephra layers as such information can be used to deduce melt generation processes.

Some work has been conducted to analyse the succession of basaltic to basaltic andesite tephra layers in the Icelandic succession (e.g. Jagan (2010) and Óladóttir *et al*. 2008). Continuing this work to develop a full geochemical reference data set for the more primitive tephra layers may not provide much benefit to the tephrochronology community as primitive magmas show minimal geochemical variation. However, the increased dataset would be of use to studies of magma generation and storage within the Icelandic volcanic systems.

Aside from geochemical analyses, we have developed a series of sedimentary logs of each tephra layer at each reference section. Initially we had planned to undertake a series of physical volcanology measurements of each tephra layer (e.g. grain size measurements, componentry and density). However, this work was not completed as the urgency of preparing and analysing samples for geochemical analyses resulted in sample integrity being compromised. A detailed study of the physical volcanology of each tephra layer would provide a wealth of information regarding the evolution of eruption processes at each volcanic system throughout the Holocene.

Climate studies focusing on sedimentary cores from the Icelandic shelf use tephrochronology to date and correlate events. However, a number of the tephra layers used are older of pre-Holocene age, thus older than the tephra layers in this study. Identification and analysis of pre-Holocene terrestrial counterparts (if any exist) would provide reliable tools for correlation with sedimentary cores. Due to extensive glaciations prior to the Holocene period, many tephra layers will not relate to a terrestrial counterpart. In which case, standardised analytical techniques must become standard practise in studies of cores to ensure collection of reliable correlatable datasets.

Finally, establishing a reference dataset for the Icelandic tephra layers of the North Atlantic region will be of great use to the tephrochronology community. The dataset could however be greatly improved by including similar data (of equal quality) sourced from other volcanic centres that influence the region i.e. Jan Mayen, the Eifel region and the Italian volcanic field. By opening up collaboration with workers from these different areas, it would be possible to establish a robust international-scale tephra stratigraphy. This might assist in classifying micro-tephra horizons identified across the North Atlantic region whose provenance is currently unknown (Fig. 8.2). Such work was commenced with the development of Tephrabase; however individual researchers need to take responsibility of ensuring that their data is incorporated into such a system.

8.5 Summary

This chapter has discussed the implications of the data presented in Chapters 5, 6 and 7 for the tephrochronology, physical volcanology, geochemistry and igneous petrogenesis research communities. The introduction of small-scale intermediate tephra layers has been discussed with reference to the 2010 eruption of Eyjafjallajökull and its influence on international aviation. The influence of the new data set on North Atlantic tephrochronology studies has been highlighted by examining studies by Eiríksson *et al* (2000, 2004) and Wastegård *et al* (2003). A brief explanation details the impacts of the data set, in particular the sedimentary logs, on our understanding eruptive processes within the five volcanic systems studied. The final section of this chapter focused on the impact of the new data set with regards to Icelandic geochemistry and igneous petrogenesis. A magma generation model is presented to explain the geochemical patterns identified in the Hekla tephra layers.

The following chapter will provide an overview of the final conclusions of this thesis.

Chapter 9:

Conclusions

9.1 Introduction

This thesis has presented new major, trace and rare earth element data and a succession of sedimentary logs for a series of Holocene Icelandic silicic tephra layers. Chapter 5 investigated whether tephra provenance could be established using major element chemistry. Chapter 6 established that tephra layers sourced within the Hekla volcanic system showed significant variations in major element chemistry to allow for reasonable discrimination. Chapter 7 confirmed that each volcanic system and tephra layer studied in this thesis show individual recognisable geochemical fingerprints using trace and rare earth element chemistry. Chapter 8 presented a discussion of the implications and developments of the new data sets to tephrochronology, physical volcanology and igneous petrogenesis research, including magma generation models at the Hekla volcanic system and puts forward further work raised by this thesis. This chapter presents the final conclusions of the thesis.

9.2 Conclusions

This section presents the final conclusions of the research conducted for this thesis.

1. Application of major element chemistry to an unknown silicic tephra layer is sufficient to establish tephra provenance (Dugmore, 1989). Plotting a TAS diagram highlights two major sub-groups: high alkali and low alkali. Volcanic systems within the sub-groups can be easily discriminated by a succession of simple bivariate plots.
2. Silicic and intermediate tephra layers sourced within the Hekla volcanic system can be easily discriminated using major element chemistry. Plotting SiO_2 against FeO highlights three distinct geochemical sub-groups: 1. H4-H5, 2. H1104-H3-HSelsund, 3. HA-HZ. Once sub-groups have been established, simple bivariate plots allow for discrimination between the tephra layers in groups 1 and 2. The intermediate tephra

layers in group 3 show consistent data overlap and cannot be discriminated using major element chemistry. The Katla Silk layers also show distinct major element chemistries that allow for identification while the Landnám and Grákolla tephra layers from the Torfajökull volcanic system show indistinguishable major element characteristics.

3. The application of trace and rare earth element chemistry to the process of identifying tephra layers allows for discrimination between the Torfajökull tephra layers. The Hekla tephra layers show similar discriminations and sub-groups as with their major element chemistry, however the intermediate layers HA-HZ remain indistinguishable.
4. Plotting multi element diagrams of trace and rare earth element data for the five volcanic systems provides information regarding melt generation at both regional and local scales. The plots indicate that minor variations from an overall trend highlight geochemical fingerprints for volcanic systems as well as individual tephra layers.
5. The compilation of a robust reference data set will influence research in tephrochronology, physical volcanology and igneous petrogenesis. The new data sets collected will provide reliable references for comparison of unknown tephra horizons across the North Atlantic region. The sedimentary logs will provide information regarding eruption processes at the five volcanic systems as well as highlighting the relationship between grain size and explosivity, establishing which eruptive phases correlate with distal micro-tephra horizons. The geochemical data will further understanding of magma generation and storage at each volcanic system.
6. Geochemical data collected for the Hekla tephra layers has provided an insight into the processes controlling magma generation and storage within the system. The data sub-groups highlighted in Chapters 6 and 7 indicate three distinct phases of melt generation. We postulate that the melt phases represent temporal vertical movement of the site of magma generation within the crust beneath the volcano. Such movement would involve interaction with different source materials i.e. young transitional alkali material from the Eastern Volcanic Zone and old, hydrated tholeiitic material from the Western Volcanic Zone.

Chapter 10:

References

ARGE, S. 1991. *The Landnám in the Faroes*. Arctic Anthropology **28**(2): 101 – 120.

AUSTIN, W. E. N., WILSON, L. J. AND HUNT, J. B. 2004. *The age and chronostratigraphical significance of North Atlantic Ash Zone II*. Journal of Quaternary Science **19**(2): 137 – 146.

BASILE, I., PETIT, J. R., TOURON, S., GROUSSET, F. E. AND BARKOV, N. 2001. *Volcanic layers in Antarctic (Vostok) ice cores: Source identification and atmospheric implications*. Journal of Geophysical Research **106**(D23): 31,915 – 31,931.

BEGÉT, J. E.. AND KESKINEN, M. J. 2003. *Trace-element geochemistry of individual glass shards of the Old Crow tephra and the age of the Delta glaciation, central Alaska*. Quaternary Research **60**: 63 – 69.

BERGMAN, J., WASTEGÅRD, S., HAMMARLUND, D., WOHLFARTH, B. AND ROBERTS, S.J. 2004. *Holocene tephra horizons at Klocka Bog, west-central Sweden: aspects of preproducibility in subarctic peat deposits*. Journal of Quaternary Science **19**(3): 241 – 249.

BIJWAARD, H. AND SPAKMAN, W. 1999. *Tomographic evidence for a narrow whole mantle plume below Iceland*. Earth and Planetary Science Letters **166**: 121 – 126.

BIRKS, H. H., S. GULLIKSEN, H. HAFLIDASON, J. MANGERUD, G. POSSENERT. 1996. *New radiocarbon dates for the Vedde Ash and Saksunarvatn Ash from western Norway*. Quaternary Research **45**: 119 – 127.

BJÖRK, S., O. INGÓLFSSON, H. HAFLIDASON, M. HALLSDÓTTIR AND N. J. ANDERSON. 1992. *Lake Torfadalsvatn: a high resolution record of the North Atlantic ash zone 1 and the late glacial-interglacial environmental changes in Iceland*. Boreas **21**:15 – 22.

BLACKFORD, J. J., EDWARDS, K. J., DUGMORE, A. J., COOK, G. T. AND BUCKLAND, P. C. 1992. *Icelandic volcanic ash and the mid-Holocene Scots pine (Pinus sylvestris) pollen decline in northern Scotland*. The Holocene **2**(3): 260 – 265.

BLAKE, S. 1984. *Magma mixing and hybridization processes at the alkalic, silicic, Torfajokull central volcano triggered by tholeiitic Veidivotn fissuring, South Iceland*. Journal of Volcanology and Geothermal Research **22**: 1 – 31.

BLOCKLEY, S. P. E., PYNE-O'DONNELL, S. D. F., LOWE, J. J., MATTHEWS, I. P., STONE, A., POLLARD, A. M., TURNEY, C. S. M. AND MOLYNEUX, E. G. 2005. *A new and less*

destructive laboratory procedure for the physical separation of distal glass tephra shards from sediments. Quaternary Science Reviews **24**(16-17): 1952 – 1960.

BOND, G. C., MANDEVILLE, C. AND HOFFMAN, S. 2001. *Were rhyolitic glasses in the Vedde Ash and in the North Atlantic's Ash Zone 1 produced by the same volcanic eruption?* Quaternary Science Reviews **20**: 1189 – 1199.

BORGMARK, A. 2005. *Holocene climate variability and periodicities in south central Sweden, as interpreted from peat humification analysis*. The Holocene **15**(3): 387 – 395.

BOYGLE, J. 1998. *A little goes a long way: discovery of a new mid-Holocene tephra in Sweden*. Boreas **27**: 195 – 199.

BOYGLE, J. 1999. *Variability of tephra in lake catchment sediments, Svínavatn, Iceland*. Global and Planetary Change **21**: 129 – 149.

BOYGLE, J. 2004. *Towards a Holocene tephrochronology for Sweden: geochemistry and correlation with the North Atlantic tephrastratigraphy*. Journal of Quaternary Science **19**: 103 – 109.

BRADWELL, T., DUGMORE, A. J. AND SUGDEN, D. E. 2006. *The Little Ice Age glacier maximum in Iceland and the North Atlantic Oscillation: evidence from Lambatungnajökull, southeast Iceland*. Boreas **35**: 61 – 80.

BUCKLAND, P. C., DUGMORE, A. J. AND EDWARDS, K. J. 1997. *Bronze Age myths? Volcanic activity and human response in the Mediterranean and North Atlantic regions*. Antiquity **71**: 581 – 593.

CAREY, R. J., HOUGHTON, B. F. AND THORDARSON, T. 2009. *Abrupt shifts between wet and dry phases of the 1875 eruption of Askja Volcano: microscopic evidence for macroscopic dynamics*. Journal of Volcanology and Geothermal Research **184**: 256 – 270.

CAREY, R. J., HOUGHTON, B. F. AND THORDARSON, T. 2010. *Tephra dispersal and eruption dynamics of wet and dry phases of the 1875 eruption of Askja Volcano, Iceland*. Bulletin of Volcanology **72**(3): 259 – 278.

CAREY, S. AND SIGURDSSON, H. 1989. *The intensity of Plinian eruptions*. Bulletin of Volcanology **51**: 28 – 40.

CARMICHAEL, I. S. E. 1964. *The Petrology of Thingmuli, a Tertiary Volcano in Eastern Iceland*. Journal of Petrology **5**(3): 435 – 460.

CAS, R. A. F. AND WRIGHT, J. V. 1987. *Volcanic Successions, Modern and Ancient*. Allen and Unwin, London.

CASELDINE, C., HATTON, J., HUBER, U., CHIVERRELL, R. AND WOOLLEY, N. 1998. *Assessing the impact of volcanic activity on mid-Holocene climate in Ireland: the need for replica data.* The Holocene **8**: 105 – 111.

CHAMBERS, F. M., DANIELL, J. R. G., HUNT, J. B., MOLLOY, K. AND O'CONNEL, M. 2004. *Tephrostratigraphy of An Loch Mór, Inis Oírr, western Ireland: implications for Holocene tephrochronology in the northeastern Atlantic region*. The Holocene **14**(5): 703 – 720.

CHARMAN, D. J., WEST, S. AND KELLY, A. 1995. *Environmental change and tephra deposition: the STrath of Kildonan, Northern Scotland*. Journal of Archaeological Science **22**: 799 – 809.

CHEKOL, T. A., KOBAYASHI, K., YOKOYAMA, T., SAKAGUCHI, C. AND NAKAMURA, E. 2011. *Timescales of magma differentiation from basalt to andesite beneath Hekla volcano, Iceland: Constraints from U-series disequilibria in lava flows from the last quarter-millennium flows*. GEochimica et Cosmochimica Acta **75**: 256 – 283.

CHURCH, M. J., DUGMORE, A. J., MAIRS, K. A., MILLARD, A. R., COOK, G. T., SVEINBJARNARDÓTTIR, G., ASCOUGH, P. A. AND ROUCOUX, K. H. 2007. *Charcoal production during the Norse and early medieval periods in Eyjafjallahreppur, Southern Iceland*. Radiocarbon **49**(2): 659 – 672.

CLAUSEN, H. B., HAMMER, C. U., HVIDBERG, C. S., DAHL-JENSEN, D. AND STEFFENSEN, J. P. 1997. *A comparisson of the volcanic records over the past 4000 year from the Greenland Ice Core Project and Dye 3 Greenland ice cores*. Journal of Geophysical Research **102**: 26,707 – 26,723.

DAVIES, S. M., TURNEY, C. S. M. AND LOWE, J. J. 2001. *Identification and significance of a visible basalt-rich Vedde Ash layer in a Late-glacial sequence on the Isle of Skye, Inner Hebrides, Scotland*. Journal of Quaternary Science **16**: 99 – 104.

DAVIES, S. M., BRANCH, N. P., LOWE, J. J. AND TURNEY, C. S. M. 2002. *Towards a European tephrochronoligcal framework for Termination 1 and the Early Holocene*. Philosophical Transactions of The Royal Society London **360**: 767 – 802.

DAVIES, S. M., WASTEGÅRD, S. AND WOHLFARTH, B. 2003. *Extending the limits of the Borrobol Tephra to Scandinavia and detection of new early Holocene tephras*. Quaternary Research **59**: 345 – 352.

DAVIES, S. M., HOEK, W. Z., BOHNCKE, S. J. P. AND PYNE-O'DONNEL, S. 2005. *Detection of Late-glacial distal tephra in the Netherlands*. Boreas **34**: 123 – 135.

DAVIES, S. M., ELMQUIST, M., BERGMAN, J., WOHLFARTH, B. AND HAMMARLUND, D. 2007. *Cryptotephra sedimentation processes within two lacustrine sequences from west central Sweden*. The Holocene **17**(3): 319 – 330.

DAVIES, S. M., WASTEGÅRD, S., ABBOTT, P. M., BARBANTE, C., BIGLER, M., JOHNSEN, S. J., RASMUSSEN, T. I., STEFFENSEN, J. P. AND SNENSSON, A. 2010. *Tracing volcanic events in the NGRIP ice-core and synchronising North Atlantic marine records during the last glacial period*. Earth and Planetary Science Letters **294**: 69 – 79.

DUGMORE, A. 1989. *Icelandic volcanic ash in Scotland*. Scottish Geographical Magazine **105**(3): 168 – 172.

DUGMORE, A. J. AND NEWTON, A. J. 1992. *Thin tephra layers in peat revealed by X-radiography*. Journal of Archaeological Sciences **19**:163 - 170.

DUGMROE, A., LARSEN, G. AND NEWTON, A. J. 1995. *Seven tephra isochrones from Scotland*. The Holocene **5**: 257 – 266.

DUGMORE, A.J. AND NEWTON, A.J. 1996. *Ideas and evidence from studies of tephra in The Outer Hebrides: the last 14,000 years* (ed. D.D. Gilbertson, M. Kent and J.P. Grattan), Sheffield Academic Press, Sheffield p.45-51

DUGMORE, A. J. AND NEWTON, A. J. 1998. *Holocene tephra layers in the Faroe Islands*. Fródskaparrit **46**: 191 – 204.

DUGMORE, A. J., NEWTON, A. J., LARSEN, G. AND COOK, G. T. 2000. *Tephrochronology, environmental change and the Norse settlement of Iceland*. Environmental Archaeology **5**: 21 – 34.

EIRÍKSSON, J., KNUDSEN, K. L., HAFLIDASON, H. AND HEINEMEIER, J. 2000. *Chronology of late Holocene climatic events in the northern North Atlantic based on AMS 14C dates and tephra markers from the volcano Hekla, Iceland*. Journal of Quaternary Science **15**(6): 573 – 580.

EIRÍKSSON, J., LARSEN, G., KNUDSEN, K., HEINEMEIER, J. AND SÍMONARSON, L. A. 2004. *Marine reservoir age variability and water mass distribution in the Iceland Sea*. Quaternary Science Reviews **23**: 2247 – 2268.

ENACHE, M. D. AND CUMMING, B. F. 2006. *The morphological and optical induced properties of volcanic glass: a tool to assess density induced vertical migration of tephra in sediment cores*. Journal of Palaeolimnology **35**: 661 – 667.

FISHER, R. V. 1961. *Proposed classification of volcaniclastic sediments and rocks*. Bulletin of the Geological Society of America **72**(9): 1409 – 1414.

FISHER, R. V. AND SCHIMNKE, H-U. 1984. *Pyroclastic rocks*. Springer, Berlin Heidelberfg, New York, Tokyo.

FITTON, J. G., SAUNDERS, A. D., LARSEN, L. M., HARDARSON, B. S. AND NORRY, M. J. 1998. *Volcanic rocks from the southeast Greenland margin at 63ºN: composition, petrogenesis, and mantle sources*. Proceedings of the Ocean Drilling Programme, Scientific Results **152**.

FRANCIS, P. AND OPPENHEIMER, C. 2004. *Volcanoes*. Oxford University Press, Antony Rowe Ltd, Chippenham.

GOVINDARAJU, K. 1994. *Compilation of working values and sample descriptions for 383 geostandards*. Geostandards Newsletter 18: 1 – 158.

GRÖNVOLD, K., LARSEN, G., EINARSSON, P., THORARINSON, S. AND SÆMUNDSSON, K. 1983. *The Hekla eruption of 1980 – 1981*. Bulletin of Volcanology **46**: 349 – 363.

GRÖNVOLD, K., ÓSKARSSON, K., JOHNSES, S. J., CLAUSEN, H. B., HAMMER, C. U. BOMD, G. AND BARD, E. 1995. *Ash layers from Iceland in the Greenland GRIP ice core correlated with oceanic and land sediments*. Earth and Planetary Science Letters **135**: 149 – 155.

GUDMUNDSÓTTIR, E. R., LARSEN, G. AND EIRÍKSSON, J. 2011. *Two new Icelandic tephra markers: The Hekla Ö tephra layer, 6060 cal. yr BP, and Hekla DH tephra layer, ~ 6650 cal. yr BP Land-sea correlation of mid-Holocene tephra markers*. The Holocene ******: **-**.

GUDMUNDSSON, A. 1987. *Formation and mechanics of magma reservoirs in Iceland*. Geophys. JR. Astr. Soc. **91**: 27 – 41.

GUDMUNDSSON, A. 1995. *Infrastructure and mechanics of volcanic systems in Iceland*. Journal of Volcanology and Geothermal Research **64**(1-2): 1 – 22.

GUDMUNDSSON, A. 2000. *Dynamics of volcanic systems in Iceland: example of tectonism and volcanism at juxtaposed hot spot and mid-ocean ridge systems*. Annual Review of Earth and Plantetary Science **28**: 107 -140.

GUNNARSON, B., MARSH, B. D. AND TAYLOR JR, H. P. 1998. *Generation of Icelandic rhyolites: silicic lavas from the Torfajökull central volcano*. Journal of Volcanology and Geothermal Research **83**: 1 – 45.

HALL, V. A., MCVICKER, S. J. AND PILCHER, J. R. 1994a. *Tephra-linked landscape history around 2310 BC in some sites in County Antrim and Down, N. Ireland*. Biology and Environment: Proceedings of the Royal Irish Academy **94**B: 245 – 253.

HALL, V. A., PLICHER, J. R. AND MCCORMAC, F. G. 1994b. *Icelandic volcanic ash and the mid-Holocene Scots pine (Pinus sylvestris) decline in the north of Ireland: no correlation*. The Holocene **4**(1): 79 – 83.

HALL, V. A. AND PILCHER, J. R. 2002. *Late-Quaternary Icelandic tephras in Ireland and Great Britain: detection, characterisation and usefulness*. The Holocene **12**(2): 223 – 230.

HALL, V. A. AND MAUQUOY. D. 2005. *Tephra-dated and climate- and human-impact studies during the last 1500 years from a raised bog in central Ireland*. The Holocene **15**(7): 1086 - 1093.

HAYWARD, C. L. (in reviw). *High spatial resolution electron probe microanalysis of tephras and melt inclusions without beam-induced chemical modification*. The Holocene.

HINTON, R. W. 1995. *Ion microprobe analysis in geology*. Microanalytical Techniques, Eds. Reed and Potts. Chapman and Hall: 235 – 289.

HOLMES, J., HALL, V. A. AND WILSON, P. 1999. *Volcanoes and peat bogs*. Geology Today: 60 – 63.

HUNT, J. B. AND HILL, P. G. 1993. *Tephra geochemistry: a discussion of some persistent analytical problems*. The Holocene **3**: 271 – 278.

HUNT, J. B. AND HILL, P. G. 1996. *An inter-laboratory comparison of the electron probe microanalysis of glass chemistry*. Quaternary International **34**: 229 – 241.

JAKOBSSON, S.P. 1979. *Outline of the petrology of Iceland*. Jökull **29**: 57 – 73.

JENNINGS, A. E., GRÖNVOLD, K., HILBERMAN, R., SMITH, M. AND HALD, M. 2002. *High-resolution study of Icelandic tephras in the Kangerlussuaq Trough, southeast Greenland, during the last de-glaciation*. Journal of Quaternary Science **17**(8): 747 – 757.

JOHANNESSON, H., JAKOBSSON, S. P., SÆMUNDSSON, K. 1982. *Geological map of Iceland, sheet 6, S-Iceland, sheet 6, S-Iceland, 2nd edn*. Icelandic Museum of Natural History and Icelandic Geodetic Survey, Reykjavik

JÓHANNESSON, H., JAKOBSSON, S.P., S&MUNDSSON, K., 1990. *Geological map of Iceland, sheet 6, South-Iceland. (third edition)* Icelandic Museum of Natural History and Iceland Geodetic Survey, Reykjavík.

JÓHANNSDÓTTIR. G. E. 2006. *Mid Holocene to late glacial tephrochronology in West Iceland as revealed in three lacustrine environments*. Unpublished thesis. University of Iceland.

JÓNASSON, K. 2006. *Silicic volcanism in Iceland: composition and distribution within the active volcanic zones*. Journal of Geodynamics.

KIRKBRIDE, M. P. AND DUGMORE, A. J. 2001. *Timing and significance of mid-Holocene glacier advances in northern and central Iceland*. Journal of Quaternary Science **16**(2): 145 – 153.

KIRKBRIDE, M. P. AND DUGMORE, A. J. 2003. *Glaciological response to distal tephra fallout from the 1947 eruption of Hekla, south Iceland*. Journal of Glaciology **49**(166): 420 – 428.

KIRKBRIDE, M. P. AND DUGMORE, A. J. 2006. *Responses of mountain ice caps in central Iceland to Holocene climate change*. Quaternary Science Reviews **25**: 1692 – 1707.

KIRKBRIDE, M. P. AND DUGMORE, A. J. 2008. *Two millennia of glacier advances from southern Iceland dated by tephrochronology*. Quaternary Research **70**: 398 – 411.

KRISTJÁNSDÓTTIR, G. B., STONER, J. S., JENNINGS, A. E., ANDREWS, J. T. AND GRÖNVOLD, K. 2007. *Geochemistry of Holocene cryptotephras from the North Iceland Shelf (MD99-2269): intercalibration with radiocarbon and palaeomagnetic chronostratigraphies*. The Holocene **17**(2):155 – 176.

KVAMME, T., MANGERUD, J., FURNES, H. AND RUDDIMAN, W. F. 1989. *Geochemistry of Pleistocene ash zones in cores from the North Atlantic*. Norsk Geologisk Tidsskrift **64**: 251 – 272.

LACASSE, C., SIGURDSSON, H., JÓHANNESSON, H., PATERNE, M. AND CAREY, S. 1995. *Source of Ash Zone 1 in the North Atlantic*. Bulletin of Volcanology **57**:18 – 32.

LACASSE, C. 2000. *Influence of climate variability on the atmospheric transport of Icelandic tephra in the subpolar North Atlantic*. Global and Planetary Change **29**: 23 – 30.

LACASSE, C. AND GARE-SCHÖNBERG, C.-D. 2001. *Explosive silicic volcanism in Iceland and the Jan Mayen area during the last 6 Ma: sources and timing of major eruptions*. Journal of Volcanology and Geothermal Research **107**: 113 – 147.

LANGDON, P. G. AND BARBER, K. E. 2001. *Rapid Communication: New Holocene tephras and a proxy climate record from a blanket mire in northern Skye, Scotland*. Journal of Quaternary Science **16**(8): 753 – 759.

LANGDON, P. G. AND BARBER, K. E. 2004. *Snapshots in time: precise correlations of peat-based proxy climate records in Scotland using mid-Holocene tephras*. The Holocene **14**(1): 21- 33.

LARSEN, G. 1982. *Tephrochronology of Jökuldalur and the surrounding areas*. In: Thorarindóttir, H. (ed) Eldur er í Nordir. Reykjavik, Sögufélag Reykjaviku, 51 – 66.

LARSEN, G. 1982. *Gjoskutimatal Jokuldals og nagrennis (tephrochronology of Jökuldalur and the surrounding areas)*. In: THORARINSDOTTIR, H., OSKARSSON, O. H., STEINTHORSSON, S. AND EINARSSON, TH. editors, *Eldur er i Nordri*. Reykjavik: Sogufelag: 51 – 66.

LARSEN, G. 1984. *Recent volcanic history of the Veiðivötn fissure swarm, southern Iceland*. Journal of Volcanology and Geothermal Research **22**: 33 – 58.

LARSEN, G. 1992. *Gjoskulagaid ur Heklugosinu 1158 (The tephra layer from the 1158 AD eruption of Hekla)*. Jardfrædafelag Islands, Vorradstefna, Yfirlit of Agrip. Reykjavik: Geoscience Society of Iceland: 25 – 27.

LARSEN, G. 2000a. *Holocene eruptions within the Katla volcanic system, south Iceland: Characteristics and environmental impact*. Jokull **49**: 1 – 27.

LARSEN, G. 2000b. *Holoce volcanism in Iceland and tephrochronology as a tool in volcanology*. In ICELAND 2000: Modern Processes and Past Environments, Russel A, Marren P (eds) D. Reidel: Dorodrecht: 95 – 102.

LARSEN, G. AND THORARINSSON, S. 1977. *H4 and other acid Hekla tephra layers*. Jökull **27**: 28 – 46.

LARSEN, G., GUDMUNSSON, M. T. AND BJÖRNSSON, H. 1998. *Eight centuries of periodic volcanism at the center of the Iceland hotspot revealed by glacier topostratigraphy*. Geology **26**(10): 943 – 946.

LARSEN, G., DUGMORE, A. AND NEWTON, A. 1999. *Geochemistry of historical-age tephras in Iceland*. The Holocene **9**: 463 – 471.

LARSEN, G., NEWTON, A. J., VILMUNDARDOTTIR, EG. 2001. *Geochemistry, dispersal, volumes and chronology of Holocene slicic tephras from the Katla volcanic system, Iceland*. Journal of Quaternary Science **16**: 119 – 132.

LARSEN, G., EIRÍKSSON, J. KNUDSEN, K. L. AND HEINEMEIER, J. 2002. *Correlation of the late Holocene terrestrial and marine tephra markers, north Iceland: implications for reservoir age changes*. Polar Research **21**(2): 283 – 290.

LARSEN, G. AND EIRÍKSSON, J. 2008a. *Late Quaternanry terrestrial tephrochronology of Iceland – frequency of explosive eruptions, type and volume of tephra deposits*. Journal of Quaternary Science **23**(2): 109 – 120.

LARSEN, G. AND EIRKÍKSSON, J. 2008b. *Holocene tephra archives and tephrochronology in Iceland – a brief overview*. Jökull **58**: 229 – 250.

LARSEN, G., THORDARSON, TH., HOSKULDSSON, A., GUDMUNDSSON, M. T., SVERRISDOTTIR, G., ODDSON, B., OSKARSSON, B. V., JONSDOTTIR, I., OLADOTTIR, B., THORSTEINSSON, T., HARTLEY, M. E. AND MEARA, R. 2010. *On-land distribution and modes of deposition of the Eyjafjallajökull 2010 tephra*. American Geophysical Union, Fall Meeting 2010, abstract #V53F-04.

LE MAITRE, R. W., WALTER, R. 1989. *A classification of Igneous Rocks and Glossary of terms, recommendations of the International Union of Geological Sciences,* Sub commission on the Systematics of Igneous Rocks. Bibliografia: 130 – 171. Blackwell Scientific, Oxford.

LOWE, J. J. AND TURNEY, C. S. M. 1997. *Vedde Ash discovered in a small lake basin on the Scottish mainland*. Journal of the Geological Society of London **154**: 605 – 612.

R. MACDONALD, R. J. S. SPARKS, H. SIGURDSSON, D. A. MCGARVIE AND R. L. SMITH, 1987. *The 1875 eruption of Askja volcano, Iceland: combined fractional crystallisation and selective contamination in the generation of rhyolotic magma,* Mineral Mag, **51**(2): 183 - 202.

MANGERUD, J., LIE, S. E., FURNESS, H., KRISTIANSEN, I. L., LØMO, L. 1984. *A Younger Dryas Ash Bed in Western Norway, its possible correlations with tephra in cores from the Norwegian Sea and the North Atlantic*. Quaternary Research **21**: 85 – 104.

MARTIN, E. AND SIGMARSSON, O. 2007. *Crustal thermal state and origin of silicic magma in Iceland: the case of Torfajökull, Ljósufjöll and Snæfellsjökull volcanoes*. Contributions to mineralogy and petrology **153**(5): 593 – 605.

MARTIN. E. AND SIGMARSSON, O. 2007. *Low-pressure differention of tholeiitic lavas as recorded in segregation veins from Reykjanes (Iceland), Lansarote (Canary Islands)*

and Masaya (Nicaragua). Contributions to Mineralogy and Petrology **154**(5): 559 – 573.

MATTSSON, H. AND HÖSKULDSSON, Á. 2003. *Geology of the Heimaey volcanic centre, south Iceland: early evolution of a central volcano in a propagating rift?* Journal of Volcanology and Geothermal Research **127**: 55 – 71.

MCDONOUGH, W. F. AND SUN, S.-S. 1995. *The composition of the Earth*. Chemical Geology **120**: 223 – 253.

MCDOUGALL, I., KRISTJANSSON, L. AND SÆMUNDSSON, K. 1984. *Magnetostratigraphy and geochronology of Northwest Iceland*. Journal of Geophysical Research 89(8):7029 – 7060.

MCGARVIE, D. W. 1984. *Torfajökull: a volcano dominated by magma mixing*. Geology **12**: 685 – 688.

NARANJO, J. A. AND STERN, C. R. 2004. *Holocene tephrochronology of the southernmost part (42 30'-45 S) of the Andean Southern Volcanic Zone*. Revista Geológica de Chile **31**(2): 225 – 240.

NEWHALL, C. G. AND SELF, S. 1982. *The Volcanic Explosivity Index (VEI): an estimate of explosive magnitude for historical volcanism*. Journal of Geophysical Research **87**(C2): 1231 – 1238.

NICHOLSON, H., CONDOMINES, M., FITTON, J. G., FALLICK, A. E., GRÖNVOLD, K AND ROGERS, G. 1991. *Geochemical and isotopic evidence for assimilation beneath Krafla, Iceland*. Journal of Petrology 32(5): 1005 – 1020.

NORDDAHL, H. AND HAFLIDASON, H. 1991. *The Skogar Tephra, a Younger Dryas marker in North Iceland*. Boreas **21**: 23 – 41.

OLDFIELD, F., THOMPSON, R., CROOKS, P. R. J., GEDYE, S. J., HALL, V. A., HARKNESS, D. D., HOUSLEY, R. A., MCCORMAC, F. G., NEWTON, A. J., PILCHER, J. R., RENBERG, I. AND RICHARDSON, N. 1997. *Radiocarbon dating of a recent high latitude peat profile: Stor Åmyrân, northern Sweden*. The Holocene **7**(3): 283 – 290.

ÓLADÓTTIR, B. A., LARSEN, G., THORDARSON, TH. AND SIGMARSSON, O. 2005. *The Katla volcano S-Iceland: Holocene tephra stratigraphy and eruption frequency*. Jökull **55**: 53 – 74.

ÓLADÓTTIR, B. A., OLGEIR SIGMARSSON, GUDRUN LARSEN AND THOR THORDARSON. 2008. *Katla volcano, Iceland: magma composition, dynamics and eruption frequency as recorded by Holocene tephra layers*. Bulletin of Volcanology **70**: 475 – 493.

O'NIONS, R. K. AND GRÖNVOLD, K. 1973. *Petrogenetic relationships of acid and basic rocks in Iceland: Sr-isotopes and rare-earth elements in late and post-glacial volcanics*. Earth and Planetary Science Letters **19**: 397 – 409.

ÓSKARSSON, N., SIGVALDASSON, G. E. AND STEINTHÓRSSON, S. 1982. *A dynamic model of rift zone petrogenesis and the regional petrology of Iceland*. Journal of Petrology **23**(1): 28 – 74.

PALAIS, J. M., TAYLOR, K., MAYEWSKI, P. A. AND GROOTES, P. 1991. *Volcanic ash from the 1362 Öræfajökull eruption (Iceland) in the Greenland Ice Sheet*. Geophysical Research Letters **18**(7): 1241 – 1244.

PAWES, A., BESKE-DIEHL, S. AND MARSHALL, S. A. 1998. *Use of magnetic hysteresis properties and electron spint resonance spectroscopy for the identification of volcanic ash: a preliminary study*. Geophys. J. Int. **132**: 712 – 720.

PEARCE, N.J.G., WESTGATE J.A. AND PERKINS W.T. 1996. *Developments in the analysis of volcanic glass shards by Laser Ablation ICP-MS: quantitative and single internal standard-multi-element methods*. Quaternary International ,**34-36**: 213-227.

PEARCE, N.J.G., PERKINS W.T., WESTGATE J.A., GORTON M.P., JACKSON S.E., NEAL C.R. AND CHENERY S.P. 1997. *A compilation of new and published major and trace element data for NIST SRM 610 and NIST SRM 612 glass reference materials*. Geostandards Newsletter, **21**: 115-144

PEARCE N.J.G., WESTGATE J.A., PERKINS W.T., EASTWOOD W.J. AND SHANE P. 1999. *The application of laser ablation ICP-MS to the analysis of volcanic glass shards from tephra deposits: bulk glass and single shard analysis*. Global and Planetary Change, **21**: 151-171

PEARCE, N. J. G., WESTGATE, J. A., PERKINS, W. T. AND PREECE, S. J. 2004. *The application of ICP-MS methods to tephrochronological problems*. Applied Geochemistry **19**: 289 – 322.

PEARCE , N. J. G., WESTGATE, J. A., PREECE, S. J., EASTWOOD, W. J. AND PERKINS, W. T. 2004b. *Identification of Aniakchak (Alaska) tephra in Greenalnd ice core challenges the 1645 BC date for Minoan eruption of Santorini*. Geochemsitry Geophysics Geosystems **5**(3): 1 – 10.

PILCHER, J. R. AND HALL, V. A. 1992. *Towards a tephrochronology for the Holocene of the north of Ireland*. The Holocene **2**(3): 255 – 259.

PILCHER, J. R. AND HALL, V. A. 1996. *Tephrochronological studies in northern England*. The Holocene **6**(1): 100 – 105.

PILCHER, J. R., HALL, V. A. AND MCCORMAC, F. G. 1995. *Dates of Holocene eruptions from tephra layers in Irish peats*. The Holocene **5**: 103 – 110.

PILCHER, J. R., HALL, V. A. AND MCCORMAC, F. G. 1996. *An outline tephrochronology for the Holocene of the north or Ireland*. Journal of Quaternary Science **11**(6): 485 – 494.

PILCHER, J., BRADLEY, R. S. AND ANDERSON, L. 2005. *A Holocene tephra record from the Lofoten Islands, Arctic Norway*. Boreas **34**: 136 – 156.

POLLARD, A. M., BLOCKLEY, S. P. E. AND WARD, K. R. 2003. *Chemical alteration of tephra in the depositional environment: theoretical stability modelling*. Journal of Quaternary Science **18**(5): 385 – 394.

PRESTVIK, T. 1985. *Petrology of Quaternary volcanic rocks from Öræfi, southeast Iceland*. Rep. **21**Geological Institute, NTH: 81.

PRESTVIK, T., GOLDBERG, S., KARLSSON, H., GRÖNVOLD, K. 2001. *Anomalous strontium and lead isotope signatures in the off-rift Öræfajökull central volcano in south-east Iceland. Evidence for enriched endmember(s) of the Iceland mantle plume?* Earth and Planetary Science Letters **190**: 211 – 220.

PYNE-O'DONNELL, S. D. F. 2006. *Three new distal tephras in sediments spanning the Last Glacial-Interglacial Transistion in Scotland*. Journal of Quaternary Science (in press).

RANNER, P. H., ALLEN, J. R. M. AND HUNTLEY, B. 2005. *A new early Holocene cryptotephra from northwest Scotland*. Journal of Quaternary Science **20**(3): 201 – 208.

ROLLINSON H. R. 1993. *Using Geochemical Data: Evaluation, Presentation, Interpretation* (Longman, Harlow).

ROSE, N. L., GOLDING, P. N. E. AND BATTARBEE, R. W. 1996. *Selective concentration and enumeration of tephra shardsf rom lake sediment cores*. The Holocene **6**(2): 243 – 246.

SAUNDERS, A. D., FITTON, J. G., KERR, A. C., NORRY, M. J. AND KENT, R. W. 1997. *The North Atlantic Igneous Province*. in: Large Igneous Provinces: Continental, Oceanic and Planetary Flood Volcanism. Geophysical Monograph 100.

SÆMUNDSSON, K. 1978. *Fissure swarms and central volcanoes of the neovolcanic zones of Iceland*. Geological Journal Special Issue 10: 415 – 432.

SÆMUNDSSON, K. 1979. *Outline of the geology of Iceland*. Jökull **29**: 7 – 28.

SÆMUNDSSON, K. 1980. Outline of the geology of Iceland. Jökull **29**: 7 – 28

SÆMUNDSSON, K. 1986. *Subaerial volcanism in the western North Atlantic*. In: Vogt, P. R., Tucholke, B .E. (eds). The Geology of North America, The Western North Atlantic Region, vol. M. The Geological Society of America: 69 – 86.

SÆMUNDSSON, K. 1988. *Strcuture and evolutionary trends of volcano systems within the neovolcanic zones of Iceland*. Symposium of Geologic and Geochemical Evidence.

SELBEKK, R. S. AND TRØNNES, R. G. 2007. *THE 1362 AD Öræfajökull eruption, Iceland: Petrology and geochemistry of large-volume homogeneous rhyolite.* Journal of Volcanology and Geothermal Research **160**: 42 – 58.

SHARMA, K., SELF, S., BLAKE, S., THORDARSON, T. AND LARSEN, G. 2008. *The AD 1362 Öræfajökull eruption, S.E. Iceland: Physical volcanology and volatile release*. Journal of Volcanology and Geothermal Research **178**(4): 719 – 739.

SIGMARSSON, O., HÉMOND, C., CONDOMINES, M., FOURCADE, S. AND OSKARSSON, N. 1991. *Origin of silicic magma in Iceland revealed by Th isotopes*. Geology **19**(6): 621 – 624.

SIGMARSSON, O., CONDOMINES, M. AND FOURCADE, S. 1992. *A detailed Th, Sr and O isotope study of Hekla: a differentiation process in an Icelandic volcano*. Contributions to Mineralogy and Petrology **112**: 20 – 34.

SIGURDSSON, H. 1977. *Generation of Icelandic rhyolites by melting of plagiogranites in the oceanic layer*. Nature **269**: 25 – 28.

SIGURDSSON, H. AND SPARKS, R. S. J. 1978. *Rifting episodes in northern Iceland in 1874-75 and the eruption of Askja and Sveinagja*. Bulleting of Volcanology **41**: 1 – 19.

SIGURDSSON, H. AND SPARKS, R. J. S. 1978. *Lateral magma flow within rifted Icelandic crust*. Nature **274**: 126 – 130.

SIGURDSSON, H. AND R. J. S. SPARKS. 1980. *Petrology of rhyoltitic and mixed magma ejecta from the 1875 eruption of Askja, Iceland*. Journal of Petrology **22**(1): 41- 84.

SIGURDSSON, H. AND SPARKS, R. S. J. 1981. *Petrology of rhyolitic and mixed magma ejecta from the 1875 eruption of Askja, Iceland*. Journal of Petrology **22**: 41 – 84.

SIGVALDASON, G. E. 1974. *The petrology of Hekla and origin of silicic rocks in Iceland. The eruption of Hekla 1947 – 1948*. 5. Reykjavík: Societas Scientarium Islandica: 3 – 44.

SIGVALDASON G. E. 1979. *Rifting, magmatic activity and interaction between acid and basic liquids*. Nordic Volcanological Institute Report 7903: 54.

SIGVALDASSON, G. E. 2002. *Volcanic and tectonic processes coinciding with glaciation and crustal rebound: an early Holocene rhyolitic eruption in the Dyngjufjöll volcanic centre and the formation of the Askja caldera, north Iceland*. Bulletin of Volcanology **64**: 192 – 2005.

SJØHOLM, J., SEJRUP H. P. AND FURNESS, H. 1991. *Quaternary volcanic ash zones on the Iceland Plateau, southern Norwegian Sea*. Journal of Quaternary Science **6**:159 – 173.

SOOSALU, H AND EINARSSON, P. 2004. *Seismic constraints on magma chambers at Hekla and Torfajökull volcanoes, Iceland*. Bulletin of Volcanology **66**: 276 – 286.

SPARKS, S. R. J., WILSON, L. AND SIGURÐSSON, H. 1981. *The pyroclastic deposit of the 1875 eruption of Askja, Iceland*. Philos Trans R Soc Lond **299**(1447): 241 – 273.

STEVENSON, J. A., MCGARVIE, D. W., SMELLIE, J. L. AND GILBERT, J. S. 2006. *Subglacial and ice-contact volcanism at the Öræfajökull stratovolcano, Iceland*. Bulletin of Volcanology **68**: 737 – 752.

SVERRISDOTTIR, G. 2007. *Hybrid magma generation predecing Plinian silicic eruptions at Hekla, Iceland: evidence from mineralogy and chemistry of two zoned deposits*. Geological Magazine **144**(4): 643 – 659.

TALWANI, M. AND ELDHOLM, O. 1977. *Evolution of the Norwegian Greenland Sea*. Geological Society of America Bulletin **88**: 969 – 999.

THORARINSSON, S. 1944. *Tefrokronologiska studier på Island. Thjórsárdalur och dess förödelse*. Geografiska Annaler **26**: 1 – 217.

THORARINSSON, S. 1949. *Some tephrochronological contributions to the volcanology and glaciology of Iceland*. Geografiska Annaler, **31**: Glaciers and Climate: Geophysical and Geomorphological Essays: 239 – 256.

THORARINSSON, S. 1951. *Laxárgljúfur and Laxárhaun. A tephrochronological study*. Geografiska Annaler **1-2**: 1 – 89.

THORARINSSON, S. 1954. *The tephra fall from Hekla on March 29th, 1947*. The eruption of Hekla 1947 – 48 II(3): 1 – 68.

THORARINSSON, S. 1958. *The Öræfajökull eruption of 1362*. Acta Naturalia Islandica. **II** 2 99.

THORARINSSON, S. 1961. *Uppblastur i lj6si bskulagarannsokna*. Arsrit Skograektat$lags Islands*:* 17-54.

THORARINSSON, S. 1963. *Nedansjávargos við Island*. Natturufrædingurinn **35**: 49 – 74.

THORARINSSON, S. 1967. *The eruptions of Hekla in historical times*. The eruptions of Hekla, 1947 – 1948 I: 1 – 183.

THORARINSSON, S. 1970. *Hekla.* Reykjavik: Almenna Bokafelagid: 59.

THORARINSSON, S. 1974, *Vötnin stríð. Saga Skeiarárhlaupa og Grímsvatnagosa (The swift flowing rivers. The history of Grímsvötn jökulhlaups and eruptions)*: Reykjavík, Menningarsjódur, 254 p.

THORARINSSON, S. 1981. *Greetings from Iceland, ash-falls and volcanic aerosols in Scandinavia*. Geografiska Annaler. Series A, Physical Geography 65(3-4): 109 – 118.

THORDARSON, T. AND HÖSKULDSSON, A. 2002. *Iceland*. Classic Geology in Europe. Terra Publishing, Hertfordshire, England.

THORDARSON, T. AND HÖSKULDSSON, A. 2008. *Postglacial volcanism in Iceland*. Jökull **58**: 197 – 228.

THORDARSON, T. AND LARSEN, G. 2007. *Volcanism in Iceland in historical time: Volcano types, eruptions styles and eruptive history*. Journal of Geodynamics **43**:118 – 152.

THY, P., BEARD, J. S. AND LOFGREN, G. E. 1990. *Experimental constraints on the origin of Icelandic rhyolites*. Journal of Geology **98**: 417 – 421.

TOMASSON, J. 1967. *Hekla's magma* in: Iceland and Mid-Oceanic Ridges (ed. S. Björnsson). Societas Scientarium Islandica **38**: 180 – 189.

TURNEY, C. S. M., HARKNESS, D. D. AND LOWE, J. J. 1997. *Rapid Communication: The use of microtephra horizons to correlate Late-glacial lake sediment successions in Scotland*. Journal of Quaternary Science **12**(6): 525 – 531.

TURNEY, C. S. M., LOWE, J. J., WASTEGÅRD, S., COOPER, R., ROBERTS, S. J. 2001. *The development of a tephrochronological framework for the last glacial - Holocene transition in NW Europe*. In: Tephras: Chronology and Archaeology, Juvinge J, Raynal, J-P (eds). Les Dossiers de l-Archéo-Logis, No. 1, Goudet, CRDP: Clermont Ferrand; 101-109.

TURNEY, C. S. M., VAN DEN BURG, K., WASTEGÅRD, S., DAVIES, S. M., WHITEHOUSE, N. J., PILCHER, J. R. AND CALLAGHAN, C. 2006. *North European last glacial-interglacial transition (LGIT; 15 – 9 ka) tephrochronology: extended limits and new events*. Journal of Quaternary Science **21**(4): 335 – 345.

VAN DEN BOGAARD, C., DÖRFLER, W., SANDGREN, P. AND SCHMINKE, H.-U. 1994. *Correlating the Holocene records: Icelandic tephra found in Schleswig-Holstein (Northern Germany)*. Naturwissenschaften **81**: 554 – 556.

VAN DEN BOGAARD, C., DÖRFLER, W., GLOS, R. NADEAU, M., GROOTES, P. M. AND ERLENKEUSER, H. 2002. *Two tephra layers bracketing late Holocene palaeoecological changes in Northern Germany*. Quaternary Research **57**: 314 – 324.

VAN DEN BOGAARD, C. AND SCHMINKE, H-U. 2002. *Linking the North Atlantic to central Europe: a high resolution Holocene tephrochronological record from northern Germany*. Journal of Quaternary Science **17**(1): 3 – 20.

VINTHER, B. M., CLAUSEN, H. B., JOHNSEN, S. J., RASMUSSEN, K. K., ANDERSEN, S., BUCHART, L., DAHL-JENSEN, D., SEIERSTAD, I. K., SIGGAARD-ANDERSEN, S., STEFFENSEN, J. P. AND SVENSSON, A. 2006. *A synchronised dating of three Greenland ice cores throughout the Holocene*. Journal of Geophysical Research.

VORREN, K., BLAAUW, M., WASTEGÅRD, S., VAN DER PLICHT, J. AND JENSEN, C. 2007. *High-resolution stratigraphy of the northernmost concentric raised bog in Europe: Sellevollmyra, Andøya, northern Norway*. Boreas **36**(3): 253 – 277.

WALKER, G. P. L. 1966. *Acid volcanic rocks in Iceland*. Bulletin of Volcanology 29: 375 – 406.

WALLRABE-ADAMS, H-J. AND LACKSCHEWITZ, K. S. 2003. *Chemical composition, distribution, and origin of silicic volcanic ash layers in the Greenland-Iceland-Norwegian Sea: explosive volcanism from 10 to 300 ka as recorded in deep-sea sediments*. Marine Geology **193**: 273 – 293.

WASTEGÅRD, S. 2001. *The Mjáuvøtn tephra and other Holocene tephra horizons from the Faroe Islansa: a link between Icelandic source region, the Nordic Seas and the European continent*. The Holocene **11**(1): 101 – 109.

WASTEGÅRD, S. 2002. *Rapid Communication: Early to middle Holocene silicic tephra horizons from the Katla volcanic system, Iceland: new results from the Faroe Islands*. Journal of Quaternary Science 17(8): 723 – 730.

WASTEGÅRD, S. 2005. *Late Quaternary tephrochronology of Sweden: a review*. Quaternary International **130**: 49 – 62.

WASTEGÅRD, S., HALL, V. A., HANNON, G.E., VAN DEN BOGAARD, C., PILCHER, J. R., SIGURGEIRSSON, Á. AND HERMANNS – AUÐARDÓTTIR, M. 2003. *Rhyolitic tephra horizons in northwestern Europe and Iceland from the AD 700s – 800s: a potential alternative for dating first human impact*. The Holocene **13**(2): 277 – 283.

WASTEGÅRD, S., RUNDGREN, M., SCHONING, K., ANDERSSON, S., BJÖRK, BORGMARK, A. AND POSSNERT, G. 2008. *Age, geochemistry and distribution of the mid-Holocene Hekla-S/Kebister tephra*. The Holocene **18**(4): 539 – 549.

WASTEGÅRD, S. AND DAVIES, S. M. 2009. *An overview of distal tephrochronology in northern Europe during the last 1000 years*. Journal of Quaternary Science **24**(5): 500 – 512.

WATTS, W. L. 1876. *Across the Vatnajökull*. Longmans and Co. London.

WENTWORTH, C. K. 1922. *A Scale of Grade and Class Terms for Clastic Sediments*. The Journal of Geology 30(5): 377 – 392.

WOLFE, C. J., BJARNASSON, I. T., VANDECAR, J. C. AND SOLOMON, S. C. 1997. *Seismic structure of the Iceland mantle plume*. Nature **385**(6613): 245 – 247.

WOLFFE-BOENISCH, D., GISLASON, S. R., OEKLERS, E. H. AND PUTNIS, C. V. 2004. *The dissolution rates of natural glasses as a function of their composition at pH 4 and 10.6, and temperatures from 25 to 74 C*. Geochemical et Cosmochemica Acta **68**(23): 4843 – 4858.

ZIELINSKI, G. A., GERMANI, M. S., LARSEN, G., BAILLE, M. G. L., WHITLOW, S., TWICKLER, M. S. AND TAYLOR, K. C. 1997. *Volcanic aerosol records and tephrochronology of the Summit, Greenland, ice cores*. Journal of Geophysical Research **102**: 26625 – 26640.

ZILLÉN, L. M., WASTEGÅRD, S. AND SNOWBALL, I. F. 2002. *Calendar year ages of three mid-Holocene tephra layers identified in varved lake sediments in west central Sweden*. Quaternary Science Reviews **21**: 1583 – 1591.